

The Delta Barrier

A climate robust preliminary design
of the Delta21 storm surge barrier

B.L. Verschoor



The Delta Barrier

A climate robust preliminary design
of the Delta21 storm surge barrier

by

B.L. (Bob) Verschoor

to obtain the degree of Master of Science
at the Delft University of Technology,

February 6, 2023

Studentnumber: 4596331

Thesis committee:	Prof. Dr. ir. S.N. Jonkman,	<i>Chairman</i>	TU Delft
	Dr. ing. M.Z. Voorendt,	<i>First supervisor</i>	TU Delft
	Dr. ir. G.A. van Nederveen,	<i>Supervisor</i>	TU Delft
	Ing. D. van der Wiel,	<i>Supervisor</i>	Van Hattum en Blankevoort
	MSEng. G. Visser,	<i>Supervisor</i>	Van Hattum en Blankevoort

An electronic version of this thesis is available at <http://repository.tudelft.nl/>



Preface

This thesis concludes my Master of Science program in Hydraulic Engineering - Hydraulic Structures at Delft University of Technology. This design was conducted as part of the Delta21 initiative in collaboration with Van Hattum en Blankevoort and Delft University of Technology. I am grateful for the opportunity to work on such an innovative and ambitious project and I would like to extend my gratitude to the initiators of Delta21, Huub Lavooij and Leen Berke. I hope that this preliminary design and the gathered insights can aid you in the further development of this challenging project.

While studying at the Delft University of Technology, I have grown passionate about flood protection. This thesis has been a personal reminder of the many challenges the world faces regarding flood protection as a result of the climate crisis. It is my hope to contribute in finding solutions, such as the Delta21 concept, for these global flood protection challenges through the discipline of civil engineering.

This design would not have been possible without the expertise, time, critical feedback and support of my graduation committee. I would like to thank Bas Jonkman for giving me the opportunity to work on this topic and for the valuable comments during the progress meetings. My sincere gratitude goes to Mark Voorendt for introducing me to the Delta21 project and being my first supervisor (again). I enjoyed our meetings and your in depth feedback regarding both the structure of my report and the overall design process has been extremely helpful. Sander van Nederveen, thank you for being prepared to participate in my committee at a later stage and for the feedback on the integral design process in particular. Thank you to Daan van der Wiel and Gert Visser for being my supervisors at Van Hattum en Blankevoort. Many thanks for always remaining critical while reminding me not to get lost in the details and to look at the bigger picture. Daan van der Wiel, thank you for your constructive feedback throughout my thesis and sharing your knowledge about designing hydraulic structures. I enjoyed our fruitful meetings and lunch break walks in Vianen and IJmuiden. Gert Visser, thank you for all our discussions and your advice during my thesis. Your knowledge about structural design and the accompanying design process has helped me a great deal.

I would also like to thank my fellow students and friends in Delft, with whom I have spent most of my time while working on my thesis. Special thanks to Quintes van Horick, I am grateful for your company during this journey. Thank you for motivating me and most importantly for having a laugh.

Last but certainly not least, this achievement would not have been possible without the support of my family and friends, for which I am very grateful. Thank you for being patient with me and for surrounding me with positivity.

Bob Verschoor
Delft, February 6, 2023

Abstract

The world is heating up quickly. Since 1901, the temperature in the Netherlands has risen about twice as fast as the global average and the effects of climate change seem clearly noticeable. With sea levels rising and peak river discharges increasing an enormous pressure is mounting on the current Flood Protection Programme in the Netherlands and measures to prepare for an uncertain future are being developed. Although expensive, the most commonly used strategy as in the current Flood Protection Programme is to increase the retaining heights of the existing dikes. A new method to improve the flood defence system in the South West Delta of the Netherlands is the Delta21 concept. With discharging instead of raising the dikes in mind, Delta21 poses an alternative strategy to reinforcing dike sections for the downstream area of the Rhine and Meuse. The idea of Delta21 is a future-proof solution for the Southwestern Delta of the Netherlands. A solution for not only flood risk management, but energy transition and nature restoration as well.

Between the coastline of the Tweede Maasvlakte and that of the island of Goeree-Overflakkee, the Delta21 project aims to construct a flood defence in the form of a row of dunes, multiple pumping stations and a closable storm surge barrier. Considering protection against flooding, Delta21 strives to limit the water level at Dordrecht to a maximum of NAP + 2.5 m. The flood defence ensures that a lake of about 20 km² is created in the sea, as it were. By closing off the newly created Tidal Lake by means of a storm surge barrier and opening up a spillway to the Energy Storage Lake, pumping stations are able to pump excess river water from the Energy Storage Lake into the sea. The dunes and the closable storm surge barrier together provide sufficient protection against high seawater levels.

This thesis aims to come up with a preliminary, integral design for the Delta21 storm surge barrier taking into account the new Delta21 landscape design as such that the required functionality of Delta21 is met. This design must fulfil the functional and structural requirements and must fit within the ideology of Delta21. To achieve this, the hydraulic engineering design method is used. The first step in this cycle is to analyse the system with the purpose to better understand the situation in order to formulate the requirements and boundary conditions more accurately. The first design phase is concluded with the basis of design where the processes and functions of the Delta21 system explored in the system analysis are translated into the requirements and boundary conditions used for the design. The Basis of Design provides mostly "SMART" formulated functional- and structural requirements and boundary conditions. Boundary conditions at sea have been determined using Hydra-NL software. Climate change plays a vital role in this, as mostly sea level rise influences the boundary conditions significantly. Wishes from stakeholders, which are also explored in the system analysis, are translated either in requirements or evaluation criteria.

In the second step a gate type variant study is conducted. From an inventory of multiple concepts, the vertical lift gate and the segment gate remained after verification. After evaluation of the two remaining concepts using the functional requirements and criteria from stakeholders, the vertical lift gate came out as most suitable for the Delta Barrier.

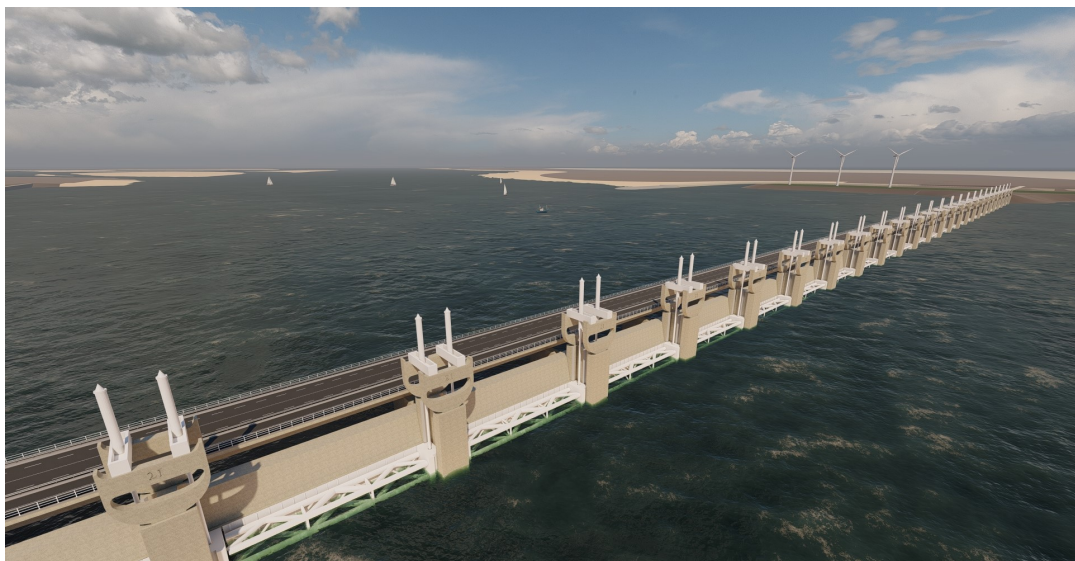
Subsequently, in the second step, a spatial and functional design is presented which satisfies all functional requirements. A new Delta21 flood protection process is proposed in order to more effectively protect the hinterland from flooding. The reliability of the closure operation has been researched after which is concluded that the closure procedure can be considered reliable until a sea level rise of ca. 1 m. It is verified with a hydrodynamic model that an effective flow area of 6000 m², defined below NAP, is to be preferred where mostly the impact on the ecosystem was governing. In order to enable passage of shipping, a location of a separate lock complex is proposed and bridge girders are incorporated into the design in order to enable the passage of road-traffic over the barrier. Furthermore, it is concluded that using tidal turbines to generate electricity with tidal flow behind the Delta Barrier is unfeasible due to the shallow water depth behind the barrier and the relatively low tidal flow velocities through the barrier. Hydraulic cylinders are chosen as driving mechanisms for the gates as it is expected that hydraulic cylinders are less expensive and have a lower failure probability than e.g. a rack and pinion

system.

Lastly, using a climate adaptive pathway approach, three general strategies are presented to the closure reliability problem of the Delta Barrier after ca. 1 m of sea level rise. Firstly, the barrier could be closed permanently as part of the "protected closed" strategy. Secondly, the dikes in the hinterland could be strengthened, the bottom protection could be strengthened, the probability that the closure of gates fail could be decreased and the Tidal Lake water level could be increased during a non-closure event. Additionally, the Water Act allows for redistribution of failure probabilities over dike segments and failure mechanisms. Changes in the closure regime could also prove beneficial. These solutions are part of the "protected open" strategy. Thirdly, inhabitants of the lower lying areas of the Netherlands could be stimulated to move to higher ground in the Netherlands as part of the "move along" strategy. It should be noted that a combination of either three strategies is very much possible and perhaps to be preferred. The Delta21 project enables the adaptation of any climate adaptive pathway where especially the "protected closed" and "protected open" strategies seem in line with the ideology of Delta21. Whereas the solutions above are presented within the context of the Delta21 flood protection system and the Delta Barrier, the problem is not specific to the Delta Barrier alone and a solution placed within an integral flood protection strategy for the entire (South West) Netherlands might be preferred.

As the third step, a structural design is presented which satisfies all structural requirements. Firstly, it is determined that a prefab construction method suits the construction of the Delta Barrier best, where the piers are to be sunk on to a prepared bed and most of the assembly of the barrier is to take place from the water using specialised vessels and equipment. Secondly, the 40 m long and 10.4 m high steel gates (25 in total) are designed. Thirdly, all main elements of the concrete civil superstructure are designed consisting of the 25 top beams, 25 sill beams and the 26 piers. In general, all concrete elements are restrained from cracking and post-tensioned. Finally, the global stability of the Delta Barrier is verified, taking into account horizontal, vertical and rotational stability, uplift, scour and internal erosion. A geometrically closed granular bottom protection is designed to tackle the latter two failure mechanisms. In a structural sense, the Delta Barrier is able to withstand a sea level rise of 3.81 m corresponding to the median projection of climate scenario SSP5-8.5 and has a design life of 200 years. The construction of the Delta Barrier will take ca. 5 years, is assumed to be completed in 2050 and will cost between ca. 2.67 and 3.50 billion euro (price level 2022).

It is recommended to further investigate the ecological impact of the Delta Barrier. Furthermore, a detailed driving mechanisms design and as such a more profound estimate for the probability that the closure of the gates fail is to be recommended.



Final design Delta Barrier

Contents

Preface	v
Abstract	vii
Part 1: Problem Analysis	1
1 Introduction	1
1.1 Thesis Motivation	1
1.2 Introduction to Delta21	3
1.3 Problem Statement	4
1.4 Design Objective	4
1.5 Scope	4
1.6 Methodology and Report Outline	4
2 System Analysis	8
2.1 Proposed Solution: Delta21	8
2.1.1 The Concept	8
2.1.2 Objectives & Purposes	9
2.2 Stakeholder Analysis	12
2.2.1 Stakeholder Inventory	12
2.2.2 Stakeholder Interests	13
2.2.3 Stakeholder Involvement	14
2.3 Process and Functional Analysis	15
2.3.1 Process Analysis	15
2.3.2 Functional Analysis	16
3 Basis of Design	18
3.1 Requirements	18
3.1.1 Functional Requirements	18
3.1.2 Structural Requirements	20
3.2 Boundary Conditions	21
3.2.1 Climate Adaptivity and Climate Scenarios	21
3.2.2 Spatial Conditions	22
3.2.3 Geotechnical Conditions	24
3.2.4 Meteorological Conditions	25
3.2.5 Sea Level	27
3.2.6 Wave Conditions	30
3.2.7 Discharge Through the Haringvliet	31
3.2.8 Tidal Lake Water Level	32
3.2.9 Discharge Through the Delta Barrier	34
3.3 Overview of Design Parameters	34
3.3.1 Functional Design	34
3.3.2 Structural Design	36
Part 2: Variant Study and Spatial and Functional Design	39
4 Gate Type Variant Study	39
4.1 Inventory of Concepts	39
4.2 Verification	42
4.3 Evaluation	42
4.4 Selection	45

5	Spatial and Functional Design	46
5.1	Proposed Delta21 Flood Protection Process	46
5.1.1	Closure Regime	46
5.1.2	Closure Frequency Delta Barrier	48
5.1.3	Closure and Opening Strategy Delta Barrier	49
5.1.4	Opening the Spillway	50
5.1.5	Overview Proposed Process Delta21 Flood Protection System	50
5.2	Reliability of the Closure Operation	51
5.3	Effective Flow Area	55
5.4	Morphological Impact of the Delta Barrier	57
5.5	Impact on the Ecological System	58
5.5.1	Tidal Flats	58
5.5.2	Tidal Range	59
5.5.3	Passage of Aquatic Creatures	59
5.6	Retaining Height	61
5.7	Passage for Shipping	63
5.8	Passage for Road-traffic	64
5.9	Tidal Turbines	66
5.10	Driving Mechanisms	68
5.11	Climate Adaptive Pathways	70
5.12	Layout & Main Dimensions	72
Part 3:	Structural Design	75
6	Construction Method	75
6.1	Prefab Instead of In-situ	75
6.2	Initial Construction	76
6.3	Building Dock	80
7	Gate Design	81
7.1	Design Strategy	81
7.2	Limit States & Load Combinations	82
7.3	Force Flow	82
7.4	Cross-section Classification	83
7.5	Strength Verifications	84
7.5.1	Normal Force	84
7.5.2	Bending Moment	85
7.5.3	Shear Force	85
7.5.4	Torsion	86
7.5.5	Bending and Shear Force	86
7.5.6	Bending and Normal Force	87
7.5.7	Bending, Shear and Normal Force	87
7.5.8	Buckling	87
7.5.9	Joints	88
7.6	Deflection	89
7.7	Natural Frequencies and Resonance	89
7.8	Final Gate Design	90
8	Civil Superstructure Design	92
8.1	Design Strategy	92
8.2	Limit States & Load Combinations	93
8.3	Concrete Cover	93

8.4	Duct and Bar Spacing	94
8.5	Losses in Pre-stress	94
8.6	Maximum Pre-stressing	96
8.7	Strength Verifications	97
8.7.1	Bending and Normal Force	97
8.7.2	Shear Force	98
8.7.3	Torsion	98
8.7.4	Shear and Torsion	99
8.7.5	Local Spalling	99
8.8	Deflection	100
8.9	Final Civil Superstructure Design	101
8.9.1	Top Beam	101
8.9.2	Sill Beam	103
8.9.3	Pier	105
9	Global Stability Verification	108
9.1	Design Strategy	108
9.2	Limit States & Load Combinations	108
9.3	Verifications	109
9.3.1	Horizontal Stability	109
9.3.2	Vertical Stability: Bearing Capacity	110
9.3.3	Vertical Stability: Settlements	111
9.3.4	Rotational Stability	112
9.3.5	Uplift	112
9.3.6	Scour	113
9.3.7	Internal Erosion	117
10	Construction Planning and Costs	119
10.1	Construction Planning	119
10.2	Construction Costs	121
Part 4:	Discussion, Conclusion and Recommendations	123
11	Discussion	123
12	Conclusion	126
12.1	Preliminary Design	126
12.2	Conclusions	129
13	Recommendations	131
References		133
Appendices		138
I	Climate Change	139
I.1	Introduction	139
I.2	Climate Scenarios	140
I.3	River Discharges	141
I.4	Sea Level Rise	142
I.5	Wind and Storms	144
I.6	Uncertainties	145

II Dutch Flood Defence Policy	146
II.1 Water Act 2017	146
II.2 The Building Decree	147
II.3 Flood Protection Programme (HWBP)	147
II.4 Knowledge Agenda of the Delta Programme	149
III Energy Transition	150
III.1 Introduction	150
III.2 Renewable Energy	150
III.3 Energy Storage Problem	150
IV Elaboration Current Process Delta21 Flood Protection System	152
V Substantiation Functional Requirements	161
VI Safety Standard Delta21	164
VI.1 Estimation of Flood Protection Standard Delta21 Dike Ring	164
VI.2 Proposed Delta21 Dike Segments with Failure Mechanisms	169
VI.3 Maximum Failure Probabilities on Object Level	172
VII Wind Data	174
VIII Geotechnical Soil Profile	176
IX Creation of a Hydrodynamic Model	179
IX.1 Tidal Lake (Storage-Basin Model)	179
IX.2 Haringvliet - Hollandsch Diep (1D Channel Model)	182
IX.3 Numerical Computation	184
IX.4 Validation and Discussion	185
X Elaboration on Design Parameters	187
X.1 Functional Design	188
X.2 Structural Design	189
XI Simulations Proposed Delta21 Flood Protection Process	193
XII Exceedance Probability of Water Storage Capacity	196
XIII Limit States Building Decree	201
XIV Complete Verification Gate Design	207
XIV.1 External Forces on the Gate	207
XIV.2 Verification per Gate Component	214
XIV.2.1 Stiffened Skin Plate (nr.1)	214
XIV.2.2 Vertical Girders: HEB240 (nr.2)	219
XIV.2.3 Stump Connectors (nr.3)	223
XIV.2.4 Truss System	228
XIV.3 Natural Frequencies and Resonance	233
XV Complete Verification Civil Superstructure	238
XV.1 Materials	238
XV.2 External Forces	239
XV.3 Top Beam	242
XV.3.1 Overview of Forces	244

XV.3.2 Bending and Normal Force	247
XV.3.3 Shear and Torsion	248
XV.3.4 Spalling Reinforcement	249
XV.3.5 Deflection	252
XV.4 Sill Beam	252
XV.4.1 Overview of Forces	255
XV.4.2 Bending and Normal Force	258
XV.4.3 Shear and Torsion	258
XV.4.4 Spalling Reinforcement	259
XV.4.5 Deflection	261
XV.5 Pier	262
XV.5.1 Flow of Forces	262
XV.5.2 Global Analysis Reinforcement Plan	265
XVI Complete Global Stability Verification	276
XVI.1 External Forces	276
XVI.2 Verifications	296
XVI.2.1 Horizontal Stability	296
XVI.2.2 Vertical Stability: Bearing Capacity	297
XVI.2.3 Vertical Stability: Settlements	300
XVI.2.4 Rotational Stability	303
XVI.2.5 Uplift	305
XVI.2.6 Scour	306
XVII Monte Carlo Simulation Construction Costs	312

1 Introduction

1.1 Thesis Motivation

The world is heating up quickly. Since 1901, the temperature in the Netherlands has risen about twice as fast as the global average. The effects of climate change seem clearly noticeable. In the last two decades the number of days with extreme precipitation has increased. The dry seasons in three consecutive years (2018, 2019 and 2020) also stood out, with the relevant question looming whether this will occur more often and/or more intensively in the future (KNMI, 2021). Reports from the KNMI in 2014 and 2021 have shown that global temperature rise can have a significant impact on the Dutch climate (see Appendix I). The most significant impact seems the accelerating sea level rise due to the melting of large ice sheets in Antarctica (and Greenland). The KNMI reports that, if no measures are taken to reduce fossil fuel emissions, the sea level could rise between 54 cm and 121 cm in 2100 compared to 1995-2014 (KNMI, 2021). Hence, climate change could have a significant impact on the way we, in the Netherlands, manage our defences and water systems. Great changes in our climate could translate to great changes in our Flood Protection Programme.

Throughout history the Netherlands has often suffered from floods. The usual response was to strengthen the levees such that the hinterland would be protected against the highest observed water level ever. Since the Watersnoodramp of 1953 (and knowledge of statistics) the way of thinking and decision making regarding flood risk has been revolutionised. Flood defences in the Netherlands had to apply to stricter requirements since the storm surge. Whereas, in the past, levees would be raised to 50 centimetres above the highest previously recorded local water level, from now on levee reinforcements would be based on the probability that a certain high water level would occur. Hence, a shift from reactive to proactive protection (Vergouwe, 2014).



Figure 1.1: Reconstruction of the 1953 Watersnoodramp (Wayenberg, 2023)

Since the Waterlaw update from the first of January 2017, new and stricter standards apply to primary flood defences (Figure 1.2). As a result, it turned out that in a number of areas significantly more of the primary flood defences did not meet the new standards (or suddenly did), in addition to some flood defences which did not even meet the old standards. Traditionally, once a new national flood risk analysis concludes that certain segments of dike rings do not meet the required annual probability of flooding, the specific dike segment would be strengthened accordingly. Therefore, a new Flood Protection Programme as part of the current Dutch flood defence policy (see Appendix II), was started in order to attain the maximum individual risk of 1:100000 everywhere. In this Flood

Protection Programme (HWBP in Dutch), the 21 Dutch water boards and the central government are working together on the largest dike improvement operation since the Delta Works. The aim of the programme is that by 2050 the primary flood defences managed by the water boards and Rijkswaterstaat will meet the new standards. This concerns almost 1500 km of dikes and almost 500 structures (Rijkswaterstaat, 2021a).



Figure 1.2: Safety standards (signaling values) of primary dike segments since 2017 (Rijkswaterstaat, 2021b)

However, areas outside of the dikes are not considered in the current Flood Protection Programme. In Rijnmond-Drechtsteden, the area around Rotterdam and Dordrecht, ca. 60000 people are living in areas outside of the dikes (Berke & Lavooij, 2018c). Furthermore, for the area of Rijnmond-Drechtsteden, the water comes from four sides: from the sea, the rivers, the air (precipitation) and the soil (seepage). It is a densely populated area with great economic significance for the Netherlands. All these things make the area rather vulnerable. Rijnmond-Drechtsteden is an area of extremes: with port activities, an urban area, the Greenports (horticulture), Groene Hart and nature reserves such as De Biesbosch. Economic and spatial development is only possible here if flood risk management is in order, now and in the future. The anticipated effects of climate change resulting in a certain expected sea level rise and a growth of the population and economy in flood-prone areas are expected to result in an increase of flood risk levels in the future (Jonkman, Kok, & Vrijling, 2008).

In December 2015, The Paris Climate Agreement was concluded, in which it was agreed that the world should not warm by more than 2°C compared to the pre-industrial era (1850-1900) and aim for 1.5°C. In order to reach the Net Zero Emissions by 2050 a stronger commitment is needed to limit global temperature rises to 1.5°C (see Appendix III).

1.2 Introduction to Delta21

With discharging instead of raising (the dikes) in mind, Delta21 poses an alternative strategy to reinforcing dike sections for the downstream area of the Rhine and Meuse. The idea of Delta21 is a future-proof solution for the Southwestern delta of the Netherlands. A solution for not only flood risk management, but energy transition and nature restoration as well.

Between the coast of the Tweede Maasvlakte and that of the island of Goeree-Overflakkee, the Delta21 project aims to construct a flood defence in the form of a row of dunes, multiple pumping stations and a closable storm surge barrier (Figure 1.3). The flood defence ensures that a lake of about 20 km² is created in the sea, as it were. The Pumping Stations in the flood defence system have more than sufficient capacity to pump the excess water into the sea at the highest expected river water levels. By temporarily lowering the water level of the Tide Lake and discharging excess river water to the sea via the Spillway of the Energy Storage Lake the water level can be kept at a maximum of NAP + 2.5 m at Dordrecht, even with a rise in sea level due to climate change (Delta21, 2021a). The dunes and the closable storm surge barrier together provide sufficient protection against high seawater levels.

Fortunately, the current water levels at the North sea are rarely too high (in combination with a high river discharge). For these daily circumstances, the lake is also useful. If there are no high water levels, the pumping station can be used to give the lake the function of an energy storage lake. The new Delta21 landscape design by van Eeden (2021) is designed as such that nature will be restored and enhanced. The recovery of fish migration in the Haringvliet is addressed with the incorporation of a fish migration river bypassing the Haringvlietsluizen. With an environmentally friendly design, the Energy Storage Lake and the salt spray present can provide unique vegetation, somewhat comparable to the Voornes Duin (Delta21, 2021a).

This thesis focuses on the design of one of the components of the Delta21 concept: the storm surge barrier between the North Sea and the current Haringvliet estuary, connecting the Energy Storage Lake and the island of Goeree-Overflakkee (number 3 in Figure 1.3).



Figure 1.3: Landscape design Delta21 (modified from van Eeden (2021))

1.3 Problem Statement

Based on the thesis motivation and Delta21 introduction, the following problem statement can be formulated:

Delta21 still lacks a design of a structure which can effectively close of the Tidal Lake from the North Sea, taking into account the new Delta21 landscape design as such that the required functionality of Delta21 is met and to prevent flooding of the hinterland.

1.4 Design Objective

Given the requirement that the Haringvliet estuary is to be open to the sea under daily conditions the solution to the problem statement as stated above should come in the form of a closable storm surge barrier. Hence, the objective of this thesis is to make a preliminary, integral design for the storm surge barrier between the Energy Storage Lake and the island of Goeree-Overflakkee at the inflow point of the Delta21 Tidal Lake (i.e. between the North Sea and the Tidal Lake).

Focus of the design will mostly be on the required functionality, both regarding the Delta Barrier individually and as a part of the Delta21 flood protection system as a whole. Nonetheless, from the required functionality, a structural substantiation should follow. Furthermore, the storm surge barrier design ought to be climate robust in the broadest sense, i.e. should be able to withstand new boundary conditions as a result of climate change. The barrier should enable a proper functioning water management system of the Delta21 concept for at least the entire lifetime of the storm surge barrier.

1.5 Scope

This thesis focuses on the preliminary design of the storm surge barrier connecting the Energy Storage Lake and the island of Goeree-Overflakkee. The preliminary design should be integrated into the Delta21 concept in such a way that at the least all primary and preserving functions (see Section 2.3.2) are satisfied. Components such as the gates, piers, foundation, bed protection, passage for shipping and road-traffic and the incorporation of tidal turbines are considered in the design. Furthermore, aspects such as the closure regime, closure and opening strategy, the required wet cross-section and failure due to non-closure are considered in depth in order to ensure the required functionality. Other elements of the Delta21 concept are in general outside of the scope of this thesis (e.g. the Spillway, Pumping Stations and adjacent dike sections).

1.6 Methodology and Report Outline

Figure 1.4 shows the design cycles used in this thesis to go from a general to a more detailed design.

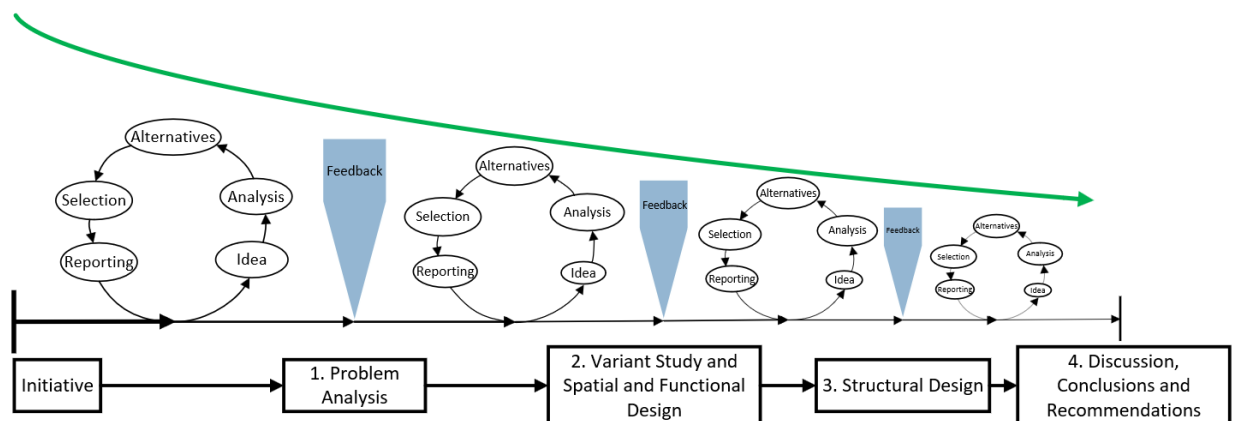


Figure 1.4: Design cycles from general to more detailed level (based on Molenaar & Voorendt, 2019)

As indicated in Figure 1.4, this report is structured in four parts, going from a general to a more detailed design:

- *Part 1: Problem Analysis*
After the initiative, the first design cycle encompasses the problem analysis. This part starts with Chapter 1 giving an introduction of the topic after which the problem statement and design objective are defined. Chapter 2 presents a system analysis considering the whole Delta21 system aimed to achieve a greater understanding of the situation in order to better formulate the requirements, evaluation criteria and boundary conditions. The Basis of Design, Chapter 3, concludes this first design cycle with "SMART" formulated functional- and structural requirements and boundary conditions. Wishes from stakeholders, which are also explored in the System Analysis, are translated either in requirements or evaluation criteria.
- *Part 2: Variant Study and Spatial and Functional Design*
After the Basis of Design concludes Part 1, Part 2 starts with Chapter 4 in which a gate type variant study is conducted. Chapter 4 is concluded with the selection of the most suitable gate type which provides the foundation for the further design cycles. Subsequently, Part 2 is continued with Chapter 5: the Spatial and Functional Design. The purpose of the Spatial and Functional Design is to ensure complete functionality of the Delta21 flood protection system where all established functions from Chapter 2 and hence all functional requirements from Chapter 3 should be met. Chapter 5 covers a newly proposed closure regime of the Delta Barrier, the reliability of the closure operation, the required effective flow area, the morphological and ecological impact of the Delta Barrier, the required retaining height, passage for shipping and road-traffic, tidal turbines, driving mechanisms, climate adaptive pathways to ensure functionality in the future and lastly presents the general lay-out based on the choices made thus far.
- *Part 3: Structural Design*
After complete functionality is ensured in Part 2, the purpose of Part 3: the Structural Design is to ensure that all structural requirements from Chapter 3 are met. The Structural Design consists of multiple subsystems. Firstly, Chapter 6 discusses the construction method, whereas knowledge of the intended construction method is of paramount importance to the further structural design. After the construction method is discussed, a gate design is presented in Chapter 7. The gate design includes a dynamic analysis. After the gate design, the civil superstructure is designed in Chapter 8. Finally, only now, the complete barrier is defined and the global stability of the Delta Barrier can be verified in Chapter 9. As part of the global stability verification not only vertical, horizontal and rotational stability but also scour and piping measures are considered. Chapter 10 concludes Part 3 with estimates of the construction planning and costs of the Delta Barrier .
- *Part 4: Discussion, Conclusions and Recommendations*
After all structural requirements are verified in Part 3, Part 4 commences with a discussion in Chapter 11. The discussion treats important steps in the design approach and assumptions which had an impact on the preliminary design. Part 4 is continued with Chapter 12 presenting the preliminary design of the Delta Barrier and the most important conclusions. Last but not least, Chapter 13 advises recommendations for further research and concludes the final design cycle.

The hydraulic engineering design method as shown by Figure 1.5 is used throughout the entire thesis. Said design method is an iterative process as indicated by the iterative jumps. However, not explicitly reported in that way to keep the report understandable.

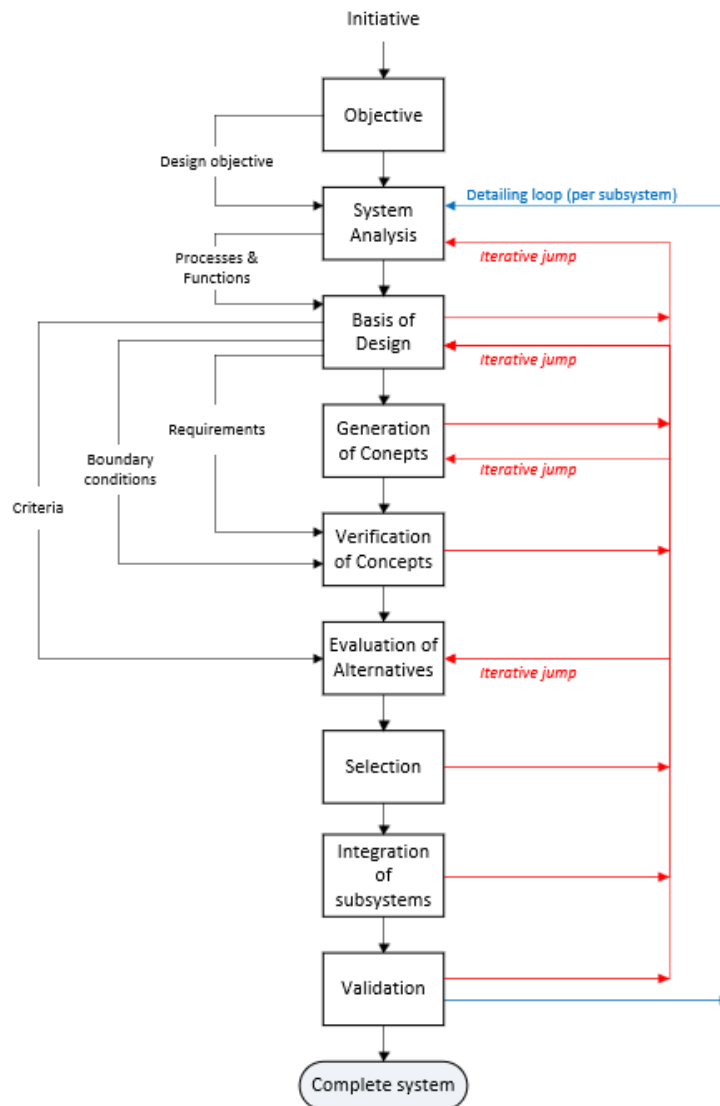


Figure 1.5: Hydraulic engineering design method (modified from Molenaar and Voorendt (2019))

Throughout all design cycles the notion of climate change is considered as such that the Delta21 flood protection system is able to function properly in the future as well. In order to account for climate change in both the functional and structural design of the Delta Barrier, choices regarding climate change scenarios ought to be made. Phenomena which (could) occur as a result of climate change are discussed in Appendix I. From this exploration, the boundary conditions regarding climate change (such as sea level rise) are deduced.

However, designing the whole storm surge barrier on a stringent climate scenario from the get go might not be feasible, or even necessary at all in hindsight. It might be more feasible to design taking into account a less stringent climate scenario with the possibility to adapt the structure when (or if) the need arises. This consideration is made in the spatial and functional design, where for the retaining height both a stringent and less stringent climate scenario is considered. Finally a choice is made as to whether a climate adaptive design is most feasible or an initial design based on a more stringent climate scenario. For the structural design, climate adaptivity is not considered as structural adaptations on a structure of this scale and importance is generally not desirable and feasible.

This thesis mostly applies Level I methods (semi-probabilistic approach) for design purposes. In a semi-probabilistic approach, the uncertainty in parameters is accounted for by means of applying partial safety factors. In this semi-probabilistic approach, design values are used for a unity check.

The structure is considered safe, if the design value of the resistance is greater than the design value of the load. Partial factors (γ) are used to derive these design values. It is hence important that the design values are defined or calibrated such that meeting the unity check implies that the probability of failure complies with the target failure probability (Jonkman, Jorissen, Schweckendiek, & van den Bos, 2021).

Governing water levels and wave conditions at sea are determined with Hydra-NL software, though adjusted due to a difference in considered location and additional sea level rise. Hydra-NL is a full probabilistic model that calculates the statistics of the hydraulic loads for the assessment of the primary dikes and structures in the Netherlands. It is consistent with the "Beoordelings- en Ontwerpinstrumentarium" (BOI) (Heldesk Water, 2022b). Due to the fact that Hydra-NL is a full probabilistic model and adjustments are made for a more accurate representation of the considered boundary conditions, no partial safety factors are applied for the boundary conditions at sea determined with Hydra-NL.

2 System Analysis

This chapter describes the system analysis, used as a predecessor to the basis of design. The aim of this chapter is to better understand the situation in order to formulate the requirements and boundary conditions more accurately. Here, Delta21 and corresponding stakeholders are discussed. Furthermore, a process analysis is presented regarding the flood protection system of Delta21 and the functions of both the integral Delta21 project and the new storm surge barrier (from now on: the Delta Barrier) are presented in the functional analysis.

2.1 Proposed Solution: Delta21

2.1.1 The Concept

The idea of Delta21 is a future-proof solution for the Southwestern Delta of the Netherlands. The Delta21 project aims to construct a lake between the Tweede Maasvlakte and the island of Goeree-Overflakkee. The lake will be bounded by dunes, multiple pumping stations and a spillway and is as such capable of removing excess water from the Rhine- and Meuse system resulting in lower water levels of the rivers upstream. When the Rhine-Meuse discharge with or without a combination of a high storm surge at sea causes the Tidal inlet to the Tidal Lake to have insufficient capacity to discharge the river water freely, excess water is able to flow into the lake by means of the Spillway and can be pumped out using the Pumping Stations. The Pumping Stations ought to have a discharge capacity of 10000 m³/s and the Spillway has a discharge capacity of 20000 m³/s (Donkers, 2021). The Pumping Stations and Spillway are situated within the Delta21 project as depicted by Figure 2.1 by numbers 1 and 2 respectively. Furthermore, the Pumping Stations will be able to generate electricity by letting water into the lake, hence the Energy Storage Lake.

In order to be able to effectively lower the water level in the Haringvliet, a closable storm surge barrier has to be constructed between the Energy Storage Lake and the island of Goeree-Overflakkee, or rather between the North Sea and the current Haringvliet estuary (number 3 in Figure 2.1). The storm surge barrier will close under storm conditions and during extreme river discharge to ensure flood protection of the South West Delta. When the barrier is closed, the water level upstream of the barrier will rise due to the disruption of the Rhine and Meuse discharge to sea. By using the Spillway of the Delta21 concept, water at the Tidal Lake side of the new storm surge barrier can be discharged out of the river system into the Energy Storage Lake. With the construction of the closable storm surge barrier, a part of the Voordelta is changed into the so called Tidal Lake.



Figure 2.1: Landscape design Delta 21 concept (modified from van Eeden (2021))

Last but not least, the Delta21 project aims to construct a fish migration river to boost fish migration between the North Sea and the Rhine/Meuse Delta. The fish migration river would mostly target and benefit the salmon, twaite shad, river lamprey, eel, flounder, herring and three-spined stickleback (Delta21, 2021b). Furthermore, the Delta21 project could prove beneficial for nature development and tourism, both on the new dike stretches itself and the newly created Tidal Lake.

2.1.2 Objectives & Purposes

Flood risk management is the leading theme of Delta21. However, the subjects of energy transition and nature restoration are strongly intertwined and cannot be viewed separately within the Delta21 concept. In the first place, Delta21 is an integral spatial development plan that is primarily aimed at protecting the Netherlands against flooding. By also using the facilities required for flood risk management in an alternative way, a large-scale battery becomes available to store electrical energy. Integration of the concept with the Haringvliet ensures that the fish migration can recover while the freshwater supply in the area is guaranteed (Berke & Lavooij, 2018c).

Flood protection

The Delta21 project promises dry feet for the entire South West Delta, including the city of Dordrecht. The project creates a catchment basin that more than doubles the existing catchment capacity of the South West Delta and excess water in the delta can always be discharged to the sea using the Pumping Stations (and Spillway) with a capacity of 10000 m³/s, regardless of the discharge, wind and tidal conditions. According to Berke and Lavooij (2018c), even with a major water set-up and a high river discharge, with Delta21, the water level in the entire downstream area around Dordrecht will not be able to rise higher than NAP + 2.5 m.

With Delta21, raising the dikes in the South West Delta due to sea level rise and higher discharges is no longer strictly required to ensure the safety of the Netherlands. Berke and Lavooij (2018c) argue that, besides monetary values taking into account nature restoration, CO₂ reduction and even the yield of the Energy Storage Lake, the Delta21 project seems economically feasible.

Energy transition

Besides the main function of the lake being the ability to pump out large amounts of excess water to the sea, it is also capable of storing energy on a large scale. Since the Paris Climate Agreement, the construction of wind farms and the installation of solar panels is growing exponentially. As a result of this transition and its uncertainties, there is on the one hand an enormous overcapacity on the supply side, but also more often temporary shortages. This imbalance is related to the weather dependence on renewable energy sources, but also to overcapacity of conventional sources. In order to be able to offer electricity in the event of a shortage, contracts have been concluded that ensure sufficient emergency power from conventional power stations. This expensive and inefficient approach to balancing supply and demand is mainly perpetuated by the low electricity price, lack of storage capacity and unfavourable energy storage laws and regulations. Energy storage would be much more logical and much less wasteful (Berke & Lavooij, 2018a).

With wind and solar energy on the rise and the need for storage soaring, Delta21 offers a concept of energy storage using the Energy Storage Lake. For several decades, hydro-power has also been increasingly used to temporarily store energy in water, usually referred to as Pumped Hydro Storage (PHS). With PHS, water from a lower basin is pumped back up at night and used repeatedly at attractive rates. Despite the high investments, hydro-power and PHS appear to be able to operate at very competitive production costs. Hydro-power is relatively clean, successful, proven and also fits perfectly within the Dutch water context (Berke & Lavooij, 2018a).

The current Delta21 plan aims to construct 93 pumps, 20 MW each, combining to a total of 1860 MW. Berke and Lavooij (2018a) estimate that, based on assumptions from 2017, the annual revenue for the exploitation of the Energy Storage Lake is approximately 48 million euro. Incorporating 40 tidal turbines in the storm surge barrier design of 1.5 MW each, would give an additional 12 million euro of revenue according to Berke and Lavooij (2018a). Based on this situation considering the price level in 2017, the lake represents a capital value of approximately 0.85 billion euro for the private electricity industry (Berke & Lavooij, 2018a).

Nature restoration

The closure of the Haringvliet in 1970 as part of the Delta Works brought an end to the Haringvliet as the Netherlands most important and ecologically rich estuary, where the salty tide had free access and the river water was drained to the sea naturally. After the closure, the area became drier and less salty, causing reeds and rushes to disappear and make way for trees and shrubs. The bird population changed as a result: swamp birds came, geese and ducks stayed, but of the waders only the meadow birds remained and most of the shorebirds have disappeared (Berke & Lavooij, 2018a). Furthermore, the Delta Works complicated the migration of fish upstream of the Rhine. With a discharge of less than 1100-1500 m³/s for low and high tide respectively (ca. 50% of the year), the Haringvlietsluizen are closed, which results in the Nieuwe Waterweg as the only remaining migration option for the majority of the fish (Noordhuis, 2017). Since 2018, the Kierbesluit ensures that the Haringvliet locks open at high tide so that migratory fish can swim with the salt water into the Haringvliet. For the Delta21 project the Kierbesluit will be maintained, as opening the Haringvlietsluizen completely would cause significant salt intrusion negatively impacting multiple stakeholders.

Because biodiversity in Europe had been declining for decades, Europe published the "Birds Directive" in 1979 and the "Habitats Directive" in 1992 in order to further sustain Dutch flora and fauna (Berke & Lavooij, 2018b). In accordance, the Netherlands assigned certain areas as specific habitat for flora and fauna, which together formed the Natura 2000 network. The "Voordelta" is one of many areas which are labeled as a Natura 2000 area. The Kierbesluit marks the start of the recovery of the dynamic delta nature, which has virtually disappeared from the Netherlands.

Delta21 aims to construct a fish migration river (FMR) in order to further reinstate the migration of fish. The FMR in the Delta21 project would mainly consider five target species, three of which are anadromous (Atlantic salmon, twaite shad and European river lamprey) and two being catadromous (European eel and flounder). Migratory behavior, life cycle and seven environmental conditions (water temperature, critical water velocity, salinity, turbulence, turbidity, light and migratory environment) are of importance for the construction of an FMR regarding these target species. As every fish species demands specific conditions, an optimal FMR needs to be heterogeneous (van den Tweel et al., 2021). The migration river must meet the requirements of flow (100 m³/s), water quality and a permanent attraction flow ought to be created. The advice is to construct several channels with a total length of at least 6 km, a width of 20-50 m and one with a depth of 5 m, with an abundance of shelters, a sand/gravel bed, substrate, artificial reefs and sea grass with shellfish banks. Both the north side and the south side (via the Zuiderdiep) are suitable for the construction of the fish migration river (Delta21, 2021b).

An ecology-oriented spatial design of the dune rows bordering the Energy Storage Lake could prove rather beneficial for flora and fauna development in the region. The dynamic landscape design for the Haringvliet including Delta21 by van Eeden (2021) has shown that a specific implementation of the dune area in stages could set the stage for rare flora and fauna. Figure 2.2 presents this implementation and the natural processes which define the development of the landscape.

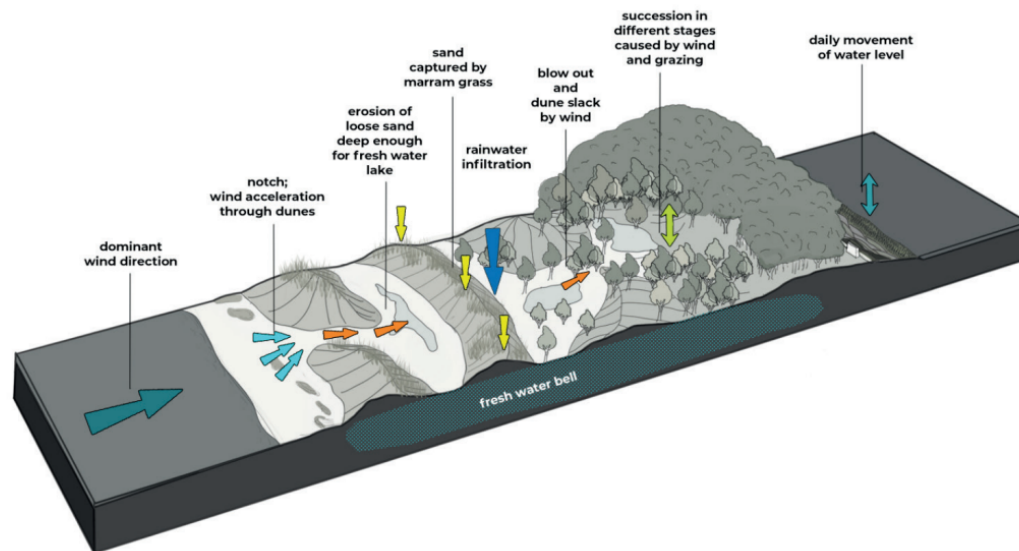


Figure 2.2: Natural processes that shape the landscape (van Eeden, 2021)

As a last, significant step, vegetation and the low lying areas between the dunes will capture rainwater and cause the water to infiltrate. After a few years, a freshwater bell will form in the subsoil between the dunes. As this happens, freshwater ponds will provide habitat for rare flora and fauna. This spatial design would specifically create habitat for the Kentish Plover (*Anarhynchus Alexandrinus*) and the Sand Lizard (*Lacerta Agilis*) besides many other species of birds, crustaceans and plants (van Eeden, 2021). Besides creating habitat, the spatial design as presented by van Eeden (2021) also creates ample possibilities for recreation.

2.2 Stakeholder Analysis

Within every project there are parties involved with an interest in the project, some of these even have some degree of power within the project. All these parties are therefore stakeholders. A stakeholder analysis for the Delta Barrier of the Delta21 project is compiled below. Eventually, stakeholder's interest can be converted into wishes and requirements for the project. In order to reach the most important and relevant stakeholders, the stakeholder analysis is divided into several steps. Firstly, all stakeholders of this project are identified and a relationship diagram is made to outline the position of the stakeholders in relation to the project. Secondly, the general interests of the stakeholders are presented on the basis of eight general interests. Thirdly, the degree of interest is plotted against the degree of influence to arrive at a combined importance, after which the most relevant and important stakeholders and their interests is discussed more thoroughly.

2.2.1 Stakeholder Inventory

Below, the relevant stakeholders are identified and listed regarding the Delta21 Barrier. The numbers indicate the position of the parties within Figure 2.3 in relation to the project. The letters per stakeholder are used to indicate their respective general interests in Table 2.1.

1. *Project:* Delta21 Barrier
2. *Client:*
 - **A:** Rijkswaterstaat
3. *Executives:*
 - **B:** Contractors & Engineering firms
4. *Responsibility:*
 - **A:** Rijkswaterstaat
 - **C:** Waterboard Hollandse Delta
5. *Consulted:*
 - **D:** Ministry of Infrastructure and Water Management
 - **E:** Ministry of Agriculture, Nature and Food Quality
 - **F:** Ministry of Economic Affairs and Climate Policy
 - **G:** Ministry of Climate and Energy
 - **H:** Province South-Holland
 - **I:** Province North-Brabant
 - **J:** Municipality of Goeree-Overflakkee
 - **K:** Municipality of Westvoorne
 - **L:** Municipality of Dordrecht
 - **M:** Delta Commission
6. *Supportive:*
 - **N:** Local residents
 - **O:** Local fishing companies
 - **P:** Natura 2000

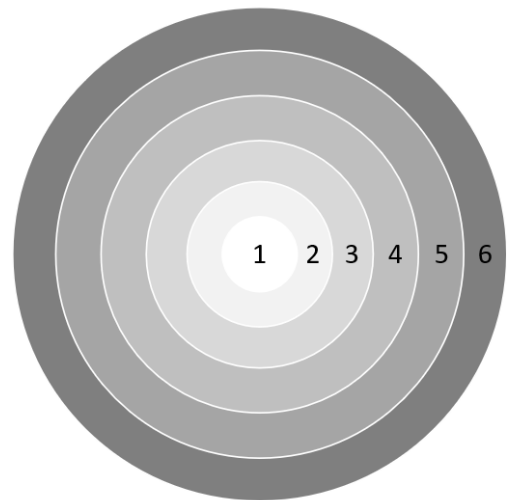


Figure 2.3: Relationship scheme

2.2.2 Stakeholder Interests

Below, Table 2.1 presents the interests of the stakeholders. The stakeholders are indicated by letters.

Interest	A	B	C	D	E	F	G	H	I	J	K	L	M	N	O	P
<i>Flood protection</i>	++	-	++	++	-	+	+	++	++	++	++	++	++	++	+	+
<i>Economic potential</i>	+	-	-	-	-	++	++	+	+	++	++	-	+	-	-	--
<i>Sustainability</i>	+	-	+	-	++	+	++	+	+	+	+	--	+	+	-	++
<i>Nature impact</i>	++	-	++	-	++	+	+	+	+	++	++	--	++	++	++	++
<i>(Construction) hindrance</i>	++	+	+	+	+	-	+	+	+	++	++	--	+	++	++	++
<i>Maintainability</i>	++	-	++	-	--	--	-	-	-	-	-	--	+	--	--	-
<i>Adaptability</i>	++	--	++	++	--	+	+	+	+	+	+	+	++	+	-	-
<i>Costs project</i>	++	+	-	-	--	+	-	-	-	-	-	--	++	--	--	--

Table 2.1: General interests of stakeholders (++ very strong; + strong; - average; -- no interest)

The interests are expressed in a broad sense in the table and defined as follows:

Flood protection

The flood protection interest expresses whether a stakeholder is bothered by the increase in safety regarding a possible flood event due to the new Delta21 project and interventions. As Delta21 mostly aims to improve flood protection from the Haringvliet to Dordrecht, stakeholder adjacent to said area would generally be most bothered whereas stakeholders further away would not gain the same amount of safety improvement - if any.

Economic potential

The interest regarding economic potential expresses the amount in which a stakeholder is bothered by economic growth. Delta21 aims to increase the economic potential of the areas directly adjacent to the project, say the coasts of Goeree-Overflakkee and Vorne-Putten. Furthermore, the newly developed area in the Voordelta should create an attractive environment for specific, mostly recreational based, industries.

Sustainability

The concept of sustainability in this context mostly regards the goals of Delta21 with respect to enabling the energy transition and the generation of green energy. Besides on helping to reach net zero emissions on a more global scale, locally generated energy could supply the nearby regions with green electricity.

Nature impact

Nature impact in this sense is actually a form of hindrance, but with respect to nature. Here considered explicitly due to the relative importance of nature impact. It generally regards the impact on flora and fauna by the Delta21 project and interventions, also including the new landscape to be created.

(Construction) hindrance

(Construction) hindrance represents the hindrance due to the Delta21 project in a more broad sense, excluding nature impact. This is the hinder during all life cycle stages of the project, from the construction stage until the end of life stage. Hindrance includes hindrance to shipping, fishing (both professionally and recreational), all kinds of surfing and canoeing and hindrance during construction such as hindrance due to noise and vibrations.

Maintainability

The interest regarding maintainability expresses whether a stakeholder is bothered by a design which can be maintained with relative ease or not. Besides direct maintenance considerations, maintainability is also closely connected to flood protection in a more indirect sense as maintenance (or repairing) should not take too long to an extent where flood protection could not be guaranteed.

Adaptability

In this context, adaptability mainly considers the extent to which the Delta Barrier is climate adaptable. For this reason adaptability can be considered an interest with on one hand flood protection and on the other hand the costs of the project.

Costs project

This interest considers all costs of the project taking into account the design stage, construction phase and use phase (management and maintenance). Sunk costs regarding nature impact is not included in this interest.

2.2.3 Stakeholder Involvement

Each stakeholder generally needs a tailor made involvement and communication approach. The way of involvement depends on the influence and the interest of the stakeholder. In Figure 2.4, the estimated influence and interest in the project can be found for every respective identified stakeholder. All stakeholders, but especially the most involved ones, should be approached in the project right from the initiative. Identifying the wishes of the most involved stakeholders and incorporating these in the design is key for the success of a project.

Figure 2.4 depicts the degree of importance vs. the degree of influence for all stakeholder identified above. This visually shows which stakeholders are the most important (top right) and which are the least important (bottom left).

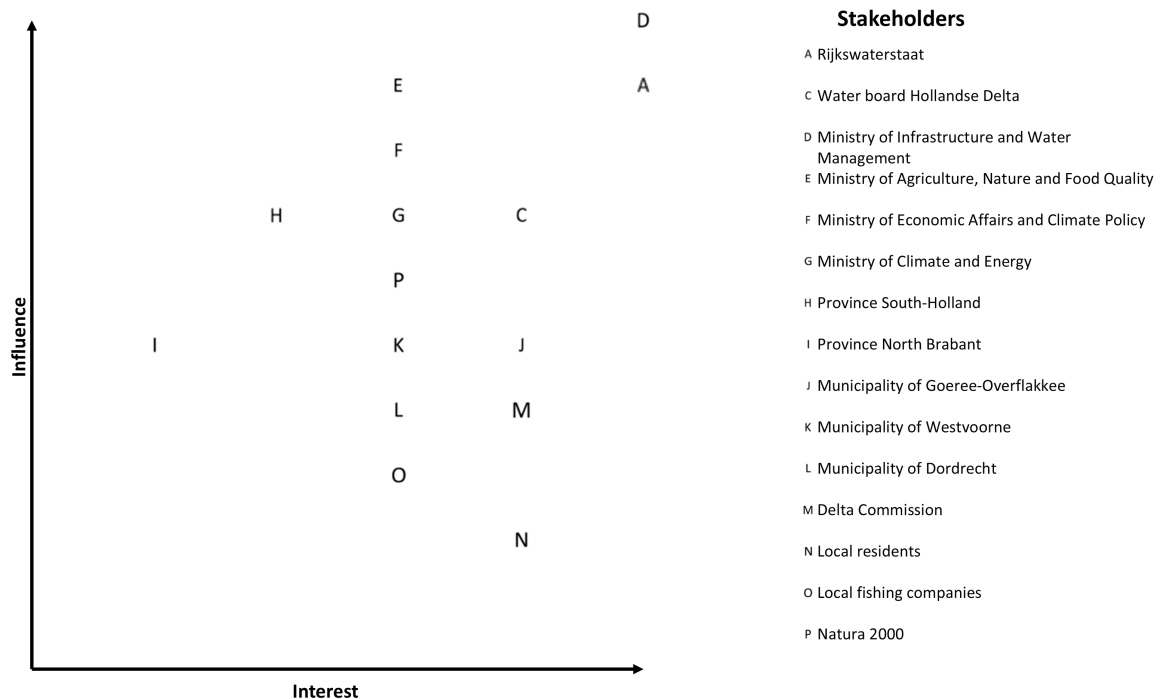


Figure 2.4: Stakeholder Classification Matrix

From Figure 2.4 it clearly shows that the Ministry of Infrastructure and Water Management is the most important stakeholder, closely followed by Rijkswaterstaat and the Ministry of Agriculture, Nature and Food Quality.

Ministry of Infrastructure and Water Management

"The Ministry of Infrastructure and Water Management is committed to improving quality of life, access and mobility in a clean, safe and sustainable environment. The Ministry strives to create an efficient network of roads, railways, waterways and airways, effective water management to protect against flooding, and improved air and water quality" (Government of the Netherlands, 2022b). The ministry is responsible for the legislation and rules in the Netherlands regarding flood protection and therefore has the most influence (i.e. power) when considering Delta21. Delta21 shares the main values of the ministry, especially regarding flood protection.

Rijkswaterstaat

Rijkswaterstaat is the executive agency of the Ministry of Infrastructure and Water Management in the Netherlands. The organisation manages and develops the main roads, main waterways and main water systems on behalf of the Ministry. Rijkswaterstaat ensures that the Netherlands is safe (against flooding), liveable and accessible. Rijkswaterstaat is responsible for the construction and the maintenance of the Dutch primary flood defence structures and is therefore the client of the Delta21 project (see Figure 2.3) and is to maintain the Delta Barrier once constructed. As a direct result, Rijkswaterstaat is heavily involved within the project. Delta21 shares the main value of Rijkswaterstaat and therefore of the Ministry of Infrastructure and Water Management. The Delta21 project would positively influence flood protection, hence the interest of Rijkswaterstaat in this project is very high.

Ministry of Agriculture, Nature and Food Quality

The Ministry of Agriculture, Nature and Food Quality wants to ensure good prospects for the Dutch farming, horticulture and fishing sectors. It aims for good-quality, safe and affordable food. In addition, the Ministry is working to restore and maintain natural areas. It aims to consolidate the agriculture sectors leading international position, strengthen the link between nature and agriculture, and improve farmers economic situation (Government of the Netherlands, 2022a). As depicted in Table 2.1 the ministry mainly has sustainability and nature impact in mind. As the Delta21 project is situated in a Natura 2000 area some conflict or disagreement can be expected. It is of grave importance that the needs of the Ministry of Agriculture, Nature and Food Quality are met, due to their significant influence in the project.

2.3 Process and Functional Analysis

In this section the process and function analysis are presented for the Delta21 project, respectively. Firstly, the process analysis is conducted, in which the current process of the Delta21 flood protection system as proposed by Berke and Lavooij (2018c) is presented by means of a process tree and table. It should be noted that in Section 5.1 a new Delta21 flood protection process is proposed essentially replacing the process as presented here. Lastly, the functional analysis describes the primary, preserving and additional functions for both the whole Delta21 project and the Delta Barrier in detail. The purpose of the process analysis, considering the current flood protection system, is to give an insight in the desired use and behaviour of the Delta Barrier within the Delta21 flood protection system. Furthermore, the functional analysis provides the foundation for the Spatial and Functional Design.

2.3.1 Process Analysis

The process analysis aims to give an accurate overview of all the stages in which the relevant elements of Delta21 occur during different scenarios for the Delta21 flood protection system as proposed by Berke and Lavooij (2018c). The overview is depicted using the flow chart as presented by Figure 2.5. In general the Delta21 flood protection system by Berke and Lavooij (2018c) considers three main scenarios: high discharge of the Nieuwe Waterweg and the Haringvliet combined ($> 9000 \text{ m}^3/\text{s}$) without a storm surge at Hoek van Holland, high discharge of the Nieuwe Waterweg and the Haringvliet combined ($> 5000 \text{ m}^3/\text{s}$) with an expected storm surge at Hoek van Holland ($> 1.5 \text{ m}$) and only an expected storm surge at Hoek van Holland ($> 1.5 \text{ m}$) (Berke & Lavooij, 2018c).

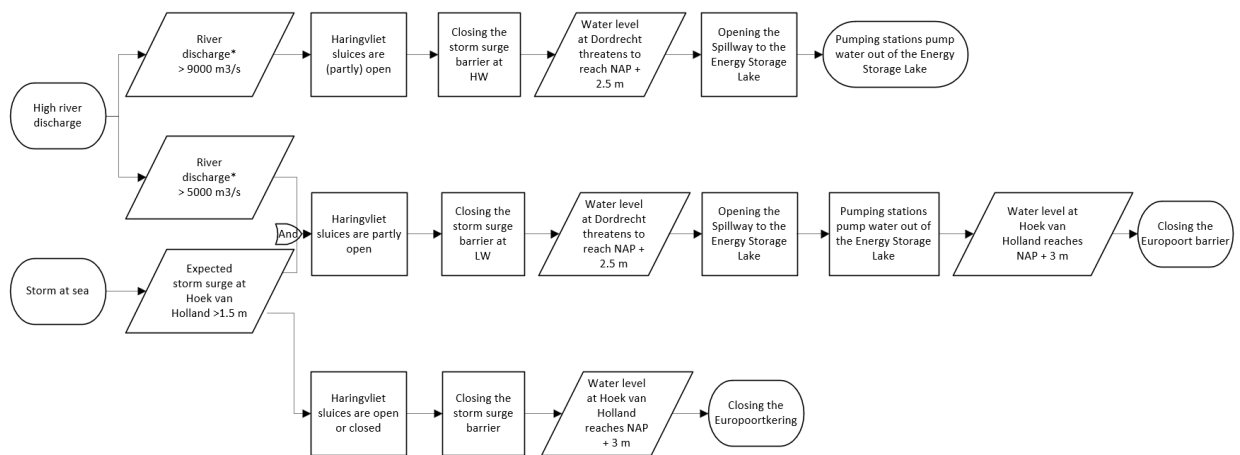


Figure 2.5: Process of the Delta21 flood protection system for different scenarios
 * River discharge represents the sum of Nieuwe Waterweg and Haringvliet discharge

The three main scenarios as depicted by Figure 2.5 are indicated by the three separate branches respectively. Table 2.2 presents the states of all relevant structures for the different (sub)scenarios. It should be noted that the Europoortkering represents both the Maeslantkering and the Hartelkering. A full elaboration on every (sub)scenario can be found in Appendix IV.

Scenarios	Haringvlietsluizen *	Storm surge barrier	Spillway	Pumping Stations **	Europoortkering
0. Daily circumstances	Open or closed	Open	Closed	Not pumping	Open
1.1. Discharge > 9000 m ³ /s	Open	Closed	Closed	Not pumping	Open
1.2. Discharge > 9000 m ³ /s WL at Dordrecht NAP + 2.5 m	Open	Closed	Open	Pumping	Open
2.1. Discharge > 5000 m ³ /s Expected storm surge HvH > 1.5 m	Open	Closed	Closed	Not pumping	Open
2.2. Discharge > 5000 m ³ /s Storm surge at HvH > 1.5 m WL at Dordrecht NAP + 2.5 m	Open	Closed	Open	Pumping	Open
2.3. Discharge > 5000 m ³ /s Storm surge at HvH > 1.5 m WL at Dordrecht NAP + 2.5 m WL at HvH NAP + 3 m	Open	Closed	Open	Pumping	Closed
3.1. Storm surge at HvH > 1.5 m	Open or closed	Closed	Closed	Not pumping	Open
3.2. Storm surge at HvH > 1.5 m WL at HvH NAP + 3 m	Open or closed	Closed	Closed	Not pumping	Closed

Table 2.2: States of structures for different scenarios of the current Delta21 flood protection system

* The opening of the Haringvlietsluizen depends on the upstream discharge of the Rhine according to Figure 3.12

** Here, the state of the Pumping Stations is presented for flood protection purposes only. Note that the Pumping Stations might be pumping or turbining as part of the energy storage cycle of the Energy Storage Lake

2.3.2 Functional Analysis

Delta21

For the integral Delta21 project the following functions can be distinguished:

Primary functions:

- Protecting the South West Delta from flooding
- Generating sustainable energy

Preserving functions:

- Allowing passage of ships from- and to the sea.
- Preserve ecology
- Allowing passage of water, ice and sediments
- Restoring fish migration to the Haringvliet

- Nature restoration of the Voordelta

Additional functions:

- Allowing passage of road-traffic
- Enabling recreation in the Delta21 dune landscape

The objectives and purposes of the Delta21 project can be observed directly in the functions. The primary goals are to increase the flood protection of the Netherlands, mainly in the South West Delta, and enabling the generation of sustainable hydro-power.

Preserving functions originate from the fact that the system created to fulfil the main function can interfere with other functions. The new system should therefore inherit these functions from the other systems. Additional functions do not originate from the motivation for creating a system or preserving other systems, but are extra opportunities created by the intervention (Molenaar & Voorendt, 2020a). The precise allocation of the additional functions depends on the scope of this thesis, which will be specified in a later design stadium and are therefore optional for now.

Delta Barrier

As the main purpose of this thesis is the design of the closable storm surge barrier between the Energy Storage lake and the Island of Goeree-Overflakkee, it is useful to look with more detail at the functions and sub-functions of said storm surge barrier.

The following functions for the storm surge barrier can be distinguished:

Primary functions:

1. Protecting the South West Delta from flooding from land and sea
 - 1.1 Ability to retain water
 - 1.2 Allowing passage of river discharge, ice and sediments¹

Preserving functions:

2. Allowing passage of ships from- and to the sea²
3. Allowing passage of tidal flow, ice and sediments
4. Preserving of ecological system
 - 4.1 Allowing safe passage for aquatic creatures
 - 4.2 Minimizing impact on ecological system

Additional/Optional functions:

5. Generating sustainable hydro-power
6. Allowing passage of road-traffic

For obvious reasons, the Delta Barrier shares the same primary function as the integral Delta21 concept in protecting the South West Delta from flooding. It should be noted that storm surge barriers generally have two opposing functions, namely retaining water and allowing passage of ships and/or water (tidal flow, or river discharge). Besides the integration of a lock complex, said functions are mostly not fulfilled at the same time (Molenaar & Voorendt, 2019).

¹This could also be considered a preserving function, in this case presented as a primary function due to flood protection reasons

²Note that the actual design of a sluice, if needed, is outside the scope of this thesis

3 Basis of Design

In this chapter, the last design phase of part 1 is described: the basis of design. In this phase, the processes and functions of the Delta21 system explored in the system analysis (Section 2) are translated into the requirements for the design. Furthermore, after analysing the general impact of climate change on boundary conditions in Appendix I, future boundary conditions required for the design are posed in a climate robust way.

3.1 Requirements

The requirements which the Delta Barrier should fulfill are formulated here. The functional requirements are derived from the problem analysis taking into account the Delta21 processes and functions and all stakeholders as established in the stakeholder analysis. The structural requirements ought to be met in order for the Delta Barrier to conform to all relevant codes, laws and regulations. Note that all requirements as stated below must suffice including climate change, which can be seen as a changing boundary condition. Section 3.2.1 presents the climate change scenarios (including accompanying sea level rise) which are taken into account.

3.1.1 Functional Requirements

All functional requirements enumerated here are directly related to the functional analysis (see Section 3.1.1). The functional requirements are substantiated and quantified in a "SMART" manner in Appendix V, allowing for direct verification. Part of said substantiation follows from the safety standard of the newly introduced Delta21 dike ring (1:3333 per year), which is determined and elaborated in Appendix VI. Functional requirements which can not reasonably be described in a SMART manner for this thesis, but are of significant importance (viz. certain ecological requirements), are mentioned after the enumeration. The verification of the design with regard to these requirements is conducted qualitatively, as evaluation criteria.

FR-1. Flood protection

FR-1.1. The Delta Barrier must prevent the hinterland from flooding

FR-1.2. Water-retaining function

FR-1.2.1. The Delta Barrier must be sufficiently high

FR-1.2.2. The Delta Barrier must conform to the 2017 Water Act

FR-1.3. Closure reliability

FR-1.3.1. The closing procedure must be reliable

FR-1.3.2. The Delta Barrier must conform to the 2017 Water Act

FR-1.4. Ability to discharge water, ice and sediments

FR-1.4.1. The Delta Barrier must have sufficient effective flow area

FR-1.4.2. The Delta Barrier must be able to discharge ice

FR-1.4.3. The Delta Barrier must not cause excessive erosion or accretion

FR-1.4.4. The Delta Barrier must conform to the 2017 Water Act

FR-2. Preserving passage of ships

FR-2.1. Allowing passage of ships

FR-2.2. Enable sport- and recreational ships

FR-2.3. Enable professional fishing vessels

FR-2.4. Enable sport- and recreational fishing vessels

FR-3. Allowing passage of tidal flow, ice and sediments

FR-4. Preserving ecological system

FR-4.1. Allow safe passage of aquatic creatures

- FR-4.1.1. Accommodate migrating fish
- FR-4.1.2. Allow seals to pass
- FR-4.1.3. Allow passage of harbour porpoise
- FR-4.2. Allow safe passage of land mammals, birds and insects
- FR-5. Allowing passage of road-traffic
 - FR-5.1. All motorised road-traffic must be able to pass safely
 - FR-5.2. Cyclists must be able to pass safely
 - FR-5.3. Pedestrians must be able to pass safely
- FR-6. The Delta Barrier must be maintainable
 - FR-6.1. Regular maintenance and inspection
 - FR-6.2. Maintenance after (storm event) damages
- FR-7. The Delta Barrier must be stiff enough
 - FR-7.1. The Delta Barrier must conform to the 2012 Building Decree
 - FR-7.2. The Delta Barrier must conform to the relevant European norms and regulations including the National Annexes (NEN-EN)
- FR-8. The Delta Barrier must have a functional lifetime of 200 years with regard to functions FR-1.1, FR-1.2, FR-1.3, FR-1.4, FR-4, FR-5, FR-6 and FR-7
- FR-9. FR-3 is subordinate to FR-1.3

It should be noted that, with regard to requirement FR-9, FR-3 has a service life which depends on climate change and more specifically sea level rise. If conforming to FR-3 leads to conflict with FR-1.2 at any given point in time, the current Delta Barrier can no longer fulfill all posed functional requirements and a choice must be made on how to handle this conflict. Section 5.11, gives an impression of some possible solutions to said conflict following a climate adaptive pathway approach.

Besides the requirements as stated above, the impact of the Delta Barrier on the ecological system should be minimised. All relevant ecological requirements are listed below:

- The ecological footprint of the Delta Barrier should be minimised where possible in all life cycle stages of the structure (product, construction, use, and end of life stage).
- The Delta Barrier should not negatively impact growing up juvenile fish, shellfish, crustaceans, insects, birds and small land mammals in the Voordelta.
- Both during the construction- and use stage of the Delta Barrier there should be minimal impact on e.g. the Hinderplaat, Garnalenplaat, Slikken van Voorne, Voornes Duin, Kwade Hoek, Bollen van de Ooster and Duinen Goeree.
- The Delta Barrier should minimise the negative impact on all plant species in the Voordelta.
- The Delta Barrier should minimise the negative impact on all fauna in the Voordelta.
- The water quality in the Voordelta should not be negatively influenced.
- Any loss in nature or habitat due to the Delta Barrier ought to be compensated for before the structure is operational.
- The Delta Barrier should minimise the negative impact on all fishing industry activities and target species amount, quality and behaviour.
- The Delta Barrier should minimise the negative impact on sport- and recreational fishing activities and target species amount, quality and behaviour.

3.1.2 Structural Requirements

- SR-1. The Delta Barrier must be strong enough, stable and have sufficient rigidity of shape.
 - SR-1.1. The Delta Barrier must conform to the 2012 Building Decree
 - SR-1.2. The Delta Barrier must conform to the relevant European norms and regulations including the National Annexes (NEN-EN)
 - SR-1.3. The Delta Barrier must conform to the ROK
 - SR-1.4. The Delta Barrier must conform to the 2017 Water Act
- SR-2. The Delta Barrier must be constructible
 - SR-2.1. The Delta Barrier must be constructible in the initial construction phase
 - SR-2.2. The climate adaptability adjustments to the Delta Barrier must be constructible
- SR-3. The Delta Barrier must have a certain level of redundancy
 - Failure of one individual gate of the Delta Barrier must not lead directly to flooding of the hinterland.*
- SR-4. The Delta Barrier must be completed and operational in 2050
- SR-5. The Delta Barrier must have a sufficient design life
 - SR-5.1. Foundation
 - The foundation must have a design life of 200 years.*
 - SR-5.2. Piers
 - The piers must have a design life of 200 years.*
 - SR-5.3. Gates
 - The gates must have a design life of 200 years.*
 - SR-5.4. Bottom protection
 - The bottom protection must have a design life of 200 years.*
- SR-6. The Delta Barrier must be designed with consequence class CC3 and reliability class RC3.

One should note that all mechanical and electrical components needed for proper functioning of the Delta Barrier should also be designed for. In the context of this thesis though, mechanical and electrical components will only be considered where there is intersection with the civil sub- and super structures (e.g. integration of technical rooms).

3.2 Boundary Conditions

3.2.1 Climate Adaptivity and Climate Scenarios

This section provides the climate scenario or scenarios which are taken into account in the further design steps, both regarding the functional and structural design.

Functional design

For the functional design, when determining the retaining height, the feasibility of a climate adaptive design is researched. I.e. the required retaining height is calculated for a stringent and less stringent climate scenario. The feasibility is evaluated in terms of functional, structural and financial considerations. The stringent climate scenario considered is SSP5-8.5 representing a continuing rise in greenhouse gas emissions. The less stringent climate scenario considered, in combination with a climate adaptive design, is the intermediate scenario SSP2-4.5.

Structural design

The structural design is made with reference period 2250 and climate scenario SSP5-8.5 for all elements as we can confidently state a priori that structural adaptations on a structure of this scale and importance is generally not desirable and feasible.

Overview of used climate scenario(s)

Table 3.1 presents an overview of the used climate scenarios in this thesis for both the functional and structural design.

	Climate scenario	Sea level rise [m] ³	
		2050	2250
Functional design	SSP2-4.5	0.28	2.29
	SSP5-8.5	0.32	3.88
Structural design	SSP5-8.5	0.32	3.88

Table 3.1: Overview of used climate scenarios

³The median value of sea level rise with respect to 2005 is presented for the respective climate scenarios

3.2.2 Spatial Conditions

Figure 3.1 by van Eeden (2021) gives an impression of the integration of the new Delta21 project into the current Dutch South West peninsula. Knowledge of the location of Delta21 and more specifically the storm surge barrier is need to determine remaining boundary condition on site.



Figure 3.1: New Dutch South West peninsula with Delta21 (van Eeden, 2021)

With the location of the Delta Barrier in mind (red dot in Figure 3.1), it is clear that barrier only experiences waves from ca. the south-west (SW) to the west-southwest (WSW) and is sheltered from all other directions. The most southwestern tip of the (to be constructed) spit forming the Energy Storage Lake shelters the Delta Barrier from the waves more north of WSW, whereas the overall shape and orientation of the peninsula itself south of Delta21 shelters the barrier from waves more south of SW.

Figure 3.2 gives an indication of the depth-profile directly after construction of the Delta21 project as modeled by van Horick (2023) based on the landscape design of van Eeden (2021). At the location of the Delta Barrier the bed level is situated at roughly NAP - 7 m.

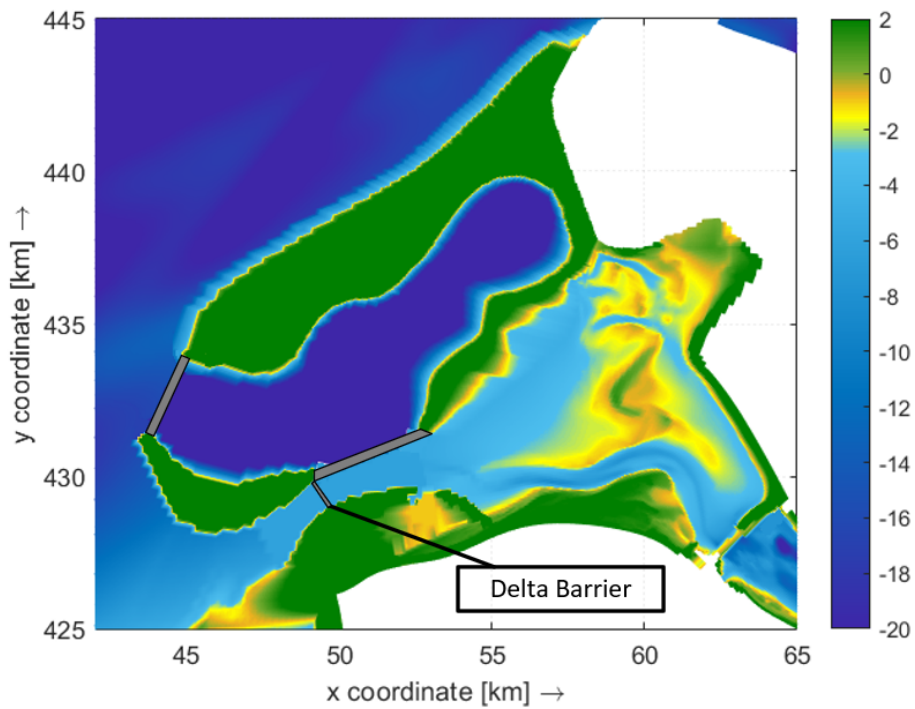


Figure 3.2: Indicative bed level at the Delta Barrier (modified from van Horick (2023))

From Figure 3.2 (also Figure 2.1) it is clear that the Delta Barrier is oriented 247.5° clockwise from the true north, i.e. the face of the Delta Barrier is facing the west-southwest. Hence, waves from 247.5° can be considered normally incident. The new Delta21 project however, is not available as a database for Hydra-NL. Therefore, one should find a similar location with similar characteristics (viz. similar orientation, depths and hydrodynamic forcing). A location at the most northern tip of the Oosterscheldekering represents the location of the Delta Barrier quite well. Said location is presented in Figure 3.3.

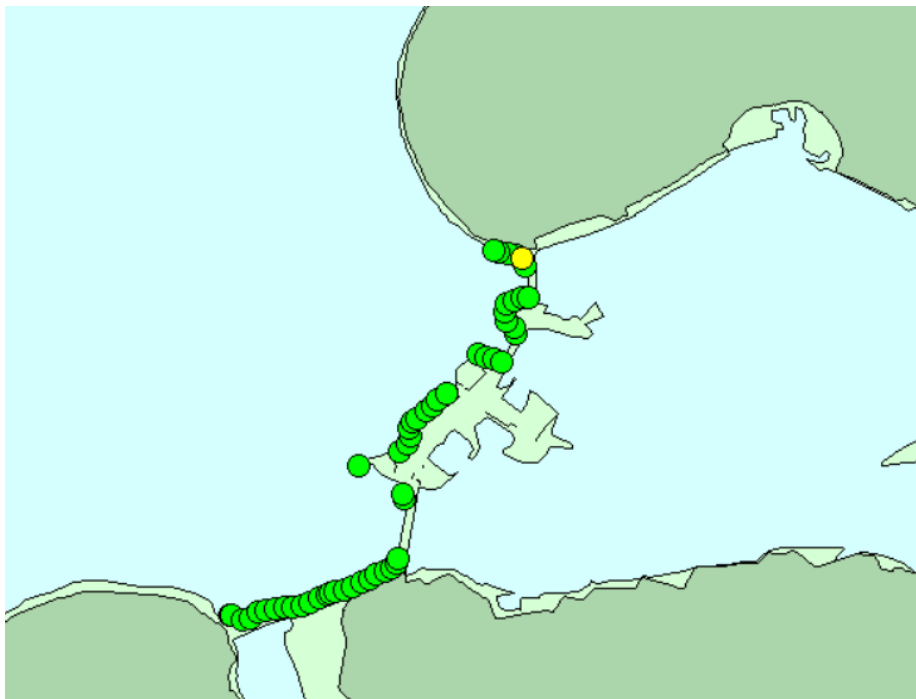


Figure 3.3: Chosen Hydra-NL boundary condition location at the Oosterscheldekering

As we can see, the Hydra-NL boundary condition depicted as the yellow dot in Figure 3.3 is roughly sheltered from the same direction and also experiences normally incident waves from the WSW. Furthermore, it can easily be verified that the depths in west-southwest direction of the yellow dot are similar to the depths as depicted in Figure 3.2. Finally, roughly similar hydrodynamic forcing can be expected due to the fact that the Oosterscheldekering is relatively close to the Delta Barrier (besides similar orientation and depths).

3.2.3 Geotechnical Conditions

Knowledge of the geotechnical conditions is a must in order to design any structure. The soil characteristics as determined here are important when determining the most suitable construction method (see Chapter 6) and are used for the global stability verification of the Delta Barrier in Chapter 9.

The soil conditions at the site of the Delta Barrier are estimated by means of two cone penetration test (CPT) results. These CPTs are retrieved from the database of the Dinoloket (2022). Appendix VIII presents the locations and results of the two most relevant CPTs.

From the CPTs it can be concluded that the soil profile near the site consists mostly of sandy soils, some with a silty to clayey admixture to a certain degree. Figure Figure 3.4 depicts the soil type per specified soil layer. The characteristic soil parameters are derived using Table (2.b) from the National Annex to NEN-EN 1997-1 (2019) and are shown in Table 3.2.

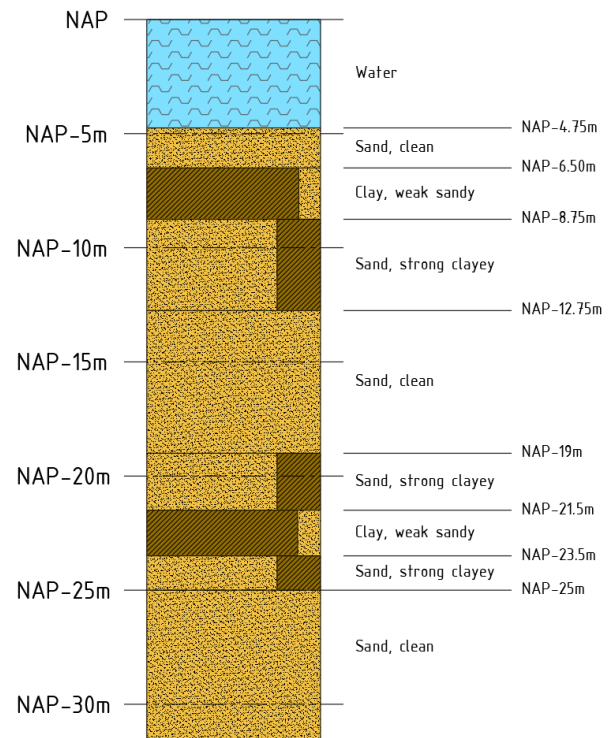


Figure 3.4: Soil profile with specified layers

Name	Admixture	Consistency	γ [kN/m ³]	γ_{sat} [kN/m ³]	c' [kPa]	ϕ [°]
Sand	Clean	Loose	17	19	0	30
Clay	Weak sandy	Moderate	18	18	5	22,5
Sand	Strong silty, clayey	-	18	20	0	27,5

Table 3.2: Characteristic soil parameters

It should be noted that for this preliminary design these CPTs give a reasonably accurate indication of the soil profile at the storm surge barrier, however more tests should be conducted in the future at the exact location for the final design stage.

3.2.4 Meteorological Conditions

Wind direction and corresponding velocity are of paramount important for the design of the storm surge barrier. Besides plain wind loads, the wind dictates some of the most important hydraulic loads on the structure, especially wave loads and wave set-up are heavily dependent on both the wind direction and accompanying velocity. The phenomena as mentioned above are influenced by the waves on different time scales though. The largest wind loads naturally occur for the strongest wind gusts. Wind waves generally need time to develop as they are created by the wind blowing along the water surface, setting it in motion and are therefore more strongly related to hourly mean wind speeds. Whereas wave set-up requires an even longer time to develop as the entire North Sea plays a role resulting in a greater importance of daily mean wind speeds.

For the purpose of quantifying the direct wind forces on the structure and determining wind waves at the Tidal Lake, wind data from Hoek van Holland between 01-01-1972 and 01-01-2022 is retrieved from the KNMI database (2022). The retrieved data gives for every day the mean wind direction, the maximum wind gust, the daily mean wind speed and the hourly mean wind speed (besides other variables). All data has been measured at a height of 10 metres in m/s (KNMI, 2022).

Figure 3.5 presents the wind rose for Hoek van Holland between 1972 and 2022 for the daily mean wind speed. It depicts the daily mean wind speeds for every wind direction with a cumulative percentage of occurrence for every wind direction.

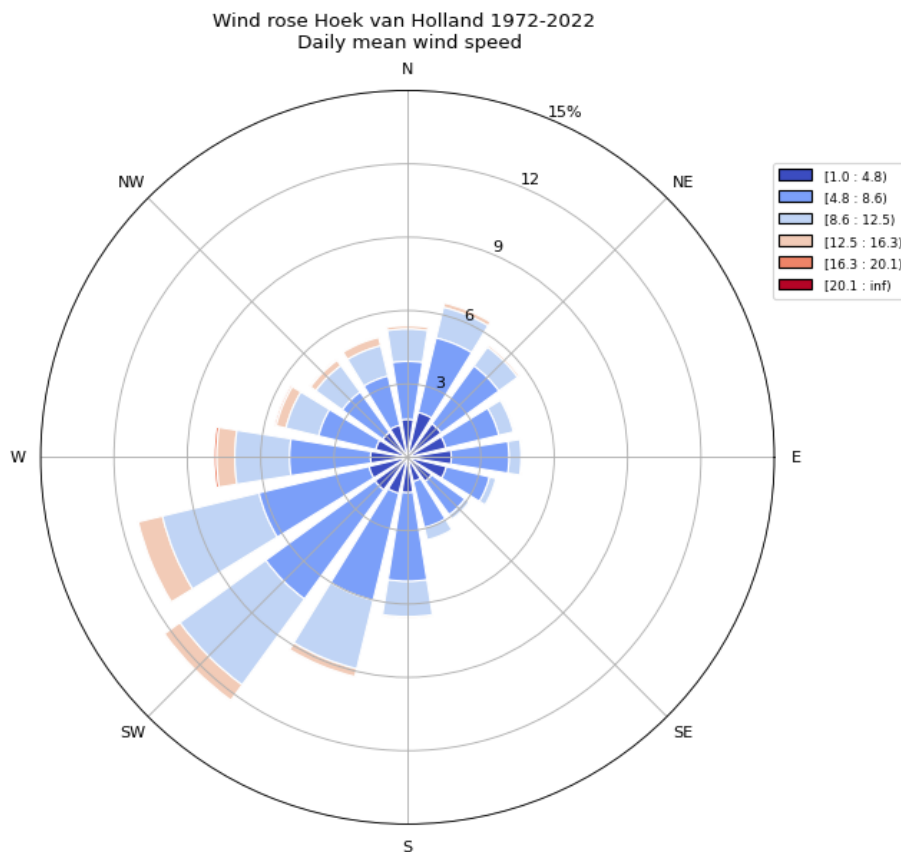


Figure 3.5: Wind rose for the daily mean wind speed

From Figure 3.5 it can be concluded that wind from the south-west has the highest percentage of occurrence (12,3%) over the 50 year reference period, closely followed by wind from the west-southwest (11,3%). Furthermore, it can be seen that the daily mean wind speed rarely exceeds ca. 16 m/s.

One should note that, besides acting on different timescales, wind waves and set-up are also strongly correlated through the wind direction. The maximum wind wave at the structure is to be expected with a wind direction from ca. the West-southwest (WSW) due to the structure orientation, whereas the largest overall set-up generally occurs for more northern wind blowing up the North Sea towards the south. This strong correlation results in the fact that the maximum wind waves and hence wave loads generally do not occur simultaneously with the maximum set-up (i.e. storm surge). In order to account for this correlation, Hydra-NL is used to generate the design water levels, significant wave heights with corresponding spectral periods and potential wind speeds at sea.

In addition, to gain insight on the strongest wind gusts and corresponding direction, Figure 3.6 presents the wind rose for Hoek van Holland between 1972 and 2022 for the maximum daily wind gusts over 30 m/s.

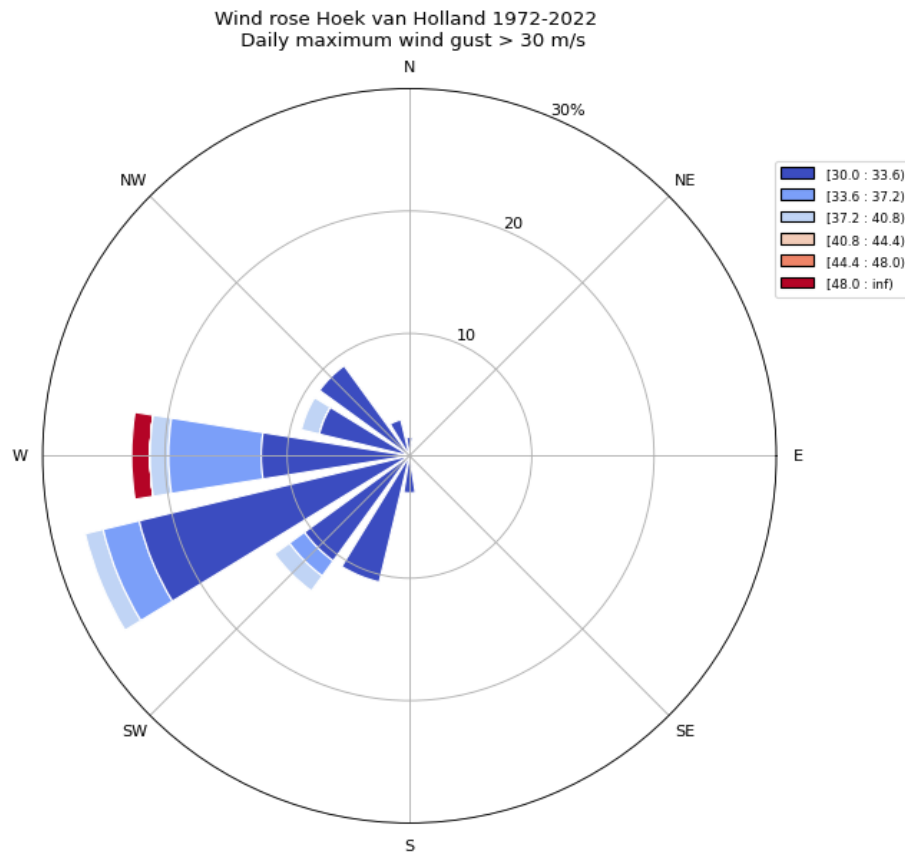


Figure 3.6: Wind rose for the maximum daily wind gusts over 30 m/s

Now, from Figure 3.6 one can see that the strongest wind gusts originate more from the west and west-southwest. As the direction normal to the Delta Barrier is mostly west-southwest oriented, it is expected that the latter direction contributes strongest to direct wind loads on the structure.

A Three-parameter Weibull distribution is fitted through all wind data. Said distributions can be found in Appendix VII. The Weibull distributions can be represented by Equation (3.1).

$$R = \exp \left(- \left(\frac{v - \gamma}{\alpha} \right)^\beta \right) \quad (3.1)$$

where:	R	[years]	=	return period
	v	[m/s]	=	maximum daily wind speed at 10 m height
	γ	[-]	=	location parameter = 3.83 for WSW
	α	[-]	=	scale parameter = 13.85 for WSW
	β	[-]	=	shape parameter = 2.57 for WSW

Now, after rewriting Equation (3.1), one is able to compute the maximum daily wind speed for every given return period using Equation (3.2).

$$v = \alpha \sqrt[\beta]{\ln R} + \gamma \quad (3.2)$$

Plotting the maximum daily wind speed for the WSW as a function of the return period on a logarithmic x-axis yields Figure 3.7.

It should be noted that Equation (3.2) and Figure 3.7 only serve for quantifying the direct wind forces on the structure and the wind waves generated at the Tidal Lake. Hydra-NL is used for the design value of the wind speed at sea in order to account for the correlation between the water level and wave height which are both a function of the wind speed.

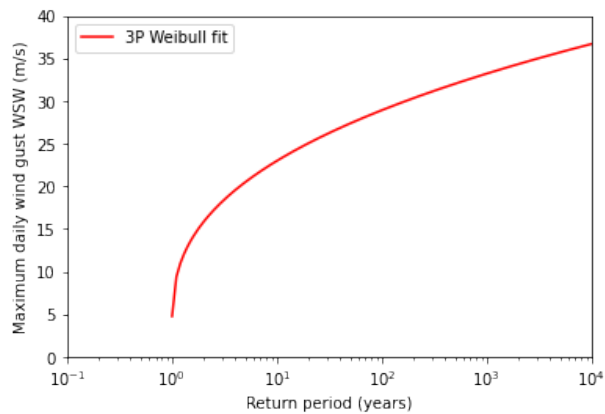


Figure 3.7: Wind velocity as a function of the return period for the WSW

3.2.5 Sea Level

In general, the sea level depends on the tidal signal and over time also on sea level rise. Here, the tidal signal is presented, different climate scenarios are elaborated upon and the approach for determining the design water levels using Hydra-NL is discussed. The design water levels are presented in Section 3.3, only after following the approach as presented here.

Tidal signal

The Dutch coast experiences a dominant semi-diurnal tide. The dominant semi-diurnal lunar tide has a period of 44700 s. The Dutch and British coast form the boundaries of the North Sea giving rise to an amphidromic system fed by the Coriolis phenomenon. Said system causes the tide to propagate from south to north along the Dutch coast with increasing tidal amplitudes. Colina Alonso (2018) found the tidal signal during January and February 2018 in front of the coast of Goeree-Overflakkee including four spring-neap tidal cycles (see Figure 3.8). It should be noted that the tidal levels as indicated in Figure 3.8 are based on the tide of said months and may vary when analysing the tidal signal for a longer period.

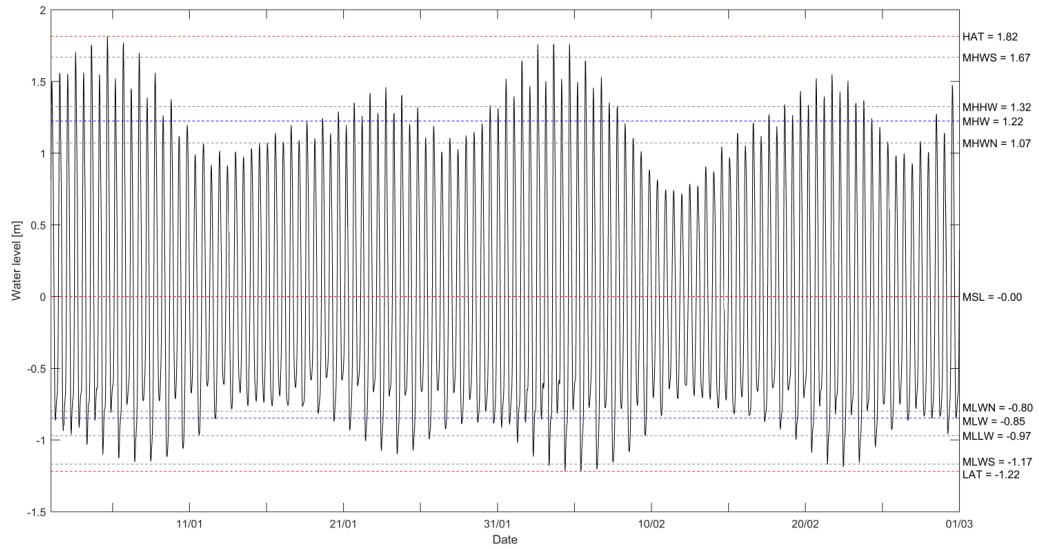


Figure 3.8: Tidal signal containing four spring-neap tidal cycles in front of the Haringvliet outer delta (Colina Alonso, 2018)

From Figure 3.8 a governing vertical tidal signal during spring tide is formulated as presented in Equation (3.3).

$$h_1(t) = a + SLR + S + b \sin(\omega_{M2} \cdot t) \quad (3.3)$$

where:

a	[m]	=	offset from MSL (skewness) ≈ 0.3
SLR	[m]	=	offset due to sea level rise
S	[m]	=	total (wind and wave) set-up
b	[m]	=	tidal amplitude ≈ 1.52
ω_{M2}	[rad/s]	=	principal lunar tide angular velocity $\approx 1.4 \cdot 10^{-4}$

A governing mean tidal signal yields:

a	[m]	\approx	0.185
b	[m]	\approx	1.035

The horizontal tide offshore of the Delta Barrier has readily been analysed by Zaldivar Piña (2020) and can roughly be formulated by Equation (3.4).

$$v_1(t) = v_0 + v \sin(\omega_{M2} \cdot t + \frac{\pi}{2}) \quad (3.4)$$

where:

v_0	[m/s]	=	offset from zero velocity (skewness) ≈ 0.05
v	[m/s]	=	velocity amplitude ≈ 0.65

Note that the vertical tide leads the horizontal tide by 90° , verified by Zaldivar Piña (2020). Furthermore, although Zaldivar Piña (2020) stated that the water surface develops a vertical asymmetry with a steeper face, for this qualitative description of the tidal signal, any vertical asymmetry in both the vertical and horizontal tidal signal has been neglected.

Sea level rise

Naturally, when designing a structure, one should take changes of boundary condition during the design life into account. The Delta Barrier is to retain direct sea water and therefore sea level rise ought to be taken into account. Climate change induced sea level rise has readily been introduced in Appendix I.4. The latest KNMI report (2021) has presented indicative sea level rise scenarios for the Dutch coast corresponding to three different emission scenarios (see Table I.1). Said indicative values for sea level rise per climate scenario are used to extrapolate to the end of design life of the Delta Barrier (viz. 2250).

In Figure 3.9 the sea level rise according to Hydra-NL is presented as well. The Hydra-NL measurement points (green) correspond to the KNMI2006 W+ scenario sea level rise for the years 2023, 2050 and 2100 respectively. The sea level rise as from Hydra-NL is extrapolated linearly, as advised in the WOWK (2018) for determining hydraulic boundary conditions using Hydra-NL⁴. The indicative values for sea level rise per climate scenario (SSP1-2.6, SSP2-4.5 and SSP5-8.5) are extrapolated quadratically as sea level rise is most certainly not a linear process and is thought to be accelerating in time.

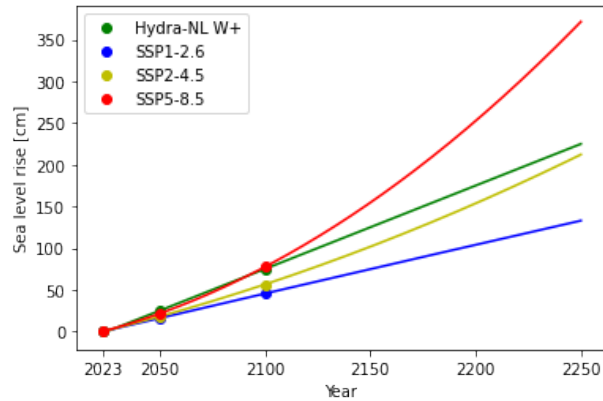


Figure 3.9: Indicative sea level rise per scenario for the Dutch coast

Design water levels

Hydra-NL is used to generate the water levels corresponding to specific return periods as needed for the assessments according to the 2017 Water Act and the 2012 Building Decree. Said water levels include set-up (also locally). Furthermore, as stated in the ROK (2017), additions for storm-oscillations and gusts and seiches should be taken into account, if relevant. Van Hijum (1999) proposes an addition of 0.5 m for vertical structures in tidal inlets to take into account storm-oscillations and gusts. The occurrence of seiches in the Haringvliet inlet however, is hard to prove and distinguish from overtides and human interference according to Reijmerink (2017). Therefore the effect of seiches is neglected for this preliminary design. It should be noted that Reijmerink (2017) reported a seiche-amplitude of only 0.25 m for a return period of 10000 years (which could not be distinguished with certainty from overtides and human interference).

The Hydra-NL location has different fetches and accompanying average depths than the actual location of the Delta Barrier due to the slight difference in allocation. Additionally, there is a difference in future depths due to sea level rise between the Hydra-NL W+ climate scenario linear extrapolation and the climate-scenarios quadratic extrapolations (see Figure 3.9). In order to account for said differences resulting in a different actual set-up than the set-up which Hydra-NL provides as output, Equation (3.5) is used.

$$S = C_2 \frac{U_{10}^2}{gd} F \cdot \sin \phi \quad (3.5)$$

⁴The WOWK (2018) recognises that this linear extrapolation leads to underestimation.

in which:	S	[m]	=	total wind set-up
	C ₂	[-]	=	coefficient taking into account various effects (e.g. temperature, humidity) $\approx 3.75 \cdot 10^{-6}$ for Dutch circumstances
	F	[m]	=	fetch
	U ₁₀	[m/s]	=	wind velocity at an altitude of 10 m
	g	[m/s ²]	=	gravitational acceleration
	d	[m]	=	average depth over the fetch
	ϕ	[°]	=	angle of incidence of the waves, where 90 ° is normally incident

With the "Wave conditions for revetments" module in Hydra-NL the correlation between water level and wave height can be taken into account. The revetment type "Asphalt wave impact zone" is chosen in order to disregard the influence of the wave period and angle of incidence of the waves. Section 3.3 presents the governing adjusted design water levels for every relevant combination of climate scenario, reference year and return period. Water levels from Hydra-NL with 0.5 m increments are presented in Appendix X with corresponding significant wave height, peak wave period, wind speed and dominant wind direction, from which the normative combination is indicated.

3.2.6 Wave Conditions

Hydra-NL is used to generate the significant wave heights given the sea water level corresponding to specific return periods as needed for the assessments according to the 2017 Water Act and the 2012 Building Decree. Accounting for the difference in fetches and accompanying average water depths between the Hydra-NL location and the actual location and sea level rise, the Bretschneider equations improved by Young and Verhagen (1996) (Equation (3.6) and Equation (3.7)) are used. The Bretschneider equations are also used to calculate the governing significant wave height and peak wave period at the Tidal Lake.

$$\tilde{H} = \tilde{H}_{\infty} \left\{ \tanh(0.343\tilde{d}^{1.14}) \cdot \tanh\left(\frac{4.41 \cdot 10^{-4} \tilde{F}^{0.79}}{\tanh(0.343\tilde{d}^{1.14})}\right) \right\}^{0.572} \quad (3.6)$$

$$\tilde{T} = \tilde{T}_{\infty} \left\{ \tanh(0.10\tilde{d}^{2.01}) \cdot \tanh\left(\frac{2.77 \cdot 10^{-7} \tilde{F}^{1.45}}{\tanh(0.10\tilde{d}^{2.01})}\right) \right\}^{0.187} \quad (3.7)$$

in which:	\tilde{H}	[-]	=	$\frac{gH_{m0}}{U_{10}^2}$	\tilde{T} [-]	=	$\frac{gT_p}{U_{10}}$
	\tilde{F}	[-]	=	$\frac{gF}{U_{10}^2}$	\tilde{d} [-]	=	$\frac{gd}{U_{10}^2}$
	F	[m]	=	fetch			
	d	[m]	=	average water depth over the fetch			
	U ₁₀	[m/s]	=	wind velocity at an altitude of 10 m			
	T _p	[s]	=	peak wave period			
	\tilde{H}_{∞}	[-]	=	dimensionless deep water wave height = 0.24			
	\tilde{T}_{∞}	[-]	=	dimensionless deep water wave period = 7.69			
	H _{m0}	[m]	=	significant wave height, from wave spectrum ($H_{m0} \approx H_s$)			

Section 3.3 presents the adjusted significant wave heights (and peak periods) given the water levels from Hydra-NL. Again, the complete Hydra-NL output and adjustments is reported in Appendix X from which the most normative are indicated.

3.2.7 Discharge Through the Haringvliet

The discharge through the Haringvliet is an important boundary condition influencing the Delta21 flood protection system. The presented residual discharge and the Kierbesluit is used as input for the hydrodynamic model as presented in Section 3.2.8. The fresh water discharge distribution over the different river-arms in the Rhine-Meuse estuary is actually quite a complicated system.

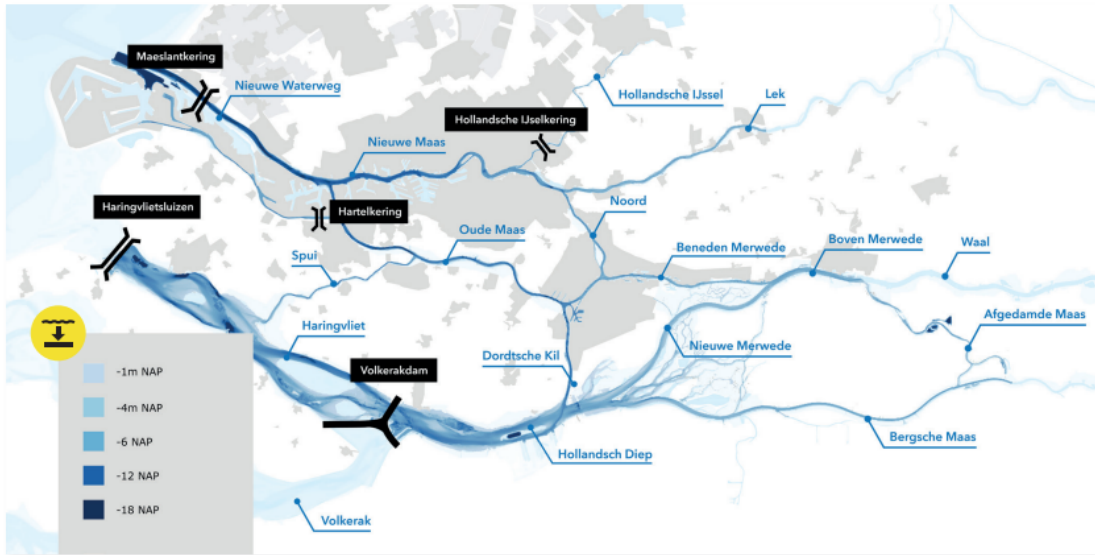


Figure 3.10: Overview with the names of the waterways and the Delta Works in the Rhine-Meuse estuary (Balla et al., 2019)

In a nutshell, the discharge in the Haringvliet river comes from the Hollandsch Diep via the Nieuwe Merwede and the Bergsche Maas. Note that the Spui river flows from the Haringvliet river towards the Nieuwe Waterweg since the Delta Works and the Dordtsche Kil can be characterised as a typical tidal river (Balla et al., 2019). After damming of the Meuse towards the Boven Merwede, the Meuse flows in entirety towards the Hollandsch Diep. The Nieuwe Merwede river is fuelled by a part of the Waal, which in turn discharges a certain part of the Rhine river. Further complicating the picture is the incorporation of the Haringvlietsluizen and the accompanying (ever changing) discharge program.

Figure 3.11 presents the residual discharge through the Haringvliet as a function of the Rhine discharge at Lobith. It should be noted that Figure 3.11 is calculated using SOBEK for the current situation (without Delta21) and with the current Kierbesluit (Figure 3.12) as operational programme of the Haringvlietsluizen.

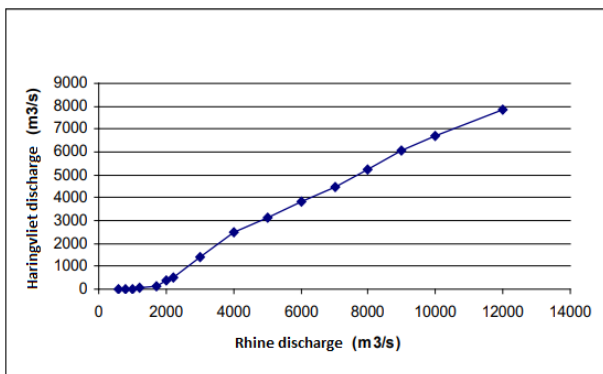


Figure 3.11: Residual Haringvliet discharge depending on the Rhine discharge calculated with SOBEK (Beeldman, 2011)

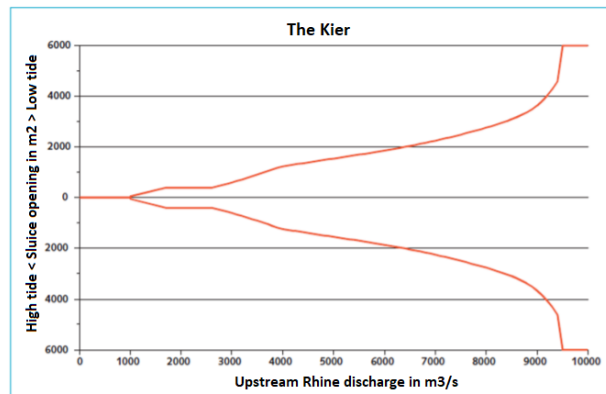


Figure 3.12: Haringvlietsluizen opening according to the Kierbesluit (Noordhuis, 2017)

3.2.8 Tidal Lake Water Level

For a closed Delta Barrier, the water level seaward of the storm surge barrier is solely dictated by the water level at the North Sea and the water level at the Tidal Lake is governed by the incoming river discharge and the management of the Spillway. For an open barrier though, the water level of the Tidal Lake depends on the tidal signal, river discharge and both of the geometry (effective flow area) of the storm surge barrier and of the Tidal Lake.

The effective flow area of the Delta Barrier has a significant impact on a multitude of hydrological and morphological processes in the Haringvliet estuary. A hydrodynamic model, as proposed by Onwuachu (2021), is used in order to assess the impact of the effective flow area of the storm surge barrier and make a sound choice for said flow area (say effective width and depth). For a total elaboration of the hydrodynamic model see "The New Haringvliet Barrier. Conceptual design for the storm surge barrier of the Delta21 project." (2021) and Appendix IX.

The water level in the Tidal Lake can be modeled by means of a one-dimensional continuity equation. The Haringvliet and Hollandsch Diep river can be modeled by means of a one-dimensional conservation of streamwise momentum equation in addition to again a one-dimensional continuity equation. Figure 3.13 presents the domain of the model. The river section of the model Haringvliet - Hollandsch Diep is taken until Moerdijk with a total length measured from the Haringvlietsluizen of 43 km.



Figure 3.13: Hydrodynamic model domain (Onwuachu, 2021)

It should be noted however that due to the large geometries and complexity of the structure in all dimensions, a 2D or even 3D approach ought to be taken for at least the final design stages. Furthermore, in order to capture all relevant hydrodynamic aspects (such as discharge distribution and influence of the Nieuwe Waterweg) a larger (SOBEK) model might be more suitable. For this preliminary design though, a much simpler 1D approach is chosen to give a more qualitative than quantitative insight into the water level in the Tidal Lake.

Tidal Lake (storage-basin model)

The storage-basin model (Equation (3.10)) may only be used if the basin can be considered a short basin, which is only valid when inertia and friction can be neglected. If this is the case we can expect the water level in the basin (Tidal Lake) to immediately follow the water level at sea (Bosboom & Stive, 2021). A short basin has a length that is short relative to the tidal wavelength. Bosboom and Stive (2021) proposed the short basin criterion as presented in Equation (3.8).

$$L_b < \frac{1}{20}L \quad (3.8)$$

where: L_b [km] = basin length ≈ 13
 L [km] = tidal wave length

The tidal wave length for shallow water conditions⁵ can be calculated using Equation (3.9).

$$L = \sqrt{gh} T_{M2} \quad (3.9)$$

where: L [m] = tidal wave length
 g [m/s²] = gravitational acceleration = 9.81
 h [m] = water depth
 T_{M2} [s] = principal lunar tide period ≈ 44700

Using Equation (3.9), it can easily be verified that the short basin criterion (Equation (3.8)) holds for all depths in the Dutch Voordelta. Hence, the one-dimensional continuity equation (Equation (3.10)) may be used. This means that the Tidal Lake effectively only has a storage function and that the water level at the Tidal Lake is directly dependent on the incoming and outgoing discharges through the Delta Barrier and the Haringvlietsluizen.

$$\frac{dQ(t)}{dx} + B_T(t) \frac{dh_3(t)}{dt} = 0 \quad (3.10)$$

where: $Q(t)$ [m³/s] = discharge
 $B_T(t)$ [m] = surface area of the Tidal Lake
 $h_3(t)$ [m] = water level in the Tidal Lake

A complete expansion of Equation (3.10) is presented in Appendix IX.

Haringvliet - Hollandsch Diep (1D channel model)

The short basin approximation is not valid for the Haringvliet - Hollandsch Diep. Onwuachu (2021) has proposed a exponentially decreasing cross-section and a length of 43 km. The model functions by the repeated execution of the shallow water wave equations: the 1D continuity equation (Equation (3.11)), and the streamwise momentum equation (Equation (3.12)). As the model proposed by Onwuachu (2021) is a simplified model, both the Spui and the Dordtsche Kil are left outside of the domain of the model, as can be seen in Figure 3.13.

$$\frac{\delta Q(x,t)}{\delta x} + B_H(x,t) \frac{\delta h_4(x,t)}{\delta t} = 0 \quad (3.11)$$

where: $Q(x,t)$ [m³/s] = discharge
 $B_H(x,t)$ [m] = surface area of the Haringvliet - Hollandsch Diep
 $h_4(x,t)$ [m] = water level in the Haringvliet - Hollandsch Diep

$$\frac{\delta Q(x,t)}{\delta t} + \frac{\delta}{\delta s} \left(\frac{Q(x,t)^2}{A_c(t)} \right) + g A_c(x) \frac{\delta h_4(x,t)}{\delta s} + c_f \frac{|Q(x,t)| Q(x,t)}{A_c(t) R(x)} = 0 \quad (3.12)$$

where: $Q(x,t)$ [m³/s] = discharge
 $A_c(x)$ [m²] = conveyance area
 g [m/s²] = gravitational constant = 9.81
 $h_4(x,t)$ [m] = water level in the Haringvliet - Hollandsch Diep
 c_f [-] = friction coefficient = 0.004
 $R(x)$ [m] = hydraulic radius of the Haringvliet - Hollandsch Diep

The complete hydrodynamic model is elaborated upon in Appendix IX.

⁵Note that for the relatively shallow North Sea a tidal wave can always be considered under shallow water conditions

3.2.9 Discharge Through the Delta Barrier

The discharge through the open storm surge barrier has already been introduced by means of Equation (IX.1a) and expanded to Equation (IX.1c) in Appendix IX. Once the water level in the Tidal Lake ($h_3(t)$) is solved we can therefore solve for the discharge through the barrier ($Q_S(t)$), provided the flow condition (sub-or super critical flow) is known.

$$Q_S(t) = \mu_1 B s h_2(t) \sqrt{2g\Delta H_1(t)} \quad (3.13)$$

in which:	Q_S	[m ³ /s]	=	discharge through the barrier
	μ_1	[-]	=	discharge coefficient of the Delta Barrier ≈ 0.7
	B	[m]	=	effective width of the Delta Barrier
	$h_2(t)$	[m]	=	water level at the sill
	$\Delta H_1(t)$	[m]	=	head difference over the Delta Barrier

The maximum discharge occurs in the super critical flow regime when the water level in the Tidal Lake is maximum (i.e. at the transition from sub- to super critical flow). For super critical flow, the flow is only dependent on the upstream water level (see Equation (IX.2)).

Furthermore, also the depth-averaged flow velocity through the barrier can now readily be solved.

$$U_1(t) = \mu_1 \sqrt{2g\Delta H_1(t)} \quad (3.14)$$

3.3 Overview of Design Parameters

The final design parameters, collected from Hydra-NL and adjusted accordingly for various effects - viz. fetch and depth differences and sea level rise - as discussed, are presented for the structural design of the Delta Barrier. These design parameters ought to be used for designing the structure with regards to the respective limit states and elements of the storm surge barrier.

With regard to the functional design, design parameters are presented where possible at this stage. As for the reliability of the closure operation (see Section 5.2), the design parameters are presented later in this thesis, as described.

3.3.1 Functional Design

The functional design is directly coupled to the functional requirements as set in Section 3.1.1. With regard to said functions, the retaining height and effective flow area are the most important dimensions of the structure. Furthermore, the reliability of closure is of importance and is discussed.

Parameters to determine the retaining height

The retaining height can be determined using Hydra-NL for specified return period and overtopping/overflow discharge using the "hydraulic load level" module. The return period with regard to overtopping or overflow comes from the failure mechanism overtopping in the 2017 Water Act (see Figure VI.12 in Appendix VI); $R = 83333$ years. The allowable overtopping discharge depends mostly on the fulfillment of the functional requirements. The WOWK (2018) states that considering a storm surge barrier a maximum overtopping discharge (q) of 1000 l/s/m is generally acceptable. This is a general rule of thumb, based on both the strength of the bottom protection and the available storage capacity. With greater specific overtopping discharges, dynamic aspects as a result of air pockets under the overflowing jet may play a role (Rijkswaterstaat, 2018). Here, Table 3.3 provides the input for Hydra-NL.

Parameter		
Climate-scenario	W+	-
Reference year	2100	
R	83333	years
q	1000	l/s/m/

Table 3.3: Hydra-NL input

table 3.4 and Table 3.5 present the adjusted design parameters used to calculate the required retaining height in Section 5.6 for climate scenario SSP2-4.5 and SSP5-8.5 respectively. Where $h_{1;d}$ is the design water level at sea and $H_{S;d}$ is the design value for the significant wave height. The adjustments made can be found in Appendix X.

$h_{1;d}$ [m NAP]	$H_{S;d}$ [m]
7.83	3.17

Table 3.4: Design parameters for SSP2-4.5 reference period 2250, R=83333

$h_{1;d}$ [m NAP]	$H_{S;d}$ [m]
9.52	3.34

Table 3.5: Design parameters for SSP5-8.5 reference period 2250, R=83333

Parameters to determine the effective flow area

Input for determining the best suitable effective flow area of the Delta Barrier (determined in Section 5.3) comes in the form of the average tidal signal ($h_1(t)$), considered climate scenarios and the discharge at Lobith (Q_{Lob}) and through the Haringvlietsluizen (Q_R). The required effective flow area for climate scenario SSP2-4.5 and SSP5-8.5 are compared. The final effective flow area is determined under daily conditions which are governing for the functionality of the storm surge barrier. Finally, both 2050 (after completion) and 2250 (end of design life) are considered in order to assess the impact of the Delta Barrier on the hydrodynamic characteristics of the area and the impact of climate change respectively. The input as described above is presented in Table 3.6.

Parameter		
Climate-scenario	SSP2-4.5	-
	SSP5-8.5	-
Reference year	2050	-
	2250	-
$h_1(t)$	$0.185 + SLR + 1.035 \sin(1.4 \cdot 10^{-4} \cdot t)$	m NAP
Q_{Lob}	2200	m^3/s
Q_R	500	m^3/s

Table 3.6: Overview design parameters effective flow area

Parameters to assess the reliability of the closure operation

The effects of a non-closure event of a barrier or barriers - when consisting of multiple barriers - is strongly dependent on the final gate type and design. Whether the Delta Barrier consists of one relative wide gate or multiple smaller ones influences the general behaviour and functioning of the barrier and as such also the effects of a non-closure event. Verification of the failure probability due to non-closure can be conducted as a function of sea level rise. The greater the sea level rises the greater the probability of flooding given a failed closure. Said verification is conducted in Section 5.2.

3.3.2 Structural Design

As has been established in Section 3.2.1, for the structural design only climate scenario SSP5-8.5 is considered with the reference year 2250. The reference year 2050, at completion of the storm surge barrier, is also included.

ULS

The relevant return periods for the ultimate limit state are 10 and 100000 years corresponding to the return periods as prescribed in the ROK (2021) for maximum positive head and ship collision (see Appendix XIII). Note that the Building Decree is governing over the 2017 Water Act considering structural failure (return period of 100000 vs. 52632 years, respectively).

Positive head

The tables below give the governing -adjusted- design parameters for a positive head situation for their respective climate-scenarios, reference periods and return periods. All combinations from which said governing parameters arise can be found in Appendix X". The adjustments made in order to account for fetch and depth differences and sea level rise are listed in Appendix X as well.

$h_{1;d}$ [m NAP]	$h_{3;d}$ [m NAP]	Δh [m]	θ [°]	$H_{S;d}$ [m]	$T_{p;d}$ [s]	U_p [m/s]	r [°]
6.49	1.00	5.49	246.6	2.35	8.64	37.3	300

Table 3.7: Design parameters for SSP5-8.5 reference period 2050, R=100000

$h_{1;d}$ [m NAP]	$h_{3;d}$ [m NAP]	Δh [m]	θ [°]	$H_{S;d}$ [m]	$T_{p;d}$ [s]	U_p [m/s]	r [°]
7.01	1.00	6.01	248.4	2.11	7.76	21.4	270

Table 3.8: Design parameters for SSP5-8.5 reference period 2250, R=10

$h_{1;d}$ [m NAP]	$h_{3;d}$ [m NAP]	Δh [m]	θ [°]	$H_{S;d}$ [m]	$T_{p;d}$ [s]	U_p [m/s]	r [°]
9.97	1.00	8.97	246.6	2.81	9.20	37.3	300

Table 3.9: Design parameters for SSP5-8.5 reference period 2250, R=100000

in which:	$h_{1;d}$	[m NAP]	=	design value sea water level
	$h_{3;d}$	[m NAP]	=	design value tidal lake water level
	Δh	[m]	=	head
	θ	[°]	=	wave angle of incidence w.r.t. north
	$H_{S;d}$	[m]	=	design value significant wave height
	$T_{p;d}$	[s]	=	design value peak wave period
	U_p ⁷	[m/s]	=	potential wind velocity
	r	[°]	=	wind direction w.r.t. north

Negative head

A negative head can generally only occur in two situations:

- Between the first and second peak of a storm while the Delta Barrier is closed.
In this situation negative head occurs during a storm surge, where generally for the smaller surges and larger discharges. One should note though, that in this situation waves approach the structure from the sea essentially reducing the hydraulic load caused by the negative head over the structure. For this reason, this situation will not be normative.
- For the case when the Delta Barrier has permanently closed, during LAT.
In this situation the storm surge barrier has closed permanently as sea level rise has resulted in a probability of flooding which exceeds the maximum regarding the reliability of the closure operation requirement. For the case of easterly wind, this situation is normative. Note that the governing situation is when the Delta Barrier has only just closed permanently, as this yield the lowest LAT. Permanent closure is not strictly required to keep the Netherlands safe against flooding and other solutions are also possible (see Section 5.11). Nonetheless, if the Delta Barrier were to be closed permanently, this would give the governing situation regarding negative head.

It is assumed that, given permanent closure, the water level at the Tidal Lake is managed at a level of NAP + 1 m by means of the Spillway and if necessary the Pumping Stations. Table 3.10 presents the design parameters for the Tidal Lake side as determined in Appendix X.

For the final calculation of the head over the barrier, the lowest astronomical tide (LAT) should be known for the situation when the Delta Barrier has only just closed permanently after a certain sea level rise. From Section 5.2 it follows that after a sea level rise of 1 m the closure operation is considered unreliable. Hence, directly after permanent closure incorporating a sea level rise of 1 m yields LAT = NAP - 0.22 m.

$h_{1;d}$	$h_{3;d}$	Δh	θ	$H_{S;d}$	$T_{p;d}$	U_p	r
[m NAP]	[m NAP]	[m]	[°]	[m]	[s]	[m/s]	[°]
-0.22	1.64	1.86	247.5	1.16	3.85	18.65	90

Table 3.10: Design parameters for negative head, SLR = 1 m, R=100000

⁷The potential wind velocity output from Hydra-NL can be converted to a wind speed at 10 m altitude (U_{10}) by the method from de Waal (2003)

SLS

As for the serviceability limit state, two stages are treated in this thesis. It is assumed that the characteristic combination, i.e. an irreversible SLS limit state, will not occur.

Frequent combination

As for the verification of the durability of the concrete (concrete crack widths), the frequent combination is used with loads corresponding to a return period of 100 years (see Appendix XIII).

$h_{1;f}$ [m NAP]	$h_{3;f}$ [m NAP]	Δh [m]	θ [°]	$H_{S;f}$ [m]	$T_{p;f}$ [s]	U_p [m/s]	r [°]
7.93	1.00	6.93	247.3	2.38	8.07	24.0	300

Table 3.11: Design parameters for SSP5-8.5 reference period 2250, R=100

in which:	$h_{1;f}$	[m NAP]	=	frequent value sea water level
	$h_{3;f}$	[m NAP]	=	frequent value tidal lake water level
	Δh	[m]	=	head
	θ	[°]	=	wave angle of incidence w.r.t. north
	$H_{S;f}$	[m]	=	frequent value significant wave height
	$T_{p;f}$	[s]	=	frequent value peak wave period
	U_p	[m/s]	=	potential wind velocity
	r	[°]	=	wind direction w.r.t. north

Quasi-permanent combination

As for the verification of the appearance of the structure (deflection), the quasi-permanent combination should be used with loads corresponding to a return period of 2 years (see Appendix XIII). However, as Hydra-NL can only be used for return periods between 10 and 1000000 years, the quasi-permanent combination is used with loads corresponding to a return period of 10 years. Note that the governing design parameters corresponding to R = 10 years have readily been presented for the ULS positive head combination (Table 3.8).

$h_{1;q}$ [m NAP]	$h_{3;q}$ [m NAP]	Δh [m]	θ [°]	$H_{S;q}$ [m]	$T_{p;q}$ [s]	U_p [m/s]	r [°]
7.01	1.00	6.01	248.4	2.11	7.76	21.4	270

Table 3.12: Design parameters for SSP5-8.5 reference period 2250, R=10


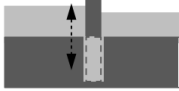
in which:	$h_{1;q}$	[m NAP]	=	quasi-permanent value sea water level
	$h_{3;q}$	[m NAP]	=	quasi-permanent value tidal lake water level
	Δh	[m]	=	head
	θ	[°]	=	wave angle of incidence w.r.t. north
	$H_{S;q}$	[m]	=	quasi-permanent value significant wave height
	$T_{p;q}$	[s]	=	quasi-permanent value peak wave period
	U_p	[m/s]	=	potential wind velocity
	r	[°]	=	wind direction w.r.t. north

4 Gate Type Variant Study

Having defined the Basis of Design, the second design step commences with the variant study in order to arrive at the most suitable gate type. Here, different standard concepts are inventoried after which they are verified against the most stringent functional requirements. The remaining concepts are subsequently evaluated. Finally, the highest scoring gate type is chosen to work out in a more detailed, yet preliminary, functional and structural design.

4.1 Inventory of Concepts

Table 4.1 presents an overview of the hydraulic gate types suitable for a storm surge barrier. For this thesis, the hydraulic gate types are categorised by their direction of movement (e.g., vertical, rotating horizontally) and type of structure. Short descriptions of the gate concepts, advantages and disadvantages are included in the table.

Hydraulic gate type	Pictogram *	Description *	Advantages	Disadvantages
Vertical lift		Vertical lift gates are moved vertically from the sill. A tower supports the gate during its operation. Overhead cables, sheaves and bull wheels can enable lifting. Alternatively, hydraulic cylinders could lift the gate.	<ul style="list-style-type: none"> - Simple shape - Can retain head from both sides - Easy fabrication - Large span possible - Double gate possible - Avoid long piers - Short erection time - Accessibility - Height is adaptable - Sill depth is adaptable - Width is adaptable - Gates easily replaceable - Suitable for km long barrier 	<ul style="list-style-type: none"> - Heavy mechanical system - Complex mechanical system - Mechanical system obsolete after permanent closure - High friction forces - Needs a hoisting tower - Large slots in piers - Moving loads in slots - Under water mechanism - Complex hoisting system - Sensitive to vibrations - Sensitive to sediments - Clearance for navigation - Towers always visible - Towers obsolete after permanent closure
Vertical rising		Vertical rising gates lie beneath the sill in open position. The gates are lifted vertically to close the barrier. Both in open and in closed position the gates are positioned largely under water. In most applications, gates can be lifted above water to allow maintenance.	<ul style="list-style-type: none"> - Simple shape - Can retain head from both sides - Large span possible - Double gate possible - Avoid long piers - Short erection time - Clearance for navigation - Width is expandable - Gates easily replaceable - Suitable for km long barrier 	<ul style="list-style-type: none"> - Complex foundation required - Heavy mechanical system - Complex mechanical - Mechanical system obsolete after permanent closure - High friction forces - Large slots in piers - Moving loads in slots - Under water mechanism - Complex hoisting system - Accessibility - Accumulation risk in sill - Height adaptability not flexible - Sill depth adaptability not flexible - Recess obsolete after permanent closure

Segment



The segment gate rotates around a horizontal axis, which passes through the bearing center. In closed position, the segment gate rests on the sill and in open position it is lifted. In literature, this type of gate is often referred to as a radial or tainter gate.

- Robustness and high stiffness
- Concentrated loads
- Low hoisting capacity
- No slot
- Width is expandable
- Suitable for km long stretch
- Allows for bridge integration
- Extensive trunnion anchoring required
- Not suitable for large negative head
- Large downstream piers
- Sensitive to vibrations
- Visible when open
- Clearance for navigation
- Gates difficult to (re)place
- Height adaptability gates challenging
- Sill depth adaptability challenging

Rotary segment



The rotary segment gate also has a horizontal axis. However, in recess, it lies in a concrete sill in the bed of the river. Thus, it is possible to sail over the gate in opened position. Operation of the gate is achieved by the rotation through approximately 90° thus raising the gate to the 'defence' position. A further 90° of rotation of the gate positions it ready for inspection or maintenance.

- Large torsion stiffness
- Light operating mechanisms
- Clearance for navigation
- Can retain head from both sides
- Facilitates maintenance when rotated above water
- Not visible when open
- Suitable for km long stretch
- Width is expandable
- Allows for bridge integration
- Complex engineering
- Forces on pivoting points
- Sensitive to waste and sediments
- Sensitive to vibrations
- Gates difficult to replace
- Height adaptability gates challenging
- Sill depth adaptability challenging
- Recess obsolete after permanent closure

Sector



A sector gate consists of a double gate. Each gate has a circular shape, transferring forces through a steel frame to the hinges at each side of the opening. It operates by rotating around two vertical axes. During operation the doors will rest on the river bed. In non-operational condition, the doors are stored in special docks constructed in the river banks.

- Simple structural concept
- Not visible
- Large recesses at sides
- Not suitable for km long barrier
- Not suitable for large negative head
- Usually expensive
- Heavy steel structure
- Friction in underwater slots
- Big and complex ball joints for hinges
- Sensitive to abrasion
- Gates difficult to replace
- Width not expandable
- Height adaptability gates challenging
- Sill depth adaptability challenging
- Recesses obsolete after permanent closure

Inflatable



An inflatable gate is basically a sealed tube made of a flexible material, such as synthetic fiber, rubber, or laminated plastic. It is anchored to the sill and walls by means of anchor bolts and an air- and watertight clamping system. The gate is inflated with air, water, or a combination of the two.

- Light weight
- Suitable for km long barrier
- Width is expandable
- Short erection time
- Not visible when open
- Simple foundation
- No "metallic" degradation
- Can resist limited head
- Strength strongly depends on material
- Risk of ship propeller collision when open
- Shorter service life for rubber
- Vandalism risk
- Sensitive to debris abrasion
- "Gate" not climate adaptive
- "Gate" difficult to replace
- Sill depth adaptability challenging

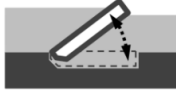
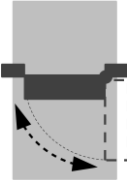
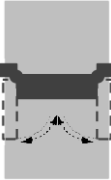
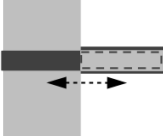
Flap		<p>Flap gates consist of a straight or curved retaining surface, pivoted on a fixed axis. In Venice, the gates are operated by filling or emptying them with air. At Venice and Stamford, the gates pivot around an axis at the sill, while at the Billwerder Bucht the axis lies above the water table.</p>	<ul style="list-style-type: none"> - Economic - Simple civil work - Simple hoist equipment - Forces transmitted to floor - Not visible when open 	<ul style="list-style-type: none"> - Can resist limited head - Not suitable for km long barrier - Lack of torsion rigidity - Difficulty of alignment - Sensitive to vibrations - Corrosion risk for hinges - Sensitive to abrasion - Accessibility issues - Clearance for shipping - Gate difficult to replace - Height adaptability gates challenging - Sill depth adaptability challenging - Recess obsolete after permanent closure
Barge		<p>A barge gate is a caisson stored on one side of a waterway, pivoting around a vertical axis to close. A barge gate may be buoyant or equipped with gated openings to reduce hinge and operating forces. In literature this type of gate is often referred to as a swing gate.</p>	<ul style="list-style-type: none"> - Clearance for navigation - Shallow gate recess - Can retain head from both sides - Suitable for narrow width - Gate easy to replace - Width is expandable - Gate height is adaptable - Sill depth is adaptable 	<ul style="list-style-type: none"> - Not suitable for km long barrier - High blockage risk - Heavy operating mechanism - Operating mechanism obsolete after permanent closure - Recesses obsolete after permanent closure
Mitre		<p>A mitre gate is in essence a barge gate but with two - mostly steel - gates, pivoting around two vertical axes to close. When closed, the two gates form a triangle (mitre) pointing towards high water. This hydraulic gate type is mostly and often seen in locks. Openings can be made in the gates for watering and dewatering purposes during the locking process.</p>	<ul style="list-style-type: none"> - Clearance for navigation - Quick opening and closing - Shallow gate recess - Suitable for narrow width - Gate easy to replace - Width is expandable - Gate height is adaptable - Sill depth is adaptable - Widely known concept 	<ul style="list-style-type: none"> - High blockage risk - Sensitive to ship collision - Not suitable for km long barrier - Not suitable for negative head - Manual closure more difficult - Two operating mechanism needed at both sides - Operating mechanism obsolete after permanent closure - Recesses obsolete after permanent closure
Rolling		<p>Rolling gates are sliding panels stored adjacent to the waterway. They are rolled into position in anticipation of a flood event. The new Panama locks are equipped with rolling gates.</p>	<ul style="list-style-type: none"> - Light operating mechanism - Can retain head from both sides - Forces transmitted to floor - Clearance for navigation - Gates easy to replace - Height is adaptable 	<ul style="list-style-type: none"> - Large construction area gate chamber - Not suitable for km long barrier - Width adaptability challenging - Sill depth adaptability challenging - Gate guiding system - Accumulation risk in sill - Sensitive to waves - Recess obsolete after permanent closure

Table 4.1: Overview of hydraulic gate types

* Adapted and modified from Mooyaart and Jonkman (2017)

4.2 Verification

The verification of the concepts presented in Table 4.1 is based on the most stringent functional requirements, here length suitability and height adaptability. In other words, all other functional requirements as posed in Section 3.1.1 can reasonably and economically be fulfilled by all the inventoried concepts. Though, not all concepts are suitable for a barrier with a length in the order of one kilometre or can enable an economic and feasible height adaptation. These functional requirements are treated here as knock-out criteria. Table 4.2 present the verification of the single gate concepts with respect to the established knock-out criteria.

	Hydraulic gate type	Length suitability	Height adaptability
→	Vertical lift gate	+	+
	Vertical rising	+	-
→	Segment	+	+
	Rotary segment	+	-
	Sector	-	-
	Inflatable	+	-
	Flap	-	-
	Barge	-	+
	Mitre	-	+
	Rolling	-	+

Table 4.2: Verification of single gate concepts (+ suitable; - not suitable)

As follows from Table 4.2 by the arrows (→), only the vertical lift gate and segment gate can fulfill all posed functional requirements.

4.3 Evaluation

The concepts remaining after the verification: the vertical lift gate and segment gate, are evaluated by means of quantitatively scoring how easily the specific concept is able to fulfill certain functional requirements as posed in Section 3.1.1 and certain criteria from the stakeholder analysis (see Section 2.2). All relevant verification criteria, i.e. requirements in which specific concepts can differ from one another, are presented below.

- 1 Retaining water
 - 1.1 Positive head
 - 1.2 Negative head
 - 1.3 Ice resistance
- 2 Future proof
 - 2.1 Height adaptability
 - 2.2 Width adaptability
 - 2.3 Depth adaptability
 - 2.4 Obsolete parts after permanent closure
- 3 Reliability & Maintenance
 - 3.1 Closure reliability w.r.t. malfunction
 - 3.2 Closure reliability w.r.t. external event
 - 3.3 Maintenance requirements
 - 3.4 Maintainability
 - 3.5 Complexity of closure and opening

- 4 Constructability
 - 4.1 Length suitability
 - 4.2 Impact on surroundings
 - 4.3 Technical feasibility
 - 4.4 Construction time
 - 4.5 Construction space needed
- 5 Ecology
 - 5.1 Environmental footprint
 - 5.2 Fish passage
 - 5.3 Seal passage
 - 5.4 Impact on flora and fauna
 - 5.5 Morphology
- 6 Spatial quality
 - 6.1 Spatial optimisation (road)
 - 6.2 Incorporation technical rooms
 - 6.3 Simplicity and coherence
 - 6.4 Integration into the environment

After the concepts are scored considering the evaluation criteria, the total score is computed on a scale from 0 to 10. Finally, the weighted score takes into account the different weights for the evaluation criteria. The greater the weight of a specific criteria, the more it is taken into account when computing the total weighted score. The different weights follow from engineering judgement regarding the posed functional requirements (see Section 3.1.1) and the stakeholder analysis (see Section 2.2). As weighted scores can transcend the 10 mark, the highest weighted score will receive a reference score of 10 from which the second concept is scaled. The evaluation is presented in Figure 4.1.

In order to make a clear comparison, the reference score representing the benefits is compared with the costs for both the vertical lift gate and the segment gate. The most expensive concept gets a monetary reference score of 10, from which the other variant is in a relative sense. The total costs comprise of initial costs and operational costs and do not represent so called "hidden costs" caused by e.g. the environmental footprint. The scores for both concepts are presented in Table 4.3.

	Vertical lift gate	Segment gate
Costs	9	10

Table 4.3: Monetary reference scores regarding total costs

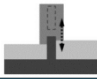
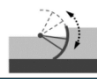
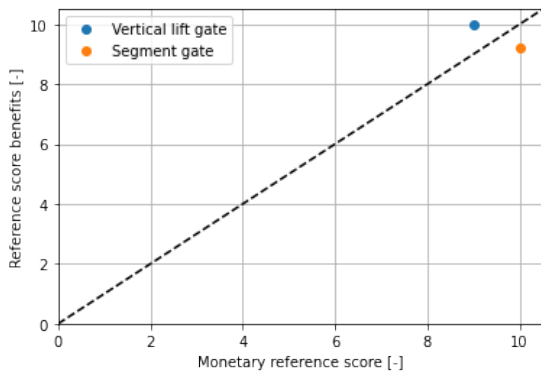
LEGENDA SCORE		Vertical lift gate		Segment gate	
Zeer goed	4				
Goed	3	Remarks		Remarks	
Redelijk	2				
Slecht	1				
1 Retaining water					
1.1 Positive head		Load transfer to piers (and sill possible)	4 / 4	Load transfer to trunnion	3 / 4
1.2 Negative head		No change in load transfer scheme	4 / 4	Tension forces on trunnion points	1 / 4
1.3 Ice resistance		Less controlled underflow	3 / 4	More controlled underflow	4 / 4
Total			11 / 12		8 / 12
2 Future proof					
2.1 heigh adapt.		Gate easily adaptable/replaceable	4 / 4	Gate difficult to adapt/replace	1 / 4
		Movement works easier to replace		Movement works difficult to replace	
		Concrete superstructure adaptable		Curved slots in concrete difficult	
		<i>Not distinguishable</i>			
2.2 width adapt.		Only if load transfer is not to the sill	4 / 4	Difficult due to curved gate	3 / 4
2.3 depth adapt.		Heavy mechanical system and towers	2 / 4	Lighter mechanical system	4 / 4
2.4 permanent closure					
Total			10 / 12		8 / 12
3 Reliability & Maintenance					
3.1 Closure reliability w.r.t. malfunction		Gravity driven closure very reliable	4 / 4	Trunnion wear due to friction	3 / 4
		Complex mechanical system		Less complex mechanical system	
3.2 Closure reliability w.r.t. ext. Event		Movement works shielded	4 / 4	Strutt arms susceptible to buckling	1 / 4
		More distributed load transfer to piers		Unshielded hydraulic cylinder	
				Load transfer to trunnion	
3.3 Maintenance requirements		Heavy and complex mechanical system	3 / 4	Lighter mechanical system	4 / 4
		Many complex seals and guiding systems		Complex, curved seals	
		High friction forces and loads in slots			
3.4 Maintainability		Under water mechanisms	3 / 4	Trunnion easily accessible	4 / 4
		Gates easier to inspect/maintain		Gates more difficult to inspect/maintain	
3.5 Complexity of opening and closure		Gravity driven closure	4 / 4	Susceptible to vibrations for underflow	3 / 4
		Closure/opening under flow possible		Relatively constant hoisting loads	
		High lift forces for no counterweights		Relatively faster opening/closing	
		Slower opening/closing for gears			
Total			18 / 20		15 / 20
4 Constructibility					
4.1 Length suitability		<i>Not distinguishable</i>			
4.2 Impact on surroundings		<i>Not distinguishable</i>			
4.3 Technical feasibility		Very well-proven technology	4 / 4	Well-proven technology	3 / 4
4.4 Construction time		Gate (de)installation relatively complex	4 / 4	Gate (de)installation relatively complex	3 / 4
		Gate transport relatively complex		Gate transport relatively complex	
				High installation accuracy trunnion	
4.5 Construction space needed		Avoids wide piers	4 / 4	Relatively wide piers required	2 / 4
Total			12 / 12		8 / 12
5 Ecology					
5.1 Environmental footprint		Towers require much material	3 / 4	Wider piers require much material	4 / 4
		Heavy mechanical system		Lighter mechanical system	
5.2 Fish passage		Less controlled underflow	3 / 4	More controlled underflow	4 / 4
		passage opening in gate possible		Fish passage opening in gate possible	
5.3 Seal passage		Less controlled underflow	3 / 4	More controlled underflow	4 / 4
5.4 Impact on flora & fauna		Less controlled underflow	3 / 4	More controlled underflow	4 / 4
5.5 Morphology		Less controlled underflow	3 / 4	More controlled underflow	4 / 4
Total			15 / 20		20 / 20
6 Spatial quality					
6.1 Road connection		Bridge girder integration difficult	3 / 4	Bridge girder integration possible	4 / 4
		Better installation conditions for bridge		Poor installation conditions for bridge	
6.2 Incorporation of technical rooms		Heavy mechanical system	2 / 4	Lighter mechanical system	4 / 4
		room in towers		Much room in wide piers	
		<i>Less</i>			
6.3 Simplicity and coherence		<i>Not distinguishable</i>			
6.4 Integration into the environment		Towers often seen as distortion	2 / 4	Less visual distortion	4 / 4
Total			7 / 12		12 / 12
Overall	Weight	1. Vertical lift gate		2. Segment gate	
1. Retaining water	2		11 / 12		8 / 12
2. Future proof	2		10 / 12		8 / 12
3. Reliability & maintenance	1.5		18 / 20		15 / 20
4. Constructibility	1		12 / 12		8 / 12
5. Ecology	1.5		15 / 20		20 / 20
6. Spatial quality	1		7 / 12		12 / 12
Total score		Total score	8.31	Total score	7.92
Selection		Weighted score	12.60	Weighted score	11.60
		Reference score	10	Reference score	9.21

Figure 4.1: Evaluation

4.4 Selection



From Figure 4.1 and Figure 4.2 it shows that the vertical lift gate is the most suitable hydraulic gate type for the Delta Barrier.

Figure 4.2: Costs vs. benefits gate concepts

5 Spatial and Functional Design

This chapter presents the spatial and functional design, the second phase of part 2 of the design cycle. The aim of this chapter is to enable the Delta Barrier to satisfy all functional requirements and present a final layout with main dimensions for which it does. Firstly, in order for the storm surge barrier to effectively protect the the South West Delta from flooding, a new Delta21 flood protection process is proposed as opposed to the current process (see Appendix IV). Secondly, the reliability of the closure operation is discussed. Thirdly, in order to preserve sufficient discharge capacity, the required effective flow area of the Delta Barrier is determined by means of a hydrodynamic model. Hereafter, the impact of the implementation of Delta21 and the Delta Barrier on the morphology and ecological system of the Haringvliet estuary is discussed. Subsequently, the required retaining height is determined after which possible solutions for enabling the passage for shipping and road-traffic are given. Finally, the feasibility of using tidal turbines to generate electricity with tidal flow is researched and a brief description on the chosen driving mechanisms is given. Additionally, climate adaptive pathways are presented which enable the flood protection function of Delta21 in the future, after a continuously rising sea level. This chapter is concluded with a final layout of the Delta Barrier with main dimensions for which all functional requirement are met.

5.1 Proposed Delta21 Flood Protection Process

The current Delta21 flood protection process (see Appendix IV) seems ill defined and formulated closure criteria for the storm surge barrier are rather ambiguous. A new Delta21 flood protection process is proposed with clear closure criteria in order to effectively protect the hinterland against flooding. Furthermore, the estimated closure frequency considering the new flood protection process is presented as a function of sea level rise. In addition, the proposed closure and opening strategy of the Delta Barrier is presented and it is researched when to open the Delta21 Spillway as part of the proposed Delta21 flood protection process.

5.1.1 Closure Regime

Here, new operational scenarios are proposed instead of the scenarios as proposed by Berke and Lavooij (2018c) and presented in Section 2.3.1. In order to set-up such operational scenarios, i.e. scenarios in which the Delta Barrier ought to close, the current Europoortkering closure regime is compared to the cases for which the water level at Dordrecht reaches NAP + 2.50 m in Figure 5.1. The line for which Dordrecht reaches NAP + 2.50 m and the line representing the current Europoortkering closure regime is adapted from De Bruijn (2022) and Projectbureau Europoortkering met Open Beerdam (1992), respectively.

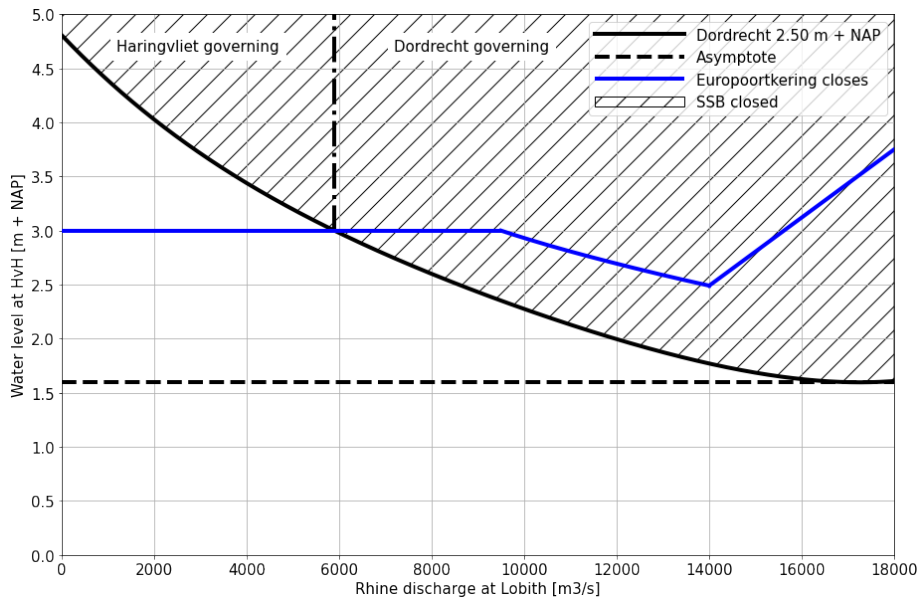


Figure 5.1: Comparison current Europoortkering regime and Dordrecht NAP + 2.50 m (adapted from De Bruijn (2022) and Projectbureau Europoortkering met Open Beerdam (1992))

In Figure 5.1 the hatched area represents the cases for which the Delta Barrier should be closed, either to protect the hinterland of the Haringvliet from a storm surge only (Haringvliet governing), or to ensure that the water level at Dordrecht stays beneath NAP + 2.50 m (Dordrecht governing).

It should be noted however, that the Delta21 flood protection system is unable to effectively lower the water level at Dordrecht when the Europoortkering (the Maeslantkering and the Hartelkering) is still open. In other words, assuming an unchanged Europoortkering closure regime (blue line in Figure 5.1), Delta21 will be ineffective in keeping the water level at Dordrecht below NAP + 2.50 m for discharges greater than ca. 5800 m³/s until the Europoortkering has to close as well. This conflict is presented in Figure 5.2, where the hatched area represents the cases for which the Delta21 flood protection system can not guarantee a water level at Dordrecht below NAP + 2.50 m.

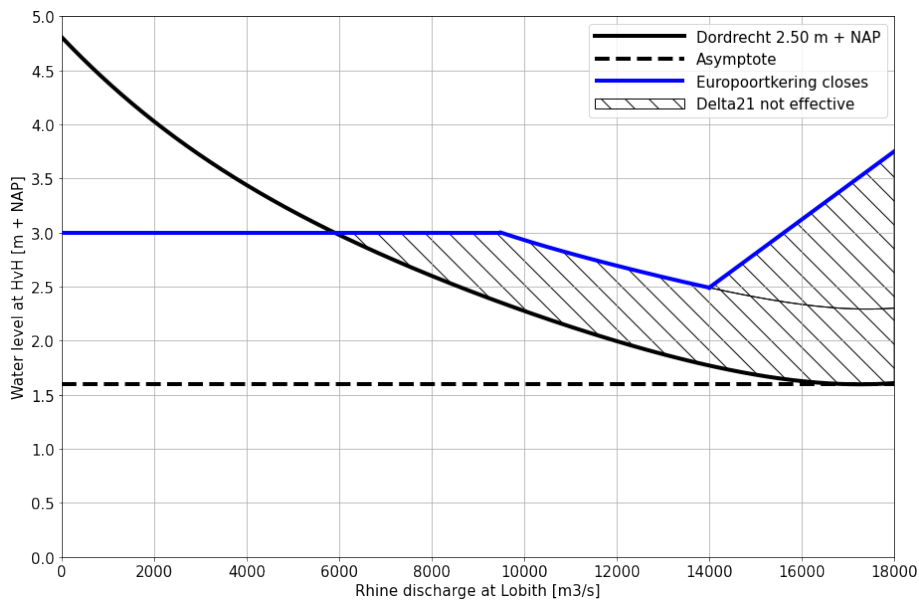


Figure 5.2: Cases for which Delta21 is ineffective given the current Europoort closure regime (adapted from De Bruijn (2022) and Projectbureau Europoortkering met Open Beerdam (1992))

Hence, in order for the Delta21 flood protection system to work properly, the closure regime of the

Europoortkering should be adapted. Figure 5.3 presents the newly proposed closure regime of the Europoortkering.

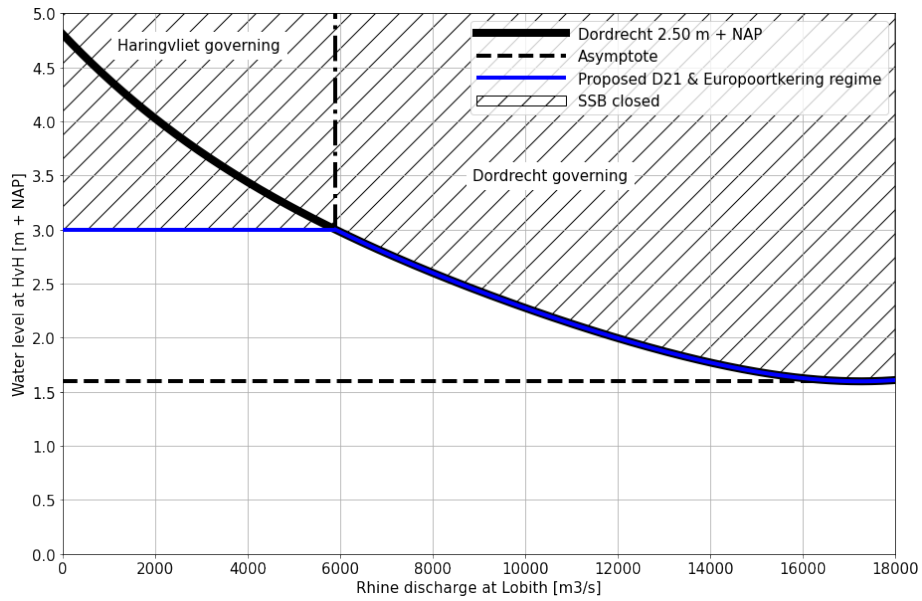


Figure 5.3: New Delta21 and Europoortkering operational regime (adapted from De Bruijn (2022) and Projectbureau Europoortkering met Open Beerdam (1992))

As a result, Figure 5.3 depicts the newly proposed Delta21 operational regime, which is the same as the adapted Europoortkering closure regime. Do note that the newly proposed operational regime translates to more frequent closures for the Europoortkering. While it should be acknowledged that this might not be beneficial for the service life of the Europoortkering, this is outside the scope of this thesis.

5.1.2 Closure Frequency Delta Barrier

The Delta Barrier should close for either an expected water level of NAP + 3.0 m at Hoek van Holland or an expected water level of NAP + 2.50 m at Dordrecht. The closure frequency of the Delta Barrier, taking into account the newly proposed Delta21 operational regime (see Figure 5.3), is estimated by means of Hydra-NL. Figure 5.4 presents said estimation as a function of sea level rise (w.r.t. 2022) where, additionally, Figure 5.5 zooms in on the closure frequency till a sea level rise of 1.0 m.

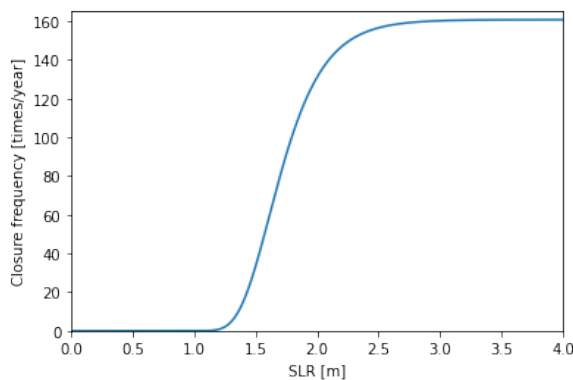


Figure 5.4: Closure frequency of the Delta Barrier as a function of sea level rise

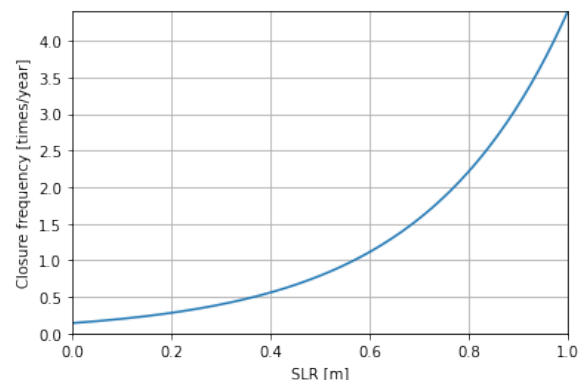


Figure 5.5: Closure frequency as a function of sea level rise till 1.0 m

Assuming 0.24 m of sea level rise in 2050 (SSP5-8.5), the closure frequency of the Delta Barrier would approximately be 1/3 times per year and for 0.5 m of sea level rise ca. 4/5 times per year.

Furthermore, the newly proposed Delta21 operational regime results in a change of operational regime of the Europoortkering, viz. the closure regime of the Europoortkering mirrors the Delta Barrier. To grasp the impact on the closure frequency of the Europoortkering, Figure 5.6 presents the current closure frequency of the Europoortkering as a function of sea level rise, again by using Hydra-NL. Lastly, Figure 5.7 zooms in on the closure frequency till a sea level rise of 1.0 m.

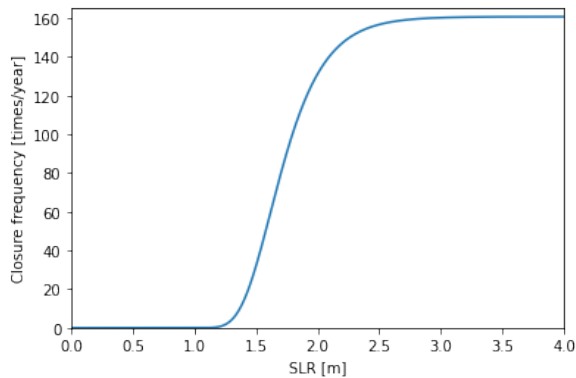


Figure 5.6: Current closure frequency of the Europoortkering as a function of sea level rise

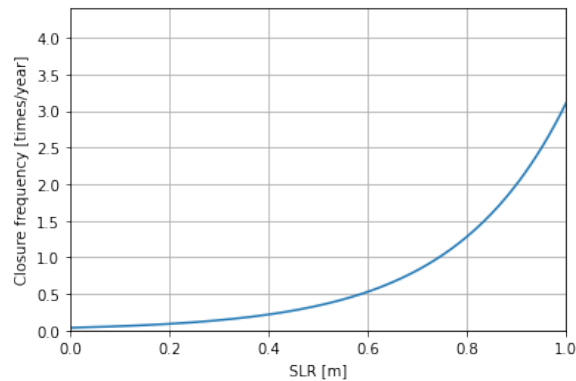


Figure 5.7: Closure frequency as a function of sea level rise till 1.0 m

As for the case of 0.24 m of sea level rise (SSP5-8.5, 2050), the closure frequency of the Europoortkering, considering the current closure regime, would approximately be $1/9$ times per year and for 0.5 m of sea level rise ca. $1/3$ times per year.

5.1.3 Closure and Opening Strategy Delta Barrier

Closure strategy

If a storm surge is to be expected which threatens the NAP + 3.0 m mark at Hoek van Holland or if a combined storm surge at sea and discharge threatens the NAP + 2.50 m mark at Dordrecht, the Delta Barrier ought to close beforehand of said storm surge's first peak. Now for the cases of a requested closure while no storm surge is present (i.e. only a high discharge), the Delta Barrier should close during low water at the moment that opening the Spillway to the Energy Storage Lake yields a greater discharge capacity than the natural capacity under gravity flow. It should be noted that, depending on the discharge at Lobith, a different water level at sea could lead to a requested closure and vice versa as can be seen in Figure 5.3.

Furthermore, closure should preferably take place when there is no head over the barrier resulting in zero flow velocity through the barrier in order to relieve the moving works from great pressures and forces. Closure should take place before the first peak of the storm surge at sea at the lowest possible water level in order to either use the maximum still available storage capacity of the Tidal Lake or in order to limit the initial amount of artificial lowering of the water level using the Spillway.

Opening strategy

When the storm surge has blown over and the water level at sea is dropping below the signalling value of NAP + 3.0 m or the water level at Dordrecht below NAP + 2.5 m, the Delta Barrier can - theoretically - be re-opened. It is advisable to always wait out the development of the second peak of the storm and hence open only when the second peak has gone by. Naturally, for the case of a requested closure while no storm surge is present, the Delta Barrier can be re-opened when the river discharge gets below the signalling value again. Additionally, opening should preferably take place under no head over the barrier again, when the flow velocity through the barrier is zero. This point of no flow velocity depends on the development of the water level at the Tidal Lake while the barrier is closed. When the latter is equal to the water level at sea, the Delta Barrier should be re-opened.

5.1.4 Opening the Spillway

When only high river discharges in combination with the tide (no significant storm surge) results in a closure, using the Tidal Lake as a first measure is not economic. Due to the fact that river discharges are relatively constant within the range of a few tidal cycles, the storm surge barrier is to remain closed for a relatively long time. As a result, for these cases, it is only a matter of time before the capacity of the Tidal Lake is reached and the Spillway should be opened. Under said cases, using the Tidal Lake as a first measure for additional storage capacity is unfeasible. Any anticipated profit gained as a result of waiting to open the Spillway is non-existent as the Energy Storage Lake should be prepared (i.e. emptied) in advance of the expected closure. For this reason, the Spillway should be opened immediately after closure of the Delta Barrier in order to provide the head for discharging the river water towards the Energy Storage Lake. First decreasing the head by waiting to open the Spillway is not beneficial in any sense.

Though, when it is expected that the water level of the Tidal Lake after closure stays beneath the closure criteria⁸ during storm duration, the Spillway does not have to be opened and the Tidal Lake only has sufficient storage capacity to store the incoming river water.

5.1.5 Overview Proposed Process Delta21 Flood Protection System

The consideration as described above are translated into the newly proposed flow chart for the Delta21 flood protection system in Figure 5.8. In the flow chart, the two main scenarios of the Delta21 flood protection system are depicted by means of a cross-section over the Tidal Lake indicating the states of the Delta Barrier, the Spillway and the Haringvlietsluizen. Additional simulations further clarifying the closure and opening strategy of the Delta Barrier and when to open the Spillway to the Energy Storage Lake can be found in Appendix XI.

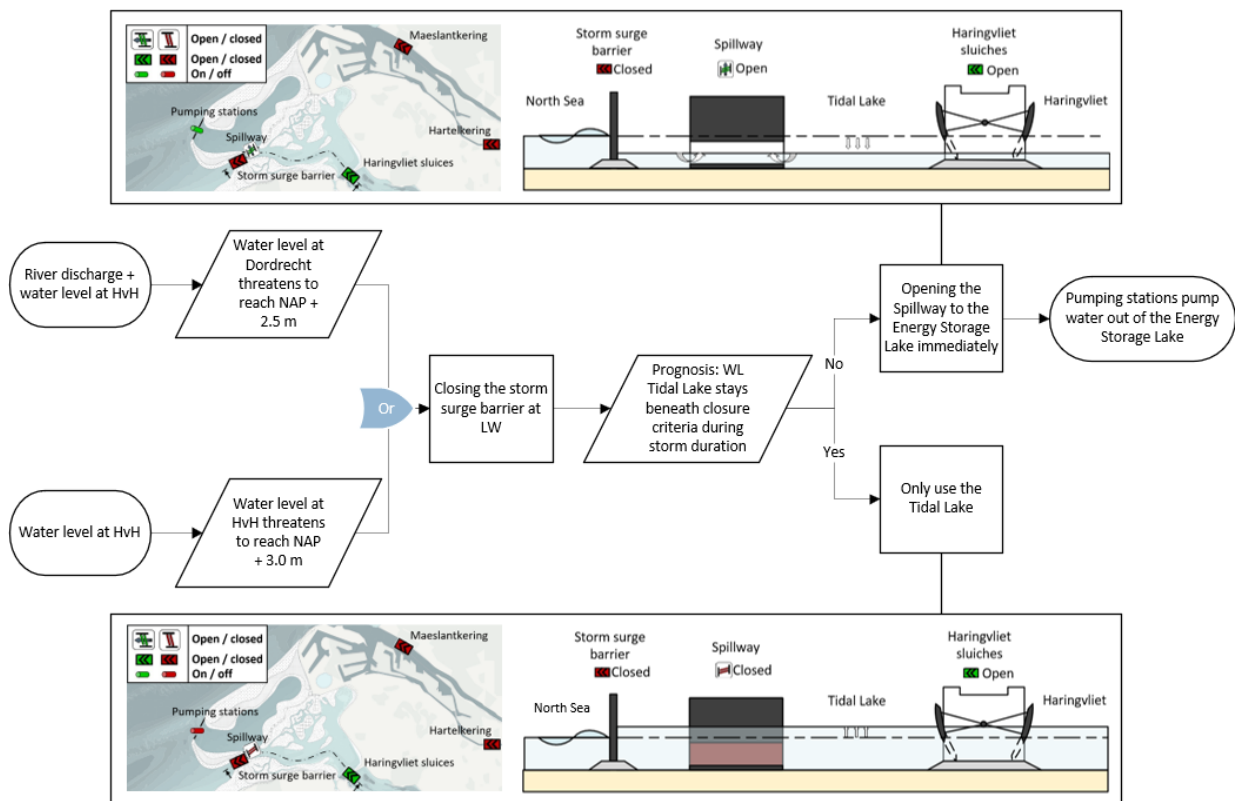


Figure 5.8: Proposed process of the Delta21 flood protection system

⁸The closure criteria here is equal to the closure criteria for the water level at HvH given a specific discharge (see Figure 5.3)

5.2 Reliability of the Closure Operation

This section presents the verification to the functional requirement regarding the reliability of the closure operation (FR-1.3 in Section 3.1.1). The failure mechanism of non-closure can be schematized as in Figure 5.9.



Figure 5.9: Failure mechanism of non-closure (Onwuachu, 2021)

The maximum failure probability regarding the failure of the barrier due to non-closure ($1/52632$ per year) is a function of the maximum failure probability of the Delta21 flood protection system, the proposed Delta21 dike segments and the distribution of probabilities over the relevant failure mechanisms per the 2017 Water Act (see Appendix VI.1). Figure 5.10 depicts the fault tree with scenarios which could lead to failure of the barrier due to non-closure.

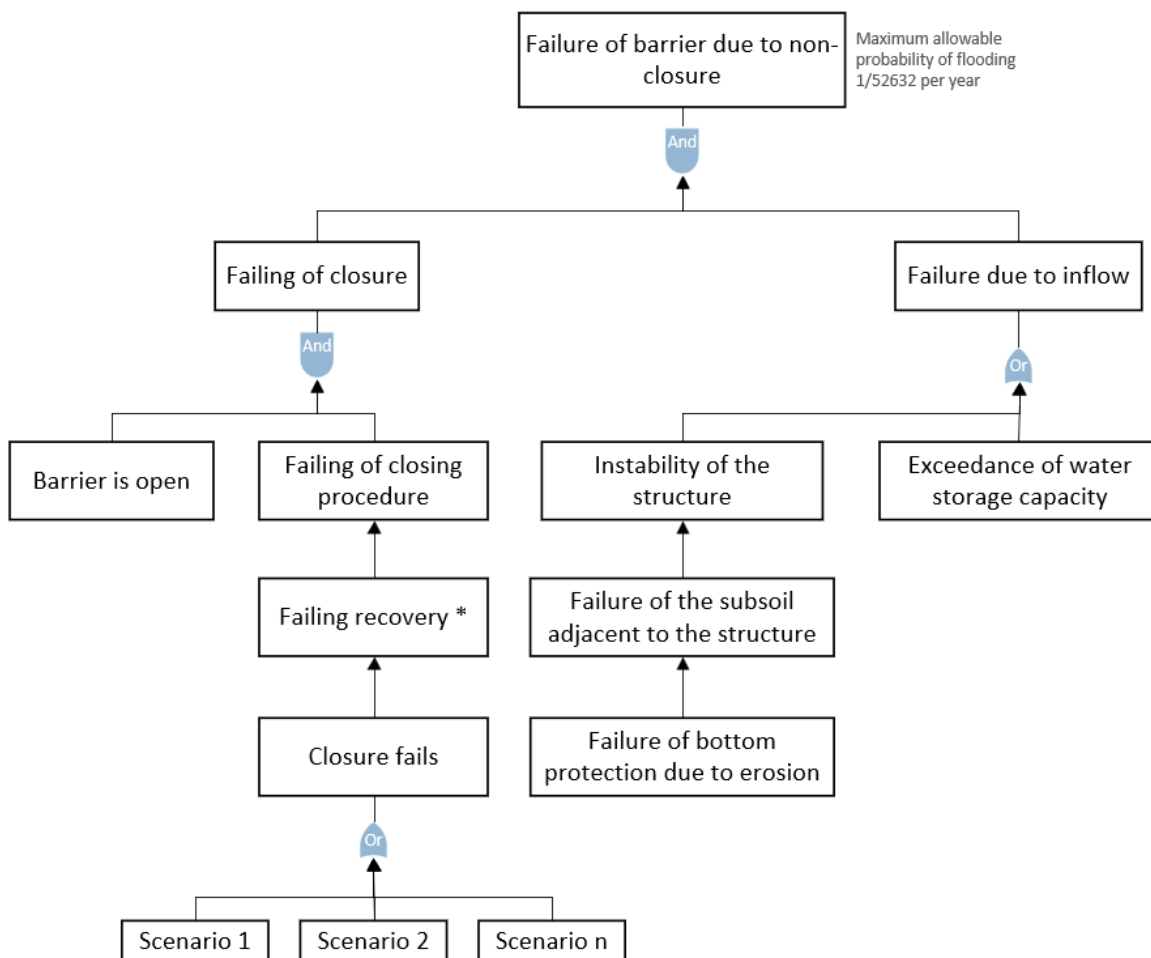


Figure 5.10: Fault tree failure of barrier due to non-closure

* The probability of recovery (or ability to repair) depends on the scenario and failing component

Note that failure of the barrier here represents flooding of the hinterland. In general, the probability of flooding after a non-closure event can be described by Equation (5.1).

$$P_{f,NC} = \sum_{i=1}^n P(fl \cap sc_i) \quad (5.1)$$

where: $P_{f,NC}$ is the probability of flooding after non-closure [per year]
 $P(fl \cap sc_i)$ is the probability of flooding and scenario i [per year]

Subsequently, the probability of flooding after a non-closure event can be elaborated into Equation (5.2a). Assuming that flooding never occurs given a successful closure yields Equation (5.2b). Elaboration of Equation (5.2b) according to the presented fault tree (Figure 5.10) gives Equation (5.2c). Note that it is assumed here that the barrier is always completely open before a requested closure and that no recovery of a failed closure is possible. Finally, assuming that the structure always fails if the bottom protection fails resulting in flooding, yields Equation (5.2d).

$$P_{f,NC} = P(fl|cf) \cdot P(cf) + P(fl|cs) \cdot P(cs) \quad (5.2a)$$

$$\approx P(fl|cf) \cdot P(cf) \quad (5.2b)$$

$$= P(Z_{NC1} < 0|cf \cap Z_{NC2} < 0|cf \cup Z_{NC3} < 0|cf) \cdot P(cf) \quad (5.2c)$$

$$\approx P(\min(Z_{NC1}; Z_{NC3}) < 0|cf) \cdot P(cf) \quad (5.2d)$$

where: $P(fl|cf)$ is the probability of flooding given that the closure fails [per year]
 $P(cf)$ is the probability that the closure fails [-]
 $P(fl|cs)$ is the probability of flooding given that the closure is a success [per year] ≈ 0
 $P(cs)$ is the probability that the closure is a success [-] ≈ 1
 $P(Z_{NC1} < 0)$ is the probability that the bottom protection fails [per year]
 $P(Z_{NC2} < 0)$ is the probability that the structure fails [per year]
 $P(Z_{NC3} < 0)$ is the probability of exceedance of the water storage capacity [per year]

Let us now consider all possible scenarios as the sum of failure of any number of gates as in Equation (5.3a). It is argued here that failure of one gate is governing considering independent failure. Regarding dependent failure, the scenarios of two gates failing and all (25) gates failing are assumed to be governing. Now, regarding the considered failure mechanisms, one should note that for the two scenarios of one failing gate and two failing gates the failure of the bottom protection (Z_{NC1}) is assumed to be governing. For the scenario that all (25) gates fail, failure due to the exceedance of water storage capacity (Z_{NC3}) is governing. Finally, the flow velocity through the barrier and therefore the load on the bottom protection is not expected to be significantly different for the case of 2 gates failing w.r.t. the case of 1 gate failing to close. Hence, we may simplify to Equation (5.3d).

$$P_{f,NC} = \sum_{i=1}^{n=25} P(fl|cf_i) \cdot P(cf_i) \quad (5.3a)$$

$$\approx n \cdot P(fl|cf_1) \cdot P(cf_1) + \binom{25}{2} \cdot P(fl|cf_2) \cdot P(cf_2) + P(fl|cf_{25}) \cdot P(cf_{25}) \quad (5.3b)$$

$$= n \cdot P(Z_{NC1} < 0|cf_1) \cdot P(cf_1) + \frac{25!}{23!2!} \cdot P(Z_{NC1} < 0|cf_2) \cdot P(cf_2) + P(Z_{NC3} < 0|cf_{25}) \cdot P(cf_{25}) \quad (5.3c)$$

$$\approx n \cdot P(Z_{NC1} < 0|cf_1) \cdot P(cf_1) + \frac{25!}{23!2!} \cdot P(Z_{NC1} < 0|cf_1) \cdot P(cf_2) \quad (5.3d)$$

$$+ P(Z_{NC3} < 0 | cf_{25}) \cdot P(cf_{25})$$

where: $P(fl cf_1)$	is the probability of flooding given that the closure of one gate fails [per year]
$P(cf_1)$	is the probability that the closure of one gate fails [-]
$P(fl cf_2)$	is the probability of flooding given that the closure of two gates fails [per year]
$P(cf_2)$	is the probability that the closure of two gates fails [-]
$P(fl cf_{25})$	is the probability of flooding given that the closure of 25 gates fail [per year]
$P(cf_{25})$	is the probability that the closure of 25 gates fail [-]

The probability that the bottom protection fails depends on the bottom protection used and the head over the failed gate. The top layer of the bottom protection which is applied, having a nominal diameter of 1.82 m, can withstand a flow velocity of 7.88 m/s according to Izbash and a head over the open gate of 5.10 m (see Section 9.3.6). Assuming a fixed Tidal Lake water level of NAP + 1 m, a water level at sea of at least NAP + 6.10 m is needed to arrive at the critical maximum head.

The probability of exceedance of the water storage capacity can be found by finding the normative primary dike section, i.e. the dike section which yields the highest failure probability taking into account the consequences of flooding (see Appendix XII). If no significant consequences occur (regarding individual risk) given a flooding as the result of the failure of a section, this section is considered not governing. The normative section, comparing the 'dike rings' of Voorne-Putten, Goeree-Overflakkee, West-Brabant, Hoeksche Waard and Eiland van Dordrecht, is a structure (Inlaatsluis Brakelsveer) which is part of segment 21-1 from the Hoeksche Waard ring. The failure probability of that section, hence an estimate of the probability of exceedance of the water storage capacity, is 0.002 per year as concluded in Appendix XII. Using Hydra-NL, a failure probability of 0.002 per year translates to a water level at Inlaatsluis Brakelsveer of NAP + 2.57 m.

Finally, Equation (5.4) describes the final equation needed for verification.

$$P_{f,NC} \approx 25 P(h_1 \geq 6.10) \cdot P(cf_1) + 300 P(h_1 \geq 6.10) \cdot P(cf_2) \quad (5.4)$$

$$+ P(h_V \geq 2.57) \cdot P(cf_{25}) < \frac{1}{52632}$$

where: $P(h_1 \geq 6.10)$	is the probability that the water level at sea is greater than or equal to NAP + 6.10 m [per year]
$P(h_V \geq 2.57)$	is the probability that the water level at Inlaatsluis Brakelsveer is greater than or equal to NAP + 2.57 m [per year]

The probability of a certain water level at sea is greatly dependent on sea level rise. Moreover, the water level at Inlaatsluis Brakelsveer is a function of the water level at Hoek van Holland and the discharge of the Rhine at Lobith and as such a function of both sea level rise and a changing discharge distribution.

Assuming that the probability of one gate failing to close is 10^{-3} , two gates failing to close is 10^{-4} and 25 gates failing to close is 10^{-4} , Figure 5.11 depicts the range for which the probability of flooding due to non-closure remains lower than the maximum allowable failure probability (1/52632 per year). The probabilities of the gates failing to close are somewhat based on the Oosterscheldekering design (2003). The probabilities of exceedance of the respective water levels at the x and y-axis are indicated by means of the dotted lines in Figure 5.11 for specific values of sea level rise (SLR). Hydra-NL is used to solve for the probability that the water level is greater than or equal to NAP + 6.10 m level at sea

and greater than or equal to $\text{NAP} + 2.57 \text{ m}$ at 21-1-VNK.21.03.003, both as a function of sea level rise. The black dots in Figure 5.11 indicate the probabilities of exceedance given a certain sea level rise. With the colourbar legend one is able to verify if the probability of flooding due to non-closure is lower than the maximum allowable failure probability ($1/52632$ per year) for the different values of sea level rise. It should be noted that for the calculations above, the change in discharge distribution over the year as a result of climate change has not been taken into account.

From Figure 5.11, it follows that for a sea level rise below 1 m the failure probability due to non-closure is below to allowable maximum ($1/52632$ per year) and hence the closure operation is still reliable considering the 2017 Water Act. For a sea level rise which rises above the 1 m mark, conforming to the closure reliability requirement as derived from the 2017 Water Act (see Appendix VI.1) becomes problematic, given the assumptions made here.

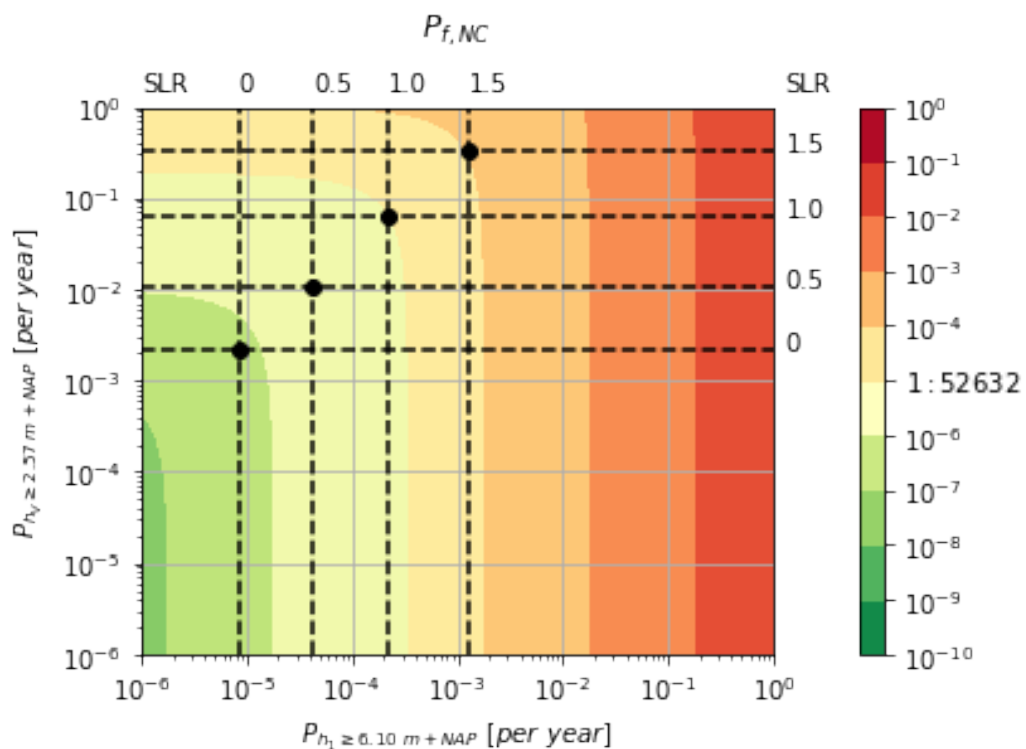
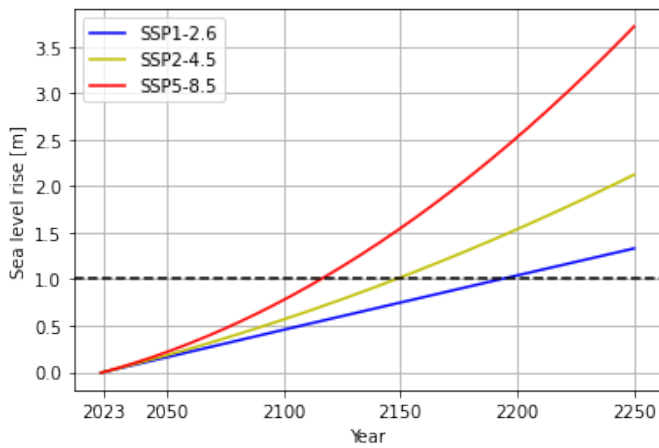


Figure 5.11: Probability of flooding due to non-closure

In conclusion, after a sea level rise of 1 m ⁹ the Delta Barrier can no longer fulfill all posed functional requirements and a decision must be made on how to handle this. From this point onwards, the closure operation is considered unreliable. Possible solutions are presented in Section 5.11, following a climate adaptive pathways approach. The exact point in time for which this occurs is rather unclear and depends on the climate scenario which actually occurs. Figure 5.12 gives an indication of when sea level rise exceeds the 1 m mark for the SSP1-2.6, SSP2-4.5 and SSP5-8.5 climate scenarios as argued by KNMI (2021). Finally Table 5.1 denotes the year and after how many years of service life (Δt) sea level rise exceeds 1 m per scenario.

⁹Sea level rise with respect to 2022



Scenario	Year	Δt [years]
SSP1-2.6	2194	144
SSP2-4.5	2149	99
SSP5-8.5	2117	67

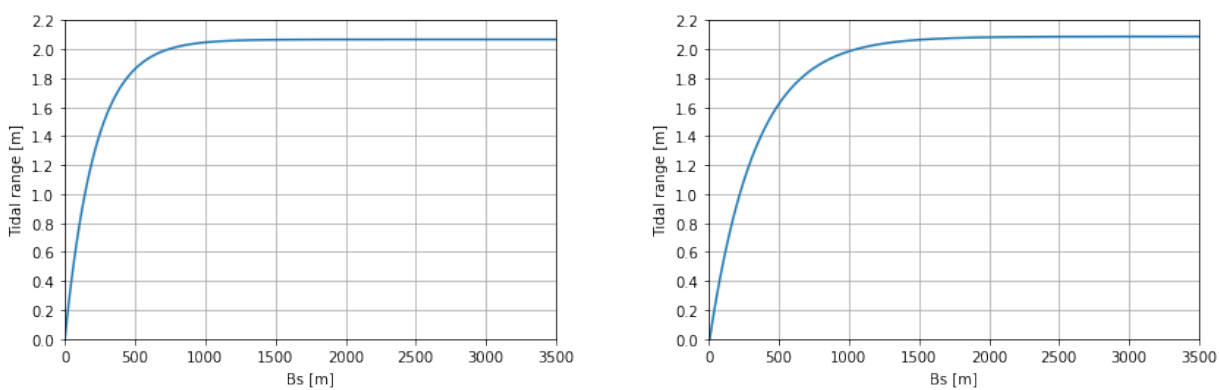
Table 5.1: Indicative year for which sea level exceeds 1 m per scenario

Figure 5.12: Indicative sea level rise per scenario for the Dutch coast

5.3 Effective Flow Area

In order to be able to preserve the passage of river discharge, tidal flow and hence the ecological system as much as possible, the Delta Barrier must have a sufficient total wet cross-section. Preserving of the functions as stated above are evaluated by means of calculating the tidal range, water level development and flow velocities through the barrier as a function of the effective flow area. The hydrodynamic model as described in Section 3.2.8 (see Appendix IX for full elaboration) is used for the evaluation. The parameters needed for evaluation are calculated by the model for daily circumstances, i.e. no storm surge and a Rhine discharge at Lobith of $2200 \text{ m}^3/\text{s}$ for climate scenarios SSP2-4.5 and SSP5-8.5 with reference years 2050, 2150 and 2250 under a mean tidal signal (see Section 3.2.5).

Figure 5.13a and Figure 5.13b depict the tidal range in the Tidal Lake as a function of the effective width (sill depth constant at NAP - 6 m) of the Delta Barrier for SSP2-4.5 and years 2050, 2150 respectively. As can be deduced from Figure 5.13, the effect of sea level rise on the tidal range is not significant. For this reason, only the model output of the tidal range for climate scenario SSP2-4.5 years 2050 and 2150 are presented.

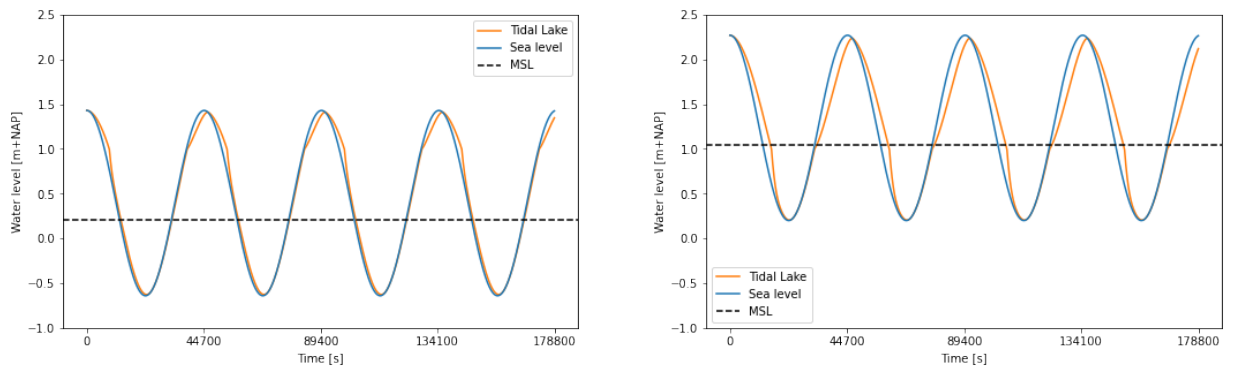


(a) Tidal range in Tidal Lake for SSP2-4.5, 2050 (0.21 m SLR) (b) Tidal range in Tidal Lake for SSP2-4.5, 2150 (1.05 m SLR)

Figure 5.13: Tidal range in the Tidal Lake under daily circumstances

For an effective cross-section of 6000 m^2 (defined below NAP), with a sill at NAP - 6 m and an effective width of 1000 m, Figure 5.14 presents the water level at the Tidal Lake under daily circumstances considering climate scenario SSP2-4.5 for the year 2050 and 2150 respectively as made using the hydrodynamic model described in Section 3.2.8. The mean tidal signal is used as opposed to the

astronomical tidal signal. It should be noted that the Haringvlietsluizen have an effective cross-section of 6000 m^2 as well (Ferguson, Blokland, & Kuiper, 1970).

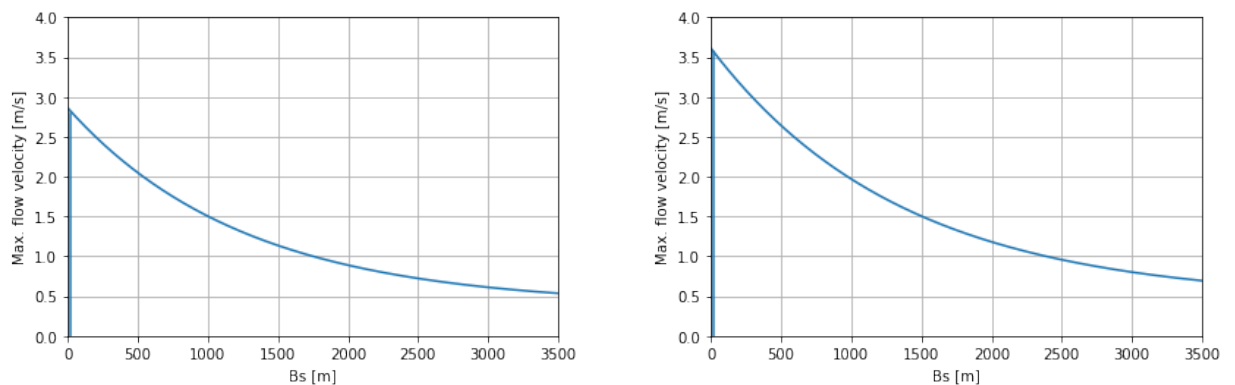


(a) Water level at Tidal Lake for SSP2-4.5, 2050 (0.21 m SLR)

(b) Water level at Tidal Lake for SSP2-4.5, 2150 (1.05 m SLR)

Figure 5.14: Water level at the Tidal Lake under daily circumstances

Figure 5.15 depicts the maximum flow velocity through the Delta Barrier as a function of the effective width (sill depth constant at NAP - 6 m) of the barrier for SSP2-4.5 for daily conditions and years 2050, 2150 respectively.



(a) Flow velocity through barrier for SSP2-4.5, 2050 (0.21 m SLR)

(b) Flow velocity through barrier for SSP2-4.5, 2150 (1.05 m SLR)

Figure 5.15: Flow velocity through the barrier under daily circumstances

Firstly, Figure 5.14b clearly shows additional sea level rise in 2150 with respect to 2050. However important, this phenomenon is not influenced by the effective cross-sectional area of the Delta Barrier. As for the impact of the Delta Barrier, Table 5.2 presents some main hydrodynamic characteristics of the Haringvliet mouth pre-barrier and post-barrier for the year 2050. The post-barrier mean tidal range and maximum flow velocity through the barrier are calculated using the before established hydrodynamic model (Section 3.2.8). Pre-barrier area change of tidal flats follow from van Horick (2023).

		Pre-barrier	Post-barrier	% change
Total surface	[km ²]	120*	120	0
Water surface at LW	[km ²]	106	106	≈ 0
Tidal flats (H1140)	[km ²]	14**	14	≈ 0
Effective cross-section	[m ²]	n.a.***	6000	n.a.
Mean tidal range	[m]	2.07	2.04	-1
Max. flow velocity	[m/s]	0.7	1.5	114

Table 5.2: Hydrodynamic characteristics Haringvliet mouth pre-barrier and post-barrier for 2050

* Tidal Lake area from Berke and Lavooij (2018c)

** Tidal flats area from Arcadis (2022)

*** Pre-barrier the Haringvliet mouth is an estuary

5.4 Morphological Impact of the Delta Barrier

An increase of the maximum flow velocity during daily circumstances at the Haringvliet mouth could induce significant morphological changes to the area considered. Either an increase or decrease of the total area of tidal flats could prove detrimental for the existing ecosystem in the Voordelta. van Horick (2023) has analysed the morphological changes in the Tidal Lake given a newly proposed Slijkgat channel design and incorporating the Delta Barrier.

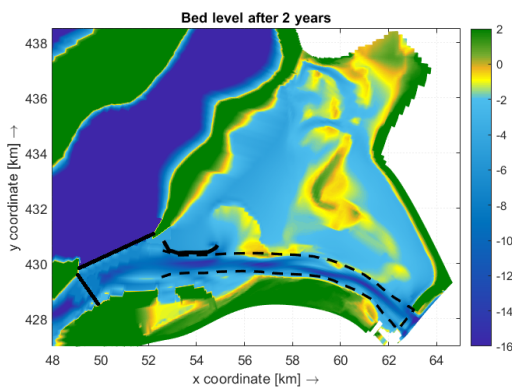


Figure 5.16: New Slijkgat channel design (van Horick, 2023)

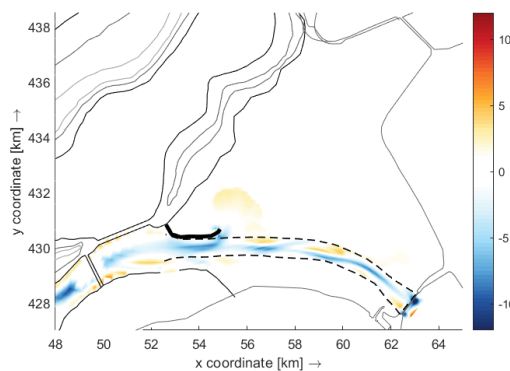


Figure 5.17: Bed level change after one average year (van Horick, 2023)

After simulation of an average year regarding river discharge, van Horick (2023) has found a net bed level change due to erosion (blue) adjacent to the bottom protection of the Delta Barrier of ca. 5 m (see Figure 5.17) one year after implementation of Delta21. Furthermore, van Horick (2023) concluded that the new Slijkgat channel design (see Figure 5.16) is rather stable with regard to the river banks and has a non-meandering character. Nonetheless, the new Slijkgat channel should be carefully assessed and dredged yearly to ensure enough draught for navigation (van Horick, 2023).

Although significant net erosion can be expected at the edges of the bottom protection near the barrier and sedimentation in the channel, the net total tidal flats area remains mostly unchanged (van Horick, 2023).

5.5 Impact on the Ecological System

As per one of the functions of both the integral Delta21 project and the Delta Barrier, the ecological system should be preserved and the impact of the Delta Barrier on the ecology must be minimized. Although rather difficult to quantify, whether the Delta Barrier has significantly minimized impact on ecology is verified by means of evaluating impact on the tidal flats and the tidal range in the Haringvliet estuary. Furthermore, the requirement that safe passage of aquatic creatures through the barrier should be enabled is treated.

5.5.1 Tidal Flats

The tidal flats in the Voordelta are important foraging and feeding grounds for birds, mostly waders and are frequently used by the common seal as resting grounds (Arcadis, 2022). Therefore, any reduction of the tidal flats directly influences the available habitat for said species. Here, the tidal flats (or intertidal area) are defined as the area between NAP - 1 m and NAP + 1 m (viz. habitat type H1140 (Arcadis, 2022)).

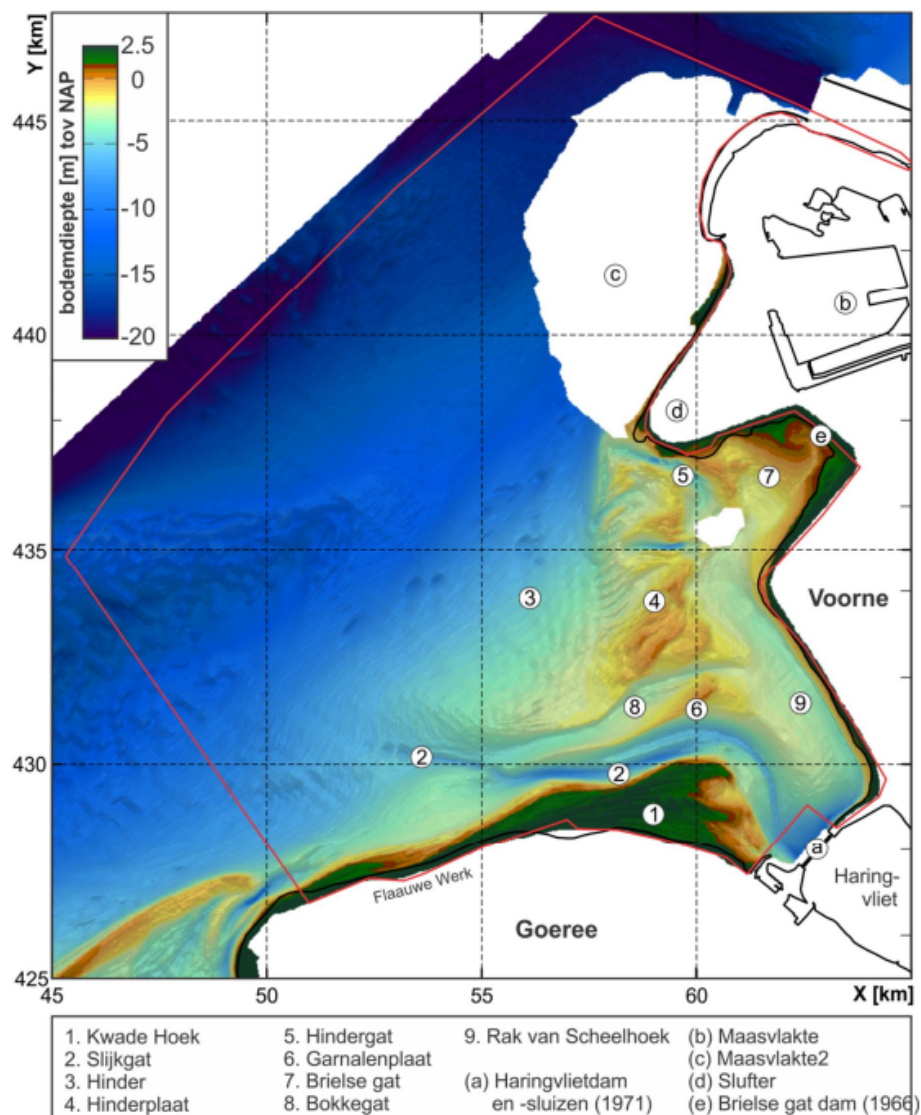


Figure 5.18: Overview of the plates in the Haringvliet mouth (Elias & van der Spek, 2014)

As can be seen from Table 5.2 and as has been concluded by van Horick (2023), it is expected that the tidal flats in the Haringvliet mouth remain mostly unchanged in area right after construction of

the Delta Barrier when considering daily circumstances.

Do note that until now, relative sea level rise has not been taken into account as said phenomenon is not a function of the Delta Barrier. Nonetheless, relative sea level rise will change the amount of available habitat for e.g. waders and common seals. For 1 m of relative sea level rise (approximately coinciding with SSP2-4.5 reference year 2150) the tidal flats should be defined as the area between NAP + 0 m and NAP + 2 m. Arcadis (2022) has tabulated the areas for different depth zones in the Haringvliet mouth.

	2050	2150	% change
Tidal flats [km ²]	14	10	-29

Table 5.3: Intertidal area in 2050 and 2150 after 1 m of relative sea level rise

Hence, in 2150, there is significant habitat loss regarding the intertidal area due to relative sea level rise only. In Table 5.3, morphological changes induced by sea level rise have not been taken into account. Considering climate scenario SSP2-4.5 in 2150 (1.05 m SLR w.r.t. 2018), mean low water will only reach a minimum of NAP + 0.2 m at the Tidal Lake. This results in permanent flooding of most parts of the plates in the Haringvliet mouth (e.g. the Hinderplaat and the Garnalenplaat) and strongly reduced foraging times at said plates. The loss of plates due to 1 m of sea level rise will only partly be compensated by the area between NAP + 1 m and NAP + 2 m mostly situated at the Slikken van Voorne and the Kwade Hoek.

5.5.2 Tidal Range

A changing tidal range in the Tidal Lake as a consequence of the interventions in the Haringvliet mouth indicate a changing tidal prism. As the Haringvliet mouth shifts from an open estuary towards a tidal lake, a decreasing tidal range and hence tidal prism results in less sea water exchange between the Haringvliet mouth and the North Sea. A reduced salt water exchange affects water quality parameters in the Haringvliet mouth (now Tidal Lake) and could significantly alter the ecological system. Furthermore, less dynamic conditions at the Tidal Lake could result in changes in the composition of the microphytobenthos community in the Haringvliet mouth (Nienhuis & Smaal, 1994).

As for the chosen effective cross-section of Delta Barrier, the mean tidal range barely changes ca. -1%. Furthermore, Figure 5.14a and Figure 5.14b indicate that the Delta Barrier enables sufficient salt water exchange between the newly formed Tidal Lake and the North Sea.

5.5.3 Passage of Aquatic Creatures

As stated by functional requirement FR-4.1, safe passage of aquatic creatures through the Delta Barrier should be enabled. Such aquatic creatures are e.g. (migrating) fish, seals and harbour porpoise. Note that, although maximum tidal flow velocities increase twofold (see Section 5.3), flow velocities under daily conditions (average discharge at Lobith of 2200 m³/s) still conform to the substantiation of FR-4.1 in Appendix V. During closure of the gates once requested, the function to preserve safe passage of aquatic creatures can temporarily not be fulfilled until re-opening.

The construction of the Delta Barrier could deter small migrating fish from entering the Tidal Lake (or leaving for that matter). Furthermore, a possible permanent closure of the Delta Barrier in the future due to sea level rise (see Section 5.11) would cut off the Tidal Lake from the North Sea completely. For both these reasons, constructing a fish migration river might be highly beneficial for the overall ecosystem. van Eeden (2021) has readily proposed a possible location for such a river.



Figure 5.19: Possible location for a fish migration river (modified from van Eeden (2021))

While a fish migration river is mostly designed for fish, it might be possible to integrate the function for passage of seals in the future. Although the construction of such a river implies some challenging structures at the interface between sea and land, a fish (and possibly seal) migration river could ensure the safe passage of aquatic creatures in the far future irrespective of the fate of the Delta Barrier.

5.6 Retaining Height

In order to ensure that the Delta Barrier is able to fulfill the function of retaining water and does not fail regarding the failure mechanism of overtopping (see Figure 5.20), the water retaining body as a whole should have sufficient retaining height.



Figure 5.20: Failure mechanism of overtopping (Onwuachu, 2021)

As for the top retaining element of the Delta Barrier, a concrete beam is chosen for the following reasons:

- Height adaptability
- Lower gate height required
- Lighter driving mechanisms required

The bottom of the top beam is situated at NAP + 3 m as such that before a requested closure (see Section 5.1) the tidal flow through the barrier is virtually never restricted by the height of the effective opening.

The retaining height, i.e. the highest part of the concrete top beam, is determined by means of Equation (5.5) as proposed in the 'Leidraad Kunstwerken' (2003) and used by Hydra-NL.

$$h_{kr} = -\frac{1}{3}\gamma_{\beta}\gamma_{\eta}H_{S;d} \ln \left(\frac{q}{0.13\sqrt{gH_{S;d}^3}} \right) \quad (5.5)$$

where:	h_{kr}	[m]	=	overtopping height
	γ_{β}	[-]	=	influence factor taking into account oblique waves
	γ_{η}	[-]	=	reduction factor for nose structure
	$H_{S;d}$	[m]	=	design value significant wave height
	q	[m ³ /s/m]	=	overtopping discharge
	g	[m/s ²]	=	gravitational constant

The WOWK (2018) states that considering a storm surge barrier a maximum overtopping discharge (q) of 1 m³/s/m is generally acceptable. This is a general rule of thumb, based on both the strength of the bottom protection and the available storage capacity. With greater specific overtopping discharges, dynamic aspects as a result of air pockets under the overflowing jet may play a role (Rijkswaterstaat, 2018).

With $\gamma_{\beta} = 1$ for roughly normally incident waves, $\gamma_{\eta} = 1$ for no nose structure and a maximum overtopping discharge of 1 m³/s/m, the overtopping height can be calculated. Note that the overtopping height ought to be calculated using the adjusted design parameters (see Section 3.3 and Appendix X).

From the overtopping height, one is able to calculate the retaining height as follows:

$$h_r = h_{1;d} + h_{kr} \quad (5.6)$$

where: h_r [m NAP] = the retaining height
 $h_{1;d}$ [m NAP] = the design water level at sea

The retaining height should conform to the water retention function FR-1.2 as presented in Section 3.1.1. With the final design parameters, the retaining height (h_r) is calculated for climate scenario SSP2-4.5 and SSP5-8.5, reference period 2250 and a return period of 83333 years.

$h_{1;d}$ [m NAP]	$H_{S;d}$ [m]	h_r [m NAP]
7.83	3.17	8.71

Table 5.4: Retaining height for SSP2-4.5

$h_{1;d}$ [m NAP]	$H_{S;d}$ [m]	h_r [m NAP]
9.52	3.34	10.50

Table 5.5: Retaining height for SSP5-8.5

Regarding climate adaptability, one should note that heightening the concrete top beams is very much possible, given that a new structural design and adjustments to the top beams allows for it. Nonetheless, as the additional required height of the concrete top beam for scenario SSP5-8.5 w.r.t. SSP2-4.5 would result in only a marginal percentage of added costs relative to the whole Delta Barrier let alone the entire Delta21 project, it is chosen to construct the concrete top beam with the crest at a height of $NAP + 10.50\text{ m}$ according to scenario SSP5-8.5.

It should furthermore be noted that an additional heightening of the concrete top beam in the future, if it were chosen to initially construct taking into account climate scenario SSP2-4.5, would be significantly more expensive. These additional expenses are mostly due to additional engineering, project management, mobilisation of equipment and inflation.

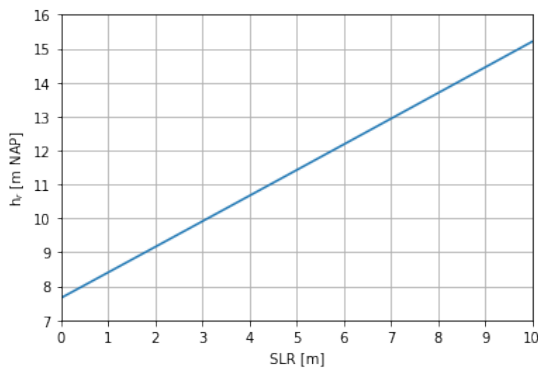


Figure 5.21: Retaining height as a function of sea level rise

Figure 5.21 depicts the retaining height as a function of sea level rise. Figure 5.21 follows from linear inter- and extrapolation of the design water levels and design values for the significant wave heights for SSP2-4.5 and SS5-8.5 corresponding to a sea level rise of 1.40 m and 3.81 m with respect to 2018, respectively.

5.7 Passage for Shipping

As posed by functional requirement FR-2 in Section 3.1.1, the passage of ships from and to the Haringvliet should be preserved. For the design of the Delta Barrier it is chosen to not integrate the function of ship passage into the gated barrier design, in other words a separate lock should be designed as the Delta Barrier itself is not designed for the passage of ships. The following considerations underlie this choice:

- **Vertical clearance is in conflict with climate adaptability retaining height**
Regarding the vertical clearance for all relevant ships, a top beam as the upper retaining part of the barrier - while climate robust considering the retaining height - brings great restrictions. The bottom level of the top beam would restrict the vertical clearance and the higher the beam the higher the supporting parts of the piers would need to be. Furthermore, with sea level rise this vertical clearance would become ever so smaller. A higher bottom level of the top beam also requires a higher gate for proper closure. For these reasons, if one wanted a vertical lift gate barrier also assigned for navigation purposes, it would seem preferable to have the gates as the sole water-retaining part of the structure once closed. However, steel gates do not lend themselves as well to heightening as a concrete top beam. Furthermore, using only gates as the sole retaining part requires rather large gates.
- **Vertical clearance for ships is costly**
The governing ship, CEMT-class Va (see Appendix V), has a height of 7.1 m from the water level when empty for which Koedijk, van der Sluijs, and Steijn (2017) prescribes a free vertical clearance of 9.1 m during MHWS. An assumed MHWS of NAP + 1.67 m would require a minimum level of NAP + 10.77 m for vertical clearance. Hence, if one wanted a vertical lift gate barrier also assigned for navigation purposes, a gate should be hoisted till the bottom of the gate is at NAP + 10.77 m which requires rather high lift shafts as part of the piers.
- **Draught for shipping is costly**
Koedijk et al. (2017) prescribes a required draught of 4.9 m for a CEMT-class Va vessel, which implies a freeboard of 0.9 m. The governing ship, OD1 Maarten-Jacob (see Appendix V) with a draught of 5 m when fully loaded, would therefore require a draught of at least 5.9 m at all times. An assumed LAT of NAP - 1.22 m, would require a maximum top level of NAP - 7.12 m of the lowest member of the storm surge barrier. The current channel design by van Horick (2023) has a bottom level of NAP - 7.0 m which leads to a complex sill structure.
- **More complex operations**
Bringing yet another function into the operational scheme of the Delta Barrier results in more complex operational systems. This greater complexity could result in a lower closure reliability.
- **Haringvliet estuary not heavily trafficked**
The Haringvliet estuary is not heavily trafficked as only a handful of relatively small shipping vessels and recreational vessels sail the area. Furthermore, the Goereese sluis adjacent to the Haringvlietsluizen, having a sill depth of only NAP - 5 m, does not allow for large vessels to pass (Waterkaart.net, 2023).

The reasons above pose enough means to choose for a separate lock complex to fulfill the function of ship passage. While important for functionality of the barrier as a whole, the design of a lock complex is not within the scope of this thesis. As for the location of the lock complex, a sheltered location would be best suitable. Furthermore, it might be preferable to have the lock complex far removed from the Spillway and from the Delta Barrier in order to keep turbulent flow as far away from vessels as possible. Hence a location south of the Delta Barrier, sheltered by means of the southern dunes of Goeree-Overflakkee (and possibly jetties) is proposed. Figure 5.32 presents the layout of the Delta Barrier including the location of said lock complex.

5.8 Passage for Road-traffic

In order to fulfill the function to enable the passage of road-traffic over the Delta Barrier, concrete bridge girders are incorporated into the barrier design. As a result, a connection is realised between the Island of Goeree-Overflakkee and the Energy Storage Lake by means of the adjacent dike sections, abutments and bridge girders. In general, the design of the concrete bridge girders is outside the scope of this thesis, however assumed imposed loads as a result of the girders are taken into account.

Regarding the required functionality, the bridge girder design as for the Oosterscheldekering (1989) is taken as a guide (Figure 5.22), which not only fulfills the function for the passage of road-traffic but also includes space for technical installations and serves as a maintenance road both during and after construction.

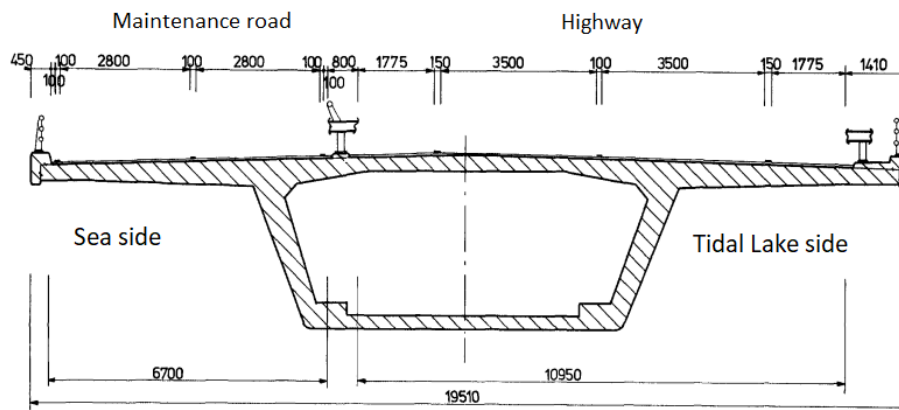


Figure 5.22: Bridge girders (Visser, 1986b)

As depicted in Figure 5.22, the bridge girders consist of a maintenance road on the sea side and a highway consisting of two lanes, one for each direction. The maintenance road can be used by cyclists and pedestrians. Furthermore, two emergency lanes of 1.775 m are included in the design at both sides of the highway in order to ensure the safety of the road users during strong wind gusts.

The height of the top of the bridge deck should be as such that users of the bridge girders, mostly vehicles but also cyclists and pedestrians, can cross the barrier safely most of the time. Furthermore, it is to be preferred that a maintenance crew is able to reach the piers if e.g. the closure of a or more gates fail. In general, two aspects may affect the safe passage over the bridge girders: overtopping itself and overtopping spray. Under still conditions or light onshore winds, overtopping spray will seldom contribute significantly to overtopping volumes, but might cause local hazards. Spray on coastal highways (particularly when intermittent) can cause sudden loss of visibility, leading drivers to veer suddenly (Allsop, Bruce, Pullen, & van der Meer, 2008).

A maximum specific overtopping discharge of 0.01 m³/s is allowed according to EurOtop (2018) for vehicles driving at low speeds. Additionally, EurOtop (2018) states that well trained and protected staff could also endure a specific overtopping discharge of 0.01 m³/s. Constructing the bridge deck well above the concrete top beam would ensure that the piers of the Delta Barrier are safely accessible even during the governing storm regarding structural integrity of the barrier. Furthermore, given enough horizontal clearance from the top beam, wave impact loads on the bridge girders are less.

To this day, there is little guidance on the effects of overtopping spray (Allsop et al., 2008). Nonetheless, the occurrence of spray is assessed in a qualitative sense by means of distinguishing between non-impulsive and impulsive waves on the near-vertical concrete top beam. For non-impulsive waves, waves run over the crest in (relatively) coherent water mass (i.e. "green water") (EurOtop, 2018). In contrast, for impulsive waves, spray overtopping tends to occur when waves break onto the seaward

face of the structure, producing non-continuous overtopping, and/or significant volumes of spray (i.e. "white water") (EurOtop, 2018). EurOtop (2018) states that if Equation (5.7a) holds, waves can be considered non-impulsive and if Equation (5.7b) holds, waves can be considered impulsive.

$$\frac{h^2}{H_{m0}L_{m-1,0}} > 0.23 \quad (5.7a)$$

$$\frac{h^2}{H_{m0}L_{m-1,0}} \leq 0.23 \quad (5.7b)$$

where: h [m] = water depth in front of toe of structure
 H_{m0} [m] = significant wave height, from wave spectrum ($H_{m0} \approx H_s$)
 $L_{m-1,0}$ [m] = spectral wave length in deep water

Note that for the governing parameters regarding overtopping of the concrete top beam, with $h = 16.52$ m and $H_{m0} = 3.34$ m for 2250 SSP5-8.5 and a return period of 83333 years, the waves can be considered non-impulsive and no overtopping spray is expected. Impulsive conditions are only to be expected for relatively shallow water or relatively high waves. For shallow water, overtopping spray is not expected to reach the bridge deck if constructed well above the concrete top beam. Furthermore, greater wave heights would occur for greater return periods which is acceptable for a serviceability limit state regarding the passage of road-traffic.

From the arguments as presented above, it chosen to construct the bridge girders with the top of the deck at NAP + 13.5 m and a horizontal clearance from the concrete top beams of 1.5 m as depicted in Figure 5.23. This configuration ensures that the piers are always safely accessible from the maintenance road for return period less than 100000 years in 2250 assuming climate-scenario SSP5-8.5. Furthermore, it allows for heightening of the concrete top beam in the far future if necessary.

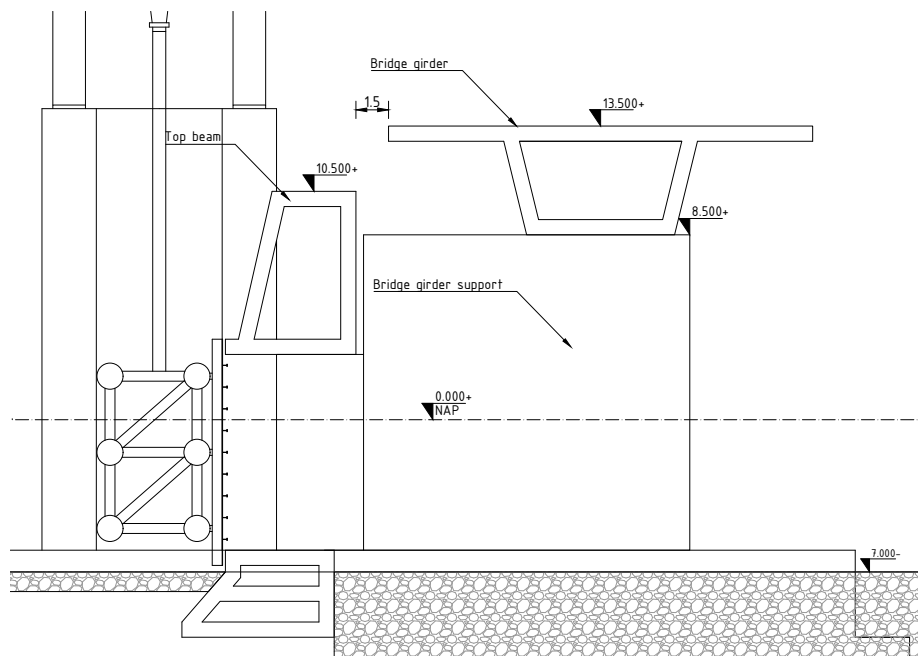


Figure 5.23: Bridge girder configuration

It should be noted that, if storm conditions arise, traffic should be forced to drive at low speeds by means of e.g. matrix boards, traffic lights and megaphones connected to the piers. Furthermore, traffic should be stopped completely before either overtopping itself or overtopping spray can cause harm to traffic.

5.9 Tidal Turbines

In this preliminary design stage, the incorporation of tidal turbines into the design is considered. The sustainably generated electricity from power turbines could serve multiple purposes:

- **Functioning of the barrier**

Firstly, the daily generated electricity could serve as the primary power source for the so called "slumber-state" of the Delta Barrier. During this slumber-state, the storm surge barrier is open and, besides other trivial processes, power is merely used for the system interpreting the incoming data on water level and discharge. For now, it is assumed that said slumber-state of the Delta Barrier requires ca. 300 kW, deduced from data presented by Visser (2003). Given a requested closure and a closure operation, it is assumed that the barrier would require ca. 3700 kW.

- **Over-capacity**

Any over-capacity (if any) could be used for a variety of other purposes, such as (partly) supplying the Spillway with electricity or supplying other local buildings and infrastructure.

The power production of a number of horizontal tidal flow turbine can be calculated using Equation (5.8) (Guijt, 2018).

$$P_t = \frac{1}{2} \cdot C_p \cdot B \cdot \rho_w \cdot n \cdot A_r \cdot u_r^3 \quad (5.8)$$

where:	P_t	[W]	=	power production of the turbines
	C_p	[-]	=	efficiency parameter
	B	[-]	=	blockage parameter
	ρ_w	[kg/m ³]	=	density of sea water = 1025
	n	[-]	=	number of turbines
	A_r	[m ²]	=	swept area of the rotor blades
	u_r	[m/s]	=	tidal flow velocity

The efficiency parameter C_p , according to Bet'z law, is maximised to ca. 0.59 due to a loss of kinetic energy after the turbines (Guijt, 2018). The blockage parameter is defined using Equation (5.9) as proposed by Garrett and Cummins (2007).

$$B = \left(1 - \frac{(n \cdot A_r)}{A_c} \right)^{-2} \quad (5.9)$$

in which: A_c [m²] = total cross-sectional flow area

Furthermore, tidal turbines should not be placed closer together than two times the rotor diameter and one diameter from an object (centre-to-centre) and should always be completely submerged with a clearance from the bottom of at least 1 m in order to ensure functionality. Due to the limited depth of the bottom behind the Delta Barrier, only rather small turbines can be used. Taking into account the requirements as stated above, the average yield of two Tidal turbine configurations between two piers are presented in Table 5.6. The total power production is calculated using the flow velocity from the hydrodynamic model (see Appendix IX), with a discharge at Lobith of 2200 m³/s and MSL = NAP + 0.22 m corresponding with the year 2050 at completion assuming climate scenario SSP2-4.5.

n	D [m]	P_t [kW]
4	5	13.83
5	4	11.02

Table 5.6: Total power production of two Tidal turbine configurations

From Table 5.6, it shows that the configuration with 4 tidal turbines having a rotor diameter (D) of 5 m yields the best power production of the two configurations. Figure 5.24 depicts said configuration.

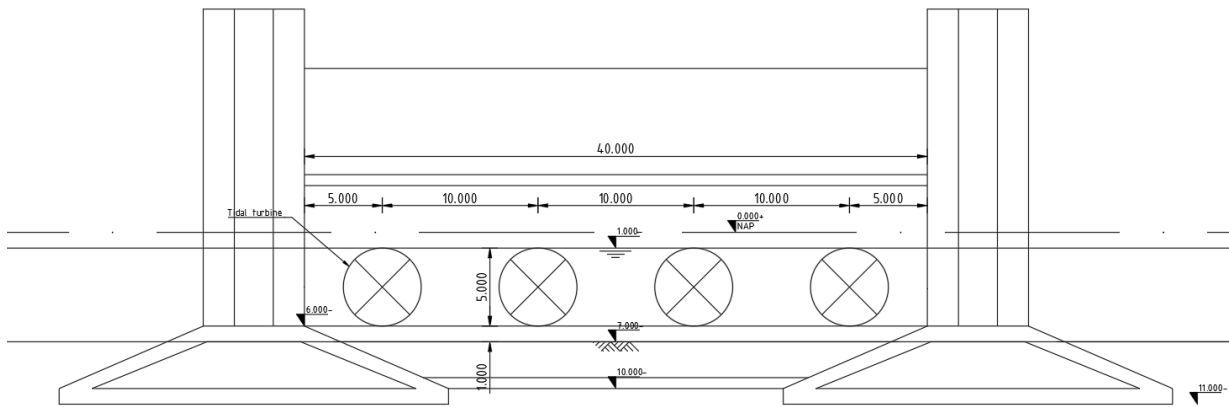


Figure 5.24: Tidal turbine configuration: 4 x 5 m

The yields for the 4 x 5 m configurations is solved with the hydrodynamic model for three tidal cycles, from which the average is computed. As the power production of a tidal turbine varies in time as a non-linear function of the tidal flow velocity, the yield is solved for every time step (a second). Figure 5.25 and Figure 5.26 present the tidal flow velocity through the Delta Barrier and the corresponding power production of the 4 x 5 m configuration, respectively.

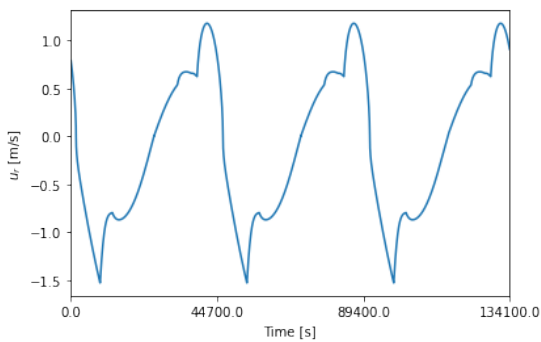


Figure 5.25: Tidal flow through the barrier

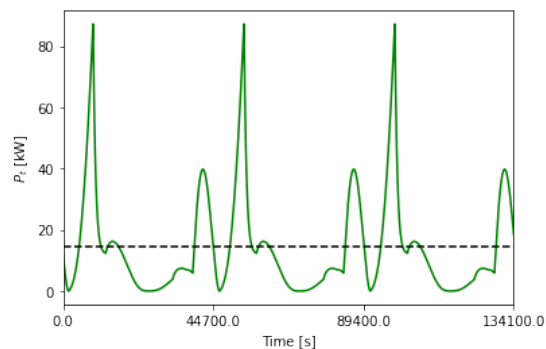


Figure 5.26: Power production of the 4 x 5 m configuration

Comparing the average yield of the configuration as presented in Figure 5.24 to the yield of the 5 Tocardo tidal turbines behind one of the openings of the Oosterscheldekering result in significant differences, in favor of the Tocardo turbines. Namely, the 5 Tocardo turbines produce ca. 1250 kW (Omroep Zeeland, 2022) to the estimated 14 kW of the Delta Barrier configuration. Although filling all 25 openings of the Delta Barrier could be enough to provide power for the slumber state of the barrier, the relatively low yield of the tidal turbines in this specific case plead for the case that generating sustainable electricity using the tide behind the barrier is rather unfeasible.

Two aspects can be identified which make tidal turbines such an inefficient method to generate electricity with tidal flow for this specific project: the relatively low water depth behind the barrier restricts the rotor size and flow velocities through the barrier are relatively low. These aspects together prove that applying tidal flow turbines is unfeasible in this case and will hence not be considered in the further design.

5.10 Driving Mechanisms

In general, two types of driving mechanisms are suitable for raising and lowering the steel gates of the Delta Barrier: using either hydraulic cylinders or a rack and pinion (or gear rack) system. Whereas both systems have their pros and cons, the system using hydraulic cylinders is chosen for this preliminary design. It is expected that the hydraulic cylinders are less expensive and have a lower failure probability than the rack and pinion system (Visser, 2003). Additionally, hydraulic cylinders are considered to be more aesthetically pleasing. A schematic overview of the hydraulic system is presented in Figure 5.27.

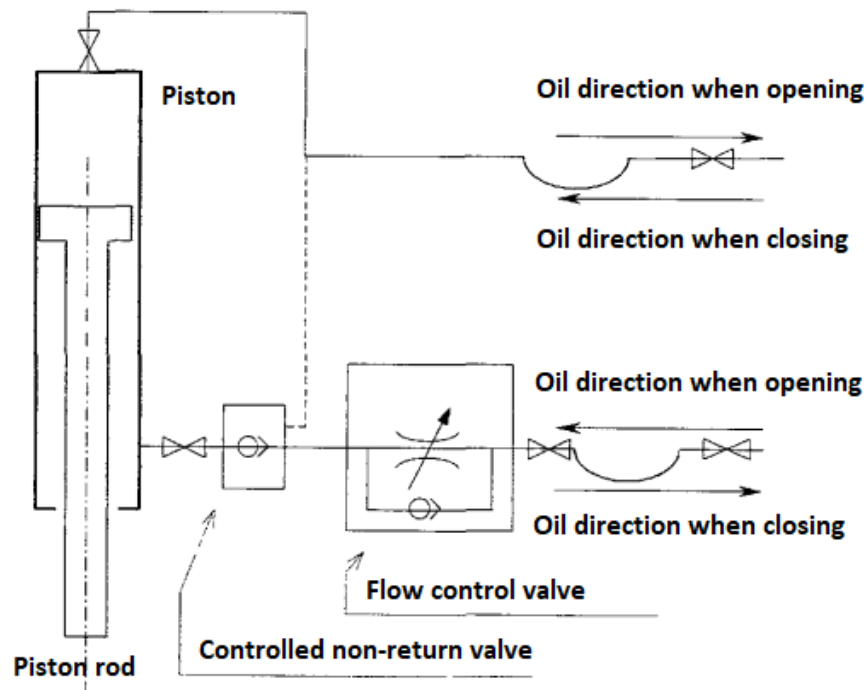


Figure 5.27: Schematic overview of the hydraulic system (modified from Visser (2003))

Finally, a brief description of the system is presented. This description is given by means of the required functionality of the driving mechanisms.

- **Keep the gate in the raised position**

There are no actions when the gate is raised. Inside the cylinder is the piston, which is integrated with the piston rod, to which the sliding end is attached. In the raised position, the piston is situated high up in the cylinder and the weight of the gate hangs on the oil column below the piston. The pressure in that oil column is mainly determined by the weight of the gate. For the Oosterscheldekering, the pressure in the oil column is now ca. 90 bar (Visser, 2003). The (controlled) non-return valve at the bottom of the cylinder prevents the oil from flowing out of the cylinder.

- **Closing the gate**

When closing, the hydraulic aggregate pumps oil into the cylinder above the piston. The pressure with which that oil is supplied opens the controlled non-return valve, so that oil can flow out under the piston. The speed at which this happens is controlled by a flow control valve. The setting of this flow control valve determines the closing speed of the relevant gate end. The closing speed is expected to be ca. 3 mm/sec which means that closing a gate would take around an hour (Visser, 2003).

- **Keep the closed gate pressed against the bottom**

When the gate has reached its stop at the bottom of the pier, the pressure at the top of the cylinder via the piston and the piston rod keeps the gate pressed against the bottom. Pressure is no longer required under the piston and the pressure generated by the tensioning pump. For the Oosterscheldekering, ca. 3 bar is generated here (Visser, 2003).

- **Opening the gate**

When the gate is opened, the pressure above the piston is released and pressurized oil is supplied below the piston. Through the piston, the oil pressure lifts the gate. The required pressure below the piston is mainly determined by the cylinder dimensions, the weight of the gate and the friction that occurs, while the pressure above the piston is determined by the flow resistance of the returning oil (Visser, 2003).

5.11 Climate Adaptive Pathways

In Section 5.2, it has been established that after a sea level rise of ca. 1 m, the closure operation of the Delta Barrier is considered unreliable. From this point onwards, the storm surge barrier can no longer conform to the functional requirement regarding FR-1.3 closure reliability (see Appendix V). Hence, a choice must be made on how to adapt to said sea level rise. In general, this choice lies with policy makers and is not specific to the Delta Barrier alone. Figure 5.28 presents three possible pathways in line with the overall adaptation strategies as proposed by Haasnoot and Diermanse (2003). It should be noted that the Delta21 project itself could be characterised as a combination of the "protected open" and "seaward" strategies.

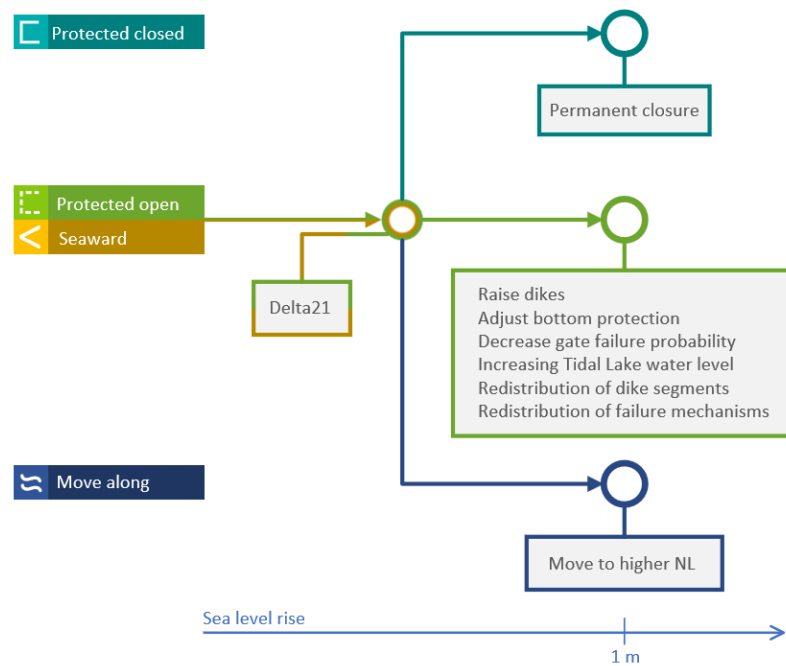


Figure 5.28: Climate adaptive pathways Delta Barrier

The three adaptive pathways as depicted in Figure 5.28 give possible, non-exhaustive, solutions to the closure reliability problem of the Delta Barrier after ca. 1 m of sea level rise. Though depicted as three separate branches in Figure 5.28, a combination of either three pathways and hence overall strategies is very much possible. Furthermore, a solution placed within an integral flood protection strategy for the entire South West Netherlands might be preferred. The Delta21 project enables the adaptation of any climate adaptive pathway where especially the "protected closed" and "protected open" strategies seem in line with the ideology of Delta21. The focus here is mostly on the "protected open" strategy as said strategy implies adjustments to the Delta Barrier.

Protected closed

As part of the general "protected closed" strategy, it is possible to permanently close the Delta Barrier. By permanently closing the barrier, the reliability of the closure operation is no longer of any importance and hence the flood protection function can be fulfilled for a sea level rise up to 3.81 m¹⁰ instead of ca. 1 m (see Section 5.2). However, by permanently closing the storm surge barrier, the tide is no longer able to propagate into the Tidal Lake resulting in severe ecological impact. Furthermore, the Energy Storage Lake should now continuously pump river discharge into the sea and can as such not be used to store energy in water with the Pumped Hydro Storage concept.

¹⁰With respect to 2018

Protected open

As part of the general "protected open" strategy, many adjustments can be made to the Delta Barrier or the overall Delta21 flood protection system. The 'protected open' strategy is characterised by enabling full functionality of the Delta Barrier, though relatively costly.

- Raise dikes

Raising and/or strengthening the dikes in the hinterland effectively increases the storage capacity of the South West Delta. An increase of the storage capacity is beneficial to the reliability of the closure operation, mainly for the scenario where all gates fail to close. Furthermore, the closure regime of the Delta Barrier can be adjusted accordingly and the closure frequency can be lowered.

- Adjust bottom protection

Adjusting, i.e. strengthening the bottom protection increases the resistance of the bottom protection to large flow velocities. As a result, adjusting the bottom protection is beneficial to the reliability of the closure operation, mainly for the scenario where one or two gates fail to close. Note that after increasing the nominal diameter of the top layer of the bottom protection, the filter layout should most probably be adjusted as well in order for the filter to remain sand-tight and functional.

- Decrease gate failure probability

However challenging, decreasing the probability that the closure of a gate or multiple gates fail increases the reliability of the closure operation. Decreasing the probability that the closure of one, two and all 25 gates fail to closure with a factor of 10, results in the closure procedure to be reliable until a sea level rise of ca. 1.6 m (*ceteris paribus*). It should however be noted that decreasing the probability that the closure of gates fail by a factor 10 seems highly unfeasible.

- Increasing Tidal Lake water level

Increasing the Tidal Lake water level once either one or two gates fail to close reduces the water head over the structure given the non-closure event. Hence, a greater water level at sea is needed to result in the critical flow velocity at which the top layer of the bottom protection starts to erode. A downside of increasing the Tidal Lake water level during a non-closure event, though temporarily, is a lower discharge capacity from the Rhine-Meuse system through the Tidal Lake towards the Energy Storage Lake.

- Redistribution of dike segments

Where the possible solutions as presented above concern mostly changing characteristics of the Delta Barrier or the Delta21 flood protection system, a complete redistribution of failure probabilities over the Delta21 dike segments could increase the maximum failure probability regarding non-closure. It should be noted however that e.g. increasing the maximum failure probability of dike segment DI (see Appendix VI.2), which includes the Delta Barrier, in turn decreases the maximum failure probability of another Delta21 dike segment. There is also a possibility to assign an even greater maximum failure probability to the storm surge barrier and less to the adjacent dike sections.

- Redistribution of failure mechanisms

Another way to increase the maximum failure probability regarding non-closure is to redistribute the failure probabilities over the different failure mechanisms. Though again, it should be noted that an increase of the maximum failure probability regarding non-closure results in less failure probability to be redistributed over the other failure mechanisms (see Appendix VI.2).

Move along

A last and most controversial strategy comes with the general "move along" strategy. This strategy encompasses moving along with sea level rise, adjusting land use to give the water more space and stimulating people in the lower lying areas of the Netherlands to move to higher areas. This strategy comes with severe economical and societal impact.

5.12 Layout & Main Dimensions

This section discusses the layout of the Delta Barrier and main dimensions following from the functional requirements. After determining the effective flow area in Chapter Section 5.3, the retaining height of the barrier in Section 5.6 and ways to enable passage for shipping and road-traffic in Section 5.7 and Section 5.8 respectively, the layout and main dimensions of the Delta Barrier are largely determined.

Lastly, the height of the gates and vertical lift shafts which hold the gates have to be determined. As the height to be closed by the steel gates is 9 m (sill at NAP - 6 m at top beam at NAP + 3 m) the gates should at least be 9 meters in height. In order to ensure a tight closure an overlap of two times 0.7 m is applied to the gate. The overlap is necessary to compensate for height differences between the piers and dimensional deviations of the sill and top beam. Hence the gates have a total height of 10.4 m.

Finally, in order to ensure the accessibility of the gates during inspection or maintenance, it should be enabled for the gates to be hoisted till at least NAP + 3 m. Hence, the lift shaft should at the least reach till NAP + 13.4 m. Applying an additional 0.9 m for the guiding systems for the gates and some leeway, results in the top of the lift shafts at NAP + 14.3 m.

Assuming a gate length of 40 meters, Figure 5.29 and Figure 5.30 presents the main dimensions between two piers from a top and front view, respectively.

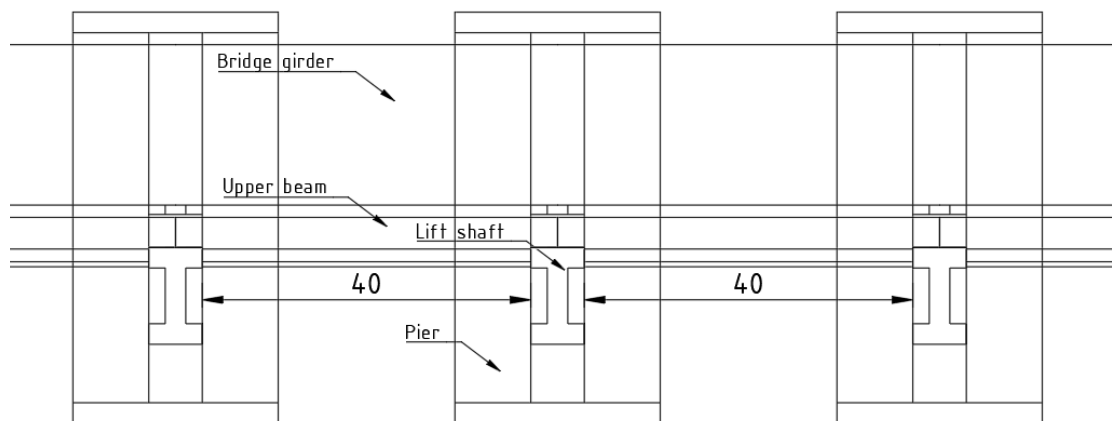


Figure 5.29: Top view. Main dimensions between two piers

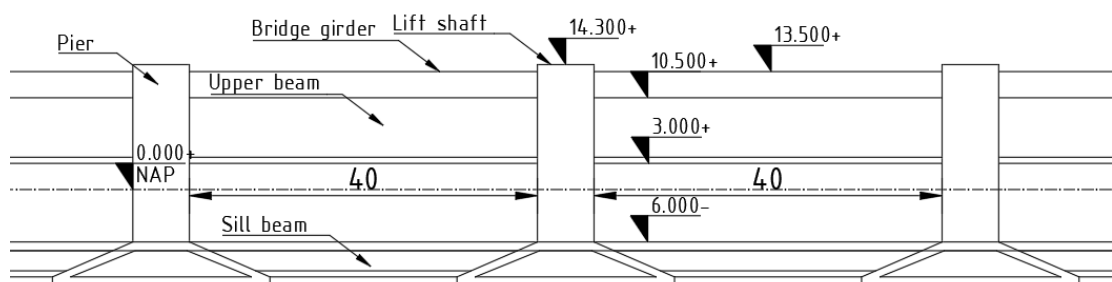


Figure 5.30: Front view. Main dimensions between two piers

With a gate length of 40 meters, a total of 25 gates are needed to arise at the required 1000 m of effective flow width as determined in Section 5.3.

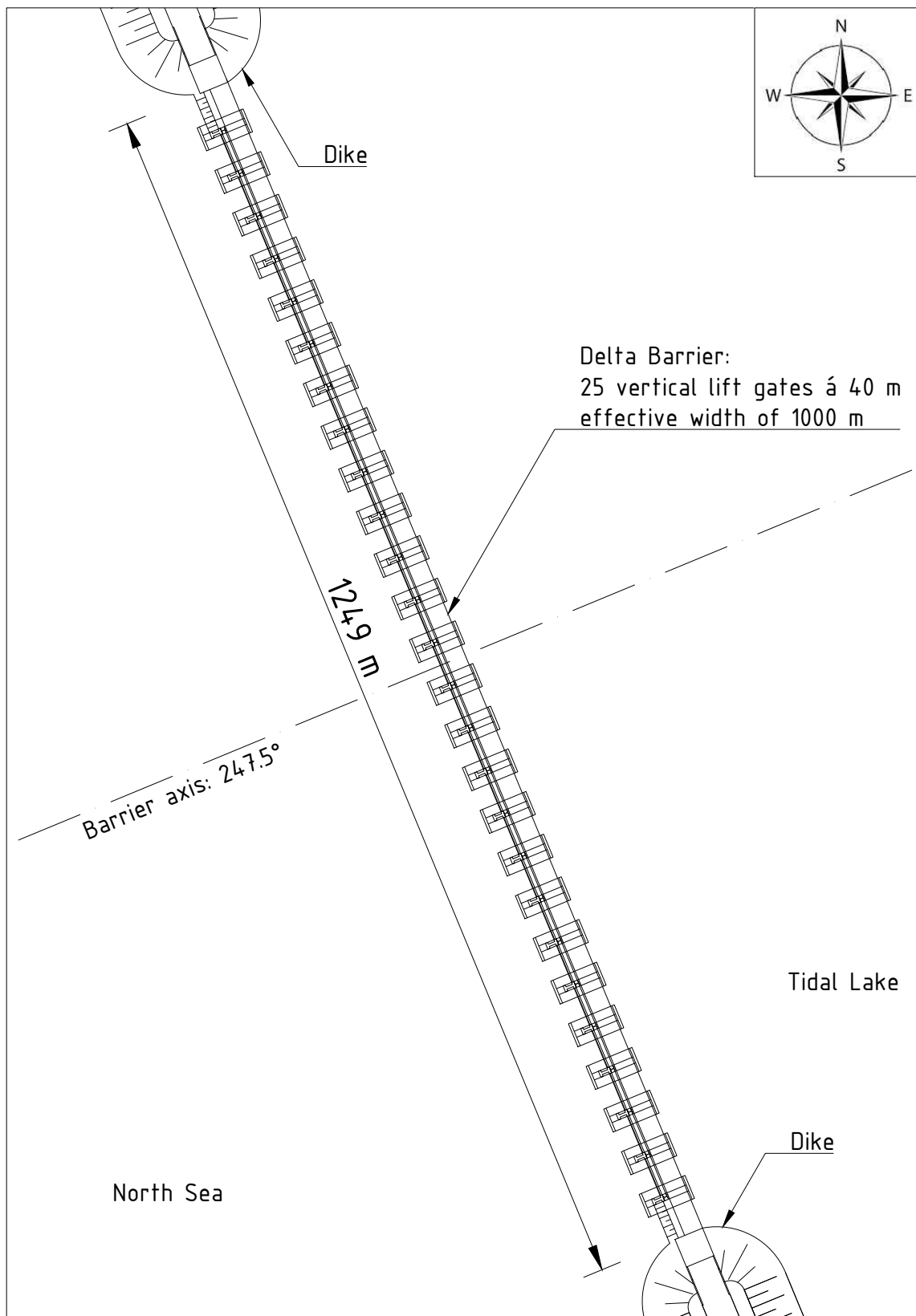


Figure 5.31: Top view. Total barrier consisting of 25 gates, each 40 meters

Finally, Figure 5.32 presents the layout of the Delta Barrier in which all implementations of the relevant functions of the barrier are indicated.

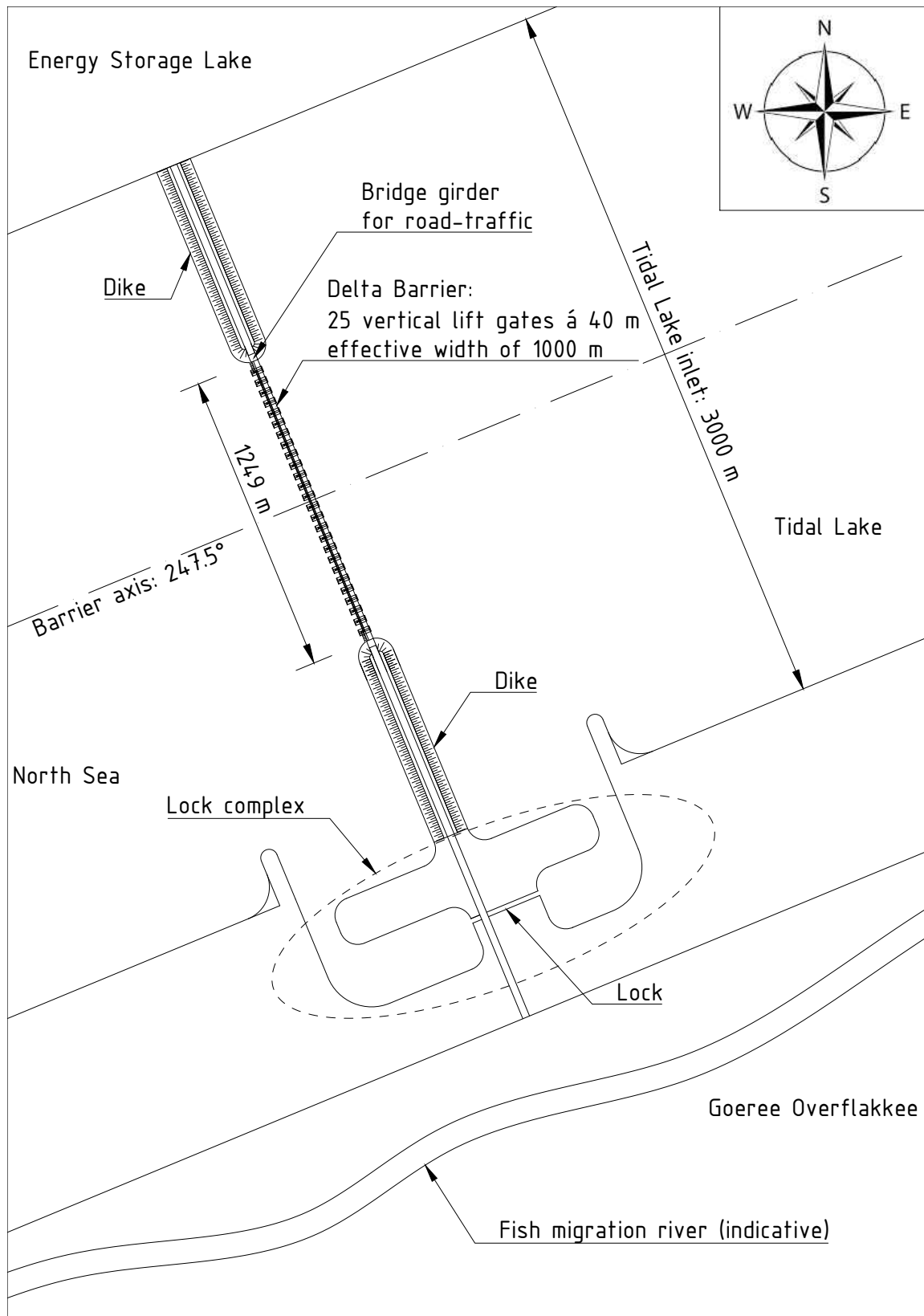


Figure 5.32: Top view. Layout including all functional requirements

6 Construction Method

In this chapter, as the first stage of the structural design, the applied construction method is discussed. First, the choice between either a prefab or an in-situ construction method is substantiated. Hereafter, with the consequences for the design carrying over from the chosen construction method, the initial construction sequence is presented. The section on the initial construction sketches an image as to how the Delta Barrier will be constructed, which main elements the barrier consists of and what the general construction sequence should be. Thirdly, the need for a building dock is discussed and some possible locations are proposed.

6.1 Prefab Instead of In-situ

Whether the Delta Barrier will be mostly prefabricated or build in-situ at the final location plays a significant part in the overall design of the structure. In order to establish which construction method would be preferable, both the advantages and disadvantages regarding a prefab or in-situ method are listed.

Prefab construction

A (mostly) prefab construction method implies that the fabrication of the greater parts of the structure will take place at a controlled and specialised location which is not the final construction location. After the prefabrication of the elements, said elements will be transported to the final building site after which the Delta Barrier will be constructed. For the elements needed to construct a large hydraulic structure such as a storm surge barrier, a building dock (or dry dock) is mostly used for the prefabrication processes. After completion of the elements, the dry dock may be flooded enabling transport over water of the element to the final construction location.

Advantages

- No need for a (complex and expensive) building pit at the final location
- Fabrication of elements in more controlled and specialised facilities
- Less activities influenced by conditions on site (currents, waves, wind)
- Less construction time in the Haringvliet estuary
- Experience from the Oosterscheldekering construction

Disadvantages

- Less freedom in design
- Increased complexity for the final assembly of the storm surge barrier
- Challenging to make in-situ adjustments
- Much expensive custom equipment needed for transport and placement of elements

In-situ construction

A (mostly) in-situ construction method implies that, in general, all fabrications take place at the final construction location. Such a construction method, considering the construction of a hydraulic structure in open water, requires a dry building pit. After transport of raw materials to the building pit, the actual elements and storm surge barrier will be fabricated at the dry building site.

Advantages

- Enables more design and construction possibilities a priori and a posteriori
- General construction on site is less complex

Disadvantages

- Need for a (complex and expensive) building pit at the final location
- More activities influenced by conditions on site (currents, waves, wind)
- More construction time and presence in the Haringvliet estuary
- Many small transport movements needed of raw material

Applying the prefab method

Given that a building pit at the final location at sea is highly unfeasible and that less presence and activities in the Haringvliet estuary is both beneficial regarding risk reduction (of personnel) during construction and regarding impact on the ecosystem and fishing activities, a prefab construction method seems preferable. Moreover, much experience has already been gathered from the prefab Oosterscheldekering construction.

A direct consequence of choosing for the prefab construction method is that a foundation on piles is no longer feasible (if possible at all). Given that the subsoil consists mostly of sand (see Section 3.2.3) and that it is very much possible to replace local weak layers and to compact the subsoil, a shallow foundation is feasible and is considered. The latter steers towards a pier design such as for the Oosterscheldekering. The piers and other required large elements will be made out of (pre-stressed) concrete at a dry dock in a more controlled location (see Section 6.3).

6.2 Initial Construction

Here, the initial construction method is discussed. That is, the construction of the Delta Barrier before climate change proves any additional measures to be necessary. Note that, although an important part of the construction sequence, activities regarding the preparation and testing are excluded. Firstly, the main activities are discussed after which an overview of the main activities - regarding the main components of the storm surge barrier - is presented by means of listed and specific activities. Although the numbering is somewhat in line with the construction sequence, it should be noted that most activities will be conducted parallel and not all activities regarding one specific element will be conducted in direct succession. Section 10.1 yields the planning of the activities presented here.

1. Foundation

In advance to placing the abutments and piers on their shallow foundation, the subsoil should be prepared for the increase in load. In this stage, the subsoil is altered as such that the bearing capacity is increased, mostly beneficial for the global stability of the structure.

2. Abutments

The abutments provide the connection between the Delta Barrier and the adjacent dikes. Furthermore, from the abutments road-traffic is able to cross the barrier. The abutments - two on each side of the barrier - are prefabricated in the dry dock, transported over water towards the construction site and placed on the improved foundation. As opposed to all other elements to be sunk in place, the two abutments will be placed during high water slack ensuring the greatest draught for the specialised vessel. It should be noted that before construction of the abutments, the adjacent dike sections ought to be realised.

3. Piers

The monolithic, concrete piers provide the main skeleton of the Delta Barrier and serve as parts of the frame in which the gates are placed. The sheer weight of the piers provide stability to the structure as a whole on the shallow foundation. The 26 identical piers are prefabricated in the dry dock, transported over water towards the construction site and placed on the improved foundation during low water slack. After placement, the piers are undergrouted to provide additional (horizontal) stability and are ballasted with sand. It should be noted that, especially for the transport and sinking of the large piers, specialised vessels are required.

4. Bottom protection

After placement of a pier, part of the bottom protection between the piers and under the, yet to be placed, sill beam is constructed to avoid direct erosion. The granular open filter is build up of a prefab geotextile mattress in which smaller gravel layers are present. The prefab mattresses are sunk at location by means of special equipment. The geotextile mattresses solely serve this purpose regarding constructability and are, due to the service life requirement, of no structural value. On the mattresses, a variety of larger rocks are dumped. The total area to be covered by a bottom protection is ca. 1250 x 2050 m². The realisation of the parts of the bottom protection further from the structure, both seaward and towards the Tidal Lake side, is conducted throughout the entire construction and parallel to various other activities (c.q. elements).

5. Bridge girders

Bridge girders will be placed on the piers over the entire barrier to serve the purpose of allowing road-traffic over the Delta Barrier. Additionally, the bridge girders provide room for technical and electrical installations. The girders - a total of 27 - are prefabricated in the dry dock, transported over water towards the construction site and placed on the piers (and two abutments) by a specialised vessel from the Tidal Lake side during low water slack. After construction of the bridge girders, said girders are used for transport of equipment and personnel and can be used for the construction of the other elements.

6. Driving mechanisms supports

The Driving mechanisms supports serve as supports for the driving mechanisms and as such for the gates connected to the driving mechanisms. While not as large in size as the other concrete elements, also the driving mechanisms supports - a total of 52; two per pier - can be prefabricated in the dry dock. The elements are transported over water towards the construction site and placed on the piers from the Tidal Lake, taking into account the future position of the gates. Finally, the driving mechanisms supports are connected to the piers by means of pre-stressing steel in ducts.

7. Gates

Construction of the steel gates can be conducted by parts. After importing individual steel parts, the parts can be connected (welded) together until 25 identical gates are constructed. After welding, an extensive conservation (say coating) should be applied in order to make the gate resistant to the saline environment. Now, after the piers have been prepared with the required guiding system, the gates are transported over water and placed between the piers in the guiding system during low water slack. Note that, in order to enable construction in less rough conditions, the gates ought to be placed from the Tidal Lake side. This implies that the gates should be hoisted over the bridge girders, which has been done with the construction of the Oosterscheldekering as well. Note that, similar to the Oosterscheldekering construction, a specialised vessel is required for the hoisting and placement from the water. The gates will be held by temporary measures (hooks) until they can be connected to the driving mechanisms. Note that the gates will be placed with the skin plate towards the Tidal Lake and hence the truss consisting of large tubular section towards the North Sea. Said configuration is chosen to enable construction of the top beams from the Tidal Lake side. Construction from the Tidal Lake side ensures better circumstances during construction.

8. Driving mechanisms

The driving mechanisms, enable the gates to move and close the barrier when necessary and enable the gates to re-open once the conditions allow for this. The driving mechanisms consist of a total of 50 hydraulic cylinders, two for each gate, connected to cardan beams on the driving mechanisms supports. After installing bearing seats on the driving mechanisms supports (besides other preparations), the driving mechanisms can be transported over water towards the construction site. Two cardan beams will be placed on the bearing seats connected to the driving mechanisms supports after which the hydraulic cylinders can be installed, all to be conducted during low water slack. Once two hydraulic cylinders are installed, on each side of the gate, the driving mechanisms can be connected to the

gate and the gate can be lifted from their temporary hooks. Finally, the driving mechanisms can be connected to the electrical installations in the bridge girders.

9. Sill beams

The sill beams, situated between two piers (and two abutment - pier connections), serve as the lower part of the frame on which the gates can be closed. They provide a (not so tight) connection between a closed gate and the foundation. The sill beams, a total of 25, are prefabricated in the dry dock, transported over water towards the construction site and placed between two piers from the Tidal Lake side during low water slack. Before transportation and before actual placement, the slots in the piers specifically serving as sill beams supports, are to be inspected and if necessary cleaned thoroughly. After sinking the sill beams in their slots by a specialised vessel and fine positioning the beams, the supports are to be grouted. Finally, the sill beams are ballasted with sand to provide additional stability.

10. Top beams

The top beams, also situated between two piers (and two abutment - pier connections), serve as the highest and final part of the frame which, together with the two piers and sill beam, provide the seal for a closed gate. The top beams, a total of 25, are prefabricated in the dry dock, transported over water towards the construction site and placed between two piers from the Tidal Lake side. Before transportation, supports for the top beams on the slots in the piers are to be prepared. Furthermore, the slots are thoroughly inspected and if necessary cleaned. Finally, the top beams will be placed in their slots during low water slack behind a closed gate by, again, a specialised vessel.

Overview of construction activities

1 Foundation

- 1.1 Dredge subsoil till under foundation level
- 1.2 Remove and replace (local) weak spots
- 1.3 Compacting the subsoil
- 1.4 Applying foundation mats

2 Abutments

- 2.1 *Realise dikes*
- 2.2 *Prefab construction in dry dock*
- 2.3 *Transport from building dock*
- 2.4 *Additional dredging before final placement*
- 2.5 *Place abutment*
- 2.6 *Finishing of abutment*

3 Piers

- 3.1 *Prefab construction in dry dock*
- 3.2 *Transport from building dock*
- 3.3 *Additional dredging before final placement*
- 3.4 *Place pier*
- 3.5 *Undergrouting pier*
- 3.6 *Applying sand ballast*

4 Bottom protection

- 4.1 *Dredge and flatten subsoil*
- 4.2 *Compacting the subsoil*
- 4.3 *Apply prefab gravel mats*
- 4.4 *Additional dredging before dumping*
- 4.5 *Applying rock bed*

- 5 Bridge girders
 - 5.1 *Prefab construction in dry dock*
 - 5.2 *Prepare supports on piers*
 - 5.3 *Transport from building dock*
 - 5.4 *Place bridge girder*
 - 5.5 *Fine positioning and adjusting*
- 6 Driving mechanisms supports
 - 6.1 *Prefab construction in dry dock*
 - 6.2 *Prepare supports on pier*
 - 6.3 *Transport from building dock*
 - 6.4 *Place tuning fork*
 - 6.5 *Fine positioning and adjusting*
 - 6.6 *Tension to pier*
- 7 Gates
 - 7.1 *Prefab gate elements*
 - 7.2 *Realising connections*
 - 7.3 *Applying conservation*
 - 7.4 *Prepare piers*
 - 7.5 *Transport*
 - 7.6 *Place gate*
- 8 Driving mechanisms
 - 8.1 *Fabrication*
 - 8.2 *Prepare driving mechanisms supports*
 - 8.3 *Transport*
 - 8.4 *Place movements works*
 - 8.5 *Final assembly and attachment to gate*
 - 8.6 *Connecting to electrical installations*
- 9 Sill beams
 - 9.1 *Prefab construction in dry dock*
 - 9.2 *Inspect and clean slots in piers*
 - 9.3 *Transport from building dock*
 - 9.4 *Additional inspection before final placement*
 - 9.5 *Place sill beam*
 - 9.6 *Grouting supports*
 - 9.7 *Applying sand ballast*
- 10 Top beams
 - 10.1 *Prefab construction in dry dock*
 - 10.2 *Prepare supports on piers*
 - 10.3 *Inspect top beam slots in piers*
 - 10.4 *Transport from building dock*
 - 10.5 *Additional inspection before final placement*
 - 10.6 *Place top beam*
 - 10.7 *Fine positioning and adjusting*

6.3 Building Dock

As established, a direct consequence of the prefab construction method is the need for a building dock (or dry dock) in which the large concrete elements of the Delta Barrier can be fabricated under relatively calm and controlled conditions. Most preferably, the dry dock would be realised as close to the final construction site as possible in order to limit transportation distance and time. Due to the large scale of the overall Delta21 project, a number of potential dry dock sites can be identified. In this section, the two most feasible and nearby locations are presented.

At this preliminary stage, the two most feasible and nearby locations are presented in Figure 6.1 and Figure 6.2 which represent a location in the Energy Storage Lake (location 1) and a location at the future location of the Spillway (location 2), respectively.

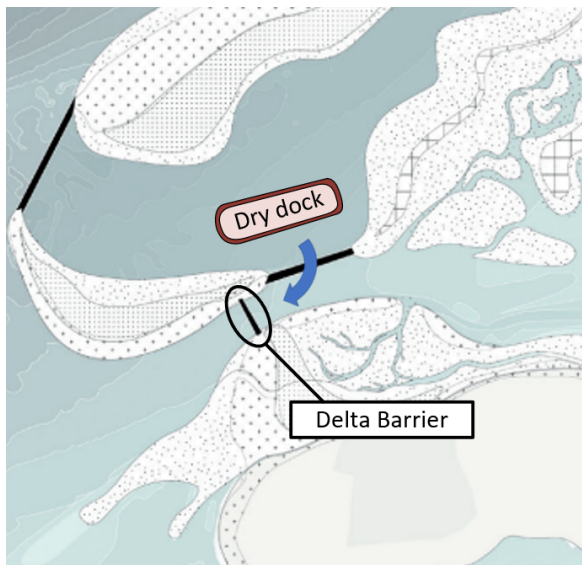


Figure 6.1: 1. Building dock location in the Energy Storage Lake (modified from van Eeden (2021))



Figure 6.2: 2. Building dock location at the Spillway location (modified from van Eeden (2021))

Location 1: In the Energy Storage Lake

Construction of the Energy Storage Lake requires reclaiming large quantities of sand to construct the outer 'dike ring', either consisting of a soft or hard line of defence. Construction of the outer defence line, in essence, creates the perfect circumstances for a building pit. The building pit could be built at any spot in the Energy Storage Lake, depending on the use of the lake at this stage. Finally, a connection should be realised from the dry dock to the final construction site by means of a lock, a dredged channel with sufficient draught and a small harbour if necessary. Additionally, it might be preferable to construct multiple compartments in the building pit for the different concrete elements.

Location 2: At the Spillway location

Given that construction of the overall Delta21 project might consist of two main phases: the Energy Storage Lake and Pumping Stations first and the Delta Barrier (including the adjacent dikes) and Spillway second, the dry dock can be constructed at the future location of the Spillway. Furthermore, a dry dock which encompasses the final construction location of the Spillway gives rise to the opportunity to construct the Spillway in the dry. Again, a connection should be realised from the dry dock to the final construction site by means of a lock, a dredged channel with sufficient draught and a small harbour if necessary. Compartmentalisation of the dry dock for the various different concrete elements to be constructed might again be preferable.

7 Gate Design

This chapter presents the gate design, as part of the structural design. First, the design strategy is discussed as certain engineering principles are pursued throughout the gate design. Secondly, all relevant limit states and load combinations are presented. Thirdly, the force flow through the gate is presented as a basis for the structural verifications. Hereafter, the way cross-sections and joints are classified is discussed. Subsequently, the verifications which ought to be made for all structural gate components regarding the strength and stiffness are presented. The actual verifications can be found in Appendix XIV. Lastly, the final design is depicted. The final design presents all components of the gate including important characteristics.

7.1 Design Strategy

Throughout the gate design, the following engineering principles are pursued:

- *A quasi-static approach*
A quasi-static approach is followed for the gate design. This can be justified as the waves approaching the structure have already broken on the foreshore, i.e. there is merely a standing wave.
- *A Torsional weak gate*
Torsional weakness of the gate is necessary in order to be able to absorb rotational and settlement differences between two piers without significant stresses. Torsional slackness of the gate means that the structure as a whole must be 'open'. Imposed deformations must not lead to large coercive forces. In order to limit the torsional stiffness, the aim is to keep the distance between the vertical truss and the skin plate as small as possible.
- *Skin plate on Tidal Lake side*
With the skin plate on the Tidal Lake side (i.e. truss-system on the sea side), it is able to construct the top beam from the Tidal Lake side. If the skin plate of the gate were to be situated at the sea side, the top beams had to be hoisted over the gates in order to be constructed from the Tidal Lake side. Furthermore, with the skin plate on the Tidal Lake side, the top beams can be placed behind closed gates. Construction from the Tidal Lake side ensures better circumstances during construction.
- *Truss with tubular sections*
As opposed to a truss with web plates, the use of tubular sections greatly reduces wave impact loads on the structure. With tubular sections, water is better able to flow around and through the structure.
- *Plastic capacity*
Cross-sections in which a plastic hinge is able to develop can reach a greater resistance. Plastic hinges can only develop in so called class 1 (or partly in class 2) cross-sections which provide sufficient rotational capacity to ensure the redistribution of loads. For the gate design, the possibility to use the plastic capacity is pursued throughout.
- *"Full strength" welds*
All welds should be designed "full strength", i.e. the strength of the weld should not be governing over the strength of the mother material. In order to be able to use the EC3 model to calculate the resistance of a welded connection to an unstiffened flange it is essential that large local deformations can occur in the plate. The tips of the flanges are much more flexible than the centre zone, so compared to the centre zone there is much more deformation required to activate the tips. Full strength welds guarantee that the plate can yield before the weld breaks, so large deformation are possible to redistribute the load along the length of the weld.

7.2 Limit States & Load Combinations

As for the structural design of the gate, the limit states regarding internal failure or excessive deformation of the structure or of structural elements (STR) and the SLS quasi-permanent combination from the Building Decree are considered.

The STR limit state represents the failure mechanism of structural failure (see Figure 7.1) and the SLS combination is used for the stiffness verification. Note that for structural failure, the Building Decree is governing over the Water Act as a result of the maximum failure probability of the Delta21 flood protection system, the proposed Delta21 dike segments and the failure probability distribution over the failure mechanisms as presented in Appendix VI.



Figure 7.1: Failure mechanism of structural failure (Onwuachu, 2021)

The Building Decree prescribes a maximum failure probability of 1:100000 per year and the Water Act, based on the substantiation in Appendix VI, 1:52632 per year for structural failure.

With regard to the STR limit state, the following load combinations as proposed in the ROK (2017) are considered:

- A: Maximum positive head is dominant
- B: Maximum negative head is dominant
- H: Ship collision¹¹

All relevant limit states and corresponding load combinations are presented in Appendix XIII.

7.3 Force Flow

In general, the loads on the gate are transferred from the skin plate (nr.1) to the vertical girders (nr.2). The vertical girders, subsequently, transfer the loads to the global truss system via the stump connectors (nr.3). The force flow as described is presented in Figure 7.2. Note that the number of elements in Figure 7.2 are significantly less than in the actual verified design, as Figure 7.2 merely serves the purpose of presenting the force flow assumed in order to design the respective elements. The complete, final gate design is presented in Section 7.8.

¹¹Note that this load combination is considered an accidental event, say a calamity by the ROK (2017)

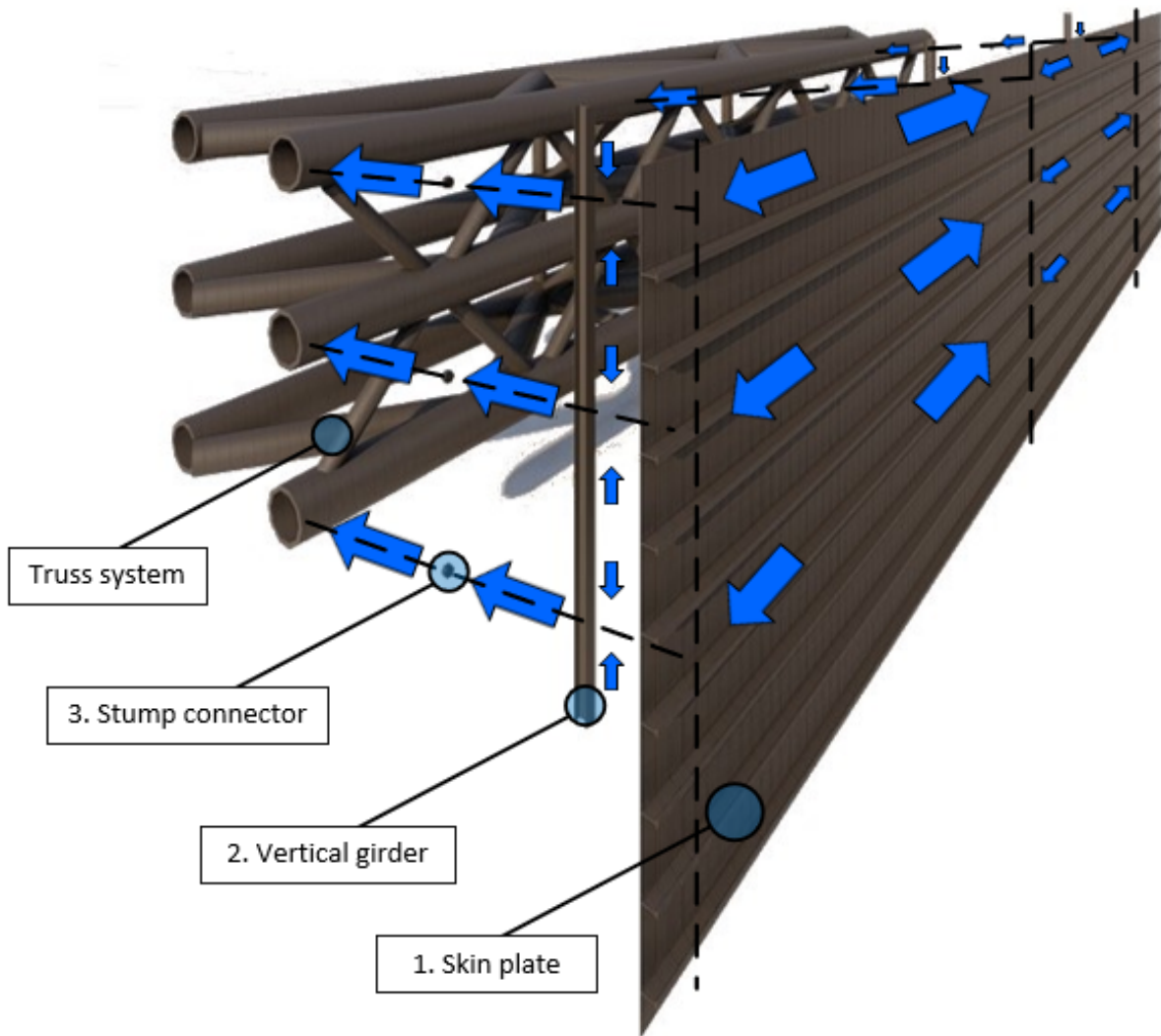


Figure 7.2: Simplified force flow through the gate

7.4 Cross-section Classification

The purpose of cross-section classification is to find out how much the resistance and rotational capacity of a cross-section are limited by its bending resistance. As for this design, the possibility to use the plastic capacity is pursued, only cross-section class 1 elements are used. Class 1 cross-sections are cross-sections in which a plastic hinge can form where the rotational capacity is sufficient for the plastic calculation without loss of resistance.

Table (5.2) from NEN-EN 1993-1-1 (2016) yields the maximum width to thickness ratios for components under compression per cross-section class.

Webs of I, H and rectangular cross-sections

For the webs of I, H and rectangular cross-sections Equation (7.1a) and Equation (7.1b) should hold (both from NEN-EN 1993-1-1 (2016) Table (5.2)) for the cross-section to be classified as a class 1 cross-section, in the case of pure bending and compression respectively.

$$\frac{c}{t} \leq 72 \sqrt{\frac{235}{f_y}} \quad (7.1a)$$

$$\frac{c}{t} \leq 33 \sqrt{\frac{235}{f_y}} \quad (7.1b)$$

where: c [mm] = length of the web
 t [mm] = thickness of the web
 f_y [N/mm²] = yield strength of the web

Flanges of I, H and rectangular cross-sections

For the flanges of I, H and rectangular cross-sections Equation (7.2) should hold (from NEN-EN 1993-1-1 (2016) Table (5.2)) for the cross-section to be classified as a class 1 cross-section, in the case of the ultimate fibre being only under compression.

$$\frac{c}{t} \leq 9 \sqrt{\frac{235}{f_y}} \quad (7.2)$$

$$(7.3)$$

where: c [mm] = length of the flange
 t [mm] = thickness of the flange
 f_y [N/mm²] = yield strength of the flange

Tubular cross-sections

For tubular cross-sections Equation (7.4) should hold (from NEN-EN 1993-1-1 (2016) Table (5.2)) for the cross-section to be classified as a class 1 cross-section.

$$\frac{d}{t} \leq 50 \cdot \frac{235}{f_y} \quad (7.4)$$

where: d [mm] = diameter of the tubular cross-section
 t [mm] = thickness
 f_y [N/mm²] = yield strength

7.5 Strength Verifications

This section merely presents the general equations which ought to be used for the respective strength verifications. The actual and complete verifications for every distinguished gate component can be found in Appendix XIV.

7.5.1 Normal Force

According to NEN-EN 1993-1-1 (2016) Equation (6.10), the design resistance of a cross-section under uniform axial pressure (i.e. normal force) of a class 1, 2 or 3 cross-section is calculated as follows:

$$N_{pl,Rd} = \frac{A f_y}{\gamma_{M0}} \geq N_{Ed} \quad (7.5)$$

where: $N_{pl,Rd}$ [Nmm] = plastic normal force resistance of a cross-section
 A [mm²] = area of the cross-section
 f_y [N/mm²] = yield strength
 γ_{M0} [-] = partial factor for resistance of cross-sections = 1
 N_{Ed} [N] = design value of normal force

7.5.2 Bending Moment

Plastic

As stated by NEN-EN 1993-1-1 (2016) Equation (6.13), the moment resistance of a class 1 or 2 cross-section for bending around one of its major axes is calculated as follows:

$$M_{pl,Rd} = \frac{W_{pl}f_y}{\gamma_{M0}} \geq M_{Ed} \quad (7.6)$$

where: $M_{pl,Rd}$ [Nmm] = plastic bending moment resistance of a cross-section
 W_{pl} [mm³] = plastic section modulus
 M_{Ed} [N] = design value of bending moment

Elastic

As for the longitudinal stiffened skin plate of the gates, the verification regarding uniaxial bending (without axial force) should be conducted according to Equation (6.29) from NEN-EN 1993-1-5 (2022), here Equation (7.7).

$$\sigma = \frac{M_{Ed}x\gamma_{M0}}{I_{xx}} \leq f_y \quad (7.7)$$

where: σ [N/mm²] = stress at location x in the cross-section
 I_{xx} [mm⁴] = mass moment of inertia
 x [mm] = distance to the outer fibre from the centre of gravity

Note that the elastic moment resistance ($M_{el,Rd}$) is defined as in Equation (7.8).

$$M_{el,Rd} = \frac{W_{eff,x}f_y}{\gamma_{M0}} \quad (7.8)$$

in which: $W_{eff,x}$ [mm³] = $\frac{I_{xx}}{x}$

7.5.3 Shear Force

Plastic

Equation (7.9) follows from Equation (6.18) of NEN-EN 1993-1-1 (2016).

$$V_{pl,Rd} = \frac{A_v(f_y/\sqrt{3})}{\gamma_{M0}} \geq V_{Ed} \quad (7.9)$$

where: $V_{pl,Rd}$ [N] = plastic shear resistance of a cross-section
 A_v [mm²] = shear surface
 V_{Ed} [N] = design value of shear force

Elastic

As for the longitudinal stiffened skin plate of the gates, the verification regarding the resistance to shear should be conducted according to Equation (7.1) from NEN-EN 1993-1-5 (2022), here Equation (7.10).

$$V_{el,Rd} = \frac{\chi_w f_{yw} h_{w,eff} t_w}{\sqrt{3}\gamma_{M1}} + \frac{b_f t_f^2 f_{yf}}{c\gamma_{M1}} \left(1 - \left(\frac{M_{Ed}}{M_{f,Rd}} \right)^2 \right) \geq V_{Ed} \quad (7.10)$$

where: $V_{el,Rd}$	[N]	=	elastic shear resistance of a plate member
χ_w	[-]	=	shear buckling factor
f_{yw}	[N/mm ²]	=	yield strength of the web
h_w	[mm]	=	height of the web
t_w	[mm]	=	thickness of the web
f_{yf}	[N/mm ²]	=	yield strength of the flange
b_f	[mm]	=	width of the flange
t_f	[mm]	=	thickness of the flange
c	[mm]	=	$a \left(0.25 + \frac{1.6b_f t_f^2 f_{yf}}{t h_{w,eff}^2 f_{yw}} \right)$
a	[mm]	=	length of the plate member
$M_{f,Rd}$	[Nmm]	=	the design plastic moment of resistance of the cross-section consisting of the effective area of the flanges only
γ_{M1}	[-]	=	partial factor for resistance to shear = 1

7.5.4 Torsion

As the self weight of the gate is orders less than the resulting loads from the water and wave pressures, any eccentrically introduced vertical loads are neglected. Note that although vertical wave impact loads can develop when water becomes entrapped under (parts of) the structure, e.g. around the still water line with vertical movement of the water, such wave impact loads are neglected in this preliminary design. Provisions are made though to decrease such wave impact loads by means of mostly using tubular cross-sections and by providing the longitudinal stiffeners with recesses. Furthermore, as the gate is designed mostly 'open', relatively large deformations can occur while not leading too large coercive forces.

7.5.5 Bending and Shear Force

Generally, when shear force is present, its influence on the moment resistance should be taken into account. Though, NEN-EN 1993-1-1 (2016) 6.2.8 (2) and NEN-EN 1993-1-5 (2022) 9.1 (1) state that when the shear force is less than half the shear force at yielding (i.e. when Equation (7.11) holds), its influence on the moment resistance may be neglected.

$$\frac{V_{Ed}}{V_{Rd}} < 0.5 \quad (7.11)$$

Plastic

If Equation (7.11) is not satisfied, for the reduced moment resistance, the design value of the cross-sectional resistance should be taken, calculated with a reduced yield strength for the shear surface. Said reduced yield strength can be calculated using Equation (7.12) as stated by NEN-EN 1993-1-1 (2016) Equation (6.29).

$$f_{y,red} = \left(1 - \left(\frac{2V_{Ed}}{V_{pl,Rd}} - 1 \right)^2 \right) f_y \quad (7.12)$$

where: $f_{y,red}$ [N/mm²] = reduced yield strength due to shear force

Elastic

For the longitudinal stiffened skin plate, if Equation (7.11) is not satisfied, the combined effects of bending and shear in the web of an I girder should satisfy Equation (7.13) (according to NEN-EN 1993-1-5 (2022) Equation (9.1)).

$$\frac{M_{Ed}}{M_{el,Rd}} + \left(1 - \frac{M_{f,Rk}}{M_{eff,Rk}}\right) \left(\frac{2V_{Ed}}{\frac{\chi_w f_{yw} h_{w,eff} t_w}{\sqrt{3}\gamma_{M1}}} - 1\right)^\mu \leq 1 \quad (7.13)$$

where: $M_{f,Rk}$ [Nmm] = the characteristic plastic moment of resistance of the cross-section consisting of the effective area of the flanges only

$M_{eff,Rk}$ [Nmm] = $W_{eff} f_y$

$W_{eff,x}$ [mm³] = the effective section modulus

μ [-] = $\left(\frac{M_{f,Rk}}{M_{eff,Rk}} + 0.2\right)^{15} + 1$

7.5.6 Bending and Normal Force

Generally, when a normal force is present, its influence on the moment resistance should be taken into account. For cross-section classes 1 and 2, the reduced moment resistance can be calculated using Equation (7.14) as stated by NEN-EN 1993-1-1 (2016) Equation (6.32).

$$M_{N,Rd} = M_{pl,Rd} \left(1 - \left(\frac{N_{Ed}}{N_{pl,Rd}}\right)^2\right) \quad (7.14)$$

where: $M_{N,Rd}$ [Nmm] = reduced moment resistance due to normal force

Note that throughout the gate design bi-axial bending has been neglected due to the fact that the self weight of the gate is orders less than the resulting loads from the water and wave pressures.

7.5.7 Bending, Shear and Normal Force

According to NEN-EN 1993-1-1 (2016) 6.2.10 (1), when both a shear force and normal force is present, the influence of both the shear force and the normal force on the moment resistance should be taken into account. Note that this implies using both Equation (7.12) and Equation (7.14) in order to determine the reduced moment resistance.

7.5.8 Buckling

Buckling stability for a bar under compression classified as a cross-section class 1 should be verified according to Equation (7.15) as per NEN-EN 1993-1-1 (2016) 6.3.1.1.

$$N_{b,Rd} = \frac{\chi A f_y}{\gamma_{M1}} \geq N_{Ed} \quad (7.15)$$

where: $N_{b,Rd}$ [N] = resistance to buckling

χ [-] = reduction factor for the appropriate buckling shape

A [mm²] = cross-sectional area of the rod

f_y [N/mm²] = yield strength of the rod

γ_{M1} [-] = partial factor for resistance of members to instability = 1

N_{Ed} [N] = design value of compression force

7.5.9 Joints

Full strength welds

In order to ensure the redistribution of forces over the structure, the strength of the welds should not be governing over the mother material adjacent to the connection.

$$C_1 \cdot \frac{F_{Ed}}{a \cdot l_{eff}} \leq \frac{f_u}{\beta_w \gamma_{M2}} \quad (7.16a)$$

$$C_2 \cdot \frac{F_{Ed}}{l_{eff} t} \leq f_y \quad (7.16b)$$

where: C_1	[-]	=	factor to determine the tension in the throat of the weld from a general force
F_{Ed}	[N]	=	design value of the general force
a	[mm]	=	throat thickness of the weld
l_{eff}	[mm]	=	effective length of the weld
f_u	[N/mm ²]	=	nominal ultimate tensile strength of the part joined, which is of lower strength grade
β_w	[-]	=	correlation factor depending on the lowest steel grade used
γ_{M2}	[-]	=	partial factor for resistance of welds = 1.25
C_2	[-]	=	factor to determine the tension in the component of the mother material from a general force
t	[mm]	=	thickness of the component of the mother material
f_y	[N/mm ²]	=	yield strength of the component of the mother material

Subsequently, after rewriting Equation (7.16a) using Equation (7.16b), a criterion can be formulated which states a minimum value for the throat thickness (a) of the weld in order for the weld to be full strength.

$$a \geq \frac{C_1}{C_2} \cdot t \beta_w \gamma_{M2} \frac{f_y}{f_u} \quad (7.17)$$

Weld failure

For the verification of the welds, the directional method (combined stress method) is used as described in NEN-EN 1993-1-8 (2021) 6.5.3.2. Equation (7.18a) and Equation (7.18b) from Equation (6.1) of NEN-EN 1993-1-8 (2021) should be satisfied.

$$\sqrt{\sigma_{\perp}^2 + 3(\tau_{\perp}^2 + \tau_{\parallel}^2)} \leq \frac{f_u}{\beta_w \cdot \gamma_{M2}} \quad (7.18a)$$

$$\sigma_{\perp} \leq \frac{0.9 f_u}{\gamma_{M2}} \quad (7.18b)$$

where: σ_{\perp}	[N/mm ²]	=	normal stress perpendicular to throat section
τ_{\perp}	[N/mm ²]	=	shear stress acting in the throat section perpendicular to axis of the weld
τ_{\parallel}	[N/mm ²]	=	shear stress acting in the throat section parallel to axis of the weld

Do note that if the weld is designed full strength (i.e. Equation (7.17) is satisfied), weld failure is not governing.

7.6 Deflection

As part of the stiffness verification, the maximum deflection of the gate should satisfy Equation (7.19), as stated by Vrijburcht (2000).

$$w_{max,x} \leq \frac{1}{200} L_i \quad (7.19)$$

where: $w_{max,x}$ [mm] = maximum deflection of the gate in x-direction (lengthwise)
 L_i [mm] = length of the gate (element)

7.7 Natural Frequencies and Resonance

In general, in order to avoid resonance, the lowest natural frequency of the gate should be greater than the corresponding excitation frequency. Table 7.1 presents the lowest natural frequency for load combination A and the quasi-permanent combination (SLS) respectively, with corresponding excitation frequency for wave loading. For the complete derivation of the natural frequencies, see Appendix XIV.3.

	f_1 [Hz]	f [Hz]
A	0.20	0.11
SLS	0.23	0.12

Table 7.1: Fundamental natural frequencies and corresponding excitation frequencies

Note that the fundamental natural frequencies in Table 7.1 result from a conservative approach. The total stiffness of the gate in reality is greater (and hence the natural frequencies greater) than estimated due to the contribution of the stiff connections to the piers and the bracings which have not been taken into account.

Besides wave impact loading, drag forces due to flow under gates can give rise to resonance phenomena. Although not considered here specifically, unstable detachment of flow should be prevented (preferably do not design curved structures); the flow should preferably detach from an edge at the downstream side. Furthermore, any rubber seals should preferably have no rounded shape.

7.8 Final Gate Design

After all verifications as established above are conducted (see Appendix XIV), the final gate design is presented here.

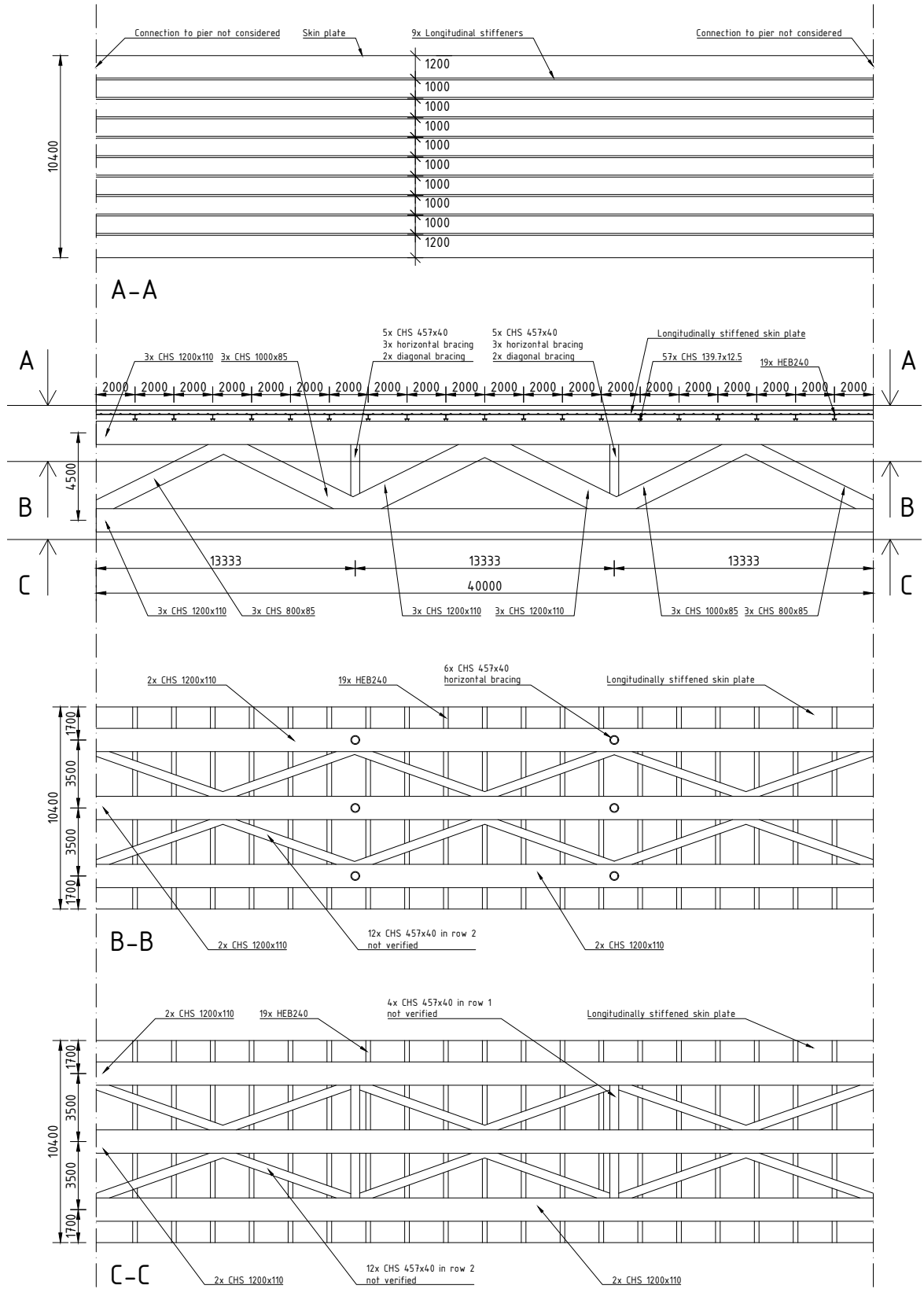
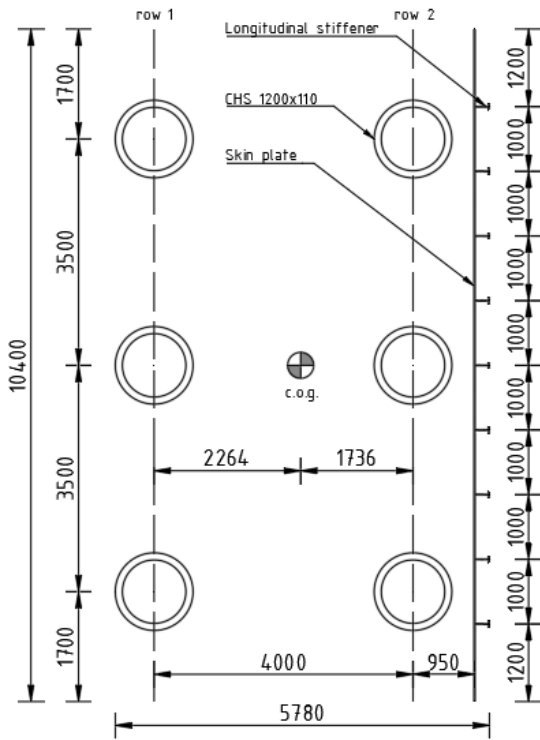


Figure 7.3: Complete gate design. Front views A-A to C-C indicated in top view



L	40	m
H	10.4	m
B	5.78	m
m_G	1116899	kg
$I_{xx,tot}$	1.12	10^{13} mm ⁴

Table 7.2: Total gate characteristics

where: L is the length
 H is the height
 B is the width
 m_G is the dry mass
 $I_{xx,tot}$ is the total mass moment of inertia

Figure 7.4: Cross-section of the gate only elements perpendicular to flow direction

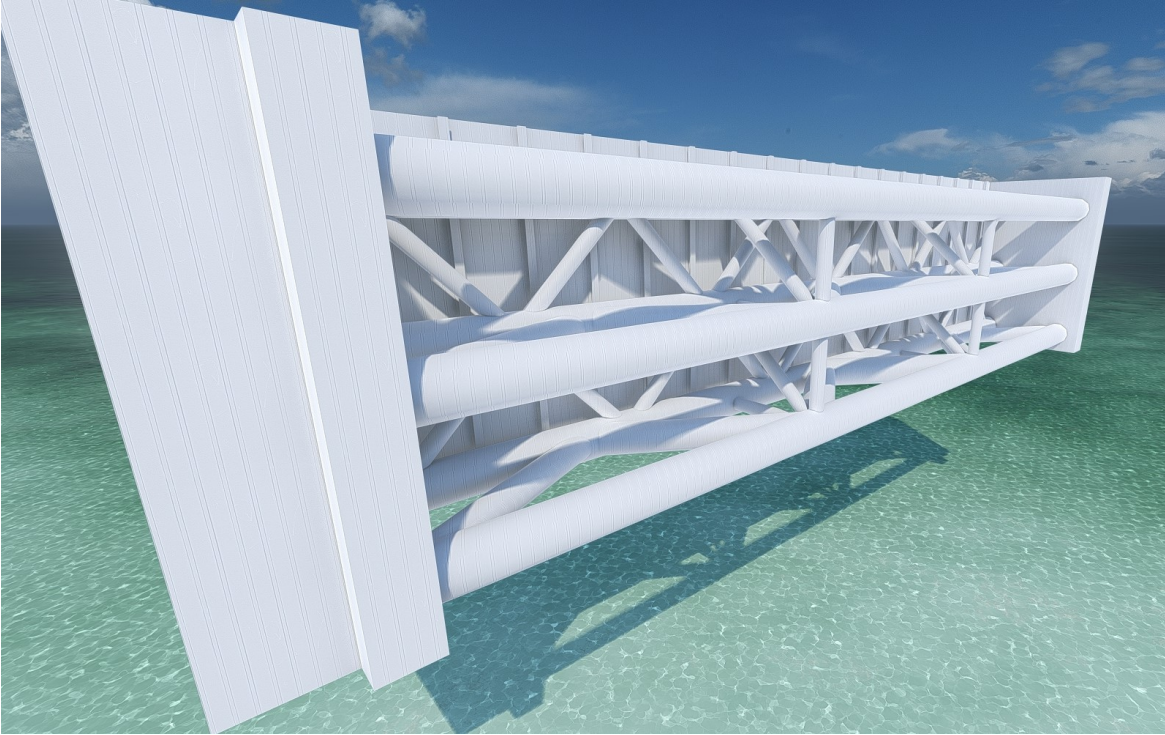


Figure 7.5: 3D render of final gate design

8 Civil Superstructure Design

This chapter presents the design of the concrete civil superstructure, as part of the structural design. First, the design strategy is discussed as certain engineering principles are pursued throughout the entire superstructure design. Secondly, all relevant limit states and load combinations are presented. Thirdly, the required concrete cover and duct and bar spacing is discussed. Subsequently, the verifications which ought to be made for all civil superstructure members regarding the strength and stiffness are presented. The complete verification for every distinguished member can be found in Appendix XV. Lastly, the final civil superstructure design is depicted. The final design presents all distinguished components of the concrete civil superstructure: the top beam, sill beam and the piers.

8.1 Design Strategy

Throughout the civil superstructure design, the following engineering principles are pursued:

- *Minimise number of cracks*
In order to ensure durability of the structure, especially in saline environment, the number of cracks in the concrete superstructure is minimised. In a global sense, no cracks are allowed and hence no tension should occur in any cross-section of any member.
- *Pre-stressing (or rather post-stressing)*
In order to counteract the tensile stresses in the structure, the concrete elements are pre-stressed as such such that no global tensile stresses are present. Besides ensuring structural integrity, this approach ensures a minimum number of cracks as well. As for the pre-stressing method, tendons grouted in ducts (bonded) are considered. A bonded system provides more protection in corrosive environments. Note that this is actually a post-tensioning system, though for simplicity called pre-stressing throughout this thesis.
- *Spalling reinforcement*
Introduction of a local pre-stressing force leads to local tension stresses in the concrete member from the anchoring point until the point where the load is evenly distributed (the so-called Discontinuity or Deep-region). In this D-region shear strains are non-linearly distributed and Bernoulli's hypothesis that plane sections remain plane is not valid. Provisions, viz. local spalling reinforcement, should be in place in order to account for the local tension stresses until the introduced load is spread evenly throughout the cross-section.
- *Skin-reinforcement*
Skin-reinforcement is applied to avoid local spalling of the concrete as rather large prestressing steel ducts are present with significant concrete cover. This measure greatly enhances the durability of the concrete civil superstructure.
- *No shear reinforcement*
The concrete members of the civil superstructure are designed as such that the concrete cross-section itself is strong enough to withstand the shear (including torsional-induced) stresses without the application of rather complicated shear reinforcement.

8.2 Limit States & Load Combinations

As for the structural design of the civil superstructure, the limit states regarding internal failure or excessive deformation of the structure or of structural elements (STR) and the SLS quasi-permanent combination from the Building Decree are considered.

The STR limit state represents the failure mechanism of structural failure (see Figure 8.1) and the SLS combination is used for the stiffness verification. Note that for structural failure, the Building Decree is governing over the Water Act as a result of the maximum failure probability of the Delta21 flood protection system, the proposed Delta21 dike segments and the failure probability distribution over the failure mechanisms as presented in Appendix VI.

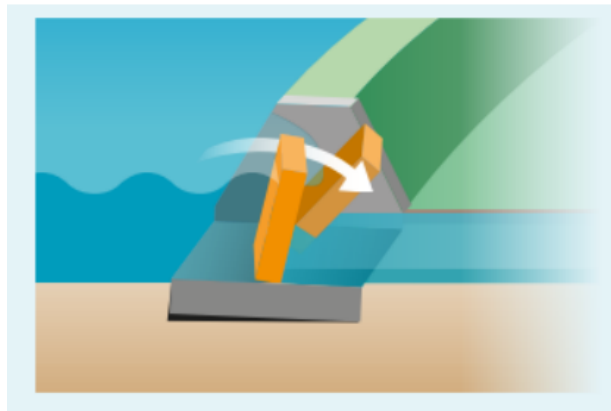


Figure 8.1: Failure mechanism of structural failure (Onwuachu, 2021)

The Building Decree prescribes a maximum failure probability of 1:100000 per year and the Water Act, based on the substantiation in Appendix VI, 1:52632 per year for structural failure.

With regard to the STR limit state, the following load combinations as proposed in the ROK (2017) are considered:

- A: Maximum positive head is dominant
- B: Maximum negative head is dominant
- H: Ship collision¹²

All relevant limit states and corresponding load combinations are presented in Appendix XIII.

8.3 Concrete Cover

In order to ensure the durability of the concrete civil superstructure, a sufficient concrete cover on the reinforcement bars should be applied. Said concrete cover mostly protects the reinforcement from corrosion and ensures a safe transmission of the bonding forces. As stated in NEN-EN 1992-1-1 (2011b) 4.4.1.1 (2)P, the nominal concrete cover to be applied consists of a required minimum cover and an addition regarding construction tolerance:

$$c_{nom} = c_{min} + \Delta c_{dev} \quad (8.1)$$

in which: c_{nom} [mm] = nominal concrete cover to be applied
 c_{min} [mm] = minimum concrete cover
 Δc_{dev} [mm] = addition for execution tolerance

The minimum concrete cover should be determined using Equation (8.2) as stated by Equation (4.2) from NEN-EN 1992-1-1 (2011b).

$$c_{min} = \max(c_{min,b}; c_{min,dur} + \Delta c_{dur,\gamma} - \Delta c_{dur,st} - \Delta c_{dur,add}; 10 \text{ mm}) \quad (8.2)$$

¹²Note that this load combination is considered an accidental event, say a calamity by the ROK (2017)

where:	$c_{min,b}$	[mm]	=	the minimum cover depending on the bond requirement
	$c_{min,dur}$	[mm]	=	the minimum cover depending on the environmental conditions
	$\Delta c_{dur,\gamma}$	[mm]	=	additional safety margin = 0
	$\Delta c_{dur,st}$	[mm]	=	reduction when using stainless steel = 0
	$\Delta c_{dur,add}$	[mm]	=	reduction when using additional protection measures = 0

In Equation (8.2), the minimum cover depending on the bond requirement ($c_{min,b}$) is equal to the applied bar diameter when using separate bars and is equal to the equivalent diameter when using bundled bars. The minimum cover depending on the environmental conditions ($c_{min,dur}$), depends on the structural class (to be determined using Table (4.3N) of NEN-EN 1992-1-1 (2011b)) and the environmental class (to be determined using Table (4.1) of NEN-EN 1992-1-1 (2011b) as a function of governing environmental conditions). The concrete civil superstructure is classified as environmental class XS3 for corrosion induced by chlorides from seawater in the tidal and splash zone. A design lifetime of 200 years, concrete class < C45/55, using prefab concrete built in a specialised dry dock and guaranteed specific quality control of the concrete production, results in a structural class S4.

Finally, Table (4.4N) and Table (4.5N) from NEN-EN 1992-1-1 (2011b) for rebar and pre-stressing steel respectively, yield the minimum cover depending on the environmental conditions. The latter is governing in Equation (8.1) and, with $\Delta c_{dev} = 10$ mm (NEN-EN 1992-1-1 (2011b) 4.4.1.3 (1)P), results in a nominal concrete cover to be applied of 55 mm for rebar and 65 mm for prestressing steel. However, to ensure durability in the salty environment of the Delta Barrier for the complete design life of 200 years, a concrete cover of 60 mm is considered for rebar.

8.4 Duct and Bar Spacing

NEN-EN 1992-1-1 (2011b) 8.10.1.3 (3) states that the minimum free space between pre-stressing ducts should comply with Figure 8.2. Lastly, the spacing of the rebar used as skin-reinforcement should not be greater than 150 mm. Furthermore, to ensure that the concrete can be properly poured and sufficiently compacted, the spacing between the skin-reinforcement bars should not be less than the maximum of either the applied rebar diameter or 20 mm as posed by NEN-EN 1992-1-1 (2011b) 8.2 (2).

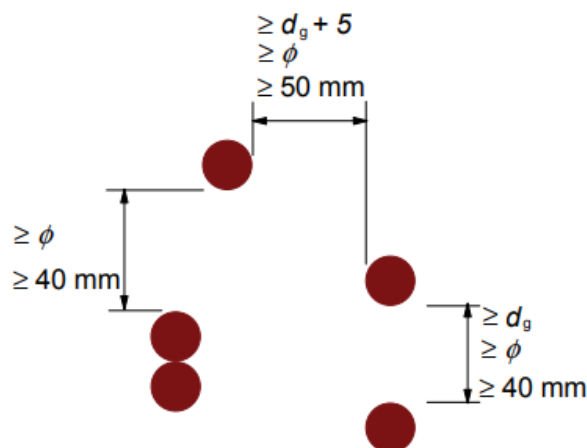


Figure 8.2: Minimum free space between pre-stressing ducts according to Eurocode 2 (2011b)

8.5 Losses in Pre-stress

Losses in pre-stress regard the slow decrease of the induced compressive stress in a pre-stressed element due to various factors. In general, losses in pre-stress of pre-stressed concrete can be divided into two categories: immediate and time-dependent. Wedge set, friction, and elastic shortening all-cause

immediate losses. Here, elastic shortening is assumed to be nil as a post-tensioning system is used. Creep, shrinkage, and relaxation losses are time-dependent.

Friction

During stretching of a tendon in a post-tensioned element, friction is formed at the interface of concrete and steel. There is a reduction in pre-stress along with the member from the stretched end(s). According to NEN-EN 1992-1-1 (2011b) 5.10.5.2 (1), losses as a result of friction may be estimated by means of Equation (8.3).

$$\Delta\sigma_{p,\mu}(x) = \sigma_i(1 - e^{-\mu(\theta+kx)}) \quad (8.3)$$

where:	$\Delta\sigma_{p,\mu}(x)$	[N/mm ²]	=	loss in pre-stress due to friction
	σ_i	[N/mm ²]	=	initial stress in pre-stressing steel
	μ	[-]	=	friction coefficient ≈ 0.19
	θ	[rad]	=	change in direction over $x = 0$, for straight tendons
	k	[rad/mm]	=	factor for accidental changes in direction (Wobble factor) ≈ 0.01
	x	[mm]	=	distance along the duct from the stretched end

Wedge set

Anchorage is a component that is used to attach the tendons to the concrete while terminating them. When the stressing process is over, the major role of anchorage is to transfer the pre-stressing force to the concrete. To transfer the pre-stressing force to the concrete, anchoring is supplied at both ends of the tendon. If the anchorage moves from its original position, the tendons loosen, resulting in pre-stress loss, also called wedge set. Losses as a result of wedge set are estimated using Equation (8.4).

$$\Delta\sigma_p(x) = l_{set} \cdot \frac{\Delta\sigma_{p,\mu}}{\Delta x} \quad (8.4)$$

where:	$\Delta\sigma_p(x)$	[N/mm ²]	=	loss in pre-stress due to wedge set
	l_{set}	[mm]	=	length over which wedge set influences the pre-stressing force
	Δx	[mm]	=	distance along the duct from the stretched end

The length over which wedge set influences the pre-stressing force (l_{set}) is determined with Equation (8.5).

$$l_{set} = \sqrt{\frac{w_{set} \cdot E_p}{\Delta\sigma_{p,\mu}/\Delta x}} \quad (8.5)$$

where:	w_{set}	[mm]	=	anchorage slip ≈ 5
	E_p	[N/mm ²]	=	Youngs Modulus of pre-stressing steel

Creep, shrinkage and relaxation

Creep is the deformation of concrete that occurs over time due to a constant force, the stress loss is aided by the shortening of tensioned wires caused by concrete shrinkage and steel relaxation is described as a decrease in stress over time when under constant tension. Due to these three mechanisms, the pressure in the tendon is reduced with time. NEN-EN 1992-1-1 (2011b) 5.10.6 (2) states that Equation (8.6) may be used to determine said time-dependent losses.

$$\Delta\sigma_{c+s+r} = \frac{\epsilon_{cs}E_p + 0.8\Delta\sigma_{p,\mu} + \frac{E_p}{E_{cm}}\phi(t, t_0)\sigma_{m,i}}{1 + \frac{E_p}{E_{cm}}\frac{A_p}{A_c}\left(1 + \frac{A_c}{I_c}z_{cp}^2\right)(1 + 0.8\phi(t, t_0))} \quad (8.6)$$

where: $\Delta\sigma_{c+s+r}$	[N/mm ²]	=	loss in pre-stress due to creep, shrinkage and relaxation
ϵ_{cs}	[-]	=	absolute strain due to creep = -0.00025
E_{cm}	[N/mm ²]	=	Youngs Modulus of concrete
$\phi(t, t_0)$	[-]	=	creep factor at time t for a load applied at $t_0 = 2.5$
$\sigma_{m,i}$	[N/mm ²]	=	stress in the concrete member after initial pre-stressing
A_p	[mm ²]	=	area of pre-stressing steel
A_c	[mm ²]	=	concrete area
I_c	[mm ⁴]	=	mass moment of inertia of the concrete cross-section
z_{cp}	[mm]	=	distance between the pre-stressing element(s) and the centre of gravity

It should be noted that in all concrete designs conducted here, it is strived for to have the point of action of the resultant pre-stressing force to coincide with the centre of gravity of the cross-section. Although optimisation of the designs could prove eccentric pre-stressing to be beneficial, the great variety in load combinations (and as a result the variety in stress distributions) seem to vow for a resultant pre-stressing force acting at the centre of gravity of the cross-section in order to keep the design from becoming overly complex.

8.6 Maximum Pre-stressing

NEN-EN 1992-1-1 (2011b) 5.10.2.1 and 5.10.3 give restrictions for the maximum stress in pre-stressing steel during stressing (Equation (8.7a)) and after the immediate losses (Equation (8.7b)), respectively.

$$\sigma_{p,max} = \min(k_1 \cdot f_{pk}; k_2 \cdot f_{p0.1k}) \quad (8.7a)$$

$$\sigma_{pm0} = \min(k_7 \cdot f_{pk}; k_8 \cdot f_{p0.1k}) \quad (8.7b)$$

where: $\sigma_{p,max}$	[N/mm ²]	=	maximum allowable stress applied to pre-stressing steel during stressing
σ_{pm0}	[N/mm ²]	=	maximum allowable stress in pre-stressing steel after immediate losses
k_1	[-]	=	0.8
k_2	[-]	=	0.95
k_7	[-]	=	0.75
k_8	[-]	=	0.85
f_{pk}	[N/mm ²]	=	characteristic yield strength of pre-stressing steel
$f_{p0.1k}$	[N/mm ²]	=	characteristic 0.1% yield strength of pre-stressing steel

8.7 Strength Verifications

8.7.1 Bending and Normal Force

The combination of a bending moment and normal force could result in both a tensile and compressive stress in the cross-section of an element. As for the concrete civil superstructure design, the restriction posed by the chosen design strategy, viz. no tensile stress in the element and the restriction regarding the maximum compressive stress in the element from the Eurocode are verified.

No tensile stress

For there to be no tensile stress in an element, Equation (8.8a) and Equation (8.8b) should hold for all cross-sections at any point in the element for bending around the z and x axis respectively.

$$\sigma_x = \frac{M_x x}{I_{xx}} - \frac{F}{A_c} - \frac{P_{m\infty}}{A_c} \leq 0 \quad (8.8a)$$

$$\sigma_z = \frac{M_z z}{I_{zz}} - \frac{F}{A_c} - \frac{P_{m\infty}}{A_c} \leq 0 \quad (8.8b)$$

where: σ_x	[N/mm ²]	= stress in x-direction
σ_z	[N/mm ²]	= stress in z-direction
M_x	[Nmm]	= bending moment in x-direction
M_z	[Nmm]	= bending moment in z-direction
x	[mm]	= distance from the centre of gravity towards the outer fibre in x-direction where tension occurs
z	[mm]	= distance from the centre of gravity towards the outer fibre in z-direction where tension occurs
I_{xx}	[mm ⁴]	= mass moment of inertia for bending around the z-axis
I_{zz}	[mm ⁴]	= mass moment of inertia for bending around the x-axis
F	[N]	= axial force (where compression is defined positive)
A_c	[mm ²]	= area of the concrete cross-section
$P_{m\infty}$	[N]	= pre-stressing force after all losses

Maximum compressive stress

According to NEN-EN 1992-1-1 (2011b) Equation (5.42), the compressive stress in a concrete element must conform to Equation (8.9a) and Equation (8.9b) for all cross-sections at any point in the element for bending around the z and x axis respectively.

$$\sigma_x = -\frac{M_x x}{I_{xx}} - \frac{F}{A_c} - \frac{P_{m0}}{A_c} \geq -0.6 f_{ck} \quad (8.9a)$$

$$\sigma_z = -\frac{M_z z}{I_{zz}} - \frac{F}{A_c} - \frac{P_{m0}}{A_c} \geq -0.6 f_{ck} \quad (8.9b)$$

where: x	[mm]	= distance from the centre of gravity towards the outer fibre in x-direction where compression occurs
z	[mm]	= distance from the centre of gravity towards the outer fibre in z-direction where compression occurs
f_{ck}	[N/mm ²]	= characteristic compressive strength of the concrete after hardening
P_{m0}	[N]	= pre-stressing force after immediate losses

8.7.2 Shear Force

According to NEN-EN 1992-1-1 (2011b) Equation 6.2.2 (2), for simply supported pre-stressed elements without shear reinforcement which are not cracked by bending, the shear resistance should be limited by the tensile strength of the concrete and should be calculated using Equation (8.10a) and Equation (8.10b) for shear in x and z-direction respectively.

$$V_{Rd,c,x} = \frac{I_{xx} \cdot b_w}{S_x} \sqrt{f_{ctd}^2 + \alpha \cdot \sigma_{cp} f_{ctd}} \geq V_{Ed,x} \quad (8.10a)$$

$$V_{Rd,c,z} = \frac{I_{zz} \cdot b_w}{S_z} \sqrt{f_{ctd}^2 + \alpha \cdot \sigma_{cp} f_{ctd}} \geq V_{Ed,z} \quad (8.10b)$$

where: $V_{Rd,c,x}$ [N]	=	shear resistance for shear in x-direction
$V_{Rd,c,x}$ [N]	=	shear resistance for shear in x-direction
b_w [mm]	=	width of the cross-section at the center of gravity
S_x [mm ³]	=	the linear surface moment relative to the median in x-direction
S_z [mm ³]	=	the linear surface moment relative to the median in z-direction
f_{ctd} [N/mm ²]	=	design value of the tensile strength of the concrete
α [-]	=	1
σ_{cp} [N/mm ²]	=	the concrete compressive stress at the center of gravity as a result of the axial force and/or the pre-stressing
$V_{Ed,x}$ [N]	=	shear force in x-direction
$V_{Ed,z}$ [N]	=	shear force in z-direction

Note that for a rectangular cross-section: $V_{Rd,c,x} = V_{Rd,c,z}$. Furthermore, if Equation (8.10a) and Equation (8.10b) are satisfied, only the minimum amount of longitudinal reinforcement is required (i.e. no shear reinforcement).

8.7.3 Torsion

St. Venant stress (pure torsion)

With Equation (6.3.2) and article 6.3.2 (5) from NEN-EN 1992-1-1 (2011b), the torsional resistance to pure torsion of a cross-section is to be calculated with Equation (8.11).

$$T_{Rd,c} = 2 \cdot A_k \cdot f_{ctd} \cdot t_{eff,i} \geq T_{Ed} \quad (8.11)$$

where: $T_{Rd,c}$ [Nmm]	=	resistance to pure torsion
A_k [mm ²]	=	area enclosed by the center lines of the connected walls, including hollow parts
$t_{eff,i}$ [mm]	=	effective wall thickness
T_{Ed} [Nmm]	=	torsional moment

If Equation (8.11) is satisfied, only the minimum amount of longitudinal reinforcement is required (i.e. no shear reinforcement).

Warping stress

NEN-EN 1992-1-1 (2011b) 6.3.3 (1) states that for closed and thin walled cross-sections and solid cross-sections, the effects due to warping of the cross-section may be neglected.

8.7.4 Shear and Torsion

According to Equation (6.31) of NEN-EN 1992-1-1 (2011b), if Equation (8.12) is satisfied, only the minimum amount of longitudinal reinforcement is required (i.e. no shear reinforcement).

$$\frac{V_{Ed,i}}{V_{Rd,c,i}} + \frac{T_{Ed}}{T_{Rd,c}} \leq 1 \quad (8.12)$$

Note that, generally for a rectangle-esque cross-section, at two sides of the cross-section the tension due to shear and due to torsion counteract each other whereas at the two other sides the shear flow due to a shear force and torsion coincide. These general characteristics of the shear flow in a cross-section on which both shear forces and torsion are present is depicted in Figure 8.3.

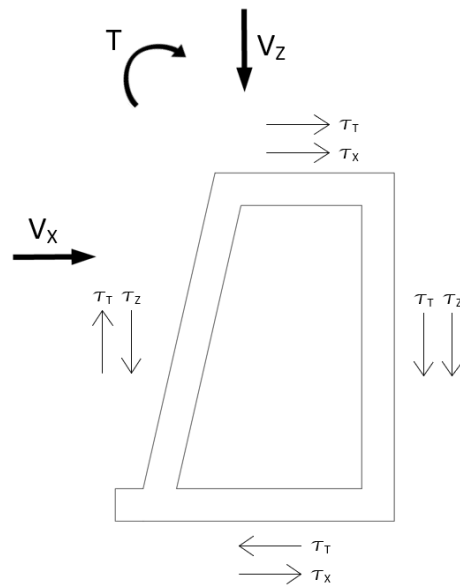


Figure 8.3: Shear flow in a concrete cross-section

8.7.5 Local Spalling

The required spalling reinforcement to resist the tension stresses which develop due to the spreading of a locally introduced (pre-stressing) force can be determined using the method of so-called strut & tie modelling. A general correct set-up of a strut & tie model is depicted in Figure 8.4. Appendix XV presents the specific strut & tie models for the elements where the need arises due to a locally introduced pre-stressing force at the supports.

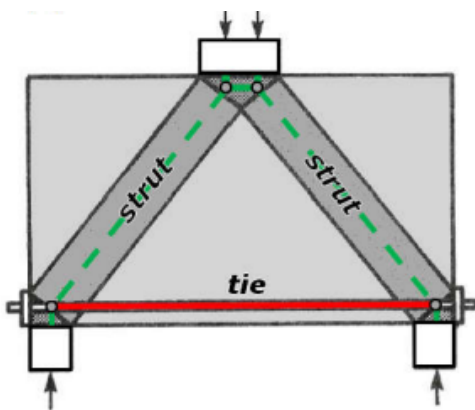


Figure 8.4: General impression of a correct strut & tie model (Molenaar & Voorendt, 2020b)

Looking at Figure 8.4, a locally introduced force at the top distributes itself over a distance equal to the half the effective beam width at the application point. Where the struts, representing the force spread under an ideal angle of 45° , meet the reaction forces developed at half the effective beam width from the introduced force, a tie is present. Said tie makes equilibrium with the inclined force in the strut and the reaction force resulting in a tension force in the tie. Finally, with the introduced force and member geometry known, one is able to proportion the ties and verify the concrete compressive strength at the strut.

Proportion the ties

In general, both transverse pre-stressing as rebar could be applied to account for the tension force in the tie. Where applicable, pre-stressing is applied and Equation (8.13a) should be satisfied. If the member geometry or available space does not allow for transverse pre-stressing, rebar is applied and Equation (8.13b) should be satisfied.

$$A_{p,tie} = \frac{F_{tie}}{\sigma_{p,max}} \quad (8.13a)$$

$$A_{s,tie} = \frac{F_{tie}}{f_{ys}} \quad (8.13b)$$

where: $A_{p,tie}$ [mm²] = required area of pre-stressing steel
 $A_{s,tie}$ [mm²] = required area of rebar
 F_{tie} [N] = tension force in the tie
 $\sigma_{p,max}$ [N/mm²] = maximum allowable stress in the pre-stressing steel
 f_s [N/mm²] = yield strength of the rebar

Strut verification

The actual compression stress in a strut should not exceed the compressive strength of the concrete.

$$\frac{F_{strut}}{w_s h_s} \geq -0.6f_{ck} \quad (8.14)$$

where: F_{strut} [N] = compression force in the strut
 w_s [mm] = strut width
 h_s [mm] = strut height, depending on the node type

8.8 Deflection

The maximum deflection of elements of the civil superstructure should satisfy Equation (8.15), as stated by Vrijburcht (2000).

$$w_{max,x} \leq \frac{1}{200} L_i \quad (8.15)$$

where: $w_{max,x}$ [mm] = maximum deflection of an element in x-direction (lengthwise)
 L_i [mm] = length of the element

8.9 Final Civil Superstructure Design

This section merely presents the final designs of the relevant elements of the civil superstructure: the top beams, sill beams and piers. A complete verification of the civil superstructure can be found in Appendix XV.

8.9.1 Top Beam

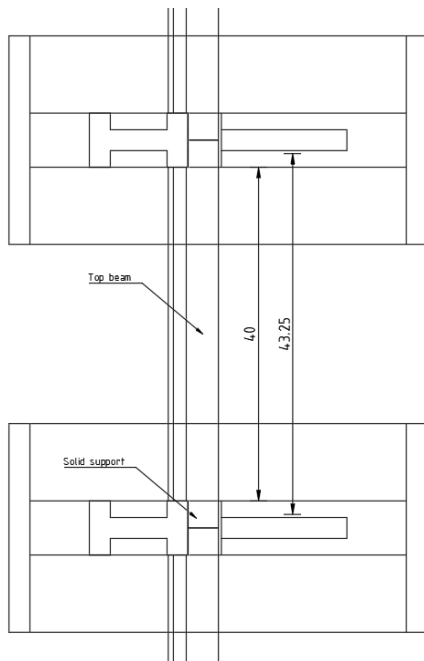


Figure 8.5: Top view. Top beam

Figure 8.5 presents a top view of the top beam with the effective width between two piers (40 m) and the distance between the supports of the top beam (43.25 m).

In order to introduce the local pre-stressing forces at the heads of the beam, the concrete parts at the supports are solid. Figure 8.6 presents a top view of said solid supports. Finally, Figure 8.7 and Figure 8.8 present the cross-sections of the hollow middle part of the top beam and the solid supports, respectively.

Appendix XV.3 presents the complete strength verification of the top beam.

The top beams consist of concrete of class C40/50, pre-stressed with Y1860 pre-stressing steel. The amount of pre-stressing steel applied and the initial pre-stressing force at which the tendons are tensioned are presented in Table 8.1

θ [mm]	strands [nr.]	ducts [nr.]	z_{cp} [mm]	A_p [mm ²]	P_{mi} [kN]	σ_{mi} [N/mm ²]
15.7	55	14	0	115500	162855	1410

Table 8.1: Pre-stressing steel and values for introduced pre-stressing force

where: θ = strand diameter
 strands = number of strand in a duct
 ducts = number of ducts applied
 z_{cp} = equivalent distance between the pre-stressing elements and the centre of gravity
 A_p = area of pre-stressing steel applied
 P_{mi} = initial pre-stressing force applied
 σ_{mi} = initial stress in pre-stressing steel

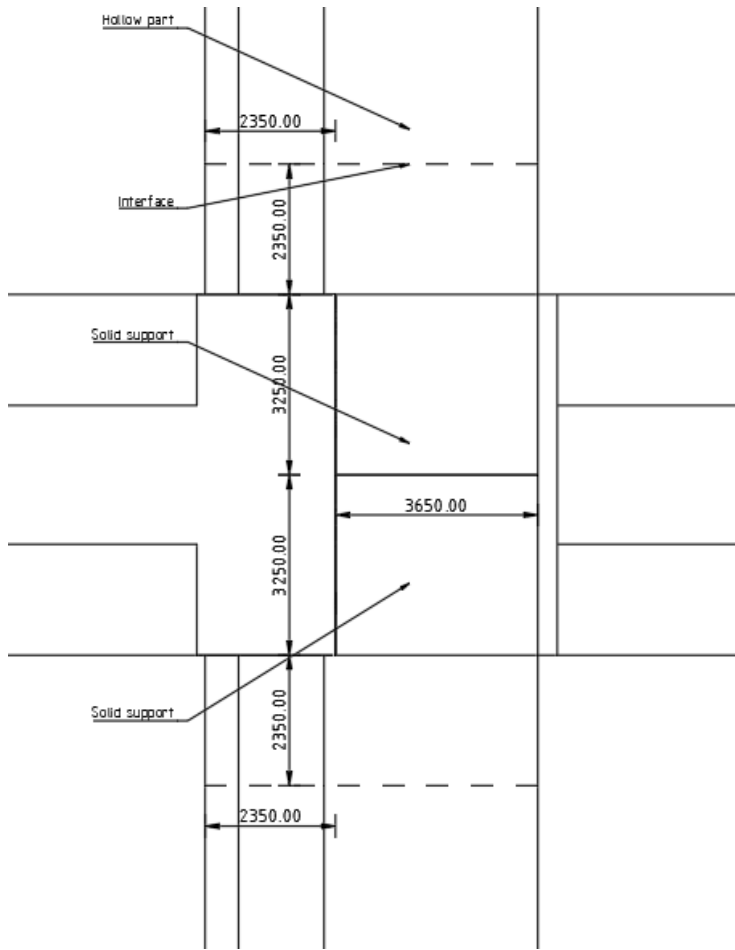


Figure 8.6: Top view. Solid support

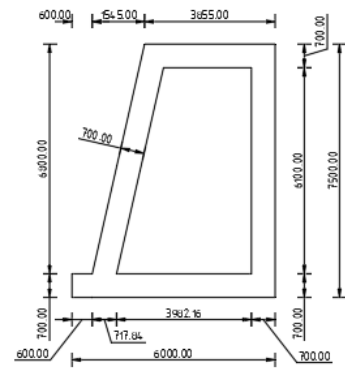


Figure 8.7: Cross-section top beam

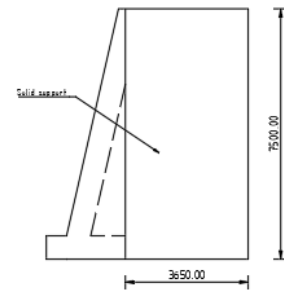


Figure 8.8: Cross-section solid support

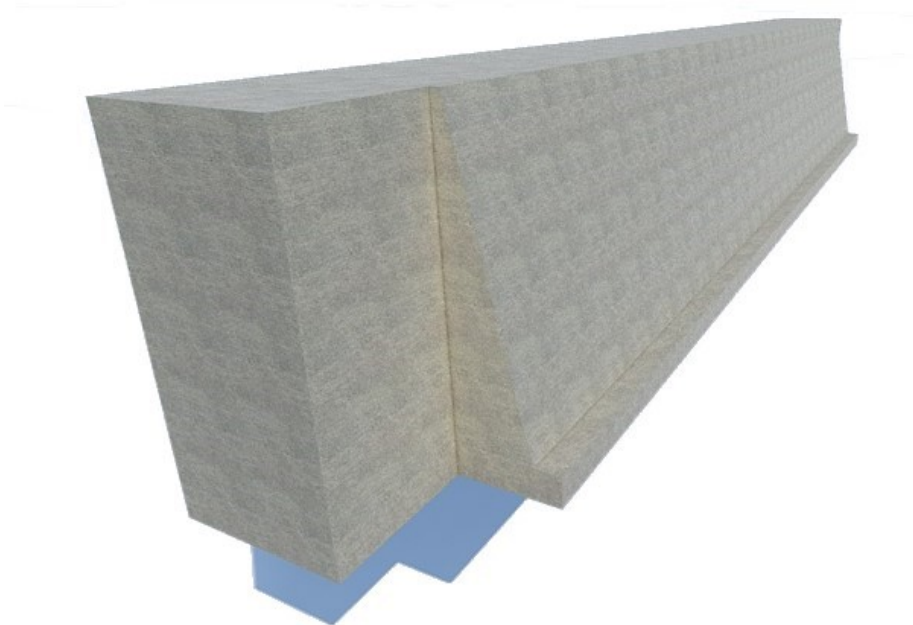


Figure 8.9: 3D render of the concrete top beam

8.9.2 Sill Beam

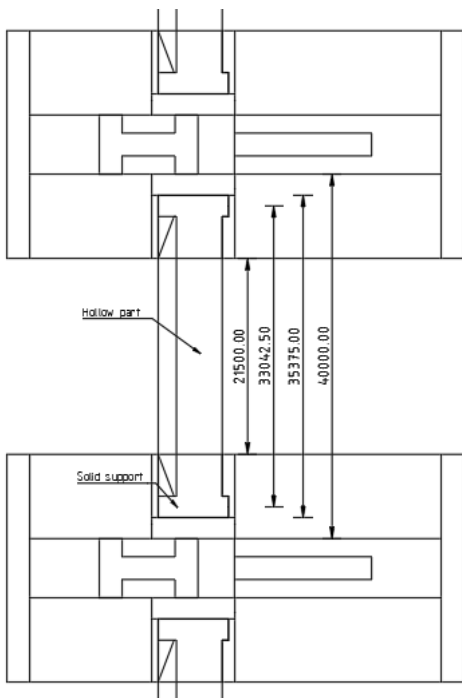


Figure 8.10 presents a top view of the sill beam with the effective width between two piers (40 m). In order to introduce the local pre-stressing forces at the heads of the beam, the concrete parts at the supports are solid. Figure 8.11 presents the front view of the sill beam alone. Finally, Figure 8.12 and Figure 8.13 present the cross-sections of the hollow middle part of the sill beam and the solid supports, respectively.

Appendix XV.4 presents the complete strength verification of the sill beam.

Figure 8.10: Top view. Sill beam

The top beams consist of concrete of class C40/50, pre-stressed with Y1860 pre-stressing steel. The amount of pre-stressing steel applied and the initial pre-stressing force at which the tendons are tensioned are presented in Table 8.2

θ [mm]	strands [nr.]	ducts [nr.]	z_{cp} [mm]	A_p [mm ²]	P_{mi} [kN]	σ_{mi} [N/mm ²]
15.7	55	8	0	66000	93060	1410

Table 8.2: Pre-stressing steel and values for introduced pre-stressing force

- where:
- θ = strand diameter
 - strands = number of strand in a duct
 - ducts = number of ducts applied
 - z_{cp} = equivalent distance between the pre-stressing elements and the centre of gravity
 - A_p = area of pre-stressing steel applied
 - P_{mi} = initial pre-stressing force applied
 - σ_{mi} = initial stress in pre-stressing steel

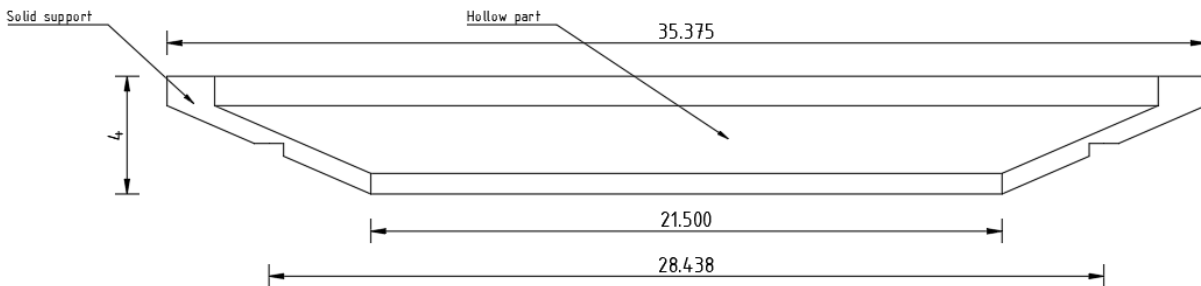


Figure 8.11: Front view. Sole sill beam

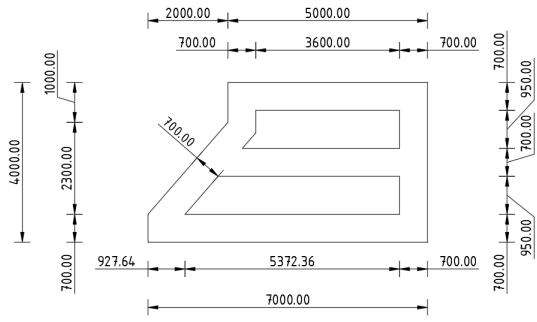


Figure 8.12: Cross-section sill beam

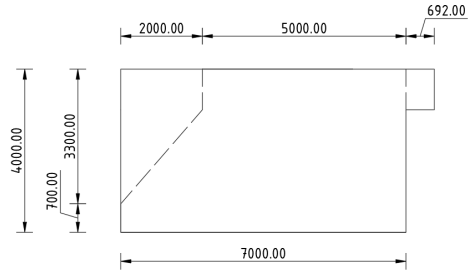


Figure 8.13: Cross-section sill beam solid support

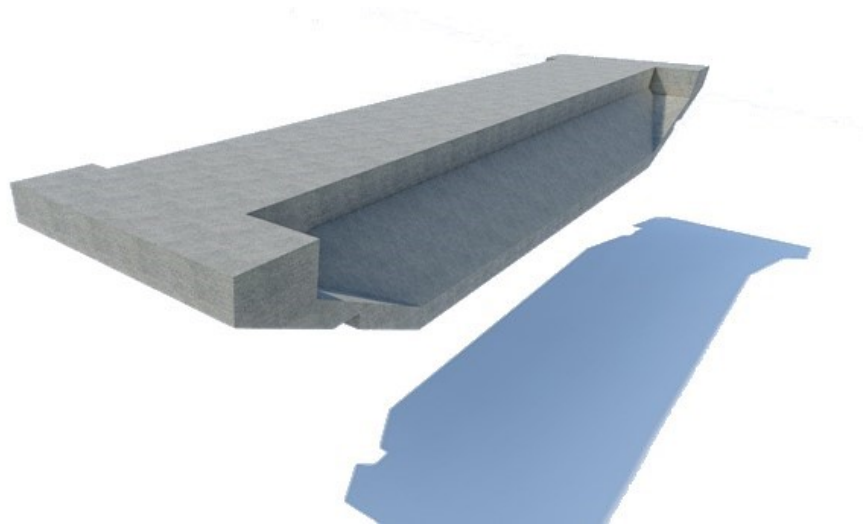


Figure 8.14: 3D render of the concrete sill beam

8.9.3 Pier

Here, only the final dimensions of the piers are presented. Said dimensions are determined as such that sufficient space is available for the required reinforcement. The reinforcement plan and the global analysis of the piers can be found in Appendix XV.5.

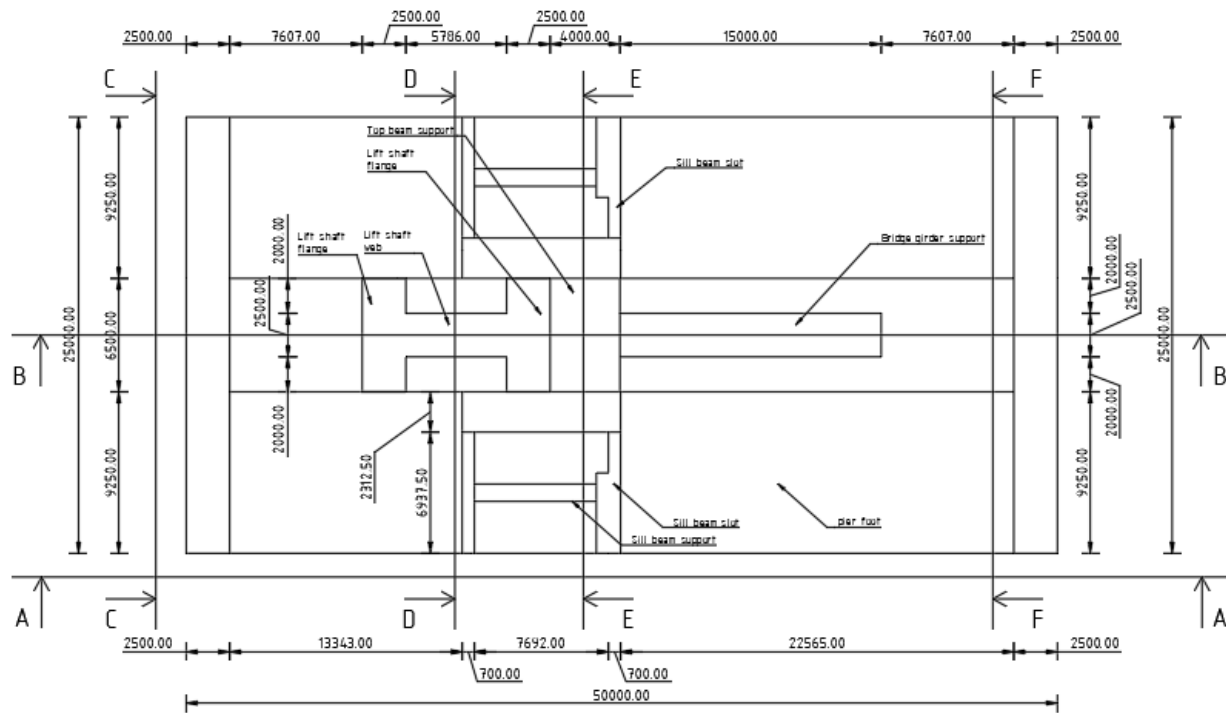


Figure 8.15: Top view. Pier

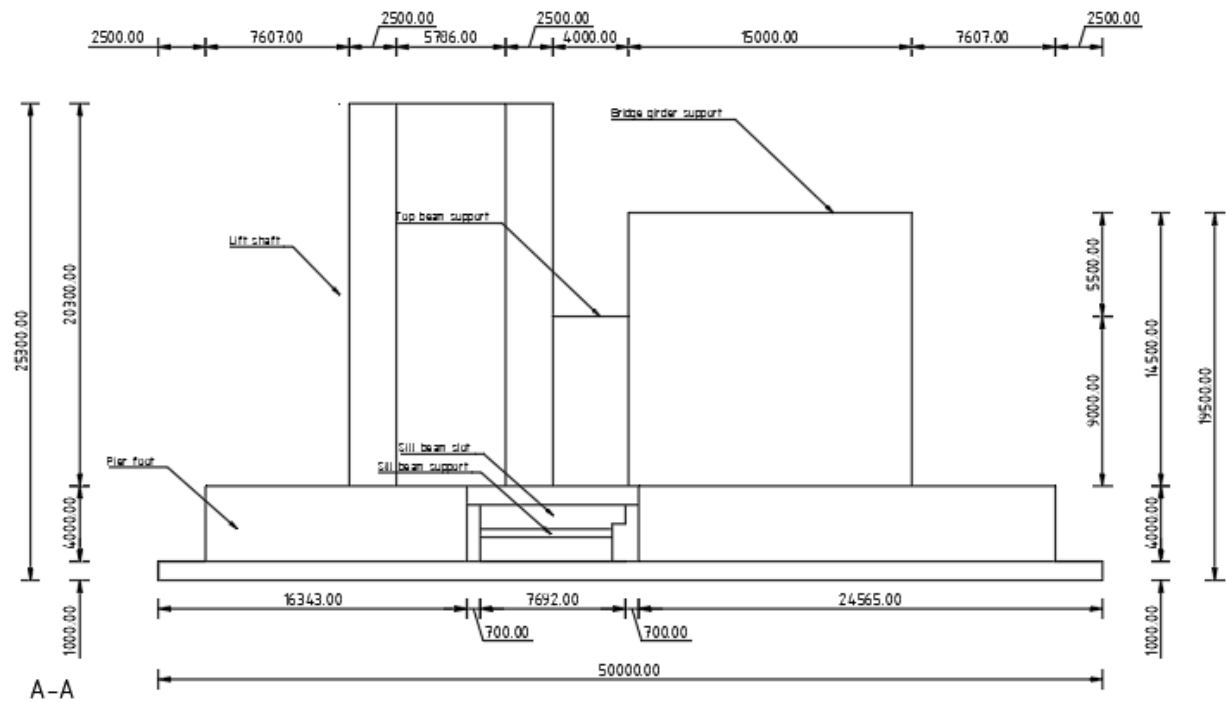


Figure 8.16: Pier (A-A)

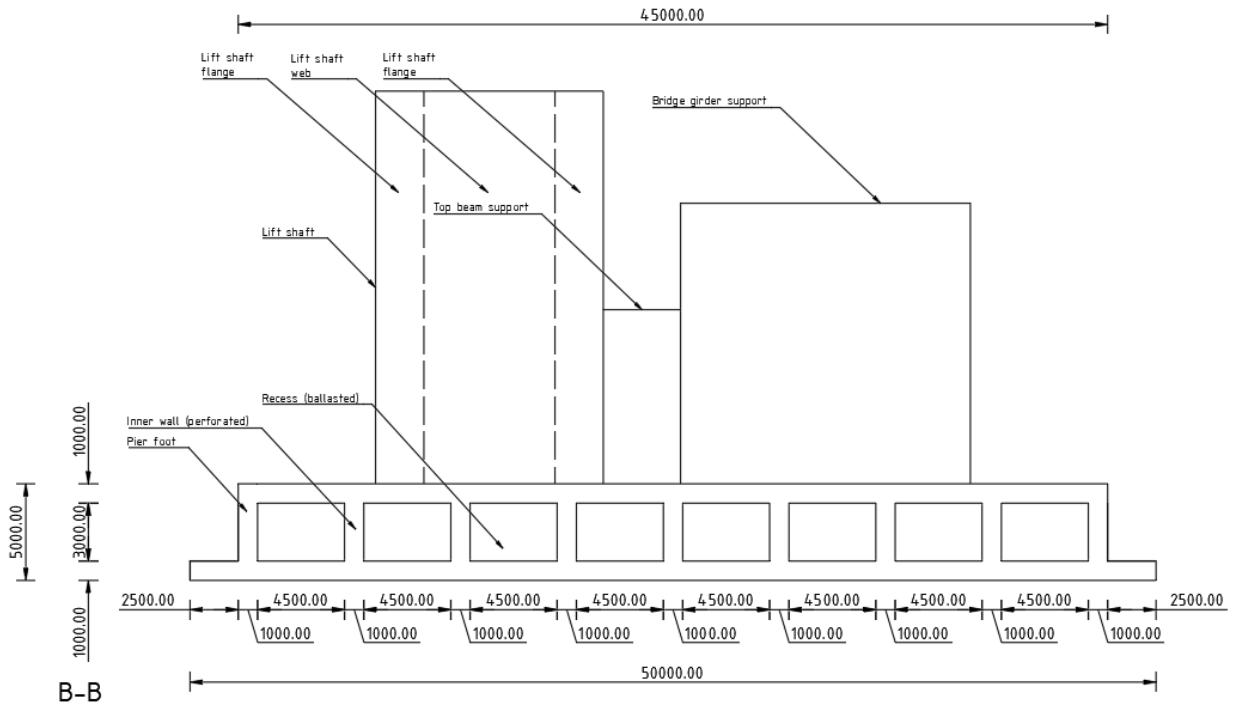


Figure 8.17: Pier (B-B)

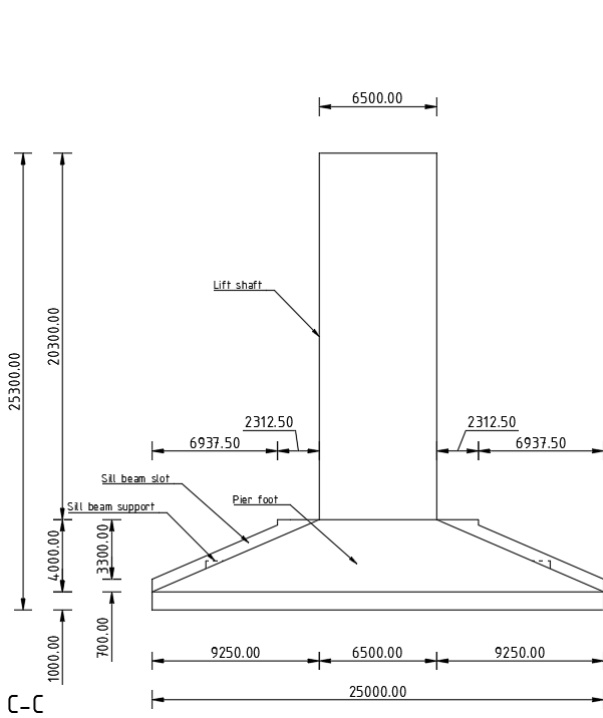


Figure 8.18: Pier (C-C)

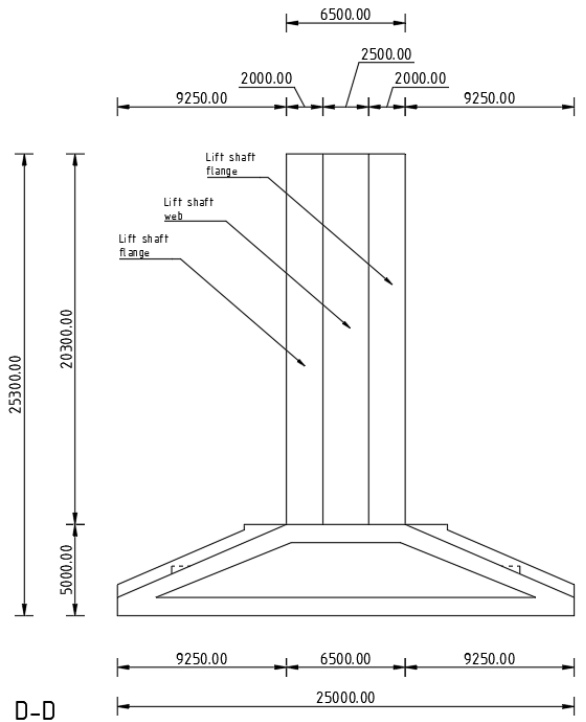


Figure 8.19: Pier (D-D)

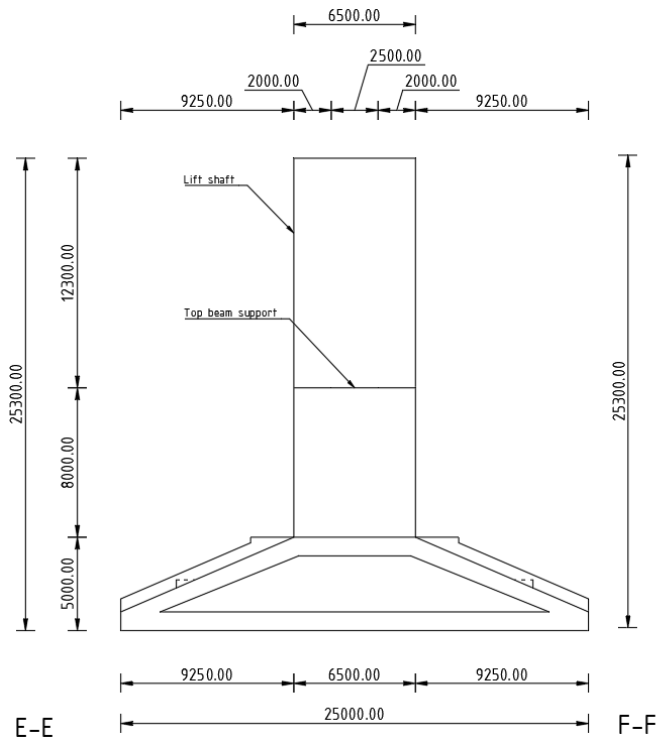


Figure 8.20: Pier (E-E)

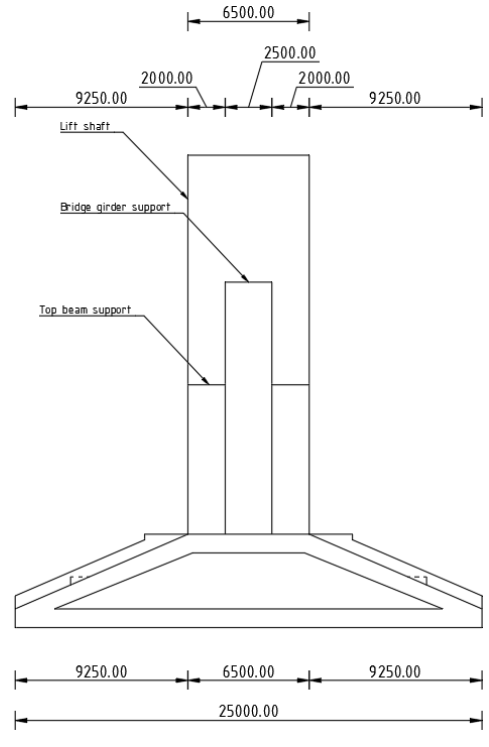


Figure 8.21: Pier (F-F)

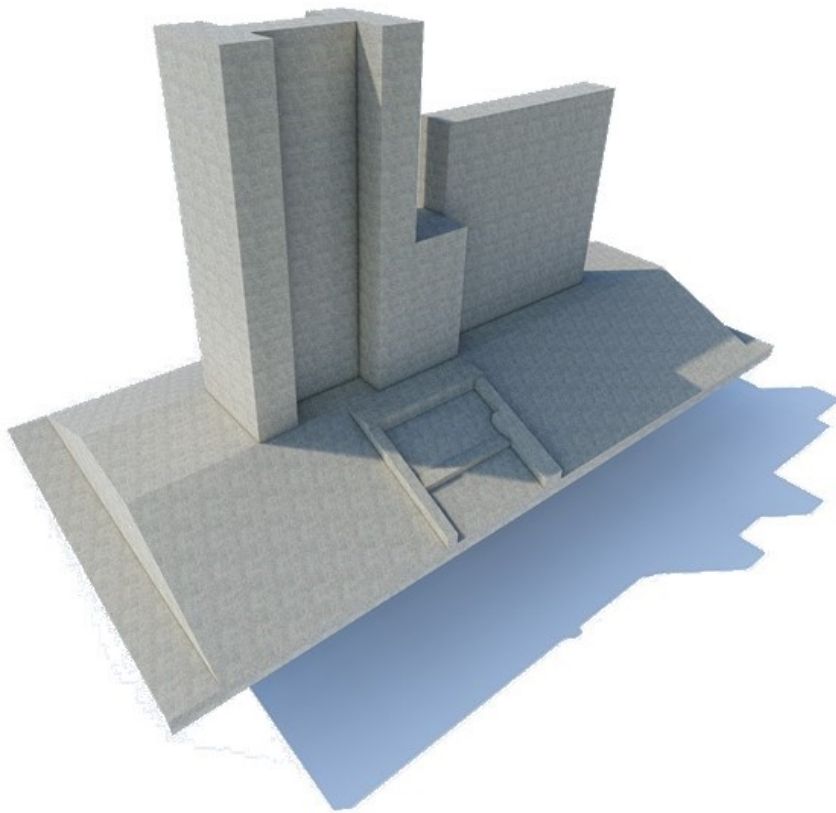


Figure 8.22: 3D render of the concrete pier

9 Global Stability Verification

This chapter presents the global stability verification, as part of the structural design. First, the design strategy is discussed as certain engineering principles are pursued throughout the design considering global stability. Secondly, all relevant limit states and load combinations are presented. Subsequently, the verifications which ought to be made considering the relevant failure mechanisms are presented. The complete verifications can be found in Appendix XVI.

9.1 Design Strategy

Throughout the design, the following engineering principles are pursued:

- *As little concrete as possible*
At the interface between costs (including hidden costs) and stability, it is pursued to keep the monolithic concrete structures as light as possible. While still maintaining - mostly horizontal - stability, said strategy proves to be both cost-efficient and climate robust. While as little concrete as possible is being pursued, the concrete piers ought to be ballasted in order to satisfy horizontal stability.
- *High friction coefficient*
In order to generate as much resistance to horizontal sliding as possible, a relatively high friction coefficient is pursued. By placing the piers on mats and undergrouting the hollow space between the piers and the mats under pressure, the interface between the pier and the seabed is extremely rough. Such a rough interface ensures that shear failure is most likely to take place at the sand body, c.q. seabed, beneath the piers resulting in a high friction coefficient.

9.2 Limit States & Load Combinations

As for the global stability verification, the limit state regarding the loss of static equilibrium of the structure (EQU), the collapse or excessive deformation of the soil where the strengths of soil or rock determine the resistance to be provided (GEO) and the design value of the load with regard to loss of equilibrium of the structure or the subsoil as a result of uplift by water pressure or other vertical loads (UPL), from the Building Decree are considered. The EQU, GEO and UPL limit states represent different failure mechanism regarding the global stability as part of structural failure. Note that for structural failure¹³, the Building Decree is governing over the Water Act as a result of the failure probability distribution as presented in Appendix VI (maximum failure probabilities of 1:100000 per year and 1:52632 per year respectively).

With regard to the EQU, GEO and UPL limit states, the following load combinations are considered:

- A: Maximum positive head is dominant
- B: Maximum negative head is dominant
- H: Ship collision¹⁴
- Lowest LAT
- During construction

All relevant limit states and corresponding load combinations as prescribed in the ROK (2017) (A, B and H) are presented in Appendix XIII. For every verification, c.q. failure mechanism, the governing load combination is determined.

¹³According to and in the Water Act, stability is treated as part of the mechanism of structural failure

¹⁴Note that this load combination is considered an accidental event, say a calamity by the ROK (2017)

9.3 Verifications

9.3.1 Horizontal Stability

In Section 6 it has been established that the prefab construction method is most suitable. A direct consequence of choosing for the prefab construction method is that a foundation on piles is no longer feasible (if possible at all). Given that the subsoil consists mostly of sand (see Section 3.2.3) and that it is very much possible to replace local weak layers and to compact the subsoil, a shallow foundation is feasible and is considered.

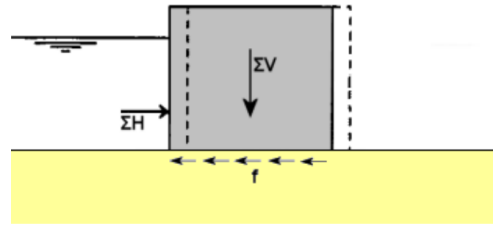


Figure 9.1: Failure mechanism of horizontal stability (Molenaar & Voorendt, 2020b)

The total of the horizontal forces acting on a hydraulic structure based on a shallow foundation should be transferred to the subsoil. The friction force of the subsoil should resist the resulting total acting horizontal force (Molenaar & Voorendt, 2020b).

$$\sum H < f \cdot \sum V \quad (9.1)$$

where: $\sum H$ [kN] = resulting horizontal force
 $\sum V$ [kN] = resulting vertical force
 f [-] = friction coefficient

Note that, due to the mats under the piers and undergrouting of the piers, the friction coefficient is determined using the angle of internal friction of the subsoil.

$$f = \frac{\tan(\phi)}{\gamma_\phi} \quad (9.2)$$

where: ϕ [°] = angle of internal friction of the subsoil
 γ_ϕ [-] = partial safety factor = 1.25

With the angle of internal friction of the newly created, greatly compacted sand layer under the pier of $\phi = 40^\circ$. The friction coefficient, following Equation (9.2), yields $f = 0.67$.

As horizontal stability concerns an EQU limit state, partial factors according to the Eurocode (2019) Table A2.4(A) are used. For the governing load combination, A: Maximum positive head is dominant, the Delta Barrier is horizontally stable (see Appendix XVI.2.1).

9.3.2 Vertical Stability: Bearing Capacity

The vertical effective soil stress, required to resist the acting loads, should not exceed the maximum bearing capacity of the soil, otherwise the soil will collapse (Molenaar & Voorendt, 2020b). Table 9.1 gives an impression of the failure mechanism regarding the collapse of soil under a structure according to Prandtl and Brinch Hansen.

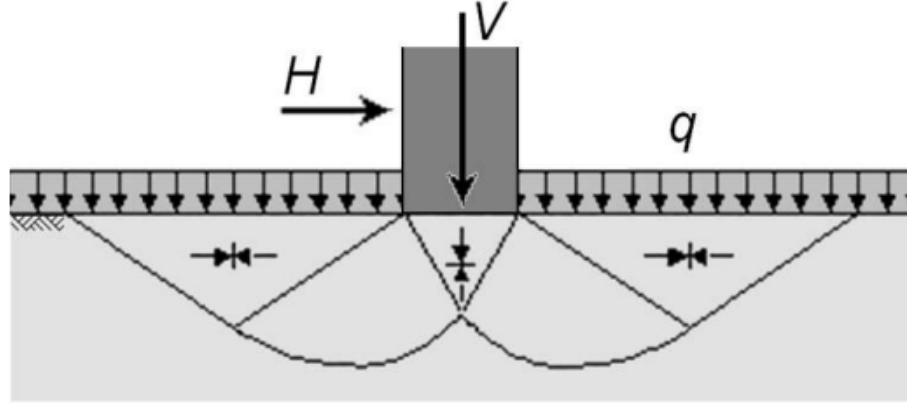


Table 9.1: Failure mechanism of vertical stability: bearing capacity (Molenaar & Voorendt, 2020b)

$$\sigma_{k,max} = \frac{\sum V}{B L} + \frac{\sum M}{\frac{1}{6} B^2 L} < p'_{max} \quad (9.3)$$

where: $\sigma_{k,max}$ [kN/m²] = maximum soil stress
 B [m] = width of the structure (parallel to the resultant horizontal force)
 L [m] = length of the structure (perpendicular to the resultant horizontal force)
 p'_{max} [kN/m²] = maximum bearing capacity of the subsoil

As the bearing capacity of the subsoil concerns a GEO limit state, partial factors according to Figure XIII.2 as proposed in the ROK(2021) are used. For the governing load combination, A: Maximum positive head is dominant, the bearing capacity of the subsoil is sufficient (see Appendix XVI.2.2).

Finally, as sand cannot or barely cope with tensile forces Equation (9.4) should be satisfied.

$$\sigma_{k,min} > 0 \quad (9.4)$$

in which: $\sigma_{k,min} = \frac{\sum V}{B L} - \frac{\sum M}{\frac{1}{6} B^2 L}$

Note that Equation (9.4) translates to Equation (9.7) as presented in Section 9.3.4 and is regarded as a verification needed to prevent rotational instability.

9.3.3 Vertical Stability: Settlements

The settlement of the subsoil as a result of the added weight of the Delta Barrier can be calculated by means of the equation as proposed by Koppejan (Molenaar & Voorendt, 2020b).

$$\epsilon = \left(\frac{U}{C'_p} + \frac{1}{C'_s} \log \left(\frac{\Delta t}{t_{ref}} \right) \right) \cdot \ln \left(\frac{\sigma'_{v;i} + \Delta \sigma'_v}{\sigma'_{v;i}} \right) \quad (9.5)$$

where:	ϵ	[-]	=	relative compression
	U	[-]	=	degree of consolidation = 1
	C'_p	[-]	=	primary compression coefficient
	C'_s	[-]	=	secondary compression coefficient
	Δt	[days]	=	duration after the application of the additional loading
	t_{ref}	[days]	=	reference duration (one day)
	$\Delta \sigma'_v$	[kPa]	=	increase of the vertical effective stress
	$\sigma'_{v;i}$	[kPa]	=	initial vertical effective pressure

After calculating the relative compression for every distinguished soil layer according to Equation (9.5), the total settlement is computed by means of Equation (9.6).

$$\Delta h = \sum_i^n \epsilon_i h_i \quad (9.6)$$

where:	Δh	[mm]	=	total settlement
	ϵ_i	[-]	=	relative compression of soil layer i
	h_i	[mm]	=	thickness of soil layer i
	n	[-]	=	number of soil layers

Finally, it is assumed that $\Delta h < 100$ mm should hold, as was in the design of the Oosterscheldekering (Visser, 1986a). As the settlement of the subsoil concerns a GEO limit state, partial factors according to Figure XIII.2 as proposed in the ROK(2021) are used. The governing load combination, is the situation with the lowest possible water level, say lowest astronomical tide (LAT) at completion 2050 where climate scenario SSP2-4.5 is considered. For this governing load combination, the total settlement remains lower than 100 mm (see Appendix XVI.2.3).

9.3.4 Rotational Stability

As per Equation (9.4), it is stipulated that the soil stresses necessary for rotational stability may only be compressive. This yields the following verification regarding the resistance to rotational stability of the structure:

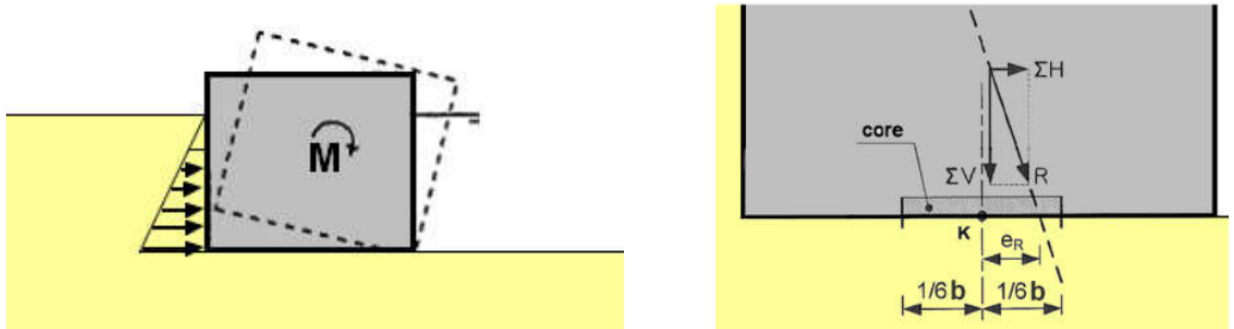


Table 9.2: Failure mechanism of rotational stability (Molenaar & Voorendt, 2020b)

$$e_R = \frac{\sum M}{\sum V} \leq \frac{1}{6} B \quad (9.7)$$

As rotational stability concerns an EQU limit state, partial factors according to the Eurocode (2019) Table A2.4(A) are used. For the governing load combination, A: Maximum positive head is dominant, the Delta Barrier is stable with regards to rotation (see Appendix XVI.2.4).

9.3.5 Uplift

For any point in time or building stage where the piers should remain stable on the bed the total self weight of the structure and the resultant downward vertical force should be greater than the upward water pressure under the pier, i.e. Equation (9.8) should hold at all times.

$$\sum V \geq 0 \quad (9.8)$$

where: V [kN] = resultant vertical force, where downwards is defined positive

As uplift concerns the UPL limit state, partial factors according to A.4 (1)P and A.4 (2)P from NEN-EN 1997-1 (2016) must be used. The governing load combination here concerns the situation during construction where only the pier has been placed and a high water event occurs with a return period of 100000 years and climate scenario SSP5-8.5. Note that during this scenario, the water levels at sea and the Tidal Lake are the same. For the governing load combination, uplift does not occur (see Appendix XVI.2.5).

9.3.6 Scour

In order to prevent scour directly adjacent to the Delta Barrier (and internal erosion) a granular, geometrically closed filter is designed. Given the consequences if the barrier subsides (e.g. distortion of the piers) for the essential function of the barrier structure as a safeguard against flooding, the failure probability of the filter must be very low. Hence, a geometrically closed filter seems appropriate.

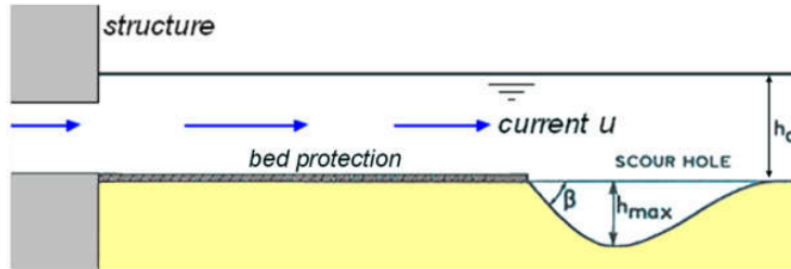


Table 9.3: Failure mechanism of scour (Molenaar & Voorendt, 2020b)

The top layer of the granular, geometrically closed filter should be stable in flow¹⁵, layering of the filter should be as such that the stability (between filter layers) and the permeability of the filter is sufficient and the bottom protection should be of sufficient length in order for the scour hole adjacent to the filter not to cause instability of the piers. This section merely presents the overall result, whereas Appendix XVI.2 gives the complete verifications and elaboration.

Critical flow patterns

The critical flow patterns, i.e. the governing flow velocities for which the bottom protection ought to be designed, are a result of plane jet flow for the case of one failing gate (Tidal Lake side) and tidal flow velocities (sea side).

After the reattachment point and after sudden broadening of the flow area behind the piers, the flow pattern can be schematized by a plane jet. Schiereck (2019) proposes Equation (9.9) for the development (say dispersion) of the flow velocity for a plane jet in x and y-direction after the reattachment point, in the region of fully developed flow.

$$\bar{u} = \frac{3.5\bar{u}_0}{\sqrt{x/B}} e^{\left(-0.693\left(\frac{y}{0.1x}\right)^2\right)} \tag{9.9}$$

where: \bar{u} [m/s] = depth-averaged flow velocity after reattachment point
 B [m] = half the effective length = 20

Finally, Figure 9.2 depicts the flow patterns at both the sea side and Tidal Lake side for their respective critical flow velocities. Until the reattachment point (at about 12B, represented by the black dashed lines), the depth-averaged flow velocity is assumed equal to the depth-averaged flow velocity at the reattachment point.

¹⁵Aspects such as stability in waves, falling and/or dragging anchors and ship collision, although of importance, have not been considered

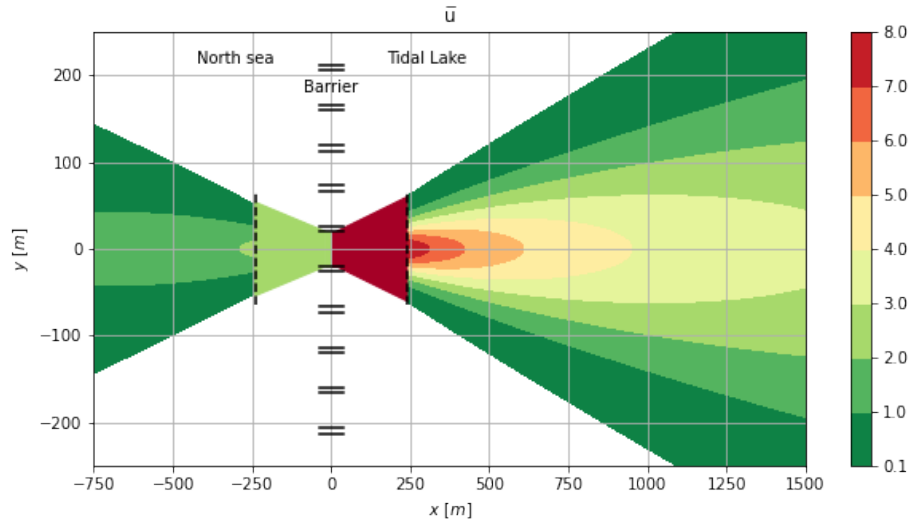


Figure 9.2: Critical flow patterns

Bed protection length

In order to ensure the stability of the Delta Barrier, a potential scour hole must be kept at sufficient length from the structure as such that a developing sliding plane can not reach the structure. Figure 9.3 gives an impression of the failure mechanism of instability due to a scour hole and all relevant parameters.

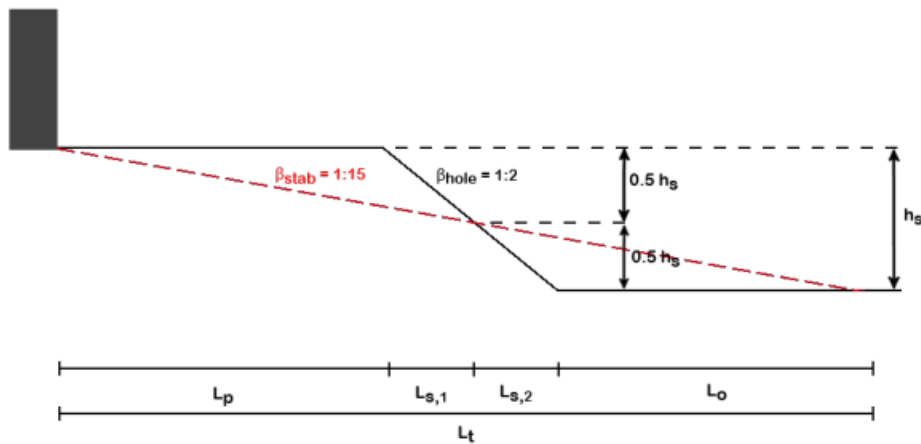


Figure 9.3: Instability due to a scour hole (Donkers, 2021)

The depth of the scour hole behind the scour protection, the consistency of the soil and the slope of the scour hole are the most important parameters which determine the required length of the scour protection. Equation (9.10), as argued by Schiereck (2019), is used to determine the required bed protection length.

$$L_p = h_s \cdot \frac{1}{2(\beta_{stab} - \beta_{soil})} \quad (9.10)$$

where: L_p [m] = required bed protection length
 h_s [m] = scour hole depth
 β_{stab} [-] = slope after sliding
 β_{soil} [-] = slope before sliding

As for the slope after sliding (β_{stab}), Schiereck (2019) indicates that a slope of 1:15 is a reasonable estimate for loosely packed sand. The slope before sliding (β_{soil}) is assumed to be 1:2.

The scour hole depth at the end of the bottom protection for the critical flow velocities (see Figure 9.2) can be estimated by finding the equilibrium (clear-water) scour depth using Equation (9.11) (Schiereck, 2019).

$$h_s = \frac{0.5\alpha\bar{u} - \bar{u}_c}{\bar{u}_c} \cdot h_0 \quad (9.11)$$

where: h_s [m] = equilibrium clear water scour hole depth
 α [-] = $1.5 + 5 \cdot r \cdot f_c$
 r [-] = relative turbulence = 0.3 for jets
 f_c [-] = $\max(C/40; 1)$
 C [\sqrt{m}/s] = Chezy coefficient
 \bar{u}_c [m/s] = critical flow velocity of the bed material
 h_0 [m] = water depth

Finally, the required bed protection lengths are calculated using Equation (9.10) for both the sea and Tidal Lake side. Table 9.4 presents all relevant parameters needed for said calculation and the required lengths for both sides. See Appendix XVI.2 for a complete elaboration.

Side	α [-]	\bar{u} [m/s]	\bar{u}_c [m/s]	h_s [m]	L_p [m]
Sea	5.13	1.38	0.29	90	600
Tidal Lake	5.13	3.24	0.29	222	1450

Table 9.4: Required bed protection length with relevant parameters

Stability of the top layer

The stability in flow of the top layer is calculated using the equation as proposed by Izbash (Equation (9.12) by Schiereck (2019)). As opposed to the standard approach proposed by Shields, the Izbash formula is used especially in cases of non-uniform flow or in cases of e.g. water jets (Schiereck, 2019). As the flow behind an opening of the Delta Barrier is all but uniform and water jets are plenty behind the piers, using the formula proposed by Izbash (instead of Shields) seems valid.

$$d = 0.7 \frac{u_c^2}{2g\Delta} \quad (9.12)$$

where: d [m] = diameter of the top layer
 u_c [m/s] = corresponding critical flow velocity
 g [m/s^2] = gravitational acceleration = 9.81
 Δ [-] = $\frac{\rho_s - \rho_w}{\rho_w}$
 ρ_s [kg/m^3] = density of the top layer stones = 2650
 ρ_w [kg/m^3] = density of the (sea) water = 1025

It should be noted that Izbash did not define the specific place of the velocity (u_c), neither is it very clear how the diameter is defined. As Izbash did his tests with big stones in relatively shallow water, one may assume that the diameter in Equation (9.12) is equal to the nominal diameter (d_n). As for the critical velocity one may assume that the near-bed velocity should be used. Though, conservatively here, the depth-averaged velocity is used.

Using the critical flow patterns from Figure 9.2 and the bed protection lengths from Table 9.4, the required stone sizes of the top layers can be determined. Table 9.5 and Table 9.6 present the top layer design for the Tidal Lake side and sea side respectively.

Section nr.	Class name	range (x) [m]	Length [m]	d_{n50} [m]	\bar{u}_c [m/s]
1	Non-standard	0 - 310	310	1.82	7.88
2	HM _A 6000-10000	310 - 375	65	1.44	7.00
3	HM _A 3000-6000	375 - 495	120	1.18	6.35
4	HM _A 1000-3000	495 - 755	260	0.90	5.54
5	HM _A 300-1000	755 - 1310	555	0.59	4.49
6	HM _A 40-200	1310 - 1450	140	0.34	3.41

Table 9.5: Top layers Tidal Lake side

Section nr.	Class name	range (x) [m]	Length [m]	d_{n50} [m]	\bar{u}_c [m/s]
7	LM _A 5 - 40	-0 - -265	265	0.17	2.41
8	CP90/250	-265 - -345	80	0.128	2.09
9	CP90/180	-345 - -525	180	0.097	1.82
10	CP45/125	-525 - -600	75	0.064	1.48

Table 9.6: Top layers sea side

Filter layering

The subsequent filter layers should obey three criteria, presented below by equations Equation (9.13a), Equation (9.13b), Equation (9.13c) considering stability, permeability and internal stability respectively (Schiereck, 2019).

$$\frac{d_{15F}}{d_{85B}} < 5 \quad (9.13a)$$

$$\frac{d_{15F}}{d_{15B}} > 5 \quad (9.13b)$$

$$\frac{d_{60}}{d_{10}} < 10 \quad (9.13c)$$

Using both standard and non-standard gradings (see Table XVI.23 for the characteristics), Table 9.7 and Table 9.8 present the filter layering per section (as specified in Table 9.5 and Table 9.6) for the Tidal Lake side and sea side respectively.

Section nr.	1	2	3	4	5	6
Layer nr.	1	2	3	4	5	6
	14000-18000	HM _A 6000-10000	HM _A 3000-6000	HM _A 1000-3000	HM _A 300-1000	LM _A 40-200
	LM _A 40-200	LM _A 40-200	LM _A 10-60	LM _A 5-40	CP90/180	CP45/125
	CP45/125	CP45/125	CP45/125	Gravel (course)	Gravel (course)	Gravel (course)
	Gravel (course)	Gravel (course)	Gravel (course)	Gravel (fine)	Gravel (fine)	Gravel (fine)
	Gravel (fine)	Gravel (fine)	Gravel (fine)			
Thickness ($\sum t$)	5.6 m	4.6 m	3.6 m	2.9 m	2.1 m	1.6 m

Table 9.7: Filter layering Tidal Lake side

Section nr.	7	8	9	10
Layer nr. 1	LM _A 5-40	CP90/250	CP90/180	CP45/125
Layer nr. 2	Gravel (course)	Gravel (course)	Gravel (course)	Gravel (course)
Layer nr. 3	Gravel (fine)	Gravel (fine)	Gravel (fine)	Gravel (fine)
Thickness ($\sum t$)	0.9 m	0.6 m	0.6 m	0.6 m

Table 9.8: Filter layering sea side

Final design

Finally, Figure 9.4 presents the final design of the bottom protection.

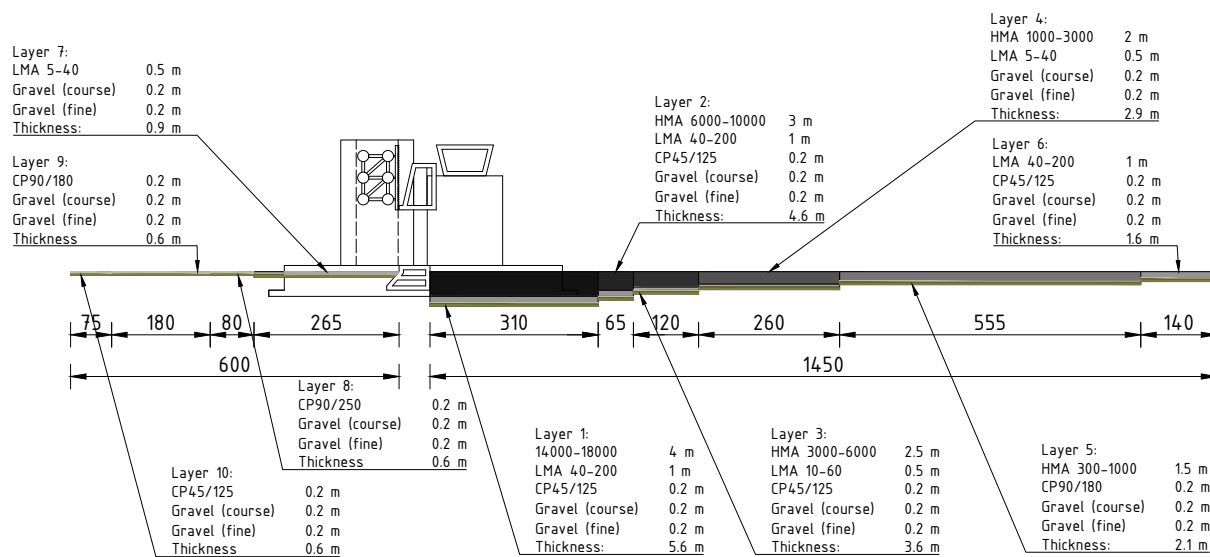


Figure 9.4: Final design bottom protection (not to scale)

9.3.7 Internal Erosion

In general, the failure mechanism of internal erosion consists of the following phases which have to occur subsequently in order to cause failure (say structural collapse) as posed by Jonkman et al. (2021):

- a) Uplift
The pore pressures in the aquifer increase due to the large hydraulic head on the river side. If the upward pressure on the low water side of the barrier exceeds the weight of the blanket layer (aquitar), the latter is lifted up and ruptures. Note that in this specific case, no impermeable blanket layer is present and the subsoil solely consists of permeable material (viz. sand and filter layers).
- b) Seepage
The pore pressures in the aquifer increase due to the large hydraulic head over the barrier. This pressure gradient results in a groundwater flow from the high to low pressure side and groundwater starts flowing upward through the blanket layer.
- c) Start of erosion (heave)
If the gradient at the exit point (also called exit gradient) exceeds a critical (heave) gradient, sand particles can start eroding.

- d) Backward Erosion

The erosion progresses upstream forming so-called "pipes", networks of erosion channels. The eroded material around the exit point starts forming sand boils. The erosion may stop even under a constant head difference depending on the ground conditions and flow pattern.

- e) Continuous Pipe

If the erosion does not stop and the pipes reach the sea side of the barrier, the flow velocity increases drastically due to the loss of hydraulic resistance.

- f) Collapse

The structure is undermined and collapses.

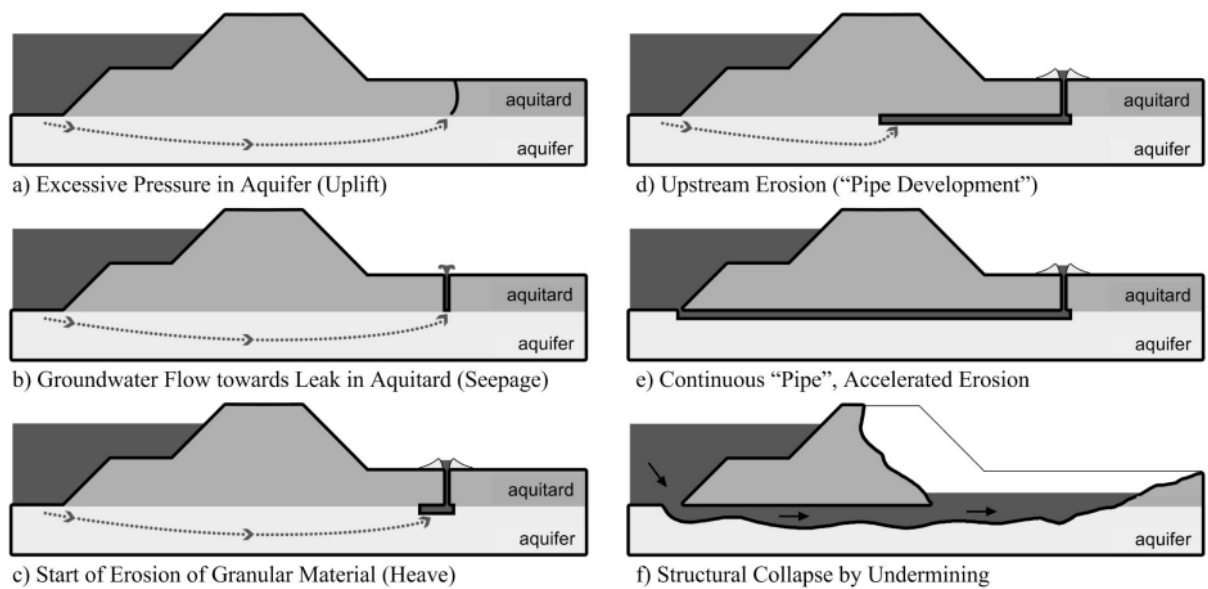


Figure 9.5: Phases of the failure mechanism of internal erosion¹⁶(Jonkman et al., 2021)

By applying a well designed granular, geometrically closed filter, the start of erosion (i.e. heave) is prevented completely and hence the failure mechanism of internal erosion can not occur. Although certain groundwater flow underneath the structure is permitted, this will not result in structural collapse by undermining. Water pressure are able to dissipate through the granular filter while soil particles are restrained from protruding.

¹⁶Note that phase a (uplift) does not occur in this specific case as the subsoil consists of solely permeable material

10 Construction Planning and Costs

This chapter provides an estimate of the construction planning (corresponding with the construction sequence presented in Chapter 6) and the accompanying costs as the last phase of the structural design. Do note that this chapter merely provides a rough indication of both construction time and costs for this preliminary design stage. The Oosterscheldekering planning by Visser (1986a) is taken as a guide.

10.1 Construction Planning

Figure 10.1 depicts the estimate of the construction planning focused on the main activities as part of the construction method (see Section 6). The year of completion coincides with the year until which the current HWBP as per the 2017 Water Act expires. In total, the construction time is estimated to be 5 years with completion in the end of 2050. The critical path of the planning encompasses all construction activities due to parallel planning of the activities. Delay in one construction activity would result in delay of the successive activity.

The large uncertainties in construction time are not presented in Figure 10.1. Nonetheless, the uncertainties in construction time are taken into account in the cost estimate of the Delta Barrier in Section 10.2.

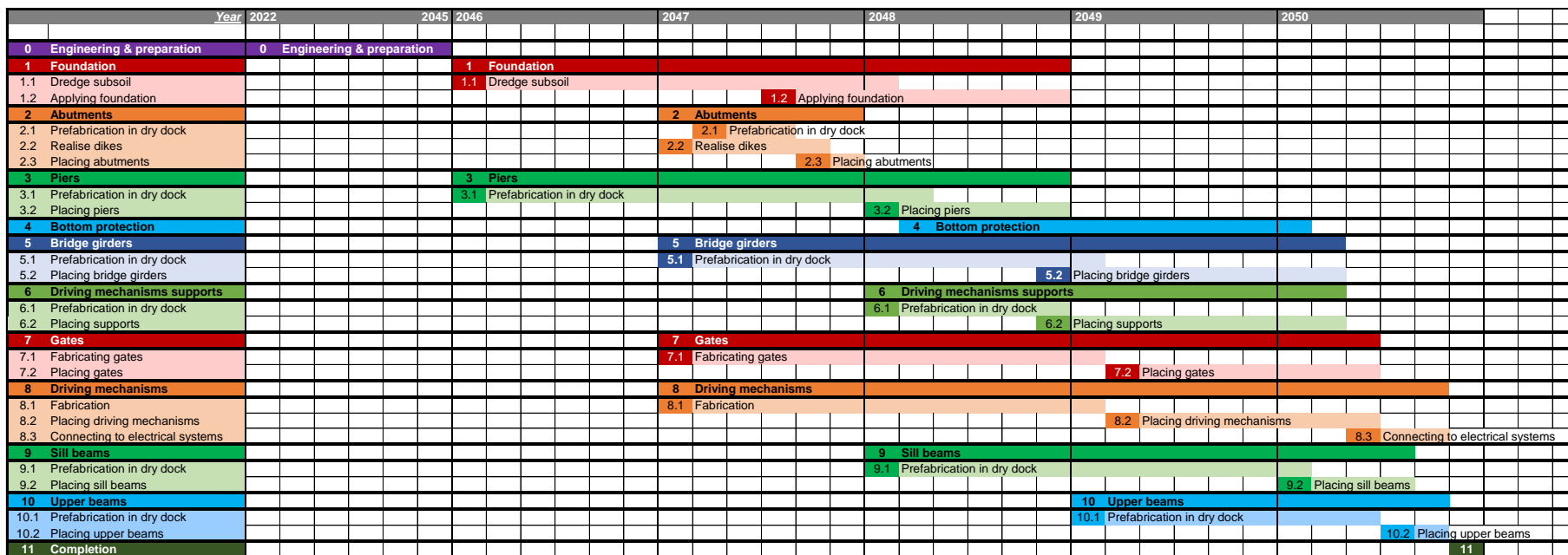


Figure 10.1: Construction planning on main activities

10.2 Construction Costs

The construction costs can generally be split in say three categories: production costs, execution costs and preparation, unforeseen and overhead costs. For the first two categories, a reasonable estimate can be made as most elements of the Delta Barrier have been designed as part of this thesis. The cost estimate (expected values) of these categories are depicted in Table 10.1. All costs represent price level 2022.

Nr.	Description	Costs [m. €]	Remarks
1	Foundation	270.5	
1.1	<i>Dredging</i>	5	ca. 740000 m ³ of soil
1.2	<i>Replacing</i>	13.5	Replacing of weak soil layers
1.3	<i>Compacting</i>	52	ca. 62450 m ² with specialised vessel
1.4	<i>Foundation mats</i>	200	ca. 62450 m ² . Sinking with specialised vessel
2	Abutments	10	
3	Piers	141.9	
3.1	<i>Prefab</i>	61.1	ca. 130000 m ³ of concrete
3.2	<i>Placing</i>	80.8	Sinking with specialised vessel
4	Bottom protection	592.97	
4.1	<i>Stones</i>	468.75	ca. 6250000 m ³ of stones
4.2	<i>Placing</i>	124.22	ca. 2.6 km ² . Appliance with specialised (fallpipe) vessel
5	Bridge girders	44.97	
5.1	<i>Prefab</i>	10.37	ca. 13500 m ³ of concrete
5.2	<i>Placing</i>	34.6	Hoisting with specialised vessel
6	Driving mechanisms supports	37.85	
6.1	<i>Prefab</i>	6.05	ca. 7800 m ³ of concrete
6.2	<i>Placing</i>	31.8	Hoisting with specialised vessel
7	Gates	311.7	
7.1	<i>Steel</i>	280	ca. 28000000 kg of steel
7.2	<i>Placing</i>	31.7	Hoisting with specialised vessel
8	Driving mechanisms	420	50 hydraulic cylinders, electrical installations included
9	Sill beams	45.3	
9.1	<i>Prefab</i>	11.1	ca. 12500 m ³ of concrete
9.2	<i>Placing</i>	34.2	Sinking with specialised vessel
10	Upper beams	43.43	
10.1	<i>Prefab</i>	11.73	ca. 16250 m ³ of concrete
10.2	<i>Placing</i>	31.7	Hoisting with specialised vessel
Subtotal (1-10)		1918.60	

Table 10.1: Construction costs excl. preparation, unforeseen and overhead costs (price level 2022)

As for the latter three categories: preparation, unforeseen and overhead costs, a reasonable estimate is rather difficult to make due to large insecurities and many assumptions which are still present in the preliminary design stage. Nonetheless, a crude estimate is given for said costs in Table 10.2. Adding the crude estimates of the preparation, unforeseen and overhead costs to the subtotal from Table 10.1 yields an estimate of the expected value of the total costs.

Nr.	Description	Costs [m. €]	Remarks
0	Preparations	550	
0.1	Engineering	191.86	10% of subtotal. Includes organisation and project management
0.2	Equipment	200	Specialised vessels, tugboats, scaffolding etc.
0.3	Dry dock	100	Construction of the dry dock
0.4	Harbour	100	Construction of a construction harbour
	Unforeseen	287.79	15% of subtotal
	Overhead	287.79	15% of subtotal
	Subtotal (1-10)	1918.60	
	Total	3086.04	

Table 10.2: Crude estimate of preparation, unforeseen and overhead costs and concluding total costs (price level 2022)

In conclusion, the expected value of the subtotal from the production and execution costs (1918.60 m. euro) added to the crude estimates for preparation, unforeseen and overhead costs (1167.44 m. euro) yields a total expected costs estimate for the Delta Barrier of *3086.04 m. euro* (price level 2022). Translated per metre barrier, for the 1249 metre long Delta Barrier, results in 2.47 m. euro/m.

It should be noted that the many insecurities in the cost estimate, e.g. the construction time per element, the cost of materials and vessels, the amount of materials to be used and the preparation costs, plead for presenting the total costs using a certain confidence interval. Hence, a Monte Carlo simulation is conducted to include the many uncertainties into the cost estimate (see Appendix XVII). The Monte Carlo simulation yields a standard deviation (σ) of the total costs of ca. 412 m. euro. Presenting the total costs by means of the bandwidth ($\mu-\sigma$; $\mu+\sigma$) results in a total cost estimate of *2674 - 3498 million euro* (price level 2022).

11 Discussion

Several assumptions and design choices have been made during the design process which have had a significant impact on the preliminary design. In this section, the assumptions and design choices with a large influence on the preliminary design are discussed.

Hydra-NL

Hydra-NL software has been used to determine boundary conditions at sea for different values of sea level rise and return periods. Delta21 however, is not incorporated in the Hydra-NL database. For this reason, a location with similar characteristics (such as sheltering from the same wind direction and incident wave angle) has been chosen to determine the characteristic water levels and wave heights at sea. In order to account for the difference between the Hydra-NL location used and the true location of the Delta Barrier, a total wind set-up formula and the Bretschneider equations improved by Young and Verhagen are used to take the differences in fetch and average depth into account. With the Hydra-NL output and the adjustments, the boundary conditions for the final design have been determined. It can not be expected that said final boundary conditions are fully representative for the true location of the Storm Surge Barrier. Nonetheless, they are treated here as design values following from a fully probabilistic approach with partial safety factors equal to 1.

Safety standard Delta21

The safety standard of Delta21 as per the 2017 Water Act is the main parameter influencing the substantiation of the functional requirements considering the retaining height and the reliability of the closure operation of the Delta Barrier. The required safety standard of Delta21 has been determined in this thesis assuming that both the Haringvlietdam and the primary dikes behind the Delta Barrier are of no value to the flood protection system, whereas in reality they are. Hence, this approach would yield a rather conservative maximum allowable failure probability of Delta21. Furthermore, the proposed Delta21 dike segments are of significant importance to the distribution of said maximum allowable failure probability over the identified dike segments. Where in this thesis the dike segments are identified from the perspective of the Delta Barrier, a different configuration of dike segments could prove beneficial to other aspects of Delta21 (e.g. the outer dune defence and pumping station) or the Delta21 project as a whole. Finally, this preliminary design deviates from the standard failure probability distribution as proposed in the WOWK (2018). Here, a rather pragmatic choice has been made by allocating more of the total allowed failure probability towards the Delta Barrier relative to the standard distribution, as it is assumed that it would be relatively expensive to have the storm surge barrier conform to a strict (low) failure probability reservation. All assumptions and design choices established above have a significant impact on the final substantiation of the functional requirements and hence on the required retaining height and the reliability of the closure operation.

Climate change

The issues regarding climate change are subjected to many uncertainties and therefore, inherently, the intended service life of 200 years for the Delta Barrier is uncertain as well. In this preliminary design the median value for sea level rise considering climate scenario SSP5-8.5 in 2250, as predicted by KNMI (2021), is taken into account. This corresponds to 3.81 m¹⁷ of sea level rise. Due to the significant intended service life of 200 years though, insecurities regarding a climate scenario are - besides the median values - extrapolated as well.

Whereas uncertainties regarding sea level rise are relatively high on the agenda and estimations are quite well-spread to a certain extent, knowledge about uncertainties regarding changes in e.g. precipitation patterns and discharge distributions as a result of climate change seem less well-spread. Due to the lack of data and significant deviations between the data and scenarios, a change in discharge distribution as a result of climate change has not been taken into account.

¹⁷With respect to 2018

Hydrodynamic model

In order to estimate the response of the Tidal Lake to different effective flow areas of the Delta Barrier, the hydrodynamic model as proposed by Onwuachu (2021) has been modified until satisfaction. Firstly, the model does not (and can not) accurately capture complex phenomena such as discharge redistribution and the influence of the Nieuwe Waterweg. Also the Spui has not been incorporated in the model. The changes in discharge distribution, either due to climate change or the implementation of Delta21 have not been taken into account. Secondly, the model houses multiple unknown and complex variables, such as discharge coefficients and friction coefficients. These coefficient have been estimated using engineering judgement. While the model is not extremely sensitive to changes in the friction coefficient for the Haringvliet - Hollandsch Diep, it is rather sensitive to changes in the discharge coefficients of both the Delta Barrier and the Haringvlietsluizen. Lastly, the response of the model is quite sensitive to the posed upstream Riemann boundary condition. The undisturbed water level for daily circumstances has been determined using Hydra-NL, which considers the present situation (without Delta21). Any sea level rise is subsequently added to said undisturbed water level. For these reasons, the impact of the Delta21 system and climate change have not properly been taken into account and results only serve as a mere estimate or indication and should be treated with care.

Gate type variant study

Focus of this thesis was specifically not on the gate type variant study, but rather on making a preliminary integral design in which all required functionality is ensured within the framework of the Delta21 concept. For this reason, the variant study conducted here might be considered not extremely thorough. Furthermore, in retrospect, the verification criteria of height adaptability can reasonably be fulfilled by all gate concepts when applying a concrete top beam. Though, it is expected that this would not significantly alter the conclusion of said verification. Furthermore, objective evaluation of the concepts left after the verification (the vertical lift gate and segment gate) can be rather challenging. As the evaluation of the concepts is done by means of quantitatively scoring how easily the specific concept is able to fulfill certain functional requirements, construction costs seem intertwined in almost all evaluation criteria. Additionally, comparing aspects regarding the ecology with costs poses a great challenge as ecological aspects can not easily be quantified. Besides the points noted above, it has followed that the vertical lift gate concept does score better regarding a cost-benefit analysis than the segment gate concept, but not by much.

Reliability of the closure operation

Quite a number of important assumptions have been made in determining the reliability of the closure operation of the Delta Barrier. Firstly, any attempts of recovery or repair during or after a failed closure have been disregarded, which is conservative. Secondly, the probability of flooding given that the closure is a success is set to nil, which overestimates the closure reliability. It should be noted however that this is most certainly not correct as e.g. local set-up before a primary dike could result in flooding irrespective of the status of the Delta Barrier. Thirdly, whereas in reality the probability of flooding after a non-closure event is the sum of the probability of flooding after failure of any number of gates, here only the failure of one and all (25) gates have been taken into account. Subsequently the impact on the hinterland after failing of one and all gates, considering a failing bottom protection and insufficient water storage capacity respectively, has been estimated. The former is estimated by means of the formula proposed by Izbash for stability of bed material in flow with its own limitations. The latter is estimated using data from the "Veiligheid Nederland in Kaart 2 (2014a)" initiative and Hydra-NL. Determining both the probability of a failing bottom protection and the probability of insufficient water storage capacity as a function of an uncertain sea level rise yields somewhat uncertain results. Finally, estimating the probability that the closure of one and all gates fail, adds to said uncertainty. It should be noted that the probability that the closure of one gate fails is assumed lower than for an Eastern Scheldt gate and the probability that the closure of all gates fail higher (Visser, 2003). At this stage it deems impossible to give a more accurate estimate of the future failure probability regarding non-closure. For the reasons established above, the concluding remarks following from the

assessment of the closure reliability of the Delta Barrier should be treated with care and merely pose as a first estimate.

Load combinations and loads considered

Throughout the entire design, only loads perpendicular to the Delta Barrier have been assumed. Lateral loads (e.g. translation waves), parallel to the Delta Barrier, have not been considered. Also coercive forces as a result of deformations, settlements and rotations have not been considered. Hence, the stresses as computed do not paint the complete picture. Furthermore, load combinations which consider both closing and opening of the gates and many temporary load combinations (e.g. handling of elements in the dry dock and transport of elements over water) have not been considered. While most certainly not governing for every elements considered in this preliminary design, said disregarded forces and load combinations could prove governing for some.

Bottom protection design

As for the bottom protection design, a geometrically closed granular filter has been designed using mostly standard grading rocks. It should be noted that this approach might not be most economic as the scale of the project might fit a completely custom bottom protection better. Furthermore, using the depth-average velocity to verify the stability of the top layer is rather conservative. Lastly, the assumed critical flow patterns which are used to determine the size of the top layer stones is uncertain and the bottom protection design as presented should serve as a starting point for further design.

Estimation of construction planning & costs

The estimations of both the construction planning and costs are made using general key figures based on engineering judgement and with reference to the Oosterscheldekering design. Both the construction planning and costs of the Delta Barrier have been estimated by means of multiplying a value for either used material or total surface area to be worked by a key figure representing the time or costs per unit. It should be noted that, for a project the size of the Delta Barrier, any changes in said key figures or used material can result in significant changes in both construction time and costs. Furthermore, an accurate estimate of preparation, unforeseen and overhead costs is deemed impossible in this stage of the design and have been estimated roughly. The costs of the Delta Barrier represent price level 2022.

Validation

Throughout this thesis, validations have occurred (more implicitly than explicitly) at numerous places in design cycles of the design process. Though in the adopted hydraulic engineering design method, validation is mentioned explicitly before the whole system - i.e. the final preliminary design - is concluded. In order to check if the design meets the expectations (of the stakeholders) and the user needs, a validation is required. This integral, preliminary design is not validated explicitly.

12 Conclusion

12.1 Preliminary Design

After the gate type variant study, it is concluded that a storm surge barrier consisting of vertical lift gates is the most suitable concept. The output of this thesis is a preliminary, integral design for the Delta Barrier between the North Sea and the current Haringvliet estuary, taking into account the new Delta21 landscape design as such that the required functionality of Delta21 is met.

The Delta Barrier design consists of a total of 25 vertical lift gates, each spanning 40 m. The effective flow area of the storm surge barrier is 6000 m² defined below NAP. The lift gates can be lowered by hydraulic cylinders, closing a recess of 9 m between the sill beam and the top beam. The storm surge barrier consists of 26 piers on a shallow foundation. The top beam serves as the highest water retaining element with a crest level of NAP + 10.5 m. Road-traffic is allowed over the barrier by means of bridge girders.

Figure 12.1 presents the cross-section of the preliminary design of the Delta Barrier.

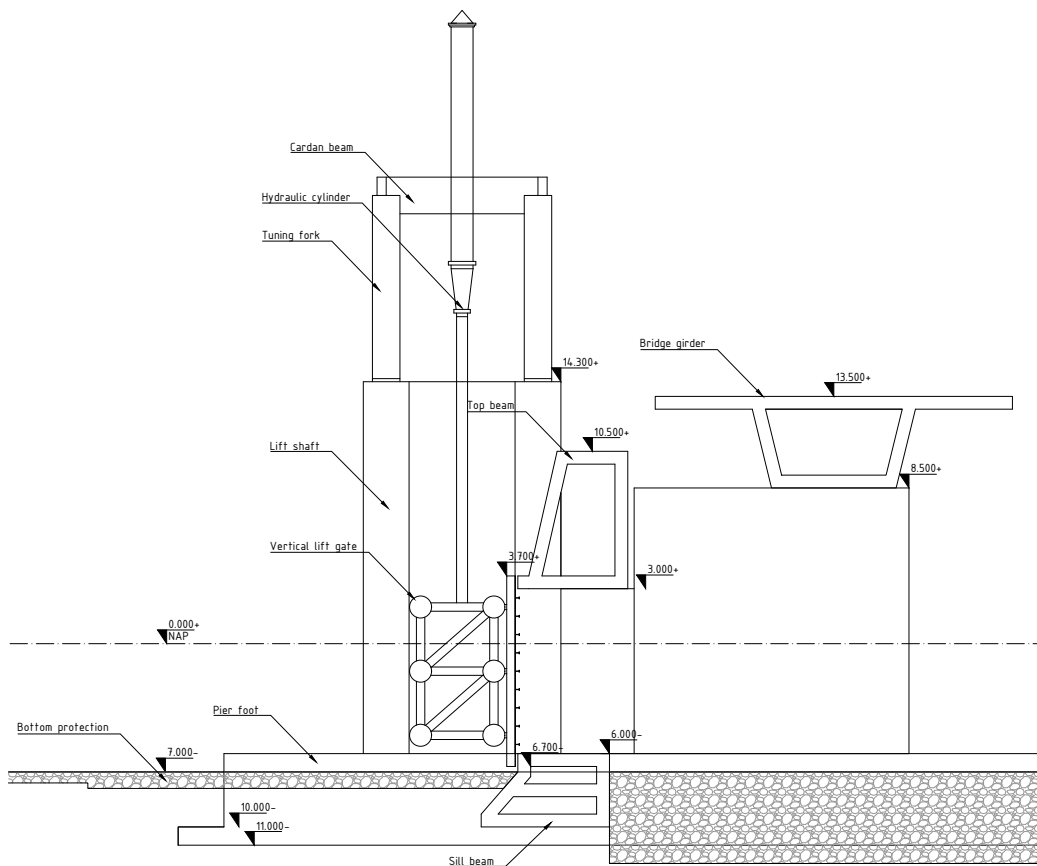


Figure 12.1: Cross-section preliminary design

Figure 12.2 presents a top view of the preliminary design of the Delta Barrier.

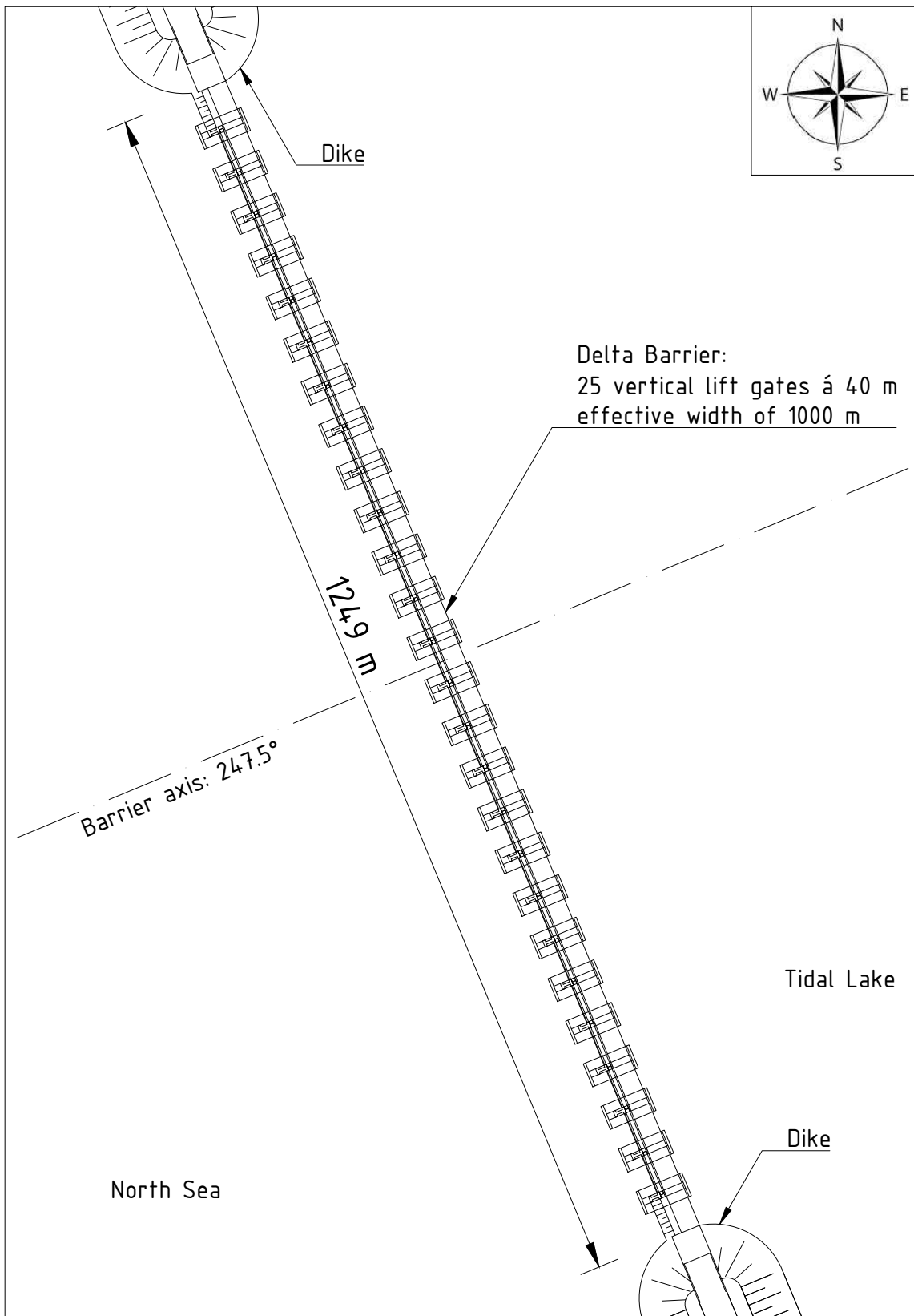


Figure 12.2: Top view. Preliminary design

Finally, Figure 12.3 and Figure 12.4 provide 3D impressions of the Delta Barrier.

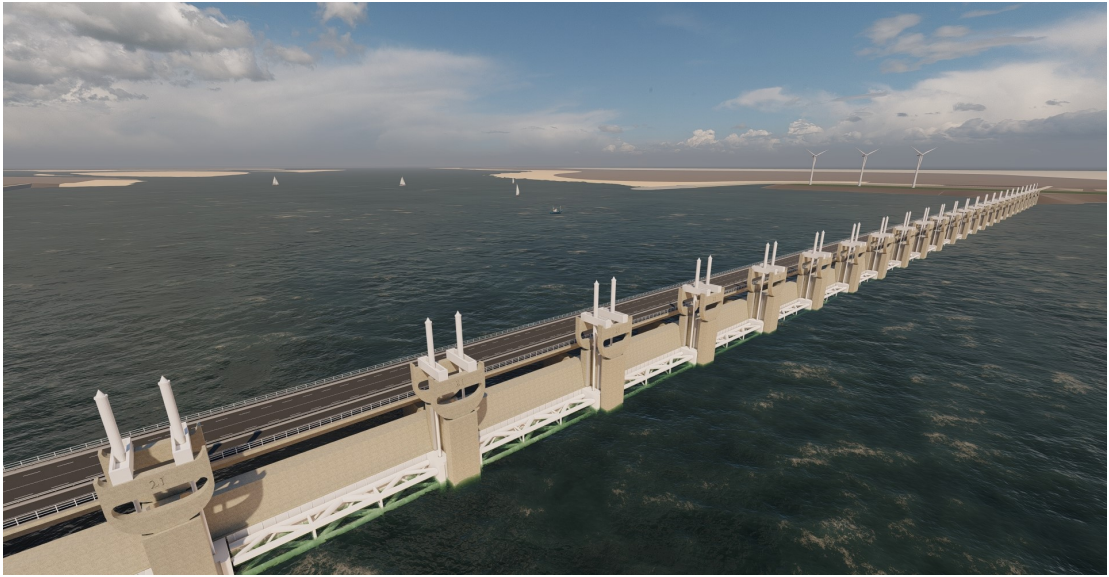


Figure 12.3: 3D impression of the Delta Barrier



Figure 12.4: 3D impression of the Delta Barrier

The main characteristics of the Delta Barrier are tabulated in Table 12.1.

Construction time	5 years
Costs	2674 - 3498 million euro (price level 2022)
Intended completion	2050
Intended service life	200 years
Climate scenario	SSP5-8.5
Closure frequency 2050	1/3 per year

Table 12.1: Main characteristics Delta Barrier

12.2 Conclusions

In order to arrive at the preliminary design as presented in this thesis, various research has been conducted resulting in notable conclusions both in regards to the Delta Barrier, as well as the overall Delta21 project. This section presents an overview of the most notable conclusions.

- **Vertical lift gates as the best concept**

Mostly due to the required size of the barrier, vertical lift gates are the most suitable gate type. The vertical lift gate is future proof, reliable, maintainable, constructable and cost efficient. Although the vertical lift gates score relatively lower with respect to segment gates considering impact on the ecological system and spatial quality, the vertical lift gate is most suitable for the Delta Barrier.

- **Proposed Delta21 flood protection process**

In this thesis, a new Delta21 flood protection process is proposed in order to prevent flooding of the hinterland and specifically Dordrecht. The proposed closure regime requires closure of the gates for a water level at Hoek van Holland of NAP + 3 m or a water level at Dordrecht of NAP + 2.5 m, depending on the discharge at Lobith. In order for Delta21 to be efficient, it is concluded that the Europoortkering should inhibit this newly proposed closure regime as well. If a closure is required, the gates should preferably be closed at low water and at a time when there is no head over the barrier. Lastly, when only high river discharges in combination with the tide (no significant storm surge) results in a closure, using the Tidal Lake as a first measure is generally not economic and the Spillway ought to be opened immediately after closure of the Delta Barrier.

- **Closure reliability**

It has been estimated that the closure operation of this preliminary Delta Barrier design can be considered reliable until a sea level rise of ca. 1 m with respect to 2022. From this point onwards, the closure operation is considered unreliable. The main aspects determining the closure reliability are: the probability that the closure of gates fail, the stability of the bottom protection and the water storage capacity.

- **Hydrodynamic impact Delta Barrier**

The hydrodynamic impact of the Delta Barrier has been evaluated using a (simplified) hydrodynamic model covering an area from the North Sea till Dordrecht. From the model it has been concluded that for this preliminary Delta Barrier design, with an effective flow area of 6000 m² defined below NAP, the mean tidal range will only diminish with ca. 1%, the maximum flow velocity at the Haringvliet estuary will increase from 0.7 m/s to ca. 1.5 m/s and the area of tidal flats will remain unchanged, all directly after completion in 2050. It should be noted however that as a result of 1 m of sea level rise only, irrespective of the construction of a storm surge barrier, ca. 29% of the tidal flats will be lost.

- **Separate lock complex**

Incorporation of the function of ship passage into the storm surge barrier design is not optimal from a flood protection point of view. Integration of the function of ship passage would result in a conflict with the overall climate robustness of the structure, is costly and negatively impacts the closure reliability.

- **Feasibility of tidal turbines**

Using tidal turbines to generate electricity with tidal flow behind the Delta Barrier is unfeasible. The relatively low water depth behind the barrier restricts the turbine size and low flow velocities through the barrier further restrict power production. It is estimated that 4 tidal turbines, all 5 m in diameter, would produce a mere 14 kW. A crude approximation yields that applying tidal

turbines behind all openings of the Delta Barrier would barely generate enough to power the slumber state of the barrier.

- **Construction method**

Prefab construction of the Delta Barrier is the most suitable construction method in the context of the overall Delta21 project. As building a construction pit at the final local of the storm surge barrier is highly unfeasible and construction of a dry dock within the whole construction of Delta21 is very much possible, prefab construction is more suitable than an in-situ construction method. Furthermore, a prefab construction method ensures less exposure time to rough conditions during construction and would therefore also mitigate the impact on the ecological system. It should be noted that, inherent to the prefab construction method, the final assembly of the barrier is rather complex. The large piers should be sunk on to a carefully dredged and prepared bed and all elements are to be transported over water and placed from the water. Placing of all the main, large element of the Delta Barrier would require specialised equipment.

- **Construction planning & costs**

It is expected that the total construction time of the Delta Barrier amounts to 5 years and will cost between ca. 2.67 and 3.50 billion euro (price level 2022). This excludes the adjacent dike sections, the sluice complex and a possible fish migration river.

- **Climate robustness & adaptability**

Regarding complete functionality of the barrier, more specifically the reliability of the closure operation, the New Storm Surge can withstand a sea level rise of ca. 1 m. After ca. 1 m of sea level rise, a decision ought to be made on how to protect people at the hinterland from flooding. Climate adaptive pathways have been drawn up for this purpose and propose three possible strategies within the framework of the climate adaptive pathway approach by Haasnoot and Diermanse (2003). The Delta Barrier could be closed permanently (protected closed), the dikes and the bottom protection could be strengthened, the probability that the closure of gates fail could be decreased, the Tidal Lake water level could be increased during a non-closure event and the Water Act allows for redistribution of failure probabilities over dike segments and failure mechanisms (protected open) and people could be stimulated to move to higher ground in the Netherlands (move along). All posed measures, provide a solution and in general the choice lies with policy makers and is not specific to the Delta Barrier alone. It should be noted that a combination of either three pathways and hence overall strategies is very much possible.

The Delta Barrier is designed to structurally withstand a sea level rise of 3.81 m. After said sea level rise, although challenging, there is ample opportunities to both heighten and strengthen the Delta Barrier. At this point, making decisions regarding flood protection within the framework of a climate adaptive pathway approach is advised.

13 Recommendations

Based on this preliminary design, the following recommendations for further research are advised:

- **Integral Delta21 design and basis of design**

The Delta21 project as a whole is a complex system consisting of multiple different and complex subjects in and of itself. Due to the sheer size and complexity of the project an integral Delta21 design, viz. a design taking into account all elements of Delta21 (storm surge barrier, spillway, energy storage lake, pumping stations ect.), would prove extremely beneficial for further designs. Such a design should at the very least include: an integral basis of design with requirements and boundary conditions to be taken into account for all future designs, a choice regarding the construction sequence and method and a quantitative description of both the Delta21 flood protection system and energy storage system.

- **Implementation of the proposed Delta21 flood protection process**

This thesis has aimed to contribute to the integral Delta21 design within the scope of the Delta Barrier. As such, a new Delta21 flood protection system is proposed describing how the Delta Barrier and partly how the Spillway should function in order to prevent flooding in the Rhine-Meuse delta and keep the water level at Dordrecht below NAP + 2.5 m. It is recommended for further designs to take this newly proposed flood protection system into account and take it as a starting point in order to further develop to a fully quantified operational scheme.

- **Integral hydrodynamic model**

In order to quantify the consequences of the implication of the Delta21 project on the Rhine-Meuse delta, a complete integral hydrodynamic model would prove very beneficial. Besides consequences due to Delta21, such a model would be able to simulate the consequences of climate change as well. Said model could e.g. provide accurate simulations of the water levels upstream as a function of the functioning of the Spillway, salt intrusion in the delta and the reduction in flooding probability as a result of Delta21. Furthermore, 2D or 3D numerical flow models could obtain more accurate results on the development of the flow velocities in order to determine the preferred effective flow area of the Delta Barrier and design the bottom protection. Such a model could also prove beneficial for quantifying parameters of importance to preserving the local ecosystem.

- **Impact on ecological system**

When determining the preferred effective flow area of the Delta Barrier, ecological considerations proved to be governing. Additionally, the construction of Delta21 is situated in a Natura 2000 area. The ecological system is e.g. impacted by a change in tidal range, morphological changes, changes in salt content and many other parameters. In order to account for the impact on the ecological system in a more quantified manner and preserve the ecological system as much as possible, it should be evaluated which (water) parameters and to what extent these parameters can change before the current ecosystem is damaged. These values can subsequently be summarised in the integral functional requirements of the Delta21 project and can as such be used for verifications of future designs.

- **Hindrance to vehicles by overtopping spray**

Overtopping spray on coastal highways can cause hindrance to vehicles by e.g. sudden loss of visibility. To this day, there is little guidance on the effects of overtopping spray and further research on this topic is recommended.

- **Detailed gate & driving mechanisms design**

A complete gate design, especially including driving mechanisms, is a rather difficult exercise. It is advised to use certain engineering software to verify and more accurately design the gates of the Delta Barrier. The driving mechanisms used to open and close the gates are of paramount importance to proper functioning of the storm surge barrier and have yet to be designed.

- **Bottom protection design**

Due to the scale of the Delta21 project, a custom bottom protection (i.e. non-standard) such as for the Oosterscheldekering, is most probably more economic over a granular bottom protection design using standard rock gradings. It is recommended that a custom bottom protection is designed for the specific case of the Delta Barrier.

- **Reliability of the closure operation**

The reliability of the closure operation is the governing functional requirement regarding a closeable storm surge barrier. In order to accurately determine the feasibility of the "protected open" strategy and after which a closeable storm surge barrier is no longer feasible, conducting a complete RAMS-analysis considering the Delta Barrier is advised.

- **Strength verifications gate and civil superstructure**

In further research, it is recommended to use computer models to examine the overall flow of forces from the gates to the civil superstructure and subsequently to the subsoil. Furthermore, a more accurate and detailed structural design can be made with the use of computer models which are able to capture a complex force flow through the structure.

- **Climate adaptive pathway approach Delta21**

As Delta21 proposes a solution to climate change within a combined strategy of "seawards" and "protected open" in order to keep the Netherlands protected against flooding in the future, it would be very much beneficial to present Delta21 within the framework of the strategies as proposed by Haasnoot and Diermanse (2003). Furthermore, the climate robustness of Delta21 can be investigated by means of such an adaptive pathway approach.

References

- AlleCijfers.nl. (2021). *Informatie buurt Nieuwe Haven en omgeving*. Retrieved 2022-06-02, from <https://allecijfers.nl/buurt/nieuwe-haven-en-omgeving-dordrecht/>
- Allsop, N. W. H., Bruce, T., Pullen, T., & van der Meer, J. W. (2008). *Direct hazards from wave overtopping - the forgotten aspect of coastal flood risk assessment?* Van der Meer Consulting B.V.
- Arcadis. (2022). *Onderzoek aanzanding kust Haringvlietmonding - Achtergrondrapport Toekomstige morfologische ontwikkelingen Effecten waterveiligheid, ecologie, economie en leefbaarheid - Eindversie blok A en B*. Arcadis.
- Arends, M., & Nieuwhof, R. T. (2011). *Veiligheid Nederland in Kaart 2 Overstromingsrisico dijkkring 34 West-Brabant*. VNK2, Rijkswaterstaat WVL.
- Balla, A., Blaas, M., van Boheemen, Y., ten Brinke, W., Broekhuizen, A., Burgers, S., R. de Goederen, ... van Zetten, R. (2019). *Het verhaal van de Rijn-Maasmonding*. .
- Beeldman, P. (2011). *Beschrijving huidige situatie Haringvliet. Achtergrondrapportage voor onderzoek naar alternatief voor het Kierbesluit*. Rijksdienst voor Ondernemend Nederland (Rijk).
- Berke, L., & Lavooij, H. (2018a). *DELTA21 en Energie*. Delta21.
- Berke, L., & Lavooij, H. (2018b). *DELTA21 en Natuurherstel*. Delta21.
- Berke, L., & Lavooij, H. (2018c). *DELTA21 en Waterveiligheid*. Delta21.
- Bisschop, C., & Karimlou, G. (2014). *Veiligheid Nederland in Kaart 2 Overstromingsrisico dijkkringgebied 25, Goeree-Overflakkee*. VNK2, Rijkswaterstaat WVL.
- Bosboom, J., & Stive, M. J. F. (2021). *Coastal Dynamics*. TU Delft Open.
- Boskalis. (2023). *Fallpipe vessels*. Retrieved 2023-01-28, from <https://boskalis.com/about-us/fleet-and-equipment/offshore-vessels/fallpipe-vessels>
- Boukhanovsky, A. V., Lopatoukhin, L. J., & Guedes Soares, C. (2007). Spectral wave climate of the north sea. *Applied Ocean Research*, 29(3), 146–154.
- Braam, C. R. (2010). *Eurocode 2 - Betonconstructies Cursusdeel 2: Belastingen op constructies*. TU Delft.
- Colin, J. A., & Lewis, T. I. (1968). Bridge piers-hydrodynamic force coefficients. *Journal of the Hydraulics Division*, 94(1), 17-30. Retrieved from <https://ascelibrary.org/doi/abs/10.1061/JYCEAJ.0001743> doi: 10.1061/JYCEAJ.0001743
- Colina Alonso, A. (2018). *Morphodynamics of the Haringvliet ebb-tidal delta*. Master's Thesis, Delft University of Technology.
- COP26. (2021). *The Glasgow Climate Pact*. Retrieved 2022-01-10, from <https://ukcop26.org/>
- De Bruijn, M. (2022). *GEGEVENS WAARUIT BLIJKT, DAT DE VEILIGHEID IN DE OMGEVING VAN DORDRECHT NA UITVOERING VAN HET DELTAPLAN VOLDOENDE IS GEWAARBORGD INDIEN DE OPENING VAN DE HARINGVLIETSLUIZEN 6000 m2 - N.A.P. BEDRAAGT*. - Nota W-174. Retrieved 2022-06-07, from https://puc.overheid.nl/PUC/Handlers/DownloadDocument.ashx?identificer=PUC_112765_31&versienummer=1
- de Groot, B. (2014a). *Veiligheid Nederland in Kaart 2 Overstromingsrisico dijkkringgebied 20, Voorne-Putten*. VNK2, Rijkswaterstaat WVL.
- de Groot, B. (2014b). *Veiligheid Nederland in Kaart 2 Overstromingsrisico dijkkringgebied 21, Hoeksche Waard*. VNK2, Rijkswaterstaat WVL.
- Delta21. (2021a). *Delta21 - Het Plan*. Retrieved 2021-12-06, from <https://www.delta21.nl/het-plan/>
- Delta21. (2021b). *Vismigratierivier en brakwater gebied passen uitstekend binnen Delta21*. Retrieved 2021-01-13, from <https://www.delta21.nl/vismigratierivier-en-brakwater-gebied-passen-uitstekend-binnen-delta21/>
- de Waal, J. P. (2003). Windmodellering voor bepaling waterstanden en golven. een analyse van de bouwstenen. *Rijkswaterstaat RIZA werkdocument*.
- Dijkzeul, J. C. M., Klatter, H. E., Hartsuiker, G., & Thabet, R. A. H. (1989). Storm surge barrier eastern scheldt: Evaluation of water movement studies for design and construction of the barrier.

- WL rapport Z0088-RWS rapport PEGESS-N-98011.
- Dinoloket. (2022). *Geologisch waterbodemonderzoek - Identificatie BS030190*. Retrieved 2022-12-06, from <https://www.dinoloket.nl/ondergrondgegevens>
- Donkers, D. H. (2021). *Conceptual Design of the Spillway into the Energy Storage Lake of Delta21*. Master's Thesis, Delft University of Technology.
- Elias, E., & van der Spek, A. (2014). *Grootschalige morfologische veranderingen in de Voordelta 1964 - 2013 - Werkdocument*. Deltares.
- EurOtop. (2018). *Manual on wave overtopping of sea defences and related structures. An overtopping manual largely based on European research, but for worldwide application*. Van der Meer, J. W., Allsop, N. W. H., Bruce, T., De Rouck, J., Kortenhaus, A., Pullen, T., Schüttrumpf, H., Troch, P. and Zanuttigh, B, www.overtopping-manual.com.
- Ferguson, H. A., Blokland, P., & Kuiper, H. (1970). The haringvliet sluices. *Rijkswaterstaat Communications 11*.
- Fugro. (2022). *Sondeeronderzoek*. Retrieved 2022-02-08, from <https://www.dinoloket.nl/ondergrondgegevens>
- Garrett, C., & Cummins, P. (2007). The efficiency of a turbine in a tidal channel. *Journal of fluid mechanics*, 588, 243–251.
- Government of the Netherlands. (2022a). *Ministry of Agriculture, Nature and Food Quality*. Retrieved 2022-01-11, from <https://www.government.nl/ministries/ministry-of-agriculture-nature-and-food-quality>
- Government of the Netherlands. (2022b). *Ministry of Infrastructure and Water Management*. Retrieved 2022-01-11, from <https://www.government.nl/ministries/ministry-of-infrastructure-and-water-management>
- Guijt, K. (2018). *Environmental impact of tidal power in the Eastern Scheldt Storm Surge Barrier: Appendix E: Impact of Tidal Energy Extraction in the Eastern Scheldt Storm Surge Barrier on Basin Hydrodynamics and Morphology*. Deltares.
- Haasnoot, M., & Diermanse, F. (2003). *Analyse van bouwstenen en adaptatiepaden voor aanpassen aan zeespiegelstijging in Nederland*. Deltares 11208062-005-BGS-0001.
- Heldesk Water. (2022a). *Afvoer*. Retrieved 2022-01-17, from <https://www.helpdeskwater.nl/onderwerpen/waterveiligheid/crisismanagement/begrippen/toelichting/afvoer/#:~:text=De%20gemiddelde%20afvoer%20van%20de,%E2%80%93%203500%20m3%2Fs>.
- Heldesk Water. (2022b). *Hydra-NL*. Retrieved 2022-01-21, from <https://www.helpdeskwater.nl/onderwerpen/applicaties-modellen/applicaties-per/omgevings/omgevings/hydra-nl/>
- Huis in 't Veld, J. C. (1987). *The closure of tidal basins: Closing of estuaries: tidal inlets and dike breaches*. Delft University Press.
- HWBP. (2021). *Projectenboek HWBP 2022*. Programmabureau HWBP.
- HWBP. (2022). *HWBP en HWBP-2: wat is het verschil?* Retrieved 2022-01-06, from <https://www.hwbp.nl/over-hwbp/wie-we-zijn-en-wat-we-doen/hwbp-en-hwbp2>
- IEA. (2020). *World Energy Balance Overview: World*. Retrieved 2022-01-10, from <https://www.iea.org/reports/world-energy-balances-overview/world>
- IEA. (2021a). *Energy Storage Tracking report*. Retrieved 2022-01-31, from <https://www.iea.org/reports/energy-storage>
- IEA. (2021b). *Global Energy Review 2021: CO2 emissions*. Retrieved 2022-01-10, from <https://www.iea.org/reports/global-energy-review-2021/co2-emissions>
- IPCC. (2021). *Summary for Policymakers. In: Climate Change 2021: The Physical Science Basis*. Intergovernmental Panel on Climate Change.
- IPCC. (2022). *About the IPCC*. Retrieved 2022-01-07, from <https://www.ipcc.ch/about/>
- Jonkman, S. N., Jorissen, R. E., Schweckendiek, T., & van den Bos, J. P. (2021). *Flood Defences Lecture notes CIE5314 (4th ed.)*. Delft University of Technology.
- Jonkman, S. N., Kok, M., & Vrijling, J. K. (2008). Flood risk assessment in the netherlands: A case study for dike ring south holland. *Risk Analysis: An International Journal*, 28(5), 1357–1374.

- Kennisagenda Deltaprogramma. (2021). *Actualisatie Kennisagenda Deltaprogramma 2021*. Deltaprogramma 2021.
- Klein Tank, A., Beersma, J., Besseminder, J., Van de Hurk, B., & Lenderik, G. (2015). KNMI'14 klimaatscenario's voor nederland; leidraad voor professionals in klimaatadaptatie. *KNMI, De Bilt*, 36.
- Klijn, F., Hegnauer, M., Beersma, J., & Sperna-Weiland, F. (2015). Wat betekenen de nieuwe klimaatscenarios voor de rivierafvoeren van rijn en maas. *Deltares: Delft, The Netherlands*.
- KNMI. (2021). *Knmi klimaatsignaal21: Hoe het klimaat in nederland snel verandert*. KNMI De Bilt, The Netherlands.
- KNMI. (2022). *Daggegevens van het weer in Nederland*. Retrieved 2022-02-02, from <https://www.knmi.nl/nederland-nu/klimatologie/daggegevens>
- Koedijk, O. C., van der Sluijs, A., & Steijn, M. L. W. (2017). Richtlijnen vaarwegen 2017: Kader verkeerskundig vaarwegontwerp rijkswaterstaat. *ISBN 978-90-9030674-2*.
- Konter, J. L. M., Klatter, H. E., & Jorissen, R. E. (1992). Afsluitdammen: Regels voor het ontwerp. *Rijkswaterstaat*.
- MarineTraffic.com. (2022a). *OD1*. Retrieved 2022-06-07, from https://www.marinetraffic.com/nl/ais/details/ships/shipid:257668/mmsi:245159000/imo:9242754/vessel:OD_1
- MarineTraffic.com. (2022b). *SL13 ZEEWOLF*. Retrieved 2022-06-07, from https://www.marinetraffic.com/nl/ais/details/ships/shipid:235885/mmsi:244650455/imo:0/vessel:SL13_ZEEWOLF
- MarineTraffic.com. (2022c). *SL4 BRANDING*. Retrieved 2022-06-07, from https://www.marinetraffic.com/nl/ais/details/ships/shipid:239996/mmsi:244671000/imo:0/vessel:SL4_BRANDING
- Masson-Delmotte, V., Zhai, P., Pirani, A., Connors, S. L., Péan, C., Berger, S., ... Zhou, B. (2021). *Summary for policymakers. in: Climate change 2021: The physical science basis. contribution of working group i to the sixth assessment report of the intergovernmental panel on climate change*. Cambridge University Press. In Press.
- Molenaar, W. F., & Voorendt, M. Z. (2019). *Hydraulic structures general lecture notes edition 2019*. TU Delft.
- Molenaar, W. F., & Voorendt, M. Z. (2020a). *Hydraulic structures general lecture notes edition 2020*. TU Delft.
- Molenaar, W. F., & Voorendt, M. Z. (2020b). *Manual hydraulic structures*. TU Delft.
- Mooyaart, L. F., & Jonkman, S. N. (2017). Overview and design considerations of storm surge barriers. *Journal of Waterway, Port, Coastal, and Ocean Engineering*, 143(4), 06017001. doi: 10.1061/(ASCE)WW.1943-5460.0000383
- Nienhuis, P. H., & Smaal, A. C. (1994, 01). The oosterschelde estuary, a case-study of a changing ecosystem: an introduction. In (p. 1-14). doi: 10.1007/978-94-011-1174-4_1
- Noordhuis, R. (2017). *Het haringvliet na de kier: Samenvatting van hydrologische prognoses ten behoeve van effectinschattingen op vis en vogels*. Deltares.
- Normcommissie 351 001. (2011a). *NEN-EN 1991-1-4+A1+C2 (nl), Eurocode 1: Belastingen op constructies - Deel 1-4: Algemene belastingen - Windbelasting*. .
- Normcommissie 351 001. (2011b). *NEN-EN 1992-1-1+C2 (nl), Eurocode 2: Design of concrete structures Part 1-1: General rules and rules for buildings*. .
- Normcommissie 351 001. (2015). *NEN-EN 1991-1-7+C1+A1 (nl), Eurocode 1: Belastingen op constructies - Deel 1-7: Algemene belastingen - Buitengewone belastingen: stootbelastingen en ontploffingen*. .
- Normcommissie 351 001. (2016). *NEN-EN 1993-1-1+C2+A1 (nl), Eurocode 3: Ontwerp en berekening van staalconstructies - Deel 1-1: Algemene regels en regels voor gebouwen*. .
- Normcommissie 351 001. (2019). *NEN-EN 1990+A1+A1/C2, Eurocode: Basis of structural design*. .
- Normcommissie 351 001. (2021). *NEN-EN 1993-1-8 (eng), Eurocode 3: Design of steel structures - Part 1-8: Design of joints*. .

- Normcommissie 351 001. (2022). *NEN-EN 1993-1-5 (eng), Eurocode 3 - Design of steel structures - Part 1-5: Plated structural elements*. .
- Normcommissie 351006. (2016). *NEN-EN 1997-1+C1+A1 (nl), Eurocode 7: Geotechnical design - Part 1: General rules*. .
- Normcommissie 351006. (2019). *NEN-EN 1997-1+C1+A1/NB (nl), National Annex to NEN-EN 1997-1 Eurocode 7: Geotechnical design Part 1: General rules*. .
- Omroep Zeeland. (2022). *Oosterscheldekering levert weer stroom uit eb en vloed*. Retrieved 2022-08-12, from <https://www.omroepzeeland.nl/nieuws/13080328/oosterscheldekering-levert-weer-stroom-uit-eb-en-vloed>
- Onwuachu, P. R. I. (2021). *The New Haringvliet Barrier. Conceptual design for the storm surge barrier of the Delta21 project*. Master's Thesis, Delft University of Technology.
- Pieterse, N., Knoop, J., Nabielek, K., Pols, L., & Tennekes, J. (2009). Overstromingsrisicozonering in nederland, hoe in de ruimtelijke ordening met overstromingsrisicos kan worden omgegaan. *Den Haag/Bilthoven, Planbureau voor de Leefomgeving*.
- Projectbureau Europoortkering met Open Beerdam. (1992). *Tracénota Europoortkering*. Rijkswaterstaat.
- Reijmerink, B. (2017). *Seiches - Analyse waterstandsmetingen en invloed opwekkingsmechanismen*. Deltares.
- Rijksdienst voor Ondernemend Nederland (Rijk). (2022). *Gids van Vissersvaartuigen*.
- Rijkswaterstaat. (2017). *Handreiking Ontwerpen met Overstromingskansen: veiligheidsfactoren en belastingen bij nieuwe overstromingskansnormen*. .
- Rijkswaterstaat. (2017). Richtlijnen ontwerp kunstwerken: Rok 1.4. *RTD 1001:2017 Rijkswaterstaat Technisch Document*.
- Rijkswaterstaat. (2018). *Werkwijzer Ontwerpen Waterkerende Kunstwerken Ontwerpverificaties voor de hoogwatersituatie*. RWS-WVL Waterkeringen.
- Rijkswaterstaat. (2021a). *Deltabeslissing Waterveiligheid*. Retrieved 2021-12-07, from <https://www.deltaprogramma.nl/themas/waterveiligheid/deltabeslissing>
- Rijkswaterstaat. (2021b). *Normering primaire waterkeringen*. Retrieved 2021-12-07, from <https://www.infomil.nl/onderwerpen/lucht-water/handboek-water/thema-s/waterveiligheid-0/normering-primaire/>
- Rijkswaterstaat. (2021). Richtlijnen ontwerp kunstwerken: Rok 2.0. *RTD 1001:2021 Rijkswaterstaat Technisch Document*.
- Schiereck, G. J. (2019). *Introduction to Bed, bank and shore protection*. Delft Academic Press / VSSD.
- Sperna Weiland, F., Hegnauer, M., Bouaziz, L., & Beersma, J. (2015). Implications of the knmi'14 climate scenarios for the discharge of the rhine and meuse; comparison with earlier scenario studies. *Deltares report*, 1220042-000.
- van den Tweel, B., Kösters, R., Boer, C., Schokker, A., Verbrugge, M., & Verweij, L. (2021). *Turning the tides in the Haringvliet*. Delta21.
- van den Wijngaard, K., Hofman, C., van Herk, J., & Wanningen, H. (2014). *Proef optimalisatie vismigratie Oranjesluizen. Eindrapportage*. .
- van der Most, H., & te Nijenhuis, A. (2019). *Nieuwe normering van waterveiligheid*. Retrieved 2022-01-06, from <https://www.stowa.nl/deltafacts/waterveiligheid/beoordelen-waterkeringen/nieuwe-normering-van-waterveiligheid>
- van Eeden, E. (2021). *A new dynamic landscape for the Haringvliet*. Master's Thesis, Delft University of Technology.
- Van Hijum, E. (1999). Leidraad zee-en meerdijken. *L3*.
- van Horick, Q. R. B. (2023). *Design of the navigation and discharge channel in the Tidal Lake of the Delta21 project - A design and morphological study*. Master's Thesis, Delft University of Technology.
- Veendorp, M., & Niemijer, J. (2003). Leidraad kunstwerken. *L15 DWW2003-059-isbn 9026955440*.

- Veenstra-Huisman, C. E. (2014). *Veiligheid Nederland in Kaart 2 Overstromingsrisico dijkkringgebied 22, Eiland van Dordrecht*. VNK2, Rijkswaterstaat WVL.
- Vergouwe, R. (2014). *The National Flood Risk Analysis for the Netherlands, Final report*. Rijkswaterstaat VNK Project Office.
- Visser, T. (1986a). *Ontwerpnota stormvloedkering oosterschelde: Boek 1: Totaalontwerp en ontwerpfilosofie (deelnota 2)*. Rijkswaterstaat.
- Visser, T. (1986b). *Ontwerpnota stormvloedkering oosterschelde: Boek 1: Totaalontwerp en ontwerpfilosofie (deelnota 4)*. Rijkswaterstaat.
- Visser, T. (1989). *Ontwerpnota stormvloedkering oosterschelde, boek 3: De betonwerken*. Rijkswaterstaat, Deltadienst.
- Visser, T. (2003). *Ontwerpnota stormvloedkering oosterschelde, boek 4: De sluitingsmiddelen*. Rijkswaterstaat, Deltadienst.
- Vrijburcht, A. (2000). *Ontwerpen van schutsluizen*. ISBN 90-369-3305-6.
- Waterkaart.net. (2023). *Schuttijden Goereeesluis*. Retrieved 2023-01-23, from <https://waterkaart.net/gids/sluis.php?naam=Goereeesluis>
- Wayenberg, S. (2023). *Waardoor overstroomde Nederland in 1953?* Retrieved 2023-01-18, from <https://npokennis.nl/longread/7562/waardoor-overstroomde-nederland-in-1953>
- Young, I. R., & Verhagen, L. A. (1996). The growth of fetch limited waves in water of finite depth. part 1. total energy and peak frequency. *Coastal Engineering*, 29(1), 47-78. Retrieved from <https://www.sciencedirect.com/science/article/pii/S0378383996000063> doi: [https://doi.org/10.1016/S0378-3839\(96\)00006-3](https://doi.org/10.1016/S0378-3839(96)00006-3)
- Zaldivar Piña, M. I. (2020). *Stability of intertidal and subtidal areas after Delta21 plan - Evaluating the consequences for the morphological development produced by the intervention*. Master's Thesis, Delft University of Technology.

Appendices

I Climate Change

This appendix introduces the topic regarding climate change and serves the purpose of analysing the general impact of climate change on boundary conditions such as the river discharges, the water level at sea and wind and storms depending on the considered climate scenario.

I.1 Introduction

The world is heating up quickly. Since 1901, the temperature in the Netherlands has risen about twice as fast as the global average. The effects of climate change seem clearly noticeable: on July 25, 2019, the mercury crossed the historical limit of 40°C and in the last two decades the number of days with extreme precipitation has increased. The dry seasons in three consecutive years (2018, 2019 and 2020) stood out, with the relevant question looming whether this will occur more often and/or more intensively in the future (KNMI, 2021). Climate change could have a significant impact on the way we, in the Netherlands, manage our defences and water systems. It is not without reason that the Knowledge Agenda of the Delta Programme seems riddled with issues regarding climate change, as great changes in our climate could translate to great changes in our Flood Protection Programme.

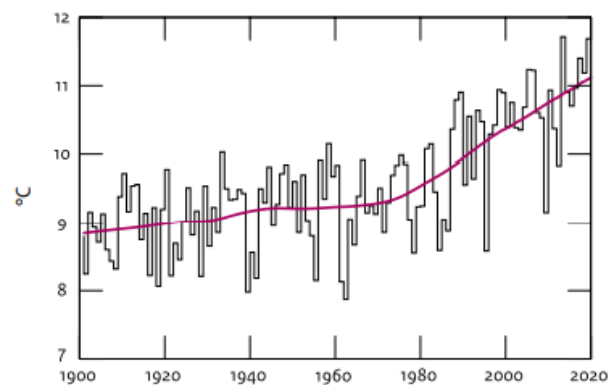


Figure I.1: Dutch annual mean temperature (KNMI, 2021)

In order to tackle said issues, the World Meteorological Organisation (WMO) and the United Nations Environment Programme (UNEP) created the IPCC in 1988. The objective of the the Intergovernmental Panel on Climate Change (IPCC) is to provide governments at all levels with scientific information that they can use to develop climate policies. The IPCC investigates and assesses drivers of climate change, its impacts and future risks, and how adaptation and mitigation can reduce those risks (IPCC, 2022). The IPCC (2021) concluded in 2021 that global warming due to human influence is an established fact and that rapid climate change has occurred on a large scale.

In order to use the data and findings of the IPCC for assessment in the Netherlands, the KNMI translates the global IPCC data and scenarios to the Netherlands using the newest European models. The most recent publication of the KNMI, including the well known climate-scenarios, stems from 2014. Since this last publication, a great deal of research has been conducted, both by the KNMI and in an (inter)national context. This research has led to a new report in oktober 2021 which presents new insights in namely sea level rise, changing precipitation patterns and drought. However, this report is not intended as a successor to the KNMI'14-scenarios for the Netherlands but gives merely an update about how the Dutch climate is developing (KNMI, 2021). The successor to the KNMI'14-scenarios for the Netherlands will likely be published in 2023.

There have also been developments on the political level: in December 2015, the Paris Climate Agreement was presented, in which it was agreed that the world should not warm by more than 2°C compared to the pre-industrial era (1850-1900) and aim for 1.5°C.

Nonetheless, both the IEA (2021b) and the Masson-Delmotte et al. (2021) state that, despite the dip in CO₂ emissions in 2020, there seems no sign of decreasing emissions in the future. In addition, during the Glasgow Climate Pact (2021) it has been urged that countries should come forward with more ambitious emission reductions targets that align with reaching net zero by the middle of the century. It seems that - at least according to the data in the present - the 2° global warming mark set by the Paris Climate Agreement is quite likely to be exceeded. It should be noted that the Masson-Delmotte et al. (2021) reports with high confidence that it would take several centuries to millennia for global mean sea level to reverse course even under large net negative CO₂ emissions. Furthermore the Masson-Delmotte et al. (2021) reports with high confidence that early responses of the climate system to reduction of emissions can be masked by natural variability and that the response of many climate variables would emerge from natural variability only later in the 21st century.

I.2 Climate Scenarios

KNMI 2014

The KNMI'14-scenarios are the four combinations of two different values for the global temperature rise, 'Moderate' and 'Warm', and two possible changes in the airflow pattern, 'Low value' and 'High value'. Together they describe the corners within which climate change in the Netherlands is likely to take place (Klein Tank et al., 2015).

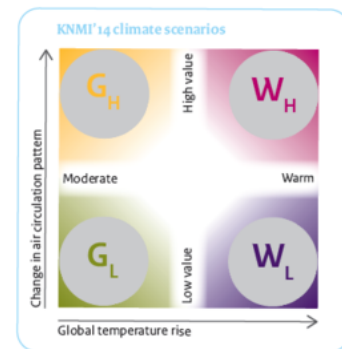


Figure I.2: KNMI'14 climate scenarios (Klein Tank et al., 2015)

KNMI 2021

The latest KNMI (2021) report treats three climate scenarios, based on the IPCC Sixth Assessment Report (Masson-Delmotte et al., 2021). The IPCC (2021) report treats an additional 2 scenarios as shown in Figure I.3. Here, the contribution to global surface temperature increase from different emissions is depicted, with a dominant role of CO₂ emissions. Figure I.3 shows the total warming (observed warming to date in darker shade), warming from CO₂, warming from non-CO₂ greenhouse gasses (GHGs) and cooling from changes in aerosols and land use in 2081-2100 relative to 1850-1900 in °C.

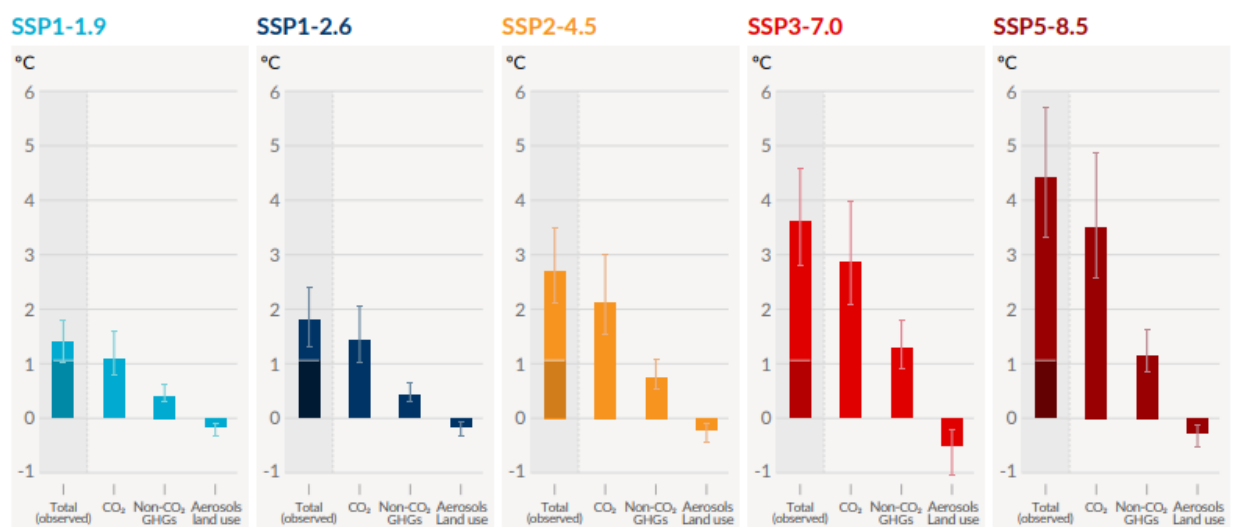


Figure I.3: Change in global surface temperature in 2081-2100 relative to 1850-1900 (°C) (IPCC, 2021)

The IPCC (2021) states that global surface temperature will continue to increase until at least the

mid-century (2041-2060) under all emissions scenarios considered. Global warming of 1.5°C and 2°C will be exceeded during the 21st century unless deep reductions in CO₂ and other greenhouse gas emissions occur in the coming decades. With the Paris Climate Agreement in mind: during the 21st century global warming of 2°C would extremely likely be exceeded in the intermediate scenario (SSP2-4.5). Under the very low and low GHG emissions scenarios, global warming of 2°C is extremely unlikely to be exceeded (SSP1-1.9), or unlikely to be exceeded (SSP1-2.6). One should note that SSP1-1.9 and SSP1-2.6 are scenarios that start in 2015 and have CO₂ emissions declining to net zero around or after 2050, followed by varying levels of net negative CO₂ emissions.

I.3 River Discharges

Climate change issues such as the changing patterns for precipitation, evaporation and melt water change the river discharge of our main rivers. In turn, these changes differ per season and per sub-basin. The Rhine catchment area is very large and complex, with many large tributaries (Main, Neckar, Moselle), whereas that of the Meuse is smaller and rather elongated. Furthermore, an important part of the Rhine area is located in the high mountains and is therefore subjected to melt water, but this does not apply to the Meuse which is a rain-river (Klijn, Hegnauer, Beersma, & Sperna-Weiland, 2015). Especially the change in precipitation is to cause a different discharge distribution for the Rhine and the Meuse throughout the year. Mostly in winter the precipitation is expected to increase, whereas in summer it is expected to decrease (Klein Tank et al., 2015). As a result, there is a general tendency towards increasing winter and spring discharge and decreasing (late) summer discharge (Sperna Weiland, Hegnauer, Bouaziz, & Beersma, 2015). One should note that this also results in a higher probability of high water events in winter and low water events in summer (KNMI, 2021).

A study by Deltares and the KNMI (2015) considered the impact of the climate scenarios of KNMI'14 on the river discharges of the Rhine and Meuse. Overviews of discharges in m³/s for specific return periods for all scenarios, including the reference situation, for both the Rhine and Meuse are shown in Figure I.4 and Figure I.5 respectively.

Return period [years]	Ref.	2050GL	2050GH	2050WL	2050WH	2050W+	2085GL	2085GH	2085WL	2085WH	2085W+
10	9100	10900	10600	10800	11100	11000	10800	10600	12000	12700	11700
30	10900	12900	12500	12700	13000	12400	12800	12400	13700	14100	13400
100	12600	14100	13900	14000	14100	13900	14000	13800	14400	14800	14300
300	13600	14700	14500	14500	14600	14500	14600	14400	15000	15600	15000
1000	14300	15700	15200	15400	15100	15100	15500	14900	16400	17000	16300
1250	14400	15900	15300	15500	15200	15300	15700	14900	16700	17100	16500
3000	14800	16700	16200	16400	16300	16400	16600	15600	17100	17300	17000
10000	15300	17200	17000	17000	17000	16900	17200	16800	17300	17500	17500
30000	15700	17300	17200	17200	17300	17200	17300	17000	17400	17500	17600

Figure I.4: Overview of discharges in m³/s for the Rhine at Lobith (Sperna Weiland et al., 2015)

Return period [years]	Ref.	2050G _L	2050G _H	2050W _L	2050W _H	2050W ₊	2085G _L	2085G _H	2085W _L	2085W _H	2085W ₊
10	2250	2550	2500	2450	2550	2400	2500	2450	2600	2750	2600
30	2750	3100	3000	3000	3100	2950	3000	2950	3150	3300	3200
100	3200	3600	3450	3500	3550	3450	3500	3400	3650	3850	3750
300	3550	4000	3850	3900	3900	3850	3900	3750	4050	4300	4200
1000	3850	4350	4200	4200	4200	4200	4250	4050	4400	4700	4550
1250	3900	4450	4250	4250	4250	4250	4350	4100	4450	4750	4650
3000	4100	4750	4500	4500	4550	4450	4600	4400	4700	4950	4850
10000	4350	5000	4700	4750	4750	4650	4900	4600	4900	5200	5050
30000	4600	5200	4850	4950	4900	4850	5050	4750	5100	5350	5200

Figure I.5: Overview of discharges in m³/s for the Meuse at Borgharen (Sperna Weiland et al., 2015)

In the model for the Rhine river the effect of upstream flooding and the correction for the flood areas along the stretch between Wesel and Lobith is included. Upstream flooding of the Rhine reduces the extreme high discharges at Lobith significantly and moreover the dampening effect of flooding between Wesel and Lobith on the peak discharges at Lobith is large. The maximum discharge at Lobith in the case flooding is taken into account is between 17500 and 18000 m³/s (Sperna Weiland et al., 2015). However, for design purposes one should note that the upstream parts of the Rhine would probably be (temporarily) reinforced or raised to prevent flooding. The study by Deltares and the KNMI (2015) states: "For the Rhine in 2050, ignoring effects of upstream flooding, for the 1250-year event the scenarios result in discharges between 19200 and 20300 m³/s. In 2085 the discharges for the 1250-year event range between 18700 and 22300 m³/s for the GH and WH scenarios respectively. The reference estimate of the 1250-year event, in the case upstream flooding is ignored, is approximately 16900 m³/s" (Sperna Weiland et al., 2015).

1.4 Sea Level Rise

Observations show that the sea level on the Dutch coast has been rising at an average rate of 1.8 mm per year since 1900 (Klein Tank et al., 2015). Figure I.6 shows the sea level rise off the Dutch coast.

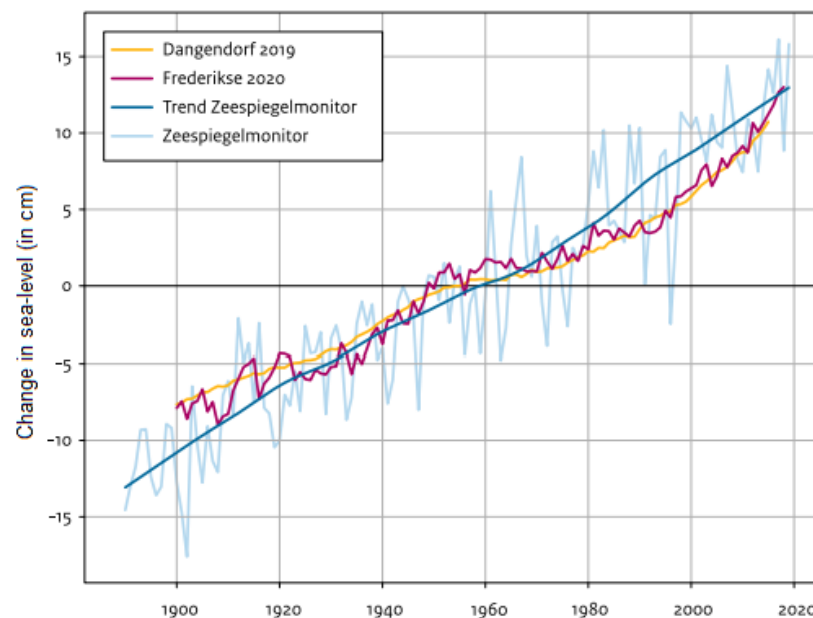


Figure I.6: Sea level rise off the Dutch coast (blue based on six tidal stations) versus two reconstructions of the global mean sea level rise (KNMI, 2021)

Globally, the sea level rise is accelerating, because the large ice sheets are melting and increasingly losing mass. One should note that locally perceived changes in mean sea level (also called relative sea level changes) can be the result of either vertical movements of the land or an absolute (relative to the earth-centre) movement of the sea level.

The world-wide distribution of sea level change is spatially non-uniform. Due to this non-uniformity the KNMI has, again, translated the assessments and predictions of the IPCC to the Netherlands by using European models in order to account for e.g. local steric changes and geoidal eustasy (Klein Tank et al., 2015).

KNMI 2013

Figure I.7 depicts the sea level rise according to the KNMI'14 scenarios as described before. The prognosis by KNMI'14 is somewhat higher compared to KNMI'06 as the land ice of Antarctica seem to melt quicker than expected (Klein Tank et al., 2015). The bandwidths as in figure Figure I.7 represent a 90% confidence interval. The upper values for the climate-scenarios represent the 95th percentile and are ca. 75 cm and 100 cm (relative to 1981-2010) for the G-and W-scenarios respectively.

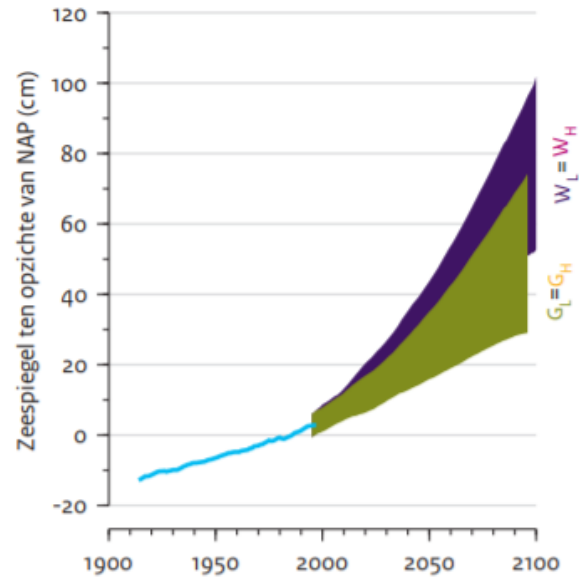


Figure I.7: Sea level on the Dutch coast as observed and according to the KNMI'14 scenarios (Klein Tank et al., 2015)

KNMI 2021

In the KNMI'21 report three indicative scenarios have been assessed, taken from the five scenarios by the sixth IPCC assessment report (see Figure I.3): SSP1-2.6 which is consistent with the maximum 2°C target, SSP5-8.5 where no measure have been taken to lower emissions (i.e. further increase in emissions) and SSP2-4.5 which is an in-between scenario. Figure I.8 depicts the sea level rise according to the KNMI'21 indicative scenarios. The blue lines show the sea level as observed. The solid lines in green, purple and red indicate the median of the different climate scenario projections (SSP1-2.6, SSP2-4.5 and SSP5-8.5 respectively) and the coloured areas the accompanying 90%-bandwidth. The zero point of the median lines is the year 2005; the bandwidth in 2005 corresponds to the natural variability (KNMI, 2021).

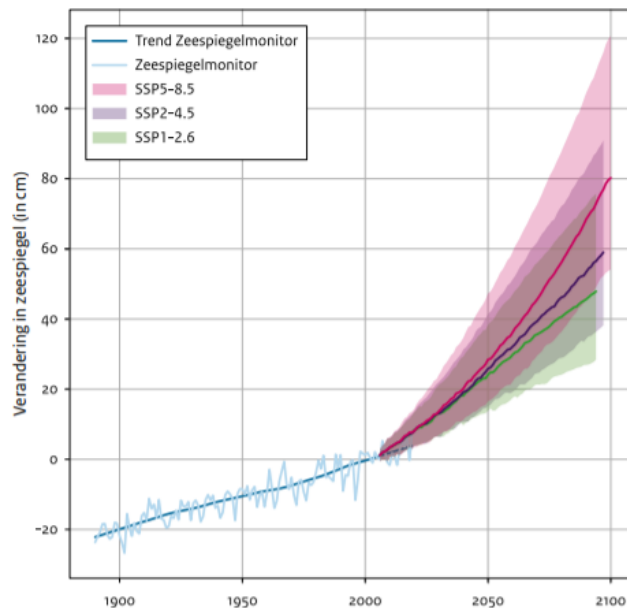


Figure I.8: Sea level on the Dutch coast as observed and according to the new, indicative sea level projections (KNMI, 2021)

When comparing Figure I.7 and Figure I.8 one can observe that, in general, the new indicative scenarios from the KNMI'21 report show a greater rise in sea level than the KNMI'14 report. This is, again, most likely due to an underestimation of the shrinkage of the Greenland and Antarctic Ice Sheets, which seems to be accelerating (KNMI, 2021). Table I.1 tabulates the indicative sea level rise for the Dutch coast under the different emission scenarios, around 2050 (2046-2055) and around 2100 (2096-2105), compared to 1995-2014, with a very probable bandwidth (90%). This includes land subsidence of 0.5 mm/year (KNMI, 2021).

Year	2050	2050	2050	2100	2100	2100
Emission-scenario	SSP1-2.6	SSP2-4.5	SSP5-8.5	SSP1-2.6	SSP2-4.5	SSP5-8.5
Sea level rise in cm	14 - 38	15 - 41	16 - 47	30 - 81	39 - 94	54 - 121
Rate of change in mm/year	2.8 - 8.7	5.2 - 10.6	5.8 - 12.1	2.9 - 9.1	4.4 - 10.5	7.2 - 16.9

Table I.1: Indicative sea level rise scenarios for the Dutch coast (KNMI, 2021)

I.5 Wind and Storms

The man-made changes in wind speed are small in the KNMI'14 scenarios. This also applied to the KNMI'06 scenarios. Changes in mean wind speed throughout the year and during winter storms are within natural variability (Klein Tank et al., 2015).

The projections from the latest generation of climate models as from KNMI'21 show only small changes in the wind climate for Western Europe. Over the southern North Sea, Denmark and southern Sweden there is an area where the maximum wind strength in winter is increasing (see Figure I.9), while the rest of the area shows a decrease. Only winter is considered, as winter is generally normative for storm-season. Furthermore, Figure I.9 is based on a high emissions scenario (SSP5-8.5). The area with the largest increase is close to the Dutch coast and is represented by the green dot in Figure I.9. The difference in maximum wind strength between 1991-2020 and 2071-2100 here is 0.35 m/s, or 2% of the average annual maximum. This change is not significant (KNMI, 2021).

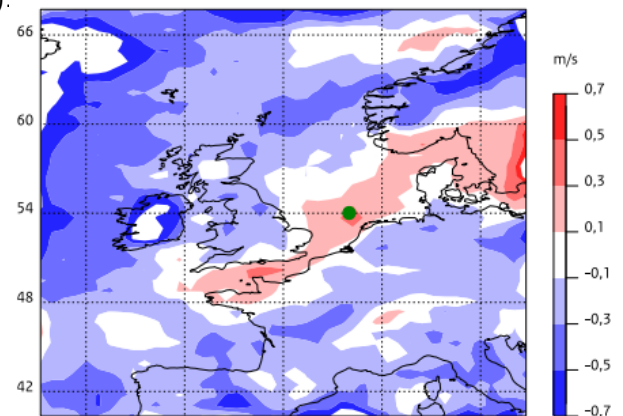


Figure I.9: Change in annual wind speed maximums (m/s) in winter (December - February) (KNMI, 2021)

In addition to the strength, the direction of the wind is important. For example, the highest water levels along the Dutch coast arise when a northern wind gives rise to set-up phenomena in the North Sea waters. The KNMI'14 scenarios show that the frequency of strong northerly winds will probably not change much in the future (Klein Tank et al., 2015).

Changing wind speeds and patterns could induce additional water set-up in front of the Dutch coast. However according to the KNMI'21 report (2021), the median of the climate models over the historical period shows a decrease, but given the large range this is not significant and the same goes for the projections. The main conclusion is that the upper limit of the 90% band in the projections does not exceed that of the historical period. But despite the fact that there is no effect of the wind on the highest water levels, the highest water levels will increase in the future because the average sea level rises.

Lastly, it should be noted that due to the rising temperature of the sea-water hurricanes could become stronger in the future. For our latitudes, that could lead to heavier hurricane remnants. Whether hurricanes could reach the North Sea in the future is yet unknown and might seem unlikely as hurricanes generally develop in regions with sea water warmer than 26.5°C. However, hurricanes do influence the

wind climate in the North Sea in the current climate. A recent study has shown that during the hurricane season (June-November) almost 9% of all severe storms in the North Sea (> 25 m/s) originate from a hurricane (KNMI, 2021). The KNMI (2021) states that current climate models are not yet sufficiently fine-grained to properly simulate hurricanes with their small eye. With increasing computing power, models with sufficient resolution will become available to answer the question about the possibility of hurricanes in the North Sea or their role as precursors to powerful extra-tropical storms.

I.6 Uncertainties

The issues regarding climate change are subjected to many uncertainties and even scepticism to some degree. The biggest uncertainties are readily introduced by the multiple climate-scenarios as established. To start off, the global temperature rise can be quite difficult to predict, mainly as it seems that the global rise in temperature is directly coupled to man-made greenhouse gas emissions. Furthermore, a prognosis for the changing air circulation pattern seems difficult to make, though it seems not of significant importance with regard to long term sea level rise (KNMI, 2021). These uncertainties translate to relatively large 90% confidentiality bandwidths and complicate design choices for structures when climate change is included in the natural boundary conditions.

In addition, some are rather sceptic about the influence of humankind on the global temperature rise. Some say that the rise in temperature as recorded till present are well within the long term natural variability for temperature change between a glacial and inter-glacial or that greenhouse gas emissions are in fact not coupled to temperature at all.

As established before, the ice sheets on both Antarctica and Greenland seem to melt faster than previously anticipated. Furthermore, Antarctica's future becomes very uncertain, due to possible major changes in ice flows and the unstable nature of parts of the Antarctic Ice Sheet which could cause a climate scenario with grave consequences (SSPS5-8.5 H++). However, accelerated melting of the Arctic could limit temperature rise in the Netherlands. Increasing Arctic precipitation and the accelerated melting of snow and land ice are causing the Arctic Ocean to become less salty. When this relatively fresh polar water flows into the northern part of the Atlantic, it weakens large-scale ocean circulation. This will slow down the Warm Gulf Stream, possibly limiting the temperature rise in the Netherlands (KNMI, 2021). One should note however that this would not (significantly) influence sea level rise at the Dutch coast. In addition, the IPCC (2021) states that there is only limited evidence, with medium agreement, of human influence on the Antarctic Ice Sheet mass loss.

Somewhat counter-intuitive, significant melting of the Greenland Ice Sheets could just as well result in a component which lowers the sea level at the Dutch coast (Bosboom & Stive, 2021). A smaller Greenland landmass has less gravitational attraction (i.e. geoidal eustasy). These uncertainties could in essence completely change the predicted climate-scenarios.

On a final note: the sheer complexity of the mechanisms and processes behind climate change and the predictions of it, results in an ongoing debate on climate change and the validity of the predictions.

II Dutch Flood Defence Policy

This appendix provides elaboration on the current Dutch flood defence policy. The way we, in the Netherlands, manage our defences and water systems from a flood safety perspective must be taken into account when designing a primary flood defence structure. Furthermore, the Delta21 flood protection process (see Section 5.1) is to follow up the current flood protection programme.

II.1 Water Act 2017

Before 2017 the safety standards for primary flood defences were based on insights from the period 1953-1960. Since then, however, flood risk and more specifically the consequences given a flood in the Netherlands has increased. Comparing the 1960s to 2017, the population has grown from 10 to 17 million and the economic value in flood-prone areas has increased sharply (van der Most & te Nijenhuis, 2019). In addition, much knowledge has been developed since the 1960s with regard to statistics and to better calculate flood risks (i.e. both probabilities and consequences). These were the main reasons for updating the previous legal standards. After the start of the Flood risk management policy in 2006 and the Delta Programme Safety, the new standards were included in the Water Act as of 2017 (van der Most & te Nijenhuis, 2019).

The new standards in the 2017 Water Act are based on a failure probability approach. The core of the Delta decision on flood risk management is based around a so-called basic protection level stating that the probability that a person will die as a result of a flood must be no greater than 1 in 100000 per year¹⁸ (i.e. 0.001%) by 2050 at the latest. This is the so-called basic protection level. This criterion makes more targeted investments possible in flood protection in the Netherlands. Everyone behind the dikes receives the same basic protection level. In places where the consequences are very large (for example, if there would be many victims, there would be significant economic damages and/or damages would occur to vital infrastructure of national importance), the level of protection will be higher (Rijkswaterstaat, 2021a). By 2050, all primary flood defences must meet the new safety standards.

A water-retaining structure does not stand alone. It is part of a dike segment which can consist of dike bodies, quays, dunes and structures. In its entirety, multiple dike segments can form a flood defence system (or dike ring) for an area behind it that must be protected against high water. The Water Act of 2017 sets a flood probability requirement per year for said dike segment. The probability of flooding of a segment must be less than this posed flood probability. The new safety standards as from 2017 are considered to be target values not to be exceeded (lower limit, i.e. the maximal acceptable failure probability). However, in practice the preparation of a dike reinforcement takes a lot of time (typically between 10 and 15 years). To cover the degradation and climate change effects during that preparation period a signal value is introduced. The signal value is three times stricter (i.e. smaller probability) than the posed lower limit safety standard. If the safety assessment shows this signal value is being exceeded, the preparation for a dike reinforcement starts. The design will aim for a lower failure probability (or higher β) than considered in the safety assessment (Jonkman et al., 2021). Hence, the design of new primary flood defence systems should conform to the lower limit values as stated in the Water Act.

Besides the legal safety requirements set by the 2017 Water Act, all structures should also comply with the Building Decree. The Water Act verification is only required in the event that a flood will occur given that the structure or a structural component collapses as a result of the considered load situation (Rijkswaterstaat, 2018). Though, in line with current design practice, if the design has been

¹⁸Within the framework of the Water Act, probabilities are expressed per year. This actually concerns a probability of failure in a continuous period (reference period) of 1 year. Therefore these probabilities are, in theory, dimensionless (Rijkswaterstaat, 2018).

verified according to the Building Decree (in CC3) it will in practice certainly also comply with the Water Act (Rijkswaterstaat, 2018).

II.2 The Building Decree

Load situations that are important for the flood defence function do not only relate to an extremely high outside water level which the Water Act considers. All load situations, which can occur during use (or errors during use), can be of importance. These 'other', less extreme load cases are considered in the Building Decree. In each load situation, it must be further examined how the different loads for the relevant failure mechanisms of structural parts should be combined (Veendorp & Niemijer, 2003).

Any new structure or new part of an existing structure should conform to the Building Decree and as such conform to all relevant codes and regulations. As a result, all new structures should conform to the relevant NEN-standards, CE-markings and recognised quality declarations as well as regulations with regard to monuments, temporary structures and the renovation and relocation of structures as dictated by the Building Decree.

In accordance with NEN-EN 1900 (2019), failure of a storm surge barrier results in major consequences in terms of loss of human life, or very large economic, social or environmental consequences. Therefore the Delta Barrier should be designed with consequence class 3 (CC3) and reliability class 3 (RC3). NEN-EN 1990 (2019) specifies a reliability index (β) for CC3 for a reference period of 50 years: $\beta=4.3$. Said reliability index translates to a probability of failure of 10^{-5} (i.e. R=100000 years). The WOWK (2018) argues that the reliability class with reference period of 50 years may also be used for greater reference periods.

II.3 Flood Protection Programme (HWBP)

In order to ensure that all primary flood defences meet the new safety standards set by the 2017 Water Act by 2050 the Flood Protection Programme (HWBP in Dutch) has been launched. In the HWBP, the 21 Dutch water boards and the government are working together on the largest dike improvement operation since the Delta Works. The aim of the HWBP is that by 2050 all the primary flood defences managed by the water boards will meet the new standards. This concerns almost 1500 km of dikes and almost 500 structures (e.g. locks and pumping stations) (HWBP, 2022). Many dike improvements are already underway (Rijkswaterstaat, 2021a). In this period, one of the milestones is that the Minister of Infrastructure and Water Management will report to the Senate and the House of Representatives on the condition of the primary flood defences before the end of 2023. This is done on the basis of the first National Assessment Round (2017 to 2023). The second National Assessment Round will run from 2023 to 2034 (Rijkswaterstaat, 2021a).

As of November 2021, 126.5 km have already been reinforced according to the new standards and 606 km are in one of the project phases (HWBP, 2021). In the coming years, various projects and activities will be carried out to implement the Delta Decision on Flood Risk Management. These projects and activities are described in the Flood Protection Programme as a part of the Delta Plan on Flood Risk Management. Figure II.1 shows the status of the dike reinforcements in kilometres with reference date 01-01-2021 on the left and a prognosis for the strengthening of primary defences in kilometres and number of structures on the right.



Figure II.1: Status of primary defence reinforcements (in km) and prognosis 2022-2027 (HWBP, 2021)

Note that the measures that the managers had to take as a result of the assessment rounds in 2001 and 2006 have been placed on the "HWBP-2". A total of 87 projects are being realized in the HWBP-2, of which 362 km of dikes and 18 engineering structures. Measures arising from the third and fourth round of assessments (2011 and 2017) are included in the "HWBP".

Hence, from Figure II.1 we can see that the last remaining dike- and structure reinforcements for the HWBP-2 programme will be in realization in the period 2022-2027. However, for the newer HWBP-programme we can see that 1324 km of dike reinforcements are not yet in the realization phase of which 745 km not considered at all. Furthermore, for the HWBP-programme still 353 structures ought to be reinforced between 2027 and 2050.

Figure II.2 gives an overview of all the projects in the Flood Protection Programme in the period 2022-2027, with the South West Delta circled and zoomed in. Furthermore, Table II.1 lists the projects as depicted by Figure II.2 in the South West Delta.

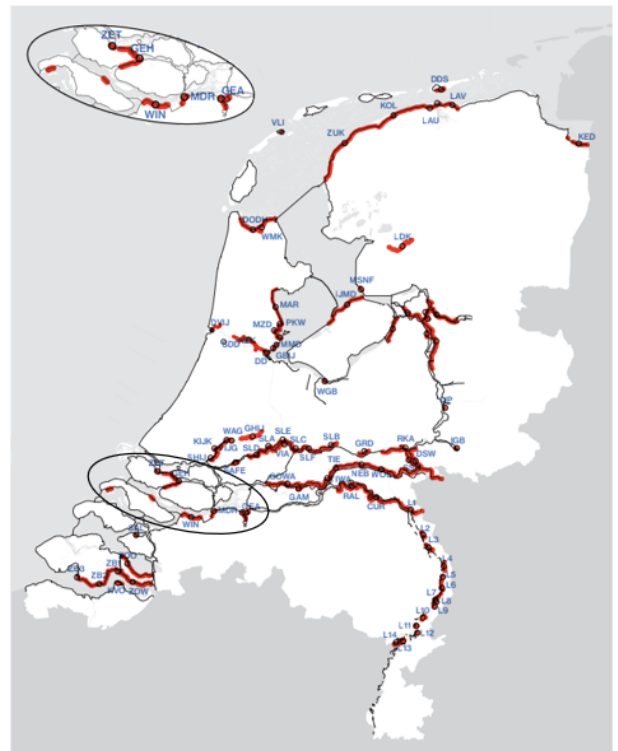


Figure II.2: Flood Protection Programme projects 2022-2027 (HWBP, 2021)

Project	Water board	Kilometres	Urgency	Status
ZET	Hollandse Delta	12.6	23	Exploration phase
GEH	Hollandse Delta	6.05	22	Exploration phase
WIN	Brabantse Delta	7.4	48	Exploration phase
MDR	Brabantse Delta	0.73	48	Realization in 2023
GEA	Brabantse Delta	7.5	108	Exploration phase

Table II.1: Projects in the South West Delta 2022-2027

As established, there are significant reinforcement projects to be undertaken after 2027 in able to meet the new standards of the Water Act by 2050. In addition, the first National Assessment Round and new insights (in e.g. climate change) could increase the pressure on the Flood Protection Programme.

II.4 Knowledge Agenda of the Delta Programme

As part of the Delta Programme the Knowledge Agenda investigates certain "knowledge questions". We continuously keep up with the ever-changing boundary conditions with regard to the Delta Programme and continue to develop our knowledge accordingly. This knowledge is important for the further elaboration, implementation or adjustment of the Delta Decisions and preferential strategies. The knowledge questions form input for the knowledge programming of the Ministry of Infrastructure and Water Management, Rijkswaterstaat, provinces, STOWA, KNMI, Deltares and universities and are partly addressed within the National Water and Climate Knowledge and Innovation Programme (NKWK) (Kennissagenda Deltaprogramma, 2021).

The knowledge question from the Knowledge Agenda can be categorised in specific themes. Below, some questions are quoted from the Knowledge Agenda (2021) per category:

a. *Flood protection:*

The category flood protection includes questions like: "What is the change in the hydraulics and morphology of the different water systems as a result of autonomous development and sea level rise?" (Kennissagenda Deltaprogramma, 2021) and "Is tightening up of the current space reservations necessary for future measures? What opportunities does it offer to take an integrated look at the entire delta and not just at the wet system?" (Kennissagenda Deltaprogramma, 2021).

b. *Water Quality and Nature:*

The category Water Quality and Nature includes questions like: "Making a fish migration plan for the entire delta, what is needed?" (Kennissagenda Deltaprogramma, 2021) and "Which nature goals are no longer (fully) achievable in the long term as a result of climate change, apart from adjustments to the design of water systems?" (Kennissagenda Deltaprogramma, 2021).

c. *Fresh Water:*

The category Fresh Water includes questions like: "Should there be a significant change in Rhine discharge in the coming decades as a result of changing meltwater discharge into stormwater discharge? And if so, does this change mainly relate to the spring discharge, or does the discharge pattern change for the whole year?" (Kennissagenda Deltaprogramma, 2021) and "What does the expected climate change such as accelerated sea level rise mean for the preferential strategy for the Rhine Meuse estuary (closing off the Nieuwe Waterweg from a safety point of view) and what effects does this have on the Preferred Strategy for Freshwater in the South West Delta?" (Kennissagenda Deltaprogramma, 2021).

It seems that the questions as from the Knowledge Agenda of the Delta Programme mostly regard climate change issues and its impact on the design of and strategy for the (fresh) water systems in the Netherlands.

III Energy Transition

This appendix introduces the topic regarding energy transition where current findings are reported regarding the transition to more sustainable energy sources, underlining the need for a greater share of renewable sources and means for energy storage in order to effectively mitigate the effects of climate change.

III.1 Introduction

The IPCC (2021) states that human influence is very likely the main driver of the global retreat of glacier and therefore the main driver of climate change. Since 2011, greenhouse gas concentrations have continued to increase in the atmosphere causing a significant rise in temperature (most likely). Changes are irreversible on centennial to millennial time scales in global ocean temperature, deep ocean acidification and deoxygenation. Therefore, in December 2015, The Paris Climate Agreement was concluded, in which it was agreed that the world should not warm by more than 2°C compared to the pre-industrial era (1850-1900) and aim for 1.5°C. The IEA (2020) reported that the production of fossil fuels decreased strongly in 2020 relative to 2019 with around -5%, most probably due to the Covid-19 pandemic measures. However, in 2021, global CO₂ emissions rebounded by nearly 5%. Again underlined by the Glasgow Climate Pact, one should strive for net zero emissions in 2050. Hence, in order to reach the Paris Climate Agreement, the emission of fossil fuels should be lowered considerably.

III.2 Renewable Energy

In 2019 fossil fuels accounted for ca. 86% of the total world energy production, whereas only 26.5% of electricity production could be assigned to renewables in 2019 (IEA, 2020). In order to reach the Paris Climate Agreement, further underlined by the Glasgow Climate Pact, the emission of fossil fuels should be lowered considerably. With the Glasgow Climate Pact, countries are being asked to come forward with ambitious 2030 emissions reductions targets that align with reaching net zero by the middle of the century. To deliver on these stretching targets, countries will need to accelerate the phaseout of coal, encourage investment in renewables and speed up the switch to electric vehicles (COP26, 2021).

In 2019 renewables increased much more than fossil fuels in relative terms (e.g. +14% for solar and +12% for wind), however Hydro-electricity production stagnated. While it did not increase in 2019, oil remained the most produced form of energy (IEA, 2020). The Net Zero Emissions by 2050 scenario mandates an even greater increase in the share of renewable energy sources. However, as the share of renewable energy such as wind, solar and hydro-power increases, energy storage systems will be critical to address the weather-dependency of said renewable sources. This hour-to-hour variability leads to an imbalance in demand and supply at certain specific moments in time.

III.3 Energy Storage Problem

Rapidly scaling up energy storage systems will be critical to address the hour-to-hour variability of wind, solar and hydro-power generation related to their weather dependency, especially as their share of generation increases rapidly in the Net Zero Emissions by 2050 Scenario. Meeting rising flexibility needs while decarbonising electricity generation is a central challenge for the power sector, so all sources of flexibility, including power plants, grids, demandside response and storage need to be tapped (IEA, 2021a).

Currently, business cases for storage can be complex, and generally not viable under unfavourable laws, policies and regulatory market conditions. Such a market does not incentivise further development, innovations and investments in the energy storage problem. Direct support for storage through mandates and policies remains the most common option to incentivise deployment, but greater emphasis

should be placed on making regulations transparent and open, and on developing markets for capacity, flexibility and ancillary services so that storage can compete with other technologies and measures (IEA, 2021a).

Nowadays, lithium-ion battery storage is most widely used, making up the majority of all new capacity installed. Some key issues now are the extent to which technology developments can spill over into grid-scale batteries and storage ownership policies and regulations. Battery storage may not always be the most attractive option, and the long lead times for other storage technologies that are competitive today imply that even if investment signals for flexibility are currently lacking, it is critical to assess country and regional capabilities that will be relevant in the long term (IEA, 2021a).

IV Elaboration Current Process Delta21 Flood Protection System

This appendix provides an elaboration on the current Delta21 flood protection system as proposed by Berke and Lavooij (2018c) and as presented in Section 2.3.1. The aim of the elaboration provided here is to gain a better understanding of how the Delta21 flood protection system should function. A new Delta21 flood protection system is presented in Section 5.1.

Scenario 0 Daily conditions

Scenario 0 represents the system and corresponding states of the relevant structures during daily conditions. Here, daily conditions are governed by a yearly average Rhine discharge of 2200 m³/s at Lobith and a yearly average Meuse discharge of 200 m³/s at Borgharen (Heldesk Water, 2022a). Furthermore, under daily circumstances it is assumed that no storm surge occurs. During daily conditions the Haringvlietsluizen are either closed or (partly) open in accordance with the Kierbesluit, depending on the Rhine discharge at Lobith. The storm surge barrier, the Maeslantkering and the Hartelkering (Europoortkering) are open as there is no storm surge. The Spillway is closed and the Pumping Stations are not pumping for flood protection purposes. Note that the Pumping Stations might be pumping or turbining as part of the energy storage cycle of the Energy Storage Lake.



Figure IV.1: Water management system in daily conditions (modified from van Eeden (2021))

Figure IV.2 depicts the cross-section over the Delta Barrier, Spillway and Haringvlietsluizen corresponding to daily circumstances. The cross-section gives a qualitative insight in the status of the structures and accompanying water levels. The Delta Barrier is open: the tide and waves can propagate into the Tidal Lake. Note that the water level at the Tidal Lake is not necessarily the same as at the North Sea. The water level at the Tidal Lake depends on the effective flow area of the Delta Barrier, the water level at sea and the discharge through the Haringvlietsluizen.

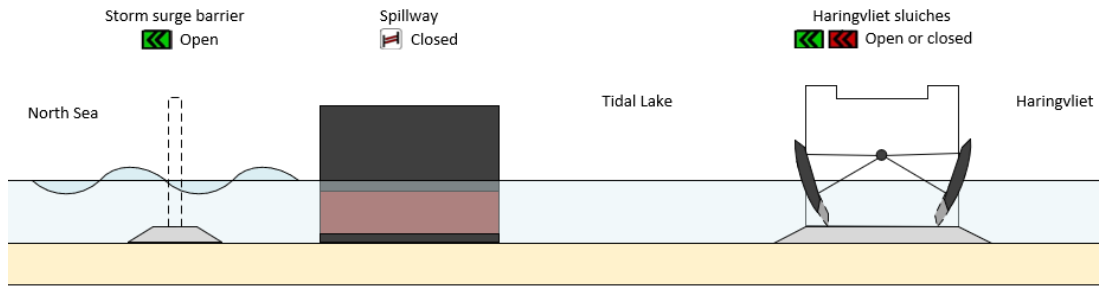


Figure IV.2: Cross-section in daily conditions

Scenario 1.1

Sub-scenario 1.1 considers the first stage of scenario 1 for a combined discharge (Haringvliet and Nieuwe Waterweg) greater than $9000 \text{ m}^3/\text{s}$. In this scenario the Haringvlietsluizen are open according to the Kierbesluit to be able to discharge the high river discharge towards the sea. The storm surge barrier will be closed during high water (HW). By closing the storm surge barrier the Tidal Lake can be used in an effective manner to capture and discharge the river water as a first resort resulting in a rising water level in the Tidal Lake. The Maeslantkering and the Hartelkering are open as for this main scenario no storm surge greater than 1.5 m is present. For now, the Spillway is still closed and the Pumping Stations are not pumping for flood protection purposes.



Figure IV.3: Water management system during scenario 1.1 (modified from van Eeden (2021))

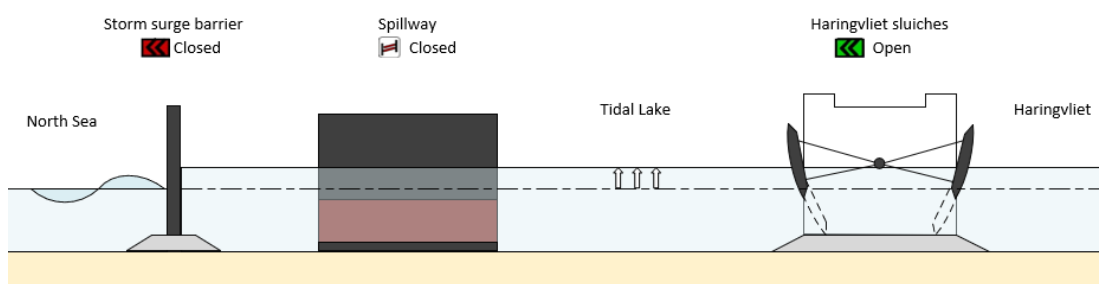


Figure IV.4: Cross-section during scenario 1.1

Scenario 1.2

Sub-scenario 1.2 considers the second and last stage of scenario 1. For this sub-scenario, the water level at Dordrecht threatens to reach NAP + 2.5 m. Excessive river discharge 'piling up' in the Tidal Lake is threatening to increase the water level at Dordrecht to NAP + 2.5 m. The Tidal Lake has insufficient capacity with regard to storing the excess river discharge and the Energy Storage Lake is used. Hence, in addition to the Haringvlietsluizen being open and the storm surge barrier being closed, the Spillway will be opened and the Pumping Stations are pumping the excess river discharge from the Energy Storage Lake to sea. The Europoortkering is still open.



Figure IV.5: Water management system during scenario 1.2 (modified from van Eeden (2021))

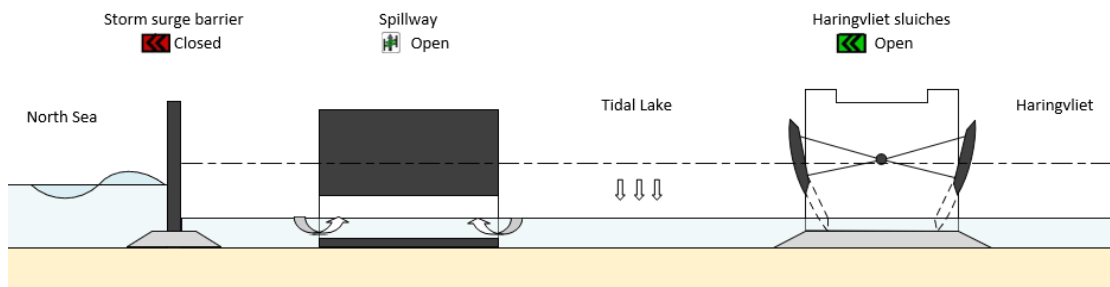


Figure IV.6: Cross-section during scenario 1.2

Scenario 2.1

Sub-scenario 2.1 considers the first stage of scenario 2 for a discharge greater than $5000 \text{ m}^3/\text{s}$ and an expected storm surge at Hoek van Holland greater than 1.5 m. In this scenario the Haringvlietsluizen are opened in accordance with the Kierbesluit, depending again on the Rhine discharge at Lobith. The storm surge barrier is closed due to the expected storm surge. The storm surge barrier will be closed during low water (LW). For now, the Spillway is still closed and the Pumping Stations are not pumping for flood protection purposes and only the Tidal Lake will be utilised. The Europoortkering is closed.



Figure IV.7: Water management system during scenario 2.1 (modified from van Eeden (2021))

Note that the general cross-section corresponding to scenario 2.1, as depicted in Figure IV.8, is the same (qualitatively) as for scenario 1.1 (see Figure IV.4). However the water level at the North Sea is greater for scenario 2.1 than for scenario 1.1 due to the storm surge at Hoek van Holland. Furthermore, the rate of increase of the water level in the Tidal Lake will be smaller due to a smaller discharge through the Haringvliet Locks.

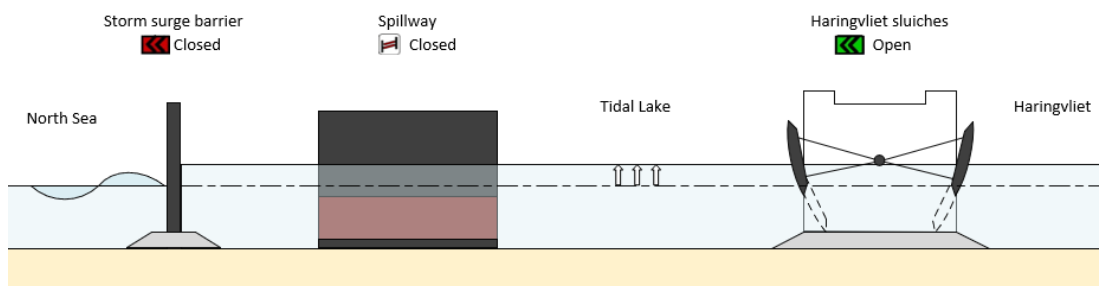


Figure IV.8: Cross-section during scenario 2.1

Scenario 2.2

After closure of the storm surge barrier in scenario 2.1, water levels will rise in the rivers upstream. Once the water level in Dordrecht threatens to reach NAP + 2.5 m the Spillway is opened and the Pumping Stations start pumping subsequently. In this stadium, the Tidal Lake only is not enough to keep the water at Dordrecht from rising to NAP + 2.5 m and the Energy Storage Lake is to be used. Note that the Maeslantkering and the Hartelkering are still open and any inflow from sea into the Nieuwe Waterweg and Hartelkanaal is pumped out by means of the Energy Storage Lake via het Spui.



Figure IV.9: Water management system during scenario 2.2 (modified from van Eeden (2021))

The general cross-section corresponding to scenario 2.2 is the same (qualitatively) as for scenario 1.2. (see Figure IV.6).

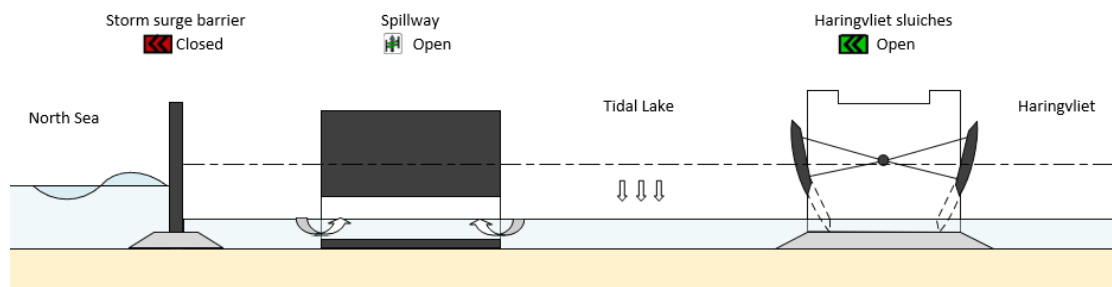


Figure IV.10: Cross-section during scenario 2.2

Scenario 2.3

If the storm conditions continue to ravage the coast of Hoek van Holland the water level at Hoek van Holland could reach NAP + 3 m. Once this happens also the Europoortkering will close in addition to scenario 2.2.



Figure IV.11: Water management system during scenario 2.3 (modified from van Eeden (2021))

Note that the closure of the Europoortkering, in addition to scenario 2.2, does not result in a changed status for the Delta Barrier, Spillway and Haringvlietssluzen with respect to scenario 2.2 in a qualitative sense. The water level at the sea side of the storm surge barrier is greater though for scenario 2.3 than for scenario 2.2.

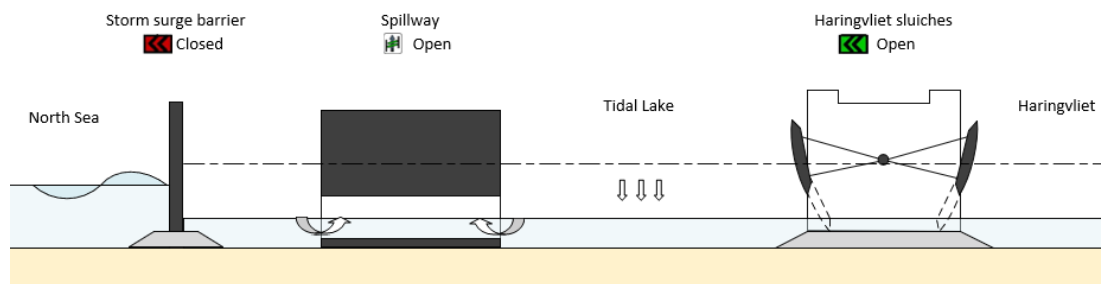


Figure IV.12: Cross-section during scenario 2.3

Scenario 3.1

Sub-scenario 3.1 considers the first stage of scenario 3 for only an expected storm surge at Hoek van Holland greater than 1.5 m, while discharges stay lower than 5000 m³/s. In this scenario the Haringvlietsluizen are either closed or (partly) open according to the Kierbesluit, depending again on the Rhine discharge at Lobith. The storm surge barrier is closed due to the expected storm surge. The Spillway is closed and the Pumping Stations are not pumping for flood protection purposes as the discharge will not result in a water level at Dordrecht of NAP + 2.5 m for the duration of a storm. The Europoortkering is still open.



Figure IV.13: Water management system during scenario 3.1 (modified from van Eeden (2021))

Figure IV.14 depicts the cross-section over the Delta Barrier, the Spillway and the Haringvlietsluizen for scenario 3.1. Note that for this scenario, the water level in the Tidal Lake will rise relatively slow compared to scenarios 1.1. and 2.1. due to the lower discharge through the Haringvlietsluizen. For this reason, it is not expected that the water level in the Tidal Lake will rise to such an extent during the storm that opening of the Spillway is necessary.

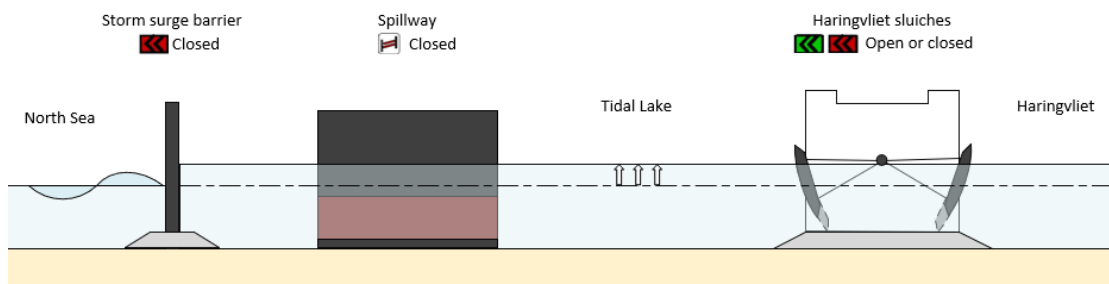


Figure IV.14: Cross-section during scenario 3.1

Scenario 3.2

Again, if the storm conditions continue to ravage the coast of Hoek van Holland the water level at Hoek van Holland could reach NAP + 3 m. Once this happens the Europoortkering will close in addition to scenario 3.1.



Figure IV.15: Water management system during scenario 3.2 (modified from van Eeden (2021))

The general cross-section corresponding to scenario 3.2 is the same (qualitatively) as for scenario 3.1. (see Figure IV.14). The water level in the Tidal Lake will be greater than for scenario 3.1, however will not reach the critical level for which the Spillway should be opened. Furthermore, the water level at the sea side of the Delta Barrier is greater for scenario 3.2 than for scenario 3.1.

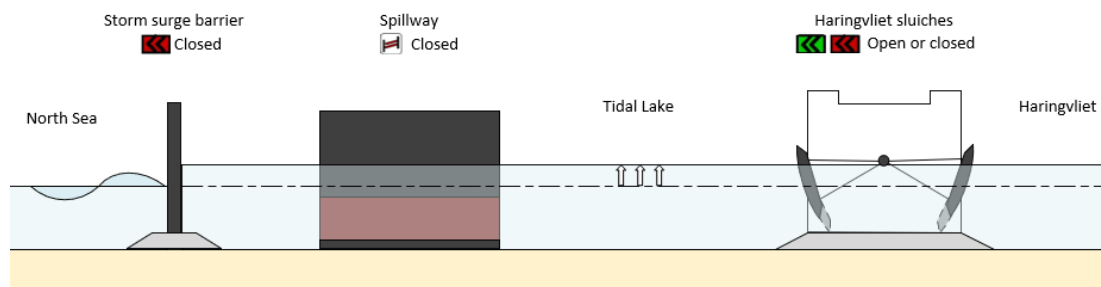


Figure IV.16: Cross-section during scenario 3.2

Overview

Figure IV.17 presents an overview of all the stages in which the relevant elements of Delta21 occur during different scenarios for the current Delta21 flood protection system as proposed by Berke and Lavooij (2018c)

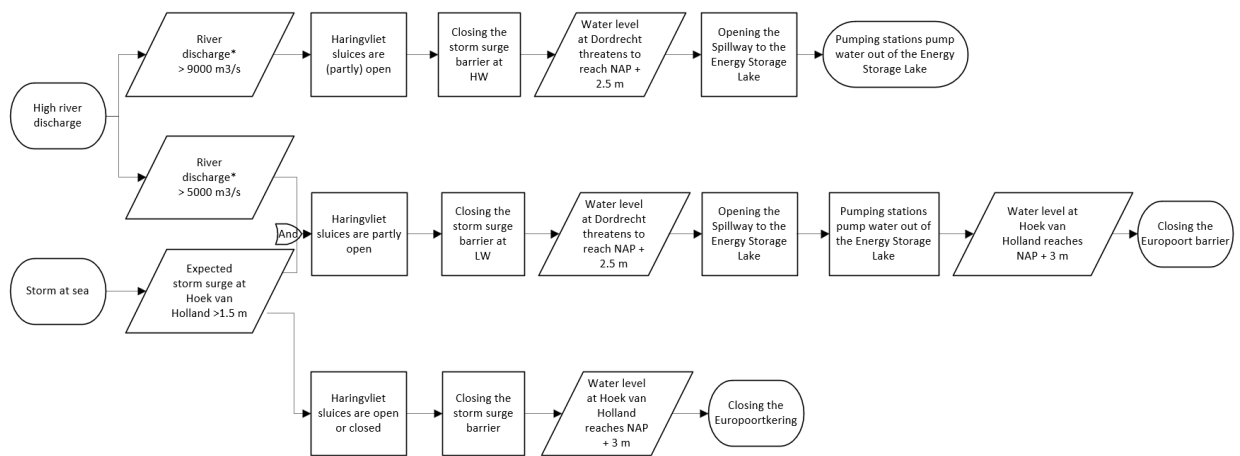


Figure IV.17: Process of the Delta21 flood protection system for different scenarios

* River discharge represents the sum of Nieuwe Waterweg and Haringvliet discharge

The current Delta21 flood protection system, as depicted in Figure IV.17, seems ill defined and formulated closure criteria for the storm surge barrier are rather ambiguous. A new Delta21 flood protection process is proposed in Section 5.1 with clear closure criteria for the storm surge barrier in order to effectively protect the hinterland against flooding.

V Substantiation Functional Requirements

This appendix provides the substantiation for the functional requirements as listed in Section 3.1.1. The functional requirements are described "SMART", allowing for direct verification. The quantified maximum failure probabilities follow from the safety standard of Delta 21 (see Appendix VI). Note that all functional requirement must also hold including climate change. For the sake of completeness, all functional requirements besides the ecological requirements are presented here.

FR-1. Flood protection

FR-1.1. The Delta Barrier must prevent the hinterland from flooding

The maximum probability of flooding due to failure of the Delta Barrier is $3.80 \cdot 10^{-5}$ per year.

FR-1.2. Water-retaining function

FR-1.2.1. The Delta Barrier must be sufficiently high

The retaining height of the structure must not lead to flooding of the hinterland for a 1:83333 per year high water and high waves event for an overtopping discharge of 1000 l/s/m.

FR-1.2.2. The Delta Barrier must conform to the 2017 Water Act

FR-1.3. Closure reliability

FR-1.3.1. The closing procedure must be reliable

Non-closure of the Delta Barrier must not lead to flooding. Probability of failure due to non-closure must not be greater than 1:526316 per year.

FR-1.3.3. The Delta Barrier must conform to the 2017 Water Act

FR-1.4. Ability to discharge water, ice and sediments

FR-1.4.1. The Delta Barrier must have sufficient effective flow area.

The effective flow area must be as such that FR-1.2 holds.

FR-1.4.2. The Delta Barrier must be able to discharge ice

Ice sheets, formed in the Tidal Lake and broken by barges, must be able to pass through the effective flow area.

FR-1.4.3. The Delta Barrier must not cause excessive erosion or accretion

When open, the Delta Barrier must not cause excessive erosion or accretion which could undermine any of the specified functions or requirements.

FR-1.4.4. The Delta Barrier must conform to the 2017 Water Act

FR-2. Preserving passage of ships

FR-2.1. Allowing passage of ships

Ships up to Cemt-class Va must be able to pass the Delta Barrier from - and to sea during both high - and low tide under daily circumstances for the entire design life of the structure.

CEMT-class Va ($L \times W \times D \times H$ [m]) = $135 \times 11,4 \times 4 \times 7,1$.

The flow velocity through the element of the Delta Barrier assigned for navigation, when open, must be less than 6 knots (≈ 3 m/s) under daily circumstances.

FR-2.2. Enable sport- and recreational ships

Sport- and recreational ships must be able to pass the Delta Barrier from - and to sea during both high - and low tide under daily circumstances for the entire design life of the structure.

The flow velocity through the element of the Delta Barrier assigned for navigation, when open, must be less than 3 knots (≈ 1.5 m/s) under daily circumstances.

FR-2.3. Enable professional fishing vessels

Professional fishing vessels must be able to pass the Delta Barrier from - and to sea during both high - and low tide under daily circumstances for the entire design life of the structure.

OD1 Maarten-Jacob ($L \times W \times D \times H$ [m])¹⁹ = $42,35 \times 8,5 \times 5 \times 5,15$.

The flow velocity through the element of the Delta Barrier assigned for navigation, when open, must be less than 5.5 knots²⁰ (≈ 2.8 m/s) under daily circumstances.

FR-2.4. Enable sport- and recreational fishing vessels

Sport- and recreational fishing vessels must be able to pass the Delta Barrier from - and to sea during both high - and low tide under daily circumstances for the entire design life of the structure.

The flow velocity through the element of the Delta Barrier assigned for navigation, when open, must be less than 5.5 knots (≈ 2.8 m/s) under daily circumstances.

FR-3. Allowing passage of tidal flow, ice and sediments

If no closure is needed for flood protection reasons, the storm surge barrier must be opened completely.

FR-4. Preserving ecological system

FR-4.1. Allow safe passage of aquatic creatures

FR-4.1.1. Accommodate migrating fish

The Delta Barrier must not interfere with migrating fish species under daily circumstances.

Provide a window of at least several hours with a maximum flow velocity of 0.60 m/s for glass eel²¹ under daily circumstances.

FR-4.1.2. Allow seals to pass

The Delta Barrier must allow for both gray- and harbour seals to pass safely from- and to sea under daily circumstances.

The flow velocity through the barrier must remain smaller than 10 m/s under daily circumstances.

The effective flow area of the barrier(s) must allow for the 100% safe passage of both gray- and harbour seals.

FR-4.1.3. Allow passage of harbour porpoise

The Delta Barrier must accommodate the safe passage of harbour porpoise from- and to sea under daily circumstances.

The flow velocity through the barrier must remain smaller than 15 m/s under daily circumstances.

The effective flow area of the barrier(s) must allow for the 100% safe passage of harbour porpoise.

FR-4.2. Allow safe passage of land mammals, birds and insects

The Delta Barrier must allow for the passage of land mammals (e.g. mice, rabbits and foxes), birds and insects from Goeree-Overflakkee towards the Energy Storage Lake and back under daily circumstances.

FR-5. Allowing passage of road-traffic

FR-5.1. All motorised road-traffic must be able to pass safely

All cars, lorries, service vehicles, special transport and maintenance vehicles and equipment must be able to pass the Delta Barrier from Goeree-Overflakkee towards the Energy Storage Lake and vice versa during daily circumstances.

FR-5.2. Cyclists must be able to pass safely

Cyclists must be able to pass the Delta Barrier from Goeree-Overflakkee towards the Energy Storage Lake and vice versa during daily circumstances.

FR-5.3. Pedestrians must be able to pass safely

Pedestrians must be able to pass the Delta Barrier from Goeree-Overflakkee towards the Energy Storage Lake and vice versa during daily circumstances.

FR-6. The Delta Barrier must be maintainable

FR-6.1. Regular maintenance and inspection

Maintenance vehicles and equipment must be able to reach the respective elements of the

Delta Barrier which require inspection or maintenance.

FR-6.2. Maintenance after (storm event) damages

Respective elements of the Delta Barrier must be maintainable or replaceable within a certain time period after (storm event) damages.

FR-7. The Delta Barrier must be stiff enough

FR-7.1. The Delta Barrier must conform to the 2012 Building Decree

FR-7.2. The Delta Barrier must conform to the relevant European norms and regulations including the National Annexes (NEN-EN)

FR-8. The Delta Barrier must have a functional lifetime of 200 years with regard to functions FR-1.1, FR-1.2, FR-1.3, FR-1.4, FR-4, FR-5, FR-6 and FR-7

FR-9. FR-3 is subordinate to FR-1.3

¹⁹The governing fishing vessel here is the OD1 Maarten-Jacob (Rijksdienst voor Ondernemend Nederland (Rijk), 2022). Dimensions adapted from MarineTraffic.com (2022a)

²⁰The governing fishing vessels here are the SL13 Zeewolf and the SL4 Branding (Rijksdienst voor Ondernemend Nederland (Rijk), 2022), with an average speed of 5.5 knots as stated by MarineTraffic.com (2022b) and MarineTraffic.com (2022c) respectively

²¹Adapted from van den Wijngaard, Hofman, van Herk, and Wanningen (2014)

VI Safety Standard Delta21

This appendix provides the reasoning and derivation of the Delta21 safety standard. First an analysis is conducted in order to derive the required safety standard for the whole Delta21 flood protection system. Secondly, the new Delta21 "dike ring" is divided into segments and the most relevant failure mechanisms are identified. Lastly from the segment containing the Delta Barrier with corresponding failure mechanisms, maximum failure probabilities are derived on object level. The maximum failure probabilities on object level are used to formulate the requirements.

VI.1 Estimation of Flood Protection Standard Delta21 Dike Ring

With regard to the main flood protection objective of the Delta21 system it could be argued that the new segments should at least inherit the lower limit failure probability of the Haringvlietdam. However, as the main purpose of the Delta21 flood protection system is mostly to improve flood protection upstream of the Rhine and Meuse at least up till Dordrecht, one might argue that a stricter requirement is needed. Furthermore, the current Haringvlietsluizen do not have a flood protection function accounting for river floods, while the new Delta21 flood protection system would.

The required maximum probability of failure for the Delta21 flood protection system can be determined analogously to determining the maximum probability of failure for a dike segment based on individual risk (see Equation (VI.1)). It is assumed that the failure probability of the dike segment corresponding with the greatest individual risk²² ought to be inherited by the Delta21 flood protection system. With this approach, it is assumed that the governing dike segment of the respective dike ring has no flood protection function after implementing the Delta21 flood protection system. In other words, it is assumed that the dikes will no longer be strengthened after the implementation of Delta21, rendering the dike unable to serve a flood protection function. The relevant dike rings in this analysis are:

- Dike ring 20: Voorne-Putten
- Dike ring 25: Goeree-Overflakkee
- Dike ring 34: West-Brabant
- Dike ring 21: Hoeksche Waard
- Dike ring 22: Eiland van Dordrecht

For every dike ring above, the governing dike segment is determined, viz. the breach with a combined high relative probability of occurrence and high relative number of casualties. Dike segments which are to be strengthened with the HWBP have not been taken into account as they will - after strengthening - most probably not be governing. For every breach, given the mortality after flooding of the area behind the breach and the evacuation fraction of the respective dike ring, one is able to determine the required maximum probability of failure for the dike segment where said breach would occur using Equation (VI.1).

$$IR(x, y) = P_i F_{D,i}(x, y)(1 - F_{E,i}) \leq 1 : 100000 \quad (\text{VI.1})$$

where: $IR(x, y)$ is the individual risk requirement at location (x,y)
 P_i is the probability of failure for dike segment i per year (to be inherited by Delta21)
 $F_{D,i}$ is the mortality at location (x,y) for a scenario i
 $F_{E,i}$ is the evacuation fraction for a scenario i

The mortality given a flood event has been assessed by Jonkman et al. (2021), interpolating between data based on historical information from several historical floods (such as the floods in the Netherlands

²²Risk is equal to probability of failure times the consequences given the breached dike segment

in 1953 and in Japan in 1959). Jonkman et al. (2021) concluded that one can distinguish three zones: a zone with rapidly rising water (most probably right after the breach location), a remaining zone further from the breach where water rises less rapidly and a transition zone between. The mortality is generally a function of flood characteristics such as the water depth after flooding (d) and the rising speed of the water in the flooded area (w). The mortality functions per zone as determined by Jonkman et al. (2021) are presented below:

Mortality in the zone with rapidly rising waters

If $d \geq 2.1$ m and $w \geq 4$ m/hr

$$F_{D,rise} = \phi \frac{\ln(d) - \mu_N}{\sigma_N} \quad (VI.2)$$

where: $F_{D,rise}$ [-] is the mortality in the zone with rapidly rising waters
 ϕ is the standard normal distribution function
 d [m] is the water depth after flooding
 μ_N [-] = 1.46
 σ_N [-] = 0.28

Mortality in the transition zone

If $d \geq 2.1$ m and 0.5 m/hr $\leq w < 4$ m/hr

$$F_D = F_{D,remain} + (w - 0.5) \frac{F_{D,rise} - F_{D,remain}}{3.5} \quad (VI.3)$$

where: F_D [-] is the mortality in the transition zone
 $F_{D,remain}$ [-] is the mortality in the remaining zone
 w [m/hr] is the rising speed of the water in the considered area after flooding

Mortality in the remaining zone

If $w \leq 0.5$ m/hr or $w \geq 0.5$ m/hr and $d \leq 2.1$ m

$$F_{D,remain} = \phi \frac{\ln(d) - \mu_N}{\sigma_N} \quad (VI.4)$$

where: $F_{D,remain}$ [-] is the mortality in the remaining zone
 d [m] is the water depth after flooding
 μ_N [-] = 7.60
 σ_N [-] = 2.75

Dike ring 20: Voorne-Putten

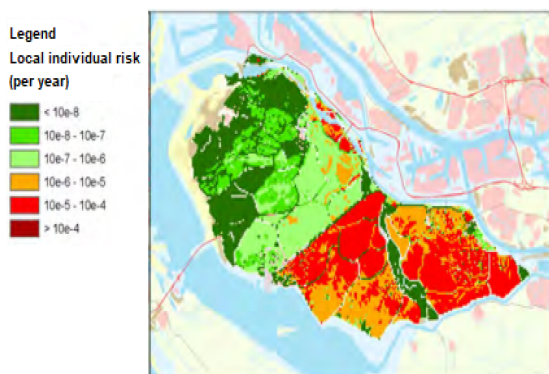


Figure VI.1: Local individual risk dike ring Voorne-Putten after HWBP2 (modified from de Groot (2014a))

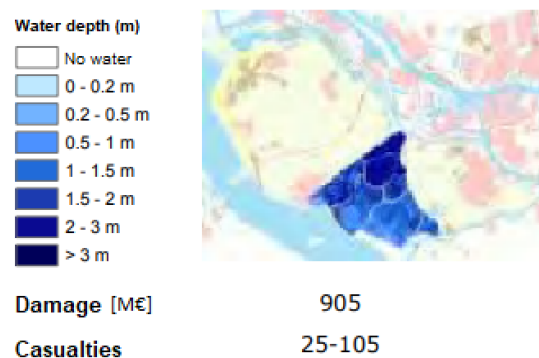


Figure VI.2: Flood map breach location 20-04 (segment 20-4) (modified from de Groot (2014a))

Governing segment	depth (d)	Rising speed (w)	$F_{D,remain}$	F_E	P [per year]
20-4	3 m	≤ 0.5 m/hr	0.0091	0.11	$1.235 \cdot 10^{-3}$

Table VI.1: Analysis dike ring Voorne-Putten

The water depth after flooding (d) follows from Figure VI.2. As for the rising speed, the location with the higher (local) individual risk (see Figure VI.1) is located far from the southern breach, hence most probably in the remaining zone. The final evacuation fraction (F_E) as stated by de Groot (2014a) is a sum of the evacuation fractions taking into account a sudden flood event with both no evacuation and an unorganised evacuation scenario and a flood event expected well in advance with an unorganised and an organised evacuation scenario. It should be noted that multiple dike reinforcements are on the HWBP programme (GEH), leaving dike segment 20-4 - not on the programme - as most probable to fail.

Dike ring 25: Goeree-Overflakkee

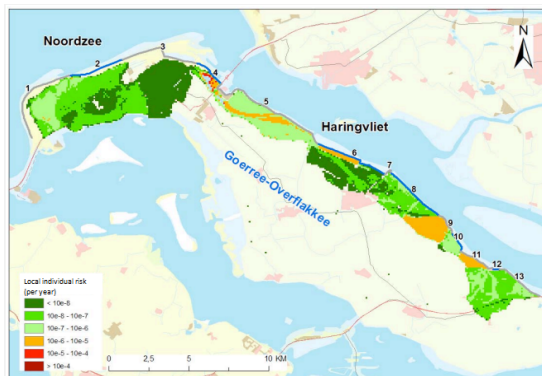


Figure VI.3: Local individual risk dike ring Goeree-Overflakkee (modified from Bisschop and Karimlou (2014))

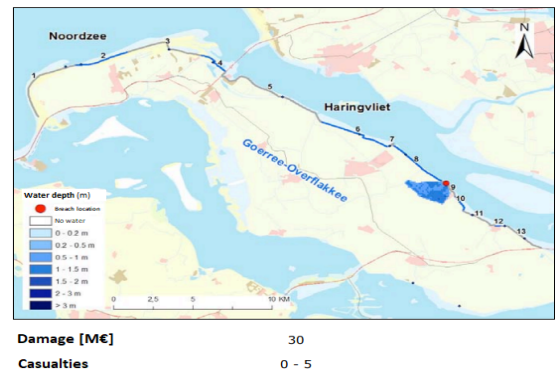


Figure VI.4: Flood map breach location 25-09 (segment 25-2) (modified from Bisschop and Karimlou (2014))

Governing segment	depth (d)	Rising speed (w)	$F_{D,remain}$	F_E	P [per year]
25-2	1.5 m	≤ 0.5 m/hr	0.0044	0.26	$3.067 \cdot 10^{-3}$

Table VI.2: Analysis dike ring Goeree-Overflakkee

The water depth after flooding (d) follows from Figure VI.4. As for the rising speed, the flooded area after the breach spans over an order of multiple kilometres, hence most probably in the remaining zone. The final evacuation fraction (F_E) as stated by Bisschop and Karimlou (2014) is a sum of the evacuation fractions taking into account a sudden flood event with both a no evacuation and an unorganised evacuation scenario and a flood event expected well in advance with an unorganised and an organised evacuation scenario. It should be noted that the breach locations with the highest probability of failure, according to Bisschop and Karimlou (2014), are not on the HWBP programme. Bisschop and Karimlou (2014) states that the breach with the highest probability of failure (breach location 25-06) would not result in any casualties. Breach location 25-09 (segment 25-2) has the second greatest probability of failure where a breach would lead to casualties as can be seen in Figure VI.4.

Dike ring 34: West-Brabant

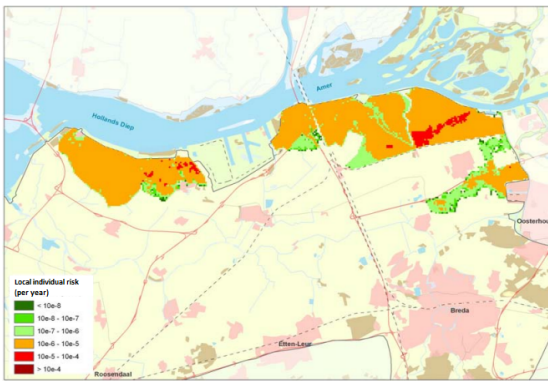


Figure VI.5: Local individual risk dike ring West-Brabant (modified from Arends and Nieuwhof (2011))

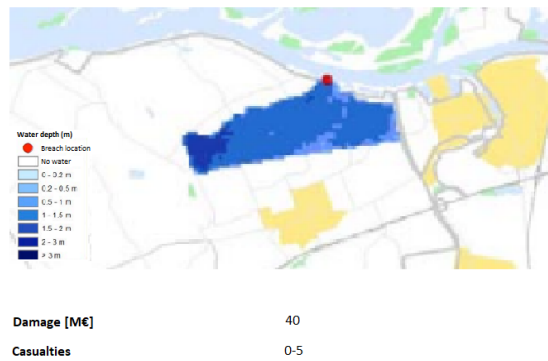


Figure VI.6: Flood map breach location 34-09 (segment 34-1) (modified from Arends and Nieuwhof (2011))

Governing segment	depth (d)	Rising speed (w)	$F_{D,remain}$	F_E	P [per year]
34-1	2 m	≤ 0.5 m/hr	0.0060	0.40	$2.778 \cdot 10^{-3}$

Table VI.3: Analysis dike ring West-Brabant

The water depth after flooding (d) follows from Figure VI.6. As for the rising speed, the flooded area after the breach spans over an order of multiple kilometres, hence most probably in the remaining zone. The final evacuation fraction (F_E) as stated by Arends and Nieuwhof (2011) is a sum of the evacuation fractions taking into account a sudden flood event with both a no evacuation and an unorganised evacuation scenario and a flood event expected well in advance with an unorganised and an organised evacuation scenario. It should be noted that the dike stretch from Willemstad till Geertruidenberg is on the HWBP programme (WIN, MDR and GEA). It is therefore assumed that the most probable breach locations will remain unchanged. The breach location near Klundert (34-03) has the highest probability of failure according to Arends and Nieuwhof (2011), with the location near Drimmelen Oost (34-09) as a close second. Flooding after a breach in segment 34-03 would give rise to a water depth after flooding which is lower than for a breach in segment 34-09. Therefore breach location 34-09 (segment 34-1) is chosen to be the governing segment with regard to the analysis. Note that this could also be deduced from Figure VI.5, comparing Drimmelen Oost to Klundert.

Dike ring 21: Hoeksche Waard

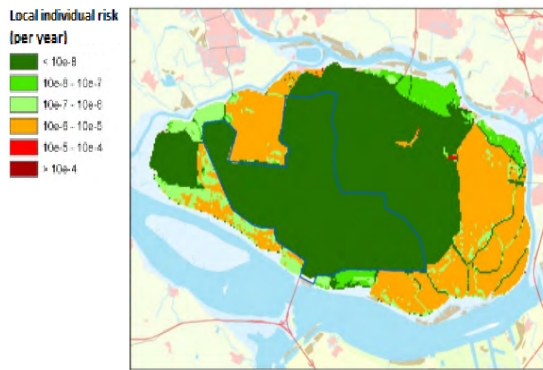


Figure VI.7: Local individual risk dike ring Hoeksche Waard (modified from de Groot (2014b))

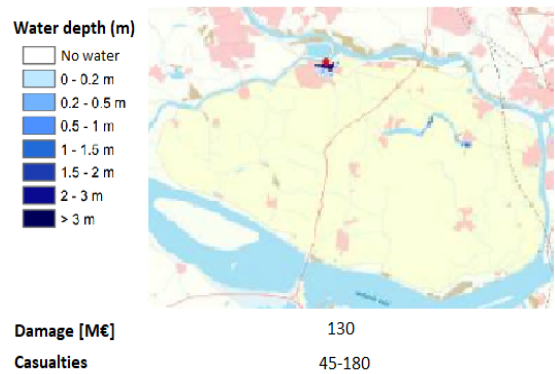


Figure VI.8: Flood map breach location 21-01 (segment 21-1) (modified from de Groot (2014b))

Governing segment	depth (d)	Rising speed (w)	F_D	F_E	P [per year]
21-1	3 m	1 m/hr	0.0219	0.11	$5.136 \cdot 10^{-4}$

Table VI.4: Analysis dike ring Hoeksche Waard

The water depth after flooding (d) follows from Figure VI.8. The rising speed for the area after a breach at breach location 21-01 is taken from Pieterse, Knoop, Nabielek, Pols, and Tennekes (2009). The final evacuation fraction (F_E) as stated by de Groot (2014b) is a sum of the evacuation fractions taking into account a sudden flood event with both a no evacuation and an unorganised evacuation scenario and a flood event expected well in advance with an unorganised and an organised evacuation scenario. It should be noted that multiple dike reinforcements are on the HWBP programme, leaving breach location 21-01 - not on the programme - as most probable to breach.

Dike ring 22: Eiland van Dordrecht

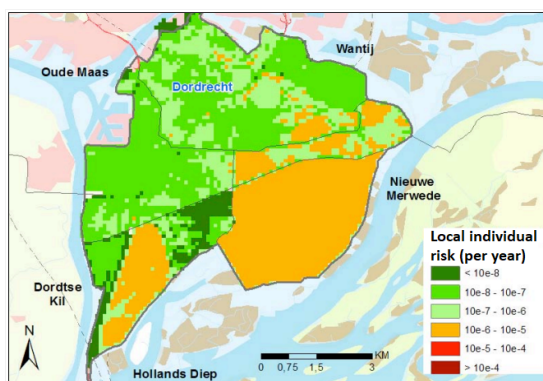


Figure VI.9: Local individual risk dike ring Eiland van Dordrecht (modified from Veenstra-Huisman (2014))

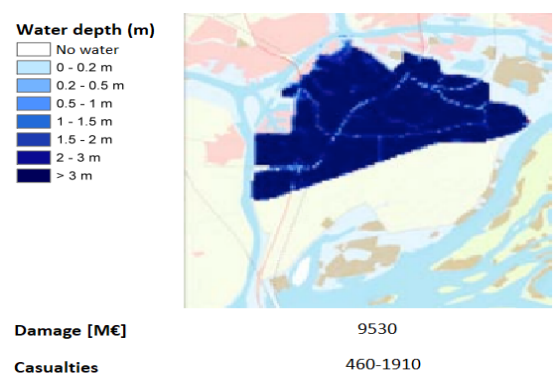


Figure VI.10: Flood map breach location 22-05 (segment 22-2) (modified from Veenstra-Huisman (2014))

Governing segment	depth (d)	Rising speed (w)	F_D	F_E	P [per year]
22-2	3.25 m	1 m/hr	0.0309	0.11	$3.636 \cdot 10^{-4}$

Table VI.5: Analysis dike ring Eiland van Dordrecht

The water depth after flooding (d) follows from Figure VI.10. The rising speed for the area after a breach at breach location 22-05 is taken from Pieterse et al. (2009). The final evacuation fraction (F_E) as stated by Veenstra-Huisman (2014) is a sum of the evacuation fractions taking into account a sudden flood event with both a no evacuation and an unorganised evacuation scenario and a flood event expected well in advance with an unorganised and an organised evacuation scenario. It should be noted that a breach at breach location 22-05 is not the most probable breach location according to Veenstra-Huisman (2014), but nonetheless has the greatest contribution to the individual risk of the dike ring.

Flood protection standard Delta21

The Delta21 flood protection system ought to inherit the most stringent maximum failure probability as calculated for every relevant dike ring, i.e. the maximum failure probability corresponding to the Eiland van Dordrecht. Hence the Delta21 flood protection system should conform to a maximum allowable failure probability of $3.636 \cdot 10^{-4}$ per year. Now, in order for the individual segments of Delta21 to stay in line with the current standard failure probability values as per the 2017 Water Act, $3.0 \cdot 10^{-4}$ per year or equivalently 1:3333 per year is chosen for the entire Delta21 flood protection system.

Individual risk Dordrecht outside the primary dikes

Delta21 aims to lower inconveniences experienced by the area of Dordrecht outside the primary dike ring by maximising the water level at Dordrecht at NAP + 2.5 m. An area outside the primary dikes is e.g. the Nieuwe Haven area, with ca. 800 inhabitants (AlleCijfers.nl, 2021).

Given the fact that there are no dike segment to breach before flooding occurs here; the water level outside the primary dikes will rise in direct response to the water level at the river. For this reason, a flood wave reaching Dordrecht will cause immediate flooding resulting in a mortality fraction of 1. Furthermore, it is assumed that within the immediate future, areas such as the Nieuwe Haven will have an effective evacuation programme in place as to be expected considering the risks of sea level rise for areas outside the primary dikes. Veenstra-Huisman (2014) gives an evacuation fraction of 0.76 for an organised evacuation given that the flood event is expected well in advance.

Using eq. (VI.1), for the determined maximum allowable failure probability of Delta21 ($3.0 \cdot 10^{-4}$ per year), yields an individual risk of $7.20 \cdot 10^{-5}$ per year (eq. 1:13888 per year). Although greater than the maximum allowable individual risk (1:100000 per year), the difference is only a factor in the order of 10 resulting in the same order of flood safety as the southwestern part of Dordrecht inside the primary dikes.

VI.2 Proposed Delta21 Dike Segments with Failure Mechanisms

Delta21 introduces a new primary flood defence system and as such a new dike ring with corresponding dike segments and dike sections. As a consequence, in addition to the already existing dike segments from the current 2017 Water Act, new segments ought to be defined. Figure VI.11 proposes the safety standards of the new Delta21 flood protection system with separate segments, incorporated in the readily defined dike segments by the 2017 Water Act.

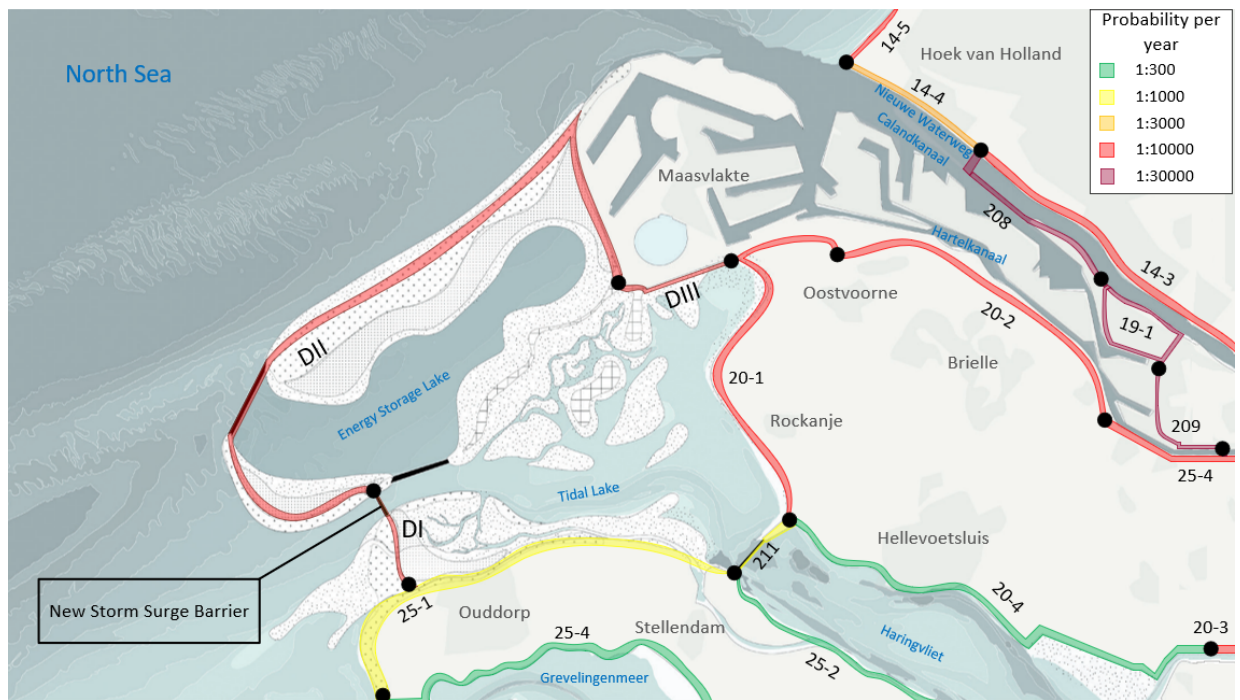


Figure VI.11: Primary flood defence standards including the Delta21 flood protection system

A decomposition of the newly defined Delta21 flood protection system with corresponding dike segments is given in Table VI.6.

It is found that a lower limit safety standard of 1:3333 is needed for the entire Delta21 flood protection system (sum of DI, DII and DIII) in order to conform to the individual risk requirement while staying in line with the current lower limit values as per the 2017 Water Act.

Segment	Sections	Safety standard
<i>DI</i>	Delta Barrier	1:10000
	Dike(s)	
<i>DII</i>	Pumping Stations	1:10000
	Dike(s)	
<i>DIII</i>	Dike(s)	1:10000
<i>Total</i>		1:3333

Table VI.6: Delta21 segments

One should note that the new segments as defined in Figure VI.11 also result in reduced hydraulic loads on the dike segments behind the new defences. Hence, one could argue that the safety standards of at least the dike segments directly behind the new defence system (i.e. 25-1, 20-1 and 211 in Figure VI.11) could be reduced. This will not be considered here in more detail as the design of the readily existing dike segments is outside the scope of this thesis.

The maximum permissible flooding probabilities from the Water Act do not relate to individual structures or dike sections, but to dike segments. A dike segment can be regarded as a series system. Note that the entire system also consists of a series system consisting of the three new dike segments. A series system is only as strong as its weakest link: if one link fails, the system fails (Rijkswaterstaat, 2018). This relationship is shown in the fault tree depicted by Figure VI.12. The probability that a structure will fail contributes to the probability of flooding of a segment. A structure fails if more water flows into the area through or over the structure than can be stored there without substantial damage or casualties (Rijkswaterstaat, 2018). This can have several causes. These causes are also known as failure mechanisms. The most important failure mechanisms treated by the Water Act are: overtopping, non-closure, internal erosion and structural failure.

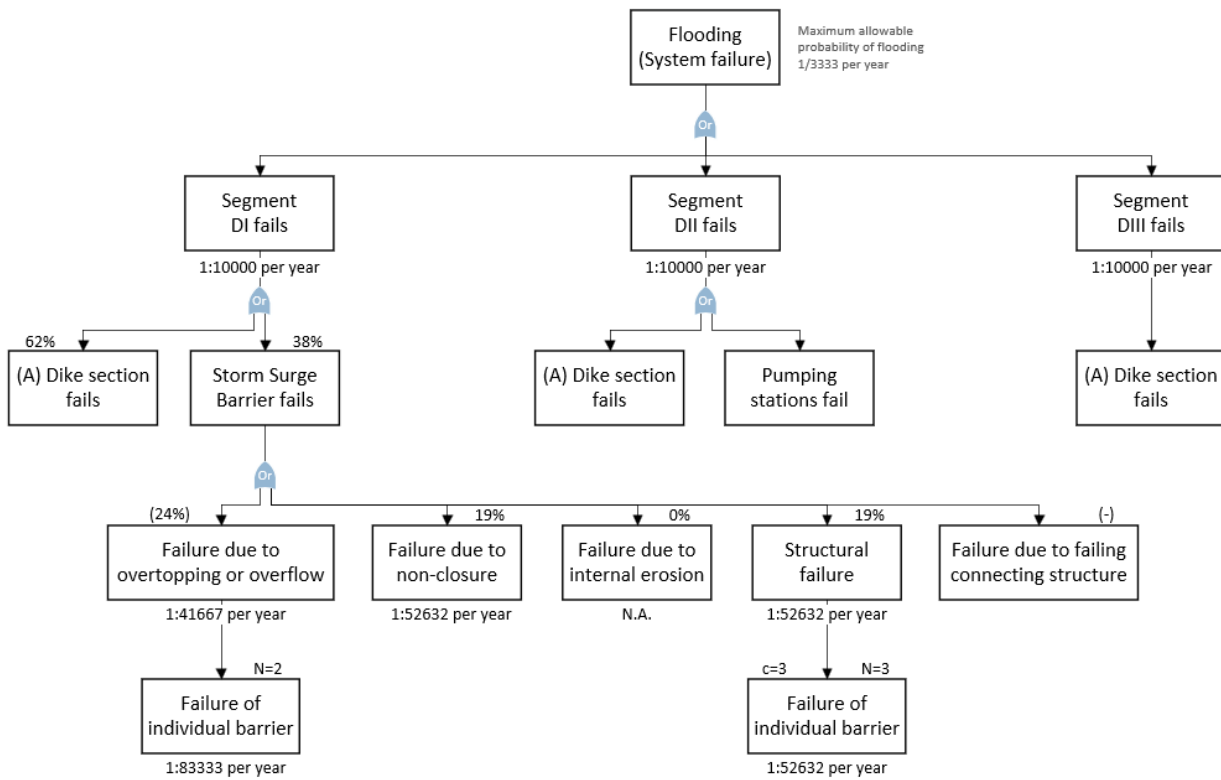


Figure VI.12: Fault tree of the new Delta21 flood protection system

As can be seen from Figure VI.12, segment DI has been divided into a dike section and the Delta Barrier. Furthermore, the storm surge barrier has been subdivided in the most important failure mechanisms. Each failure mechanism has its own maximum probability of failure, deduced from the maximum allowable probability of segment DI. Figure VI.12 is based on the standard distribution of target reliability as proposed in the WOWK (2018), however some major changes are made.

Failure probability requirements at segment level can be derived by dividing the flood probability standard over the various failure mechanisms. A default distribution of target reliability per failure mechanism has been drawn up for the WBI2017 and the OI2014v4 (Rijkswaterstaat, 2018). This is shown in Figure VI.13.

Type of structure	Failure mechanism								Total
	Overflow or overtopping	Internal erosion	Stability	Revetments	Dune erosion	Structure	Other	Reliability closure operation	
Dike	0.24	0.24	0.04	0.10	Na	0.08	0.30	Na	1.00
Structure	(0.24)	0.02	0.02	Na	Na	-	Na	0.04	0.08
Dune	Na	Na	Na	Na	0.70	Na	0.30	Na	1.00

Figure VI.13: Standard distribution of target reliability per failure mechanism (Jonkman et al., 2021)

For the case of segment DI (see Figure VI.11) consisting of only 1.2 km of structure (storm surge barrier) and a multitude of kilometres of dike, an allocation of 92% towards the dike as proposed in Figure VI.13 and in e.g. the WOWK (2018) seems illogical. While the Delta Barrier will be relatively large, it is also relatively expensive to have the storm surge barrier conform to a strict (low) failure probability reservation. For these reasons, the 30% reservation towards 'other' in Figure VI.13 is evenly distributed along the failure mechanisms of the structure.

VI.3 Maximum Failure Probabilities on Object Level

After dividing the failure probability over the relevant failure mechanisms, the failure mechanism should be evaluated for the failure of one specific, individual barrier. In practice, the chance that a structure or a part of the structure will fail is greater than the chance that *one specific* structure or part of the structure will fail. This phenomenon is also known as the length effect. In order to be able to assess the reliability of an individual structure or component, a requirement at object or component level must be derived from the requirement at segment level (Rijkswaterstaat, 2018).

In the OI2014v4 and the WBI2017 standard length effect factors are included with which a failure probability for an individual structure or component can be derived directly. In a general sense this can be written as in Equation (VI.5).

$$P_{req,i,j} = \frac{P_{req,j}}{N_j} = \frac{\omega_j}{N_j} \cdot P_{max} \quad (VI.5)$$

where: $P_{req,i,j}$	[-]	=	required annual failure probability for section i and failure mechanism j per year
$P_{req,j}$	[-]	=	failure probability for failure mechanism j at segment level per year
P_{max}	[-]	=	required annual failure probability for the dike segment
ω_j	[-]	=	contribution of failure mechanism j to the system failure probability
N_j	[-]	=	length effect factor for failure mechanism j

The contributions per failure mechanism over the storm surge barrier are depicted in Figure VI.12 by means of percentages. As for the length effect factors per failure mechanism, the OI2014v4 and the WBI2017 prescribe and advise different factors depending on the failure mechanism and the structure.

Overtopping

For overtopping the WBI2017 advises $N_h=1-3$ (Rijkswaterstaat, 2018). For simplicity, the length effect factor regarding overtopping and overflow for the Delta Barrier is assumed the same as for the Haringvlietsluizen: $N_h=2$ (Rijkswaterstaat, 2017).

$$\begin{aligned} P_{req,i,h} &= \frac{0.24}{2} \cdot \frac{1}{10000} \\ &= \frac{1}{83333} \text{ per year} \end{aligned}$$

Reliability closure operation

The length effect factor regarding a non-closure event is a function of the number of structures or components that could not be easily approved with regard to closure reliability (Rijkswaterstaat, 2018). However, the verification regarding to reliability of the closure operation of the Delta Barrier (see Section 5.2) is conducted considering the structure as a whole, i.e. taking into account all gates and not one specific gate or section. For this reason, no length effect is applied regarding a non-closure event.

Internal erosion

For the case of the Delta Barrier for Delta21 it is expected that some sort of a granular filter will be used. Hence the bottom protection on the Tidal Lake side will be designed in such a way that it is sand-tight and water-permeable, now internal erosion cannot occur. Assuming that the filter remains water-permeable and sand-tight during its design life, the WOWK (2018) states that no failure probability has to be reserved for failure due to internal erosion as can be seen in the fault tree in Figure VI.12.

Structural failure

The length effect factor regarding structural failure is set to $N_{struc} = 3$ according to the WBI2017 (Rijkswaterstaat, 2018). Furthermore, the WOWK (2018) proposes the use of an additional correlation factor (to be multiplied with Equation (VI.5)) to compute the maximum failure probability regarding structural failure.

The failure mechanisms structural failure and failure by overflow/overtopping are strongly correlated, because in both cases the hydraulic load is dominant for the failure probability over the uncertainty of strength and because the failure probability for overtopping/overflow is much greater than that for structural failure. There is therefore a good chance that a structure has already failed as a result of overtopping/overflow before structural failure occurs. In order not to unnecessarily conservatively dimension the structure, or to work with water levels that (may) extend far above the crest, the degree of correlation between the two mechanisms is taken into account using a factor c (Rijkswaterstaat, 2018).

The correction factor depends on the required annual failure probability for the dike segment (P_{max}) according to Figure VI.14.

P_{max} [-]	1/100	1/300	1/1.000	1/3.000	1/10.000	1/30.000
c [-]	7	5	4	3	3	3

Figure VI.14: Correction factor c for the correlation between structural failure and failure by overtopping/overflow (Rijkswaterstaat, 2018)

As for dike segment DI with the required maximum annual failure probability of 1/10000, fig. VI.14 gives that the correction factor concerning the correlation between structural failure and failure by overtopping/overflow should be taken as $c = 3$.

$$\begin{aligned}
 P_{req,i,struct} &= \frac{0.19}{3} \cdot 3 \cdot \frac{1}{10000} \\
 &= \frac{1}{52632} \text{ per year}
 \end{aligned}$$

Connecting structures

It should furthermore be noted that the Water Act does not reserve a failure probability for connecting structures, as there is no general applicable semi-probabilistic method due to the great variety of connecting structures (Rijkswaterstaat, 2018). In practice the Water Act states a relative requirement: A connecting structure must be designed, dimensioned, executed and maintained in such a way that it does not weaken compared to the adjacent dike body during the intended plan period, assuming that this adjacent dike body at least meets the applicable requirements during the plan period (Rijkswaterstaat, 2018). Ironically though, connecting structures are often the place where failure and breaches occur. Connecting structures adjacent to the Delta Barrier are outside the scope of the thesis.

VII Wind Data

This appendix aims to gather a general insight into the occurrence of wind speeds and to quantify both the direct wind forces on the structure and determine the height wind waves and set-up generated at the Tidal Lake. A Three-parameter Weibull distribution is fitted through data for the maximum daily wind gusts and maximum hourly mean wind speeds at Hoek van Holland measured by KNMI (2022). Figure VII.1 shows said fits through the measured data for the maximum daily wind gusts and Figure VII.2 for the maximum hourly mean wind speeds, from the KNMI (2022) data for every wind direction.

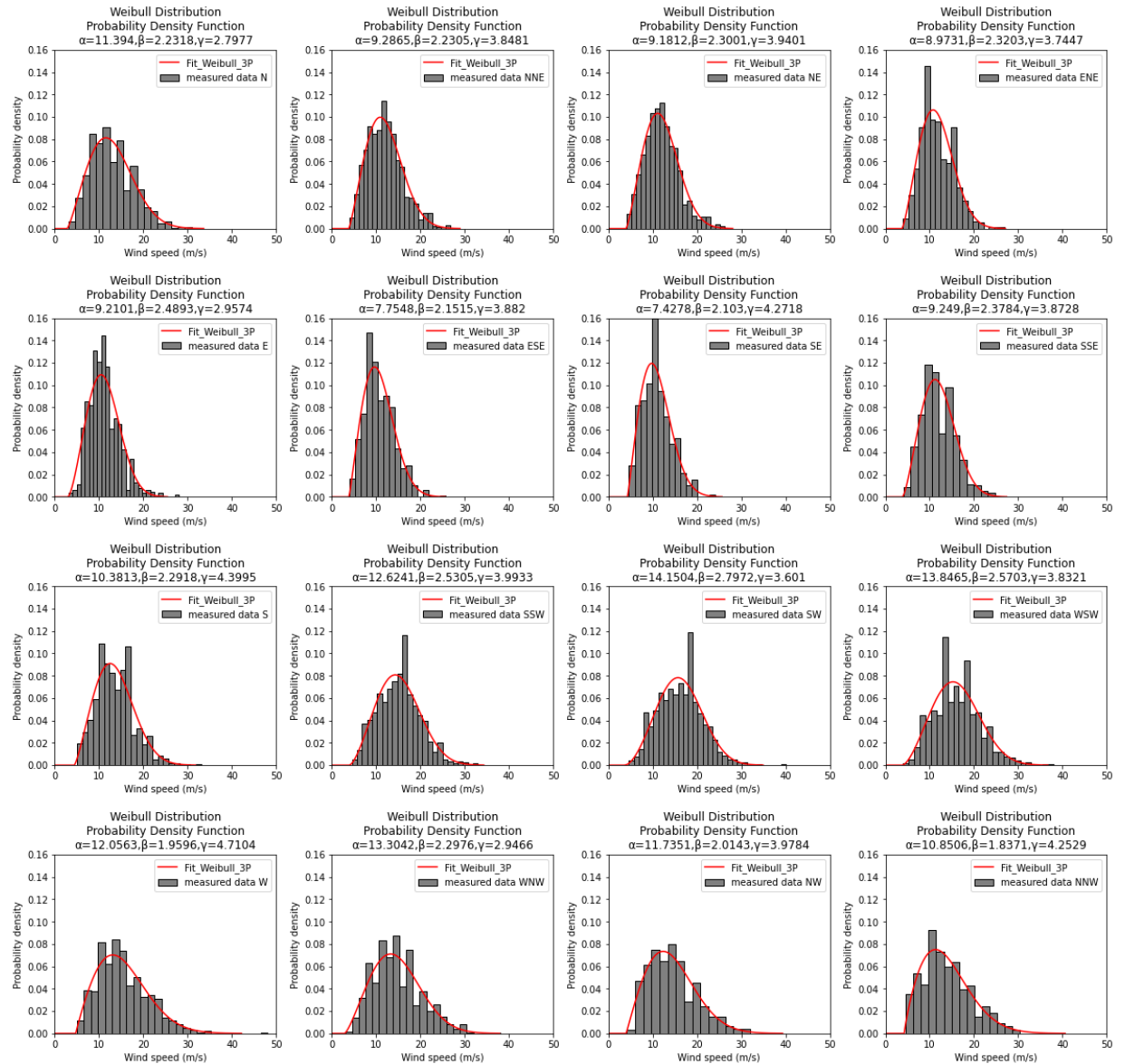


Figure VII.1: 3P Weibull fits through maximum daily wind gusts data

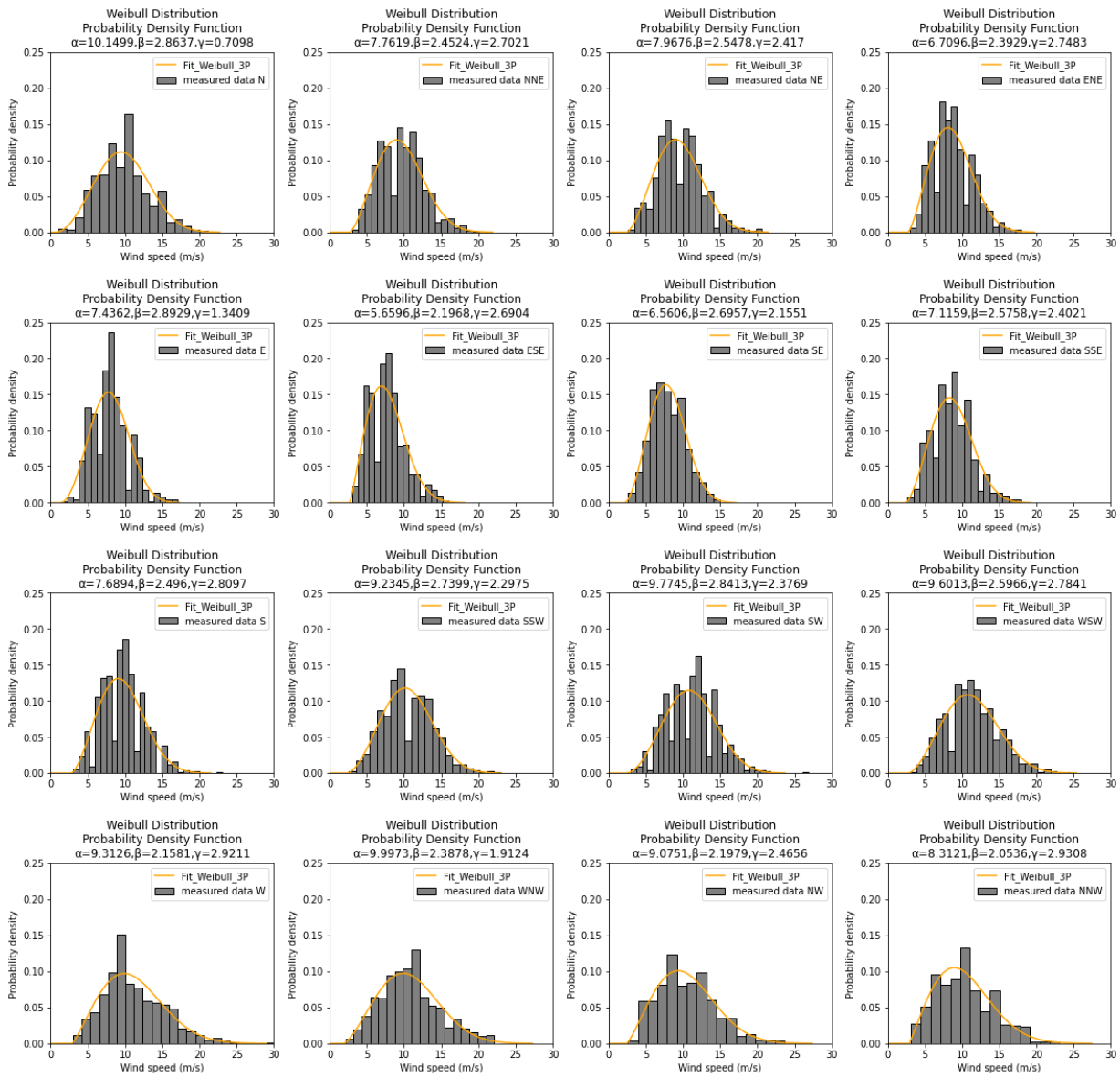


Figure VII.2: 3P Weibull fits through maximum hourly mean wind speeds data

Finally, using Equation (VII.1) one is able to compute the corresponding wind speeds for every return period and wind direction given the location, scale and shape parameters as presented in Figure VII.1 and Figure VII.2 for maximum daily wind gusts and maximum hourly wind gusts respectively.

$$v = \alpha \sqrt[\beta]{\ln R} + \gamma \quad (\text{VII.1})$$

where: R [years] = return period
 v [m/s] = respective wind speed at 10 m height
 γ [-] = location parameter
 α [-] = scale parameter
 β [-] = shape parameter

VIII Geotechnical Soil Profile

This appendix provides the cone penetration tests and corresponding locations from which, in Section 3.2.3, the soil profile and characteristic soil parameters are determined.

The soil conditions at the site of the Delta Barrier are estimated by means of two cone penetration test (CPT) results. These CPTs are retrieved from the database of the Dinoloket (2022). Figure VIII.1 shows the location of the CPTs with respect to the storm surge barrier.

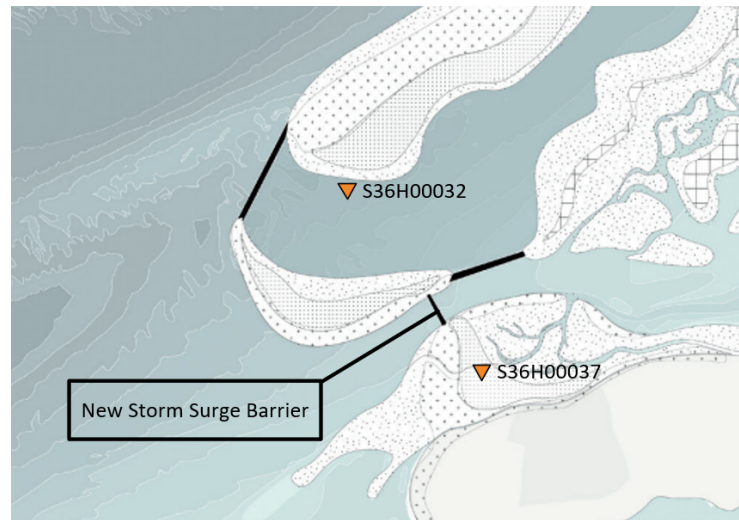


Figure VIII.1: Location of the most relevant CPTs (modified from van Eeden (2021))

Figure VIII.2 and fig. VIII.3 present the results of the two most relevant CPTs, S36H00032 and S36H00037 respectively.

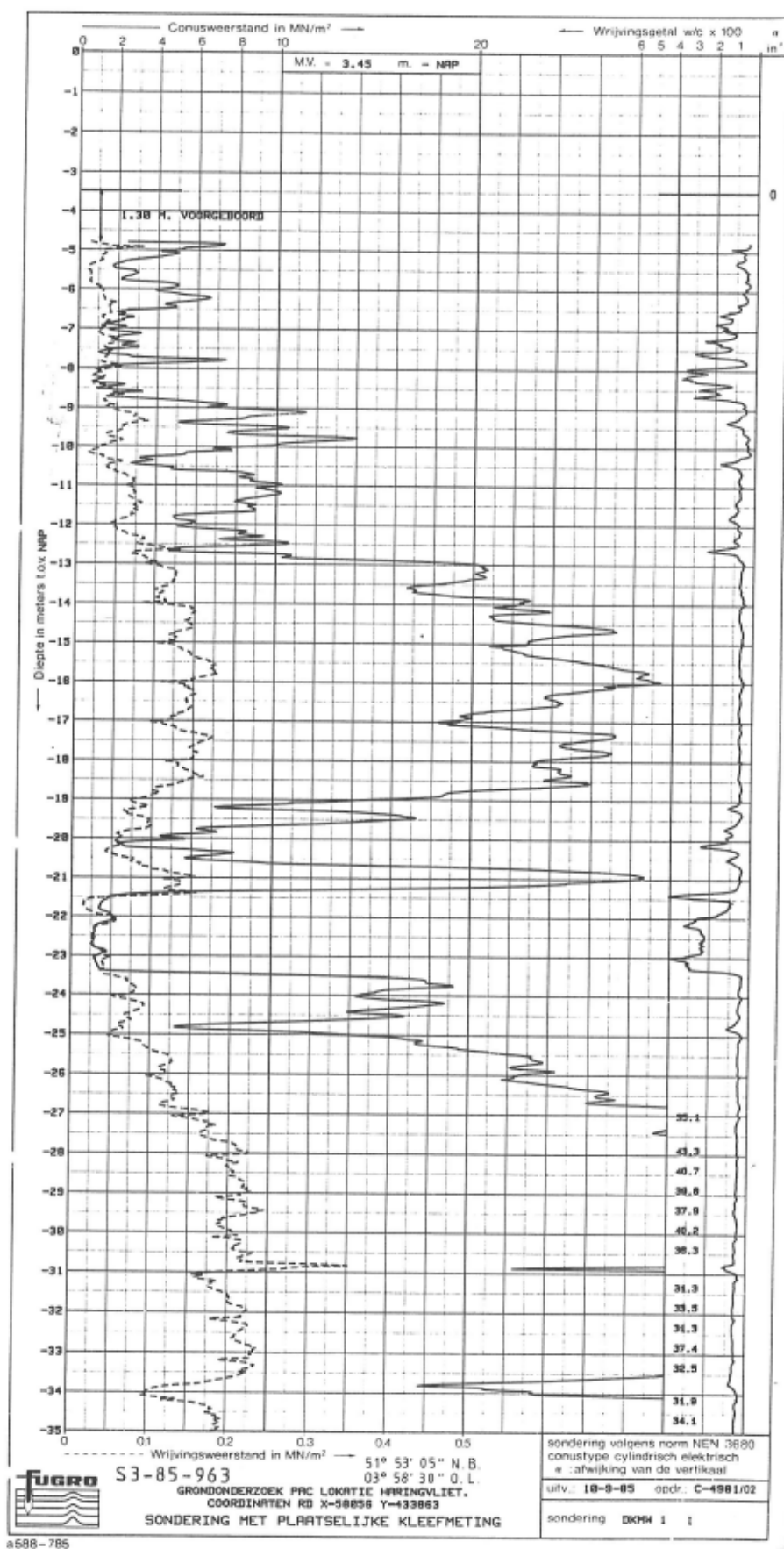


Figure VIII.2: CPT S36H00032_00 (Fugro, 2022)

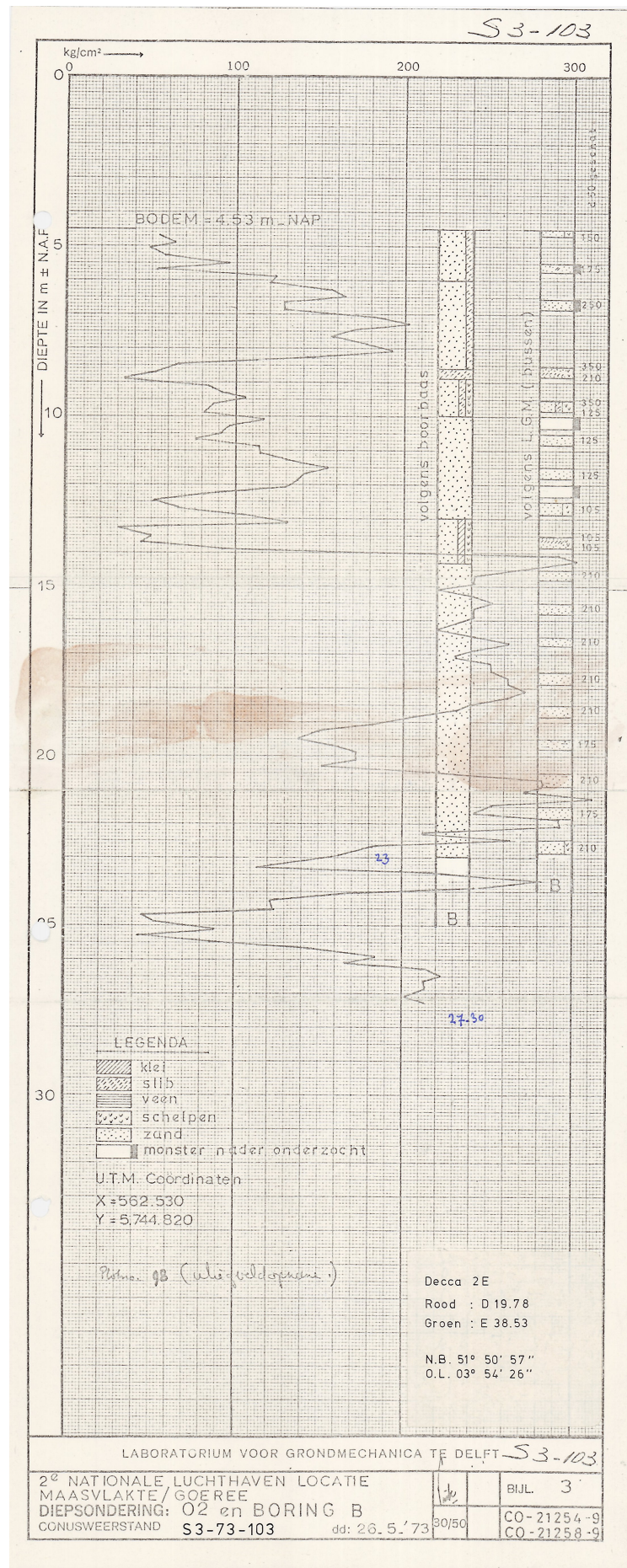


Figure VIII.3: CPT S36H00037_00 (Fugro, 2022)

IX Creation of a Hydrodynamic Model

This appendix provides an elaboration on the hydrodynamic model as presented in Section 3.2.8. For the original model, see "The New Haringvliet Barrier. Conceptual design for the storm surge barrier of the Delta21 project." (2021). The presented hydrodynamic model is used to determine the water level development at the Tidal Lake for the given tidal signal and different discharges at Lobith.

With this hydrodynamic model, the water level at the Tidal Lake is simulated in time for a certain closure and opening strategy (see Appendix XI) in order to determine if (and perhaps when) the Spillway should be opened (see Section 5.1). Furthermore, the tidal range at the Tidal Lake and the flow speeds through the barrier from which the effective flow area can be chosen (see Section 5.3) are determined using the model. Finally, the model is used to compute the discharge and flow velocity through the barrier given a failed closure (see Section 5.2).

The Python code of the hydrodynamic model is available at <http://repository.tudelft.nl/>.

IX.1 Tidal Lake (Storage-Basin Model)

An expansion of the continuity equation (Equation (3.10)) proposed by Konter, Klatter, and Jorissen (1992) and Huis in 't Veld (1987) is presented by Equation (IX.1c).

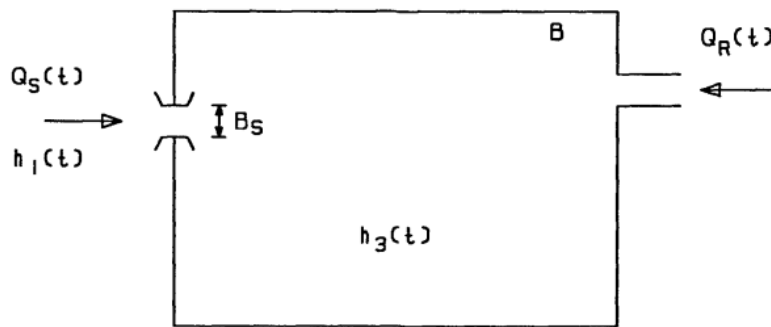


Figure IX.1: Basin capacity system

$$Q_S(t) = B(t) \frac{dh_3(t)}{dt} - Q_R(t) \quad (\text{IX.1a})$$

$$\mu_1 A_s(t) U_{0,1}(t) = B(t) \frac{dh_3(t)}{dt} - \mu_2 A_H U_{0,2}(t) \quad (\text{IX.1b})$$

$$\mu_1 B_s h_3(t) \sqrt{2g \Delta H_1(t)} = B(t) \frac{dh_3(t)}{dt} - \mu_2 A_H(t) \sqrt{2g \Delta H_2(t)} \quad (\text{IX.1c})$$

where:	$h_3(t)$	[m]	=	water level in the Tidal Lake
	$Q_S(t)$	[m ³ /s]	=	discharge through the Delta Barrier
	$B(t)$	[m ²]	=	surface area of the Tidal Lake
	$Q_R(t)$	[m ³ /s]	=	discharge through the Haringvlietsluizen
	μ_1	[-]	=	discharge coefficient of the Delta Barrier = 0.7
	$A_s(t)$	[m ²]	=	wetted cross-section at the Delta Barrier
	$U_{0,1}(t)$	[m/s]	=	the reference depth-averaged flow velocity through the Delta Barrier
	μ_2	[-]	=	discharge coefficient of the Haringvlietsluizen = 0.7
	$A_H(t)$	[m ²]	=	wetted cross-section at Haringvlietsluizen
	$U_{0,2}(t)$	[m/s]	=	the reference depth-averaged flow velocity through the Haringvlietsluizen
	B_s	[m]	=	effective width of the Delta Barrier
	$\Delta H_1(t)$	[m]	=	head difference over the Delta Barrier
	$\Delta H_2(t)$	[m]	=	head difference over the Haringvlietsluizen

For the sake of this preliminary design the discharge coefficients (μ) are for now set to 0.7. Changes in the flow field due to disruption of the flow (e.g. flow separation, energy conversion by turbulence, momentum transfer and generation of eddies, etc) and frictional losses at the floor and side walls - which are usually small relative to from losses - are represented in the discharge coefficient (Dijkzeul, Klatter, Hartsuiker, & Thabet, 1989). In addition, Dijkzeul et al. (1989) states that the coefficient of discharge, can only be obtained through measurements on a scale model of the structure. Due to the complexity of before-mentioned mentioned form loss and friction mechanisms, the coefficient of discharge is further disregarded in this thesis.

Konter et al. (1992) presents two situations, namely one for super critical overflow conditions and for sub-critical overflow conditions. The head difference to be used in Equation (IX.1c) depends on the condition.

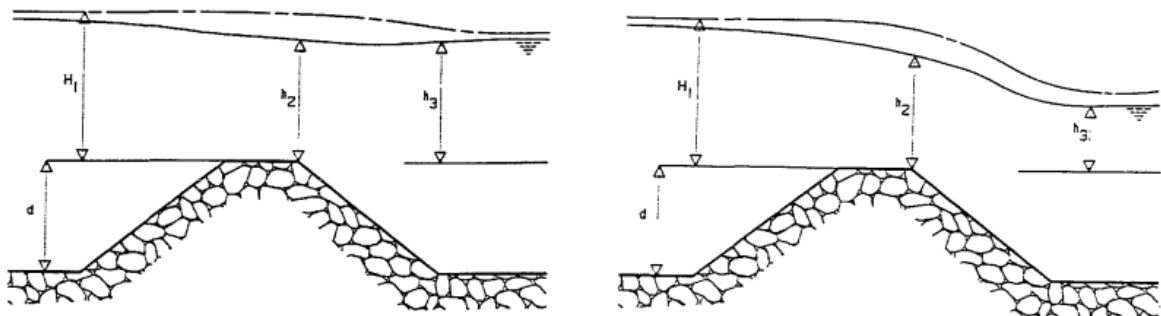


Figure IX.2: Situation for sub- and super critical flow, respectively (Konter et al., 1992)

The head difference over the structure ($\Delta H(t)$) depends on the difference of the upstream energy head and the water level at the location of the barrier ($h_2(t)$). For sub-critical overflow, the downstream water level influences the flow through the barrier whereas for super critical flow the flow through the barrier is solely governed by the upstream water level. Equation (IX.2) gives the head difference over the Delta Barrier to be used for sub- and super critical flow, for the case of water flowing seaward and landward through the barrier, respectively.

$$\Delta H_1(t) = \begin{cases} H_3(t) - h_1(t), & \text{when } h_3(t) > h_1(t) > \frac{2}{3}H_3(t) \quad \textit{sub-critical} \\ \frac{1}{3}H_3(t), & \text{when } h_1(t) < \frac{2}{3}H_3(t) \quad \textit{supercritical} \\ H_1(t) - h_3(t), & \text{when } h_1(t) > H_3(t) > \frac{2}{3}h_1(t) \quad \textit{sub-critical} \\ \frac{1}{3}H_1(t), & \text{when } h_3(t) < \frac{2}{3}H_1(t) \quad \textit{supercritical} \end{cases} \quad (\text{IX.2})$$

where: $H_1(t)$ [m] = the energy head at sea
 $H_3(t)$ [m] = the energy head at the Tidal Lake $\approx h_3(t)$

For the head difference over the Haringvlietsluizen:

$$\Delta H_2(t) = \begin{cases} H_4(t) - h_3(t), & \text{when } h_4(t) > h_3(t) > \frac{2}{3}H_4(t) \quad \textit{sub-critical} \\ \frac{1}{3}H_4(t), & \text{when } h_3(t) < \frac{2}{3}H_4(t) \quad \textit{supercritical} \\ H_3(t) - h_4(t), & \text{when } h_3(t) > H_4(t) > \frac{2}{3}h_3(t) \quad \textit{sub-critical} \\ \frac{1}{3}H_3(t), & \text{when } h_4(t) < \frac{2}{3}H_3(t) \quad \textit{supercritical} \end{cases} \quad (\text{IX.3})$$

where: $H_3(t)$ [m] = the energy head at the Tidal Lake $\approx h_3(t)$
 $H_4(t)$ [m] = the energy head at the Haringvliet - Hollandsch Diep $\approx h_4(t)$

Note that, in order to avoid an extra unknown velocity signal, the energy heads at the Tidal Lake and Haringvliet river are approximated to be equal to the respective water levels. Huis in 't Veld (1987) mentions that this simplified approach is generally valid, as can be expected for low velocity heads. The energy head at sea is calculated as follows:

$$H_1(t) = h_1(t) + \frac{v_1(t)^2}{2g} \quad (\text{IX.4})$$

Furthermore, the surface area of the Tidal Lake at the water surface ($B(t)$) is a function of time, depending on both the geometry of the lake and the water level in the lake. For simplicity, the cross-section of the Tidal Lake will here be assumed to be prismatic (Figure IX.3).

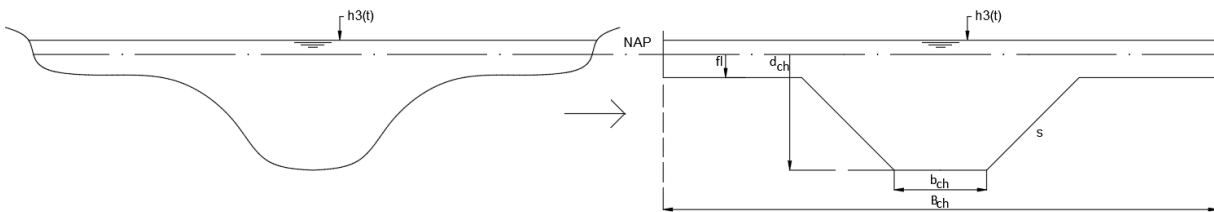


Figure IX.3: Prismatic channel approximation

For the purpose of solving Equation (IX.1c), the width of the Tidal Lake at the water surface as a function of the water level in the Tidal Lake is formulated.

$$B(t) = \left((b_{ch} + \frac{2}{s} \cdot (h_3(t) + d_{ch})) \cdot (1 - H(h_3(t) - fl)) + B_{ch} \cdot H(h_3(t) - fl) \right) \cdot L_{eq} \quad (\text{IX.5})$$

where:	b_{ch}	[m]	=	the width of the main channel = 750
	s	[-]	=	the slope of the banks = 1:4
	d_{ch}	[m NAP]	=	the depth of the main channel = - 7
	fl	[m NAP]	=	the height of the tidal flats = + 1
	B_{ch}	[m]	=	total width of the entire basin = 3500
	L_{eq}	[m]	=	equivalent length factor ≈ 34290
	$H(y)$	[-]	=	the Heaviside step function

with:

$$H(y) = \begin{cases} 1, & h_3(t) - fl > 0 \\ 0, & h_3(t) - fl \leq 0 \end{cases}$$

The equivalent length factor (L_{eq}) in Equation (IX.5) ensures that the total basin area is equal to 120 km² when the tidal flats are completely flooded (i.e. $h_3(t)-fl>0$), as specified by Berke and Lavooij (2018c).

IX.2 Haringvliet - Hollandsch Diep (1D Channel Model)

Continuity equation

The expansion of the continuity equation (Equation (3.11)) is presented by Equation (IX.6c).

$$B_H(x) \frac{dh_4(x,t)}{dt} = Q_C(t) - Q_R(t) \quad (\text{IX.6a})$$

$$B_H(x) \frac{dh_4(x,t)}{dt} = Q_C(t) - \mu_2 A_H U_{0,2}(t) \quad (\text{IX.6b})$$

$$B_H(x) \frac{dh_4(x,t)}{dt} = Q_C(t) - \mu_2 A_H(t) \sqrt{2g\Delta H_2(t)} \quad (\text{IX.6c})$$

where:	$h_4(x,t)$	[m]	=	water level in the Haringvliet - Hollandsch Diep per section
	$B_H(x)$	[m ²]	=	surface area of the Haringvliet - Hollandsch Diep per section
	$Q_C(t)$	[m ³ /s]	=	discharge at the right - upstream - boundary (Moerdijk)
	$Q_R(t)$	[m ³ /s]	=	discharge through the Haringvlietsluizen
	μ_2	[-]	=	discharge coefficient of the Haringvlietsluizen = 0.7
	$A_H(t)$	[m ²]	=	wetted cross-section at Haringvlietsluizen
	$U_{0,2}(t)$	[m/s]	=	the reference depth-averaged flow velocity through the Haringvlietsluizen
	$\Delta H_2(t)$	[m]	=	head difference over the Haringvlietsluizen

Onwuachu (2021) has proposed an exponential relationship for the surface area of the Haringvliet - Hollandsch Diep:

$$B_H(x) = B_c ds \quad (\text{IX.7})$$

$$B_H(x) = B_{H,0} e^{(-2\lambda s)} ds \quad (\text{IX.8})$$

where:	$B_{H,0}$	[m]	=	the storage width at the river mouth = 2900
	λ	[-]	=	convergence parameter = $8 \cdot 10^{-6}$
	s	[m]	=	distance from the mouth (Haringvlietsluizen)
	ds	[m]	=	section length

Furthermore, for the boundary condition at the upstream boundary ($Q_R(t)$), Onwuachu (2021) has proposed a Riemann boundary. Specifying a Riemann boundary condition avoids the occurrence of

artificial reflections within the domain by adapting to the local water level at the boundary. The local Riemann invariant is based on the assumed flow state outside of the boundary and is defined as follows (Onwuachu, 2021):

$$Q_C^n = Q_{C,0} + (B_c)_R^n (h_M^n - h_{C,0}) \quad (\text{IX.9})$$

where: $Q_{C,0}$ [m³/s] = the undisturbed discharge at the upstream boundary
 $h_{C,0}$ [m] = the undisturbed water level at the upstream boundary

The exact values of the undisturbed discharge and water level at the boundary differ, depend on e.g. the considered tidal signal at sea, river discharge and climate-scenario.

Streamwise momentum equation

The streamwise momentum equation can be written as follows:

$$\frac{\delta Q(x,t)}{\delta t} + \frac{\delta}{\delta s} \left(\frac{Q(x,t)^2}{A_c(t)} \right) + g A_c(x) \frac{\delta h_4(x,t)}{\delta s} + c_f \frac{|Q(x,t)|Q(x,t)}{A_c(t)R(x)} = 0 \quad (\text{IX.10})$$

where: $Q(x,t)$ [m³/s] = discharge
 $A_c(x)$ [m²] = conveyance area
 g [m/s²] = gravitational constant = 9.81
 $h_4(x,t)$ [m] = water level in the Haringvliet - Hollandsch Diep
 c_f [-] = friction coefficient = 0.004
 $R(x)$ [m] = hydraulic radius of the Haringvliet - Hollandsch Diep

In order to solve the streamwise momentum equation, the Haringvliet - Hollandsch Diep is subdivided into multiple sections. Figure IX.4 gives an impression of this division. Do note that Figure IX.4 by Onwuachu (2021) gives merely an impression, as actually in total 10 sections (with length $ds = 4.3$ km) is used in the hydrodynamic model.

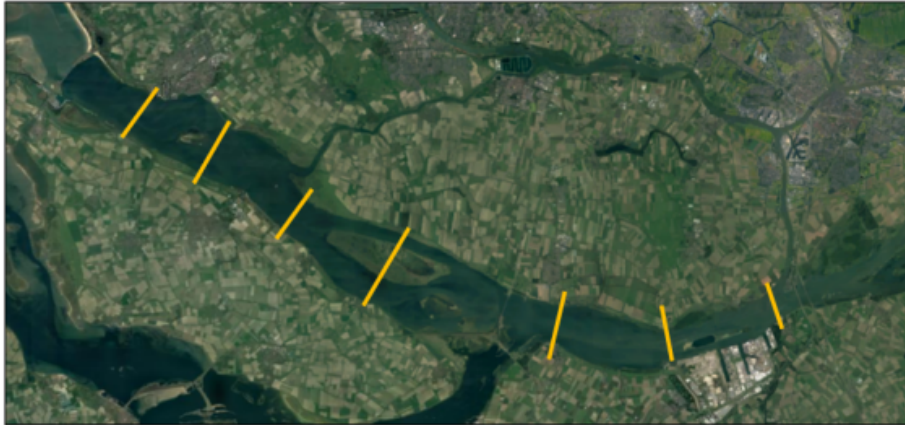


Figure IX.4: Impression of Haringvliet - Hollandsch Diep sections (Onwuachu, 2021)

Just as for the surface area, Onwuachu (2021) has proposed to use an exponential function for the conveyance area used in the streamwise momentum equation (Equation (IX.10)):

$$A_c(x) = A_{C,0} e^{(-2\lambda s)} \quad (\text{IX.11})$$

where: $A_{C,0}$ [m²] = the conveyance area at the river mouth = 21000
 λ [-] = convergence parameter = $8 \cdot 10^{-6}$
 s [m] = distance from the mouth (Haringvlietsluizen)

As for the friction coefficient in the streamwise momentum equation (Equation (IX.10)), $c_f = 0.004$ has been assumed for the Haringvliet - Hollandsch Diep. The depth of the Haringvliet - Hollandsch Diep is assumed to be a constant 7.25 m.

IX.3 Numerical Computation

In the one-dimensional hydrodynamic model, the river discharge and water level at the Haringvliet river vary both in space and time. For the numerical computation, the time domain is divided in N intervals, each of length Δt , while the channel is divided in M sections of length Δs . Each section (M) has a corresponding surface area, conveyance width, hydraulic radius and discharge specific to the section. Between every section, additional nodes specifying the respective water levels are defined. Each node has their own local storage width. The Python script starts the numerical computation from $t = 0$, where the initial conditions are defined, to $t = t_n$, by using a semi-implicit method. Firstly, the continuity equation computes an updated water level, after which an updated discharge is calculated using the streamwise momentum equation (Onwuachu, 2021).

Daily circumstances

Under daily circumstances there is no set-up at sea and an average Rhine discharge at Lobith of 2200 m^3/s , resulting in a residual discharge through the Haringvliet of 500 m^3/s (see Figure 3.11). After validation by Onwuachu (2021) this yields an upstream undisturbed water level of $h_{C,0} = 0.1$ m in 2018. In 2150, superposition of additional sea level rise (SSP2-4.5) yields $h_{C,0} = 1.15$ m. Do note that in this case the Haringvlietsluizen are only partly opened according to the Kierbesluit (Figure 3.12).

Figure IX.5 presents the results of solving the hydrodynamic model for daily circumstances in 2150 considering climate scenario SSP2-4.5. The response of the Tidal Lake water level is solved for four tidal cycles (178800 s).

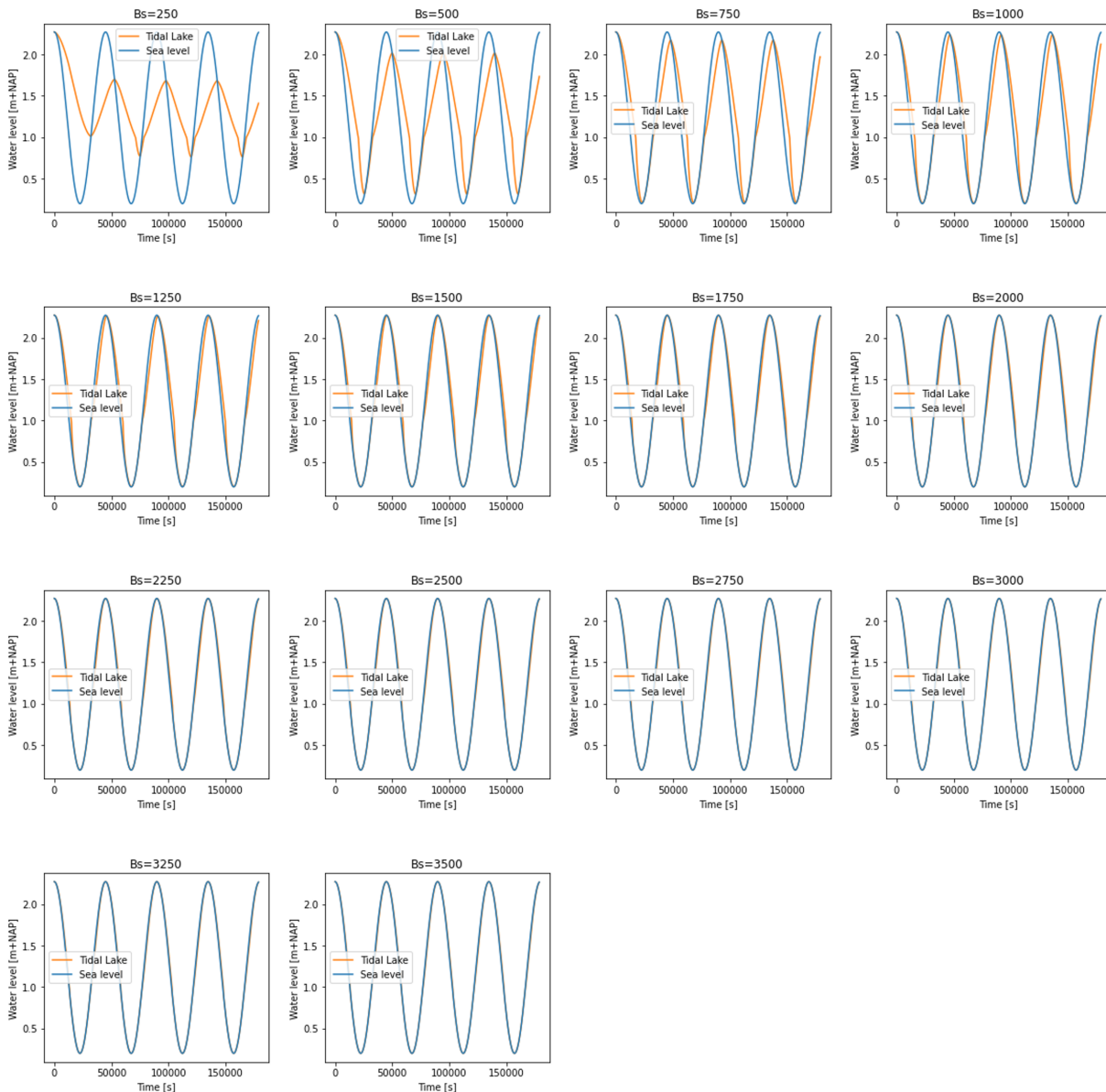


Figure IX.5: Response of the Tidal Lake water level for MSL = NAP + 1.05 m and 2200 m³/s at Lobith

From Figure IX.5 it can be seen that for small effective widths of the Delta Barrier, the barrier does not have sufficient discharge capacity resulting in a significant reduction of the tidal range at the Tidal Lake.

IX.4 Validation and Discussion

The model which is used has readily been validated by Onwuachu (2021). A few limitations of the hydrodynamic model though should be addressed.

Firstly, the model does not (and can not) accurately capture complex phenomena such as discharge redistribution and the influence of the Nieuwe Waterweg. Also the Spui is not incorporated in the model. For this reason, one can not confidently draw conclusions regarding the water level at Dordrecht from this model. However, this model can reasonably accurate estimate the response of the water level at the Tidal Lake as a function of the geometry of the Delta Barrier.

The model houses multiple unknown and complex variables, such as discharge coefficients and friction coefficients. These coefficient have been estimated using engineering judgement ($\mu_i \approx 0.7$ and $c_f \approx 0.004$, respectively). While the model is not extremely sensitive to changes in the friction coefficient for

the Haringvliet - Hollandsch Diep, it is rather sensitive to changes in the discharge coefficients of both the Delta Barrier and the Haringvlietsluizen. For this preliminary design said estimates are acceptable, however for further design stages one should accurately determine such complex and drastic variables.

The response of the model is quite sensitive to the posed upstream Riemann boundary condition. The undisturbed water level for daily circumstances has been determined using Hydra-NL by Onwuachu (2021), which considers the present situation (without Delta21). For all scenarios, the SOBEK model results as presented by Beeldman (2011) is used, also for the present situation. For this reason the impact of the Delta21 system is not properly taken into account.

X Elaboration on Design Parameters

This appendix provides further elaboration on the design parameters used in this thesis. As for the functional design, the final adjusted design parameters used to calculate the retaining height are presented. For the structural design, the final adjusted design parameters are presented for both positive and negative head.

Hydra-NL is used to generate design parameters at sea. However, the difference between the actual location of the Delta Barrier and the available Hydra-NL location translates into different fetches and average water depth over said new fetches. Adjustments are needed in order to account for the difference between the actual location of the Delta Barrier and the available Hydra-NL location. Table X.1 presents the fetches and average water depths for the directions 240, 270 and 300 degrees north for both the Hydra-NL location and the actual location.

r [°]	Hydra-NL		Actual		ΔF [km]	Δd_g [m]
	Fetch [km]	Depth [m]	Fetch [km]	Depth [m]		
240	161	16	197	17.5	36	1.5
270	191	23	179	25	-12	2
300	158	30	167	30	9	0

Table X.1: Differences Hydra-NL location and actual location

Said differences give rise to a different set-up, wind wave heights and peak wave periods. The set-up differences are calculated using Equation (X.1), the wind wave height differences using Equation (X.2) and the wave periods using Equation (X.3).

$$S = C_2 \frac{U_{10}^2}{gd} F \cdot \sin \phi \quad (\text{X.1})$$

in which: S [m] = total wind set-up
 C_2 [-] = coefficient taking into account various effects
(e.g. temperature, humidity) $\approx 3.75 \cdot 10^{-6}$ for Dutch circumstances
 F [m] = fetch
 U_{10} [m/s] = wind velocity at an altitude of 10 m
 g [m/s²] = gravitational acceleration
 d [m] = average depth over the fetch
 ϕ [°] = angle of incidence of the waves, where 90 ° is normally incident

$$\tilde{H} = \tilde{H}_\infty \left\{ \tanh(0.343\tilde{d}^{1.14}) \cdot \tanh\left(\frac{4.41 \cdot 10^{-4} \tilde{F}^{0.79}}{\tanh(0.343\tilde{d}^{1.14})}\right) \right\}^{0.572} \quad (\text{X.2})$$

$$\tilde{T} = \tilde{T}_\infty \left\{ \tanh(0.10\tilde{d}^{2.01}) \cdot \tanh\left(\frac{2.77 \cdot 10^{-7} \tilde{F}^{1.45}}{\tanh(0.10\tilde{d}^{2.01})}\right) \right\}^{0.187} \quad (\text{X.3})$$

$$\begin{aligned} \text{in which: } \tilde{H} \quad [-] &= \frac{gH_{m0}}{U_{10}^2} & \tilde{T} \quad [-] &= \frac{gT_p}{U_{10}} \\ \tilde{F} \quad [-] &= \frac{gF}{U_{10}^2} & \tilde{d} \quad [-] &= \frac{gd}{U_{10}^2} \\ F \quad [\text{m}] &= \text{fetch} \\ d \quad [\text{m}] &= \text{average water depth over the fetch} \\ U_{10} \quad [\text{m/s}] &= \text{wind velocity at an altitude of 10 m} \\ T_p \quad [\text{s}] &= \text{peak wave period} \\ \tilde{H}_\infty \quad [-] &= \text{dimensionless deep water wave height} = 0.24 \\ T_p \quad [\text{s}] &= \text{peak wave period} \\ \tilde{T}_\infty \quad [-] &= \text{dimensionless deep water wave period} = 7.69 \\ H_{m0} \quad [\text{m}] &= \text{significant wave height, from wave spectrum } (H_{m0} \approx H_s) \end{aligned}$$

X.1 Functional Design

Retaining height

Table X.2 gives the combination of water level at sea (h_1), significant wave height (H_S), wave angle w.r.t. north (θ), potential wind speed (U_p) and wind direction w.r.t. north (r) for reference period 2100, a return period of 83333 years and climate scenario W+ as gathered from Hydra-NL output using the "hydraulic load level" module to take into account the correlation between water level and wave height.

h_1 [m NAP]	H_S [m]	θ [°]	U_p [m/s]	r [°]
6.48	2.98	237.8	37.5	300

Table X.2: Hydra-NL output 2100 W+, R=83333

The Hydra-NL output is adjusted for additional sea level rise and for the difference between the actual location of the Delta Barrier and the available Hydra-NL location. Table X.3 and Table X.4 present said adjustment and final design parameters for climate scenarios SSP2-4.5 and SSP5-8.5 respectively.

h_1 [m NAP]	Adjustments		$h_{1;d}$ [m NAP]	H_S [m]	θ [°]	Adjustments		U_p [m/s]	r [°]
	<i>SLR</i> [m]	<i>Set-up</i> [m]				<i>Bretschneider</i> [m]	$H_{S;d}$ [m]		
6.48	1.37	-0.02	7.83	2.98	237.8	0.19	3.17	37.5	300

Table X.3: Design parameters for SSP2-4.5 reference period 2250, R=83333

h_1 [m NAP]	Adjustments		$h_{1;d}$ [m NAP]	H_S [m]	θ [°]	Adjustments		U_p [m/s]	r [°]
	<i>SLR</i> [m]	<i>Set-up</i> [m]				<i>Bretschneider</i> [m]	$H_{S;d}$ [m]		
6.48	2.97	0.07	9.52	2.98	237.8	0.36	3.34	37.5	300

Table X.4: Design parameters for SSP5-8.5 reference period 2250, R=83333

in which:	h_1	[m NAP]	=	sea water level Hydra-NL
	SLR	[m]	=	sea level rise adjustment
	Set-up	[m]	=	set-up adjustment
	$h_{1;d}$	[m NAP]	=	design value sea water level
	H_S	[m]	=	significant wave height Hydra-NL
	θ	[°]	=	wave angle of incidence w.r.t. north
	Bretschneider	[m]	=	wave height adjustment
	$H_{S;d}$	[m]	=	design significant wave height
	U_p	[m/s]	=	potential wind velocity
	r	[°]	=	wind direction w.r.t. north

X.2 Structural Design

ULS

The relevant return periods for the ultimate limit state are 10 and 100000 years corresponding to the return periods as prescribed in the ROK (2021) for maximum positive head and ship collision (see Appendix XIII). Note that the Building Decree is governing over the 2017 Water Act considering structural failure (return period of 100000 vs. 52632 years, respectively).

Positive head

The tables below (Table X.5, Table X.6, Table X.7 and Table X.8) give all combinations of water level at sea (h_1), significant wave height (H_S), wave angle w.r.t. north (θ), peak wave period (T_p), potential wind speeds (U_p) and wind direction w.r.t. north (r) for their respective reference periods and return periods gathered from Hydra-NL output. From Hydra-NL, the function "Wave conditions for revetments - Asphalt wave impact zone" is used in order to account for the correlation between the water level and wave height at sea. The Hydra-NL output is adjusted for additional sea level rise and for the difference between the actual location of the Delta Barrier and the available Hydra-NL location. Note that for reference periods 2050 and 2250 climate scenarios 2050 W+ and 2100 W+ are chosen in Hydra-NL respectively. The differences 2050 SSP5-8.5 - 2050 W+ and 2250 SSP5-8.5 - 2100 W+ are listed under SLR for 2050 and 2250 respectively.

With an addition for storm-oscillations and gusts (here *gusts*) as proposed by Van Hijum (1999), the above adjustments are added to the Hydra-NL output to arrive at the final design parameters. It should be noted that the governing combination of design water level and wave height depends on the total combined pressure. The normative combination is pointed out in the tables below per reference period and return period.

h_1 [m NAP]	Adjustments			$h_{1;d}$ [m NAP]	H_S [m]	θ [°]	Adjustments			$H_{S;d}$ [m]	T_p [s]	Adjustments		
	<i>Gusts</i> [m]	SLR [m]	$Set-up$ [m]				<i>Bretschneider</i> [m]	$H_{S;d}$ [m]	T_p [s]			<i>Bretschneider</i> [s]	$T_{p;d}$ [s]	U_p [m/s]
2.62	0.50	-0.04	-0.06	3.02	1.72	248.1	0.10	1.82	6.05	0.10	6.15	17.4	270	
3.10	0.50	-0.04	-0.09	3.49	1.75	248.1	0.15	1.90	6.39	0.16	6.55	21.4	270	
→ 3.50	0.50	-0.04	-0.03	3.93	1.49	249.2	0.04	1.53	7.24	0.07	7.31	22.6	300	

Table X.5: Design parameters for SSP5-8.5 reference period 2050, R=10

h_1 [m NAP]	Adjustments			$h_{1;d}$ [m NAP]	H_S [m]	θ [°]	Adjustments			$H_{S;d}$ [m]	T_p [s]	Adjustments		
	<i>Gusts</i> [m]	SLR [m]	$Set-up$ [m]				<i>Bretschneider</i> [m]	$H_{S;d}$ [m]	T_p [s]			<i>Bretschneider</i> [s]	$T_{p;d}$ [s]	U_p [m/s]
4.00	0.50	-0.04	-0.05	4.41	2.88	240	0.23	3.11	6.73	0.26	7.00	30.5	240	
4.50	0.50	-0.04	-0.27	4.69	3.07	247	0.25	3.32	7.29	0.27	7.56	33.1	270	
5.00	0.50	-0.04	0.06	5.52	2.92	248.1	0.03	2.95	8.08	0.04	8.12	33.7	300	
5.50	0.50	-0.04	-0.05	5.91	2.68	248.9	0.02	2.70	8.34	0.03	8.37	36.8	300	
→ 6.00	0.50	-0.04	0.03	6.49	2.33	246.6	0.02	2.35	8.61	0.03	8.64	37.3	300	

Table X.6: Design parameters for SSP5-8.5 reference period 2050, R=100000

h_1 [m NAP]	Adjustments				$h_{1;d}$ [m NAP]	H_S [m]	θ [°]	Adjustments			$H_{S;d}$ [m]	T_p [s]	Adjustments		$T_{p;d}$ [s]	U_p [m/s]	r [°]
	<i>Gusts</i> [m]	<i>SLR</i> [m]	<i>Set-up</i> [m]	<i>Bretschneider</i> [m]				<i>Bretschneider</i> [s]	<i>Bretschneider</i> [s]								
3.12	0.50	2.97	-0.08	6.51	1.72	248.2	0.25	1.97	6.05	0.25	6.30	17.4	270				
→ 3.60	0.50	2.97	-0.06	7.01	1.75	248.4	0.36	2.11	6.39	0.37	7.76	21.4	270				
4.00	0.50	2.97	-0.03	7.44	1.49	246.5	0.20	1.69	7.24	0.19	7.43	22.1	300				

Table X.7: Design parameters for SSP5-8.5 reference period 2250, R=10

h_1 [m NAP]	Adjustments				$h_{1;d}$ [m NAP]	H_S [m]	θ [°]	Adjustments			$H_{S;d}$ [m]	T_p [s]	Adjustments		$T_{p;d}$ [s]	U_p [m/s]	r [°]
	<i>Gusts</i> [m]	<i>SLR</i> [m]	<i>Set-up</i> [m]	<i>Bretschneider</i> [m]				<i>Bretschneider</i> [s]	<i>Bretschneider</i> [s]								
4.50	0.50	2.97	0.01	7.98	3.12	240	0.65	3.77	6.98	0.75	7.73	30.3	240				
5.00	0.50	2.97	-0.60	7.87	3.30	247.3	0.62	3.92	7.54	0.62	8.16	33.3	270				
5.62	0.50	2.97	-0.87	8.22	3.10	247.6	0.71	3.81	7.78	0.68	8.46	38.5	270				
6.00	0.50	2.97	0	9.47	2.83	246.6	0.36	3.19	8.61	0.30	8.91	36.9	300				
→ 6.50	0.50	2.97	0	9.97	2.45	246.6	0.36	2.81	8.89	0.31	9.20	37.3	300				

Table X.8: Design parameters for SSP5-8.5 reference period 2250, R=100000

in which:	h_1	[m NAP]	=	sea water level Hydra-NL
	<i>Gusts</i>	[m]	=	adjustment for storm oscillations and gusts
	<i>SLR</i>	[m]	=	sea level rise adjustment
	<i>Set-up</i>	[m]	=	set-up adjustment
	$h_{1;d}$	[m NAP]	=	design value sea water level
	H_S	[m]	=	significant wave height Hydra-NL
	θ	[°]	=	wave angle of incidence w.r.t. north
	<i>Bretschneider</i>	[m]	=	wave height adjustment
	$H_{S;d}$	[m]	=	design significant wave height
	T_p	[s]	=	peak wave period Hydra-NL
	<i>Bretschneider</i>	[s]	=	peak wave period adjustment
	$T_{p;d}$	[s]	=	design value peak wave period
	U_p	[m/s]	=	potential wind velocity
	r	[°]	=	wind direction w.r.t. north

For the final calculation of the positive head over the structure, it is assumed that during such extreme storm surges the water level at the Tidal Lake will be managed (e.g. by means of the Spillway) as such that it never drops below NAP + 1.00 m. Hence the normative situation yields $h_{3;d} = \text{NAP} + 1.00$ m.

Negative head

The significant wave height and peak wave period in the case of a situation of negative head over the structure and wind waves approaching the structure from the Tidal Lake side are determined using Equation (X.2) and Equation (X.3), respectively. The set-up due to easterly wind is using Equation (X.1).

The fetches over the Tidal Lake and accompanying average water depths for the two most relevant directions are tabulated in Table X.9. The relevant wind speeds are tabulated in Table X.10 for the most relevant wind directions for a 100000 year return period (R). Said wind speeds generating wind waves and set-up are generally speeds which last long enough in order for waves to develop (viz. maximum hourly mean wind speeds). For this reason, the wind speeds as analysed in Section 3.2.4 and Appendix VII are used to calculate the wind waves at the Tidal Lake.

r [°]	Fetch [km]	Depth [m NAP]
45	2	7
90	8.7	6.3

Table X.9: Fetches over the Tidal Lake with depths

R [years]	r [°]	U_{10} [m/s]
100000	45	23.21
	90	18.65

Table X.10: Wind speeds for wind waves and set-down

Finally, Equation (X.2), Equation (X.3), and Equation (X.1) yield the significant wave height, peak wave period and set-up at the Tidal Lake side respectively for a return period of 100000 years and assuming a managed water level at the Tidal Lake after permanent closure (see Section 5.11) of NAP + 1 m. Table X.11 presents the final design values.

h_3 [m NAP]	Adjustments		$h_{3;d}$ [m NAP]	$H_{S;d}$ [m]	$T_{p;d}$ [s]	U_p [m/s]	r [°]
	<i>Gusts</i> [m]	<i>Set-up</i> [m]					
1.00	0.5	0.04	1.54	0.80	2.86	23.21	45
→ 1.00	0.5	0.14	1.64	1.16	3.85	18.65	90

Table X.11: Design parameters for negative head, R=100000

For the final calculation of the head over the barrier, the lowest astronomical tide (LAT) should be known for the situation when the Delta Barrier has only just closed permanently after a certain sea level rise. From Section 5.2 it follows that after a sea level rise of 1 m the closure operation is considered unreliable. Hence, directly after permanent closure incorporating a sea level rise of 1 m yields $LAT = NAP - 0.22$ m. Note that the solution of permanent closure from Section 5.11 is the governing scenario considering negative head.

SLS

As for the serviceability limit state, two stages are treated in this thesis. It is assumed that the characteristic combination, i.e. an irreversible SLS limit state, will not occur.

Frequent combination

As for the verification of the durability of the concrete (concrete crack widths), the frequent combination is used with loads corresponding to a return period of 100 years (see Appendix XIII).

h_1 [m NAP]	Adjustments				$h_{1,f}$ [m NAP]	H_S [m]	θ [°]	Adjustments <i>Bretschneider</i> [m]	$H_{S,f}$ [m]	T_p [s]	Adjustments <i>Bretschneider</i> [s]	$T_{p,f}$ [s]	U_p [m/s]	r [°]
	<i>Gusts</i> [m]	<i>SLR</i> [m]	<i>Set-up</i> [m]											
3.52	0.50	2.97	-0.06	6.93	2.30	248.4	0.35	2.65	6.72	0.36	7.08	21.0	270	
4.02	0.50	2.97	-0.42	7.07	2.29	246.7	0.45	2.74	7.06	0.47	7.53	25.3	270	
→ 4.50	0.50	2.97	-0.04	7.93	2.16	247.3	0.22	2.38	7.86	0.21	8.07	24.0	300	

Table X.12: Design parameters for SSP5-8.5 reference period 2250, R=100

in which:	h_1	[m NAP]	=	sea water level Hydra-NL
	Gusts	[m]	=	adjustment for storm oscillations and gusts
	SLR	[m]	=	sea level rise adjustment
	Set-up	[m]	=	set-up adjustment
	$h_{1;f}$	[m NAP]	=	frequent value sea water level
	H_S	[m]	=	significant wave height Hydra-NL
	θ	[°]	=	wave angle of incidence w.r.t. north
	Bretschneider	[m]	=	wave height adjustment
	$H_{S;f}$	[m]	=	frequent value significant wave height
	T_p	[s]	=	peak wave period Hydra-NL
	Bretschneider	[s]	=	peak wave period adjustment
	$T_{p;f}$	[s]	=	frequent value peak wave period
	U_p	[m/s]	=	potential wind velocity
	r	[°]	=	wind direction w.r.t. north

Quasi-permanent combination

As for the verification of the appearance of the structure (deflection), the quasi-permanent combination should be used with loads corresponding to a return period of 2 years (see Appendix XIII). However, as Hydra-NL can only be used for return periods between 10 and 1000000 years, the quasi-permanent combination is used with loads corresponding to a return period of 10 years. Note that the Hydra-NL output and adjustments corresponding to $R = 10$ years have readily been presented for the ULS positive head combination (Table X.7).

XI Simulations Proposed Delta21 Flood Protection Process

This appendix serves as additional clarification regarding the closure and opening strategy of the Delta Barrier and when to close the Spillway as discussed in Section 5.1.

For the cases where the hinterland of the Haringvliet is governing, the moment of closing the Delta Barrier, the water level evolution inside the Tidal Lake and the point of re-opening are simulated using the hydrodynamic model as described in Section 3.2.8 and Appendix IX. For all simulations, the highest astronomical tide in 2150 is used according to climate scenario SSP2-4.5.

Storm surge of 0.5 m & 2200 m³/s at Lobith

During average Rhine discharge at Lobith ca. 500 m³/s flows through the Haringvliet (see Section 3.2.7). As can be seen from Figure XI.1, the Tidal Lake has more than sufficient capacity to act as a buffer during the storm when the Delta Barrier is closed at the lowest possible water level before the storm and the Spillway does not have to be opened.

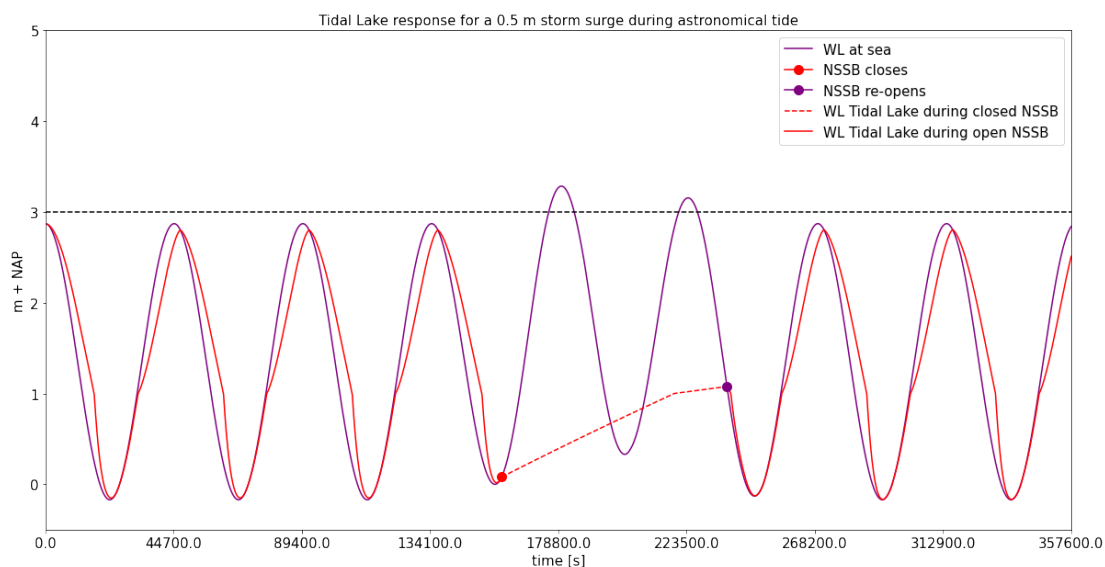


Figure XI.1: Closure and opening for a 0.5 m storm surge in 2150 SSP2-4.5 for an average Rhine discharge

Storm surge of 0.5 m & 5800 m³/s at Lobith

A Rhine discharge at Lobith of 5800 m³/s results in ca. 3750 m³/s through the Haringvliet (see Section 3.2.7). Now, the Tidal Lake only just has sufficient capacity to act as a buffer during the storm.

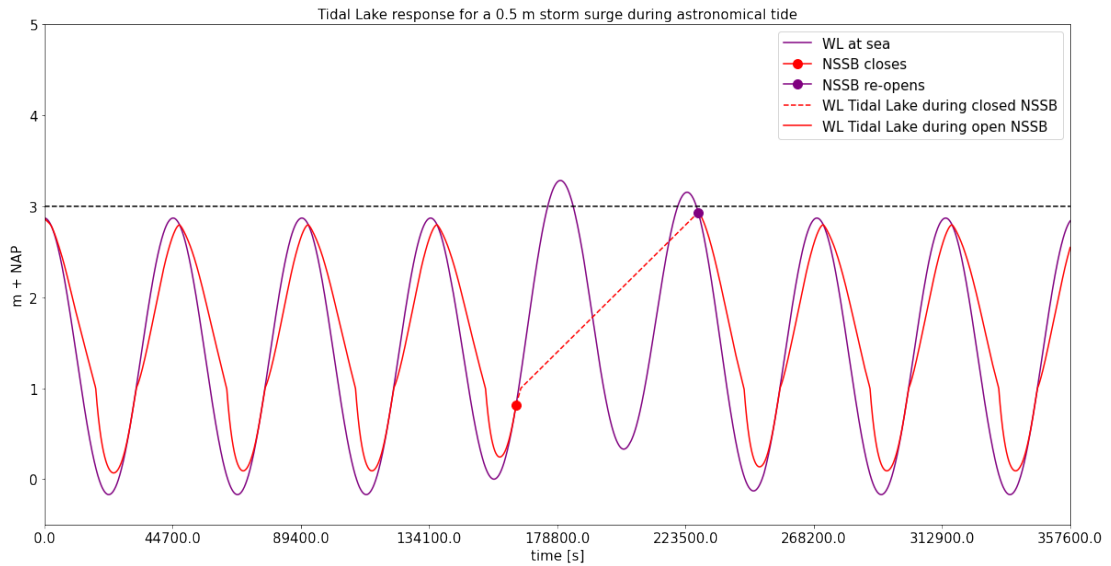


Figure XI.2: Closure and opening for a 0.5 m storm surge in 2150 SSP2-4.5 for a 5800 m³/s Rhine discharge

Storm surge of 3.0 m & 2200 m³/s at Lobith

An average Rhine discharge at Lobith of 2200 m³/s results in ca. 500 m³/s through the Haringvliet (see Section 3.2.7). Again, the Tidal Lake has more than sufficient capacity to act as a buffer during the storm.

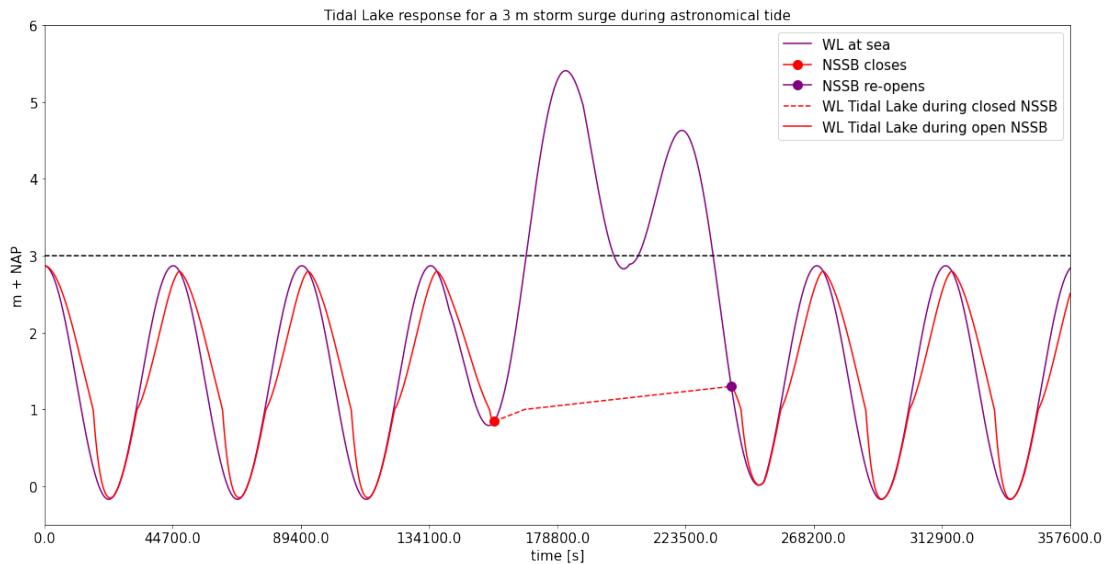


Figure XI.3: Closure and opening for a 3 m storm surge in 2150 SSP2-4.5 for an average Rhine discharge

Storm surge of 3.0 m & 5800 m³/s at Lobith

A Rhine discharge at Lobith of 5800 m³/s results in ca. 3750 m³/s through the Haringvliet (see Section 3.2.7). Now though, the Tidal Lake does not have sufficient capacity to act as a buffer during the storm as the water level inside the Tidal Lake reaches NAP + 3.0 m while the storm is still lingering. For this reason, the Spillway should be opened to keep the water level at the Tidal Lake at a maximum of NAP + 3.0 m. Note that, in Figure XI.4, the Spillway discharges a constant 3750 m³/s inside the Energy Storage Lake at the moment the water level reaches NAP + 3.0 m, resulting in the plateau, until re-opening.

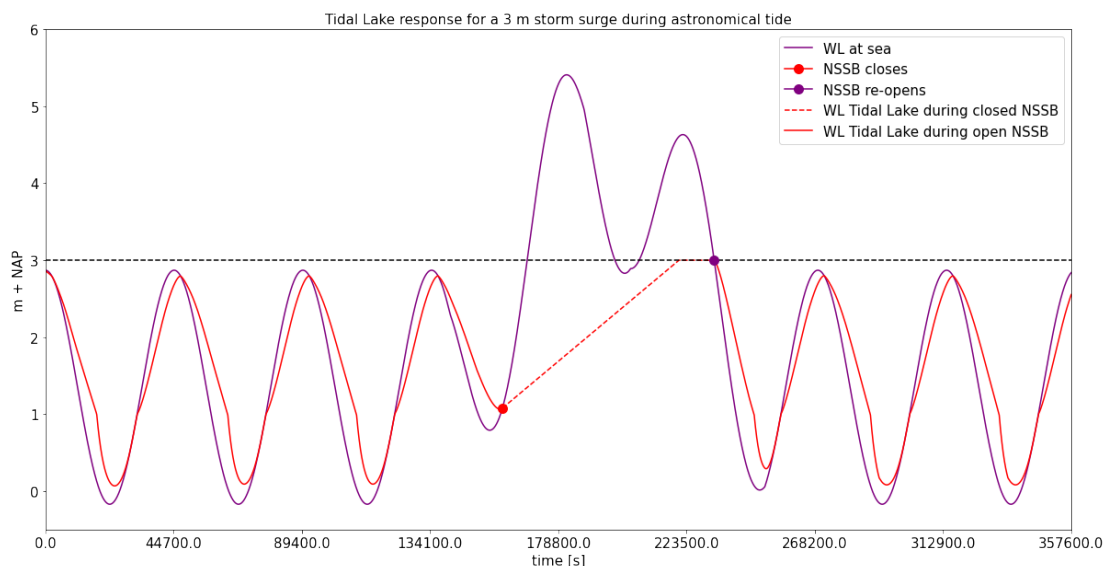


Figure XI.4: Closure and opening for a 3 m storm surge in 2150 SSP2-4.5 for a 5800 m³/s Rhine discharge
Spillway opening too late

As proposed in Section 5.1 though, the Spillway should be opened immediately after closure of the Delta Barrier. Said immediate opening of the Spillway would result in a water level at the Tidal Lake during a closed storm surge barrier which is completely dependent on the Spillway opening. For an opening resulting in exactly 3750 m³/s through the Spillway right after closure, Figure XI.5 yields the simulation.

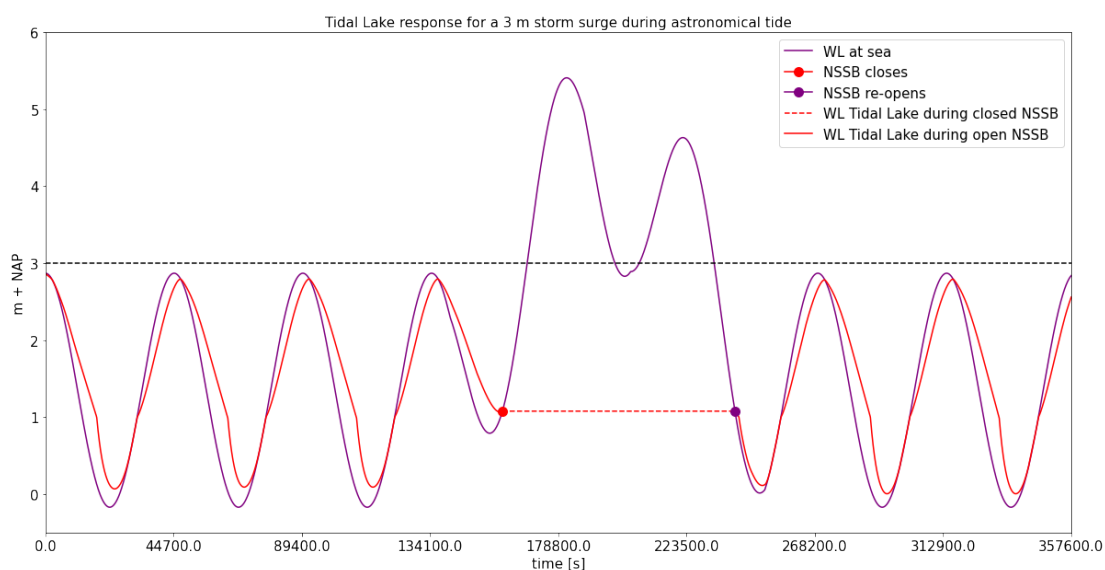


Figure XI.5: Closure and opening for a 3 m storm surge in 2150 SSP2-4.5 for a 5800 m³/s Rhine discharge
Spillway opening immediately

XII Exceedance Probability of Water Storage Capacity

The purpose of this appendix is to estimate the probability of exceedance of the water storage capacity. Said probability is used to determine the probability of flooding after a non-closure event in Section 5.2. Here, it is assumed that the water storage capacity has been exceeded once (part of) a dike segment in the hinterland fails resulting in a flooding. Furthermore, only flooding scenarios are considered which have consequences when considering individual risk. The failure of dike sections which merely result in flooding without any significant consequences are not considered.

The probability of exceedance of the water storage capacity can be found by finding the normative dike section, i.e. the dike section which yields the highest probability of failure (with significant consequences) resulting in flooding. The normative dike section is found by comparing segments of the relevant dike rings:

- Dike ring 20: Voorne-Putten
- Dike ring 25: Goeree-Overflakkee
- Dike ring 34: West-Brabant
- Dike ring 21: Hoeksche Waard
- Dike ring 22: Eiland van Dordrecht

For every dike ring established above, the governing dike section is determined, after which the greatest failure probability of said dike sections is assumed normative for the exceedance of the water storage capacity.

Dike ring 20: Voorne-Putten



Figure XII.1: Failure probabilities dike sections Voorne-Putten (modified from de Groot (2014a))

From Figure XII.1 it can be concluded that multiple dike sections pose a relative high failure probability. Table XII.1 gives the governing section, the failure mechanisms which are governing and the estimated failure probability according to de Groot (2014a).

<i>Governing section</i>	<i>Failure mechanism</i>	<i>P [per year]</i>
DV22	Uplift and piping	$7.69 \cdot 10^{-4}$

Table XII.1: Governing section dike ring Voorne-Putten

It should be noted that, according to de Groot (2014a), dike section DV22 does not have to greatest failure probability. Nonetheless, as the dike sections with greater failure probabilities (such as DV25) have yet to be reinforced in order to attain to the 2017 Water Act, dike section DV22 is governing.

Dike ring 25: Goeree-Overflakkee



Figure XII.2: Failure probabilities dike sections Goeree-Overflakkee (modified from Bisschop and Karimlou (2014))

Table XII.2 gives the governing section, the failure mechanisms which are governing and the estimated failure probability according to Bisschop and Karimlou (2014).

<i>Governing section</i>	<i>Failure mechanism</i>	<i>P [per year]</i>
DV24	Uplift and piping	$7.69 \cdot 10^{-4}$

Table XII.2: Governing section dike ring Goeree-Overflakkee

According to Bisschop and Karimlou (2014), dike section DV24 has the greatest failure probability.

Dike ring 34: West-Brabant



Figure XII.3: Failure probabilities dike sections West-Brabant (modified from Arends and Nieuwhof (2011))

From Figure XII.3 it can be concluded that multiple dike sections pose a relative high failure probability. Table XII.3 gives the governing section, the failure mechanisms which are governing and the estimated failure probability according to Arends and Nieuwhof (2011).

<i>Governing section</i>	<i>Failure mechanism</i>	<i>P [per year]</i>
DV32	Uplift and piping	$7.14 \cdot 10^{-4}$

Table XII.3: Governing section dike ring West-Brabant

It should be noted that, according to Arends and Nieuwhof (2011), dike section DV32 does not have to greatest failure probability. However, failure of the dike section with the greatest failure probability (DV19) would not have any significant consequences (Arends & Nieuwhof, 2011). Furthermore, various dike sections (e.g. DV16 and DV27) are on the HWBP2 and will be reinforced before 2050.

Dike ring 21: Hoeksche Waard



Figure XII.4: Failure probabilities dike sections Hoeksche Waard (modified from de Groot (2014b))

Table XII.4 gives the governing section, the failure mechanisms which are governing and the estimated failure probability according to de Groot (2014b).

Governing section	Failure mechanism	P [per year]
VNK.21.03.003	Piping and outflanking	0.002

Table XII.4: Governing section dike ring Hoeksche Waard

According to de Groot (2014b), structure VNK.21.03.003 (Inlaatsluis Brakelsveer) has the greatest failure probability.

Dike ring 22: Eiland van Dordrecht

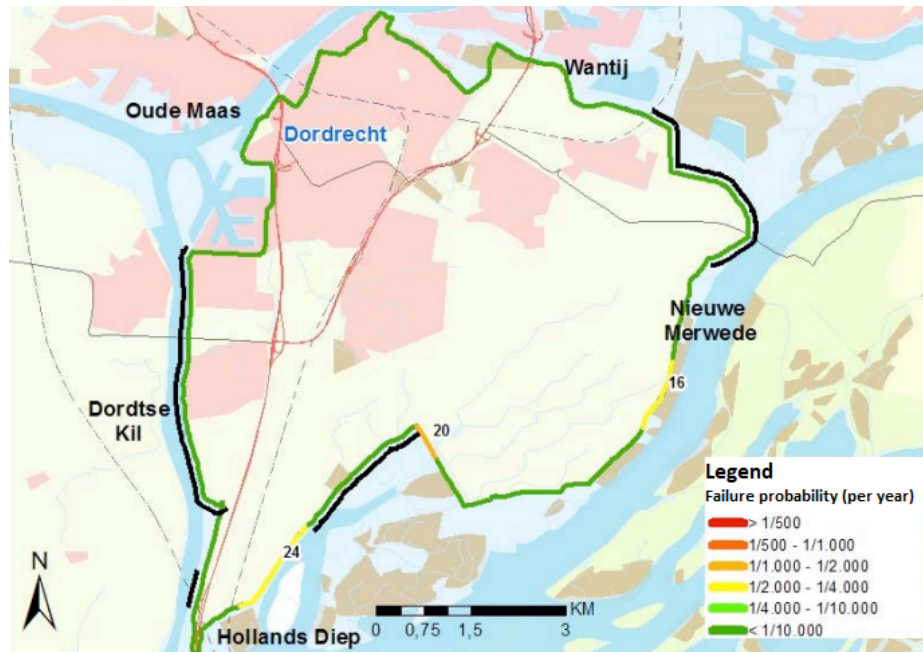


Figure XII.5: Failure probabilities dike sections Eiland van Dordrecht (modified from Veenstra-Huisman (2014))

Table XII.5 gives the governing section, the failure mechanisms which are governing and the estimated failure probability according to Veenstra-Huisman (2014).

<i>Governing section</i>	<i>Failure mechanism</i>	<i>P [per year]</i>
DV20	Uplift and piping	$5.26 \cdot 10^{-4}$

Table XII.5: Governing section dike ring Eiland van Dordrecht

According to Veenstra-Huisman (2014), dike section DV20, has the greatest failure probability.

Exceedance Probability of Water Storage Capacity

From the analysis conducted above, it follows that structure VNK.21.03.003 (Inlaatsluis Brakelsveer) at Hoeksche Waard has the greatest probability of failure and is therefore governing. Hence, the estimate of the exceedance probability of the water storage capacity is equal to the failure probability of VNK.21.03.003 of 0.002 per year or equivalently $\frac{1}{460}$ per year. It should be noted that strengthening this governing structure, although in compliance with the 2017 Water Act according to Veenstra-Huisman (2014), would not lead to significantly lowering the exceedance probability of the water storage capacity. A new governing section would arise with a failure probability of the same order of magnitude.

XIII Limit States Building Decree

This appendix provides the complete elaboration of ULS limit states. The relevant load combinations as posed in the ROK (2017) for STR, GEO and EQU are presented and SLS stages are discussed. The goal of this appendix is to determine the failure mechanisms and load combinations which ought to be used in the design of the Delta Barrier.

STR and GEO (ULS)

Water works such as storm surge barriers are not specifically mentioned in the NEN-standards. For this reason, the ROK (2017) considers said works separately in the ROK (guidelines for the design of structures). The ROK (2017) states that for internal failure or excessive deformation of the structure or of structural elements (STR) and for collapse or excessive deformation of the soil where the strengths of soil or rock determine the resistance to be provided (GEO), the load combinations as proposed in the ROK (2017) ought to be used. Said load combination in the ROK (2017) are specifically for barriers, but are also applicable for the Delta Barrier as a whole. The load combination as in the ROK are defined for CC3 with a reference period of 100 years. Greater reference periods should again be translated into greater partial safety factor for the respective characteristic variable loads. One should note that the ROK (2017) is in addition to the standards as dictated by the Building Decree, stated in the different Eurocodes and is by no means meant as a replacement to the Eurocode.

The ROK (2017) gives a total of 9 load combinations for the case in which the barrier is closed and 5 load combinations for the case in which the barrier is either opening or closing, for both limit states. For the sake of this preliminary design we will solely focus on the barrier when closed (see fig. XIII.1). With regard to the verification to the Building Decree, the following load combinations as posed in the ROK (2017) are considered:

- A: Maximum positive head is dominant
- B: Maximum negative head is dominant
- H: Ship collision²³

The load combination are based on consequence class 3 (CC3), which corresponds to major consequences in terms of loss of life, or very large economic, social or environmental consequences according to the Eurocode (2019). The New Storm Barrier is designed according to CC3, naturally. The design value of the load combinations for the case of an open storm surge barrier are all based on Equation (6.10b) from the Eurocode (2019) (Rijkswaterstaat, 2017) (here eq. (XIII.1)).

$$\sum_{j \geq 1} \xi_j \gamma_{G,j} G_{k,j} + \gamma_P P + \gamma_{Q,1} Q_{k,1} + \sum_{i > 1} \gamma_{Q,i} \psi_{0,i} Q_{k,i} \quad (\text{XIII.1})$$

- where: " + " means "to combine with"
- Σ means "the combined outcome of"
- ξ_j is a reduction factor for unfavourable permanent action j
- γ is a partial factor for the respective action j or i that produces unfavourable effects
- $\psi_{0,i}$ is a combination factor applied to variable action i to determine its combination value
- $G_{k,j}$ is the characteristic value of the permanent action j
- P is the prestressing force
- $Q_{k,1}$ is the characteristic value of the dominant variable action 1
- $Q_{k,i}$ is the characteristic value of the variable action i

When a limit state of failure or excessive deformation of a part, structural element or connection (STR and/or GEO) has been considered, it shall be verified that:

²³Note that this load combination is considered an accidental event, say a calamity by the ROK (2017)

$$E_d \leq R_d \quad (\text{XIII.2})$$

where: E_d is the design value of the loading effect, such as internal forces, internal moments or a vector representing various internal forces or internal moments
 R_d is the design value of the corresponding resistance

Figure XIII.2 presents the load combination from the ROK (2021) with specified partial factors which ought to be used. Note that the partial factors should be adjusted here for a reference period of 200 years. Additionally, the ROK (2021) states that for the hydraulic load, expressed as water pressure on the structure, it was decided not to apply a partial factor, but to prescribe the exceedance probability of the design value of the load. With this exceedance probability and the load statistics, the design value can then be determined directly. This translates to the adjustments for the partial safety factors in fig. XIII.1 for loads: F10 and F13 from 1.5 to 1 for load combination A and from 1.25 to 1 for load combination H.

belastingcombinatie	A	B	C	D	E	F	G	H	I
Belasting									
Eigen gewicht (F0,F1,F2)	7.10.2 WOWK ¹ /1,25 ⁴	7.10.3 WOWK /1,25 ⁴	1,25	1,25	1,25	1,25	1,25	1,25	1,25
Positieve vervalbelasting (F10) Windgolfbelasting bij positief verval (F13)	7.10.2 WOWK /1,5 ⁴			1,25 ²	1,25 ²	1,25 ²	1,25 ²	1,25 ²	1,25 ²
Negatieve vervalbelasting(F11) Windgolfbelasting bij negatief verval (F13)		7.10.3 WOWK /1,5 ⁴							
Vervalbelasting bij max schutpeil (F12)			1,0						
Windgolfbelasting bij max schutpeil (F13)			1,2 ³						
translatiegolf bij max schutpeil (F15)			1,2						
Verkeersbelasting /bordesbelasting (F16)	1,2	1,2	1,2	1,5	1,2	1,2	1,2	1,0	1,0
Windbelasting	1,65	1,65	0,5	0,5	0,5	0,5	0,5	0,5	0,5
Voorspankracht uit bew. Werk (F33)	1,2	1,2	1,2	1,2	1,2	1,2	1,2	1,0	1,0
Schroefstraal schip					1,5				
Utdruk (F53)					0,8	1,5			
Krachtenopbouw langs de draaiaas; zie (1.9)							1,5		
Aanvaren deur (F54)								1,0	
Lekraken drijfkist (F55)									1,0

Figure XIII.1: Load combinations with partial safety factors for a closed barrier as in the ROK (2021)

The variable loads (F_i) specified in the 9 load combinations have been defined in Ontwerp van Schutsluizen by Vrijburcht (2000). With regard to the extreme water level and wave height for load combination A (F_{10} and F_{13} respectively), the WOWK (2018) proposes loads with a frequency equal to $R = 100000$ years for CC3. Furthermore for loads due to own weight considering load combinations A and B (F_0 , F_1 and F_2), The WOWK (2018) states that a partial safety factor of 1.35 or 0.9 ought to be used for favourable and unfavourable loads respectively. Lastly, the ROK (2021) states that the loads F_{10} and F_{13} for load combinations D till I should correspond to loads with a frequency equal to $R = 10$ years.

All considerations above yields modified partial safety factors with respect to Figure XIII.1. The final partial safety factors used in this thesis for only the relevant load combinations considered for the STR and GEO verification are presented in Figure XIII.2.

belastingcombinatie	A	B	H
Belasting			
Eigen gewicht (F0,F1,F2)	7.10.2 WOWK ¹ 1.35/0.9*	7.10.3 WOWK 1.35/0.9*	1,25
Positieve vervalbelasting (F10) Windgolfbelasting bij positief verval (F13)	7.10.2 WOWK 1,0		1,0
Negatieve vervalbelasting(F11) Windgolfbelasting bij negatief verval (F13)		7.10.3 WOWK 1,5	
Vervalbelasting bij max schutpeil (F12)			
Windgolfbelasting bij max schutpeil (F13)			
translatiegolf bij max schutpeil (F15)			
Verkeersbelasting /bordesbelasting (F16)	1,2	1,2	1,0
Windbelasting	1,65	1,65	0,5
Voorspankracht uit bew. Werk (F33)	1,2	1,2	1,0
Schroefstraal schip			
IJsdruk (F53)			
Krachtsopbouw langs de draais; zie (1.9)			
Aanvaren deur (F54)			1,0
Lekraken drijfkist (F55)			

Figure XIII.2: Load combinations with partial safety factors used in this thesis (modified from Rijkswaterstaat (2021))

FAT (ULS)

The design value of the load with regard to failure of the structure or structural elements due to fatigue (FAT) should be assessed using the relevant code for the applicable material (e.g. Eurocode 3 for steel) as stated in the Eurocode (2019). For this preliminary design fatigue will not be taken into account, as fatigue verification mostly consists of verifying connections such as welds.

EQU (ULS)

The design value of the load with regard to the loss of static equilibrium of the structure (EQU) should be determined using the Eurocode (2019) Table A2.4(A) (Rijkswaterstaat, 2017). Said table is based on Equation (6.10) from the Eurocode (2019) (here eq. (XIII.3))

$$\sum_{j \geq 1} \gamma_{G,j} G_{k,j} + \gamma_P P + \gamma_{Q,1} Q_{k,1} + \sum_{i > 1} \gamma_{Q,i} \psi_{0,i} Q_{k,i} \quad (\text{XIII.3})$$

When a limit state of static equilibrium of the structure has been considered (EQU), it must be verified that:

$$E_{d,dst} \leq E_{d,stab} \quad (\text{XIII.4})$$

where: $E_{d,dst}$ is the design value of the destabilising load effect
 $E_{d,stab}$ is the design value of the stabilising load effect

For EQU the same governing load combinations by the ROK (2017): A, B and H are considered, although now with partial safety factors according to the Eurocode (2019) Table A2.4(A). Note that the partial safety factors regarding a hydraulic load, expressed as a water pressure on the structure, is again set to 1 for similar reasoning as for the limit states STR and GEO.

UPL (ULS)

The design value of the load with regard to loss of equilibrium of the structure or the subsoil as a result of uplift by water pressure or other vertical loads (UPL) and with regard to hydraulic soil fracture, internal erosion and erosion due to concentrated groundwater flow (piping) in the subsoil as a result of hydraulic gradients (HYD) are to be determined using Eurocode 7 as stated in the Eurocode (2019). For both UPL and HYD only load combination A and B are taken into account. Ice loads and ship collision will not directly cause uplift or internal erosion and hence are not relevant.

Verification of the uplift mechanism (UPL) shall consist of checking that the design value of the combination of driving permanent ($G_{dst;d}$) and variable ($Q_{dst;d}$) vertical loads is less than or equal to the design value of the resisting permanent vertical loads ($G_{stb;d}$) and/or the design value of any additional buoyancy resisting load (R_d) as stated in Eurocode 7 (2016):

$$G_{dst;d} + Q_{dst;d} \leq G_{stb;d} + R_d \quad (\text{XIII.5})$$

In eq. (XIII.5), the partial factors for $G_{dst;d}$, $Q_{dst;d}$, $G_{stb;d}$ and R_d for permanent and temporary situations from A.4 (1)P and A.4 (2)P in Eurocode 7 (2016) must be used. Note that the values of the partial factors may be specified in the national annex to Eurocode 7 (2016).

HYD (ULS)

When considering a failure limit state due to hydraulic soil fracture as a result of groundwater seepage (HYD), it must be checked for each applicable soil column that the design value of the driving total groundwater pressure ($u_{dst;d}$) at the bottom of the column or the design value of the seepage force ($S_{dst;d}$) in the column is less than or equal to the resisting vertical soil pressure ($\sigma_{stb;d}$) at the bottom of the column, or the effective weight ($G'_{stb;d}$) of that same column:

$$u_{dst;d} \leq \sigma_{stb;d} \quad (\text{XIII.6a})$$

$$S_{dst;d} \leq G'_{stb;d} \quad (\text{XIII.6b})$$

In eq. (XIII.6a) and eq. (XIII.6b) the partial factors for $u_{dst;d}$, $\sigma_{stb;d}$, $S_{dst;d}$ and $G'_{stb;d}$ for permanent and temporary situations from A.5 (1)P from Eurocode 7 (2016) must be used. Again, the values of the partial factors may be specified in the national annex to Eurocode 7.

SLS

Until now, all limit states as discussed above are ultimate limit state (ULS). For serviceability limit state (SLS) assessments (e.g. considering concrete crack width and the deflection of components) the Eurocode (2019) ought to be used. The Eurocode treats three different stages with regard to SLS assessments according to the Eurocode (2019):

- a) Characteristic combination:

The characteristic combination is normally used for irreversible limit states, where the load is defined using eq. (XIII.7). In the light of this thesis an irreversible SLS limit state will not occur.

$$\sum_{j \geq 1} G_{k,j} + "P" + "Q_{k,1}" + \sum_{i > 1} \psi_{0,i} Q_{k,i} \quad (\text{XIII.7})$$

- b) Frequent combination:

The frequent combination is normally used for reversible limit states, e.g. concrete crack widths. According to Braam (2010), this generally corresponds to the load which is surpassed 1% of the reference time, say twice per 200 years ($R = 100$ years). The load with regard to frequent combinations should be determined using eq. (XIII.8)

$$\sum_{j \geq 1} G_{k,j} + "P" + \psi_{1,1} "Q_{k,1}" + \sum_{i > 1} \psi_{2,i} Q_{k,i} \quad (\text{XIII.8})$$

- c) Quasi-permanent combination:

The quasi-permanent combination is normally used for long-term effects (e.g. creep, shrinkage) and for the appearance of the structure, corresponding to the load which is surpassed 50% of the reference time, say 100 times in 200 years ($R = 2$ years) (Braam, 2010). The load with regard to quasi-permanent combinations should be determined using eq. (XIII.9).

$$\sum_{j \geq 1} G_{k,j} + P + \sum_{i > 1} \psi_{2,i} Q_{k,i} \quad (\text{XIII.9})$$

It should be noted that for SLS assessments all partial safety factors are set to 1 and hence do not show in eq. (XIII.7), eq. (XIII.8) and eq. (XIII.9). The different stages of the serviceability limit state mostly consider variations in the variable load, using different combination factors (ψ) for every stage. An explanation for the different values of the variable load to be used per stage and corresponding combination factors (ψ) is best shown using fig. XIII.3 by Braam (2010). Though, as for water loads, these combination factors are set to 1 as well.

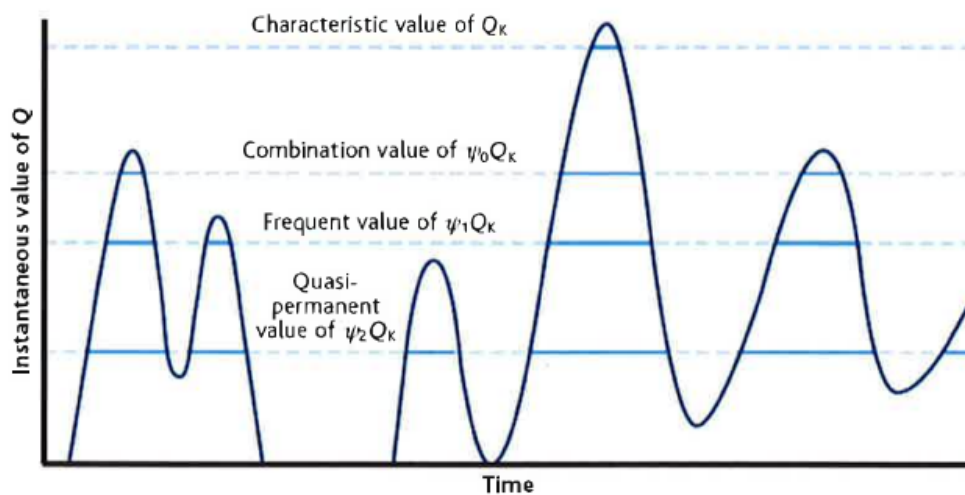


Figure XIII.3: Variable load in time (Braam, 2010)

The combination value (see ULS), frequent value and quasi-permanent value can be obtained by multiplying the characteristic value of the variable load with ψ_0 , ψ_1 and ψ_2 respectively (see fig. XIII.3).

Accidental loads

Accidental loads - or calamities - are events that may happen with a relatively small probability of occurrence and lead directly or indirectly to the occurrence of rather special loads. If the probability of a calamity is sufficiently small (less than the permissible probability of structural failure of the structure of the order of 1/100 times the safety standard), these special loads do not have to be explicitly taken into account. If this is not the case, such loads must be taken into account when checking the risk of structural failure (Veendorp & Niemijer, 2003).

The 'Leidraad Kunstwerken' (2003) considers the following accidental loads, which - if the probability of the calamity is not sufficiently small - ought to be taken into account: (ship) collision, earthquakes, explosions, ice and flow in the case of a non-closure event. Furthermore, in addition to ship collision, the ROK (2017) states that for wet civil works falling anchors, dragging anchors and a sunk ship ought to be taken into account. However, for this thesis such events have not been taken into account and it is assumed that a concrete cover is able to withstand the loads. Within the 9 load combinations specified by the ROK (2017) for the case in which the barrier is closed (for STR and GEO), 2 load combinations are already comprised of accidental loads, viz. ship collision and a leak in the floating box for the gate(s). The ROK (2017) does not consider load combinations with ice loading as a calamity.

It could be argued if ice loading is to be expected in such saline environment as the Haringvliet mouth and if so if said loading will be governing for the design. For this reason, a load combination including ice loading is not treated.

For this thesis, only the accidental event regarding ship collision is explicitly taken into account. A ship collision event, as prescribed by the ROK (2017) and Vrijburcht (2000), should correspond to the load on the closed barrier with an exceedance frequency of 1/1000 per year.

XIV Complete Verification Gate Design

This appendix presents the complete verification of the final gate design for all structural gate components regarding the strength and stiffness. First, all relevant external forces on the gate are established and an overview of the forces on the gate per load combination is presented just as the force flow through the gate. From said forces (albeit derived from pressures) and the schematized, assumed force flow all verifications are conducted per identified structural component from the final gate design. Lastly, Appendix XIV.3 presents the dynamic analysis of the gate from which the fundamental natural frequencies of the gate are determined. The Excel spreadsheet used to conduct the verifications is available at <http://repository.tudelft.nl/>.

XIV.1 External Forces on the Gate

Hydrostatic forces

$$p_h = \rho_{w,salt} g h \quad (\text{XIV.1})$$

where:	p_h	[kN/m ²]	=	hydrostatic pressure
	$\rho_{w,salt}$	[kN/m ³]	=	density of salt water = 1.025
	g	[m/s ²]	=	gravitational constant
	h	[m]	=	pressure head

Wave forces

For the calculation of the wave forces on the structure the Goda method is used. Goda's equations do not have an analytical base but rather an empirical foundation and can be used for both breaking and non-breaking waves (Molenaar & Voorendt, 2020b).

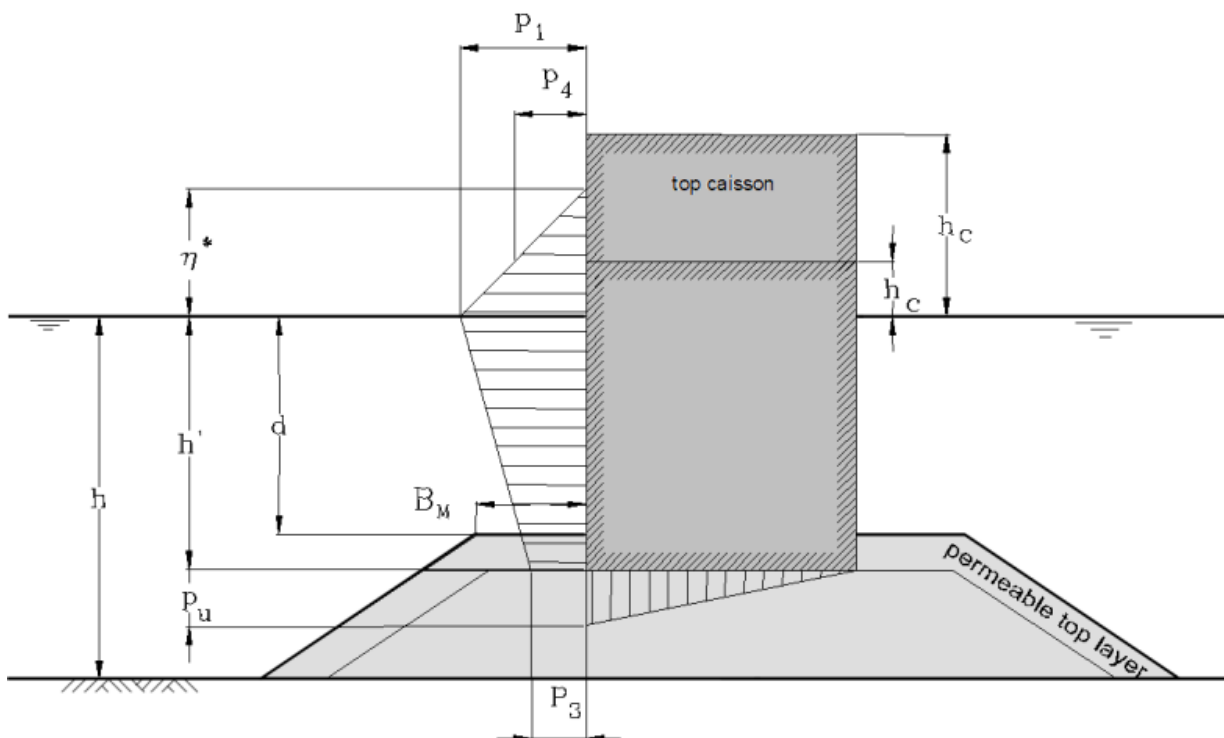


Figure XIV.1: Wave forces by Goda (modified by Tanimoto) (Molenaar & Voorendt, 2020b)

$$p_1 = 0.5 (1 + \cos(\beta)) (\lambda_1 \alpha_1 + \lambda_2 \alpha_2 \cos^2(\beta)) \rho_{w,salt} g H_{S;D} \quad (\text{XIV.2a})$$

$$p_3 = \alpha_3 p_1 \quad (\text{XIV.2b})$$

$$p_4 = \alpha_4 p_1 \quad (\text{XIV.2c})$$

$$p_u = 0.5 (1 + \cos(\beta)) \lambda_3 \alpha_1 \alpha_3 \rho_{w,salt} g H_{S;D} \quad (\text{XIV.2d})$$

in which:	p_i	[N/m ²]	=	respective wave pressures on the wall
	β	[°]	=	angle of incidence of incoming wave
	α_1	[-]	=	$0.6 + 0.5 \left(\frac{4\pi h/L_d}{\sinh(4\pi h/L_d)} \right)^2$
	α_2	[-]	=	$\min \left(\frac{(1 - d/h_b)(H_{S;d}/d)^2}{3}; \frac{2d}{H_{S;d}} \right)$
	α_3	[-]	=	$1 - (h^*/h) \left(1 - \frac{1}{\cosh(2\pi h/L_d)} \right)$
	α_4	[-]	=	$1 - \frac{h_c^*}{\eta^*}$
	h_c^*	[m]	=	$\min(\eta^*, h_c)$
	η^*	[m]	=	$0.75 (1 + \cos(\beta)) \lambda_1 H_{S;d}$
	λ_1	[-]	=	1 for vertical wall and non-breaking waves
	λ_2	[-]	=	1 for vertical wall and non-breaking waves
	λ_3	[-]	=	1 for vertical wall and non-breaking waves
	h_b	[m]	=	water depth at a distance $5H_{S;d}$ from the wall
	$H_{S;d}$	[m]	=	design significant wave height
	L_d	[m]	=	design wave length
	d	[m]	=	water depth above the sill
	h^*	[m]	=	water depth above the wall foundations plane
	h_c	[m]	=	height of the crest of the wall w.r.t. the water level
	h	[m]	=	water depth in front of the sill

For wave impact loads which develop when water becomes entrapped under (parts of) the structure, e.g. around the still water line with vertical movement of the water, some formulas have been developed. Said formulas however are not capable of taking into account the characteristics of both the waves and structure. In order to derive the governing wave impact load as accurate as possible a scale model ought to be made, subjecting it to the expected waves and subsequently measuring the wave impact forces. For the Oosterscheldekering this approach has led to a design wave impact load used in the design of 600 kN/m^2 . For this preliminary design, such wave impact loads are neglected. Nonetheless, provisions are made to decrease such wave impact loads by means of mostly using tubular cross-sections and by providing the longitudinal stiffeners with recesses.

Drag & lift forces

The general empirical formulas for drag and lift are respectively (from (Molenaar & Voorendt, 2020b)):

$$F_D = \frac{1}{2} \rho u^2 (C_D + C'_D) A \quad (\text{XIV.3a})$$

$$F_L = \frac{1}{2} \rho u^2 (C_L + C'_L) A \quad (\text{XIV.3b})$$

- in which: F_D [N] = drag force parallel to the flow direction
 F_L [N] = lift force perpendicular to the flow direction
 ρ [kg/m³] = density of water
 u [m/s] = disturbed flow velocity
 C_D [-] = static drag coefficient
 C'_D [-] = dynamic drag coefficient
 C_L [-] = static lift coefficient
 C'_L [-] = dynamic lift coefficient
 A [m²] = area facing flow, projected perpendicular to the flow direction

As for the static drag and lift coefficients, Figure XIV.2 as reported by Molenaar and Voorendt (2020b) gives a first indication for both assuming $L/D = \infty$. This yield $C_D = C_L \approx 1.25$.

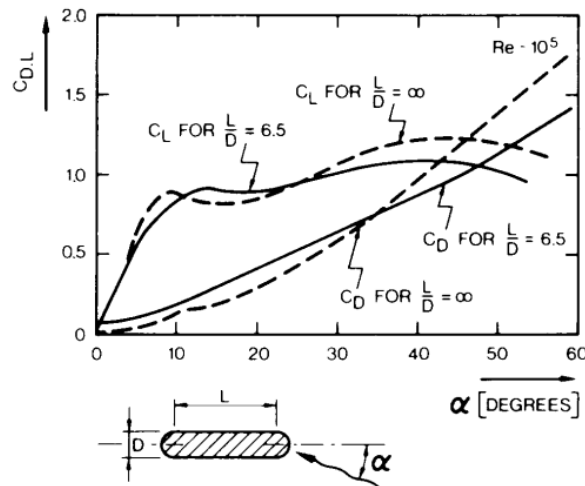


Figure XIV.2: Static drag and lift coefficients (Colin & Lewis, 1968)

As for the static structural design, the drag and lift forces are neglected as the resulting forces are significantly less than e.g. the hydrostatic and wave forces. Nonetheless it should be noted that lift forces with certain frequency can result in resonance of the gate. This is discussed in Appendix XIV.3.

Ship collision

NEN-EN 1991-1-7 (2015) C.4.4 prescribes the derivation of impact loads from ships (collision) at sea. Here, it is assumed that a frontal collision is normative.

$$F_{bow} = \begin{cases} F_0 \cdot \bar{L}(\bar{E}_{imp} + (5.0 - \bar{L})\bar{L}^{1.6})^{0.5}, & \text{for } \bar{E}_{imp} \geq \bar{L}^{2.6} \\ 2.24 \cdot F_0(\bar{E}_{imp}\bar{L})^{0.5}, & \text{for } \bar{E}_{imp} < \bar{L}^{2.6} \end{cases} \quad (XIV.4)$$

- in which: \bar{L} [-] = $\frac{L_{pp}}{275}$
 \bar{E}_{imp} [-] = $\frac{E_{imp}}{1425}$
 E_{imp} [MNm] = $\frac{1}{2}mv_r^2$
 F_{bow} [MN] = is the maximum frontal impact force
 F_0 [MN] = is the reference impact force = 210
 E_{imp} [MNm] = is the energy to be absorbed by mean of plastic deformation
 L_{pp} [m] = is the length of the ship
 m [kg] = is the (average) mass of the ship
 v_r [m/s] = is the impact speed of the ship

As for the impact speed, NEN-EN 1991-1-7 (2015) C.4.4 [C1] recommends a speed of 5 m/s. However, as the storm surge barrier will be very much in sight in case of a approaching ship and extensive warning systems will be in place, one may assume that the impact speed is less. Here, the impact speed is assumed $v_r = 2.5$ m/s, as recommended in NEN-EN 1991-1-7 (2015) C.4.4 [C1] for ships in harbours at sea.

From the established normative ships, it is chosen to regard ship impact by a CEMT-class Va as highly improbable²⁴. Therefore, Table XIV.1 presents the ship characteristics with the calculated impact load for the governing fishing trawler OD1 Maarten-Jacob only.

	m [DWT] ²⁵	L_{pp} [m]	F_{bow} [MN]
OD1 Maarten-Jacob	365	42.35	5.22

Table XIV.1: Impact loads for the normative ships

Overview of forces

- A: Maximum positive head is dominant

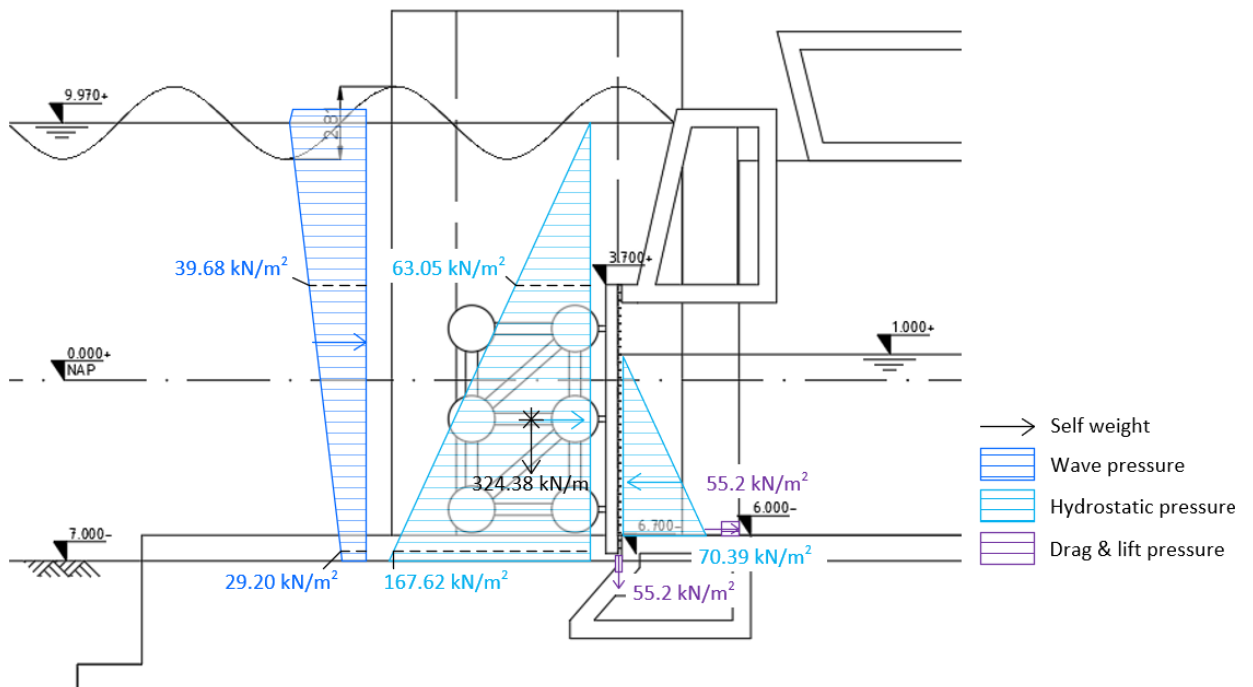


Figure XIV.3: Forces on the gate for load combination A

²⁴A ship collision event, as prescribed in the ROK (2017) and Vrijburcht (2000), should correspond to the load on the closed barrier with an exceedance frequency of 1/1000 per year

²⁵The average mass has been reported and used for the calculation as prescribed by NEN-EN-1991-1-7 (2015)

- B: Maximum negative head is dominant

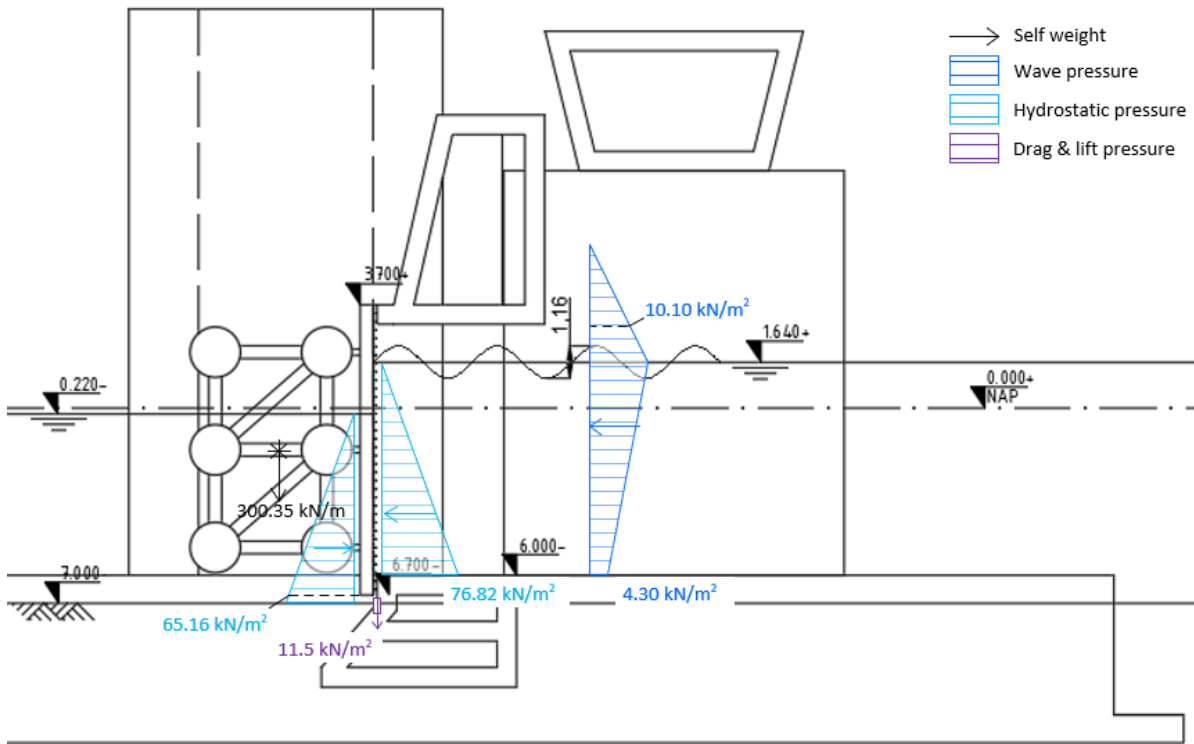


Figure XIV.4: Forces on the gate for load combination B

From Figure XIV.4, it can easily be deduced that load combination B is not governing (over load combination A) as the strength of the vertical lift gate is the same irrespective of positive or negative head and the (resultant) loads on the gate in the case of load combination A are greater.

- H: Ship collision

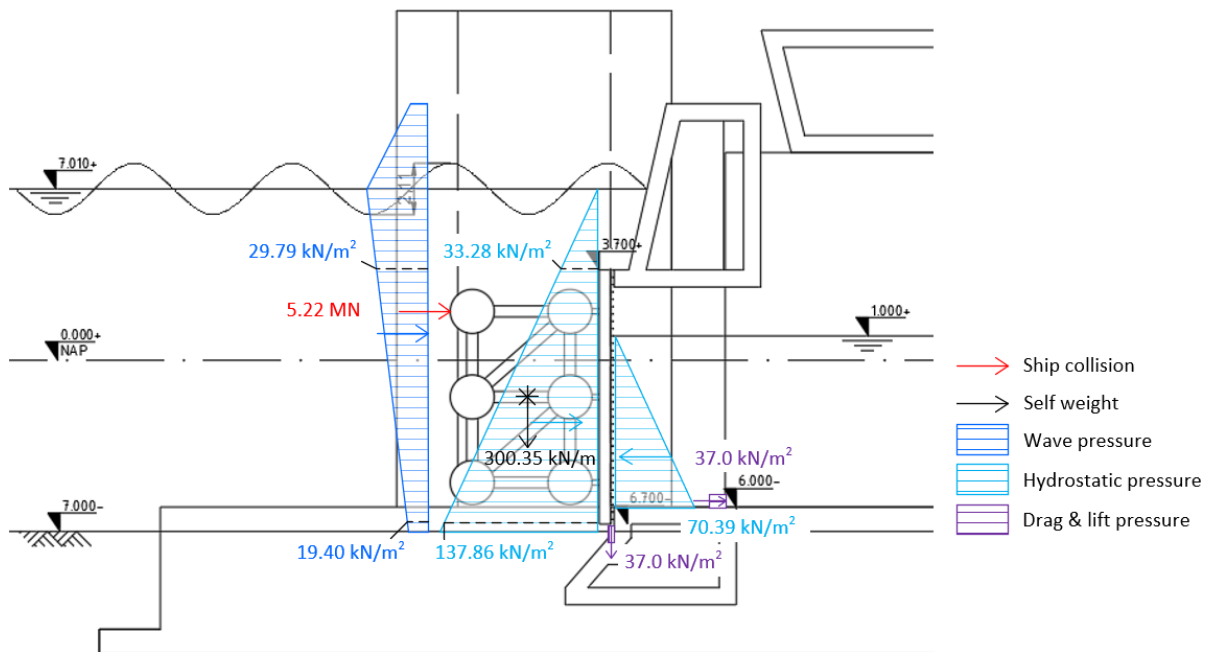


Figure XIV.5: Forces on the gate for load combination H

- SLS: Quasi-permanent combination

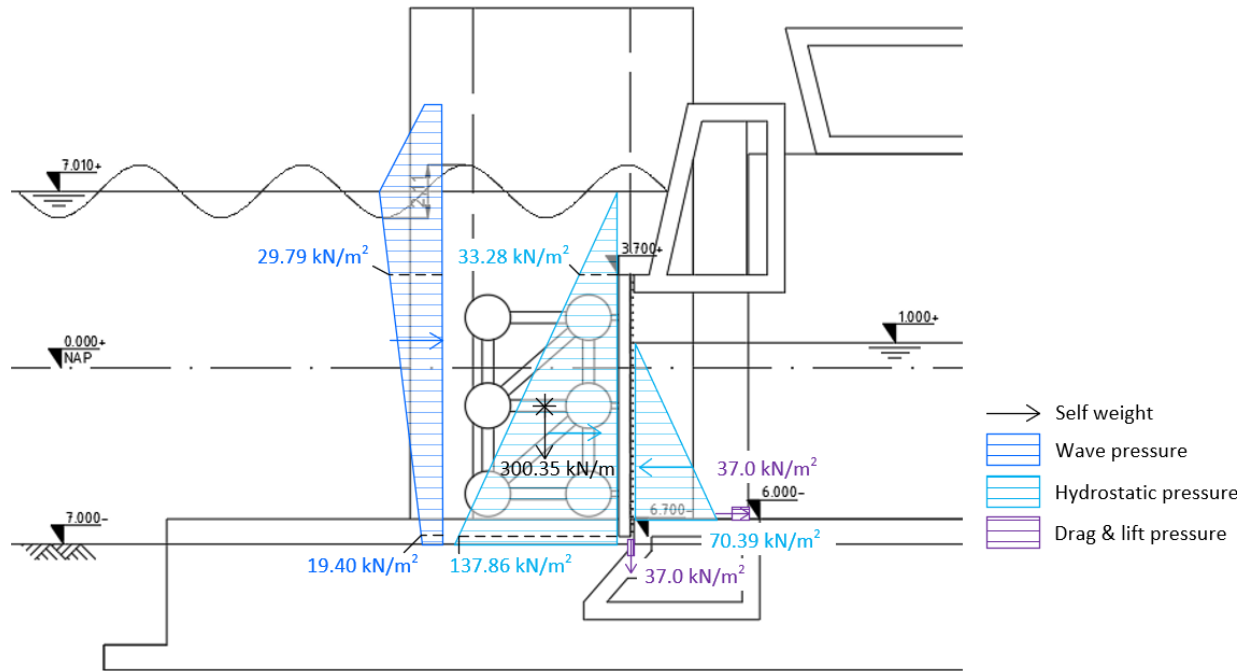


Figure XIV.6: Forces on the gate for quasi-permanent combination

Flow of forces

The loads on the gate as specified per load combination above, are transferred from the skin plate (nr.1) to the vertical girders (nr.2). The vertical girders, subsequently, transfer the loads to the global truss system via the stump connectors (nr.3). The force flow as described is presented in Figure XIV.7. Note that the number of elements in Figure XIV.7 are significantly less than in the actual verified design, as Figure XIV.7 merely serves the purpose of presenting the force flow assumed in order to design the respective elements.

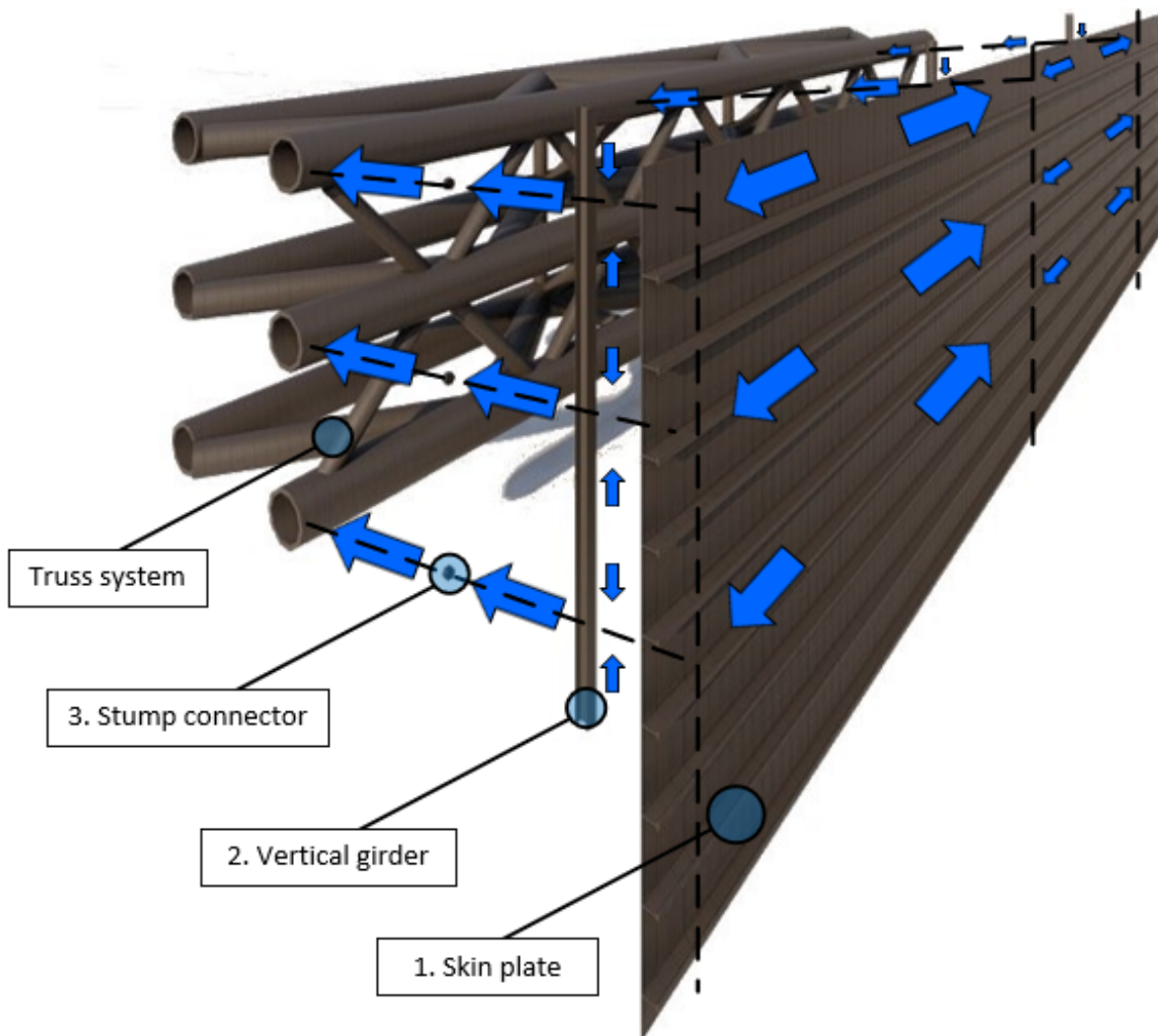


Figure XIV.7: Simplified force flow through the gate

XIV.2 Verification per Gate Component

XIV.2.1 Stiffened Skin Plate (nr.1)

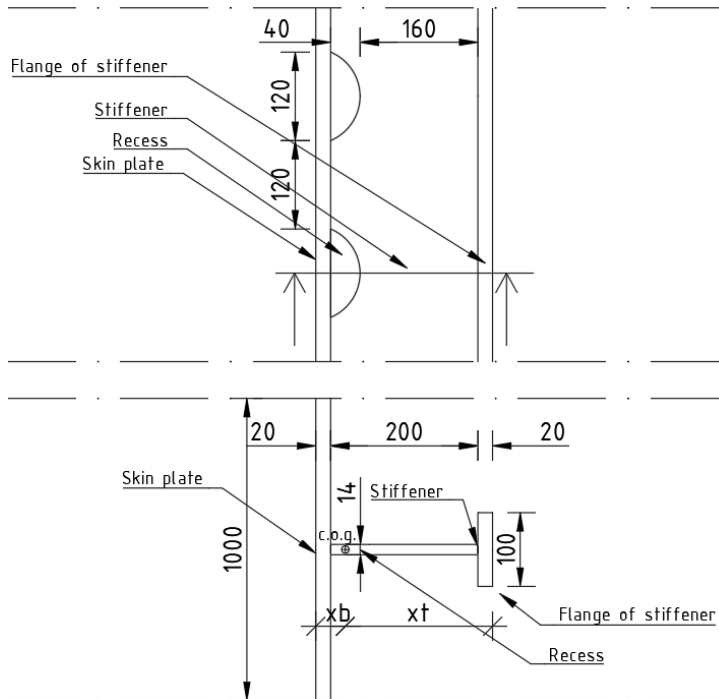


Figure XIV.8: Stiffened skin plate (nr.1)

f_y	355	N/mm ²
E	210000	N/mm ²
b_s	1000	mm
t_s	20	mm
h_w	200	mm
$h_{w,eff}$	160	mm
t_w	14	mm
b_f	100	mm
t_f	20	mm
a	2000	mm
I_{xx}	118111340	mm ⁴
x_t	200	mm
x_b	-40	mm
$M_{f,Rd}$	156.20	kNm

Table XIV.2: Stiffened skin plate characteristics

- in which:
- f_y is the yield strength
 - E is the Youngs Modulus
 - b_s is the centre to centre distance of two stiffeners
 - t_s is the thickness of the skin plate
 - h_w is the height of the web of the stiffener
 - $h_{w,eff}$ is the effective height of the web stiffener
 - t_w is the thickness of the web of the stiffener
 - b_f is the width of the flange of the stiffener
 - t_f is the thickness of the flange of the stiffener
 - a is the centre to centre distance between the supports (vertical girders)
 - I_{xx} is the mass moment of inertia of the combined elements
 - x_t is the distance from the centre of gravity to the top (right)
 - x_b is the distance from the centre of gravity to the bottom (left)

A: Maximum positive head is dominant

Bending moment skin plate

The design value for the bending moment in the skin plate is calculated assuming a pinned-pinned schematization using the maximum pressure following from Figure XIV.3. A pinned-pinned schematization gives the maximum bending moment and is hence a conservative approach. The maximum pressure (p_{max}) occurs at the Tidal Lake water level and consists of the sum of the hydrostatic pressures and wave pressure. Conservatively, it is assumed that said maximum pressure occurs over the entire length between two stiffeners (b_s). The centre to centre distance between two vertical girders (nr.2), which transfer the forces as depicted in Figure 7.2, is $a = 2000$ mm.

$$M_{Ed} = \frac{1}{8} p_{max} b_s a^2$$

$$\begin{aligned}
&= \frac{1}{8} \cdot 134.2 \cdot 1.00 \cdot 2.00^2 \\
&= 67.10 \text{ kNm}
\end{aligned}$$

where: M_{Ed} [kNm] = design value of bending moment
 p_{max} [kN/m²] = maximum pressure
 b_s [m] = centre to centre distance of two longitudinal stiffeners
 a [m] = distance between vertical girders (nr.2) (i.e. supports of the skin plate)

The verification now follows from Equation (XIV.5a) and Equation (XIV.5b) for the top fibre under tension and bottom fibre under compression, respectively.

$$\sigma_t = \frac{M_{Ed} x_t \gamma_{M0}}{I_{xx}} \leq f_y \quad (\text{XIV.5a})$$

$$\sigma_b = \frac{M_{Ed} x_b \gamma_{M0}}{I_{xx}} \leq f_y \quad (\text{XIV.5b})$$

where: σ_t [N/mm²] = stress at the outermost top fibre
 σ_b [N/mm²] = stress at the outermost bottom fibre
 x_t [mm] = distance between the centre of gravity and outermost top fibre
 x_b [mm] = distance between the centre of gravity and outermost bottom fibre
 I_{xx} [mm⁴] = mass moment of inertia of the cross-section
 γ_{M0} [-] = partial factor for resistance of cross-sections = 1
 f_y [N/mm²] = yield strength

Finally, Table XIV.3 presents the stresses at the outer fibres of the cross-section. Furthermore, the unity check (UC) is reported, defined as follows:

$$UC = \left| \frac{\sigma_i}{f_y} \right| \leq 1$$

	σ [N/mm ²]	UC [-]
x_t	114	0.32
x_b	-23	0.06

Table XIV.3: Bending moment verification

Shear force skin plate

As for the bending moment, the design value for the shear force in the skin plate is calculated assuming the pinned-pinned schematization using the maximum pressure following from Figure XIV.3. Conservatively, it is assumed that said maximum pressure occurs over the entire area consisting of the product of the length between two stiffeners (b_s) and the centre to centre distance between two vertical girders (a).

$$\begin{aligned}
V_{Ed} &= p_{max} b_s a \\
&= 134.2 \cdot 1.00 \cdot 2.00 \\
&= 268.40 \text{ kN}
\end{aligned}$$

The verification now follows from Equation (XIV.6) (NEN-EN 1993-1-5 (2022) 7.2 (1)).

$$V_{el,Rd} = \frac{\chi_w f_{yw} h_{w,eff} t_w}{\sqrt{3} \gamma_{M1}} + \frac{b_f t_f^2 f_{yf}}{c \gamma_{M1}} \left(1 - \left(\frac{M_{Ed}}{M_{f,Rd}} \right)^2 \right) \geq V_{Ed} \quad (\text{XIV.6})$$

where: $V_{el,Rd}$	[N]	=	elastic shear resistance of a plate member
χ_w	[-]	=	shear buckling factor
f_{yw}	[N/mm ²]	=	yield strength of the web
h_w	[mm]	=	height of the web
t_w	[mm]	=	thickness of the web
f_{yf}	[N/mm ²]	=	yield strength of the flange
b_f	[mm]	=	width of the flange
t_f	[mm]	=	thickness of the flange
c	[mm]	=	$a \left(0.25 + \frac{1.6 b_f t_f^2 f_{yf}}{t_w h_{w,eff}^2 f_{yw}} \right)$
a	[mm]	=	length of the plate member
$M_{f,Rd}$	[Nmm]	=	the design plastic moment of resistance of the cross-section consisting of the effective area of the flanges only
γ_{M1}	[-]	=	partial factor for resistance to shear = 1

The shear buckling factor (χ_w) depends on the the modified slenderness ($\bar{\lambda}_w$), according to Table (7.1) from NEN-EN 1993-1-5 (2022). NEN-EN 1993-1-5 (2022) 7.3 (9) states that, for webs with longitudinal stiffeners, the modified slenderness should not be taken as less than:

$$\bar{\lambda}_w = \frac{h_{w,eff}}{37.4 t_w \epsilon \sqrt{k_\tau}} \quad (\text{XIV.7})$$

where: $\bar{\lambda}_w$	[-]	=	modified slenderness
ϵ	[-]	=	$\sqrt{\frac{235}{f_y}}$
k_τ	[-]	=	shear buckling coefficient

Subsequently, according to NEN-EN 1993-1-5 (2022) A.5 (1), the shear buckling coefficient k_τ - for plates with more than two longitudinal stiffeners and if $a \geq h_{w,eff}$ - should be obtained as follows:

$$k_\tau = 5.34 + 4.00 \left(\frac{h_{w,eff}}{a} \right)^2 + k_{\tau,sl} \quad (\text{XIV.8})$$

where:

$$k_{\tau,sl} = \max \left(9 \left(\frac{h_{w,eff}}{a} \right)^2 \left(\frac{\beta_{sl} I_{sl}}{h_{w,eff} t_w^3} \right)^{0.75} ; \frac{2.1}{t_w} \left(\frac{\beta_{sl} I_{sl}}{h_{w,eff}} \right)^{\frac{1}{3}} \right) \quad (\text{XIV.9})$$

in which: β_{sl}	[-]	=	equal to 1.0 for open-section longitudinal stiffeners
I_{sl}	[mm ⁴]	=	I_{xx}

Finally, Table XIV.4 presents - besides the relevant calculated parameters as established above - the unity check (UC), which is defined as follows:

$$UC = \left| \frac{V_{Ed}}{V_{el,Rd}} \right| \leq 1$$

$k_{\tau,sl}$	13.56	-
k_{τ}	18.92	-
λ_w	0.09	-
χ_w	1.2	-
$V_{el,Rd}$	288.97	kN
UC	0.93	-

Table XIV.4: Shear force verification

Bending and shear force skin plate

NEN-EN 1993-1-5 (2022) 9.1 (1) states that when the shear force is greater than half the shear force at yielding, its influence on the moment resistance may not be neglected.

$$\frac{V_{Ed}}{V_{Rd}} = 0.93$$

$$\not\leq 0.50$$

Hence, the combined effects of bending and shear should satisfy Equation (XIV.10) (according to NEN-EN 1993-1-5 (2022) Equation (9.1)).

$$UC = \frac{M_{Ed}}{M_{el,Rd}} + \left(1 - \frac{M_{f,Rk}}{M_{eff,Rk}} \right) \left(\frac{\frac{2V_{Ed}}{\chi_w f_{yw} h_{w,eff} t_w}}{\sqrt{3} \gamma_{M1}} - 1 \right)^{\mu} \leq 1 \quad (\text{XIV.10})$$

where:

$M_{f,Rk}$	[Nmm]	=	$M_{f,Rd} \gamma_{M0}$
$M_{eff,Rk}$	[Nmm]	=	$W_{eff} f_y$
$W_{eff,x}$	[mm ³]	=	the effective section modulus
μ	[-]	=	$\left(\frac{M_{f,Rk}}{M_{eff,Rk}} + 0.2 \right)^{15} + 1$

Finally, Table XIV.5 presents - besides the relevant calculated parameters as established above - the unity check (UC) for the outermost top fibre (x_t) and outermost bottom fibre (x_b) respectively.

	W_{eff} [mm ³]	$M_{eff,Rk}$ [Nmm]	μ [-]	UC [-]
x_t	591044	209820748	1.42	0.56
x_b	2940652	1043931494	1.00	0.87

Table XIV.5: Bending and shear force verification

B: Maximum negative head is dominant

As has been concluded after presentation of the pressures on the gate corresponding with load combination B in Figure XIV.4, it can be deduced that both load combinations A and H are governing over load combination B. Note that the strength of the vertical lift gate is the same irrespective of positive or negative head.

H: Ship collision

Note that the ship collision force (see Figure XIV.5), will not act directly on the skin plate under any circumstance. Hence, as the resultant of the hydrostatic pressures and wave pressure under load combination H are less than under load combination A, load combination H is not governing and the skin plate does not have to be verified for this load combination.

SLS: Quasi-permanent combinationDeflection skin plate

The maximum deflection of the gate and therefore the skin plate should satisfy Equation (XIV.11), as stated by Vrijburcht (2000).

$$w_{max,x} \leq \frac{1}{200} a = 10 \text{ mm} \quad (\text{XIV.11})$$

where: $w_{max,x}$ [mm] = maximum deflection of the skin plate in x-direction (lengthwise)
 a [mm] = distance between two vertical girders (nr.2)

Conservatively, $w_{max,x}$ is calculated using the general forget-me-not for a pinned-pinned beam under a distributed load according to Equation (XIV.12). It should be noted that the maximum pressure considering the quasi-permanent combination is used.

$$w_{max,x} = \frac{5}{384} \frac{p_{max} b_s a^4}{EI_{xx}} \quad (\text{XIV.12})$$

where: p_{max} [N/mm²] = maximum pressure on the skin plate = 0.088
 b_s [mm] = length between two longitudinal stiffeners
 E [N/mm²] = Youngs modulus
 I_{xx} [mm⁴] = mass moment of inertia of the equivalent plate member

This yields, $w_{max,x} = 0.74 \text{ mm} \leq 10 \text{ mm}$.

XIV.2.2 Vertical Girders: HEB240 (nr.2)

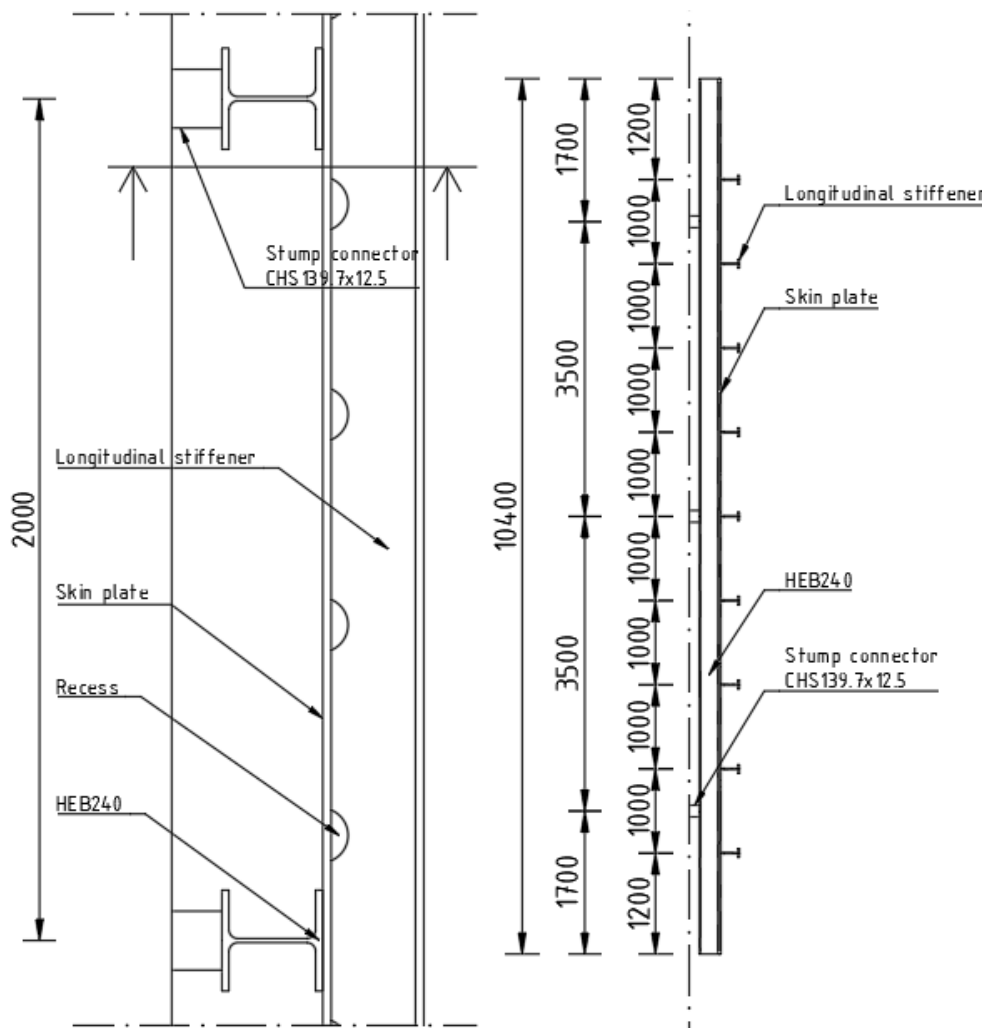


Figure XIV.9: Vertical girders: HEB240 (nr.2)

f_y [N/mm ²]	E [N/mm ²]	h [mm]	b [mm]	t_w [mm]	t_f [mm]	r [mm]
355	210000	240	240	10	17	21

Table XIV.6: HEB240 characteristics

- in which:
- f_y is the yield strength
 - E is the Youngs Modulus
 - h is the height of the profile
 - b is the width of the profile
 - t_w is the thickness of the web
 - t_f is the thickness of the flange
 - r is the rounding between the web and the flange

Cross-section classification

Table (5.2) from NEN-EN 1993-1-1 (2016) yields the maximum width to thickness ratios for components under compression per cross-section class. For H cross-sections Equation (XIV.13a) and Equation (XIV.13b) should hold (from NEN-EN 1993-1-1 (2016) Table (5.2)) for the web of the cross-section (under pure bending) and the flange of the cross-section to be classified as class 1.

$$\frac{c}{t} \leq 72 \sqrt{\frac{235}{f_y}} \quad (\text{XIV.13a})$$

$$\frac{c}{t} \leq 9 \sqrt{\frac{235}{f_y}} \quad (\text{XIV.13b})$$

Note that for the characteristics as presented in Table XIV.6, for the HEB240, both Equation (XIV.13a) and Equation (XIV.13b) are satisfied. Hence the HEB240 can be classified as a class 1 cross-section.

A: Maximum positive head is dominant

Bending moment HEB240

As stated by NEN-EN 1993-1-1 (2016) Equation (6.13), the moment resistance of a class 1 cross-section for bending around one of its major axes is calculated as follows:

$$M_{pl,Rd} = \frac{W_{pl} f_y}{\gamma_{M0}} \geq M_{Ed} \quad (\text{XIV.14})$$

where: $M_{pl,Rd}$ [Nmm] = plastic bending moment resistance of a cross-section
 W_{pl} [mm³] = plastic section modulus
 M_{Ed} [N] = design value of bending moment

The design value of the bending moment follows from the bending moment line in Figure XIV.10. The pressures on the skin plate (see Figure XIV.3) are transferred over a width of 2 m towards the HEB240 (see Figure 7.2).

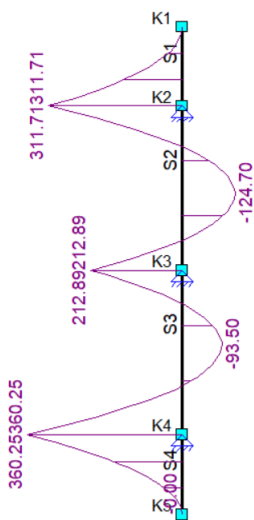


Figure XIV.10: Bending moment line HEB240 (in kNm)

Table XIV.7 presents the unity check (UC) regarding the bending moment verification defined as follows:

$$UC = \frac{M_{Ed}}{M_{pl,Rd}} \leq 1$$

M_{Ed} [kNm]	W_{pl} [mm ³]	$M_{pl,Rd}$ [kNm]	UC [-]
360.25	1053000	373.82	0.96

Table XIV.7: Bending moment verification

Shear force HEB240

Equation (XIV.15) follows from Equation (6.18) of NEN-EN 1993-1-1 (2016).

$$V_{pl,Rd} = \frac{A_v (f_y / \sqrt{3})}{\gamma_{M0}} \geq V_{Ed} \quad (\text{XIV.15})$$

where: $V_{pl,Rd}$ [N] = plastic shear resistance of a cross-section
 A_v [mm²] = shear surface
 V_{Ed} [N] = design value of shear force

The design value of the shear force follows from the shear force line in Figure XIV.11. The pressures on the skin plate (see Figure XIV.3) are transferred over a width of 2 m towards the HEB240 (see Figure 7.2).

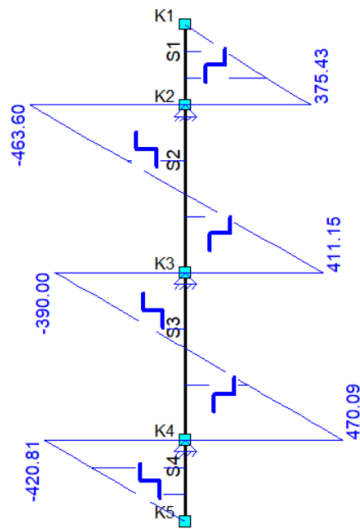


Table XIV.8 presents the unity check (UC) regarding the bending moment verification defined as follows:

$$UC = \frac{V_{Ed}}{V_{pl,Rd}} \leq 1$$

V_{Ed} [kN]	A_v [mm ²]	$V_{pl,Rd}$ [kN]	UC [-]
470.09	8160	1672.47	0.28

Table XIV.8: Shear force verification

Figure XIV.11: Shear force line HEB240 (in kN)

Bending and shear force HEB240

NEN-EN 1993-1-5 (2022) 9.1 (1) states that when the shear force is less than half the shear force at yielding, its influence on the moment resistance may be neglected.

$$\frac{V_{Ed}}{V_{Rd}} = 0.28 < 0.50$$

Hence, as the posed condition is satisfied, the influence of the shear force on the bending moment resistance may be neglected.

Welds HEB240 - skin plate

Note that, as the HEB240 is welded to the skin plate with welds along both flanges, there is no difference in stiffness over the length of the weld of the connected parts. For this reason the redistribution of loads over the length of the weld is ensured.

As for the verification of the welded connection, the self weight of the components are not taken into account as their resulting force is orders less than the resulting water and wave forces. The normal stress perpendicular to the throat section (a) and shear stress perpendicular to the axis of the weld can be calculated using Equation (XIV.16).

$$\sigma_{\perp} = \tau_{\perp} = \frac{1}{4} \sqrt{2} \frac{p_{max} \cdot 2 \cdot l_{eff}}{a l_{eff}} \tag{XIV.16}$$

Here, the stresses are calculated at the point of maximum pressure per metre length ($l_{eff} = 1$ m). Furthermore, the maximum pressure works over a width equal to the centre to centre of the HEB240 profiles (= 2 m). The HEB240 is welded continuously to the skin plate over the entire height of the gate.

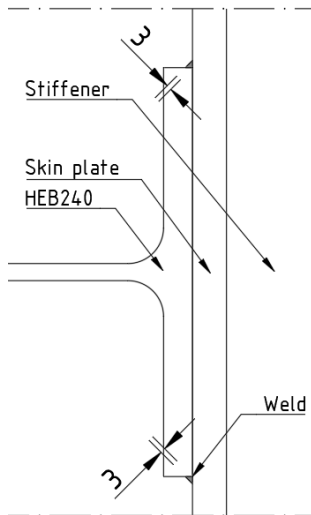


Figure XIV.12: Welded connection HEB240 - skin plate

For the verification of the welded connection, the directional method (combined stress method) is used as described in NEN-EN 1993-1-8 (2021) 6.5.3.2. Table XIV.9 presents the unity checks (UC) regarding the verification of the welded connection, defined as follows:

$$UC_1 = \frac{\sqrt{\sigma_{\perp}^2 + 3(\tau_{\perp}^2 + \tau_{\parallel}^2)} \beta_w \cdot \gamma_{M2}}{f_u} \leq 1$$

$$UC_2 = \frac{\sigma_{\perp} \cdot \gamma_{M2}}{0.9f_u} \leq 1$$

p_{max}	134.20	kN/M ²
σ_{\perp}	31.63	N/mm ²
τ_{\perp}	31.63	N/mm ²
f_u	490	N/mm ²
β_w	0.90	-
UC_1	0.15	-
UC_2	0.09	-

Table XIV.9: Verification welded connection

B: Maximum negative head is dominant

As has been concluded after presentation of the pressures on the gate corresponding with load combination B in Figure XIV.4, it can be deduced that both load combinations A and H are governing over load combination B. Note that the strength of the vertical lift gate is the same irrespective of positive or negative head.

H: Ship collision

As the ship collision force will not act directly on the skin plate under any circumstance, no ship collision forces will ever be transferred to the HEB240. For this reason, as the water and wave pressures under load combination H are less than under load combination A, load combination H is not governing and the HEB240 does not have to be verified for this combination.

SLS: Quasi-permanent combination

Deflection HEB240

The maximum deflection of the gate and hence the HEB240 vertical girders should satisfy Equation (XIV.18), as stated by Vrijburcht (2000).

$$w_{max,x} \leq \frac{1}{200} H = 53.5 \text{ mm} \quad (\text{XIV.18})$$

where: $w_{max,x}$ [mm] = maximum deflection of the HEB240 in x-direction (lengthwise)
 H [mm] = height of a HEB240 member (nr.2)

$w_{max,x}$ is calculated using Matrixframe. It should be noted that the maximum pressure considering the quasi-permanent combination is used.

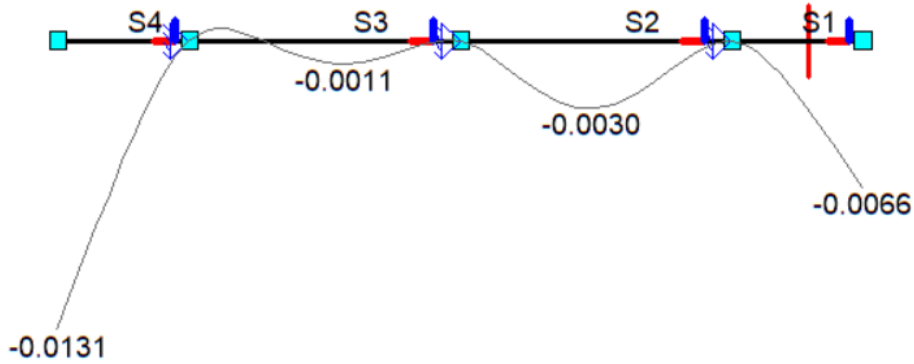


Figure XIV.13: Deflection of the HEB240 [m] (left = bottom)

From Figure XIV.13, it follows that $w_{max,x} = 13.1$ mm.

XIV.2.3 Stump Connectors (nr.3)

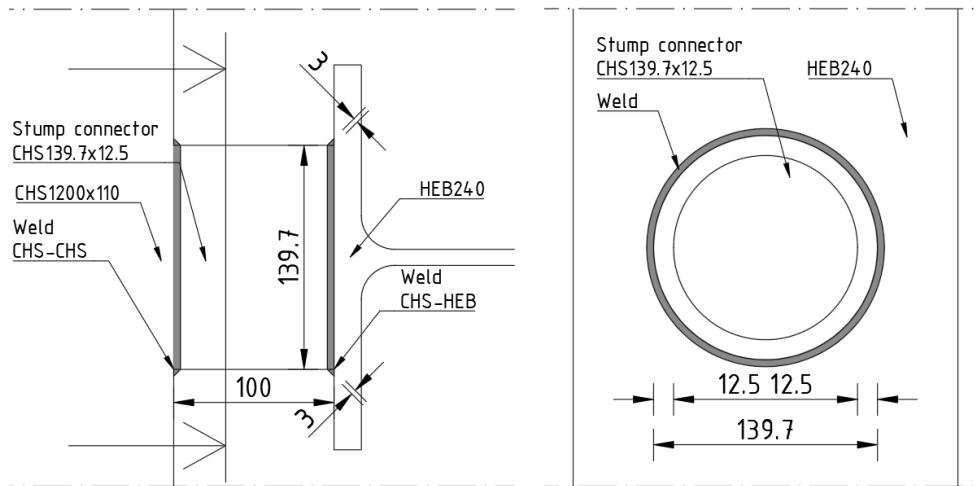


Figure XIV.14: Stump connector (nr.3)

f_y [N/mm ²]	E [N/mm ²]	d [mm]	t [mm]	L [mm]
355	210000	139.7	12.5	100

Table XIV.10: CHS 139.7x12.5 characteristics

- in which:
- f_y is the yield strength
 - E is the Youngs Modulus
 - d is the diameter of the CHS profile
 - t is the thickness of the CHS profile
 - L is the length

Cross-section classification

Table (5.2) from NEN-EN 1993-1-1 (2016) yields the maximum width to thickness ratios for components under compression per cross-section class. For tubular cross-sections Equation (XIV.19) should hold (from NEN-EN 1993-1-1 (2016) Table (5.2)) for the cross-section to be classified as class 1.

$$\frac{d}{t} \leq 50 \frac{235}{f_y} \tag{XIV.19}$$

Note that for the characteristics as presented in Table XIV.10, for the CHS 139.7x12.5, Equation (XIV.19) is satisfied. Hence the CHS 139.7x12.5 can be classified as a class 1 cross-section.

A: Maximum positive head is dominant

Here, only loads derived from the water and wave pressures are taken into account, as the resulting force from the self weight of the gate on the stump connectors are orders less. For this reason, only a normal force is present on the cross-section.

Normal force stump connectors

According to NEN-EN 1993-1-1 (2016) Equation (6.10), the design resistance of a cross section under uniform axial pressure (i.e. normal force) of a class 1 (and 2 and 3) cross-section is calculated as follows:

$$N_{pl,Rd} = \frac{A f_y}{\gamma_{M0}} \geq N_{Ed} \quad (\text{XIV.20})$$

where: $N_{pl,Rd}$ [Nmm] = plastic normal force resistance of a cross-section
 A [mm²] = area of the cross-section
 f_y [N/mm²] = yield strength
 γ_{M0} [-] = partial factor for resistance of cross-sections = 1
 N_{Ed} [N] = design value of normal force

The normal force on the stump connectors follow from the water and wave pressures on the skin plate and can be calculated directly from the shear force line of the HEB240 (see Figure XIV.11).

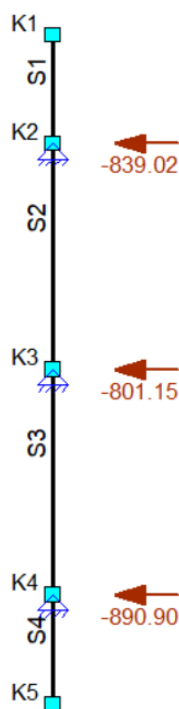


Figure XIV.15: Normal forces in the stump connectors

Table XIV.11 presents the unity check (UC) regarding the normal force verification defined as follows:

$$UC = \frac{N_{Ed}}{N_{pl,Rd}} \leq 1$$

N_{Ed} [kN]	A [mm ²]	$N_{pl,Rd}$ [kN]	UC [-]
890.90	4995	1773.27	0.50

Table XIV.11: Normal force verification

Weld CHS-HEB

As can be seen from Figure XIV.14, the CHS 139.7x12.5 is welded all around the circular hollow section to the HEB240. Table (7.20) from NEN-EN 1993-1-8 (2021) states that if $d/t \leq 50$ one only has to take the following failure mechanisms into account for a T-connection of a CHS to a H profile:

$$N_{1,Rd} = \frac{\pi}{4} \frac{f_y t_w (d + 5(t_f + r))}{\gamma_{M5}} \quad (\text{XIV.21a})$$

$$N_{1,Rd} = \frac{\pi}{4} \frac{2f_y t (t_w + 2r + 7t_f)}{\gamma_{M5}} \quad (\text{XIV.21b})$$

where: $N_{1,Rd}$ [N] = resistance of the connection to a normal force
 f_y [N/mm²] = yield strength
 t_w [mm] = thickness of the web of the HEB
 t_f [mm] = thickness of the flange of the HEB
 r [mm] = radius of the rounding of the HEB
 d [mm] = diameter of the CHS
 t [mm] = thickness of the CHS
 γ_{M5} [-] = partial factor for resistance of connections in trusses of tubular profiles = 1

The governing resistance of the connection is given by the lowest value of Equation (XIV.21a) or Equation (XIV.21b) representing failure of the HEB and the CHS profiles respectively. Finally, Table XIV.12 presents the unity check (UC) regarding the verification of the welded connection defined as follows:

$$UC = \frac{N_{Ed}}{N_{1,Rd}} \leq 1$$

$N_{1,Rd}$ [kN]	UC [-]
919.26	0.97

Table XIV.12: Welded connection verification

Do note that the failure mechanisms as presented above are irrespective of the throat section of the weld, hence the minimum $a = 3$ mm is applied.

Weld CHS-CHS

The stump connector (CHS 139.7x12.5) is welded to the horizontal CHS 1200x110. For CHS-CHS welded connections, Table (9.6) of NEN-EN 1993-1-8 (2021) gives the governing failure mechanisms to consider for T joints. Said failure mechanism are chord (face) failure and chord punching shear failure, represented by Equation (XIV.22a) and Equation (XIV.22b) respectively.

$$N_{1,Rd} = C_f \frac{f_{y0} t_0^2}{\sin \theta} (2.6 + 17.7\beta^2) \gamma^{0.2} Q_f / \gamma_{M5} \geq N_{Ed} \quad (\text{XIV.22a})$$

$$N_{2,Rd} = C_f \frac{f_{y0}}{\sqrt{3}} \pi d t_0 \frac{1 + \sin \theta_2}{2 \sin^2 \theta} / \gamma_{M5} \geq N_{Ed} \quad (\text{XIV.22b})$$

in which

$$Q_f = \left(1 - \left| \frac{N_{0,Ed}}{A_0 f_{y0}} \right| \right)^{C1} \geq 0.4$$

where:	$N_{1,Rd}$	[N]	=	design axial resistance of chord face
	$N_{2,Rd}$	[N]	=	design axial resistance for chord punching shear
	$N_{0,Ed}$	[N]	=	axial force on the chord member
	C_f	[-]	=	material factor = 0.9
	f_{y0}	[N/mm ²]	=	yield strength of a chord member
	t_0	[mm]	=	wall thickness of chord member
	A_0	[mm ²]	=	area of the chord member
	θ	[°]	=	included angle between brace member and the chord = 90
	β	[-]	=	minimum ratio of the diameter and the thickness of the brace or chord ≤ 50
	γ	[-]	=	ratio of the chord diameter to twice its wall thickness
	Q_f	[-]	=	chord stress factor
	γ_{M5}	[-]	=	partial factor for resistance of joints in hollow section lattice girders = 1
	N_{Ed}	[N]	=	design value of axial force
	d	[mm]	=	chord diameter
	C_1	[-]	=	0.20 for tension

One should note that NEN-EN 1993-1-8 (2021) 9.4.1(3) states that for $\beta > 1$, all failure modes listed in 9.2.2(1) should be considered:

- Chord (face) failure
- Chord side wall failure
- Chord shear failure
- Punching shear failure
- Brace failure
- Local buckling failure
- Brace shear failure

Although the criterion as stated above is not satisfied for the characteristics of the welded connection, only failure modes a and d are considered. The governing resistance of the CHS-CHS connection is given by the lowest value of Equation (XIV.22a) or Equation (XIV.22b). Finally, Table XIV.13 presents the unity check (UC) regarding the verification of the welded connection defined as follows:

$$UC = \frac{N_{Ed}}{\min(N_{1,Rd}; N_{2,Rd})} \leq 1$$

β	γ	Q_f	$N_{1,Rd}$ [kN]	$N_{2,Rd}$ [kN]	UC [-]
11.18	6.00	0.87	8801018	8096	0.11

Table XIV.13: Welded connection verification

Do note that the failure mechanisms as presented above are irrespective of the throat section of the weld, hence the minimum $a = 3$ mm is applied.

Buckling stump connectors

Buckling stability for a CHS under compression, classified as a cross-section class 1, should be verified according to Equation (XIV.23) as per NEN-EN 1993-1-1 (2016) 6.3.1.1.

$$N_{b,Rd} = \frac{\chi A f_y}{\gamma_{M1}} \geq N_{Ed} \quad (\text{XIV.23})$$

where:	$N_{b,Rd}$	[N]	=	resistance to buckling
	χ	[-]	=	reduction factor for the appropriate buckling shape
	A	[mm ²]	=	cross-sectional area of the rod
	f_y	[N/mm ²]	=	yield strength of the rod
	γ_{M1}	[-]	=	partial factor for resistance of members to instability = 1
	N_{Ed}	[N]	=	design value of compression force

It should be noted that Equation (XIV.23) for the resistance to buckling only differs a factor χ with Equation (XIV.20) for the plastic normal force resistance. This reduction factor can be calculated by means of the following procedure:

$$N_{cr} = \frac{\pi^2 EI_{xx}}{l_{bk}^2} \quad (\text{XIV.24a})$$

$$\bar{\lambda} = \frac{Af_y}{N_{cr}} \quad (\text{XIV.24b})$$

$$\Phi = 0.5(1 + \alpha(\bar{\lambda} - 0.2) + \bar{\lambda}^2) \quad (\text{XIV.24c})$$

$$\chi = \frac{1}{\Phi + \sqrt{\Phi^2 - \lambda^2}} \leq 1 \quad (\text{XIV.24d})$$

where:	N_{cr}	[N]	=	resistance to buckling
	E	[-]	=	Youngs modulus
	I_{xx}	[mm ⁴]	=	mass moment of inertia
	l_{bk}	[mm ²]	=	buckling length = L
	$\bar{\lambda}$	[-]	=	the relative slenderness
	α	[-]	=	imperfection factor for appropriate buckling shape = 0.21

Evaluation of the equation above yields Table XIV.14, which subsequently presents the unity check (UC) regarding the verification to buckling defined as follows:

$$UC = \frac{N_{Ed}}{N_{b,Rd}} \leq 1$$

N_{cr} [kN]	$\bar{\lambda}$ [-]	Φ [-]	χ [-]	$N_{1,Rd}$ [kN]	UC [-]
2114093	0.03	0.48	1	1773.27	0.50

Table XIV.14: Buckling verification

B: Maximum negative head is dominant

As has been concluded after presentation of the pressures on the gate corresponding with load combination B in Figure XIV.4, it can be deduced that both load combinations A and H are governing over load combination B. Note that the strength of the vertical lift gate is the same irrespective of positive or negative head.

H: Ship collision

As the ship collision force will not act directly on the skin plate under any circumstance, no ship collision forces will ever be transferred to the CHS 139.5x12.5 stump connectors. For this reason, as the water and wave pressures under load combination H are less than under load combination A, load combination H is not governing and the HEB240 does not have to be verified for this combination.

XIV.2.4 Truss System

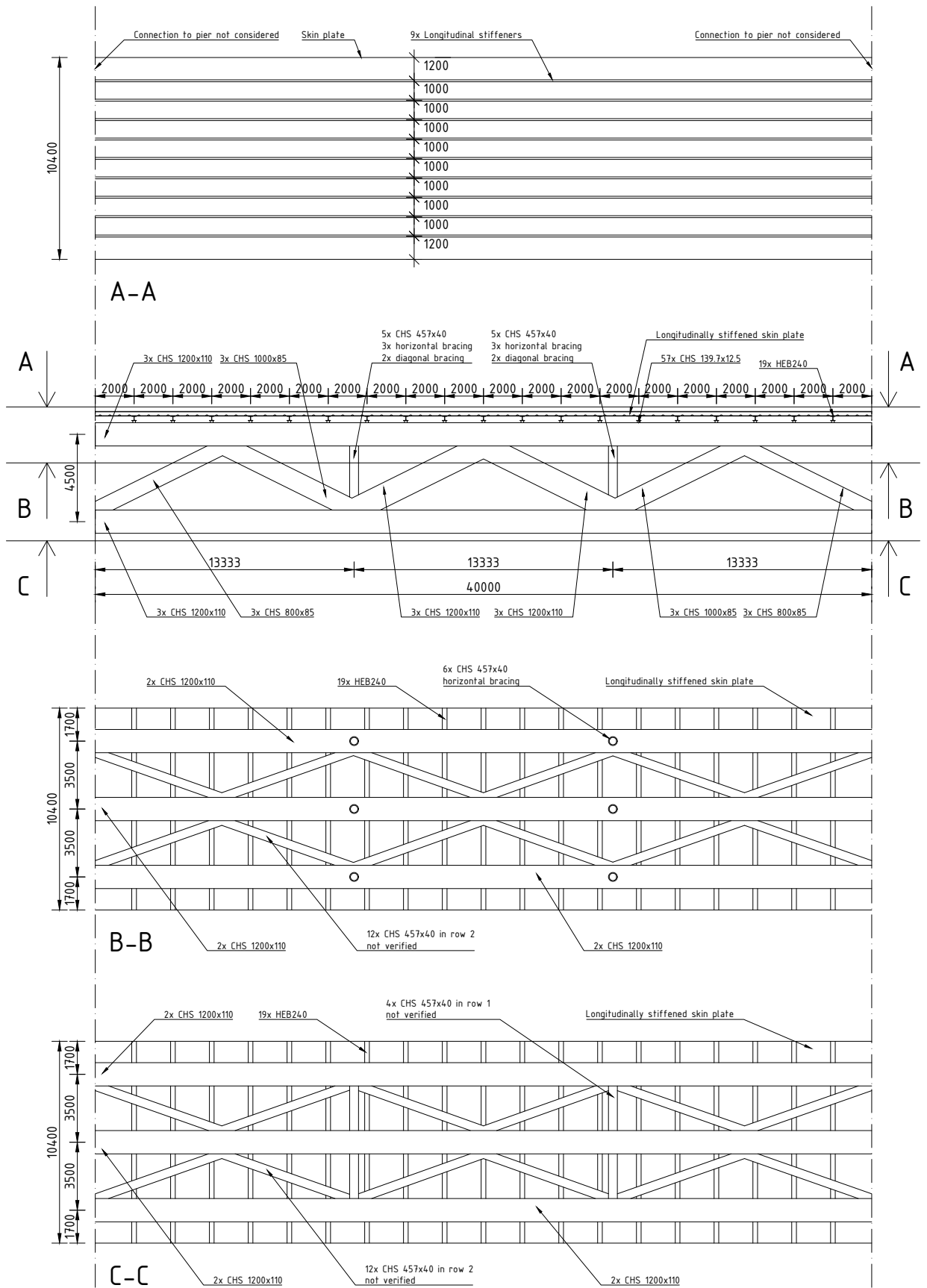


Figure XIV.16: Truss system

Cross-section classification

For tubular cross-sections, again, Equation (XIV.19) should be satisfied for a cross-section to be classified as class 1.

Normal force truss system

The design resistance of a cross section under uniform axial pressure (i.e. normal force) of a class 1 cross-section is calculated as follows:

$$N_{pl,Rd} = \frac{A f_y}{\gamma_{M0}} \geq N_{Ed}$$

Bending moment truss system

The moment resistance of a class 1 cross-section is calculated as follows:

$$M_{pl,Rd} = \frac{W_{pl} f_y}{\gamma_{M0}} \geq M_{Ed}$$

Shear force truss system

The shear force resistance of a class 1 cross-section is calculated as follows:

$$V_{pl,Rd} = \frac{A_v (f_y / \sqrt{3})}{\gamma_{M0}} \geq V_{Ed}$$

Bending, shear and normal force truss system

According to NEN-EN 1993-1-1 (2016) 6.2.10 (1), when both a shear force (if $V_{Ed} < 0.5 V_{pl,Rd}$) and a normal force is present, the influence of both the shear force and the normal force on the moment resistance should be taken into account.

$$f_{y,red} = \left(1 - \left(\frac{2V_{Ed}}{V_{pl,Rd}} - 1 \right)^2 \right) f_y$$

$$M_{N,Rd} = M_{pl,Rd} \left(1 - \left(\frac{N_{Ed}}{N_{pl,Rd}} \right)^2 \right)$$

The unity check is defined as follows:

$$UC = \frac{M_{Ed}}{M_{N,Rd}}$$

Finally, Table XIV.15 presents all required characteristics for every profile used.

Profile	Class	f_y [N/mm ²]	A [mm ²]	W_{pl} [mm ³]	A_v [mm ²]	$N_{pl,Rd}$ [kN]	$V_{pl,Rd}$ [kN]	$M_{pl,Rd}$ [kNm]
CHS 1200x110	1	355	376677	131134667	239800	133720	49149	46553
CHS 1000x85	1	355	244337	71368833	155550	86740	31881	25336
CHS 800x85	1	355	190930	43658833	121550	67780	24913	15499
CHS 457x40	1	355	52402	6976893	33360	18603	6837	2476

Table XIV.15: Truss system profiles characteristics

A: Maximum positive head is dominant

The axial loads from the stump connectors (CHS 139.7x12.5) are transferred to the horizontal CHS frame as depicted in Figure XIV.17. Again, as the resulting load from the self weight of the gate is orders less than the water and wave loads, no significant vertical loads are acting on the structure.

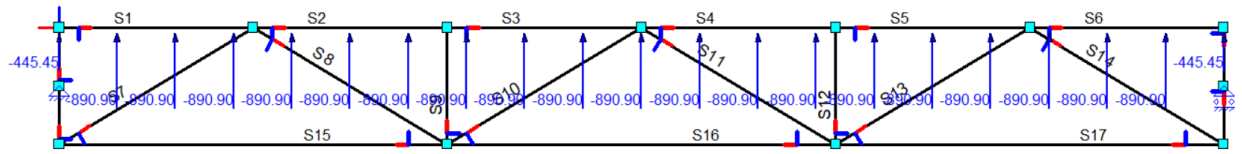


Figure XIV.17: Loads [kN] on the Truss system

Figure XIV.17 results in the normal force, shear force and bending moment line respectively as presented in Figure XIV.18.

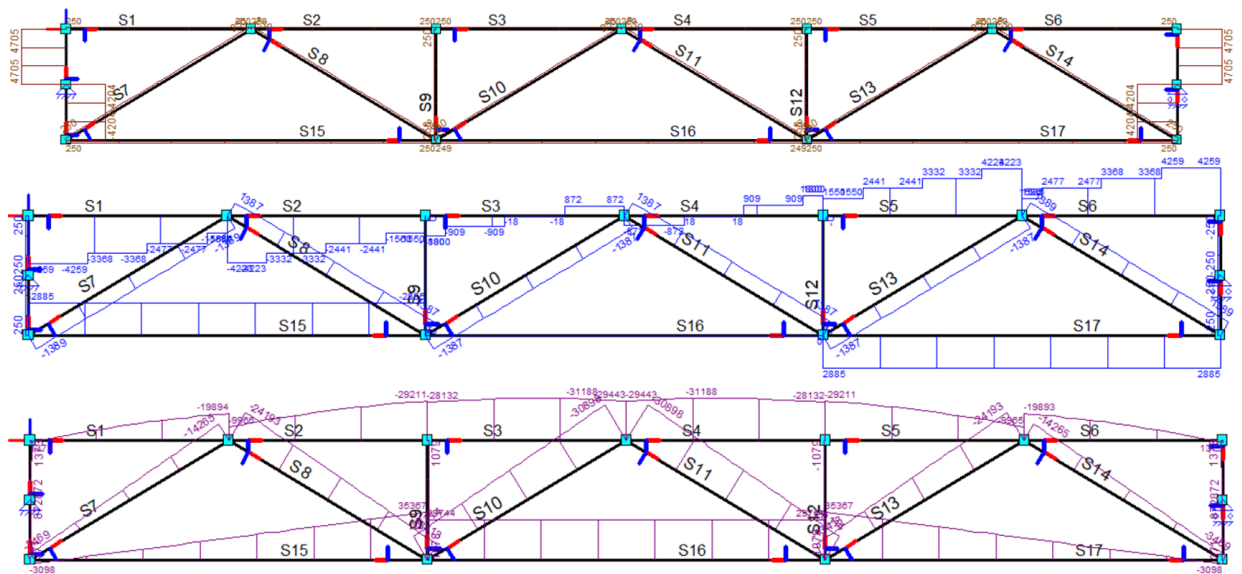


Figure XIV.18: Normal force [kN], shear force [kN] and bending moment [kNm] lines

With Figure XIV.18 the truss system is verified regarding the normal force, shear force and bending moment resistance. It should be noted that the location where the maximum bending moment and maximum shear force occur do not have to coincide for every element. Table XIV.16 presents the unity checks (UC) for the governing combination of normal force, shear force and bending moment in the cross-section for every identified element of the truss system.

Element	Profile	N_{Ed} [kN]	V_{Ed} [kN]	M_{Ed} [kNm]	$M_{N,Rd}$ [kNm]	UC [-]
S1	CHS 1200x110	250	1586	19894	46553	0.43
S2	CHS 1200x110	250	1550	29211	46553	0.63
S3	CHS 1200x110	250	872	31188	46553	0.67
S4	CHS 1200x110	250	872	31188	46553	0.67
S5	CHS 1200x110	250	1550	29211	46553	0.63
S6	CHS 1200x110	250	1586	19893	46553	0.43
S7	CHS 800x85	250	1389	14265	15499	0.92
S8	CHS 1000x85	250	1387	24193	25336	0.95
S9	CHS 457x40	250	0	1078	2476	0.44
S10	CHS 1200x110	250	1387	30898	46553	0.66
S11	CHS 1200x110	250	1387	30898	46553	0.66
S12	CHS 457x40	250	0	1079	2476	0.44
S13	CHS 1000x85	250	1387	24193	25336	0.95
S14	CHS 800x85	250	1389	14265	15499	0.92
S15	CHS 1200x110	250	2885	35367	46553	0.76
S16	CHS 1200x110	250	0	29744	46553	0.64
S17	CHS 1200x110	250	2885	35367	46553	0.76

Table XIV.16: Truss system verification load combination A

B: Maximum negative head is dominant

As has been concluded after presentation of the pressures on the gate corresponding with load combination B in Figure XIV.4, it can be deduced that both load combinations A and H are governing over load combination B. Note that the strength of the vertical lift gate is the same irrespective of positive or negative head.

H: Ship collision

The axial loads from the stump connectors (CHS 139.7x12.5) are again transferred to the truss system. Besides the water and wave loads transferred by the stump connectors, the ship collision load as determined in Appendix XIV.1 for the fishing trawler OD1 Maarten-Jacob is introduced at the most governing position (i.e. in the middle of the gate). Again, any vertical load is neglected. Figure XIV.19 presents all said forces on the truss system.

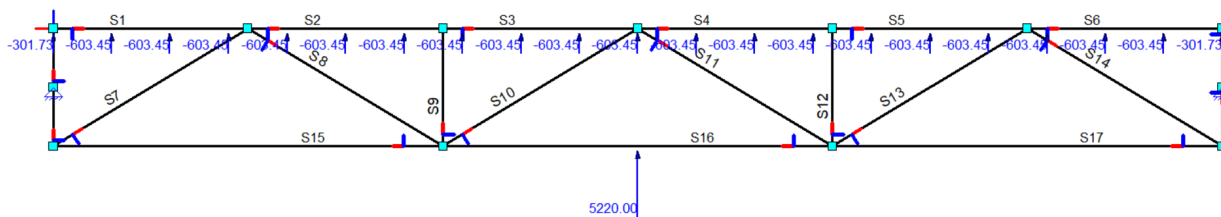


Figure XIV.19: Loads [kN] on the Truss system

Figure XIV.19 results in the normal force, shear force and bending moment line respectively as presented in Figure XIV.20.

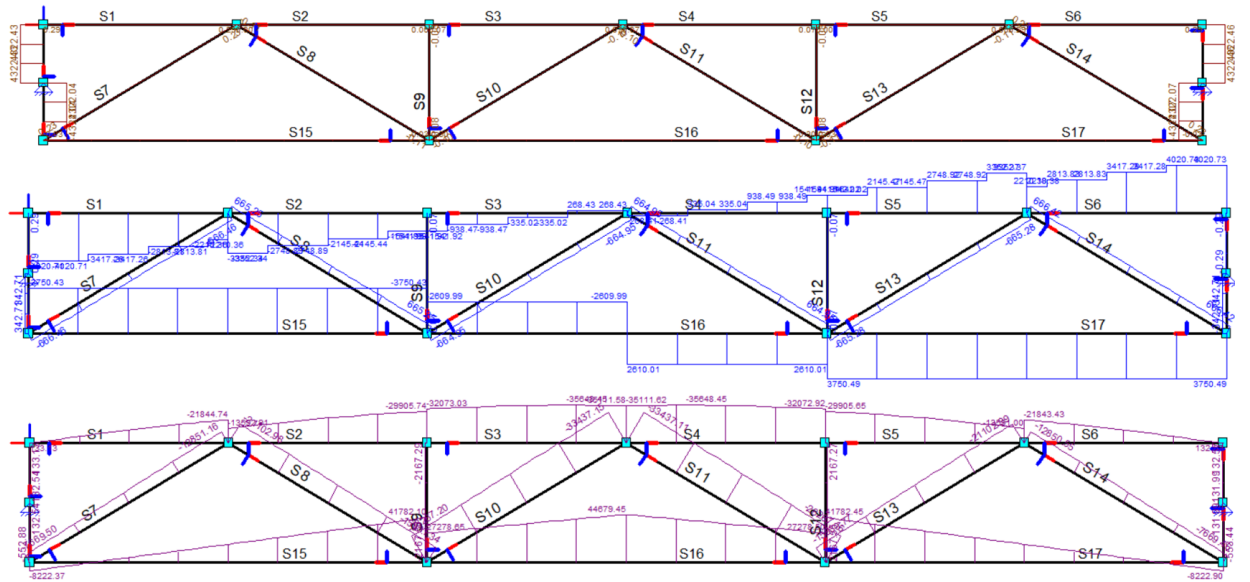


Figure XIV.20: Normal force [kN], shear force [kN] and bending moment [kNm] lines

With Figure XIV.20 the truss system is verified regarding the normal force, shear force and bending moment resistance. It should be noted that the location where the maximum bending moment and maximum shear force occur do not have to coincide for every element. Table XIV.17 presents the unity checks (*UC*) for the governing combination of normal force, shear force and bending moment in the cross-section for every identified element of the truss system.

Element	Profile	N_{Ed} [kN]	V_{Ed} [kN]	M_{Ed} [kNm]	$M_{N,Rd}$ [kNm]	<i>UC</i> [-]
S1	CHS 1200x110	0	2210	21845	46553	0.47
S2	CHS 1200x110	0	1542	29906	46553	0.64
S3	CHS 1200x110	0	335	35648	46553	0.77
S4	CHS 1200x110	0	335	35648	46553	0.77
S5	CHS 1200x110	0	1542	29906	46553	0.64
S6	CHS 1200x110	0	2210	21845	46553	0.47
S7	CHS 800x85	0	666	12851	15499	0.83
S8	CHS 1000x85	0	666	21103	25336	0.83
S9	CHS 457x40	0	0	2167	2476	0.88
S10	CHS 1200x110	0	666	33437	46553	0.72
S11	CHS 1200x110	0	666	33437	46553	0.72
S12	CHS 457x40	0	0	2167	2476	0.88
S13	CHS 1000x85	0	666	21103	25336	0.83
S14	CHS 800x85	0	666	12851	15499	0.83
S15	CHS 1200x110	0	3750	41782	46553	0.90
S16	CHS 1200x110	0	2610	44679	46553	0.96
S17	CHS 1200x110	0	3750	41782	46553	0.90

Table XIV.17: Truss system verification load combination H

SLS: Quasi-permanent combination

Deflection truss system

The maximum deflection of the gate should again satisfy Equation (XIV.25), as stated by Vrijburcht (2000).

$$w_{max,x} \leq \frac{1}{200} L_i \tag{XIV.25}$$

where: $w_{max,x}$ [mm] = maximum deflection of the gate in x-direction (lengthwise)
 L_i [mm] = length of the respective element

$w_{max,x}$ is calculated using Matrixframe. It should be noted that the maximum pressure considering the quasi-permanent combination is used.

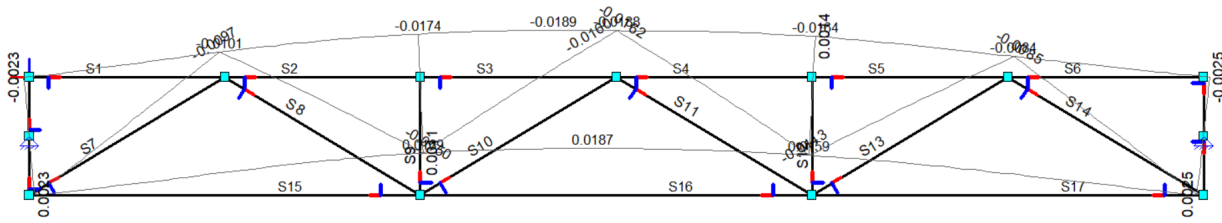


Figure XIV.21: Deflection of the truss system [m]

Note that Equation (XIV.25) is satisfied for every element in Figure XIV.21.

XIV.3 Natural Frequencies and Resonance

Regarding a single gate as a simply supported Bernoulli beam under general forcing, the equation of motion (EoM) is formulated as follows:

$$\frac{m}{L} \frac{\delta^2 w(x,t)}{\delta t^2} + EI \frac{\delta^4 w(x,t)}{\delta x^4} + c_d \frac{\delta w(x,t)}{\delta t} + k_d w(x,t) = q(t) \tag{XIV.26}$$

in which: $w(x,t)$ [mm] = deflection of the gate as a function of space and time
 m [kg] = total mass of the gate (including added water mass)
 L [mm] = length of the gate
 E [N/mm²] = Young's modulus
 I [mm⁴] = mass moment of inertia of the gate
 c_d [N/mm²] = dynamic damping coefficient
 k_d [N/mm²] = dynamic stiffness coefficient
 $q(t)$ [N/mm] = distributed load on the gate as a function of time

with initial conditions:

$$\phi = w(x, t = 0) = 0$$

$$\Psi = \frac{\delta w(x, t = 0)}{\delta t} = 0$$

and boundary conditions:

$$w(0, t) = \frac{\delta^2 w(0, t)}{\delta x^2} = 0$$

$$w(L, t) = \frac{\delta^2 w(L, t)}{\delta x^2} = 0$$

As for the distributed load in time, let us consider a hydrostatic load and a dynamic wave load:

$$q_t = \begin{cases} q_h + q_w \left(\frac{1}{2} \sin \left(-\frac{\pi}{2} + \Omega t \right) + \frac{1}{2} \right), & 0 < t \leq t_1 \\ 0, & t > t_1 \end{cases}$$

in which: q_h [N/mm] = hydrostatic load
 q_w [N/mm] = amplitude of the dynamic wave load
 Ω [rad/s] = excitation frequency of the dynamic wave load

The natural frequencies of the system are solved by considering an eigenvalue problem. The eigenvalue problem is based on the homogeneous equation of motion. Assuming a solution of the form (using separation of variables):

$$w(x, t) = \widetilde{W}(x) \widetilde{\Psi}(t) \quad (\text{XIV.27})$$

Substitution of Equation (XIV.27) into the homogeneous equation of motion yields:

$$\begin{aligned} \widetilde{W}(x) \frac{d^2 \widetilde{\Psi}(t)}{dt^2} + \frac{EIL}{m} \widetilde{\Psi}(t) \frac{d^4 \widetilde{W}(x)}{dx^4} + 2nd \widetilde{W}(x) \frac{d \widetilde{\Psi}(t)}{dt} + \frac{kdL}{m} \widetilde{W}(x) \widetilde{\Psi}(t) &= 0 \\ \frac{1}{\widetilde{\Psi}(t)} \frac{d^2 \widetilde{\Psi}(t)}{dt^2} + \frac{EIL}{m} \frac{1}{\widetilde{W}(x)} \frac{d^4 \widetilde{W}(x)}{dx^4} + 2nd \frac{1}{\widetilde{\Psi}(t)} \frac{d \widetilde{\Psi}(t)}{dt} + \frac{kdL}{m} &= 0 \end{aligned}$$

The only way to satisfy the equation above is to set:

$$\frac{1}{\widetilde{\Psi}(t)} \frac{d^2 \widetilde{\Psi}(t)}{dt^2} + 2nd \frac{1}{\widetilde{\Psi}(t)} \frac{d \widetilde{\Psi}(t)}{dt} = -\frac{EIL}{m} \frac{1}{\widetilde{W}(x)} \frac{d^4 \widetilde{W}(x)}{dx^4} - \frac{kdL}{m} = \omega^2$$

For the coordinate related part, this yields:

$$\frac{d^4 \widetilde{W}(x)}{dx^4} + \beta^4 \widetilde{W}(x) = 0 \quad (\text{XIV.28})$$

in which: $\beta^4 = \frac{\bar{k} + \omega^2}{c^2}$
 $\bar{k} = \frac{k_d L}{m}$
 $c^2 = \frac{EIL}{m}$

The general solution for $\widetilde{W}(x)$ in Equation (XIV.28):

$$\widetilde{W}(x) = C_1 \sin(\beta x) + C_2 \cos(\beta x) + C_3 \sinh(\beta x) + C_4 \cosh(\beta x) \quad (\text{XIV.29})$$

With the boundary conditions for a simply supported beam:

$$w(0, t) = \widetilde{W}(0) \widetilde{\Psi}(t) = 0 \quad \Rightarrow \widetilde{W}(0) = 0$$

$$\begin{aligned} \frac{\delta^2 w(0, t)}{\delta x^2} &= \frac{d^2 \widetilde{W}(0)}{dx^2} \widetilde{\Psi}(t) = 0 & \Rightarrow \frac{d^2 \widetilde{W}(0)}{dx^2} &= 0 \\ w(L, t) &= \widetilde{W}(L) \widetilde{\Psi}(t) = 0 & \Rightarrow \widetilde{W}(L) &= 0 \\ \frac{\delta^2 w(L, t)}{\delta x^2} &= \frac{d^2 \widetilde{W}(L)}{dx^2} \widetilde{\Psi}(t) = 0 & \Rightarrow \frac{d^2 \widetilde{W}(L)}{dx^2} &= 0 \end{aligned}$$

Substituting the general solution, Equation (XIV.29), into these boundary conditions, and imposing the non-triviality condition that the coefficients $C_1 - C_4$ may not vanish simultaneously, we obtain the frequency equation Equation (XIV.30).

$$\sin \beta L = 0 \quad \Leftrightarrow \quad \beta_n L = n\pi, \quad n = 1, 2, 3, \dots \quad (\text{XIV.30})$$

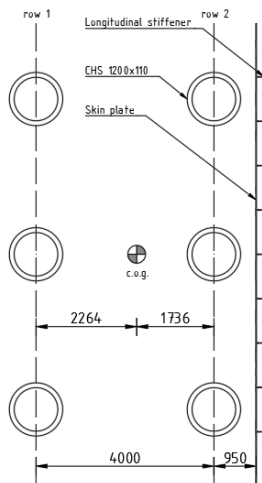
The frequency equation, Equation (XIV.30), determines the eigenvalues of the beam vibrations, which can be found as:

$$\omega_n = \sqrt{\frac{k_d L}{m} + \frac{n^4 \pi^4 EI}{mL^3}} \quad (\text{XIV.31})$$

Assuming no dynamic stiffness finally yields:

$$\omega_n = \sqrt{\frac{n^4 \pi^4 EI}{mL^3}} \quad (\text{XIV.32})$$

The total mass moment of inertia of the gate is determined using Steiner's Theorem (Equation (XIV.33)).



As for determining the total mass moment of inertia, only the elements depicted in Figure XIV.22 are taken into account. It should be noted that all elements and bracings besides the elements in Figure XIV.22 also contribute to the total mass moment of inertia. Lastly, also the stiff connections of the gate to the piers are not considered.

$$I_{xx,tot} = I_{xx} + A_i e_i^2 \quad (\text{XIV.33})$$

Figure XIV.22: Cross-section to determine total mass moment of inertia

The mass of the gate is the sum of both the self weight of the gate (m_G) and the added water mass (m_w). The added water mass for a closed gate per mode of vibration is estimated using the Orson Tieleman method (assuming no effect of surface waves or fluid compressibility):

$$p_f(y = 0, z) = -\Omega^2 \hat{w} \cdot \left(p_f \sum_{p=1}^{\infty} -1^{(p-1)} \frac{20h^2}{18(2p-1)^2 \pi^2} \cos \left(\frac{(2p-1)\pi}{2h} \right) \right) \quad (\text{XIV.34})$$

The added water mass depends both on the mode of vibration and the water head over the gate. Table XIV.18 presents the estimated added water mass for the first three modes of vibration under load combination A ($\Delta h = 8.97$ m) and under quasi-permanent combination ($\Delta h = 6.01$ m).

Δh [m]	$m_{w,1}$ [kg]	$m_{w,2}$ [kg]	$m_{w,3}$ [kg]
8.97	1141418	1992442	2485568
6.01	507512	945902	1269172

Table XIV.18: Estimated added water mass by Orson Tieleman

For the two conditions stated above, Table XIV.19 yields the first three eigenvalues of the gate:

Δh [m]	ω_1 [rad/s]	ω_2 [rad/s]	ω_3 [rad/s]
8.97	1.26	4.29	8.97
6.01	1.48	5.27	11.02

Table XIV.19: First three eigenvalues of the gate

The frequency is defined as follows:

$$f = \frac{\omega}{2\pi} = \frac{1}{T} \quad (\text{XIV.35})$$

With Equation (XIV.35), the excitation frequency per condition is calculated. Finally, in order to avoid resonance, the lowest natural frequency of the gate should be greater than the corresponding excitation frequency. Table XIV.20 presents the lowest natural frequency for both conditions considered and corresponding excitation frequency.

Δh [m]	f_1 [Hz]	f [Hz]
8.97	0.20	0.11
6.01	0.23	0.12

Table XIV.20: Fundamental natural frequencies and corresponding excitation frequencies

One a final note, as the quasi-permanent load combination has been determined with a return period of 10 years, the excitation frequencies on a daily basis could turn out greater. Figure XIV.23 by Boukhanovsky, Lopatoukhin, and Guedes Soares (2007) gives an impression of the spectral wave climate of the North Sea.

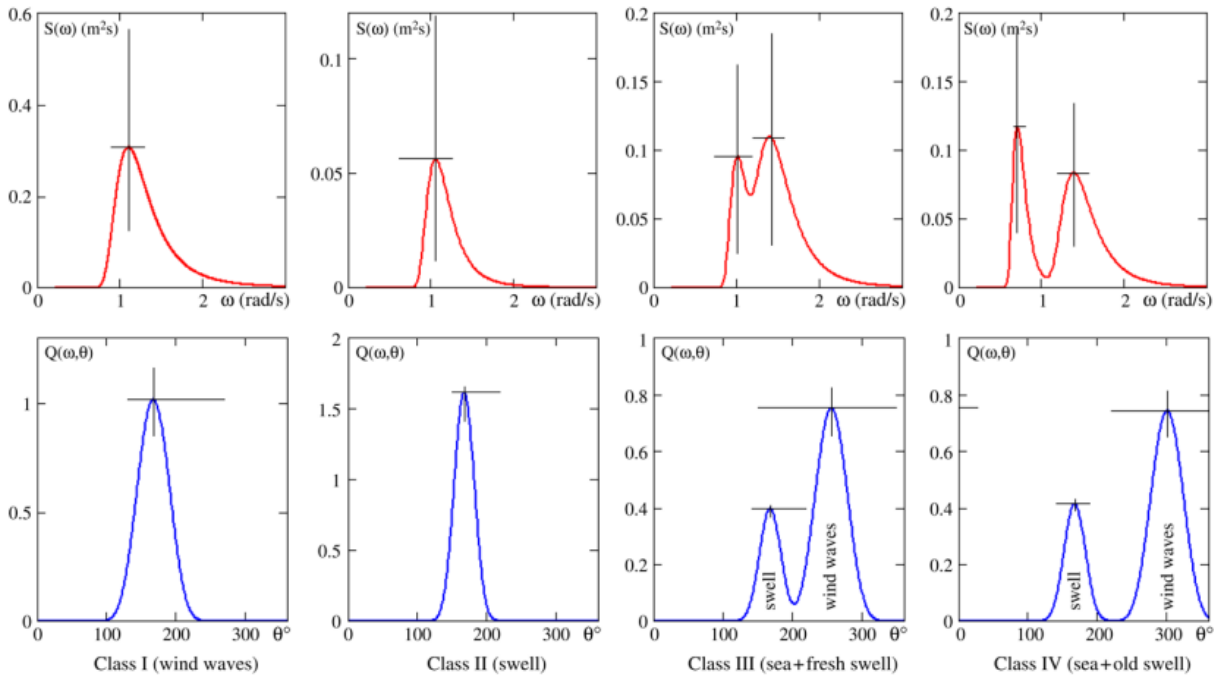


Figure XIV.23: Spectral wave climate of the North Sea (Boukhanovsky et al., 2007)

From Figure XIV.23 one could conclude that the daily excitation frequency of mostly (small) wind waves could reach the fundamental natural frequency of the gate. However, one should note that the total stiffness of the gate is greater (and hence the natural frequencies greater) than estimated due to the contribution of the stiff connections to the piers and the bracings which have not been taken into account.

Besides wave impact loading, drag forces due to flow under gates can give rise to resonance phenomena. Although not considered here specifically, unstable detachment of flow should be prevented (preferably do not design curved structures); the flow should preferably detach from an edge at the downstream side. Furthermore, any rubber seals should preferably have no rounded shape.

XV Complete Verification Civil Superstructure

This appendix presents the complete verification of the civil superstructure. First, the different materials from which the elements of the civil superstructure consist are treated. Secondly, all relevant external forces are established. Subsequently the verifications of the three most important elements of the civil superstructure are presented: the top beam, sill beam and pier, respectively. For every element an overview of all forces per load combination is presented. From said forces, the resultant horizontal and vertical force and the accompanying design values for shear, torsion and bending moment is calculated. For every load combination it is determined whether a force acts favourable or unfavourable regarding the load on the element and partial safety factors are assigned for every force accordingly. The Excel spreadsheet used to conduct the verifications is available at <http://repository.tudelft.nl/>.

XV.1 Materials

All concrete elements of the civil superstructure consist of concrete class C40/50. Table XV.1 presents the relevant characteristics regarding concrete class C40/50.

f_{ck} [N/mm ²]	f_{cd} [N/mm ²]	f_{ctm} [N/mm ²]	f_{ctd} [N/mm ²]	E_{cm} [N/mm ²]
40	26.7	3.5	1.64	35000

Table XV.1: Characteristics C40/50

in which: f_{ck} = characteristic compressive strength
 f_{cd} = design value of the compressive strength
 f_{ctm} = characteristic tensile strength
 f_{ctd} = design value of the tensile strength
 E_{cm} = Youngs modulus

All concrete elements of the civil superstructure are pre-stressed using strands of steel Y1860. Table XV.2 presents the relevant characteristics regarding pre-stressing steel Y1860.

f_{pk} [N/mm ²]	$f_{p0.1k}$ [N/mm ²]	E_p [N/mm ²]	$\sigma_{p,max}$ [N/mm ²]	σ_{pm0} [N/mm ²]
1860	1600	195000	1488	1360

Table XV.2: Characteristics Y1860

in which: f_{pk} = characteristic yield strength
 $f_{p0.1k}$ = characteristic 0.1% yield strength
 E_p = Youngs modulus
 $\sigma_{p,max}$ = maximum allowable stress applied to pre-stressing steel during stressing
 σ_{pm0} = maximum allowable stress in pre-stressing steel after immediate losses

For some local spalling reinforcement, rebar is applied when the member geometry or available space does not allow for transverse pre-stressing. Table XV.3 presents the relevant characteristics regarding rebar FeB500.

f_{ys} [N/mm ²]	E_s [N/mm ²]
435	195000

Table XV.3: Characteristics FeB500

in which: f_{ys} = characteristic yield strength
 E_s = Youngs modulus

XV.2 External Forces

Hydrostatic forces

See Appendix XIV.1.

Wave forces

See Appendix XIV.1.

Drag & lift forces

See Appendix XIV.1.

Drag and lift forces are neglected in the civil superstructure verification as said forces are negligible compared to e.g. hydrostatic and wave forces.

Ship collision

See Appendix XIV.1.

Soil pressures

For the derivation of the vertical effective soil pressure one may use Equation (XV.1).

$$\sigma'_v = \sum_{i=1}^n \gamma_{d,i} d_i + \sum_{j=1}^m \gamma_{w,j} d_j - p \quad (\text{XV.1})$$

in which:	σ'_v	[kN/m ²]	=	vertical effective soil pressure
	n	[-]	=	number of dry layers above the considered plane
	$\gamma_{d,i}$	[kN/m ³]	=	dry volumetric weight of soil layer i
	d_i	[m]	=	thickness of soil layer i
	m	[-]	=	number of wet layers above the considered plane
	$\gamma_{w,j}$	[kN/m ³]	=	wet volumetric weight of soil layer j
	d_j	[m]	=	thickness of soil layer j
	p	[kN/m ³]	=	water pressure in the considered plane

For the derivation of the horizontal effective soil pressures one may use Equation (XV.2).

$$\sigma'_h = K \cdot \sigma'_v \quad (\text{XV.2})$$

in which:	σ'_h	[kN/m ²]	=	horizontal effective soil pressure
	K	[-]	=	soil pressure coefficient

In general, the soil pressure coefficient K depends on the deformation of the soil. So called 'neutral stress' occurs when the soil is at rest. For greater soil pressures to develop the soil should be activated by means of deformation (e.g. due to deflection or sliding aside of a structure). When the soil becomes less compacted than at rest we speak of 'active stress' and when the soil is compressed we speak of 'passive stress'. The three types as described above give rise to different soil pressure coefficients, respectively K_0 , K_a and K_p for neutral, active and passive stress. Note that large shallow foundations expand due to temperature changes, so in these cases one must take a larger pressure on the vertical walls into account than predicted by Jáký ($K_0 \approx 1$) (Molenaar & Voorendt, 2020b).

Assuming a straight wall without shear stress and a non-cohesive soil, a lower limit (K_a) and upper limit (K_p) is given by Rankine's theory (Molenaar & Voorendt, 2020b).

$$K_a = \frac{1 - \sin \phi}{1 + \sin \phi} \quad (\text{XV.3})$$

$$K_p = \frac{1 + \sin \phi}{1 - \sin \phi} \quad (\text{XV.4})$$

in which: K_a [-] = active soil pressure coefficient
 K_p [-] = passive soil pressure coefficient
 ϕ [°] = angle of internal friction of the soil

The pressure of the bottom protection ($\phi = 35^\circ$) on the structure yields the following pressure coefficients:

K_a	0.27
K_p	3.69

Table XV.4: Pressure coefficients bottom protection

Wind loads

The wind loads acting perpendicular on the structure are determined according to Equation (5.3) of Eurocode 1 (2011a) (here Equation (XV.5)).

$$F_w = c_s c_d \cdot c_f \cdot q_p(z_e) \cdot A_{ref} \quad (\text{XV.5})$$

in which: F_w [kN] = wind load perpendicular on the structure (element)
 $c_s c_d$ [-] = building factor = 1
 c_f [-] = force coefficient for the structure (element)
 $q_p(z_e)$ [kN/m²] = the extreme wind pressure on height z_e
 A_{ref} [m²] = reference area of the subjected structure (element)

The force coefficient (c_f) can be determined using Equation (7.9) of Eurocode 1 (2011a) (here Equation (XV.6)).

$$c_f = c_{f,0} \cdot \psi_r \psi_\lambda \quad (\text{XV.6})$$

where: $c_{f,0}$ is the force coefficient of rectangular cross-sections with acute angles [-]
 ψ_r is the reduction factor for rectangular cross-sections with rounded corners, = 1 for acute angles [-]
 ψ_λ is the end effect factor for elements in which end effects play a role [-]

For large structure lengths (relative to the exposed height) and closed structures, $c_{f,0} \approx 1$ and $\psi_\lambda \leq 1$. Hence we may assume $c_f \approx 1$.

NEN-EN 1991-1-4 (2011a) recommends using Equation (XV.7) to determine extreme wind pressure $q_p(z_e)$.

$$q_p(z_e) = (1 + 7I_v(z)) \cdot \frac{1}{2} \rho v_m^2(z) \quad (\text{XV.7})$$

in which: $I_v(z)$ [-] = the turbulence intensity
 ρ [-] = density of air during storm conditions = 1.25 kg/m³
 $v_m(z)$ [m/s] = the average wind speed on height z above the terrain

Finally, the turbulence intensity ($I_v(z)$) and the average wind speed $v_m(z)$ can be calculated as proposed by NEN-EN 1991-1-4 (2011a) with Equation (XV.8) and Equation (XV.9) respectively.

$$I_v(z) = \begin{cases} \frac{k_l}{c_0(z) \cdot \ln(z/z_0)}, & \text{for } z_{min} \leq z \\ I_v(z_{min}), & \text{for } z < z_{min} \end{cases} \quad (\text{XV.8})$$

in which: k_t [-] = the turbulence factor = 1
 $c_0(z)$ [-] = the orography factor = 1
 z [m] = height above the terrain
 z_0 [m] = the roughness length = 0.003 for sea and coastal areas
 z_{min} [m] = minimum height = 1 for sea and coastal areas

$$v_m = c_r(z) \cdot c_0(z) \cdot v_b \quad (\text{XV.9})$$

where: $c_r(z)$ [-] = the roughness factor
 v_b [m] = 10-minute average wind speed with an annual exceedance probability of 0.02 at a height of 10 m above flat terrain

Note that v_b can be determined using the wind data gathered in Appendix VII and using Equation (3.2) from Section 3.2.4 for an annual exceedance probability of 0.02 (R=50 years). The roughness factor $c_r(z)$ should be determined using Equation (4.4) from NEN-EN 1991-1-4 (2011a) (here Equation (XV.10)).

$$c_r(z) = \begin{cases} k_r \ln(z/z_0), & \text{for } z_{min} \leq z \\ c_r(z_{min}), & \text{for } z < z_{min} \end{cases} \quad (\text{XV.10})$$

in which: k_r [-] = $0.19 \cdot \left(\frac{z_0}{0.05}\right)^{0.07}$

As all parameters are now known, one can solve for the wind load using Equation (XV.5) for all heights z .

Wind loads are neglected in the civil superstructure verification as said loads are negligible compared to e.g. hydrostatic and wave forces.

XV.3 Top Beam

Figure XV.1 presents a top view of the top beam with the effective width between two piers (40 m) and the distance between the supports of the top beam (43.25 m). In order to introduce the local pre-stressing forces at the heads of the beam, the concrete parts at the supports are solid.

Figure XV.2 presents a top view of said solid supports. Finally, Figure XV.3 and Figure XV.4 present the cross-sections of the hollow middle part of the top beam and the solid supports, respectively.

Table XV.5 and Table XV.6 present the characteristics of the hollow part of the top beam and the solid supports, respectively, in compliance with the final design.

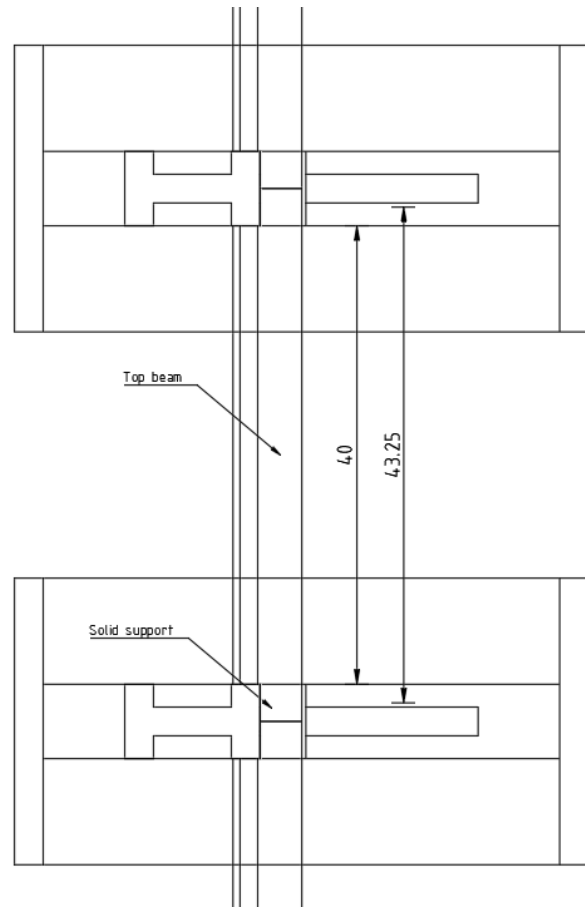


Figure XV.1: Top view. Top beam

A_c [10^6 mm^2]	I_{xx} [10^{13} mm^4]	I_{zz} [10^{13} mm^4]	S_x [10^{11} mm^3]	S_z [10^{11} mm^3]	A_k [10^6 mm^2]
15.56	3.94	11.88	5.08	25.30	26.71

Table XV.5: Characteristics of the hollow top beam

A_c [10^6 mm^2]	I_{xx} [10^{17} mm^4]	I_{zz} [10^{17} mm^4]	S_x [10^{10} mm^3]	S_z [10^{10} mm^3]	A_k [10^6 mm^2]
27.38	1.11	9.62	1.25	2.56	15.19

Table XV.6: Characteristics of the solid supports of the top beam

where: A_c = shear resistance for shear in x-direction
 I_{xx} = mass moment of inertia for bending around the z-axis
 I_{zz} = mass moment of inertia for bending around the x-axis
 S_x = the linear surface moment relative to the median in x-direction
 S_z = the linear surface moment relative to the median in z-direction
 A_k = area enclosed by the center lines of the connected walls, including hollow parts

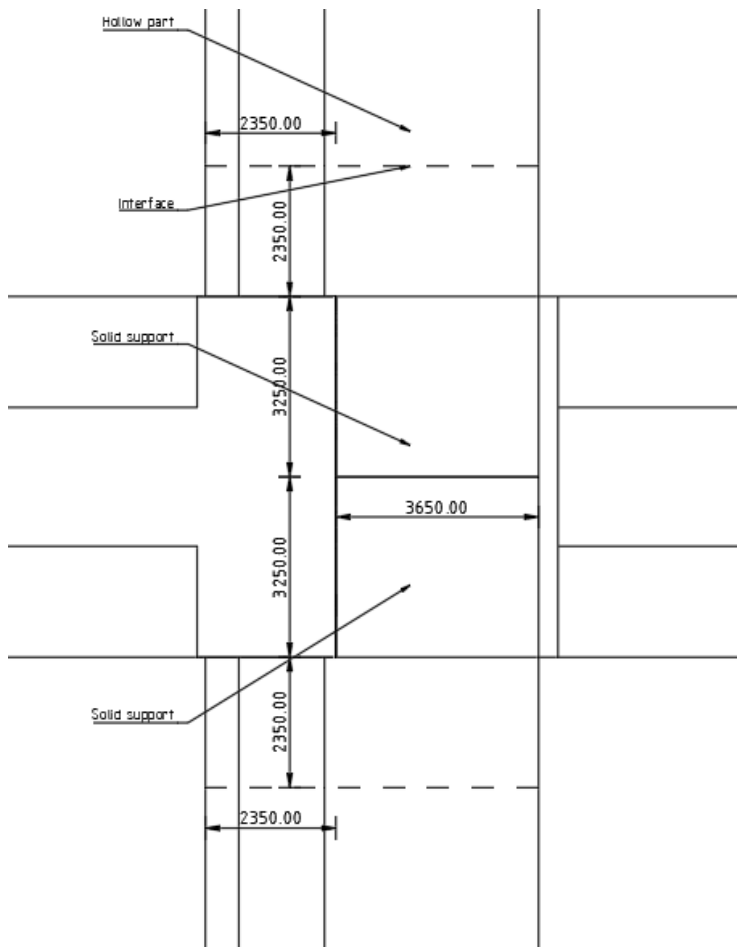


Figure XV.2: Top view. Solid support

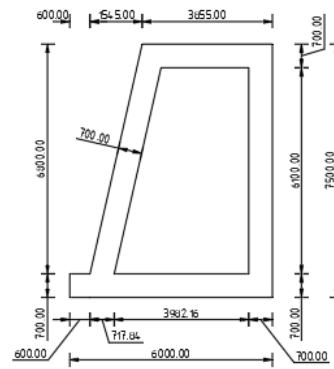


Figure XV.3: Cross-section top beam

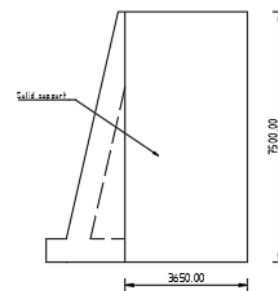


Figure XV.4: Cross-section solid support

The amount of pre-stressing steel applied and the initial pre-stressing force at which the tendons are tensioned are presented in Table XV.7

θ [mm]	strands [nr.]	ducts [nr.]	z_{cp} [mm]	A_p [mm ²]	P_{mi} [kN]	σ_{mi} [N/mm ²]
15.7	55	12	0	99000	139590	1410

Table XV.7: Pre-stressing steel and values for introduced pre-stressing force

- where:
- θ = strand diameter
 - strands = number of strand in a duct
 - ducts = number of ducts applied
 - z_{cp} = equivalent distance between the pre-stressing elements and the centre of gravity
 - A_p = area of pre-stressing steel applied
 - P_{mi} = initial pre-stressing force applied
 - σ_{mi} = initial stress in pre-stressing steel

Finally, Table XV.8 presents the immediate losses due to friction and wedge set, the time dependent losses and the pre-stressing force left after all losses.

$\Delta\sigma_{p,\mu}(L/2)$ [N/mm ²]	l_{set} [mm]	$\Delta\sigma_p(l_{set})$ [N/mm ²]	$\sigma_p(l_{set})$ [N/mm ²]	$\Delta\sigma_p(0)$ [N/mm ²]	$\sigma_p(0)$ [N/mm ²]	P_{m0} [kN]	$\Delta\sigma_{c+s+r}$ [N/mm ²]	$P_{m\infty}$ [kN]	$\sigma_{m\infty}$ [N/mm ²]
60.93	19184	10.93	1360	61.93	1309	133558	216.27	118179	1194

Table XV.8: Pre-stress losses and pre-stressing force left after losses

- where:
- $\Delta\sigma_{p,\mu}(L/2)$ = stress loss due to friction at half beam length
 - l_{set} = length over which wedge set influences the pre-stressing force
 - $\Delta\sigma_p(l_{set})$ = stress loss due to wedge set at l_{set}
 - $\sigma_p(l_{set})$ = stress at l_{set} after immediate losses
 - $\Delta\sigma_p(0)$ = stress loss due to wedge set at anchorage point
 - $\sigma_p(0)$ = stress at anchorage point after immediate losses
 - P_{m0} = pre-stressing force left after immediate losses
 - $\Delta\sigma_{c+s+r}$ = stress loss due to time dependent losses
 - $P_{m\infty}$ = pre-stressing force left after all losses
 - $\sigma_{m\infty}$ = stress left in pre-stressing steel after all losses

XV.3.1 Overview of Forces

Here, an overview of the forces on the top beam is presented for all relevant load combinations.

A: Maximum positive head is dominant

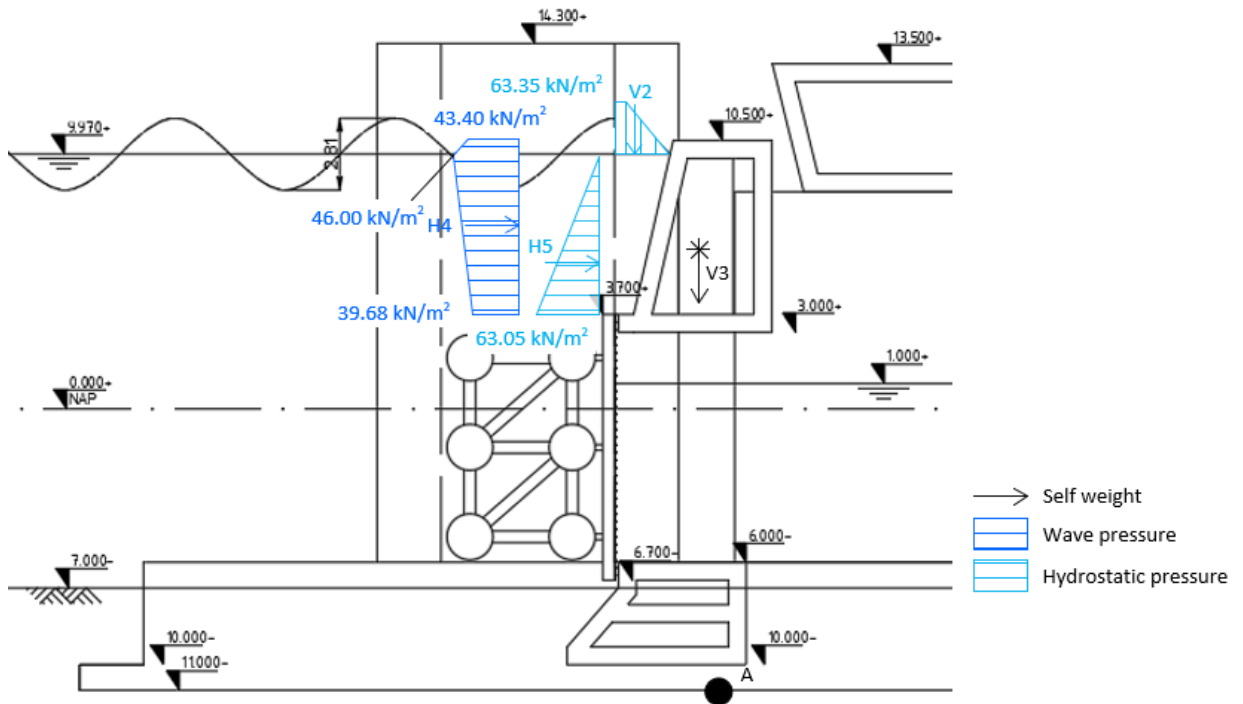


Figure XV.5: Forces on the top beam for load combination A

γ					
H4	1	11691.91	kN	e	0.74 m
H5	1	7906.47	kN	e	-0.006 m
V2	1	3319.54	kN	e	-2.34 m
V3	1.35	21000	kN	e	0 m

Table XV.9: Design forces

$q_{Ed,x}$	490	kN/m
$q_{Ed,z}$	608	kN/m
$V_{Ed,x}$	9799	kN
$V_{Ed,z}$	12162	kN
T_{Ed}	-18299	kNm
$M_{Ed,x}$	114562	kNm
$M_{Ed,z}$	142192	kNm

Table XV.10: Design values for shear, torsion and bending moment

The shear force is calculated as follows:

$$V_{Ed,i} = \frac{1}{2} \cdot q_{Ed,i} \cdot 40$$

The torsion moment is calculated as follows:

$$T_{Ed} = \sum F \cdot e$$

The total moment is calculated as follows:

$$M_{Ed,i} = \frac{1}{8} \cdot q_{Ed,i} \cdot 43.25^2$$

B: Maximum negative head is dominant

During load combination B, no hydrostatic water and wave loads act on the top beam. Besides self weight, merely a wind pressure is present which can be neglected.

H: Ship collision

As for load combination H, ship collision is only possible from the Tidal Lake side as the gates create an obstruction at the sea side. In this case, the governing combination of forces including only the ship collision force and the self weight of the top beam. Note that water and wave pressure from the sea side would have a beneficial effect in this case. It is assumed that a vessel collides with the bottom of the top beam.

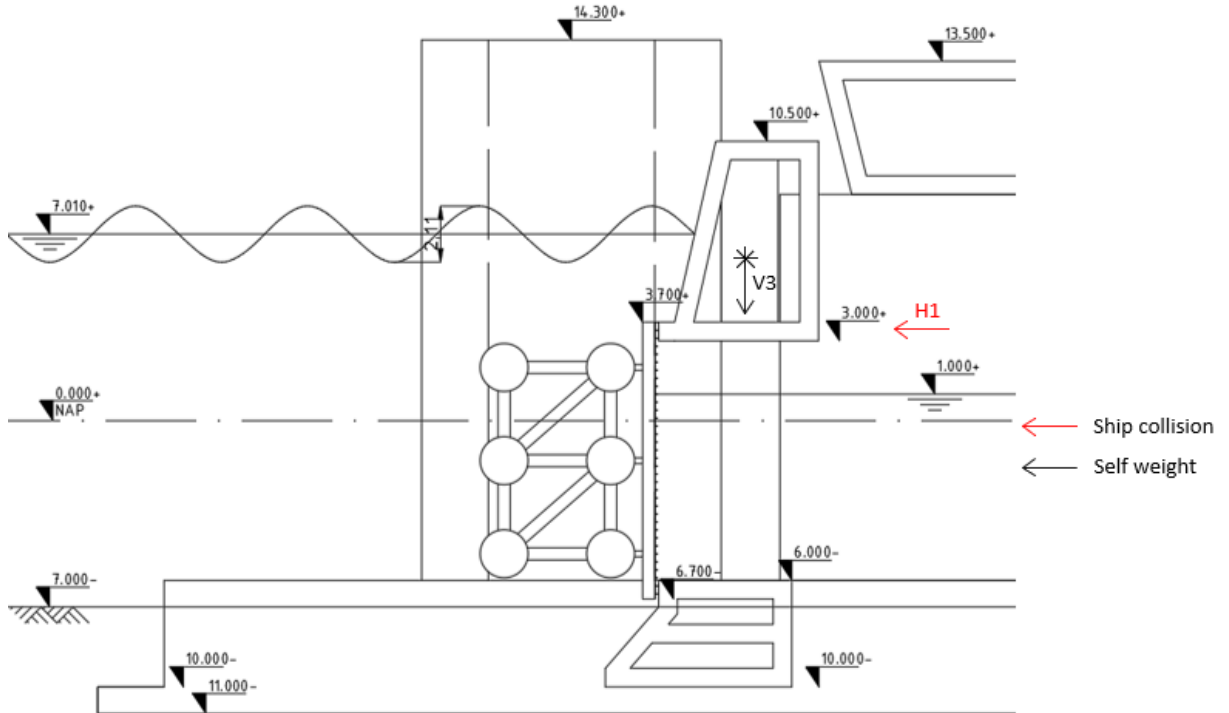


Figure XV.6: Governing forces on the top beam for load combination H

	γ				
H1	1	-5220	kN	e	2.446 m
V3	1.35	21000	kN	e	0 m

Table XV.11: Design forces

The total moment due to ship collision is calculated as follows:

$$M_{Ed,x} = \frac{1}{4} \cdot H1 \cdot 43.25$$

$q_{Ed,z}$	525	kN/m
$V_{Ed,x}$	-2610	kN
$V_{Ed,z}$	10500	kN
T_{Ed}	12768	kNm
$M_{Ed,x}$	-56441	kNm
$M_{Ed,z}$	122756	kNm

Table XV.12: Design values for shear, torsion and bending moment

Comparing Table XV.12 to Table XV.10, it can be concluded that load combination H is not governing over load combination A.

SLS: Quasi-permanent combination

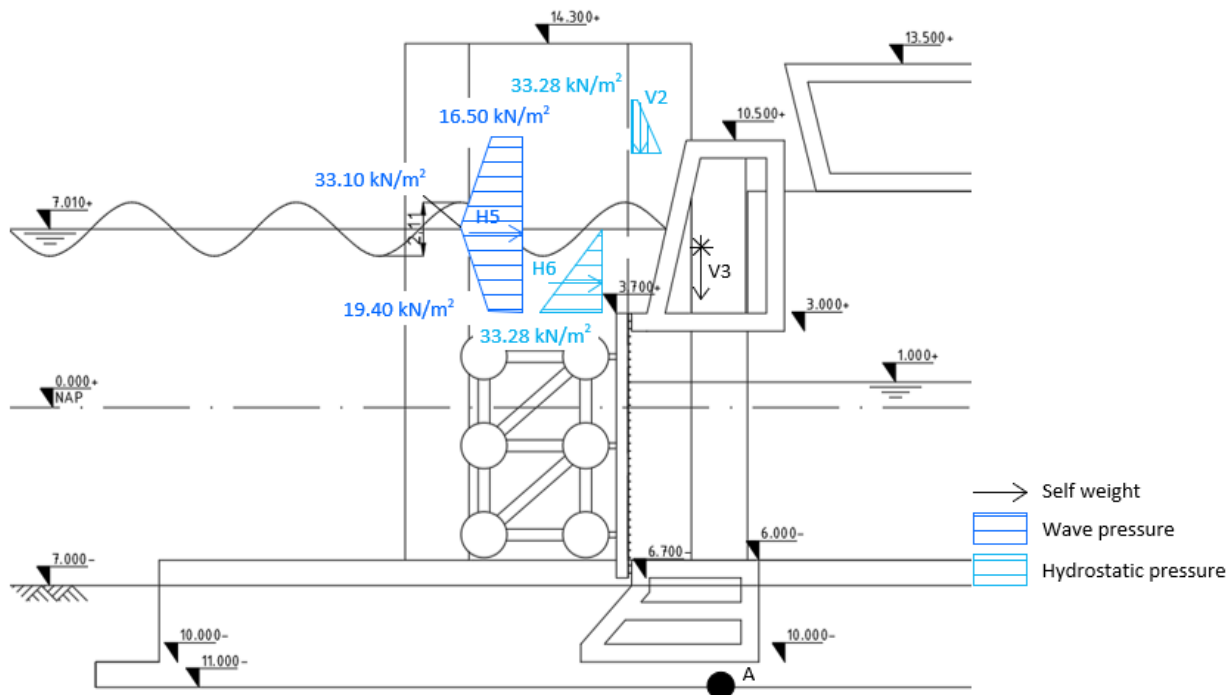


Figure XV.7: Governing forces on the top beam for load combination SLS

γ			
H5	1	6938	kN
H6	1	2203	kN
V2	1	1298	kN
V3	1	25883	kN

Table XV.13: Design forces

$q_{Ed,x}$	211	kN/m
$q_{Ed,z}$	628	kN/m

Table XV.14: Design values for distributed loads

The Quasi-permanent load combination is solely used for the deflection verification.

XV.3.2 Bending and Normal Force

No tensile stress

For there to be no tensile stress in an element, Equation (XV.11a) and Equation (XV.11b) should hold for all cross-sections at any point in the element for bending around the z and x axis respectively.

$$\sigma_x = \frac{M_{Ed,x} \cdot x}{I_{xx}} - \frac{P_{m\infty}}{A_c} \leq 0 \tag{XV.11a}$$

$$\sigma_z = \frac{M_{Ed,z} \cdot z}{I_{zz}} - \frac{P_{m\infty}}{A_c} \leq 0 \tag{XV.11b}$$

The distance to the top fibres where the maximum tensile stresses occur, $x = 2581$ mm and $z = 2796$ mm for bending around the z-axis and bending around the x-axis respectively are indicated in Figure XV.8. Finally, this yields $\sigma_x = -0.08$ N/mm² and $\sigma_z = -4.25$ N/mm².

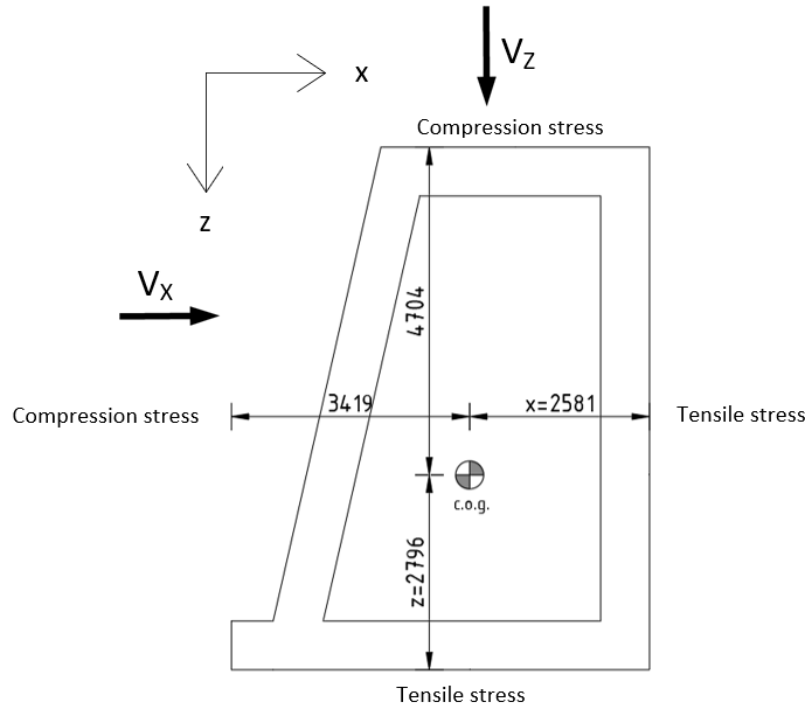


Figure XV.8: Outer fibres where maximum stresses occur

Maximum compressive stress

According to NEN-EN 1992-1-1 (2011b) Equation (5.42), the compressive stress in a concrete element must conform to Equation (XV.12a) and Equation (XV.12b) for all cross-sections at any point in the element for bending around the z and x axis respectively.

$$\sigma_x = -\frac{M_x x}{I_{xx}} - \frac{P_{m0}}{A_c} \geq -0.6 f_{ck} \quad (\text{XV.12a})$$

$$\sigma_z = -\frac{M_z z}{I_{zz}} - \frac{P_{m0}}{A_c} \geq -0.6 f_{ck} \quad (\text{XV.12b})$$

The distance to the top fibres where the maximum compressive stresses occur, $x = 3419$ mm and $z = 4704$ mm for bending around the z-axis and bending around the x-axis respectively are indicated in Figure XV.8. Finally, this yields $\sigma_x = -17.54$ N/mm² and $\sigma_z = -13.23$ N/mm².

XV.3.3 Shear and Torsion

According to Equation (6.31) of NEN-EN 1992-1-1 (2011b), if Equation (XV.13) is satisfied, only the minimum amount of longitudinal reinforcement is required (i.e. no shear reinforcement).

$$\frac{V_{Ed,i}}{V_{Rd,c,i}} + \frac{T_{Ed}}{T_{Rd,c}} \leq 1 \quad (\text{XV.13})$$

According to NEN-EN 1992-1-1 (2011b) Equation 6.2.2 (2), for simply supported pre-stressed elements without shear reinforcement which are not cracked by bending, the shear resistance should be limited by the tensile strength of the concrete and should be calculated using Equation (XV.14a) and Equation (XV.14b) for shear in x and z-direction respectively.

$$V_{Rd,c,x} = \frac{I_{xx} \cdot b_w}{S_x} \sqrt{f_{ctd}^2 + \alpha \cdot \sigma_{cp} f_{ctd}} \geq V_{Ed,x} \quad (\text{XV.14a})$$

$$V_{Rd,c,z} = \frac{I_{zz} \cdot b_w}{S_z} \sqrt{f_{ctd}^2 + \alpha \cdot \sigma_{cp} f_{ctd}} \geq V_{Ed,z} \quad (\text{XV.14b})$$

where: $V_{Rd,c,x}$ [N] = shear resistance for shear in x-direction
 $V_{Rd,c,z}$ [N] = shear resistance for shear in z-direction
 b_w [mm] = width of the cross-section at the center of gravity
 α [-] = 1
 σ_{cp} [N/mm²] = the concrete compressive stress at the center of gravity as a result of the pre-stressing

With Equation (6.3.2) and article 6.3.2 (5) from NEN-EN 1992-1-1 (2011b), the torsional resistance to pure torsion of a cross-section is to be calculated with Equation (XV.15).

$$T_{Rd,c} = 2 \cdot A_k \cdot f_{ctd} \cdot t_{eff,i} \geq T_{Ed} \quad (\text{XV.15})$$

where: $T_{Rd,c}$ [Nmm] = resistance to pure torsion
 $t_{eff,i}$ [mm] = effective wall thickness = $\frac{A_c}{u_c}$
 u_c [mm] = circumference

NEN-EN 1992-1-1 (2011b) 6.3.3 (1) states that for closed and thin walled cross-sections and solid cross-sections, the effects due to warping of the cross-section may be neglected.

The maximum shear stresses, shear and torsion combined, occur at the supports. However, the solid supports of the top beam poses the greatest resistance to both shear and torsion relative to the middle, hollow part of the beam. Therefore, the verification regarding shear and torsion is conducted for both the solid supports and at the interface between the solid support and the hollow part of the top beam.

Solid supports

$V_{Rd,c,x}$ [kN]	$V_{Rd,c,z}$ [kN]	$V_{Ed,x}$ [kN]	$V_{Ed,z}$ [kN]	$T_{Rd,c}$ [kNm]	T_{Ed} [kNm]	UC_x [-]	UC_z [-]
57043	57043	9799	12162	61180	423	0.18	0.22

Table XV.15: Shear and torsion verification top beam

Interface

$V_{Rd,c,x}$ [kN]	$V_{Rd,c,z}$ [kN]	$V_{Ed,x}$ [kN]	$V_{Ed,z}$ [kN]	$T_{Rd,c}$ [kNm]	T_{Ed} [kNm]	UC_x [-]	UC_z [-]
42256	25573	7703	9561	55794	333	0.19	0.38

Table XV.16: Shear and torsion verification top beam

XV.3.4 Spalling Reinforcement

The pre-stressing force is introduced through the 12 ducts into the solid supports of the top beam. The introduction through the 12 ducts is already somewhat distributed due to the duct spacing. Nonetheless, conservatively, it is assumed here that the total pre-stressing force is introduced at the centre of gravity of the hollow part of the top beam. Non-linear distribution of the introduced load is considered in both x- and z-direction. Local spalling reinforcement should be in place in order

to account for the local tension stresses until the introduced load is spread evenly throughout the cross-section.

X-direction

Figure XV.9 depicts the introduction of the pre-stressing force (after immediate losses) and the reaction forces from the concrete cross-section to make equilibrium. Note that a tensile reaction force is present due to the large eccentricity of the introduced load with respect to the solid support geometry. Figure XV.10 presents the strut and tie model with which the local tension forces are determined. A compression force is depicted in blue and a tension force in red in Figure XV.10.

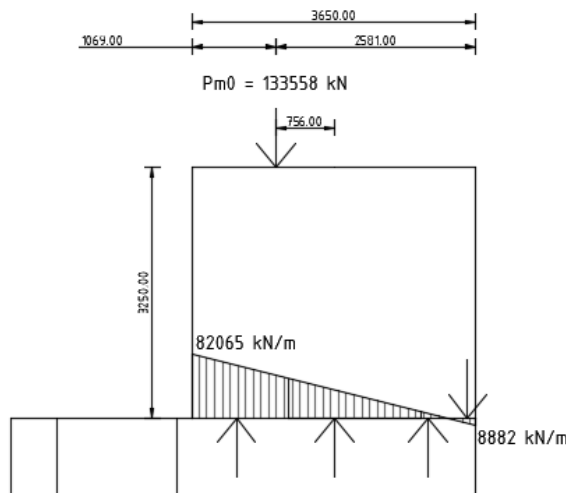


Figure XV.9: Reaction forces

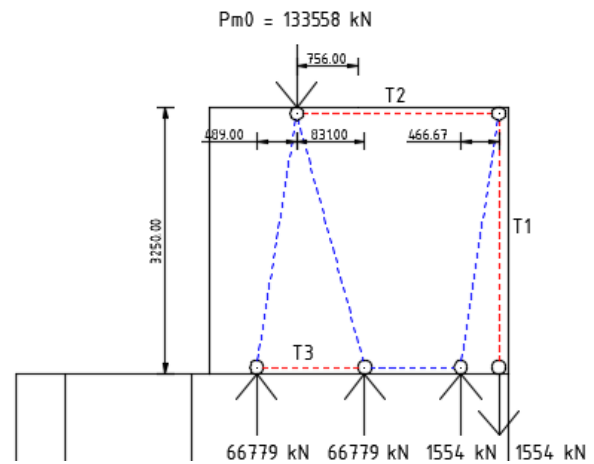


Figure XV.10: Strut and tie model

Subsequently, the local tension forces are calculated as follows:

$$T_1 = 1554 \text{ kN}$$

$$T_2 = \frac{467}{3250} \cdot 1554$$

$$= 223 \text{ kN}$$

$$T_3 = \frac{489}{3250} \cdot 66779$$

$$= 10048 \text{ kN}$$

Note that the established tension forces could be taken up by both rebar and pre-stressing steel. As the available space does not allow for transverse pre-stressing, the amount of rebar needed to withstand the tension forces is calculated by means of Equation (XV.16).

$$A_{s,i} = \frac{T_i}{f_{ys}} \quad (\text{XV.16})$$

$A_{s,1}$ [mm ²]	$A_{s,2}$ [mm ²]	$A_{s,3}$ [mm ²]
3572	513	23099

Table XV.17: Required spalling reinforcement

The calculated required rebar in Table XV.17 is to be distributed over the entire height of the top beam.

Z-direction

Figure XV.11 depicts the introduction of the pre-stressing force (after immediate losses) and the reaction forces from the concrete cross-section to make equilibrium. The eccentricity in z-direction (i.e. over the height of the beam) is minor and therefore only compression is present in the reaction forces from the cross-section. Figure XV.12 presents the strut and tie model with which the local tension force is determined. A compression force is depicted in blue and a tension force in red in Figure XV.12.

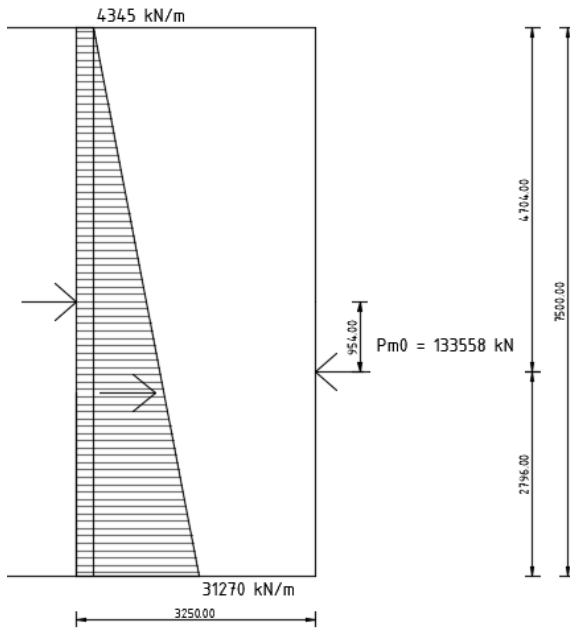


Figure XV.11: Reaction forces

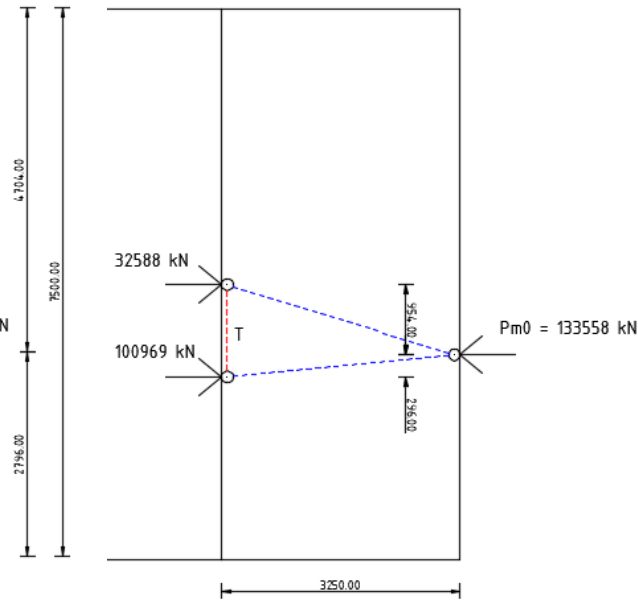


Figure XV.12: Strut and tie model

Subsequently, the local tension force is calculated as follows:

$$T = \frac{954}{3250} \cdot 32588$$

$$= 9566 \text{ kN}$$

Note that the established tension forces could be taken up by both rebar and pre-stressing steel. As the available space does not allow for transverse pre-stressing, the amount of rebar needed to withstand the tension forces is again calculated by means of Equation (XV.16).

A_s
$[mm^2]$
21991

Table XV.18: Required spalling reinforcement

The calculated required rebar in Table XV.18 is to be distributed over the entire width of the top beam.

XV.3.5 Deflection

The maximum deflection of the top beam should satisfy Equation (XV.17), as stated by Vrijburcht (2000).

$$w_{max,i} \leq \frac{1}{200} L = 216 \text{ mm} \quad (\text{XV.17})$$

where: $w_{max,i}$ [mm] = maximum deflection of the top beam in either x- or z-direction
 L [mm] = length of the top beam between two supports = 43250

Conservatively, $w_{max,i}$ is calculated using the general forget-me-not for a pinned-pinned beam under a distributed load according to Equation (XV.18).

$$w_{max,i} = \frac{5}{384} \frac{q_{Ed,i} L^4}{EI_{ii}} \quad (\text{XV.18})$$

E [N/mm²] = Youngs modulus
 I_{ii} [mm⁴] = mass moment of inertia in either x- or z-direction

This yields, $w_{max,x} = 6.98 \text{ mm}$ and $w_{max,z} = 6.88 \text{ mm} \leq 216 \text{ mm}$. Note that the top beam is assumed to be in uncracked state, as to be expected after post-tensioning.

XV.4 Sill Beam

Figure XV.13 presents a top view of the sill beam with the effective width between two piers (40 m). In order to introduce the local pre-stressing forces at the heads of the beam, the concrete parts at the supports are solid.

Figure XV.14 and Figure XV.15 present front views of the sill beam in their slots in the piers and of the sill beam alone, respectively. Finally, Figure XV.16 and Figure XV.17 present the cross-sections of the hollow middle part of the sill beam and the solid supports, respectively.

Table XV.19 and Table XV.20 present the characteristics of the hollow part of the sill beam and the solid supports, respectively, in compliance with the design as presented above.

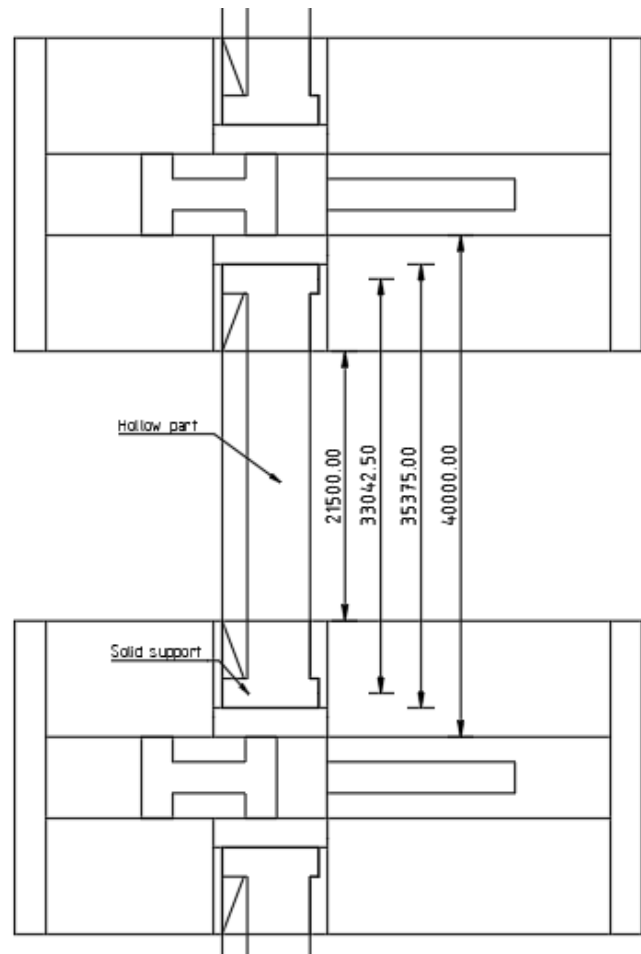


Figure XV.13: Top view. Sill beam

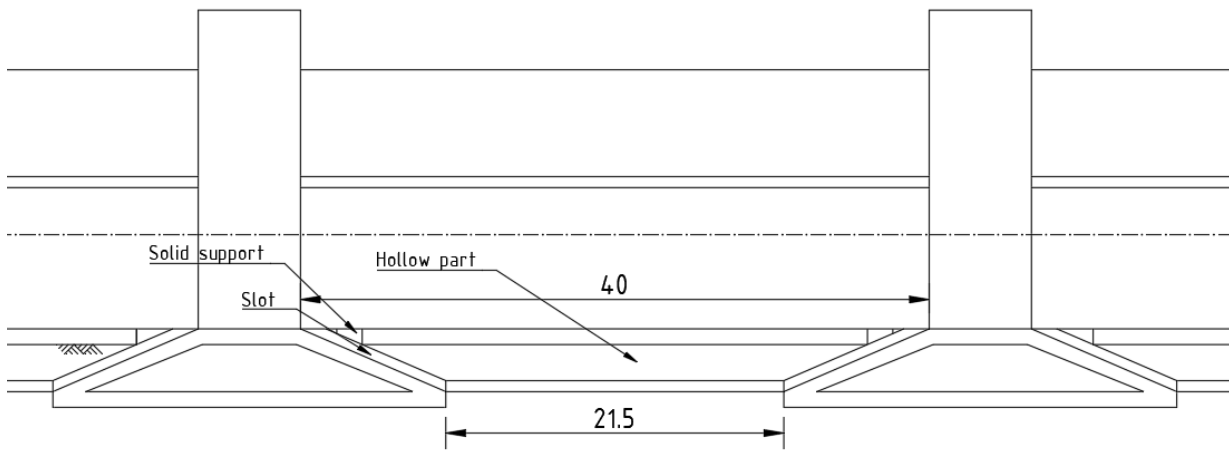


Figure XV.14: Front view. Sill beam in slots between two piers

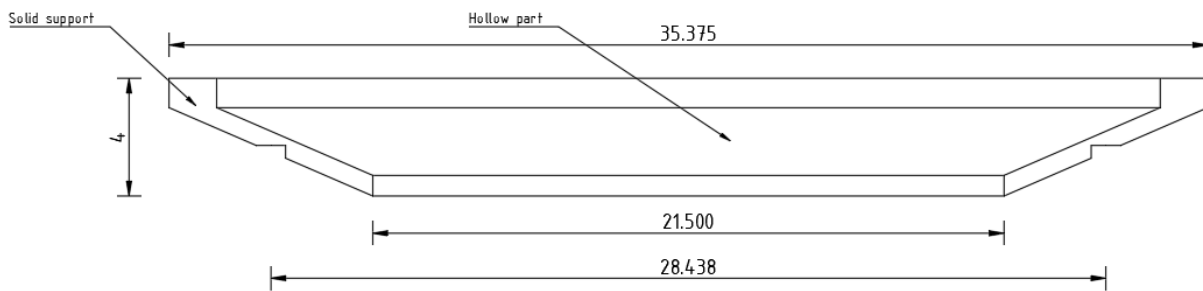


Figure XV.15: Front view. Sole sill beam

A_c [10 ⁶ mm ²]	I_{xx} [10 ¹³ mm ⁴]	I_{zz} [10 ¹³ mm ⁴]	S_x [10 ¹⁰ mm ³]	S_z [10 ¹⁰ mm ³]	A_k [10 ⁶ mm ²]
15.27	6.70	2.47	1.42	0.92	16.84

Table XV.19: Characteristics of the hollow sill beam

A_c [10 ⁶ mm ²]	I_{xx} [10 ¹³ mm ⁴]	I_{zz} [10 ¹³ mm ⁴]	S_x [10 ¹⁰ mm ³]	S_z [10 ¹⁰ mm ³]	A_k [10 ⁶ mm ²]
28	11.43	3.73	2.45	1.40	14.68

Table XV.20: Characteristics of the solid supports of the sill beam

- where:
- A_c = shear resistance for shear in x-direction
 - I_{xx} = mass moment of inertia for bending around the z-axis
 - I_{zz} = mass moment of inertia for bending around the x-axis
 - S_x = the linear surface moment relative to the median in x-direction
 - S_z = the linear surface moment relative to the median in z-direction
 - A_k = area enclosed by the center lines of the connected walls, including hollow parts

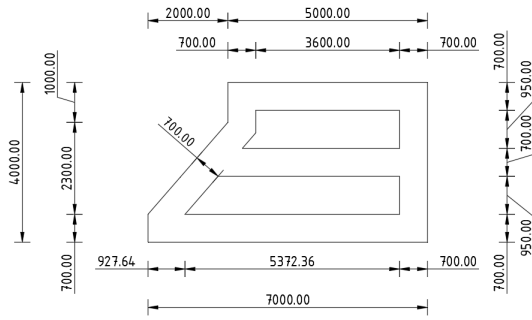


Figure XV.16: Cross-section sill beam

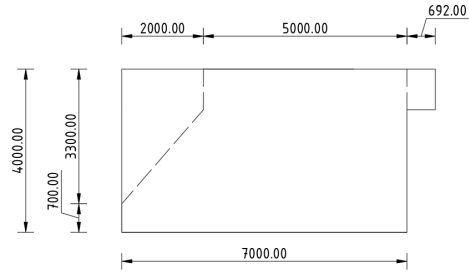


Figure XV.17: Cross-section sill beam solid support

The amount of pre-stressing steel applied and the initial pre-stressing force at which the tendons are tensioned are presented in Table XV.21

θ [mm]	strands [nr.]	ducts [nr.]	z_{cp} [mm]	A_p [mm ²]	P_{mi} [kN]	σ_{mi} [N/mm ²]
15.7	55	8	0	66000	93060	1410

Table XV.21: Pre-stressing steel and values for introduced pre-stressing force

- where: θ = strand diameter
 strands = number of strand in a duct
 ducts = number of ducts applied
 z_{cp} = equivalent distance between the pre-stressing elements and the centre of gravity
 A_p = area of pre-stressing steel applied
 P_{mi} = initial pre-stressing force applied
 σ_{mi} = initial stress in pre-stressing steel

Finally, Table XV.22 presents the immediate losses due to friction and wedge set, the time dependent losses and the pre-stressing force left after all losses.

$\Delta\sigma_{p,\mu}(L/2)$ [N/mm ²]	l_{set} [mm]	$\Delta\sigma_p(l_{set})$ [N/mm ²]	$\sigma_p(l_{set})$ [N/mm ²]	$\Delta\sigma_p(0)$ [N/mm ²]	$\sigma_p(0)$ [N/mm ²]	P_{m0} [kN]	$\Delta\sigma_{c+s+r}$ [N/mm ²]	$P_{m\infty}$ [kN]	$\sigma_{m\infty}$ [N/mm ²]
60.29	19286	10.93	1359	50	1309	89081	171.62	81733	1238

Table XV.22: Pre-stress losses and pre-stressing forces left after losses

- where: $\Delta\sigma_{p,\mu}(L/2)$ = stress loss due to friction at half beam length
 l_{set} = length over which wedge set influences the pre-stressing force
 $\Delta\sigma_p(l_{set})$ = stress loss due to wedge set at l_{set}
 $\sigma_p(l_{set})$ = stress at l_{set} after immediate losses
 $\Delta\sigma_p(0)$ = stress loss due to wedge set at anchorage point
 $\sigma_p(0)$ = stress at anchorage point after immediate losses
 P_{m0} = pre-stressing force left after immediate losses
 $\Delta\sigma_{c+s+r}$ = stress loss due to time dependent losses
 $P_{m\infty}$ = pre-stressing force left after all losses
 $\sigma_{m\infty}$ = stress left in pre-stressing steel after all losses

XV.4.1 Overview of Forces

A: Maximum positive head is dominant

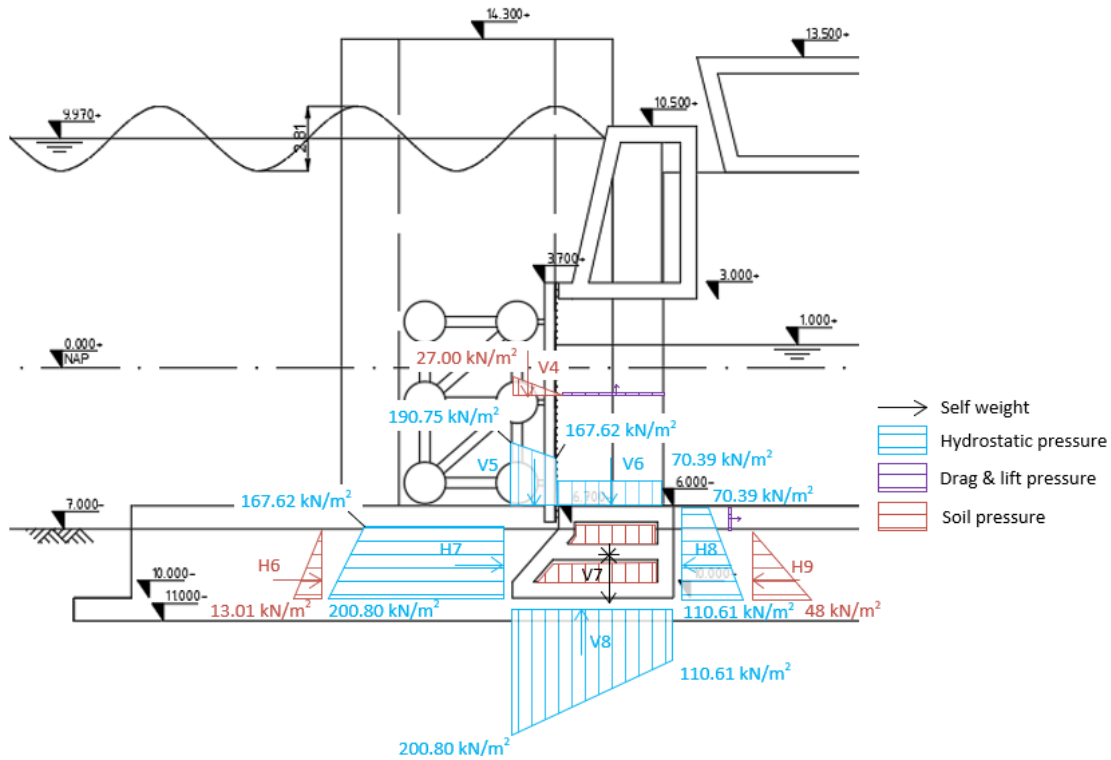


Figure XV.18: Forces on the sill beam for load combination A

γ					
H6	1.35	636.19	kN	e	-0.85 m
H7	1	19817.3	kN	e	-0.25 m
H8	1	-11801.2	kN	e	0 m
H9	0.9	-2347.2	kN	e	-0.85 m
V4	1.35	680.4	kN	e	-2.51 m
V5	1	9030.92	kN	e	-2.82 m
V6	1	14078	kN	e	0.65 m
V7	1.35	11120.9	kN	e	0 m
V8	1	-27466.4	kN	e	-0.45 m

Table XV.23: Design forces

$q_{Ed,x}$	191	kN/m
$q_{Ed,z}$	262	kN/m
$V_{Ed,x}$	3153	kN
$V_{Ed,z}$	3722	kN
T_{Ed}	-4642	kNm
$M_{Ed,x}$	26042	kNm
$M_{Ed,z}$	26461	kNm

Table XV.24: Design values for shear, torsion and bending moment

The shear force is calculated as follows:

$$V_{Ed,i} = \frac{1}{2} \cdot q_{Ed,i} \cdot 40$$

The torsion moment is calculated as follows:

$$T_{Ed} = \sum F \cdot e$$

The total moments are calculated as follows:

$$M_{Ed,x} = \frac{1}{8} \cdot q_{Ed,i} \cdot 33.0^2$$

$$M_{Ed,z} = \frac{1}{8} \cdot q_{Ed,i} \cdot 28.4^2$$

B: Maximum negative head is dominant

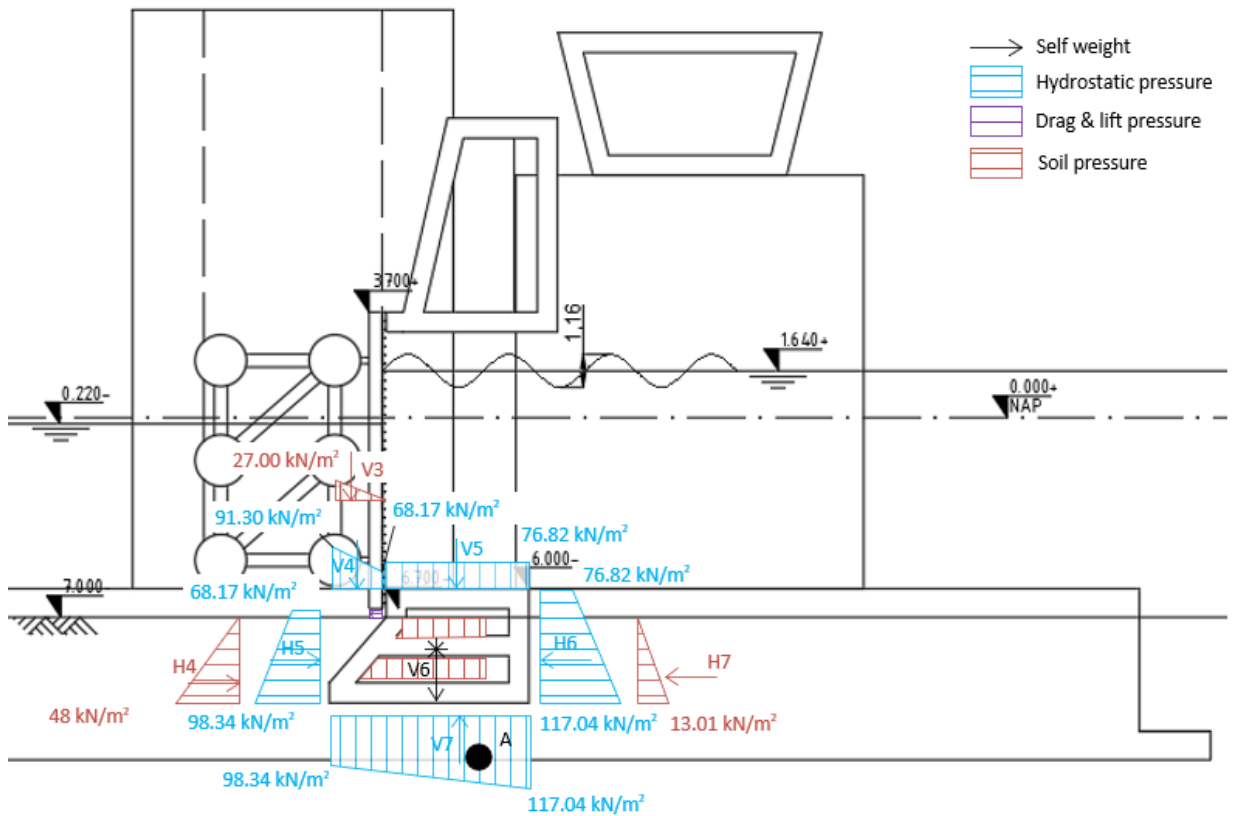


Figure XV.19: Forces on the sill beam for load combination B

	γ				
H4	0.9	2347	kN	e	-0.85 m
H5	1	8957	kN	e	-0.30 m
H6	1	-12640	kN	e	-0.01 m
H7	1.35	-636	kN	e	-0.85 m
V3	1.35	680	kN	e	-2.51 m
V4	1	5688	kN	e	-1.98 m
V5	1	15364	kN	e	0.65 m
V6	1.35	11121	kN	e	0 m
V7	1	-16735	kN	e	-0.24 m

Table XV.25: Design forces

$q_{Ed,x}$	-60	kN/m
$q_{Ed,z}$	567	kN/m
$V_{Ed,x}$	-986	kN
$V_{Ed,z}$	8059	kN
T_{Ed}	-1445	kNm
$M_{Ed,x}$	-8145	kNm
$M_{Ed,z}$	57295	kNm

Table XV.26: Design values for shear, torsion and bending moment

The shear force is calculated as follows:

$$V_{Ed,i} = \frac{1}{2} \cdot q_{Ed,i} \cdot 40$$

The torsion moment is calculated as follows:

$$T_{Ed} = \sum F \cdot e$$

The total moments are calculated as follows:

$$M_{Ed,x} = \frac{1}{8} \cdot q_{Ed,i} \cdot 33.0^2$$

$$M_{Ed,z} = \frac{1}{8} \cdot q_{Ed,i} \cdot 28.4^2$$

H: Ship collision

As for load combination H, it is assumed that ships will not collide with the sill beam. From the sea side, the sill beam is obstructed by the gates. If a ship were to sink after collision from the Tidal Lake side, a ship collision load on the sill beam would be a possibility. However, it is assumed here that the probability of a ship sinking to the sill beam level after collision is significantly low and ship collision with the sill beam is therefore neglected.

SLS: Quasi-permanent combination

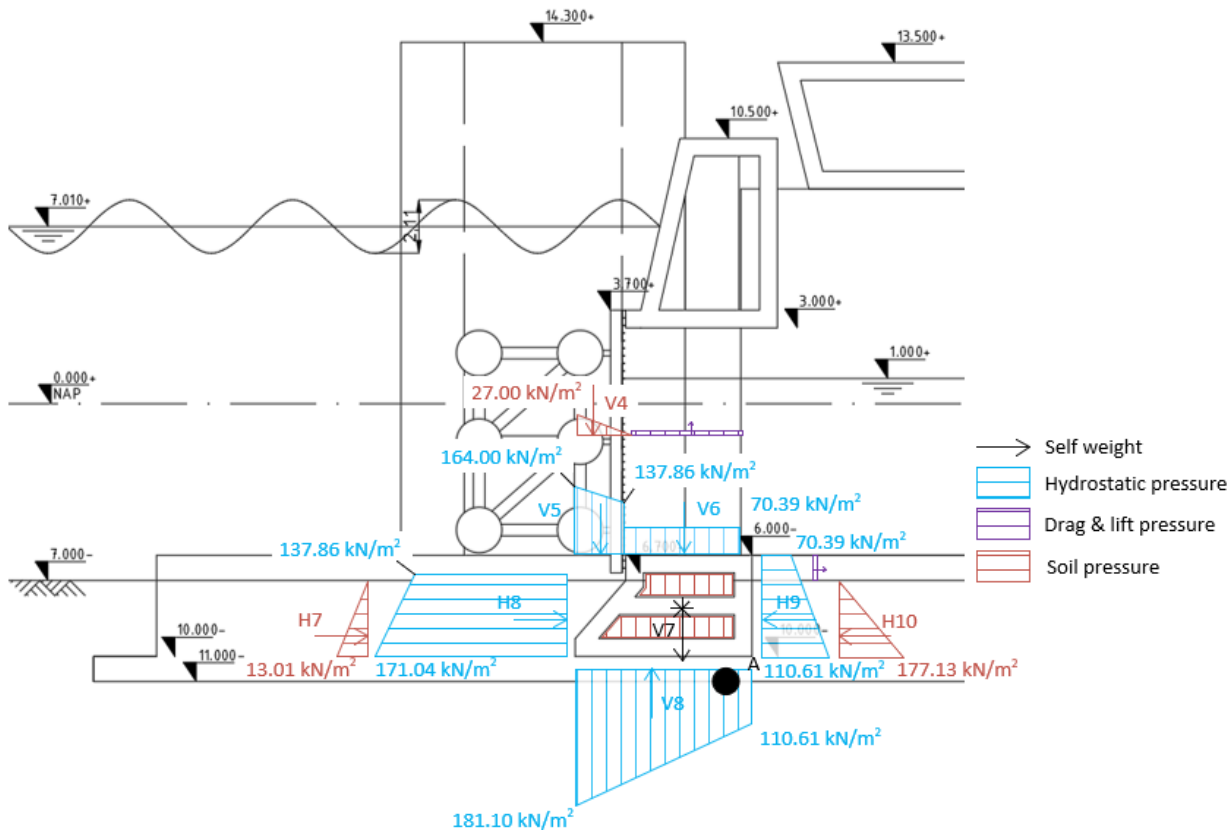


Figure XV.20: Governing forces on the sill beam for load combination SLS

	γ		
H7	1	636	kN
H8	1	16616	kN
H9	1	-11801	kN
H10	1	-8662	kN
V4	1	680	kN
V5	1	7607	kN
V6	1	14078	kN
V7	1	11121	kN
V8	1	-21337	kN

Table XV.27: Design forces

$q_{Ed,x}$	94	kN/m
$q_{Ed,z}$	427	kN/m

Table XV.28: Design values for distributed loads

The Quasi-permanent load combination is solely used for the deflection verification.

XV.4.2 Bending and Normal Force

It should be noted that load combination A is governing for bending around the z-axis and load combination B is governing for bending around the y-axis.

No tensile stress

For there to be no tensile stress in an element, Equation (XV.11a) and Equation (XV.11b) should hold for all cross-sections at any point in the element for bending around the z and x axis respectively.

The distance to the top fibres where the maximum tensile stresses occur, $x = 3154$ mm and $z = 1848$ mm for bending around the z-axis and bending around the x-axis respectively are indicated in Figure XV.21. Finally, this yields $\sigma_x = - 4.13$ N/mm² and $\sigma_z = - 0.36$ N/mm².

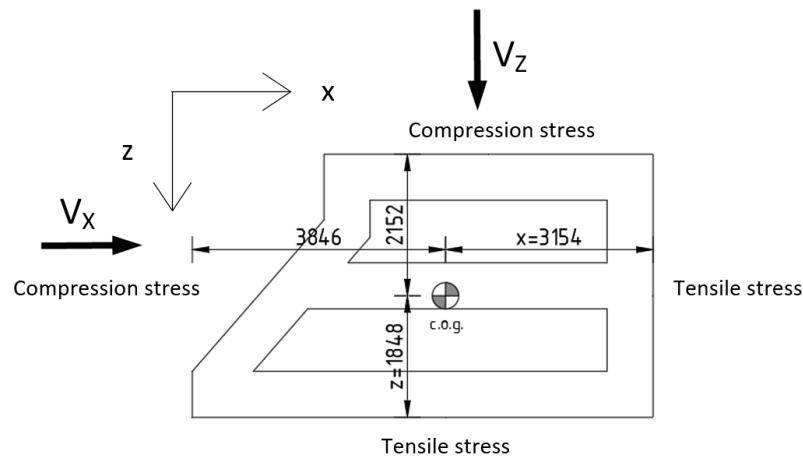


Figure XV.21: Outer fibres where maximum stresses occur

Maximum compressive stress

According to NEN-EN1992-1-1 (2011b) Equation (5.42), the compressive stress in a concrete element must conform to Equation (XV.12a) and Equation (XV.12b) for all cross-sections at any point in the element for bending around the z and x axis respectively.

The distance to the top fibres where the maximum compressive stresses occur, $x = 3846$ mm and $z = 2152$ mm for bending around the z-axis and bending around the x-axis respectively are indicated in Figure XV.8. Finally, this yields $\sigma_x = - 7.33$ N/mm² and $\sigma_z = - 10.12$ N/mm².

XV.4.3 Shear and Torsion

According to Equation (6.31) of NEN-EN 1992-1-1(2011b), if Equation (XV.13) is satisfied, only the minimum amount of longitudinal reinforcement is required (i.e. no shear reinforcement).

According to NEN-EN1992-1-1 (2011b) Equation 6.2.2 (2), for simply supported pre-stressed elements without shear reinforcement which are not cracked by bending, the shear resistance should be limited by the tensile strength of the concrete and should be calculated using Equation (XV.14a) and Equation (XV.14b) for shear in x and z-direction respectively.

With Equation (6.3.2) and article 6.3.2 (5) from NEN-EN1992-1-1 (2011b), the torsional resistance to pure torsion of a cross-section is to be calculated with Equation (XV.15).

NEN-EN 1992-1-1(2011b) 6.3.3 (1) states that for closed and thin walled cross-sections and solid cross-sections, the effects due to warping of the cross-section may be neglected.

The maximum shear stresses, shear and torsion combined, occur at the supports. However, the solid supports of the sill beam poses the greatest resistance to both shear and torsion relative to the middle, hollow part of the beam. Therefore, the verification regarding shear and torsion is conducted for both the solid supports and at the interface between the solid support and the hollow part of the sill beam.

It should be noted that load combination A is governing for shear in x-direction and load combination B is governing for shear in z-direction.

Solid supports

$V_{Rd,c,x}$ [kN]	$V_{Rd,c,z}$ [kN]	$V_{Ed,x}$ [kN]	$V_{Ed,z}$ [kN]	$T_{Rd,c}$ [kNm]	$T_{Ed,A}$ [kNm]	$T_{Ed,B}$ [kNm]	UC_x [-]	UC_z [-]
48059	48059	3153	8059	82233	-4642	-1445	0.12	0.19

Table XV.29: Shear and torsion verification sill beam

Interface

$V_{Rd,c,x}$ [kN]	$V_{Rd,c,z}$ [kN]	$V_{Ed,x}$ [kN]	$V_{Ed,z}$ [kN]	$T_{Rd,c}$ [kNm]	$T_{Ed,A}$ [kNm]	$T_{Ed,B}$ [kNm]	UC_x [-]	UC_z [-]
31801	12038	2866	7209	82233	-4221	-1293	0.20	0.63

Table XV.30: Shear and torsion verification sill beam

XV.4.4 Spalling Reinforcement

The pre-stressing force is introduced through the 8 ducts into the solid supports of the sill beam. The introduction through the 8 ducts is already somewhat distributed due to the duct spacing. Nonetheless, conservatively, it is assumed here that the total pre-stressing force is introduced at the centre of gravity of the hollow part of the sill beam. Local spalling reinforcement should be in place in order to account for the local tension stresses until the introduced load is spread evenly throughout the cross-section.

X-direction

Figure XV.22 depicts the introduction of the pre-stressing force (after immediate losses) and the reaction forces from the concrete cross-section to make equilibrium. Figure XV.23 presents the strut and tie model with which the local tension force is determined. A compression force is depicted in blue and a tension force in red in Figure XV.23.

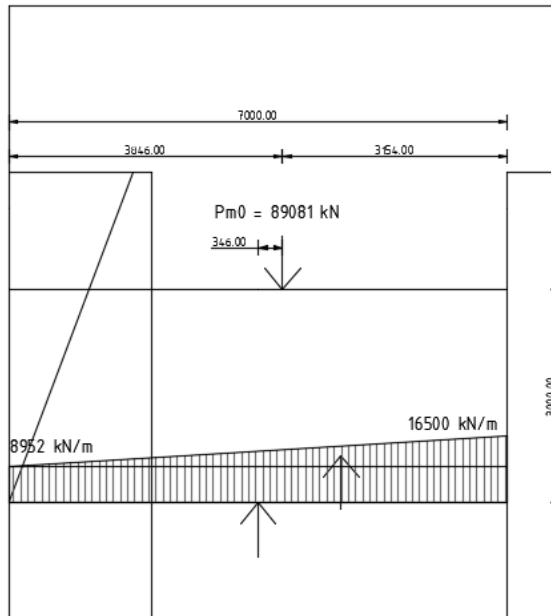


Figure XV.22: Reaction forces

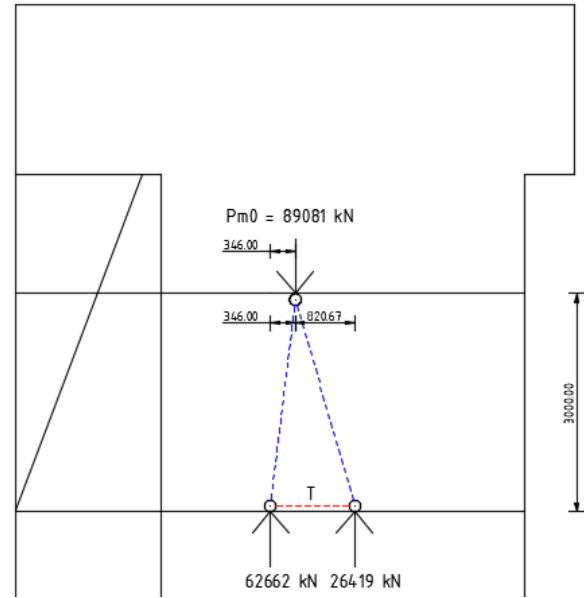


Figure XV.23: Strut and tie model

Subsequently, the local tension force is calculated as follows:

$$T = \frac{821}{3000} \cdot 26419 = 7230 \text{ kN}$$

Note that the established tension forces could be taken up by both rebar and pre-stressing steel. As the available space does not allow for transverse pre-stressing, the amount of rebar needed to withstand the tension forces is calculated by means of Equation (XV.19).

$$A_{s,i} = \frac{T_i}{f_{ys}} \tag{XV.19}$$

A_s
$[mm^2]$
16621

Table XV.31: Required spalling reinforcement

The calculated required rebar in Table XV.31 is to be distributed over the entire height of the sill beam.

Z-direction

Figure XV.24 depicts the introduction of the pre-stressing force (after immediate losses) and the reaction forces from the concrete cross-section to make equilibrium. Figure XV.25 presents the strut and tie model with which the local tension force is determined. A compression force is depicted in blue and a tension force in red in Figure XV.25.

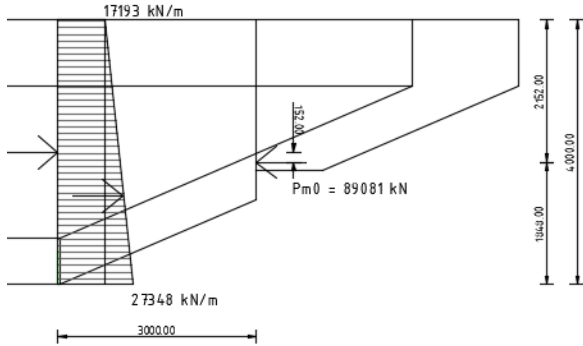


Figure XV.24: Reaction forces

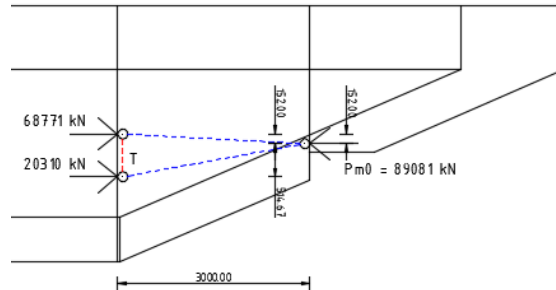


Figure XV.25: Strut and tie model

Subsequently, the local tension force is calculated as follows:

$$T = \frac{515}{3000} \cdot 20310 = 3487 \text{ kN}$$

Note that the established tension forces could be taken up by both rebar and pre-stressing steel. As the available space does not allow for transverse pre-stressing, the amount of rebar needed to withstand the tension forces is again calculated by means of Equation (XV.19).

A_s
[mm ²]
8016

Table XV.32: Required spalling reinforcement

The calculated required rebar in Table XV.32 is to be distributed over the entire width of the sill beam.

XV.4.5 Deflection

The maximum deflection of the sill beam should satisfy both Equation (XV.20a) and Equation (XV.20b), as stated by Vrijburcht (2000).

$$w_{max,x} \leq \frac{1}{200} L_x = 165 \text{ mm} \tag{XV.20a}$$

$$w_{max,z} \leq \frac{1}{200} L_z = 142 \text{ mm} \tag{XV.20b}$$

where: $w_{max,x}$ [mm] = maximum deflection of the sill beam in x-direction
 $w_{max,z}$ [mm] = maximum deflection of the sill beam in z-direction
 L_x [mm] = length of the sill beam between two supports for deflection around the z-axis = 33042.5
 L_z [mm] = length of the sill beam between two supports for deflection around the y-axis = 28438

Conservatively, $w_{max,i}$ is calculated using the general forget-me-not for a pinned-pinned beam under a distributed load according to Equation (XV.21).

$$w_{max,i} = \frac{5}{384} \frac{q_{Ed,i} L^4}{EI_{ii}} \quad (\text{XV.21})$$

E [N/mm²] = Youngs modulus
 I_{ii} [mm⁴] = mass moment of inertia in either x- or z-direction

This yields, $w_{max,x} = 0.64 \text{ mm} \leq 165 \text{ mm}$ and $w_{max,z} = 4.34 \text{ mm} \leq 142 \text{ mm}$. Note that the sill beam is assumed to be in uncracked state, as to be expected after post-tensioning.

XV.5 Pier

The strength verification of the piers is conducted by means of a global analysis. Most forces on the piers are introduced locally, these are the loads transferred by the elements connected to the piers. Said elements are: the driving mechanisms supports, gates, top beams, bridge girders and sill beams. For the loads transferred by these elements, from a flow of forces approach, strut and tie models are made in order to determine the tension forces and required reinforcement. Throughout the analysis, the pier is considered as a so-called 'deep beam', as the width of the pier far exceeds one third of the height.

XV.5.1 Flow of Forces

Here, the flow of forces are presented for the relevant load combinations considering the locally introduced loads from the established elements only. From the flow of forces, the locations where reinforcement is needed are identified.

A: Maximum positive head is dominant

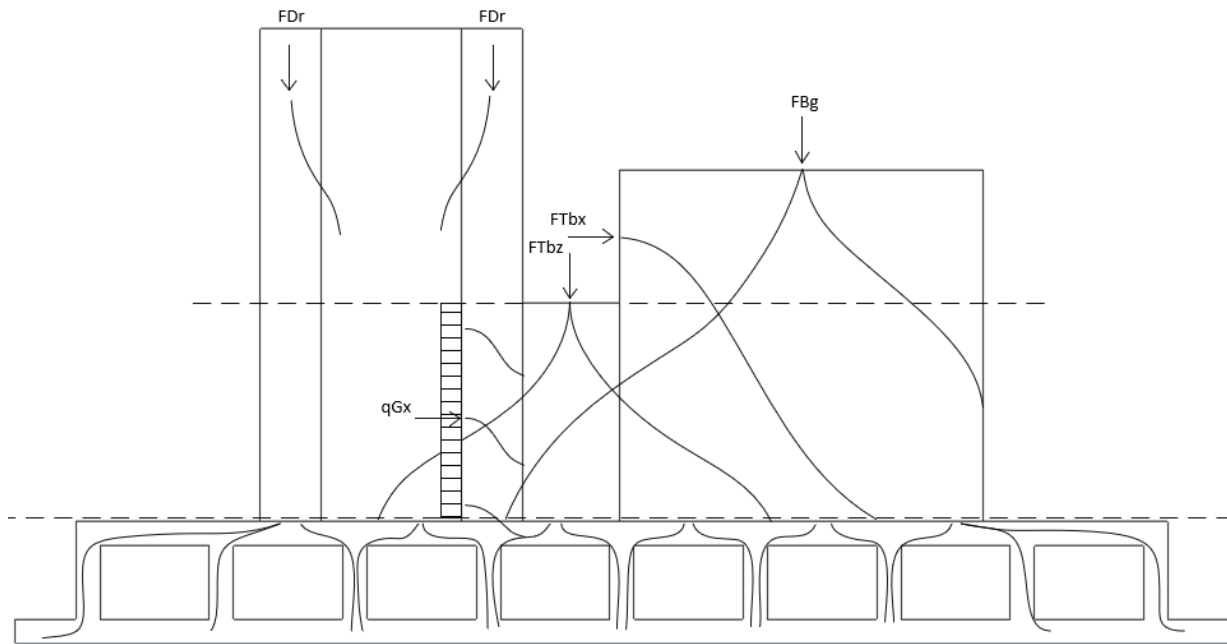


Figure XV.26: Flow of forces through the pier

F_{Dr}	1823	kN
q_{Gx}	2914	kN/m
F_{Tbx}	19598	kN
F_{Tbz}	38262	kN
F_{Bg}	16376	kN

Table XV.33: External forces, design values

- F_{Dr} = loads from driving mechanisms supports
- q_{Gx} = distributed load from gates in x-direction
- F_{Tbx} = loads from top beams in x-direction
- F_{Tbz} = loads from top beams in z-direction
- F_{Bg} = loads from bridge girders

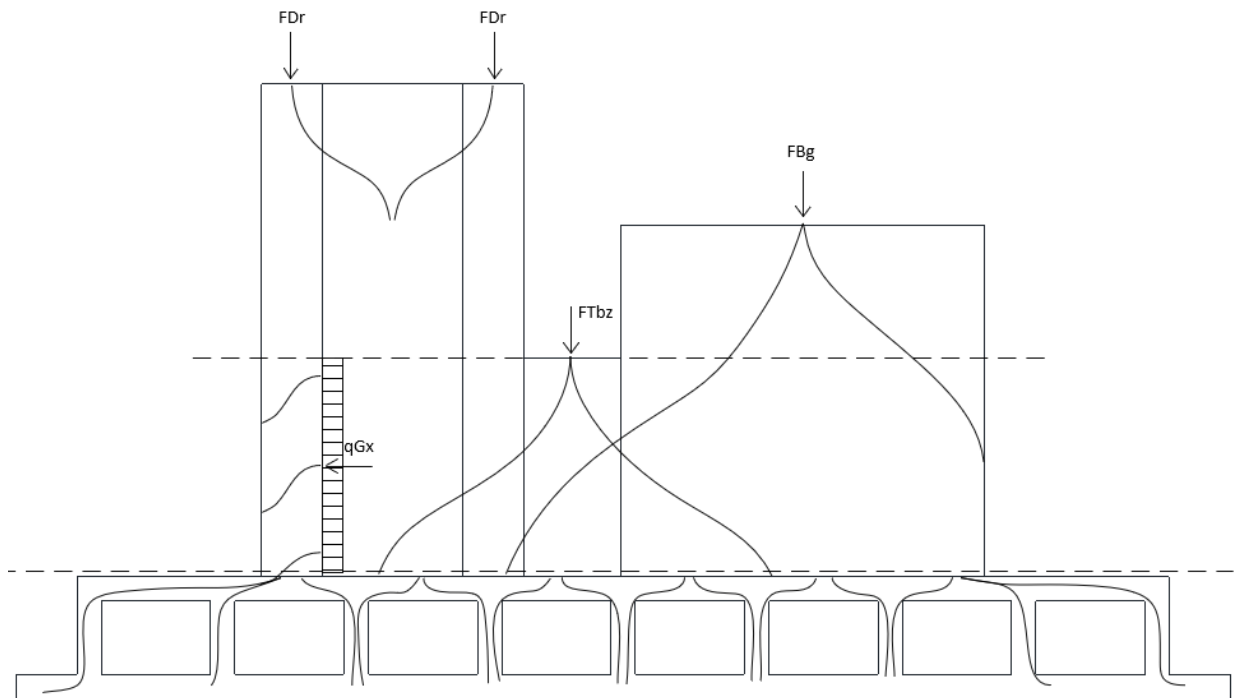
B: Maximum negative head is dominant

Figure XV.27: Flow of forces through the pier

F_{Dr}	1823	kN
q_{Gx}	633	kN/m
F_{Tbz}	34942	kN
F_{Bg}	16376	kN

Table XV.34: External forces, design values

F_{Dr} = loads from driving mechanisms supports

q_{Gx} = distributed load from gates in x-direction

F_{Tbz} = loads from top beams in z-direction

F_{Bg} = loads from bridge girders

H: Ship Collision

The load combination considering ship collision is not governing over load combinations A and B.

XV.5.2 Global Analysis Reinforcement Plan

From the flow of forces, the locations where reinforcement is required is identified. Subsequently, the global analysis is conducted for every established reinforcement location (A₁ to A₁₉) as presented in the figures below.

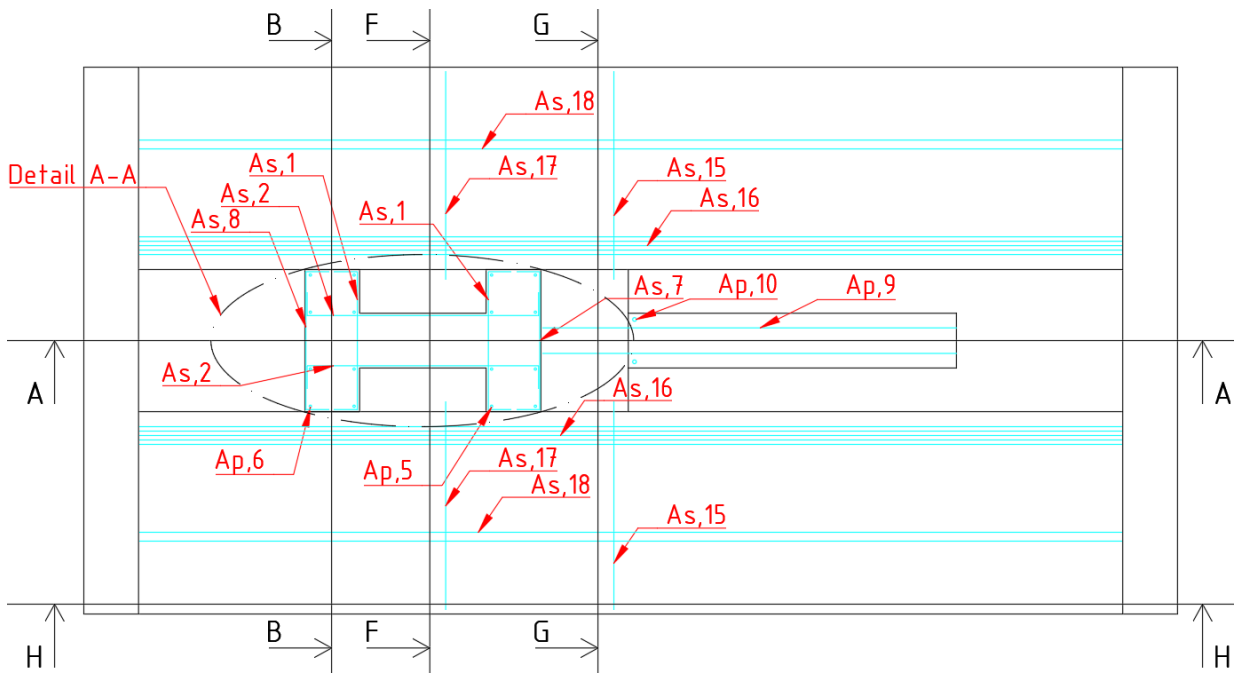


Figure XV.28: Reinforcement plan, top view

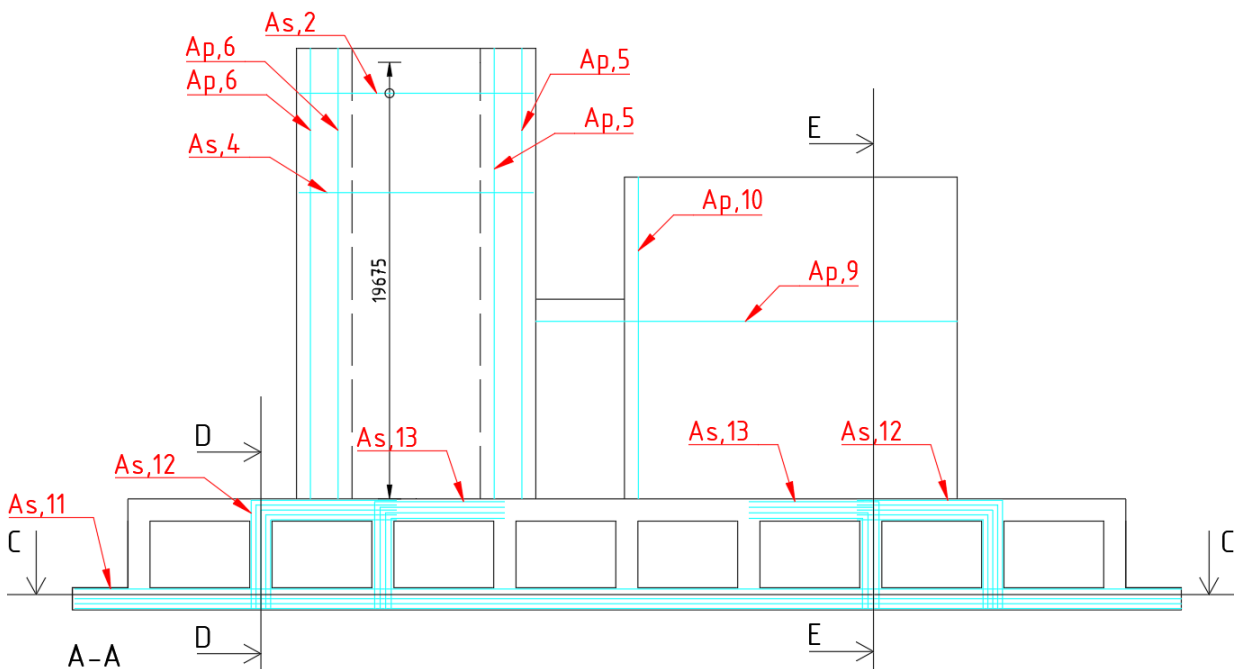


Figure XV.29: Reinforcement plan, A-A

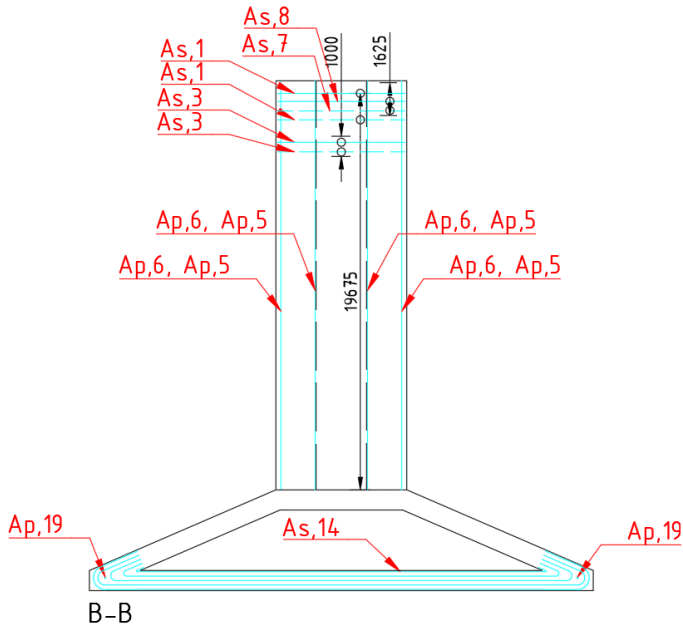


Figure XV.30: Reinforcement plan, B-B

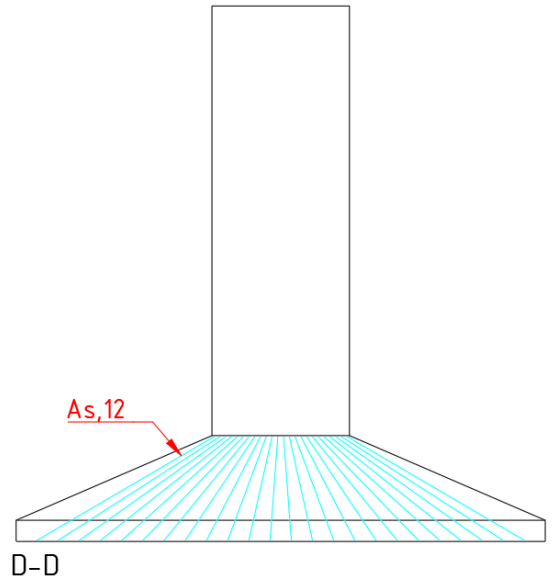


Figure XV.31: Reinforcement plan, D-D

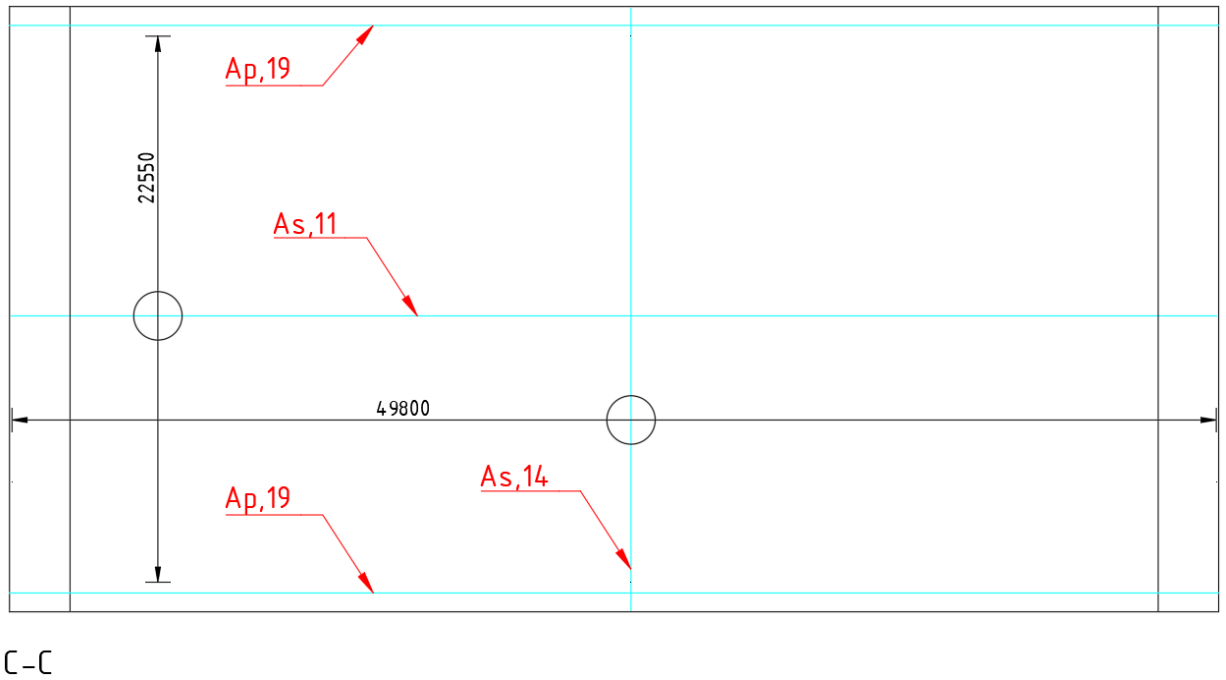


Figure XV.32: Reinforcement plan, C-C

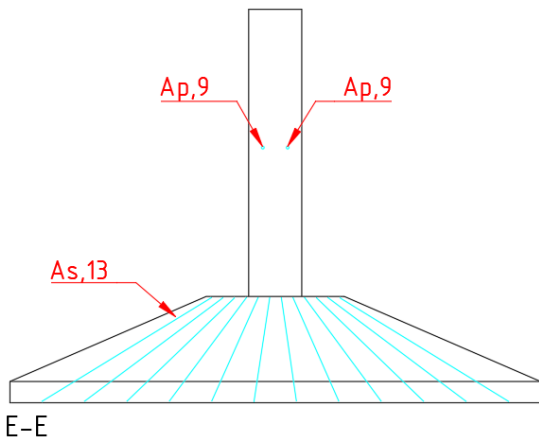


Figure XV.33: Reinforcement plan, E-E

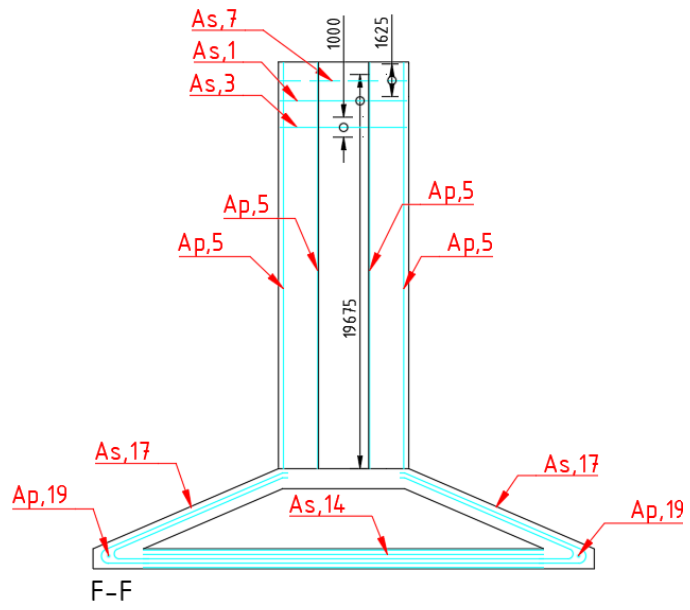


Figure XV.34: Reinforcement plan, F-F

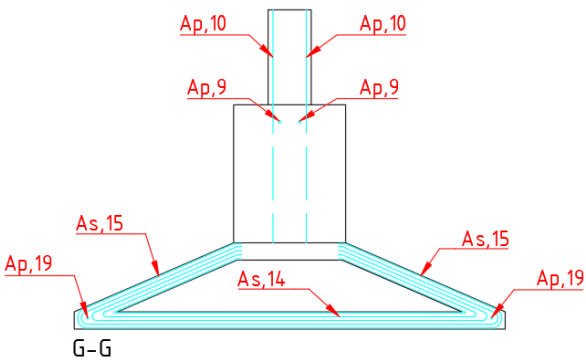


Figure XV.35: Reinforcement plan, G-G

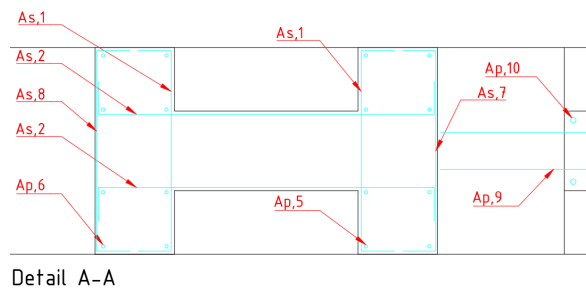


Figure XV.36: Reinforcement plan, detail A-A

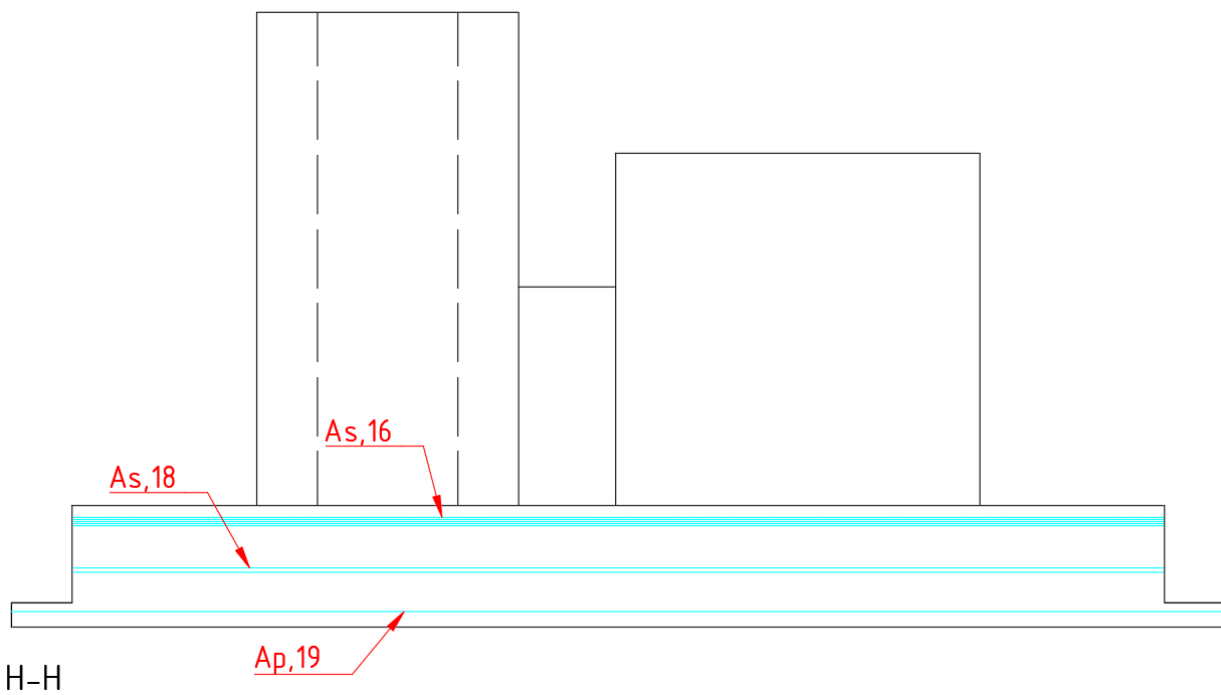


Figure XV.37: Reinforcement plan, H-H

A₁ & A₂

The distributed load transferred from the gates to the lift shaft (q_{Gx}) are introduced at the flanges of the I-shaped shaft and are to be transferred to the web of the shaft. Figure XV.38 presents the strut and tie model regarding the loads transferred from the gates in a top view of the lift shaft. It should be noted that load combination A results in the greatest load to be transferred.

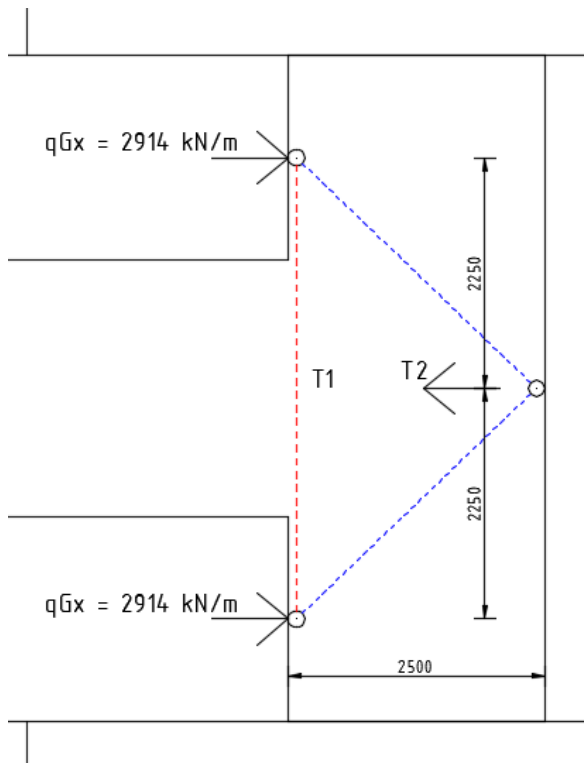


Figure XV.38: A₁ & A₂: strut and tie model

In order to make equilibrium:

$$T_1 = \frac{2250}{2500} \cdot 2914 = 2623 \text{ kN/m}$$

$$T_2 = 2 \cdot 2914 = 5828 \text{ kN/m}$$

The amount of rebar needed to withstand the tension forces is calculated by means of Equation (XV.22).

$$A_{s,i} \geq \frac{T_i}{f_{ys}} \quad (\text{XV.22})$$

	$A_{s,i} [mm^2/m]$	$\theta [mm]$	$s [mm]$
1.	6434	32	125
2.	12868	2x32	125

Table XV.35: A₁ & A₂: applied reinforcement

The reinforcement as presented in Table XV.35 are to be placed per metre height of the lift shaft.

A₃ & A₄

The driving mechanisms supports with the driving mechanisms rest on the lift shaft. The driving mechanisms supports are situated on the flanges of the shaft and the forces (F_{Dr}) are to be transferred throughout the entire cross-section, i.e. also to the webs. Figure XV.39 presents the reaction forces in the lift shaft and Figure XV.40 presents the strut and tie model regarding the loads transferred from the driving mechanisms supports per flange.

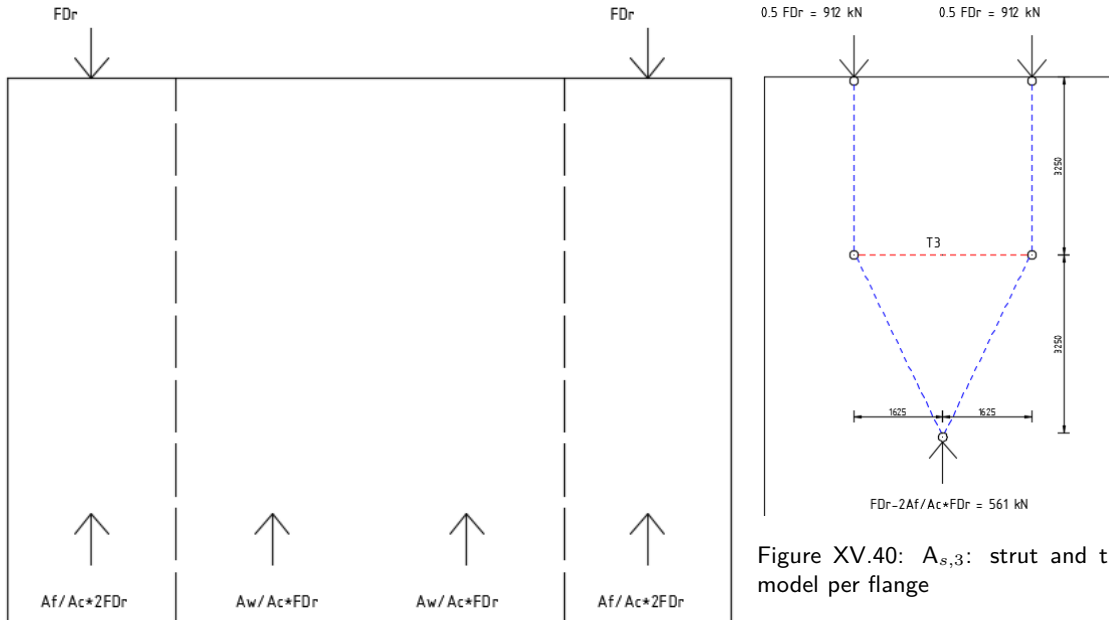


Figure XV.39: $A_{s,3}$: reaction forces

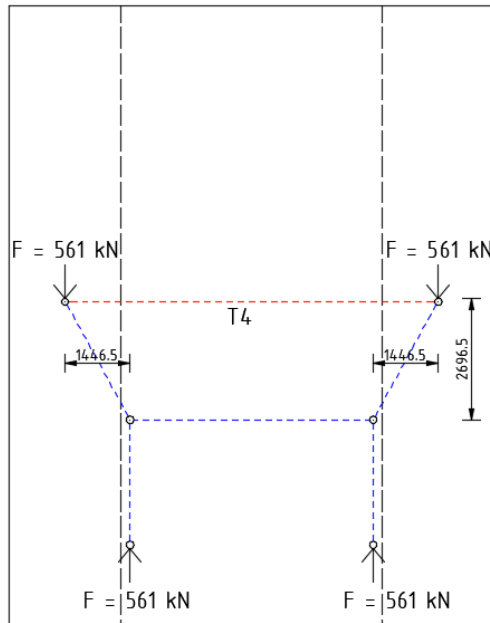
Figure XV.40: $A_{s,3}$: strut and tie model per flange

In order to make equilibrium, taking into account the reaction forces from Figure XV.39:

$$\begin{aligned}
 T_3 &= \frac{1}{4} \left(1 - 2 \cdot \frac{A_f}{A_c} \right) \cdot F_{Dr} \\
 &= \frac{1}{4} \left(1 - 2 \cdot \frac{16.25}{46.965} \right) \cdot 1823 \\
 &= 140 \text{ kN}
 \end{aligned}$$

where: A_f [m²] = area of the flange of the shaft
 A_c [m²] = total area of the lift shaft

Finally, Figure XV.41 presents the strut and tie model for the introduction of the forces from the flanges into the web. Note that the force transfer occurs for both flanges.



In order to make equilibrium:

$$T_4 = \frac{1446.5}{2696.5} \cdot 561 = 301 \text{ kN}$$

The amount of rebar needed to withstand the tension forces is calculated by means of Equation (XV.22).

	$A_{s,i} [mm^2]$	n	$\theta [mm]$	$s [mm]$
3.	339	3	12	300
4.	806	4	16	250

Table XV.36: A_3 & A_4 : applied reinforcement

Figure XV.41: $A_{s,4}$: strut and tie model per flange

As the lift shaft consists of two flanges, the applied reinforcement presented in Table XV.36 is per flange. Furthermore, as opposed to the reinforcement at location 1 and 2, A_3 and A_4 are to be applied only locally and should be applied over a height of 1 metre at the respective locations.

A_5 & A_6

The reinforcement at locations 5 and 6 are necessary to withstand tension stresses induced by the bending moments in the lift shaft for the load combinations A and B respectively. The total bending moment in the lift shaft is calculated for both load combinations. The external hydrostatic and wave forces directly on the pier are presented in Appendix XVI.1 for both load combinations. Only the concluding bending moments as a result of said external forces and loads transferred from the gates are presented here.

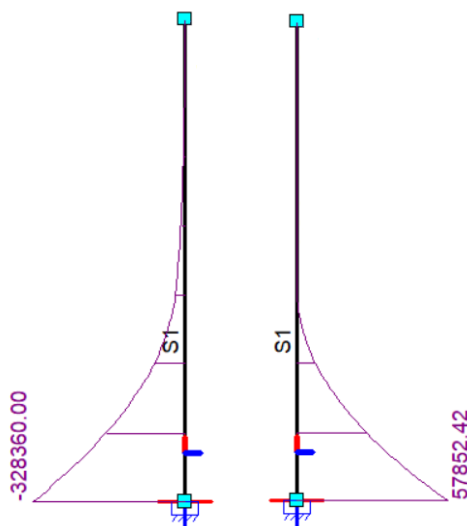


Figure XV.42: A. Moment line lift shaft [kNm] Figure XV.43: B. Moment line lift shaft [kNm]

The tension forces as a result of the occurring bending moment can be calculated by means of Equation (XV.23):

$$N_i = \frac{M_{Ed,i}}{z} \tag{XV.23}$$

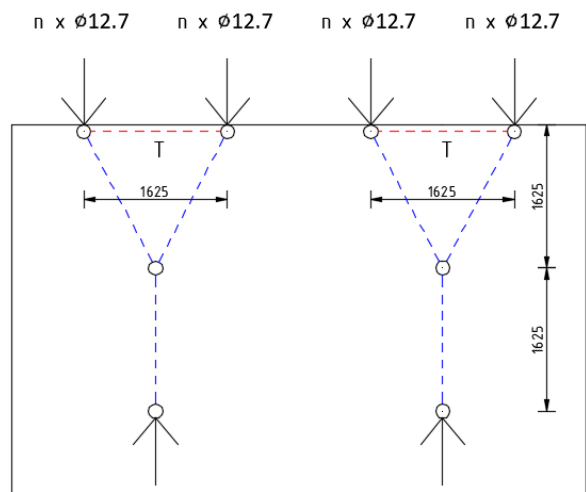
The amount of reinforcement needed to withstand the tension forces is again calculated by means of Equation (XV.22). As for the flanges of the lift shaft, it is chosen to apply pre-stressing tendons Y1860 instead of traditional rebar.

	$N_i [kN]$	$A_{p,i} [mm^2]$	ducts	strands	$\theta [mm]$	$\sigma_{m\infty} [N/mm^2]$
5.	39628	36482	8	36	12.7	1200
6.	6982	7094	8	7	12.7	1200

Table XV.37: A_5 & A_6 : applied reinforcement

A₇ & A₈

The introduction of the pre-stressing forces cause tension stresses in the flanges of the lift shaft. Figure XV.44 presents the general strut and tie model to determine the tension force and required spalling reinforcement.



In order to make equilibrium:

$$T = \frac{0.5 \cdot 1625}{1625} \cdot (strands \cdot \frac{1}{4} \cdot \pi \cdot 12.7^2) \cdot 1200$$

The amount of rebar needed to withstand the tension forces is calculated by means of Equation (XV.22).

	T_i [kN]	$A_{s,i}$ [mm ²]	n	θ [mm]	s [mm]
7.	2736	6434	8	32	200
8.	532	1257	4	20	400

Table XV.38: A₇ & A₈: applied reinforcement

Figure XV.44: A₇ & A₈: strut and tie model per flange

As the pre-stressing forces are introduced at two lines in the flange of the lift shaft, the applied reinforcement presented in Table XV.38 should be placed in two lines. Furthermore, A₇ and A₈ are to be applied only locally and should be applied over a height of 1.625 metre at the respective locations. It should be noted that A₇ and A₈ are to be placed additional to A₁ in both flanges as well.

A₉ & A₁₀

The bridge girders and the top beams transfer load to their respective supports on the piers. These loads are, again, introduced locally and strut and tie models are made for the respective elements.

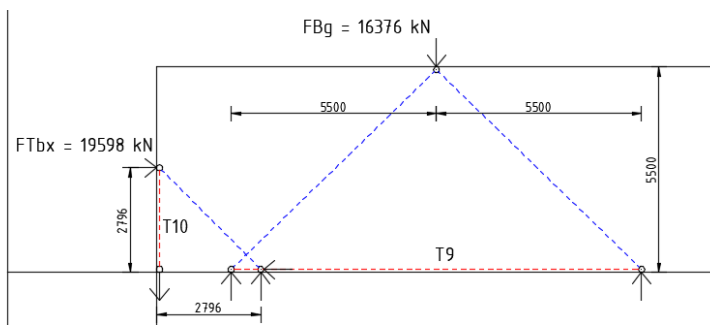


Figure XV.45: A_{s,9} & A_{s,10}: strut and tie model

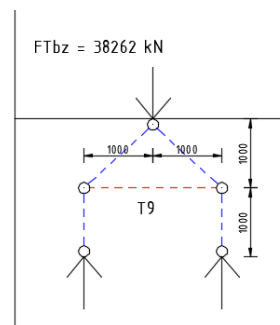


Figure XV.46: A_{s,9}: strut and tie model

Comparing Figure XV.45 and Figure XV.46, it can be seen that the vertical load transferred by the top beam (F_{Tbz}) far exceeds the vertical load transferred by the bridge girders (F_{Bg}). Therefore, for the reinforcement needed at location 9, the vertical force transferred by the top beam is governing.

In order to make equilibrium:

$$T_9 = 0.5 \cdot \frac{1000}{1000} \cdot 38262 = 19131 \text{ kN}$$

$$T_{10} = 19598 \text{ kN}$$

The amount of reinforcement needed to withstand the tension forces is calculated by means of Equation (XV.24). Due to the large locally introduced forces, it is chosen to apply pre-stressing tendons Y1860 instead of traditional rebar.

$$A_{p,i} \geq \frac{T_i}{f_{pk}} \tag{XV.24}$$

	$A_{p,i} \text{ [mm}^2\text{]}$	ducts	strands	$\theta \text{ [mm]}$	$\sigma_{m\infty} \text{ [N/mm}^2\text{]}$
9.	21295	2	55	15.7	1200
10.	21295	2	55	15.7	1200

Table XV.39: A_9 & A_{10} : applied reinforcement

A_{11} , A_{12} , A_{13} & A_{14}

The pier foot is to resist the reaction forces from the subsoil. The reaction forces from the subsoil are calculated according to Equation (XV.25). The complete bearing capacity verification is conducted in Appendix XVI.2.2.

$$\sigma_k = \frac{\sum V}{B L} + \frac{\sum M}{\frac{1}{6} B^2 L} \tag{XV.25}$$

where: $\sigma_k \text{ [kN/m}^2\text{]}$ = soil stress
 $B \text{ [m]}$ = width of the structure (parallel to the resultant horizontal force) = 50
 $L \text{ [m]}$ = length of the structure (perpendicular to the resultant horizontal force) = 25

Figure XV.47 and Figure XV.48 present the reaction forces from the subsoil on the pier foot for load combination A and B, respectively.

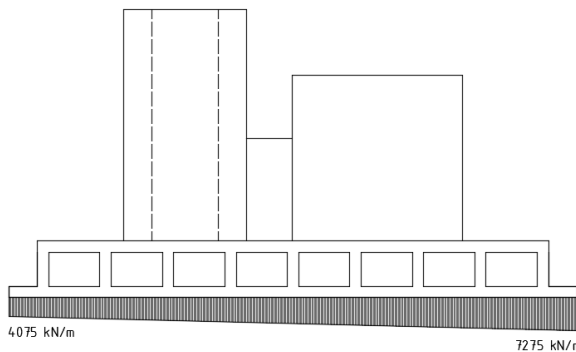


Figure XV.47: A. Reaction forces pier foot

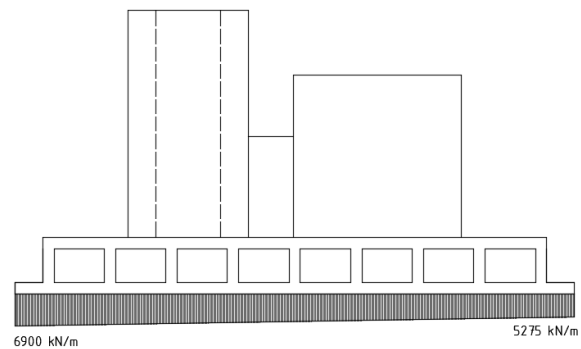


Figure XV.48: B. Reaction forces pier foot

From Figure XV.47 and Figure XV.48 it can be seen that the reaction forces under the pier foot and the allocation of the maximum soil pressure depend on the load combination considered. Conservatively, for further calculations regarding the strength of the pier foot, the maximum soil pressure is assumed to act over the entire pier foot as depicted in Figure XV.49. Additionally, Figure XV.49 presents the strut and tie model regarding the load transfer from the piers to the subsoil and Figure XV.50 presents the Matrixframe calculation of the forces in the assumed struts and ties.

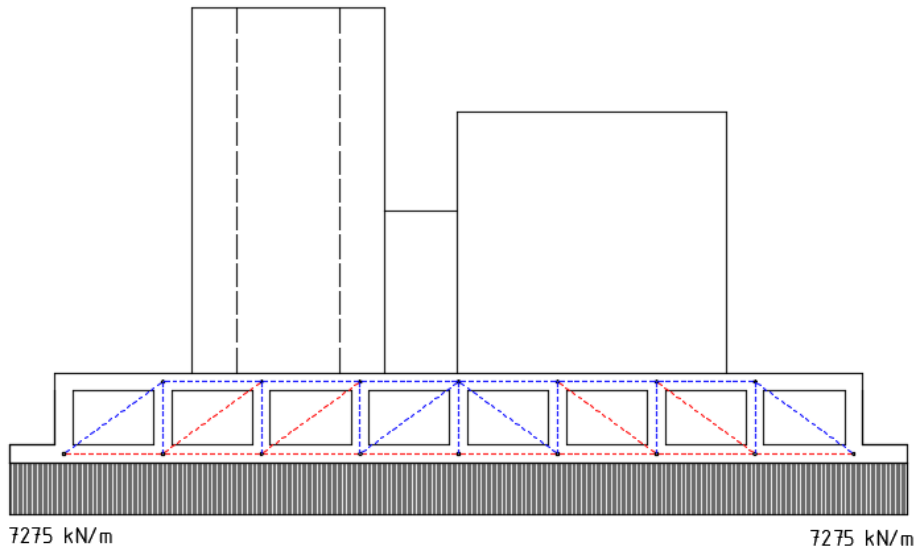


Figure XV.49: Strut and tie model pier foot

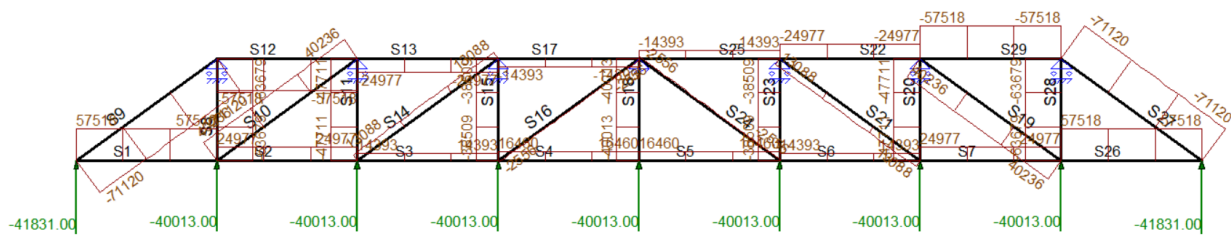


Figure XV.50: Strut and tie model pier foot Matrixframe

Finally, Table XV.40 presents all ties (elements in which a tension force occurs) for the established strut and tie model. Furthermore, the required reinforcement ($A_{s,req}$), the applied reinforcement ($A_{s,app}$), the number of applied bars (n) in both x- and z-direction, the applied rebar diameter (θ) and the spacing of rows of the applied rebar (s) in both x- and z-direction are presented in Table XV.41.

Element	N_{Ed} [kN]	$A_{s,req}$ [mm ²]
S1	57518	132225
S2	24977	57418
S3	14393	33087
S4	16460	37839
S5	16460	37839
S6	14393	33087
S7	24977	57418
S8	57518	132225
S10	40236	92497
S14	13088	30087
S19	13088	30087
S21	40236	92497

Table XV.40: A_{11} , A_{12} , A_{13} : longitudinal ties in pier foot model

Note that for the reinforcement needed in the floor of the pier foot, the governing required amount of reinforcement is applied over the entire length of the floor (A_{11}) for practical reasons. Furthermore, the reinforcement needed in the diagonal ties (S10, S14, S19 and S21) are to be placed in the dividing

walls (A_{12} and A_{13}).

	$A_{s,app} [mm^2]$	n_y	n_z	$\theta [mm]$	$s_y [mm]$	$s_z [mm]$
11.	135114	42	4	32	550	220
12.	96510	24	5	32	275	220
13.	38604	12	4	32	550	250

Table XV.41: A_{11} , A_{12} , A_{13} : applied reinforcement

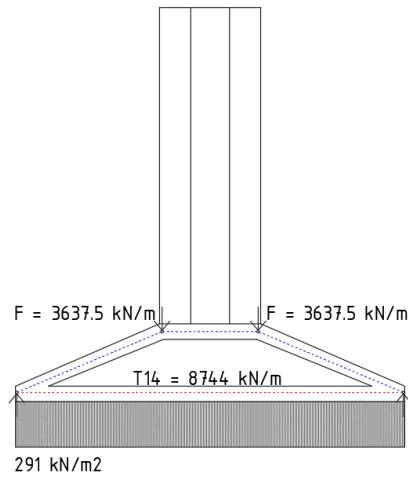


Figure XV.51: A_{14} : strut and tie model

Figure XV.51 presents the strut and tie model regarding the transfer of the loads from the pier to the subsoil in transversal direction. Table XV.42 presents the required reinforcement ($A_{s,req}$), the applied reinforcement ($A_{s,app}$), the number of applied bars (n) in both y - and z -direction, the applied rebar diameter (θ) and the spacing of rows of the applied rebar (s) in both y - and z -direction for the rebar at location 14 in the floor of the pier foot.

	$A_{s,req} [mm^2]$	$A_{s,app} [mm^2]$	n_y	n_z	$\theta [mm]$	$s_y [mm]$	$s_z [mm]$
14.	1005057	1005310	250	5	32	200	220

Table XV.42: A_{14} : applied reinforcement

A_{15} , A_{16} , A_{17} , A_{18} & A_{19}

Finally, the pier foot is to resist the locally introduced forces transferred by the sill beam. Said forces are depicted in Figure XV.52 and Figure XV.53.

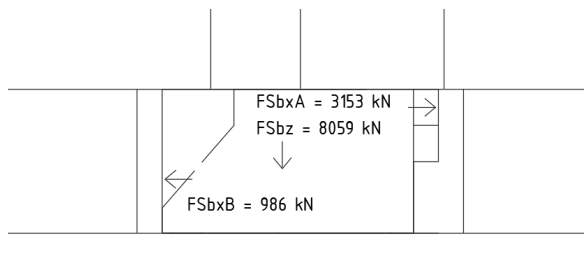


Figure XV.52: Introduced forces sill beam, side view

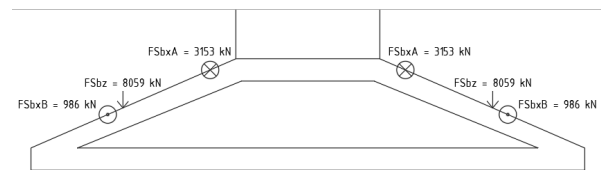


Figure XV.53: Introduced forces sill beam, front view

From Figure XV.53 it can be seen that half of the pressures acting on a singular sill beam are transferred to the pier at both sides. The walls of the pier foot should be able to accommodate spreading of the locally introduced forces. Figure XV.54 presents the strut and tie model of the pier foot regarding the transfer of the loads from the sill beam to the pier.

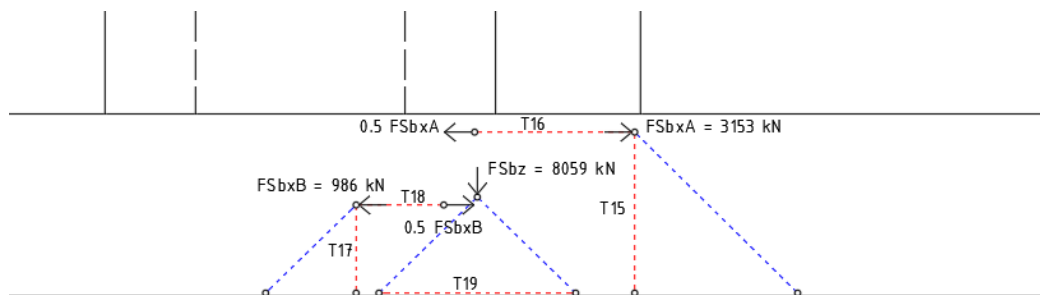


Figure XV.54: Strut and tie model pier foot

It should be noted that both load combination A regarding a maximum positive head (F_{SbxA}) and load combination B regarding a maximum negative head (F_{SbxB}) are considered. Furthermore, the maximum occurring vertical load to be transferred from the sill beam to the pier foot (F_{Sbz}) is considered. Said loads have readily been calculated in Appendix XV.4, considering the strength verification of the sill beams.

In order to make equilibrium:

$$T_{15} = 1576.5 \text{ kN}$$

$$T_{16} = 1576.5 \text{ kN}$$

$$T_{17} = 493 \text{ kN}$$

$$T_{18} = 493 \text{ kN}$$

$$T_{19} = 4029.5 \text{ kN}$$

Table XV.43 presents the required reinforcement ($A_{s,req}$), the applied reinforcement ($A_{s,app}$), the number of applied bars (n), the applied rebar diameter (θ) and the spacing of the applied rebar (s) for the rebar at locations 15, 16, 17, and 18 in the walls of the pier foot.

	$A_{s,req} [mm^2]$	$A_{s,app} [mm^2]$	n	$\theta [mm]$	$s [mm]$
15.	3624	4021	5	32	220
16.	3624	4021	5	32	220
17.	1133	1608	2	32	220
18.	1133	1608	2	32	220

Table XV.43: A_{15} , A_{16} , A_{17} , A_{18} : applied reinforcement

It should be noted that the reinforcement at locations 15, 16, 17 and 18 presented in Table XV.43 should be applied only locally in both walls of the pier foot adjacent to the sill beams.

As for the required reinforcement at location 19 at the intersection between the pier foot walls and floor, it is chosen to apply pre-stressing steel Y1860 instead of traditional rebar due to the relatively large local force to be transferred. Table XV.44 presents the applied pre-stressing steel at location 19. The amount of pre-stressing steel presented in Table XV.44 is to be placed at both intersections between the walls and the floor of the pier foot.

	$A_p [mm^2]$	ducts	strands	$\theta [mm]$	$\sigma_{m\infty} [N/mm^2]$
19.	3678	1	19	15.7	1200

Table XV.44: A_{19} : applied reinforcement

XVI Complete Global Stability Verification

This appendix presents the complete global stability verification of the Delta Barrier. First, all relevant external forces are established and an overview of all forces on the pier per load combination is presented. From said forces (albeit mostly derived from pressures), the resultant horizontal and vertical force and the resulting moment can be calculated for every failure mechanism c.q. verification. For every verification it is determined whether a force acts favourable or unfavourable regarding the specific failure mechanism and partial safety factors are assigned for every force accordingly. Note that only the verification regarding scour of the bed follows a different recipe as the latter requires no knowledge of vertical and horizontal forces. The Excel spreadsheet used to conduct the verifications is available at <http://repository.tudelft.nl/>.

XVI.1 External Forces

Hydrostatic forces

See Appendix XIV.1.

Wave forces

See Appendix XIV.1.

Drag & lift forces

See Appendix XIV.1.

Drag and lift forces are neglected in the global stability verification as said forces are negligible compared to e.g. hydrostatic and wave forces.

Ship collision

See Appendix XIV.1.

Soil pressures

See Appendix XV.2.

Wind loads

See Appendix XV.2.

Wind loads are neglected in the global stability verification as said loads are negligible compared to e.g. hydrostatic and wave forces.

Overview of forces

Here, an overview of forces (or pressures) is presented for every load combination considered. Furthermore, all numbered vertical and horizontal forces are quantified and tabulated.

- A: Maximum positive head is dominant

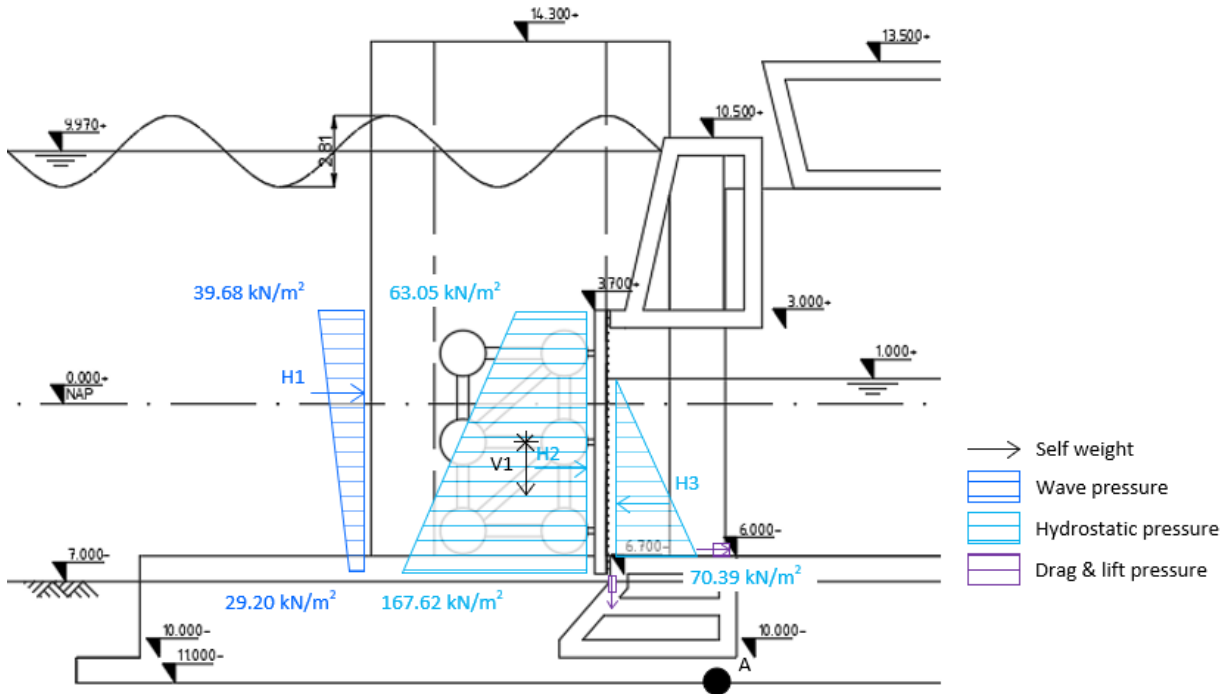


Figure XVI.1: Forces on the gate for load combination A

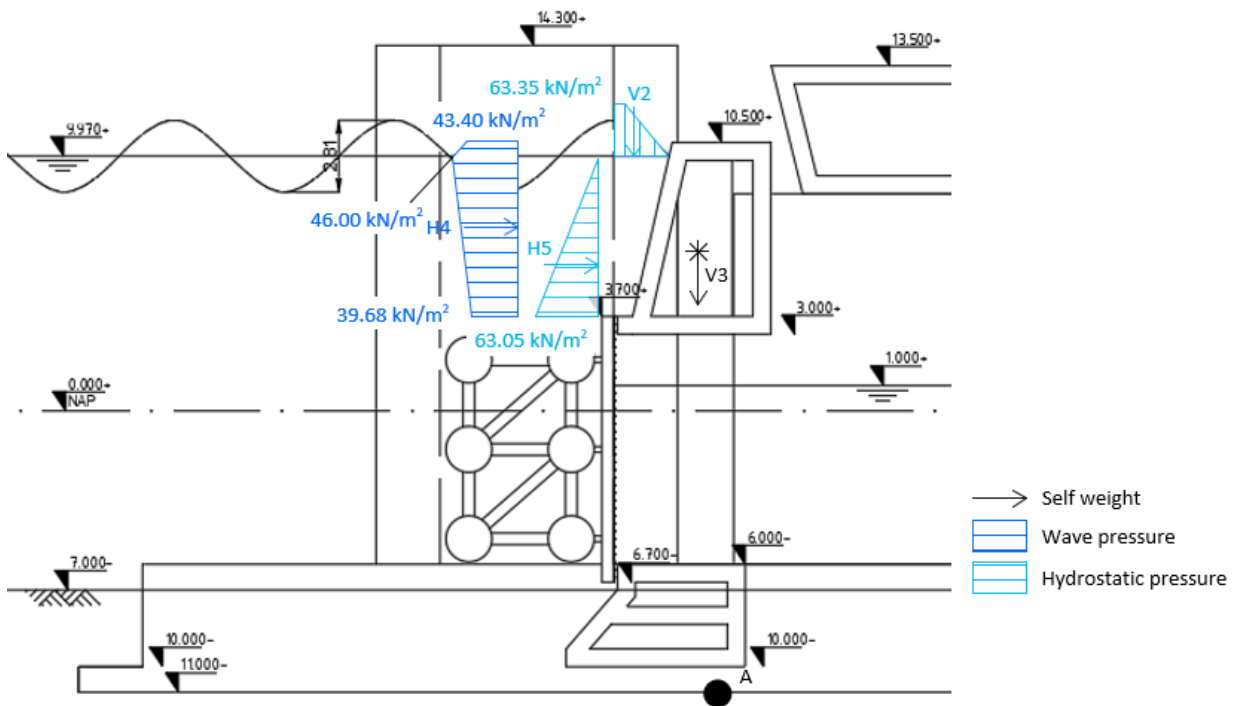


Figure XVI.2: Forces on the top beam for load combination A

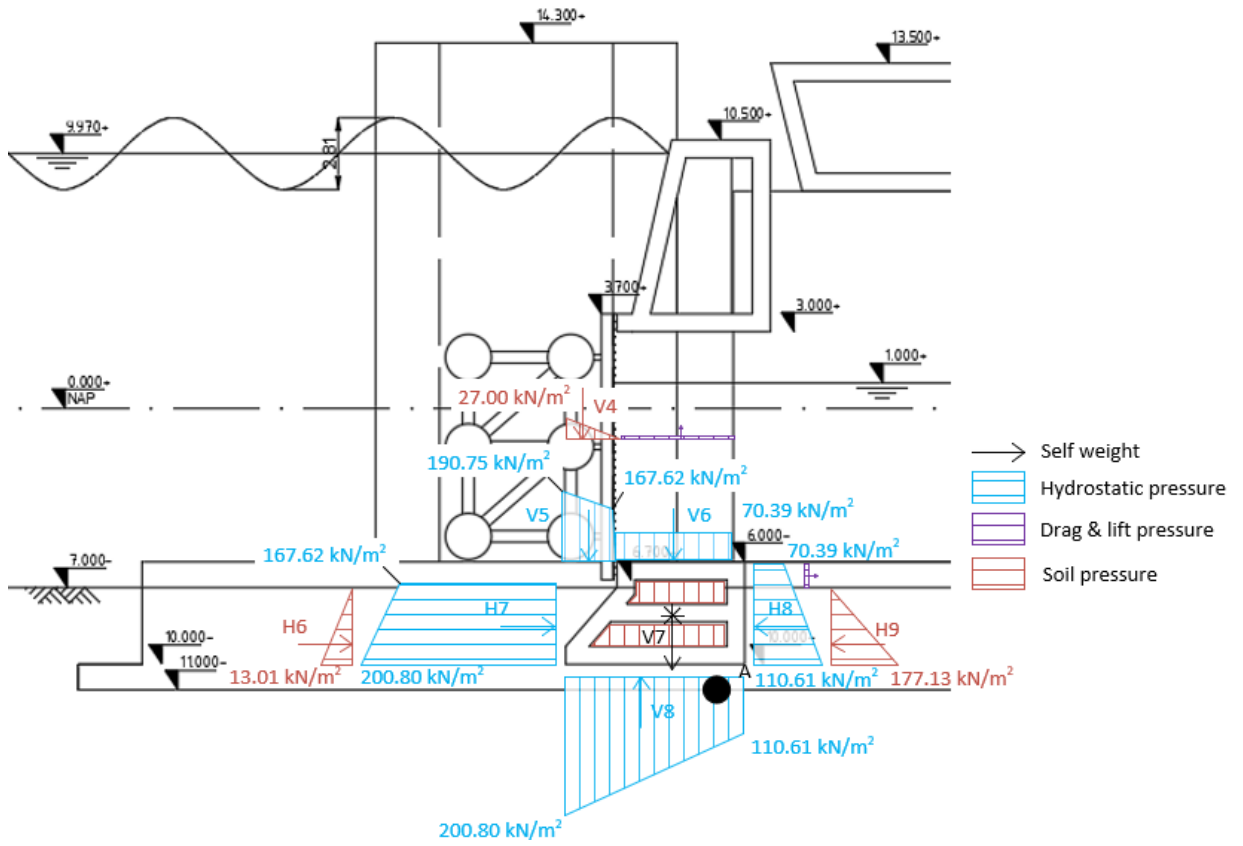


Figure XVI.3: Forces on the sill for load combination A

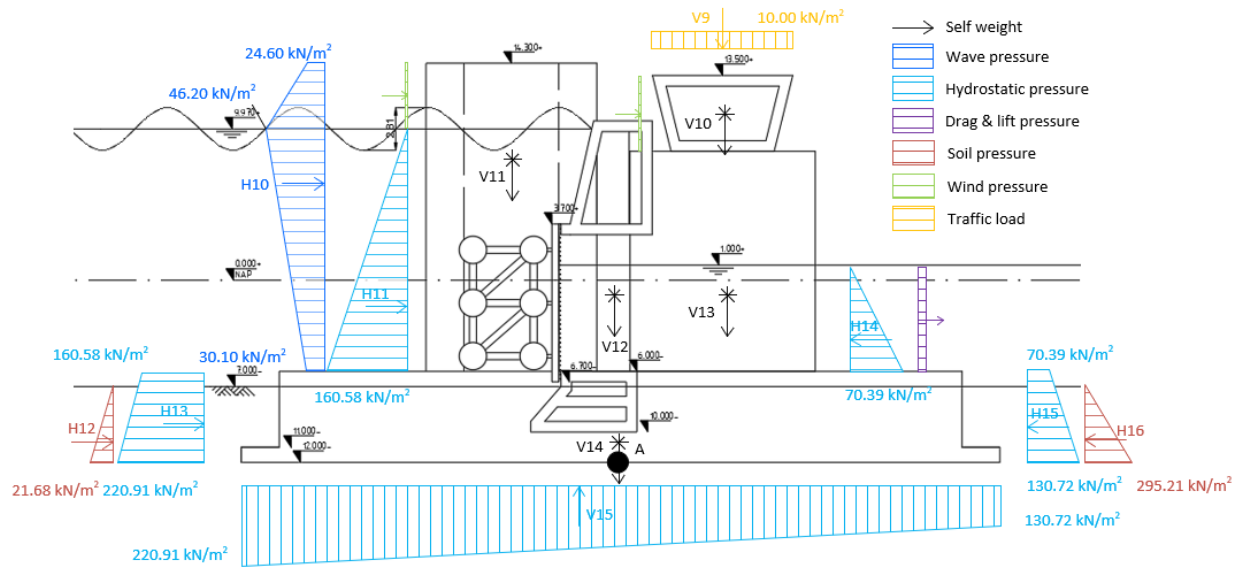


Figure XVI.4: Forces on the pier for load combination A (1)

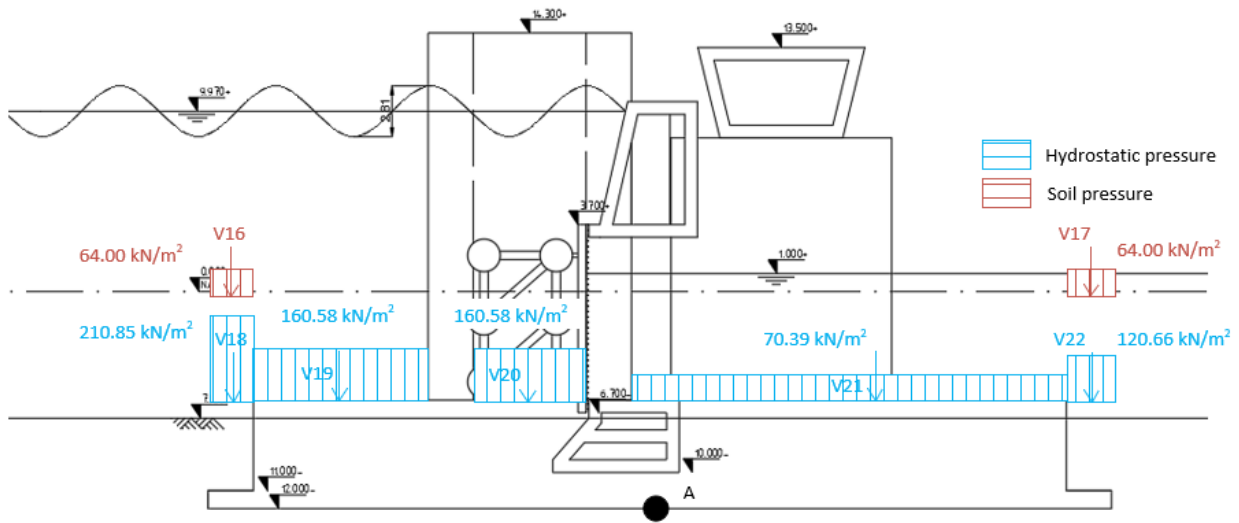


Figure XVI.5: Forces on the pier for load combination A (2)

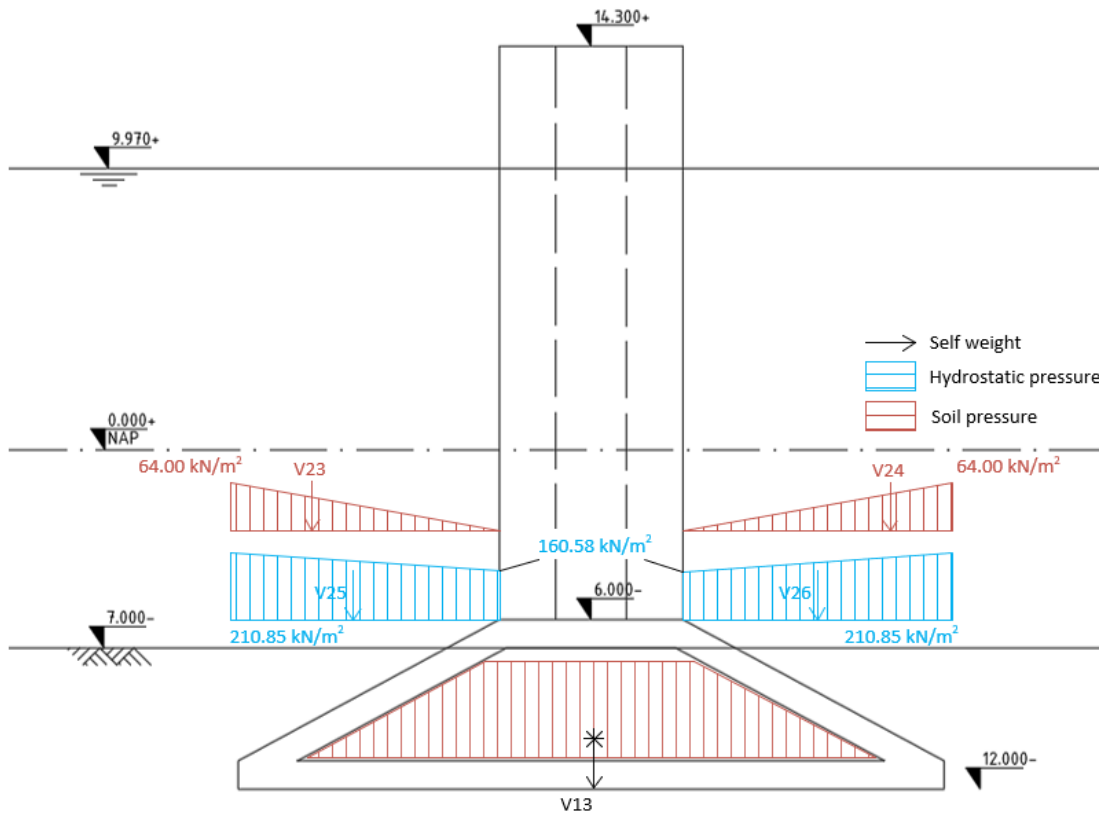


Figure XVI.6: Forces on the pier for load combination A (3)

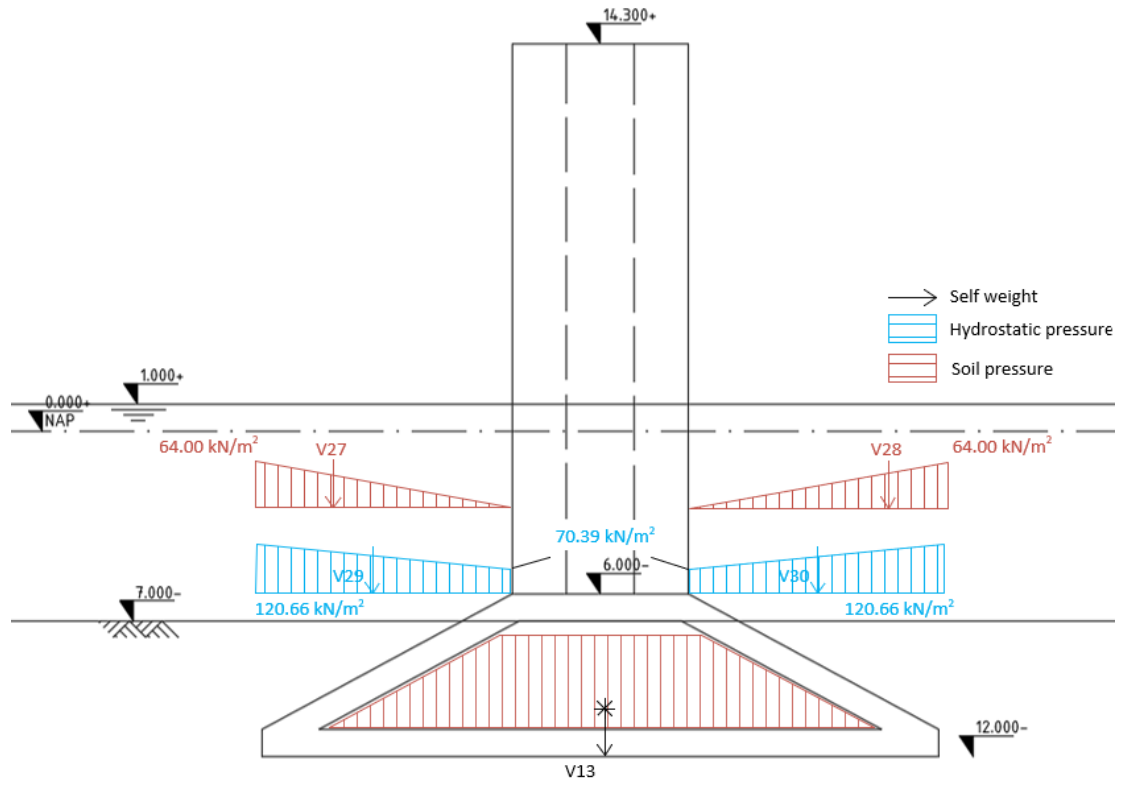


Figure XVI.7: Forces on the pier for load combination A (4)

The characteristic forces as indicated in the figures above for load combination A are tabulated in Table XVI.1 and Table XVI.2 with corresponding distances from the point of action to point A (arms). Vertical loads are positive downwards and horizontal loads are defined positive to the right. Arms are defined as such that clockwise moments are positive and anti-clockwise moments are negative.

V1	9526	kN	e	-7.47	m
V2	3320	kN	e	-3.20	m
V3	25883	kN	e	-0.51	m
V4	680	kN	e	-5.25	m
V5	9031	kN	e	-4.94	m
V6	14078	kN	e	-3.92	m
V7	11121	kN	e	-2.08	m
V8	-24197	kN	e	-2.52	m
V9	8231	kN	e	6.73	m
V10	12130	kN	e	6.73	m
V11	34503	kN	e	-7.47	m
V12	1238	kN	e	-0.47	m
V13	11056	kN	e	6.73	m
V14	126383	kN	e	0	m
V15	-207201	kN	e	-2.27	m
V16	3000	kN	e	-23.75	m
V17	3000	kN	e	23.75	m
V18	12550	kN	e	-23.75	m
V19	5871	kN	e	-17.93	m
V20	7087	kN	e	-7.47	m
V21	12148	kN	e	9.23	m
V22	6913	kN	e	23.75	m
V23	2761	kN	e	-14.21	m
V24	2761	kN	e	-14.21	m
V25	28483	kN	e	-14.21	m
V26	28483	kN	e	-14.21	m
V27	3566	kN	e	11.79	m
V28	3566	kN	e	11.79	m
V29	18927	kN	e	11.79	m
V30	18927	kN	e	11.79	m
ΣV	193825	kN			

Table XVI.1: Characteristic vertical forces with arms

H1	14327	kN	e	9.76	m
H2	47979	kN	e	8.71	m
H3	-9855	kN	e	7.33	m
H4	11692	kN	e	18.18	m
H5	7906	kN	e	16.79	m
H6	636	kN	e	2	m
H7	19817	kN	e	2.60	m
H8	-11801	kN	e	2.85	m
H9	-8662	kN	e	2	m
H10	4957	kN	e	15.43	m
H11	8335	kN	e	10.32	m
H12	680	kN	e	1.33	m
H13	14625	kN	e	2.39	m
H14	-616	kN	e	6.67	m
H15	-7523	kN	e	2.28	m
H16	-9299	kN	e	1.33	m
ΣH	83200	kN			

Table XVI.2: Characteristic horizontal forces with arms

- B: Maximum negative head is dominant

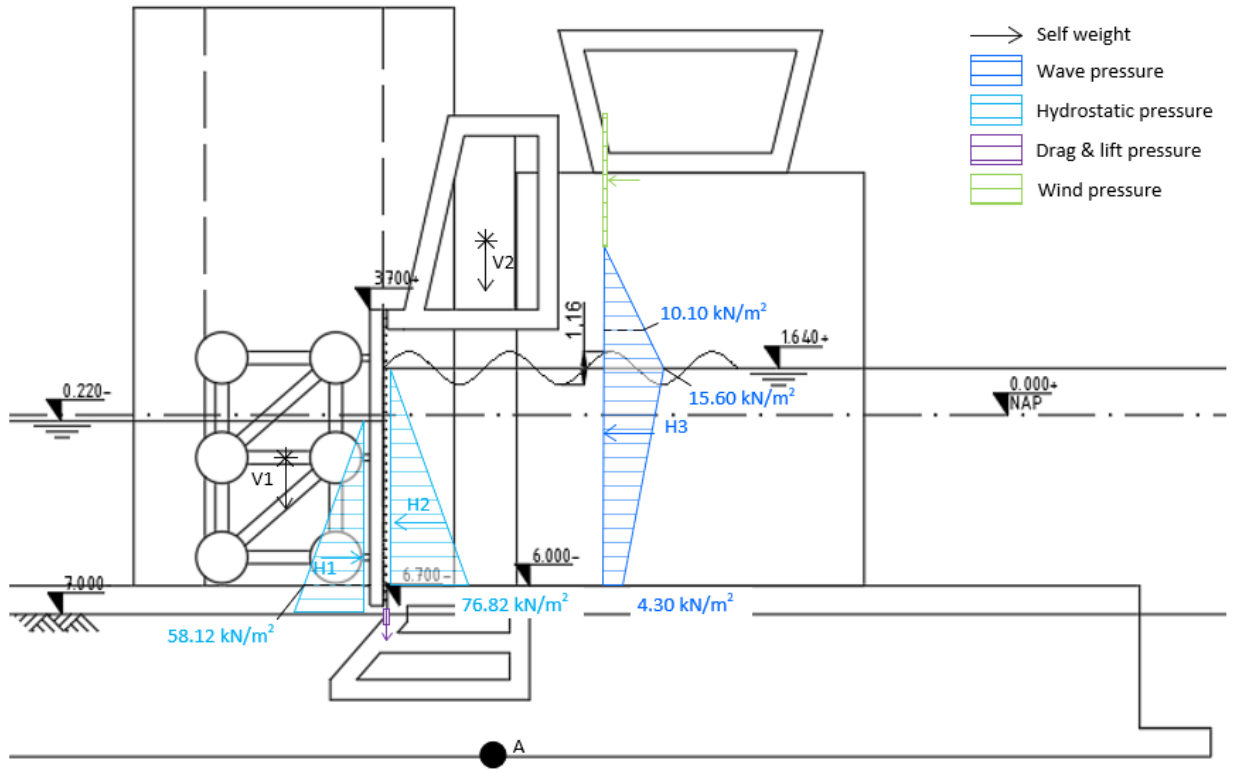


Figure XVI.8: Forces on the gate and top beam for load combination B

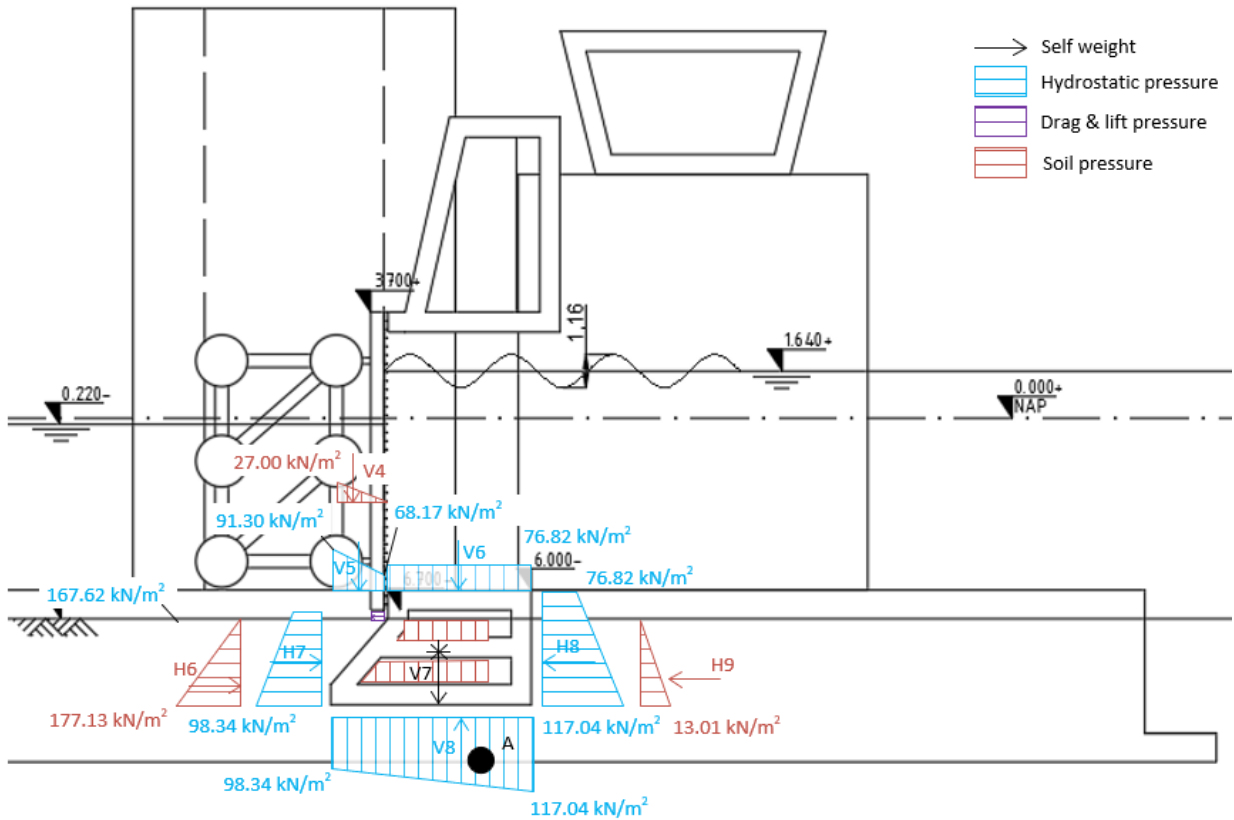


Figure XVI.9: Forces on the sill for load combination B

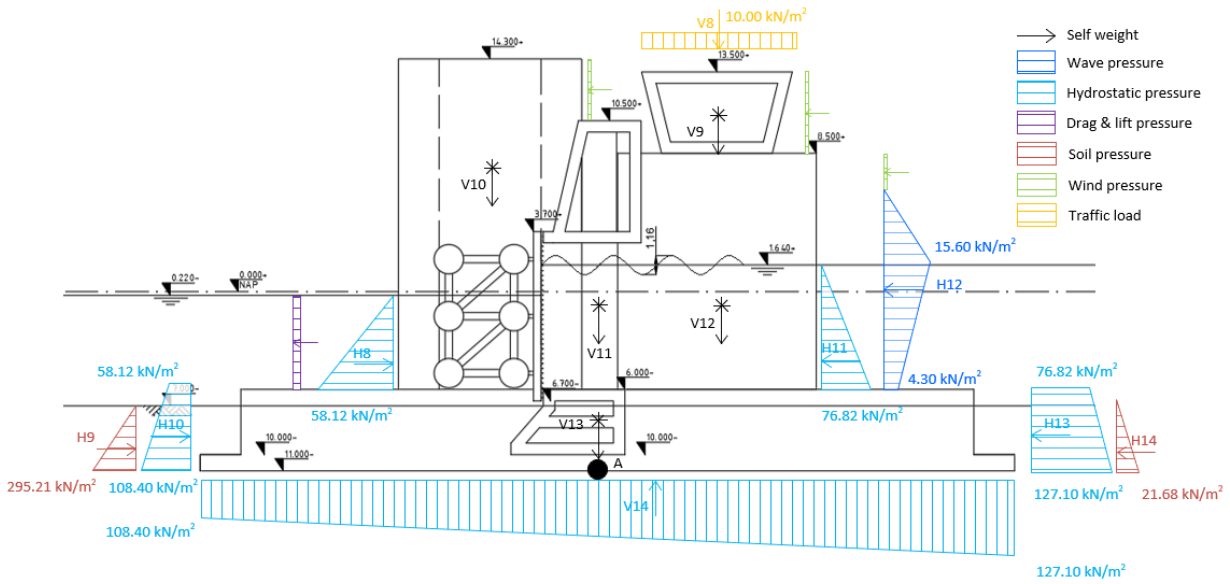


Figure XVI.10: Forces on the pier for load combination B (1)

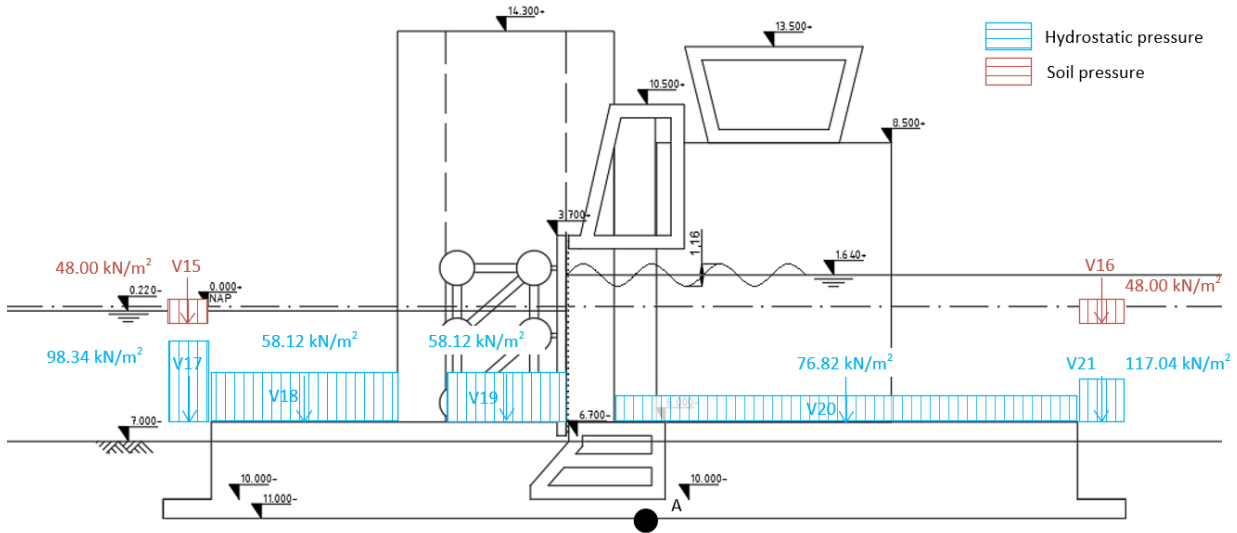


Figure XVI.11: Forces on the pier for load combination B (2)

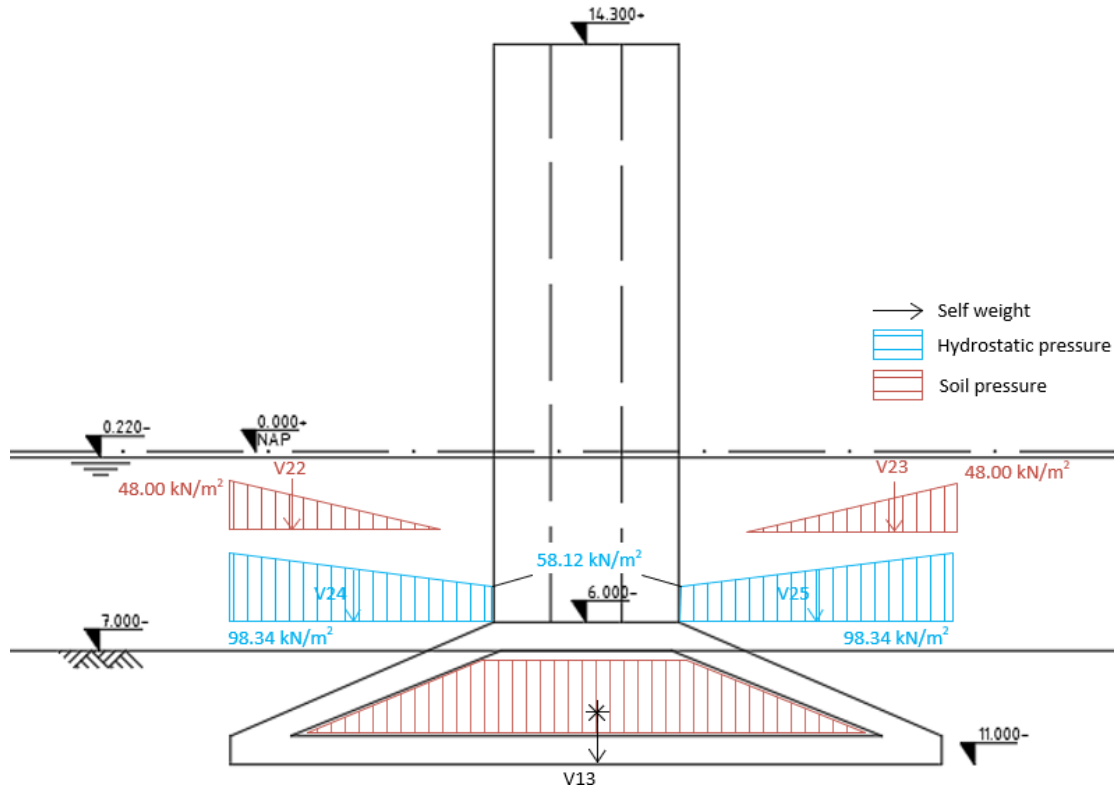


Figure XVI.12: Forces on the pier for load combination B (3)

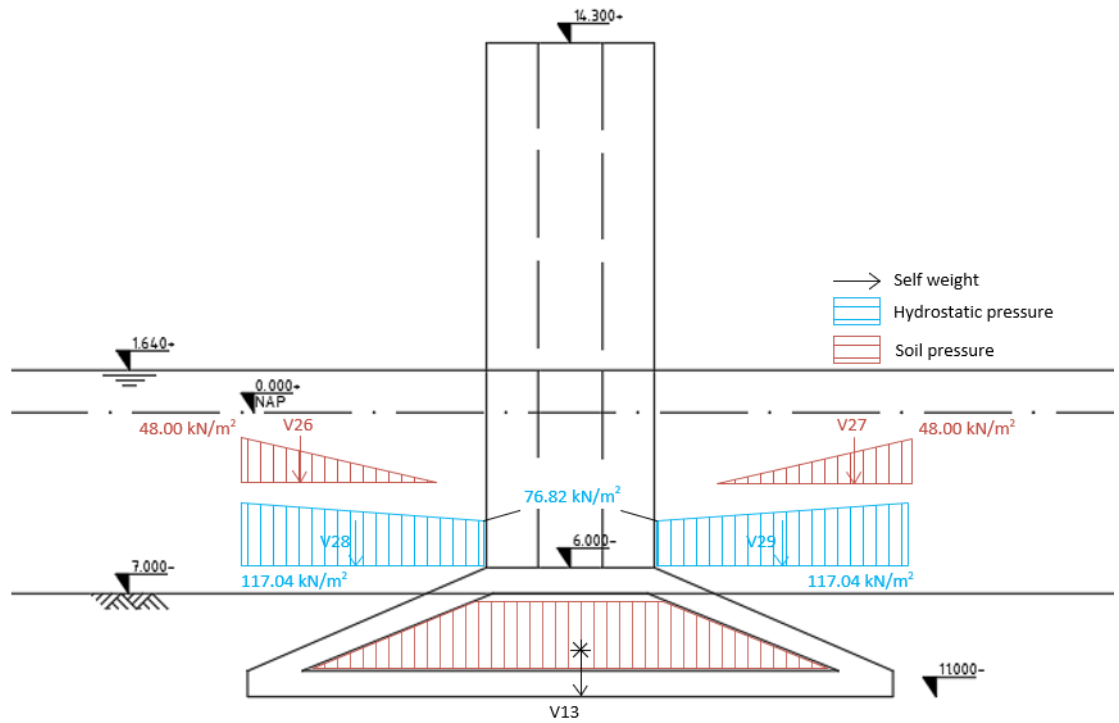


Figure XVI.13: Forces on the pier for load combination B (4)

The characteristic forces as indicated in the figures above for load combination B are tabulated in Table XVI.3 and Table XVI.4 with corresponding distances from the point of action to point A (arms). Vertical loads are positive downwards and horizontal loads are defined positive to the right. Arms are defined as such that clockwise moments are positive and anti-clockwise moments are negative.

V1	9526	kN	e	-7.47	m
V2	25883	kN	e	-0.51	m
V3	680	kN	e	-5.25	m
V4	5688	kN	e	-3.51	m
V5	15364	kN	e	-3.92	m
V6	11121	kN	e	-2.08	m
V7	-16735	kN	e	-2.21	m
V8	8231	kN	e	6.73	m
V9	12130	kN	e	6.73	m
V10	34503	kN	e	-7.47	m
V11	1238	kN	e	-0.47	m
V12	11056	kN	e	6.73	m
V13	126383	kN	e	0	m
V14	-147184	kN	e	0.66	m
V15	3000	kN	e	-23.75	m
V16	3000	kN	e	23.75	m
V17	6146	kN	e	-23.75	m
V18	3453	kN	e	-17.93	m
V19	1578	kN	e	-7.47	m
V20	13257	kN	e	-3.28	m
V21	7316	kN	e	23.75	m
V22	2761	kN	e	-14.21	m
V23	2761	kN	e	-14.21	m
V24	12769	kN	e	-14.21	m
V25	12769	kN	e	-14.21	m
V26	3566	kN	e	11.79	m
V27	3566	kN	e	11.79	m
V28	20201	kN	e	11.79	m
V29	20201	kN	e	11.79	m
ΣV	214228	kN			

Table XVI.3: Characteristic vertical forces with arms

H1	7532	kN	e	6.46	m
H2	-11738	kN	e	7.55	m
H3	-4236	kN	e	10.78	m
H4	8662	kN	e	2	m
H5	8957	kN	e	2.55	m
H6	-12640	kN	e	9.44	m
H7	-636	kN	e	2	m
H8	1224	kN	e	6.46	m
H9	9299	kN	e	1.33	m
H10	6557	kN	e	2.25	m
H11	-734	kN	e	7.55	m
H12	-265	kN	e	10.78	m
H13	-8029	kN	e	2.29	m
H14	-680	kN	e	1.33	m
ΣH	3272	kN			

Table XVI.4: Characteristic horizontal forces with arms

• H: Ship collision

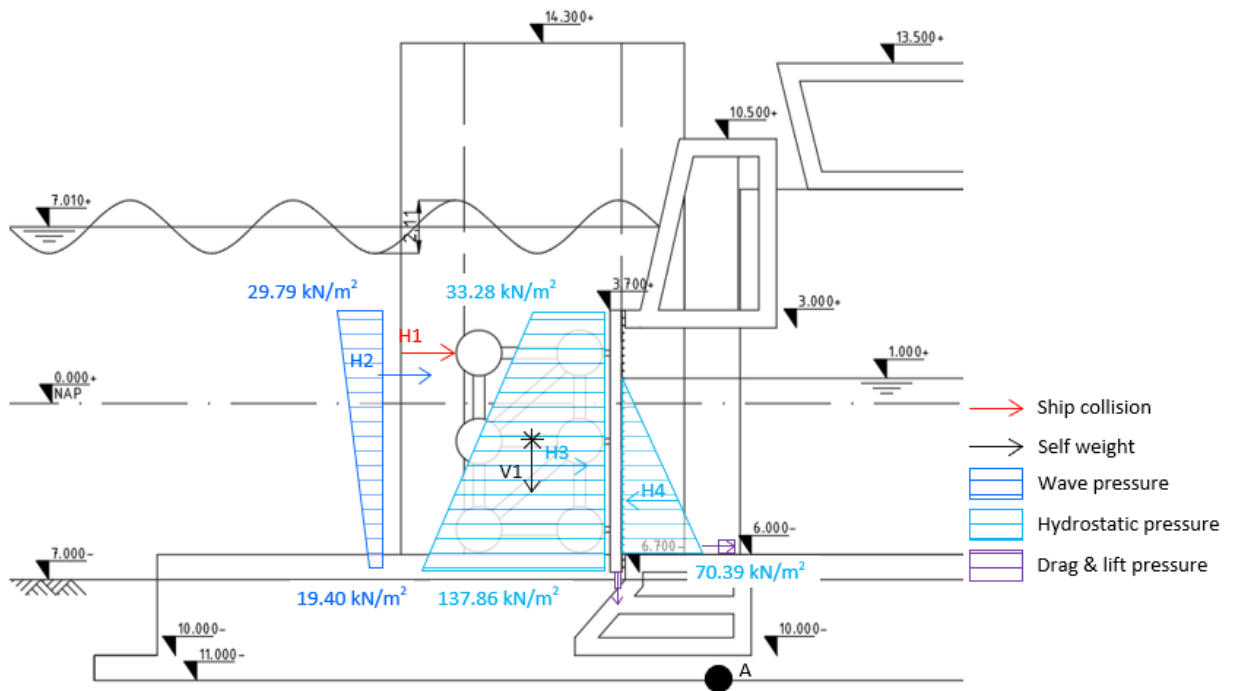


Figure XVI.14: Forces on the gate for load combination H

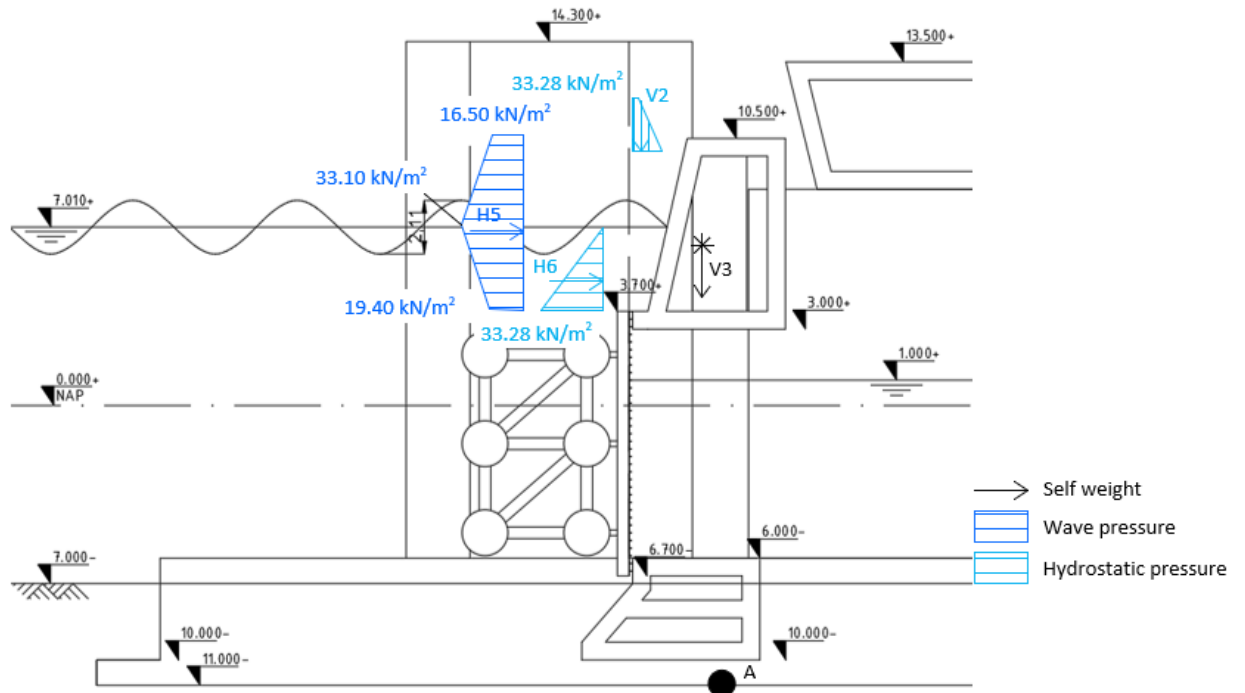


Figure XVI.15: Forces on the top beam for load combination H

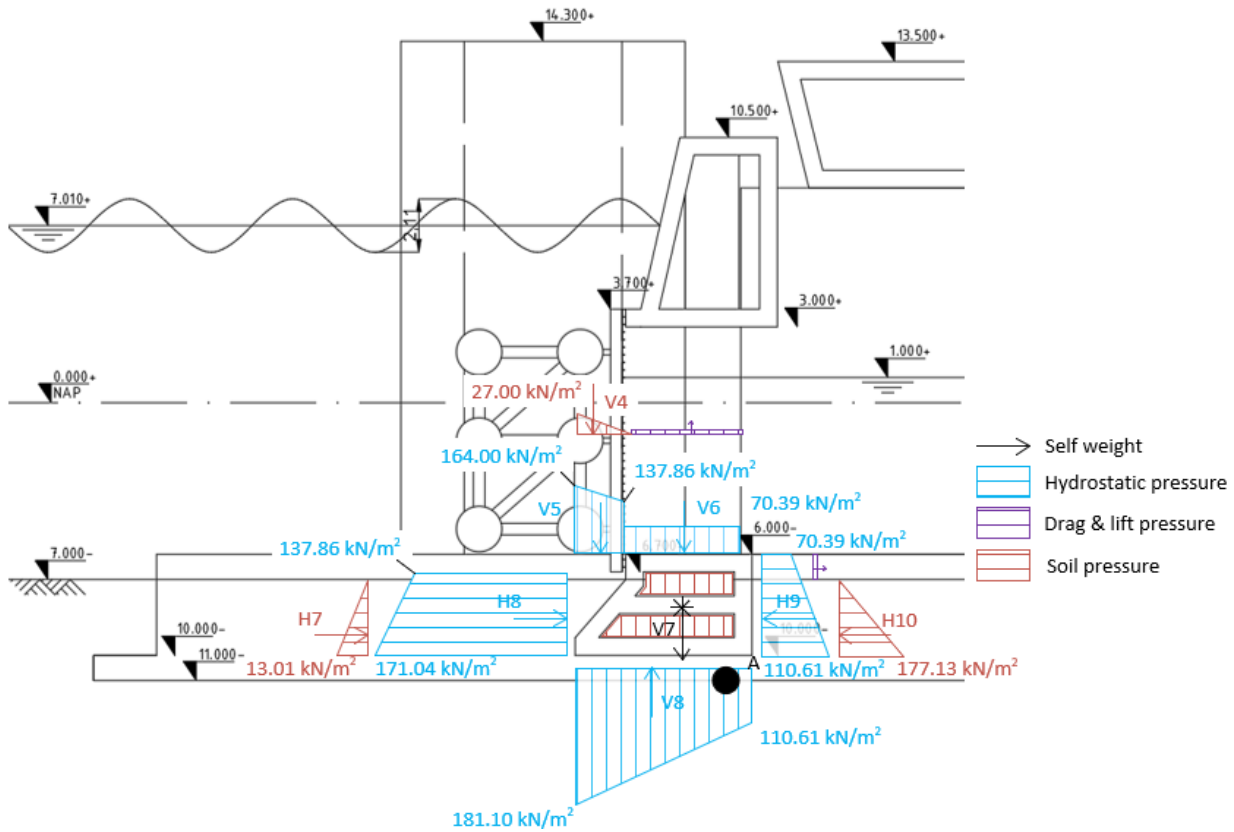


Figure XVI.16: Forces on the sill for load combination H

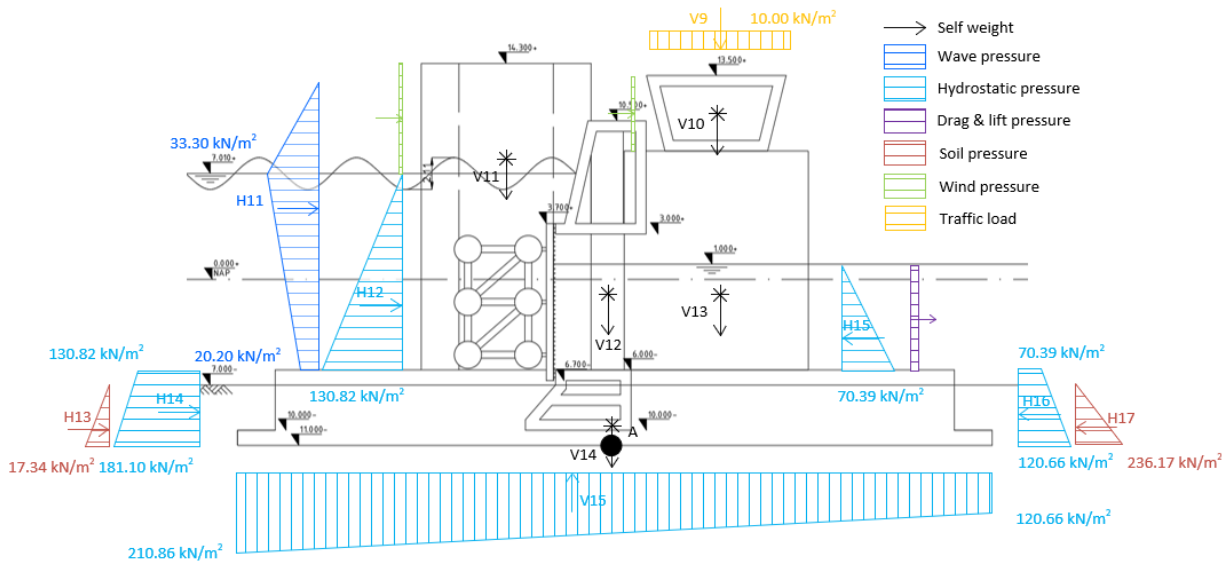


Figure XVI.17: Forces on the pier for load combination H (1)

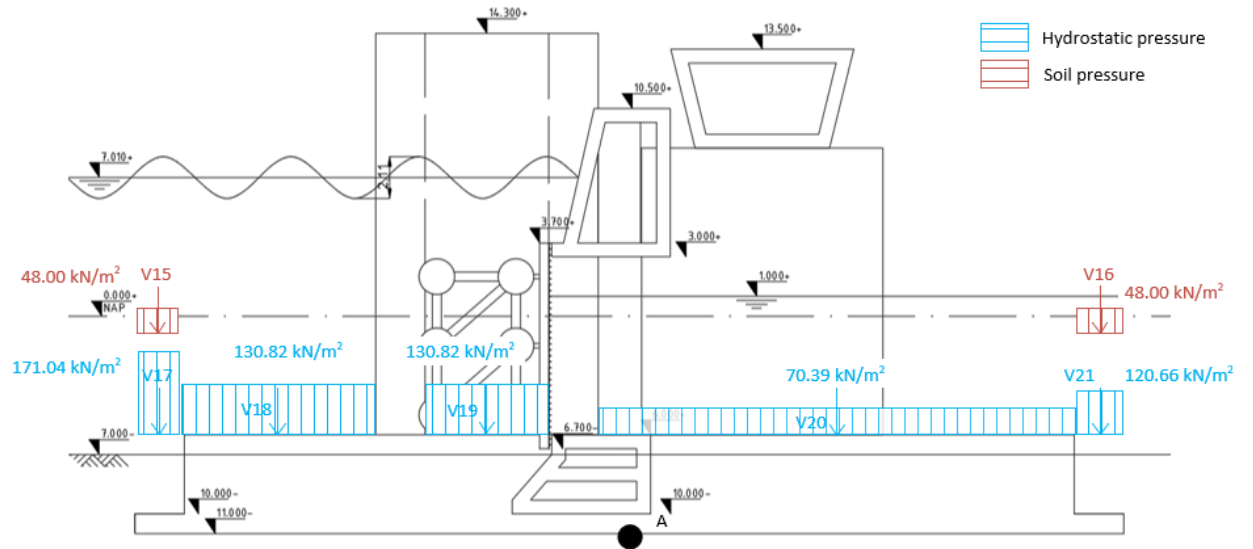


Figure XVI.18: Forces on the pier for load combination H (2)

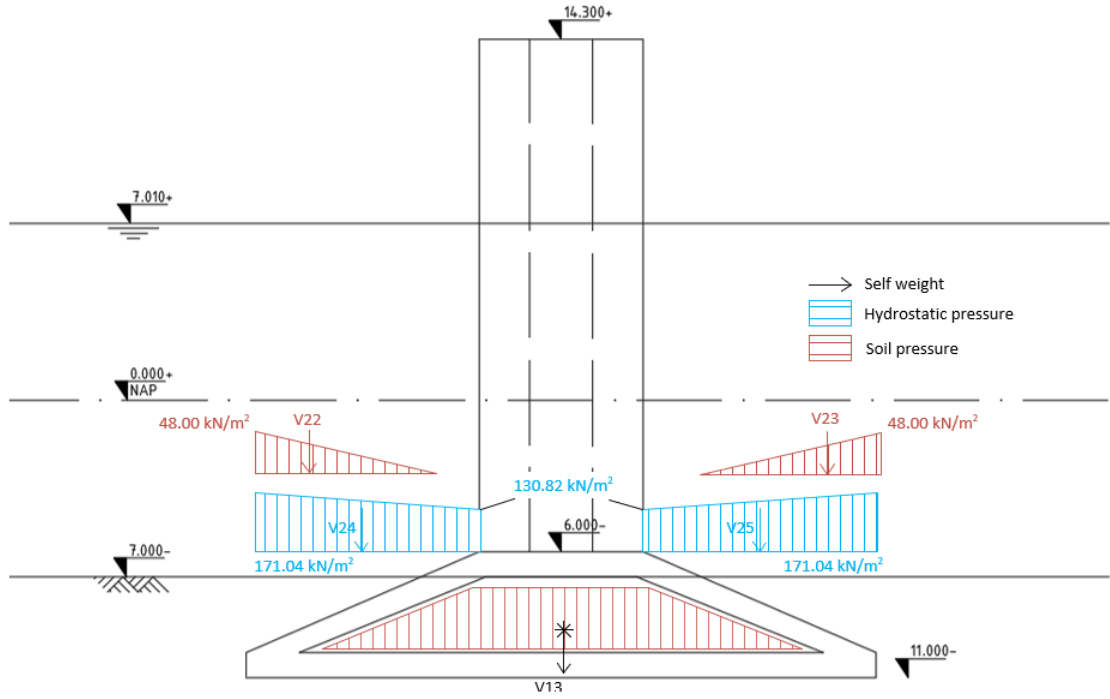


Figure XVI.19: Forces on the pier for load combination H (3)

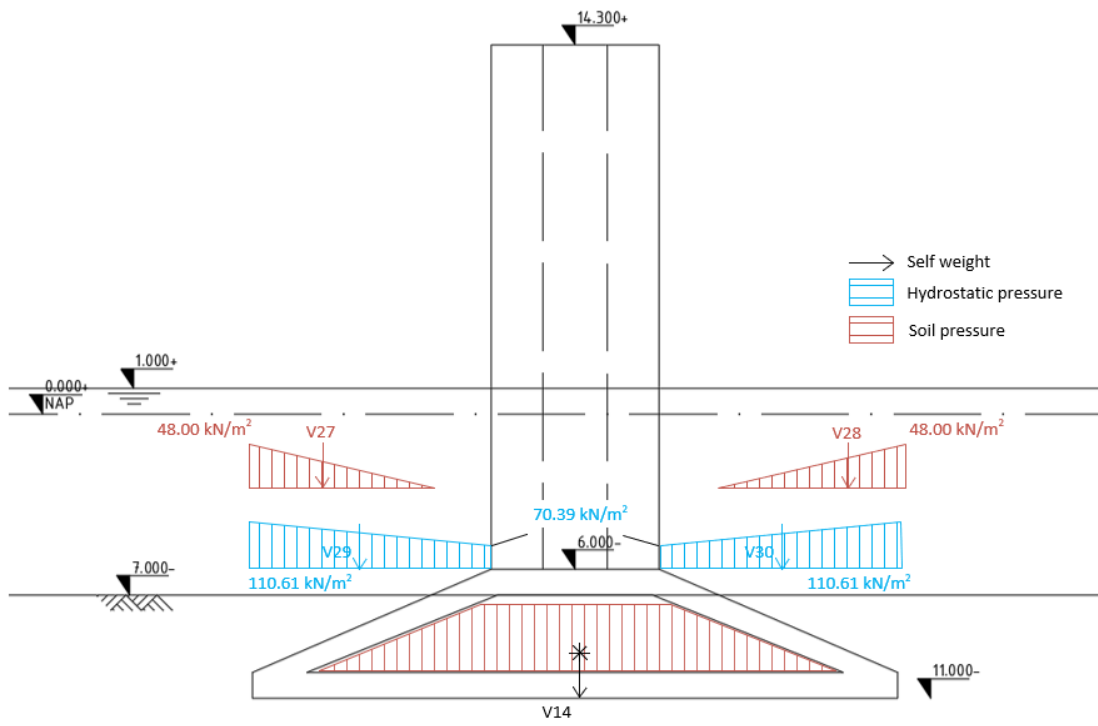


Figure XVI.20: Forces on the pier for load combination H (4)

The characteristic forces as indicated in the figures above for load combination H are tabulated in Table XVI.5 and Table XVI.6 with corresponding distances from the point of action to point A (arms). Vertical loads are positive downwards and horizontal loads are defined positive to the right. Arms are defined as such that clockwise moments are positive and anti-clockwise moments are negative.

V1	9526	kN	e	-7.47	m
V2	1298	kN	e	-3.41	m
V3	25883	kN	e	-0.51	m
V4	680	kN	e	-5.25	m
V5	7607	kN	e	-4.96	m
V6	14078	kN	e	-3.92	m
V7	11121	kN	e	-2.08	m
V8	-21337	kN	e	-2.37	m
V9	8231	kN	e	6.73	m
V10	12130	kN	e	6.73	m
V11	34503	kN	e	-7.47	m
V12	1238	kN	e	-0.47	m
V13	11056	kN	e	6.73	m
V14	126383	kN	e	0	m
V15	-188599	kN	e	-1.67	m
V16	3000	kN	e	-23.75	m
V17	3000	kN	e	23.75	m
V18	10690	kN	e	-23.75	m
V19	4783	kN	e	-17.93	m
V20	5774	kN	e	-7.47	m
V21	12148	kN	e	9.23	m
V22	6913	kN	e	23.75	m
V23	2761	kN	e	-14.21	m
V24	2761	kN	e	-14.21	m
V25	23919	kN	e	-14.21	m
V26	23919	kN	e	-14.21	m
V27	3566	kN	e	11.79	m
V28	3566	kN	e	11.79	m
V29	18927	kN	e	11.79	m
V30	18927	kN	e	11.79	m
ΣV	198451	kN			

Table XVI.5: Characteristic vertical forces with arms

H1	5220	kN	e	9	m
H2	10232	kN	e	9.87	m
H3	35597	kN	e	8.44	m
H4	-9855	kN	e	7.33	m
H5	6938	kN	e	18.03	m
H6	2203	kN	e	15.80	m
H7	636	kN	e	2	m
H8	16616	kN	e	2.59	m
H9	-11801	kN	e	2.85	m
H10	-8662	kN	e	2	m
H11	3015	kN	e	14.11	m
H12	5531	kN	e	9.34	m
H13	680	kN	e	1.33	m
H14	12282	kN	e	2.37	m
H15	-616	kN	e	6.67	m
H16	-7523	kN	e	2.28	m
H17	-9299	kN	e	1.33	m
ΣH	51195	kN			

Table XVI.6: Characteristic horizontal forces with arms

• Lowest LAT

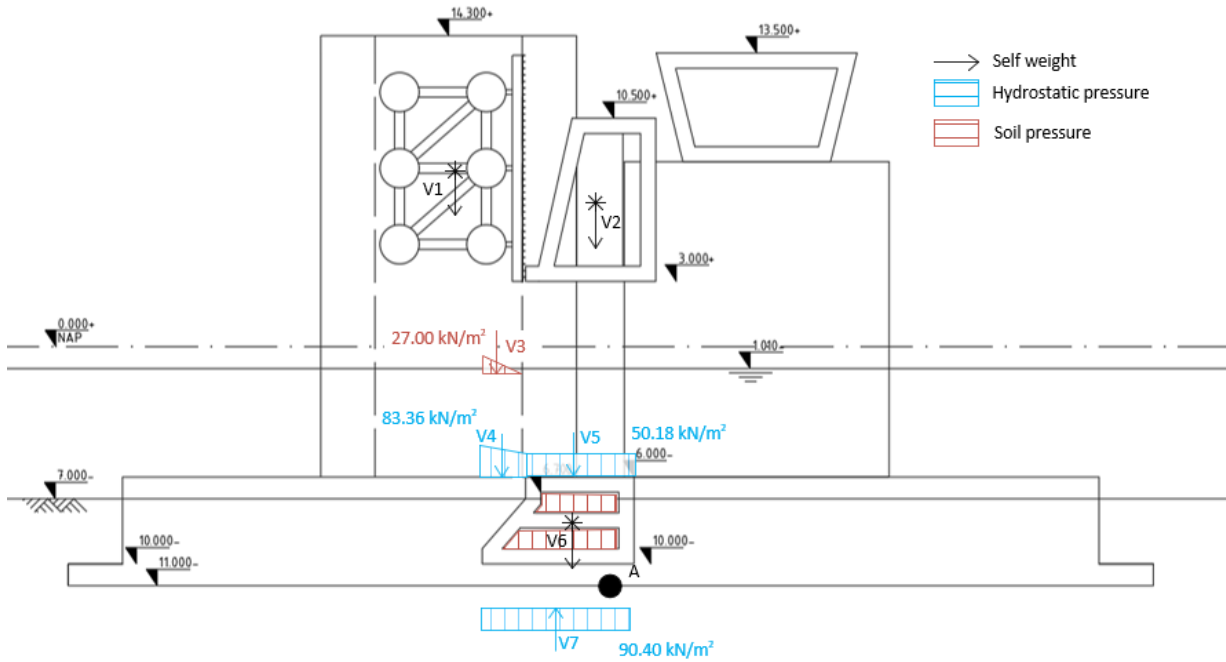


Figure XVI.21: Vertical forces on the structure for load combination Lowest LAT (1)

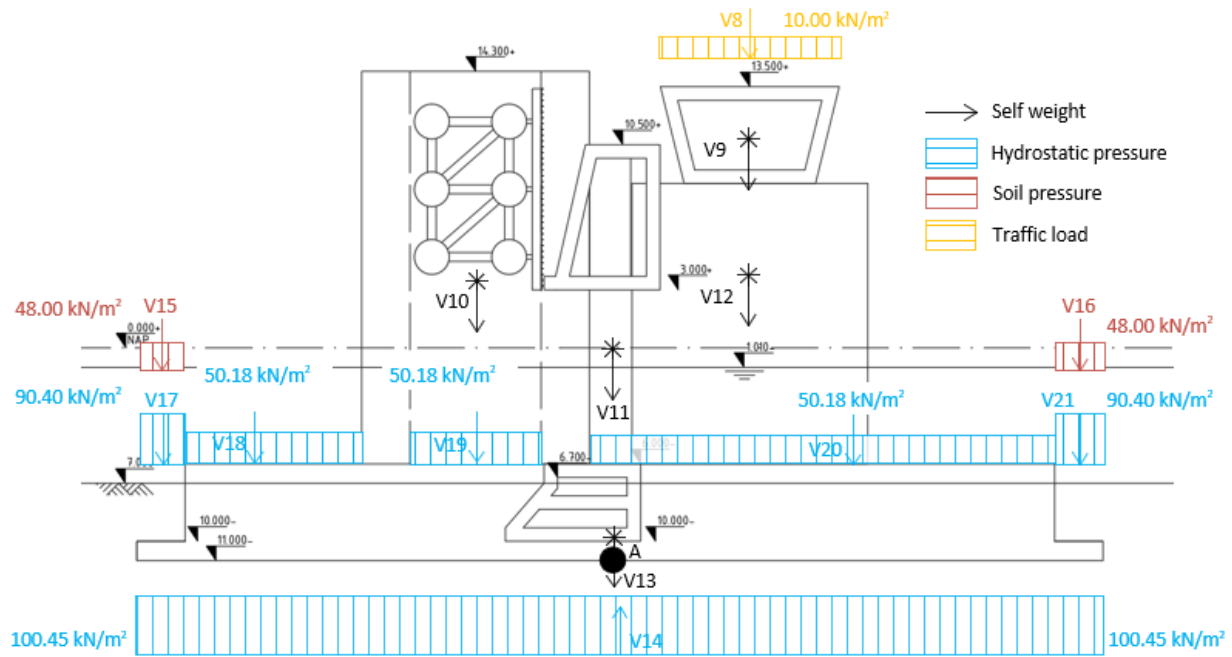


Figure XVI.22: Vertical forces on the structure for load combination Lowest LAT (2)

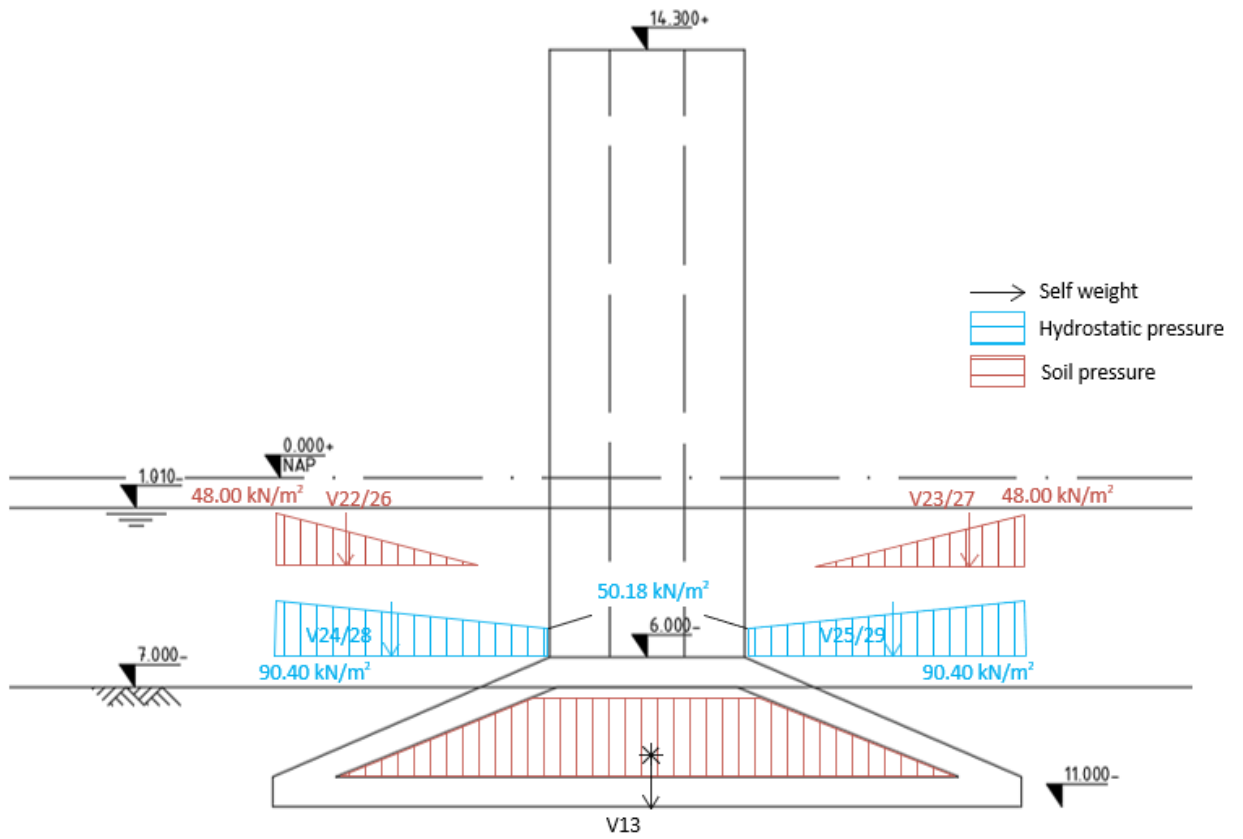


Figure XVI.23: Vertical forces on the structure for load combination Lowest LAT (3)

The characteristic vertical forces as indicated in the figures above for load combination Lowest LAT are tabulated in Table XVI.7. Vertical loads are positive downwards.

V1	10957	kN
V2	25883	kN
V3	680	kN
V4	3618	kN
V5	10036	kN
V6	11121	kN
V7	-14048	kN
V8	8231	kN
V9	12130	kN
V10	34503	kN
V11	1238	kN
V12	11056	kN
V13	126383	kN
V14	-125565	kN
V15	3000	kN
V16	3000	kN
V17	6146	kN
V18	2981	kN
V19	1362	kN
V20	8660	kN
V21	5650	kN
V22	2761	kN
V23	2761	kN
V24	11551	kN
V25	11551	kN
V26	3566	kN
V27	3566	kN
V28	14923	kN
V29	14923	kN
$\sum V$	212625	kN

Table XVI.7: Characteristic vertical forces

- During construction

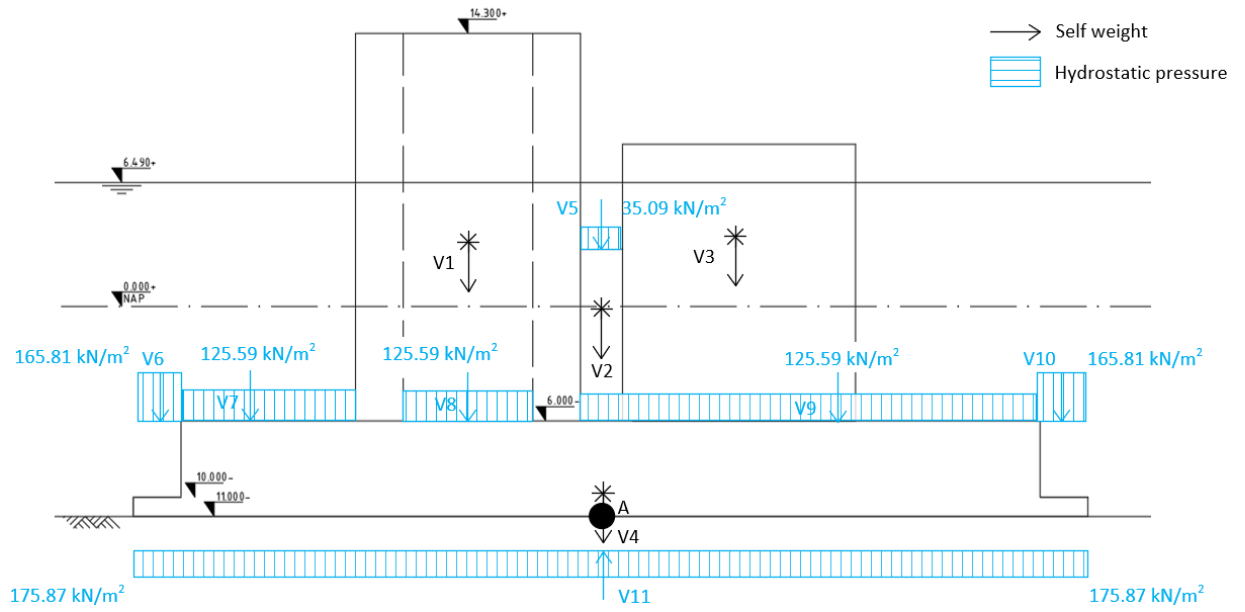


Figure XVI.24: Vertical forces on the structure for load combination Lowest During construction (1)

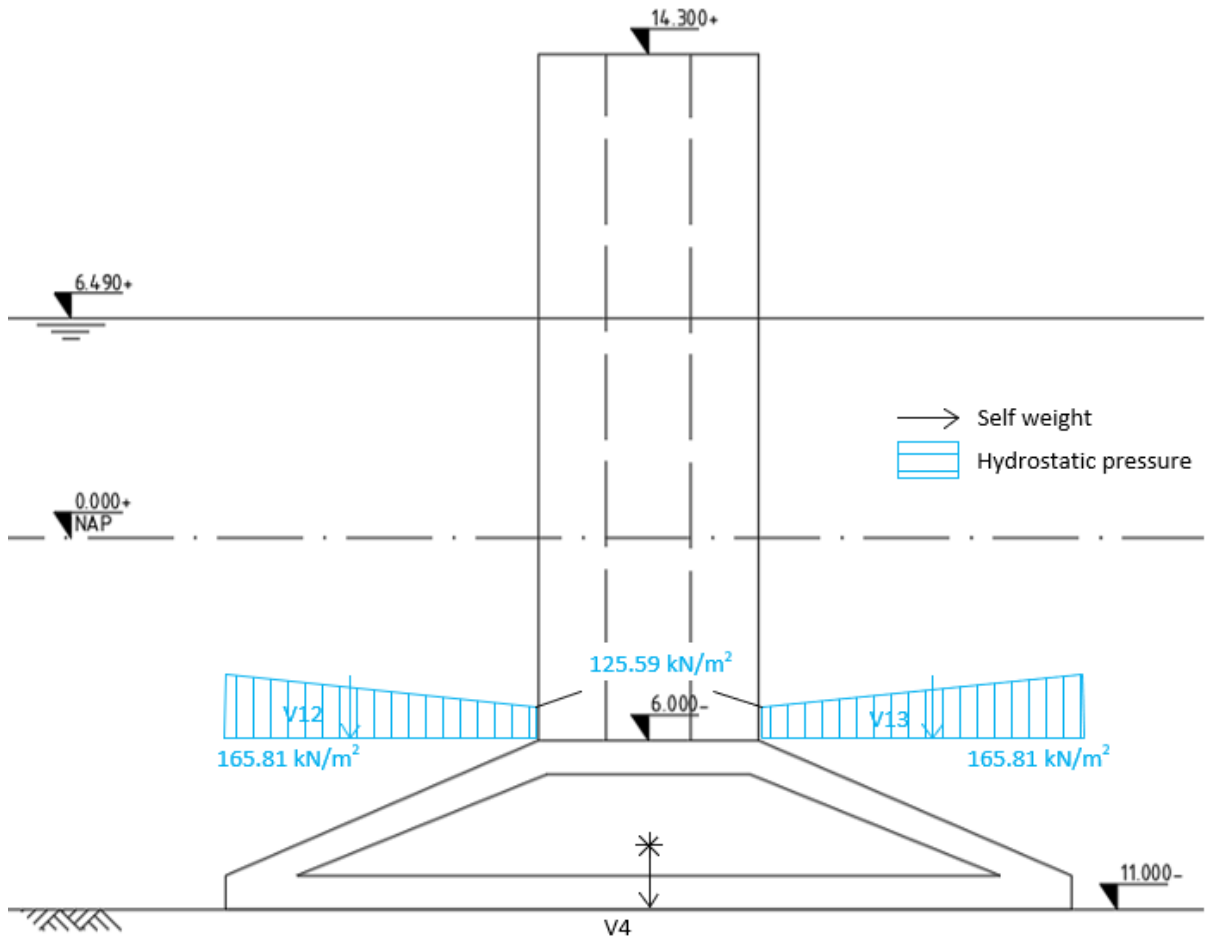


Figure XVI.25: Vertical forces on the structure for load combination Lowest During construction (2)

The characteristic vertical forces as indicated in the figures above for load combination During construction are tabulated in Table XVI.8. Vertical loads are positive downwards.

V1	25103	kN
V2	1238	kN
V3	11056	kN
V4	80086	kN
V5	193	kN
V6	10363	kN
V7	7461	kN
V8	3409	kN
V9	21673	kN
V10	10363	kN
V11	-219833	kN
V12	69712	kN
V13	69712	kN
$\sum V$	90537	kN

Table XVI.8: Characteristic vertical forces

XVI.2 Verifications

XVI.2.1 Horizontal Stability

As horizontal stability concerns an EQU limit state, partial factors according to the Eurocode (2019) Table A2.4(A) are used. The unity check regarding the horizontal stability verification now follows from Equation (XVI.1).

$$UC = \frac{\sum H}{f \cdot \sum V} \leq 1 \quad (\text{XVI.1})$$

where: $\sum H$ [kN] = resulting design horizontal force
 $\sum V$ [kN] = resulting design vertical force
 f [-] = friction coefficient = 0.67

A: Maximum positive head is dominant

	Effect	γ
V1	Unfavourable	0.95
V2	Unfavourable	1
V3	Unfavourable	0.95
V4	Unfavourable	0.95
V5	Unfavourable	1
V6	Unfavourable	1
V7	Unfavourable	0.95
V8	Favourable	1
V9	N.a.	0*
V10	Unfavourable	0.95
V11	Unfavourable	0.95
V12	Unfavourable	0.95
V13	Unfavourable	0.95
V14	Unfavourable	0.95
V15	Favourable	1
V16	Unfavourable	0.95
V17	Unfavourable	0.95
V18	Unfavourable	1
V19	Unfavourable	1
V20	Unfavourable	1
V21	Unfavourable	1
V22	Unfavourable	1
V23	Unfavourable	0.95
V24	Unfavourable	0.95
V25	Unfavourable	1
V26	Unfavourable	1
V27	Unfavourable	0.95
V28	Unfavourable	0.95
V29	Unfavourable	0.95
V30	Unfavourable	1
$\sum V$	173036	kN

Table XVI.9: Partial factors and resultant design vertical force

* This value represents $\gamma\psi_0$

	Effect	γ
H1	Unfavourable	1
H2	Unfavourable	1
H3	Favourable	1
H4	Unfavourable	1
H5	Unfavourable	1
H6	Unfavourable	1.05
H7	Unfavourable	1
H8	Favourable	1
H9	Favourable	0.95
H10	Unfavourable	1
H11	Unfavourable	1
H12	Unfavourable	1.05
H13	Unfavourable	1
H14	Favourable	1
H15	Favourable	1
H16	Favourable	0.95
$\sum H$	84164	kN

Table XVI.10: Partial factors and resultant design horizontal force

Finally, the unity check:

$$UC = \frac{\sum H}{f \cdot \sum V} = 0.73$$

B: Maximum negative head is dominant

Not governing.

H: Ship collision

Not governing.

Lowest LAT

Not governing.

During construction

Not governing.

XVI.2.2 Vertical Stability: Bearing Capacity

The vertical effective soil stress, required to resist the acting loads, should not exceed the maximum bearing capacity of the soil, otherwise the soil will collapse (Molenaar & Voorendt, 2020b).

$$\sigma_{k,max} = \frac{\sum V}{B L} + \frac{\sum M}{\frac{1}{6} B^2 L} < p'_{max} \quad (\text{XVI.2})$$

where: $\sigma_{k,max}$ [kN/m²] = maximum soil stress
 B [m] = width of the structure (parallel to the resultant horizontal force) = 50
 L [m] = length of the structure (perpendicular to the resultant horizontal force) = 25
 p'_{max} [kN/m²] = maximum bearing capacity of the subsoil

Subsequently, the maximum bearing capacity of the subsoil, is calculated by means of the Brinch Hansen method for drained conditions (Equation (XVI.3)) as proposed by (Molenaar & Voorendt, 2020b).

$$p'_{max} = c' N_c s_c i_c + \sigma'_q N_q s_q i_q + 0.5 \gamma' B N_\gamma s_\gamma i_\gamma \quad (\text{XVI.3})$$

where: p'_{max} [kN/m²] = maximum bearing capacity of the subsoil
 c' [kN/m²] = (weighted) cohesion = 0 for sand
 σ'_q [kN/m²] = effective surcharge pressure surrounding a foundation element at construction
 N_q [-] = bearing force factor to contribution of soil coverage
 s_q [-] = shape factor to contribution of soil coverage
 i_q [-] = factor for inclined loads to contribution of soil coverage
 γ' [kN/m³] = (weighted) effective volumetric weight of the soil below construction level
 N_γ [-] = bearing force factor to contribution of the specific weight of the soil below the foundation
 s_γ [-] = shape factor to contribution of the specific weight of the soil below the foundation
 i_γ [-] = factor for inclined loads to contribution of the specific weight of the soil below the foundation

Now, as $B > L$, all shape and inclined load factors are equal to 1 (Molenaar & Voorendt, 2020b). The bearing force factors are calculated as follows:

$$N_q = \frac{1 + \sin(\phi')}{1 - \sin(\phi')} \cdot e^{\pi \tan(\phi')} \quad (\text{XVI.4a})$$

$$N_\gamma = (N_q - 1) \cdot \tan(1.32 \cdot \phi') \quad (\text{XVI.4b})$$

Disregarding the stiffer and greatly compacted sand layer directly beneath the pier and the weaker soil layers at greater depth, with $\phi' = 30^\circ$ for clean loose sand, Equation (XVI.4a) and Equation (XVI.4b) yields $N_q = 18.4$ and $N_\gamma = 14.4$, respectively. Finally, with a foundation level at NAP - 11 m, a bottom protection layer ($\gamma'_s = 16 \text{ kN/m}^3$) at NAP - 7 m till NAP -12.6 m and a mean effective volumetric weight of clean loose sand below the structure of 9 kN/m^3 , Equation (XVI.3) yields:

$$\begin{aligned} p'_{max} &= \sigma'_q N_q s_q i_q + 0.5 \gamma' B N_\gamma s_\gamma i_\gamma \\ &= 64 \cdot 18.4 \cdot 1 \cdot 1 + 0.5 \cdot 9 \cdot 50 \cdot 14.4 \cdot 1 \cdot 1 \\ &= 1.18 + 3.24 \\ &= 4.42 \end{aligned}$$

Note that, when assuming that the subsoil complete consists of weakly sandy clay without cohesion and no surcharge load is present (i.e. only the third term of Equation (XVI.3) contributes to the bearing capacity), Equation (XVI.3) gives a maximum bearing capacity of 0.82 N/mm^2 .

A: Maximum positive head is dominant

	Effect	γ
V1	Unfavourable	1.35
V2	Unfavourable	1
V3	Unfavourable	1.35
V4	Favourable	0.9
V5	Unfavourable	1
V6	Unfavourable	1
V7	Unfavourable	1.35
V8	Favourable	1
V9	Unfavourable	1.25
V10	Unfavourable	1.35
V11	Unfavourable	1.35
V12	Unfavourable	1.35
V13	Unfavourable	1.35
V14	Unfavourable	1.35
V15	Favourable	1
V16	Unfavourable	1.35
V17	Unfavourable	1.35
V18	Unfavourable	1
V19	Unfavourable	1
V20	Unfavourable	1
V21	Unfavourable	1
V22	Unfavourable	1
V23	Unfavourable	1.35
V24	Unfavourable	1.35
V25	Unfavourable	1
V26	Unfavourable	1
V27	Unfavourable	1.35
V28	Unfavourable	1.35
V29	Unfavourable	1.35
V30	Unfavourable	1
$\sum V$	283488	kN

Table XVI.11: Partial factors and resultant design vertical force

	Effect	γ
H1	Unfavourable	1
H2	Unfavourable	1
H3	Favourable	1
H4	Unfavourable	1
H5	Unfavourable	1
H6	Unfavourable	1.35
H7	Unfavourable	1
H8	Favourable	1
H9	Favourable	0.9
H10	Unfavourable	1
H11	Unfavourable	1
H12	Unfavourable	1.35
H13	Unfavourable	1
H14	Unfavourable	1
H15	Unfavourable	1
H16	Favourable	0.9
$\sum H$	85457	kN

Table XVI.12: Partial factors and resultant design horizontal force

The total moment (around point A), is calculated as follows:

$$\begin{aligned}
 M &= \sum_{i=1}^{n=30} V_i \cdot e_i + \sum_{i=1}^{n=16} H_i \cdot e_i \\
 &= 668777 \text{ kNm}
 \end{aligned}$$

Finally, the unity check:

$$\begin{aligned}
 UC &= \frac{\sigma_{k,max}}{p_{max}} \leq 1 \\
 &= \frac{0.29}{4.42} \\
 &= 0.07
 \end{aligned}$$

B: Maximum negative head is dominant

Not governing.

H: Ship collision

Not governing.

Lowest LAT

Not governing.

During construction

Not governing.

XVI.2.3 Vertical Stability: Settlements

The settlement of the subsoil as a result of the added weight of the Delta Barrier can be calculated by means of the equation as proposed by Koppejan (Molenaar & Voorendt, 2020b).

$$\epsilon = \left(\frac{U}{C'_p} + \frac{1}{C'_s} \log \left(\frac{\Delta t}{t_{ref}} \right) \right) \cdot \ln \left(\frac{\sigma'_{v;i} + \Delta \sigma'_v}{\sigma'_{v;i}} \right) \quad (\text{XVI.5})$$

where:	ϵ	[-]	=	relative compression
	U	[-]	=	degree of consolidation
	C'_p	[-]	=	primary compression coefficient
	C'_s	[-]	=	secondary compression coefficient
	Δt	[days]	=	duration after the application of the additional loading
	t_{ref}	[days]	=	reference duration (one day)
	$\Delta \sigma'_v$	[kPa]	=	increase of the vertical effective stress
	$\sigma'_{v;i}$	[kPa]	=	initial vertical effective pressure

The degree of consolidation can be approximated by Equation (XVI.6) (Molenaar & Voorendt, 2020b). It should be noted that no sensible estimates can be made for general values of the coefficient of consolidation (c_v), as both the vertical permeability and the vertical soil stiffness can vary significantly per soil layer. Furthermore, the vertical permeability and the vertical soil stiffness decrease during consolidation due to their dependence on the stresses (Molenaar & Voorendt, 2020b). Nonetheless, for this preliminary design Equation (XVI.6) is used with average indicative values of the coefficient of consolidation proposed by Molenaar and Voorendt (2020b).

$$U \approx \begin{cases} \frac{2}{\sqrt{\pi}} \cdot \sqrt{\frac{c_v \cdot t}{d_c^2}}, & \text{if } U \leq 0.5 \\ 1 - \frac{8}{\pi^2} \cdot e \left(-\frac{\pi^2 \cdot c_v \cdot t}{4 \cdot d_c^2} \right), & \text{if } U > 0.5 \end{cases} \quad (\text{XVI.6})$$

where:	c_v	[m ² /year]	=	coefficient of consolidation
	d_c	[m]	=	drainage path length
	t	[years]	=	duration = 200

The calculated degrees of consolidation are presented in Table XVI.13 for every distinguished soil layer. It should be noted that for every soil layer $U = 1$, which is to be expected after a duration of 200 years.

After calculating the relative compression for every distinguished soil layer according to Equation (XVI.5), the total settlement is computed by means of Equation (XVI.7).

$$\Delta h = \sum_i^n \epsilon_i h_i \quad (\text{XVI.7})$$

where:	Δh	[mm]	=	total settlement
	ϵ_i	[-]	=	relative compression of soil layer i
	h_i	[mm]	=	thickness of soil layer i
	n	[-]	=	number of soil layers

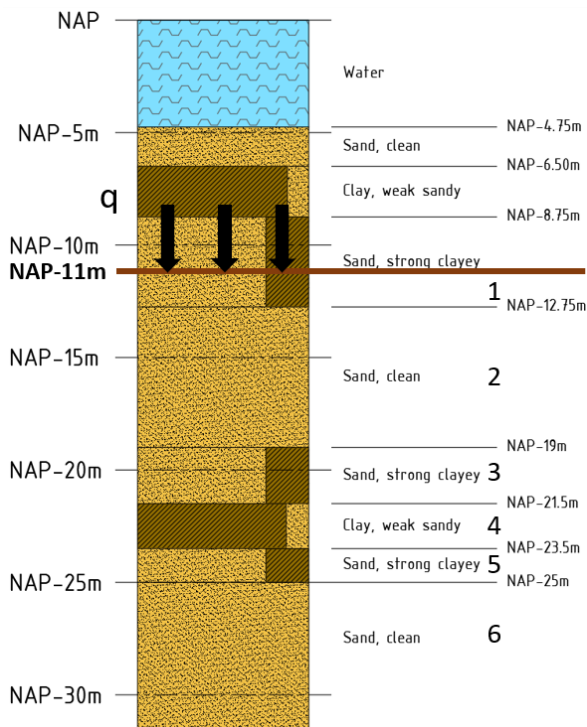


Figure XVI.26: Soil profile with specified layers

With the initial soil profile, as established in Section 3.2.3, and a foundation level of the piers at NAP - 11 m, Figure XVI.26 depicts the soil profile after construction of the Delta Barrier. The resultant vertical load which is transferred from the pier to the subsoil is converted to a pressure under the structure (q). As for this preliminary design, a spreading in depth of the surcharge stresses under an angle of 45° is assumed. Furthermore, it should be noted that the act of extensively compacting the subsoil in advance to sinking the piers in place is disregarded (i.e. assuming no dissipation of water pressure). Said approach leads to a rather conservative settlement verification.

The relevant parameters, needed to calculate the relative compression (Equation (XVI.5)) and total settlement (Equation (XVI.7)) are given in Table XVI.13 per identified soil layer under the foundation level.

Layer	h [m]	c_v [$m^2/year$]	d_c [m]	U [-]	C'_p [-]	C'_s [-]	$\sigma'_{v,i}$ [kPa]
1	1.75	25.8	1.75	1	45	1300	73.75
2	6.25	50	3.13	1	200	∞	150.63
3	1.75	25.8	1.75	1	45	1300	221.25
4	2	5.25	1	1	20	240	250.5
5	1.5	25.8	1.5	1	45	1300	283.5
6	4	50	2	1	200	∞	336.5

Table XVI.13: Relevant parameters per soil layer

In Table XVI.13, the primary and secondary compression coefficients follow from Table (2.b) in the National Annex to Eurocode 1 (2019). Average values of the coefficient of consolidation are presented in Table XVI.13 as proposed by Molenaar and Voorendt (2020b).

Finally, it is assumed that $\Delta h < 100$ mm should hold, as was in the design of the Oosterscheldekering (Visser, 1986a). As the settlement of the subsoil concerns a GEO limit state, partial factors according to Figure XIII.2 as proposed in the ROK(2021) are used.

A: Maximum positive head is dominant

Not governing.

B: Maximum negative head is dominant

Not governing.

H: Ship collision

Not governing.

Lowest LAT

	Effect	γ
V1	Unfavourable	1.35
V2	Unfavourable	1.35
V3	Unfavourable	1.35
V4	Unfavourable	1.35
V5	Unfavourable	1.35
V6	Unfavourable	1.35
V7	Favourable	0.95
V8	Unfavourable	1.25
V9	Unfavourable	1.35
V10	Unfavourable	1.35
V11	Unfavourable	1.35
V12	Unfavourable	1.35
V13	Unfavourable	1.35
V14	Favourable	0.95
V15	Unfavourable	1.35
V16	Unfavourable	1.35
V17	Unfavourable	1.35
V18	Unfavourable	1.35
V19	Unfavourable	1.35
V20	Unfavourable	1.35
V21	Unfavourable	1.35
V22	Unfavourable	1.35
V23	Unfavourable	1.35
V24	Unfavourable	1.35
V25	Unfavourable	1.35
V26	Unfavourable	1.35
V27	Unfavourable	1.35
V28	Unfavourable	1.35
V29	Unfavourable	1.35
$\sum V$	342066	kN

Table XVI.14: Partial factors and resultant design vertical force

The increase in vertical effective stress ($\Delta\sigma'_v$) in Equation (XVI.5) is a function of the resultant vertical force and the depth beneath the foundation (z) and can be written as follows:

$$\Delta\sigma'_v = \frac{\sum V}{(B + 2 \cdot z) \cdot (L + 2 \cdot z)} - \sigma'_0 \quad (\text{XVI.8})$$

where: σ'_0 [kPa]= resulting effective stress of the excavated soil = 56.25

Figure XVI.27 presents the increase in vertical effective stress per layer as specified in Figure XVI.26.

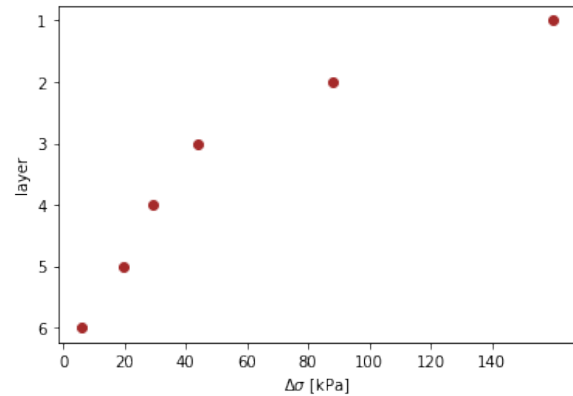


Figure XVI.27: Increase in vertical effective stress per layer

The expected decrease in $\Delta\sigma'$ in depth results in $\Delta\sigma' = 0$ somewhere in layer number 6 (the deep sand layer). Hence, said layer does not 'feel' the initial increase in vertical effective stress transferred by the pier of the Delta Barrier to the subsoil and will therefore not deform.

Finally, with the increase in vertical effective stress per layer as presented in Figure XVI.27, Figure XVI.28 and Figure XVI.29 depict the relative compression and settlement per layer, respectively.

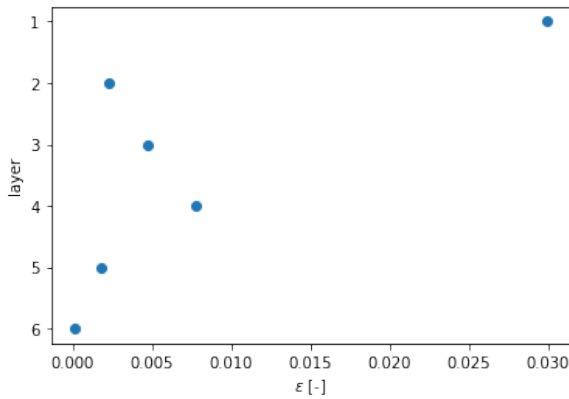


Figure XVI.28: Relative compression per layer

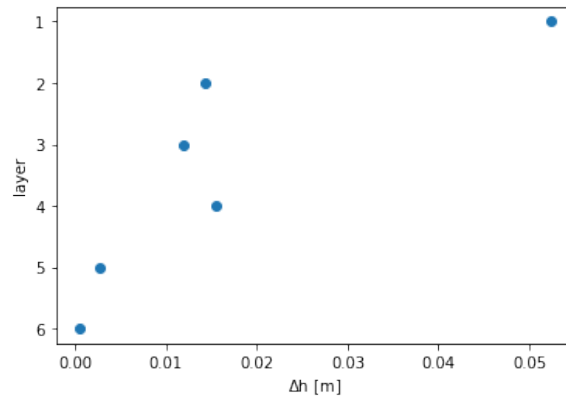


Figure XVI.29: Settlement per layer

With Equation (XVI.7), the total settlement yields 97 mm, which is smaller than the assumed maximum of 100 mm.

During construction

Not governing.

XVI.2.4 Rotational Stability

As sand cannot or barely cope with tensile forces Equation (XVI.9) should be satisfied.

$$\sigma_{k,min} > 0 \quad (\text{XVI.9})$$

$$\text{in which: } \sigma_{k,min} = \frac{\sum V}{B L} - \frac{\sum M}{\frac{1}{6} B^2 L}$$

As per Equation (XVI.9), it is stipulated that the soil stresses necessary for rotational stability may only be compressive. This yields the following verification regarding the resistance to rotational stability of the structure:

$$e_R = \frac{\sum M}{\sum V} \leq \frac{1}{6} B \quad (\text{XVI.10})$$

As rotational stability concerns an EQU limit state, partial factors according to the Eurocode (2019) Table A2.4(A) are used. The unity check regarding the horizontal stability verification now follows from Equation (XVI.11).

$$UC = \frac{6 \cdot \sum M}{B \cdot \sum V} \leq 1 \quad (\text{XVI.11})$$

A: Maximum positive head is dominant

	Effect	γ
V1	Favourable	0.95
V2	Favourable	1
V3	Favourable	0.95
V4	Favourable	0.95
V5	Favourable	1
V6	Favourable	1
V7	Favourable	0.95
V8	Favourable	1
V9	N.a.	0*
V10	Unfavourable	1.05
V11	Favourable	0.95
V12	Favourable	0.95
V13	Unfavourable	1.05
V14	Favourable	0.95
V15	Unfavourable	1
V16	Favourable	0.95
V17	Unfavourable	1.05
V18	Favourable	1
V19	Favourable	1
V20	Favourable	1
V21	Unfavourable	1
V22	Unfavourable	1
V23	Favourable	0.95
V24	Favourable	0.95
V25	Favourable	1
V26	Favourable	1
V27	Unfavourable	1.05
V28	Unfavourable	1.05
V29	Unfavourable	1.05
V30	Unfavourable	1
$\sum V$	176368	kN

Table XVI.15: Partial factors and resultant design vertical force

* This value represents $\gamma\psi_0$ **B: Maximum negative head is dominant**

Not governing.

H: Ship collision

Not governing.

Lowest LAT

Not governing.

During construction

Not governing.

	Effect	γ
H1	Unfavourable	1
H2	Unfavourable	1
H3	Unfavourable	1
H4	Unfavourable	1
H5	Unfavourable	1
H6	Unfavourable	1.05
H7	Unfavourable	1
H8	Unfavourable	1
H9	Unfavourable	0.95
H10	Unfavourable	1
H11	Unfavourable	1
H12	Unfavourable	1.05
H13	Unfavourable	1
H14	Unfavourable	1
H15	Unfavourable	1
H16	Unfavourable	0.95

Table XVI.16: Partial factors for horizontal forces

The total moment (around point A), is calculated as follows:

$$M = \sum_{i=1}^{n=30} V_i \cdot e_i + \sum_{i=1}^{n=16} H_i \cdot e_i$$

$$= 710009 \text{ kNm}$$

Finally, the unity check:

$$UC = \frac{6 \cdot \sum M}{B \cdot \sum V} \leq 1$$

$$= \frac{6 \cdot 710009}{50 \cdot 176368}$$

$$= 0.48$$

XVI.2.5 Uplift

For any point in time or building stage where the piers should remain stable on the bed the total self weight of the structure and the resultant downward vertical force should be greater than the upward water pressure under the pier, i.e. Equation (XVI.12) should hold at all times.

$$\sum V \geq 0 \quad (\text{XVI.12})$$

where: V [kN] = resultant vertical force, where downwards is defined positive

As uplift concerns the UPL limit state, partial factors according to A.4 (1)P and A.4 (2)P from Eurocode 1 (2011a) must be used.

A: Maximum positive head is dominant

Not governing.

B: Maximum negative head is dominant

Not governing.

H: Ship collision

Not governing.

Lowest LAT

Not governing.

During construction

	Effect	γ
V11	Favourable	0.9
V12	Favourable	0.9
V13	Favourable	0.9
V14	Favourable	0.9
V15	Unfavourable	1
V18	Favourable	1
V19	Favourable	1
V20	Favourable	1
V21	Favourable	1
V22	Favourable	1
V25	Favourable	1
V26	Favourable	1
$\sum V$	78596	kN

Table XVI.17: Design vertical forces

The resultant vertical force in Table XVI.17 establishes that the pier is stable regarding uplift for the load combination: during construction. As such, the piers can be considered stable regarding uplift for the entire intended lifetime of 200 years including the time during construction.

XVI.2.6 Scour

In order to prevent scour directly adjacent to the Delta Barrier (and internal erosion) a granular, geometrically closed filter is designed. Given the consequences if the barrier subsides (e.g. distortion of the piers) for the essential function of the barrier structure as a safeguard against flooding, the failure probability of the filter must be very low. Hence, a geometrically closed filter seems appropriate.

The top layer of the granular, geometrically closed filter should be stable in flow²⁶, layering of the filter should be as such that the stability (between filter layers) and the permeability of the filter is sufficient and the bottom protection should be of sufficient length in order for the scour hole adjacent to the filter not to cause instability of the piers.

Critical flow patterns

Using the concept of continuity, the depth-averaged velocity at the reattachment point can be calculated by means of Equation (XVI.13)

$$\bar{u}_0 = \frac{\mu a}{h_r} \sqrt{2g\Delta h} \quad (\text{XVI.13})$$

where:	\bar{u}_0	[m/s]	=	depth-averaged velocity at the reattachment point
	μ	[-]	=	discharge coefficient of the Delta Barrier = 0.7
	a	[m]	=	height of the flow area (i.e. distance between the sill and top beam) = 9
	h_r	[m]	=	water depth at the reattachment point
	g	[m/s ²]	=	gravitational acceleration = 9.81
	Δh	[m]	=	head difference over the Delta Barrier

After the reattachment point and after sudden broadening of the flow area behind the piers, the flow pattern can be schematized by a plane jet. Schiereck (2019) proposes Equation (XVI.14) for the development (say dispersion) of the flow velocity for a plane jet in x and y-direction after the reattachment point, in the region of fully developed flow.

$$\bar{u} = \frac{3.5\bar{u}_0}{\sqrt{x/B}} e^{\left(-0.693\left(\frac{y}{0.1x}\right)^2\right)} \quad (\text{XVI.14})$$

where:	\bar{u}	[m/s]	=	depth-averaged flow velocity after reattachment point
	B	[m]	=	half the effective width between two piers = 20

The critical flow velocity at the Tidal Lake side of the Delta Barrier is governed by the reliability of the closure operation. In order for the design to be climate robust (i.e. be functional till a sea level rise of 1 m), a head over one open - c.q. failed to close - gate of 5.10 m should not lead to failure of the structure. With a closely managed water depth of 8 m (water level at NAP + 1 m), Equation (XVI.13) yields $\bar{u}_0 = 7.88$ m/s.

The critical flow velocity at the sea side of the Delta Barrier is governed by the tidal flow where the gates of the storm surge barrier are still open. Assuming the maximum sea level rise of 1 m and a discharge at Lobith of 10000 m³/s before closure is required, the hydrodynamic model (see Appendix IX) gives a flow velocity through the barrier of 2.75 m/s. Converting to the critical depth-averaged flow velocity at the reattachment point for a water depth of again 8 m gives $\bar{u}_0 = 2.17$ m/s.

²⁶Aspects such as stability in waves, falling and/or dragging anchors and ship collision, although of importance, have not been considered

Finally, with Equation (XVI.14), Figure XVI.30 depicts the flow patterns at both the sea side and Tidal Lake side for their respective critical flow velocities. Until the reattachment point (at about 12B, represented by the black dashed lines), the depth-averaged flow velocity is assumed equal to the depth-averaged flow velocity at the reattachment point (\bar{u}_0).

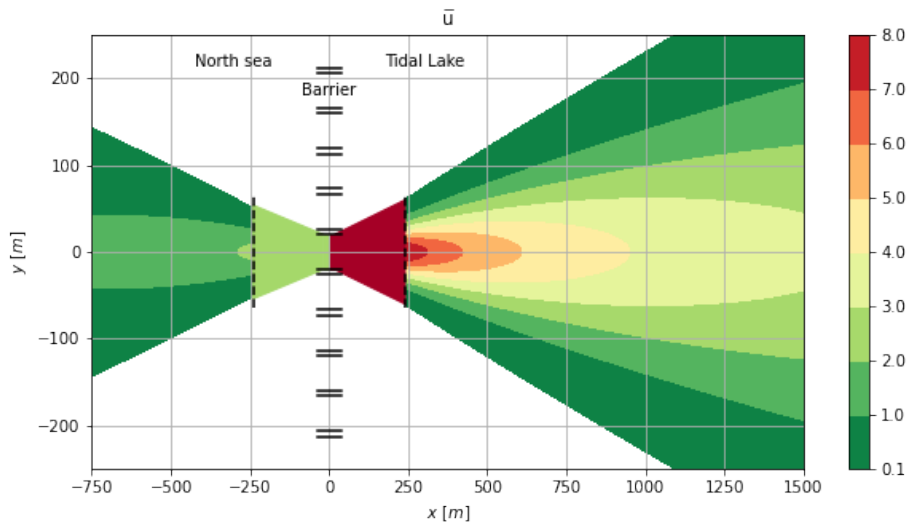


Figure XVI.30: Critical flow patterns

Bed protection length

In order to ensure the stability of the Delta Barrier, a potential scour hole must be kept at sufficient length from the structure as such that a developing sliding plane can not reach the structure. Figure XVI.31 gives an impression of the failure mechanism of instability due to a scour hole and all relevant parameters.

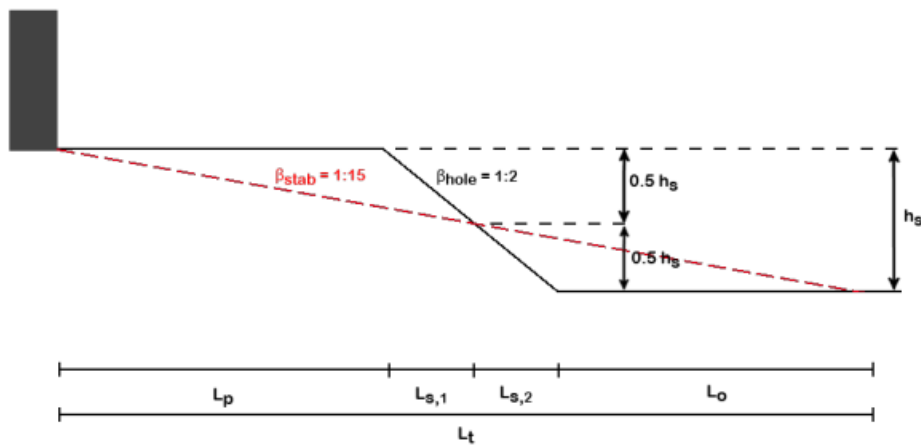


Figure XVI.31: Instability due to a scour hole (Donkers, 2021)

The depth of the scour hole behind the scour protection, the consistency of the soil and the slope of the scour hole are the most important parameters which determine the required length of the scour protection. Equation (XVI.15), as argued by Schiereck (2019), is used to determine the required bed protection length.

$$L_p = h_s \cdot \frac{1}{2(\beta_{stab} - \beta_{soil})} \quad (\text{XVI.15})$$

where: L_p [m] = required bed protection length
 h_s [m] = scour hole depth
 β_{stab} [-] = slope after sliding
 β_{soil} [-] = slope before sliding

As for the slope after sliding (β_{stab}), Schiereck (2019) indicates that a slope of 1:15 is a reasonable estimate for loosely packed sand. The slope at which sliding occurs (β_{soil}) is assumed to be 1:2.

The scour hole depth at the end of the bottom protection for the critical flow velocities (see Figure XVI.30) can be estimated by finding the equilibrium (clear-water) scour depth using Equation (XVI.16) (Schiereck, 2019).

$$h_s = \frac{0.5\alpha\bar{u} - \bar{u}_c}{\bar{u}_c} \cdot h_0 \quad (\text{XVI.16})$$

where: h_s [m] = equilibrium clear water scour hole depth
 α [-] = $1.5 + 5 \cdot r \cdot f_c$
 r [-] = relative turbulence = 0.3 for jets
 f_c [-] = $\max(C/40; 1)$
 C [\sqrt{m}/s] = Chezy coefficient
 \bar{u}_c [m/s] = critical flow velocity of the bed material
 h_0 [m] = water depth

The Chezy coefficient, according to Nikuradse-Colebrook, should be determined using Equation (XVI.17) (Schiereck, 2019):

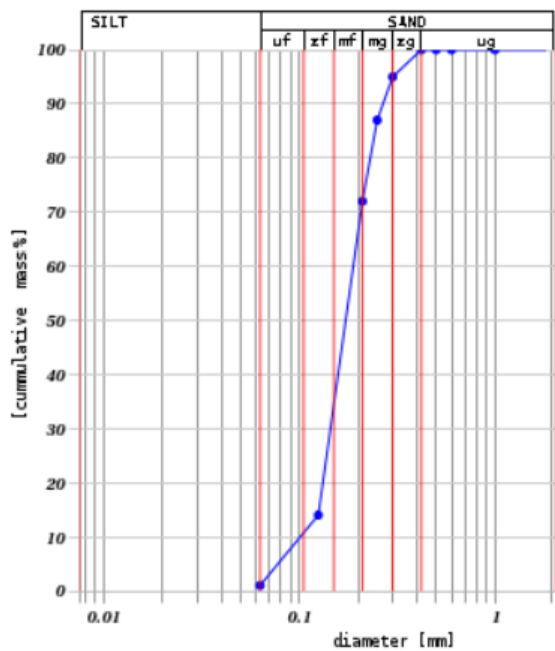
$$C \approx 18 \log \frac{12R}{k_r} \quad (\text{XVI.17})$$

where: R [m] = hydraulic radius
 k_r [m] = equivalent roughness $\approx 2d_{n50}$

The critical flow velocity of the bed material (adjacent to - and not part of - the bottom protection) is determined using the formula proposed by Shields for the stability of bed material in flow (Schiereck, 2019).

$$\bar{u}_c = \frac{C}{K_v} \sqrt{d_{n50} \psi_c \Delta} \quad (\text{XVI.18})$$

where: K_v [-] = $\frac{1 + 3r}{1 + 3 \cdot 0.1}$
 d_{n50} [m] = nominal diameter of the bed material
 ψ_c [-] = Shields parameter describing initiation of motion



The nominal diameter of the bed material can be found by looking at the sieve curve of said material found in Dinoloket (2022). Figure XVI.32 presents the sieve curve from which one can read that $d_{50} = 240 \mu\text{m}$. Using Equation (XVI.19), as proposed by Schiereck (2019), the nominal diameter (d_{n50}) is determined.

$$d_{n50} \approx 0.84 d_{50} \tag{XVI.19}$$

Equation (XVI.19) yields $d_{n50} \approx 200 \mu\text{m}$.

As for the Shields parameter (ψ_c), a nominal diameter of $200 \mu\text{m}$ results in a value $\psi_c = 0.06$ (Schiereck, 2019) as the point of initiation of motion of the bed material.

Figure XVI.32: Sieve curve of the bed material (Dinoloket, 2022)

Finally, with a water depth (h_0) of 8 m (and $R \approx h_0$), the required bed protection length can be calculated using Equation (XVI.15) for both the sea and Tidal Lake side. Table XVI.18 presents all relevant parameters needed for said calculation and the required lengths for both sides.

Side	α [-]	\bar{u} [m/s]	\bar{u}_c [m/s]	h_s [m]	L_p [m]
Sea	5.13	1.38	0.29	90	600
Tidal Lake	5.13	3.24	0.29	222	1450

Table XVI.18: Required bed protection length with relevant parameters

Stability of the top layer

The stability in flow of the top layer is calculated using the equation as proposed by Izbash (Equation (XVI.20) by Schiereck (2019)). As opposed to the standard approach proposed by Shields, the Izbash formula is used especially in cases of non-uniform flow or in cases of e.g. water jets (Schiereck, 2019). As the flow behind an opening of the Delta Barrier is all but uniform and water jets are plenty behind the piers, using the formula proposed by Izbash (instead of Shields) seems valid.

$$d = 0.7 \frac{u_c^2}{2g\Delta} \tag{XVI.20}$$

- where:
- d [m] = diameter of the top layer
 - u_c [m/s] = corresponding critical flow velocity
 - g [m/s²] = gravitational acceleration = 9.81
 - Δ [-] = $\frac{\rho_s - \rho_w}{\rho_w}$
 - ρ_s [kg/m³] = density of the top layer stones = 2650
 - ρ_w [kg/m³] = density of the (sea) water = 1025

It should be noted that Izbash did not define the specific place of the velocity (u_c), neither is it very clear how the diameter is defined. As Izbash did his tests with big stones in relatively shallow water,

one may assume that the diameter in Equation (XVI.20) is equal to the nominal diameter (d_n). As for the critical velocity one may assume that the near-bed velocity should be used. Though, conservatively here, the depth-averaged velocity is used.

Using the critical flow patterns from Figure XVI.30 and the bed protection lengths from Table XVI.18, the required stone sizes of the top layers can be determined. Table XVI.19 and Table XVI.20 present the top layer design for the Tidal Lake side and sea side respectively.

Section nr.	Class name	range (x) [m]	Length [m]	d_{n50} [m]	\bar{u}_c [m/s]
1	Non-standard	0 - 310	310	1.82	7.88
2	HM _A 6000-10000	310 - 375	65	1.44	7.00
3	HM _A 3000-6000	375 - 495	120	1.18	6.35
4	HM _A 1000-3000	495 - 755	260	0.90	5.54
5	HM _A 300-1000	755 - 1310	555	0.59	4.49
6	HM _A 40-200	1310 - 1450	140	0.34	3.41

Table XVI.19: Top layers Tidal Lake side

Section nr.	Class name	range (x) [m]	Length [m]	d_{n50} [m]	\bar{u}_c [m/s]
7	LM _A 5 - 40	-0 - -265	265	0.17	2.41
8	CP90/250	-265 - -345	80	0.128	2.09
9	CP90/180	-345 - -525	180	0.097	1.82
10	CP45/125	-525 - -600	75	0.064	1.48

Table XVI.20: Top layers sea side

Filter layering

The subsequent filter layers should obey three criteria, presented below by equations Equation (XVI.21a), Equation (XVI.21b), Equation (XVI.21c) considering stability, permeability and internal stability respectively (Schiereck, 2019).

$$\frac{d_{15F}}{d_{85B}} < 5 \quad (\text{XVI.21a})$$

$$\frac{d_{15F}}{d_{15B}} > 5 \quad (\text{XVI.21b})$$

$$\frac{d_{60}}{d_{10}} < 10 \quad (\text{XVI.21c})$$

Using both standard and non-standard gradings (see Table XVI.23 for the characteristics), Table XVI.21 and Table XVI.22 present the filter layering per section (as specified in Table XVI.19 and Table XVI.20) for the Tidal Lake side and sea side respectively.

Section nr.	1	2	3	4	5	6
Layer nr.	1	2	3	4	5	6
	14000-18000	HM _A 6000-10000	HM _A 3000-6000	HM _A 1000-3000	HM _A 300-1000	LM _A 40-200
	LM _A 40-200	LM _A 40-200	LM _A 10-60	LM _A 5-40	CP90/180	CP45/125
	CP45/125	CP45/125	CP45/125	Gravel (course)	Gravel (course)	Gravel (course)
	Gravel (course)	Gravel (course)	Gravel (course)	Gravel (fine)	Gravel (fine)	Gravel (fine)
	Gravel (fine)	Gravel (fine)	Gravel (fine)			
Thickness ($\sum t$)	5.6 m	4.6 m	3.6 m	2.9 m	2.1 m	1.6 m

Table XVI.21: Filter layering Tidal Lake side

Section nr.	7	8	9	10
Layer nr. 1	LM _A 5-40	CP90/250	CP90/180	CP45/125
Layer nr. 2	Gravel (course)	Gravel (course)	Gravel (course)	Gravel (course)
Layer nr. 3	Gravel (fine)	Gravel (fine)	Gravel (fine)	Gravel (fine)
Thickness ($\sum t$)	0.9 m	0.6 m	0.6 m	0.6 m

Table XVI.22: Filter layering sea side

	Class	d_{15} [m]	d_{85} [m]	t^* [m]
14000-18000	Non-standard	2.05	2.30	4
HM _A 6000-10000	Standard	1.72	2.06	3
HM _A 3000-6000	Standard	1.35	1.62	2.5
HM _A 1000-3000	Standard	1.01	1.41	2
HM _A 300-1000	Standard	0.69	0.96	1.5
LM _A 40-200	Standard	0.33	0.50	1
LM _A 10-60	Standard	0.22	0.32	0.5
LM _A 5-40	Standard	0.15	0.26	0.5
CP90/250	Standard	0.12	0.34	0.2
CP90/180	Standard	0.09	0.18	0.2
CP45/125	Standard	0.055	0.154	0.2
Gravel (course)	Non-standard	0.008	0.032	0.2
Gravel (fine)	Non-standard	0.0015	0.003	0.2

Table XVI.23: Grading characteristics

* $t > 2d_{n50}$ including tolerances with a minimum of 0.20 m

Final design

Finally, Figure XVI.33 presents the final design of the bottom protection.

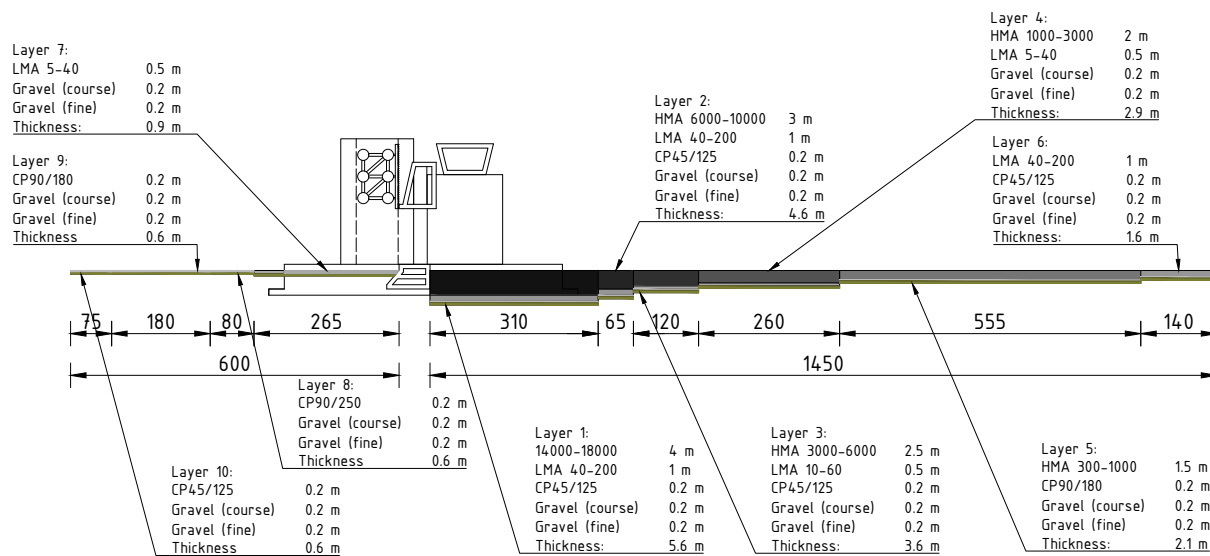


Figure XVI.33: Final design bottom protection (not to scale)

XVII Monte Carlo Simulation Construction Costs

This appendix presents the Monte Carlo simulation conducted to estimate the standard deviation of the total costs in order to present the total costs of the Delta Barrier by means of a bandwidth ($\mu-\sigma$; $\mu+\sigma$).

Variables such as the construction time per element, the cost of materials and vessels, the amount of materials to be used and the preparation costs, are stochastic in nature. Said variables are assumed to be normally distribution, all with an individually estimated expected value (μ) and standard deviation (σ). Table XVII.1 presents all stochastic parameters used in the Monte Carlo simulation. It should be noted that all presented variables are assumed to be uncorrelated.

For a total of 100000 iterations, the total costs are calculated where for every iteration a random sample is drawn from the normal distribution per stochastic variable. Finally, from all 100000 iterations, the standard deviation of the total cost estimate is calculated. With the input as presented in Table XVII.1, the Monte Carlo simulation produces a standard deviation of the total cost estimate of 412 million euro. All cost estimates represent price level 2022.

Variable	<i>Unit</i>	μ	σ
Soil to be dredged	m ³	740000	74000
Costs of dredging	€/m ³	6.75	1.69
Operations soil replacements	days	90	22.5
Soil replacements costs	€/day	150000	37500
Operations soil compacting	weeks	52	13
Soil compacting costs	€/week	1000000	250000
Costs of foundation mats	m. €	200	50
Costs of abutments	m. €	10	2.5
Amount of concrete, piers	m ³	122200	30550
Price of concrete	€/m ³	125	18.75
Amount of rebar, piers	kg/m ³	250	62.5
Price of rebar	€/kg	1.50	0.375
Operations placing piers	days	78	19.5
Standby time specialised vessel, piers	days	365	90
Costs specialised vessel, piers	€/day	200000	50000
Amount of stones bottom protection	m ³	6250000	625000
Price of stones bottom protection	€/m ³	75	18.75
Capacity fallpipe vessel*	t/hour	2000	500
Costs fallpipe vessel	€/day	120000	30000
Amount of concrete, bridge girders	m ³	12960	1296
Pre-stressing steel, bridge girders	kg/m ³	75	18.75
Operations placing bridge girders	days	108	27
Standby time lifting vessel, bridge girders	days	292	73
Costs lifting vessel	€/day	100000	25000
Amount of concrete, driving mech. sup.**	m ³	7800	1950
Amount of steel, driving mech. sup.	kg/m ³	250	62.5
Operations placing driving mech. sup.	days	52	13
Standby time lifting vessel, driving mech. sup.	days	292	73
Amount of steel, gates	kg	28000000	5600000
Operations placing gates	days	50	12.5
Standby time lifting vessel, gates	days	292	73
Amount of concrete, sill beams	m ³	12500	1250
Pre-stressing steel, sill beams	kg/m ³	72	18
Operations placing sill beams	days	100	25
Standby time lifting vessel, sill beams	days	292	73
Amount of concrete, upper beams	m ³	16250	1625
Pre-stressing steel, upper beams	kg/m ³	55	13.75
Operations placing upper beams	days	50	12.5
Standby time lifting vessel, upper beams	days	292	73
Investments specialised equipment	m. €	200	50
Costs of dry dock	m. €	100	25
Costs of harbour	m. €	100	25

Table XVII.1: Stochastic parameters used in Monte Carlo simulation

* Data from Boskalis (2023)

** Driving mechanisms supports